Polyether-based Copolymers:
From Tailored Polarity via DMC Catalysis
to Biomedical Application

Dissertation
zur Erlangung des Grades
„Doktor der Naturwissenschaften"
im Promotionsfach Chemie

am Fachbereich
Chemie, Pharmazie, Geographie und Geowissenschaften
der Johannes Gutenberg-Universität Mainz

vorgelegt von

Rebecca Ruth Matthes

geboren am 01.01.1993
in Titisee-Neustadt

Mainz, Juli 2021

JOHANNES GUTENBERG
UNIVERSITÄT MAINZ

JG|U

Referring to §10 section 3d of the Doctoral Degree Regulations (24.07.2007), I hereby declare that I wrote the dissertation submitted without any unauthorized external assistance and used only sources acknowledged in the work. All textual passages which are appropriated verbatim or paraphrased from published and unpublished texts as well as all information obtained from oral sources are duly indicated and listed in accordance with bibliographical rules. In carrying out this research, I complied with the rules of standard scientific practice as formulated in the statutes of Johannes Gutenberg University Mainz to insure standard scientific practice.

CONTENT

MOTIVATION AND OBJECTIVES

Advanced polymeric materials are supporting countless aspects of our modern life. However, the increasing demands on novel polymers necessitate precise and fully comprehended synthesis strategies. Focusing on polyethers, the multitude of applications ranging from soft components in polyurethane foaming to pharmaceutical formulations require diverse polymerization methods.

Particularly, polymers applied in a biomedical context need to fulfil the highest standards if it comes to the absence of by-products, biocompatibility and reproducibility in the respective manufacturing process. Its ideal property profile established poly(ethylene glycol) (PEG) as the "gold standard" and most prominent example of biomedically utilized polymers. Well-defined PEG is synthesized via the widely established anionic ring-opening polymerization of ethylene oxide. The resulting aliphatic polyether combines high water-solubility and non-toxicity in one distinct material due to its optimal oxygen-oxygen distances and inert chemical structure.[1] In 1977, Davis and Abuchowski[2] introduced the covalent attachment of PEG to proteins, the so-called PEGylation, which fundamentally established PEG in modern nanomedicine. The bioconjugation improves solubility and enlarges the circulation times of drugs in the blood stream via the implementation of stealth properties. These features enabled the approval of over 30 PEGylated drugs and nanocarriers by the U.S. Food and Drug Administration (FDA) to date.[3] More recently, PEGylated nanoparticles play a pivotal role in the containment of the global SARS-CoV-2 pandemic with their utilization in mRNA-based vaccines which further represent promising candidates in tomorrow's cancer treatment.[4]

In recent years however, the many advantages of PEG were impaired by the increased documentation of immune responses and the induction of anti-PEG antibodies (APA). As a result, accelerated blood clearance significantly reduces the effectiveness of PEGylated drugs and nanoparticles while causing allergic reactions up to anaphylactic shocks in rare, but severe cases. Recent studies revealed the unique recognition mechanism of APAs, relying on van-der-Waals interactions and capturing of the PEG chain by an open ring-structure.[5] The presented disadvantages have resulted in the development of PEGylation alternatives. Based on a different perspective, the following question (i) arises:

Instead of replacing PEG: Is the introduction of synthetic point mutations to PEG the solution to anti-PEG antibodies and a way for ensuring the future of PEGylated drugs?

In this context, insights of copolymerization kinetics are crucial for understanding the subsequent polymer microstructure in regard to the APA interaction. This statement is maintained regardless of the utilized polymerization method.

While the anionic ring-opening polymerization of epoxides represents the method of choice for polyethers in biomedical applications, the double metal cyanide (DMC) catalyst enables the industrial synthesis of polyether polyols in a megaton scale.[6] However, the detailed mechanistic and kinetic understanding of DMC catalysis remains obscured. Nonetheless, the unique polymerization mechanism equally opens a wide field of possibilities for the synthesis of novel materials.

Industrially, DMC catalysis is almost exclusively utilized for the synthesis of polyether polyols applied as soft components in polyurethane foaming based on poly(propylene oxide) (PPO), an amorphous, hydrophobic derivative of PEG. Herein, the modification of PPOs polarity is a crucial step to fulfil the requirements for specialized polyurethane formulations.[7] Thus, implementing the DMC catalysis to academic research, the following question (ii) arises:

Can we achieve a tailorable, evenly distributed introduction of hydrophilicity to PPO by statistical copolymerization?

Pursuing this aim, DMC catalysis is applied for the homo- and copolymerization of various monomer classes apart from epoxides i.e., lactones and carbon dioxide. In this context, the copolymerization of epoxides and siloxanes is a merely unexplored area. Block copolymers consisting of polyether as well as polysiloxane segments are established materials and a widely utilized surfactants due to their highly amphiphilic properties.[8] To this date, however, the merging of polyether and polysiloxane segments is solely achieved by coupling of the corresponding homopolymers. As common ionic polymerization techniques are inadequate in regard to this synthetic problem and keeping DMC catalysis in mind, a final question (iii) is phrased:

Is the DMC catalyst capable of realizing the statistical copolymerization of epoxides and cyclic siloxanes?
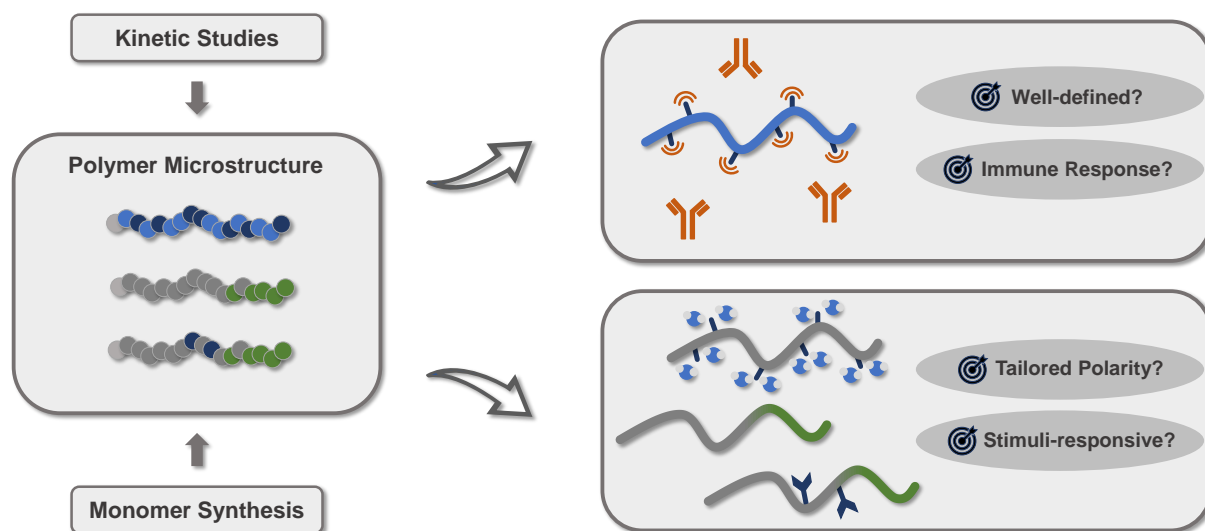
Scheme 1. Illustration of central questions characterizing the presented synthetic strategies and resulting polymer architectures.

REFERENCES

(1) Herzberger, J.; Niederer, K.; Pohlit, H.; Seiwert, J.; Worm, M.; Wurm, F. R.; Frey, H. Polymerization of Ethylene Oxide, Propylene Oxide, and Other Alkylene Oxides: Synthesis, Novel Polymer Architectures, and Bioconjugation. *Chemical reviews* **2016**, *116*, 2170–2243.

(2) Abuchowski, A.; McCoy, J. R.; Palczuk, N. C.; van Es, T.; Davis, F. F. Effect of covalent attachment of polyethylene glycol on immunogenicity and circulating life of bovine liver catalase. *Journal of Biological Chemistry* **1977**, *252*, 3582–3586.

(3) Pasut G., Z. S., Ed. Polymer-Protein Conjugates; *Elsevier*, **2020**.

(4) Pardi, N.; Hogan, M. J.; Porter, F. W.; Weissman, D. mRNA vaccines - a new era in vaccinology. *Nature reviews. Drug discovery* **2018**, *17*, 261–279.

(5) Huckaby, J. T.; Jacobs, T. M.; Li, Z.; Perna, R. J.; Wang, A.; Nicely, N. I.; Lai, S. K. Structure of an anti-PEG antibody reveals an open ring that captures highly flexible PEG polymers. *Commun Chem* **2020**, *3*.

(6) Jack Milgrom. Method of Making a Polyether using a Double Metal Cyanide Complex Compound. US 3,278,457, **1963.**

(7) Ionescu, M. Chemistry and technology of polyols for polyurethanes; Rapra Technology Ltd: *Shawbury, U.K*, **2005**.

(8) Galin, M.; Mathis, A. Structural and thermodynamic study of dimethylsiloxane-ethylene oxide PDMS-PEO-PDMS triblock copolymers. *Macromolecules* **1981**, *14*, 677–683.

GRAPHICAL ABSTRACT

CHAPTER 1.2

Polyethers based on Short-Chain Alkyl Glycidyl Ethers: From Thermoresponsive to Highly Biocompatible Materials
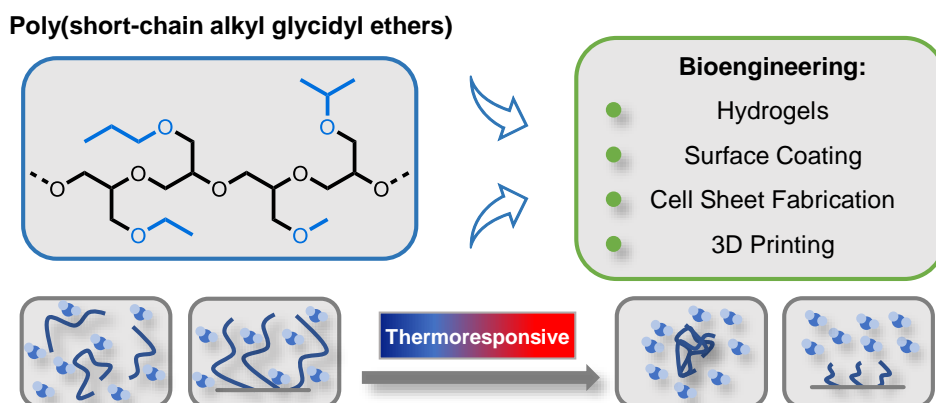
CHAPTER 2.1

Questioning a Paradigm: Random PEG Copolymers for a Better PEGylation?
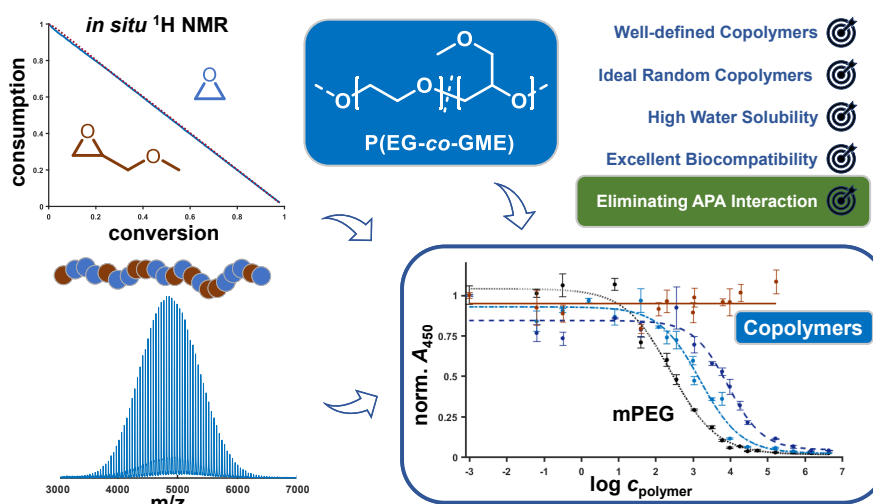
CHAPTER 2.1

In situ Kinetics is Indispensable: Influence of Solvents and Monomers on Anionic Ring-Opening Copolymerization of Epoxides
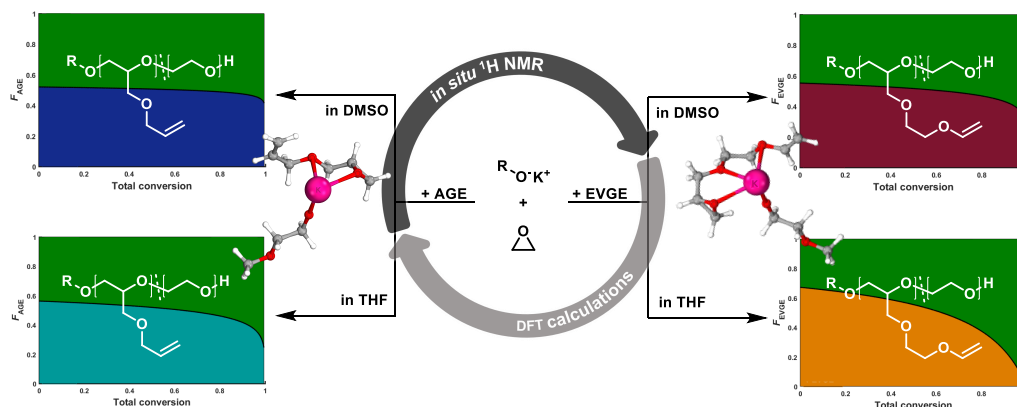
CHAPTER 3.1

Tailorable Introduction of Hydrophilicity to Polypropylene Oxide via DMC Catalyzed Copolymerization
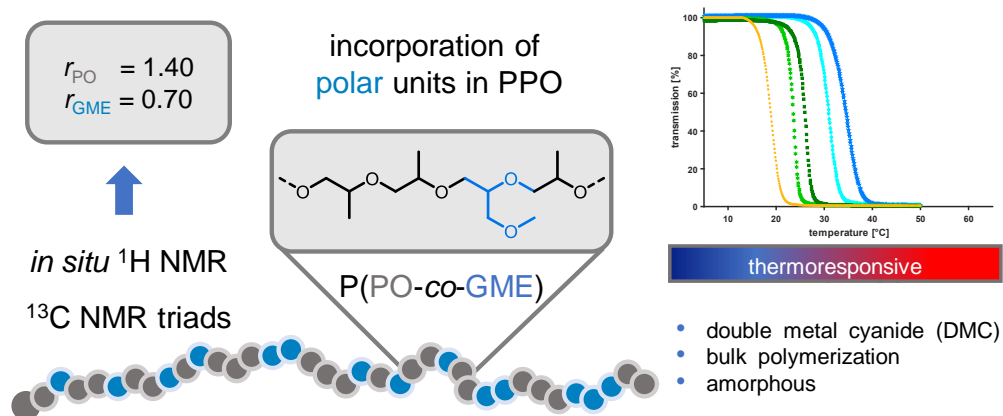
CHAPTER 3.2

The Unique Versatility of the Double Metal Cyanide (DMC) Catalyst: Introducing Siloxane Segments to Polypropylene Oxide by Ring-Opening Copolymerization
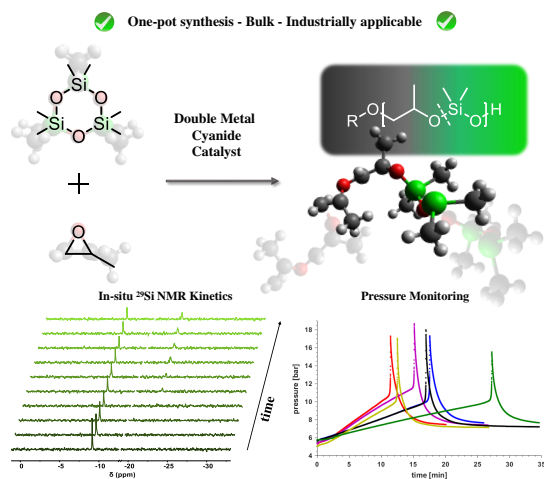
CHAPTER 3.3

Toolbox DMC Catalysis: Synthesis and Modification of Multifunctional Polyether-Polysiloxane Copolymers
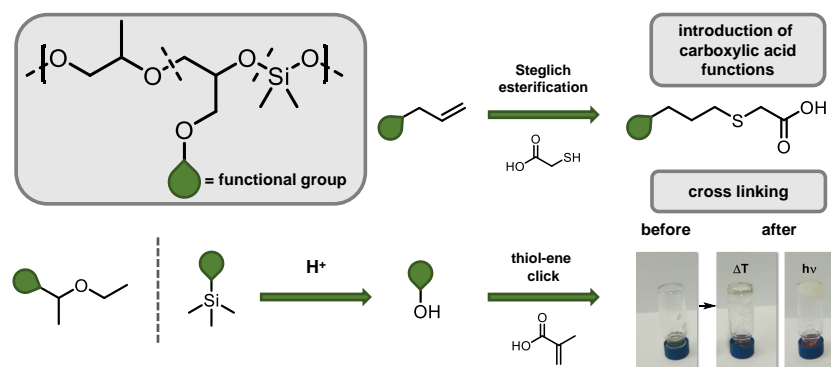
CHAPTER A1

Kinetic Investigations on DMC Catalysis of Propylene Oxide by Ring-Opening Polymerization
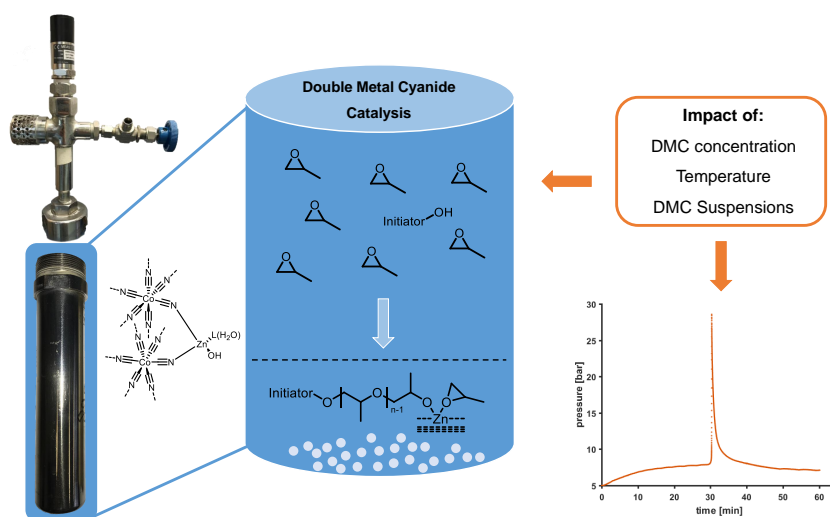
ABSTRACT

As Hermann Staudinger first discovered macromolecules in 1920, the following polymer success stories was hardly predictable. Today, polymer-based materials are omnipresent in our everyday life ranging from cosmetics, packaging materials to modern nano medicine by only naming a few examples. Throughout the course of the last century, a multitude of techniques has been introduced, enabling the precise synthesis of polymer architectures specifically manufactured for targeted applications. Among these methods, living polymerization prevailed as the method of choice for the design of well-defined multifunctional polymers whereas catalytic techniques fundamentally facilitated the industrial success of polymer materials.

Based on this, the presented thesis focuses on two parts: **(i)** the in-depth understanding of anionic epoxide copolymerization kinetics while further exploiting this knowledge for the development of biomedical polymer materials and **(ii)** the tailored variation of polarity in novel copolymeric structures facilitated by the double metal cyanide (DMC) catalyst.

**Chapter 1** introduces general aspects regarding the synthesis of polyether-based materials and their field of applications.

To give a general overview, techniques for the polymerization of epoxides and cyclic siloxanes are discussed while special interested is paid to the anionic (AROP) as well as the DMC catalyzed ring-opening polymerization in **chapter 1.1**. A detailed understanding of polymeric microstructures is crucial for design of novel materials; thus, the underlying copolymerization kinetics are outlined. Additionally, the high relevance of the most prominent polyether poly(ethylene glycol) (PEG) is described. Here, the concept of PEGylation, its significance for biomedical applications but also its limitations and possible alternatives are elucidated.

In the following, the description of the highly valuable biocompatibility of polyether-based structures is expanded by summarizing the beneficial aspects of polyethers bearing short-chain alkyl glycidyl ethers in **chapter 1.2**. The varying combination possibilities of these monomers within statistical but also block copolymers enable a finely tunable hydrophilicity, leading to highly thermoresponsive but equally biocompatible materials. Here, the polymerization techniques utilized for this purpose as well as the manifold bioapplications ranging from hydrogels, tissue engineering to 3D printability are summarized.

In the second part of this thesis, the copolymerization kinetics of varying epoxides and concepts for bioapplication of polyether-based copolymers synthesized by anionic ring-opening polymerization are described throughout **chapter 2**.

Copolymers containing ethylene oxide (EO) and glycidyl methyl ether (GME) are proposed as promising, non-immunogenic candidates for bioconjugation in **chapter 2.1**, following the established concept of PEGylation. The first successful AROP of P(EG-*co*-GME) due to a novel synthesis route of GME is introduced. The defined nature of these copolymers possessing an exceptionally high end-group fidelity is supported by NMR spectroscopy and mass spectrometry. Turbidimetric experiments illustrate the high water-solubility of P(EG-*co*-GME) which show no stimulating

effect in murine cell viability tests, therefore validating the non-toxicity of the discussed materials. One of the key aspects enabling the proposed concept is verified by *in situ* ^{1}H NMR kinetic experiments and supported by Monte-Carlo simulations: the fully random copolymerization of EO and GME. The uniform distribution of side-chains within the PEG backbone prevents the recognition of P(EG-*co*-GME) by anti-PEG antibodies (APA) which is evinced by enzyme-linked immunosorbent assays. Hence, the structural simplicity but nonetheless unstructured distribution of "chemical point-mutations" renders these copolymers highly promising candidates for preserving the future-PEGylation despite the existence of APAs.

In **chapter 2.2** the copolymerization kinetics of two selected glycidyl ethers and EO are fundamentally investigated by *in situ* ^{1}H NMR kinetics. Here, the reactivity of the respective monomers allyl glycidyl ether (AGE) and vinyloxy ethyl glycidyl ether (EVGE) in anionic copolymerization with EO is determined in dependence of the utilized solvents. Density functional theory calculations propose a crown-ether like complexation behavior of the utilized glycidyl ethers which results in the experimentally determined increased reactivity compared to EO. Further, the increase of solvent polarity (dimethyl sulfoxide) indicates a convergence of monomer reactivity while less a polar solvent (tetrahydrofuran) demonstrates the reverse effect.

The third part of this thesis depicts the multifaced potential of the industrially established DMC catalyst for synthesis of novel polymeric structures which is collected in **chapter 3**.

Here, the DMC catalyst is utilized for the synthesis of thermoresponsive copolymers composed of GME and propylene oxide (PO) in chapter **3.1**. For the first time, an almost random incorporation of polar units to a PPO backbone is achieved which is analyzed in thorough detail. The monomer reactivities are determined via bulk *in situ* ^{1}H NMR kinetics while ^{13}C triad analysis supported the transferability of the *in situ* results to the resulting polymer microstructure. Turbidimetric as well as contact angle measurements verify the introduction of polar units to the nonetheless amorphous polyether. The non-crystallinity and evenly increased polarity of P(PO-*co*-GME) copolymers synthesized via DMC catalysis are auspicious alternatives to established hydrophilic soft components in polyurethane foaming.

Chapter 3.2 further expands the versatility of the DMC catalyst as it scopes the first statistical copolymerization of a cyclic siloxane with an epoxide. Polyether-polysiloxane block copolymers are widely utilized in surfactants and other applications, however statistical copolymerization has never been realized. DMC catalysis of PO and hexamthylcyclotrisiloxane (D_3) in a bulk one-pot synthesis enable the formation of gradient copolymers which is confirmed by *in situ* ^{29}Si NMR kinetics as well as subsequent 2D NMR spectroscopy. The successful formation of statistical copolymers results in a significantly decreased glass transition temperature and equally decreased contact angle.

Subsequently, the concept of polyether-polysiloxane copolymers via DMC catalysis is enlarged by the incorporation of functional side-chains in **chapter 3.3**. The addition of AGE, ethoxy ethyl glycidyl ether (EEGE) and the rarely investigated glycidyl trimethylsilane (GlyTMS) in the copolymerization of PO and D_3 enables a multitude of modification chemistry. The addressability

of functional groups is demonstrated by the introduction of carboxylic acid substituents as well as the formation of cross linked materials via methacrylic esters. The acidic cleavability of both the in-chain functional groups and the ether-siloxane bonds is extensively studied via ^{1}H and ^{13}C NMR. Thus, the manyfold possibilities offered by the incorporation of functional, polar groups in combination with the pH-responsivity facilitate a conceivable application as degradable polyether-polysiloxane surfactants.

In **Chapter A1** of the appendix, deepening studies regarding the DMC catalyst are presented. Kinetic aspects of the industrially highly relevant DMC catalyzed ring-opening polymerization of PO are investigated via pressure monitoring and subsequent NMR spectroscopy as well as size exclusion chromatography. Throughout the exploration, the impact of catalyst concentration, temperature and the usage of polyols-catalyst suspensions is examined in regard to the polymerization efficiency and the suppression of high molecular weight tailing.

Finally, **chapter A2** describes the controlled incorporation of short-chain alkyl glycidyl ethers to poly(ethylene glycol)-based polymers. The synthesis of such copolymers, the bioconjugation as well as use thereof is hereby outlined throughout a pending European patent based on the concept introduced throughout chapter 2.1.

ZUSAMMENFASSUNG

Als Hermann Staudinger 1920 erstmals Makromoleküle entdeckte, war die folgende Erfolgsgeschichte der Polymere kaum vorhersehbar. Heute sind polymerbasierte Materialien in unserem Alltag allgegenwärtig, von Kosmetika über Verpackungsmaterialien bis hin zur modernen Nanomedizin, um nur einige Beispiele zu nennen. Im Laufe des letzten Jahrhunderts wurde eine Vielzahl von Techniken eingeführt, die die präzise Synthese von Polymerarchitekturen ermöglichen, die speziell für gewünschte Anwendungen hergestellt werden können. Unter diesen Methoden hat sich die lebende Polymerisation als die Methode der Wahl für das Design wohldefinierter multifunktionaler Polymere durchgesetzt, während katalytische Techniken den industriellen Erfolg von Polymermaterialien grundlegend ermöglicht haben.

Basierend hierauf konzentriert sich die hier vorgestellte Arbeit auf zwei Teile: **(i)** das vertiefte Verständnis der Kinetik der anionischen Epoxid-Copolymerisation bei Verwendung dieses Wissens für die Entwicklung biomedizinischer Polymermaterialien und **(ii)** die maßgeschneiderte Variation der Polarität neuartiger Copolymerstrukturen, die durch den Doppelmetallcyanid (DMC)-Katalysator ermöglicht wird.

Kapitel 1 beschreibt allgemeine Aspekte der Synthese Polyether-basierter Materialien und deren Anwendungsbereiche.

Um einen allgemeinen Überblick zu geben, werden Techniken der Polymerisation von Epoxiden und zyklischen Siloxanen in **Kapitel 1.1** diskutiert, wobei die anionischen (AROP) sowie die DMC katalysierte Ringöffnungspolymerisation detailliert betrachtet werden. Ein detailliertes Verständnis von polymeren Mikrostrukturen ist entscheidend für den Entwurf neuartiger Materialien, weshalb die zugrunde liegende Kinetik von Copolymerisationen skizziert werden. Zusätzlich zu den allgemeinen Aspekten, welche im Zuge dieses Kapitels beschrieben werden, wird die hohe Relevanz des prominentesten Polyethers Poly(ethylenglykol) (PEG) beschrieben. Hier werden das Konzept der PEGylierung, seine Bedeutung für biomedizinische Anwendungen, aber auch seine Grenzen und mögliche Alternativen erläutert.

In **Kapitel 1.2** wird die Biokompatibilität von Polyether-basierten Strukturen weiter vertieft, indem die vorteilhaften Aspekte von Polyethern, basierend auf kurzkettigen Alkylglycidylethern, zusammengefasst werden. Die unterschiedlichen Kombinationsmöglichkeiten dieser Monomere innerhalb statistischer und Blockcopolymere ermöglichen eine fein abstimmbare Hydrophilie, die zu hoch thermoresponsiven und ebenso biokompatiblen Materialien führt. Hierzu werden die dafür eingesetzten Polymerisationstechniken sowie die vielfältigen Bioanwendungen von Hydrogelen über Tissue Engineering bis hin zur 3D-Druckbarkeit zusammengefasst.

Im anschließenden Teil dieser Arbeit werden in **Kapitel 2** die zugrunde liegende Copolymerisationskinetik verschiedener Epoxide und Konzepte zur Bioanwendung von Polyether-basierten Copolymeren, die durch anionische Ringöffnungspolymerisation synthetisiert werden, beschrieben.

In **Kapitel 2.1** werden Copolymere, die Ethylenoxid (EO) und Glycidylmethylether (GME) enthalten, als vielversprechende, nicht-immunogene Kandidaten für die Biokonjugation nach dem

etablierten Konzept der PEGylierung vorgeschlagen. Die erste erfolgreiche AROP von P(EG-*co*-GME) basierend auf einer neuartigen Syntheseroute für GME wird vorgestellt. Die definierte Natur dieser Copolymere, die eine außergewöhnlich hohe Endgruppentreue besitzen, wird durch NMR-Spektroskopie und Massenspektrometrie unterstützt. Turbidimetrische Experimente veranschaulichen die hohe Wasserlöslichkeit von P(EG-*co*-GME), die in Tests zur Lebensfähigkeit von Mäusezellen keine stimulierende Wirkung zeigen und somit die Verträglichkeit der diskutierten Materialien bestätigen. Einer der Schlüsselaspekte, der das vorgeschlagene Konzept ermöglicht, wird durch *in situ* ^{1}H NMR kinetische Experimente verifiziert sowie durch Monte-Carlo-Simulationen unterstützt: die vollständig zufällige Copolymerisation von EO und GME. Die gleichmäßige Verteilung der Seitenketten innerhalb des PEG-Rückgrats verhindert die Erkennung von P(EG-*co*-GME) durch Anti-PEG-Antikörper, was durch Enzyme-Linked Immunosorbent Assays nachgewiesen wird. Die strukturelle Einfachheit und dennoch unstrukturierte Verteilung der "chemischen Punktmutationen" macht diese Copolymere daher zu vielversprechenden Kandidaten, um die PEGylierung trotz der Existenz von APAs zu erhalten.

In **Kapitel 2.2** wird die Copolymerisationskinetik von zwei ausgewählten Glycidylethern und EO mittels *in situ* ^{1}H-NMR-Kinetik grundlegend untersucht. Dabei wird die Reaktivität der jeweiligen Monomere Allylglycidylether (AGE) und Vinyloxyethylglycidylether (EVGE) bei der anionischen Copolymerisation mit EO in Abhängigkeit von den verwendeten Lösungsmitteln bestimmt. Dichtefunktionaltheoretische Berechnungen deuten auf ein Kronenether-artiges Komplexierungsverhalten der eingesetzten Glycidylether hin, das zu der experimentell ermittelten erhöhten Reaktivität gegenüber EO führt. Weiterhin zeigt sich mit zunehmender Polarität des Lösungsmittels (Dimethylsulfoxid) eine Konvergenz der Monomerreaktivität, während ein weniger polares Lösungsmittel (Tetrahydrofuran) den umgekehrten Effekt zeigt.

Im dritten Teil dieser Arbeit wird das vielseitige Potential des industriell etablierten DMC-Katalysators für die Synthese neuartiger polymerer Strukturen dargestellt, welches in **Kapitel 3** zusammengefasst ist.

Kapitel 3.1 beschreibt die Verwendung des DMC-Katalysators für die Synthese von thermoresponsiven Copolymeren aus GME und Propylenoxid (PO). Zum ersten Mal wird ein nahezu zufälliger Einbau von polaren Einheiten in ein PPO-Rückgrat erreicht, der eingehend analysiert wird. Die Reaktivitäten der Monomere werden mittels *in situ* ^{1}H-NMR-Kinetik bestimmt, während die ^{13}C- Triadenanalyse die Übertragbarkeit, der *in situ* Ergebnisse auf die resultierende Polymermikrostruktur unterstützt. Turbidimetrische sowie Kontaktwinkelmessungen verifizieren die Einführung von polaren Einheiten in den weiterhin amorphen Polyether. Die ausbleibende Kristallinität und gleichzeitig erhöhte Polarität der mittels DMC-Katalyse synthetisierten P(PO-*co*-GME)-Copolymere sind vielversprechende Alternativen zu etablierten hydrophilen Weichkomponenten in der Herstellung von Polyurethanschäumen.

Kapitel 3.2 zeigt die Vielseitigkeit des DMC-Katalysators, da es die erste statistische Copolymerisation eines zyklischen Siloxans mit einem Epoxid zeigt. Polyether-Polysiloxan-Blockcopolymere sind in Tensiden und anderen Anwendungen weit verbreitet, eine statistische Copolymerisation

wurde jedoch noch nie realisiert. Die DMC-Katalyse von PO und Hexamthylcyclotrisiloxan (D_3) in einer lösungsmittelfreien Eintopfsynthese ermöglicht die Bildung von Gradientencopolymeren, was durch *in situ* ^{29}Si und ^{1}H-NMR-Kinetik sowie anschließende 2D-NMR-Spektroskopie bestätigt wird. Die erfolgreiche Bildung von statistischen Copolymeren führt darüber hinaus zu einer deutlich verringerten Glasübergangstemperatur und einem ebenso verringerten Kontaktwinkel.

Anschließend wird das Konzept der Polyether-Polysiloxan-Copolymere mittels DMC-Katalyse durch die Einbindung funktioneller Seitenketten in **Kapitel 3.3** erweitert. Die Zugabe von AGE, Ethoxyethylglycidylether (EEGE) und dem selten untersuchten Glycidyltrimethylsilan (GlyTMS) bei der Copolymerisation von PO und D_3 ermöglicht eine Vielzahl an Modifikationmöglichkeiten. Die Adressierbarkeit der funktionellen Gruppen wird durch die Einführung von Carbonsäuresubstituenten sowie der Bildung von vernetzten Materialien über Methacrylsäureester demonstriert. Die saure Spaltbarkeit sowohl der ketteninternen funktionellen Gruppen als auch der Ether-Siloxan-Bindungen wird mittels ^{1}H- und ^{13}C NMR eingehend untersucht. Die vielfältigen Möglichkeiten des Einbaus funktioneller, polarer Gruppen in Kombination mit der pH-Empfindlichkeit ermöglichen somit eine denkbare Anwendung als abbaubare Polyether-Polysiloxan-Tenside.

In **Kapitel A1** des Anhangs werden vertiefende Studien zum DMC-Katalysator vorgestellt. Kinetische Aspekte der industriell hoch relevanten DMC-katalysierten Ringöffnungspolymerisation von PO werden mittels Drucküberwachung und anschließender NMR-Spektroskopie sowie Größenausschlusschromatographie untersucht. Dabei wird der Einfluss der Katalysatorkonzentration, der Temperatur und des Einsatzes von Polyol-Katalysator-Suspensionen auf die Polymerisationseffizienz und die Unterdrückung von hochmolekularem Tailing untersucht.

Schließlich wird in **Kapitel A2** der kontrollierte Einbau von kurzkettigen Alkylglycidylethern in Polymere auf Poly(ethylenglykol)-Basis beschrieben. Die Synthese solcher Copolymere, die Biokonjugation sowie deren Verwendung werden in einem anhängigen europäischen Patent beschrieben, welches auf dem in Kapitel 2.1 vorgestellten Konzept basiert.

Chapter 1

Introduction

Chapter 1.1

Ring-Opening Polymerization, Copolymerization Kinetics and the Concept of PEGylation

In this introductory chapter, the ring-opening polymerization (ROP) as the leading technique for the precise and controlled synthesis of polyether structures is outlined. In this context the anionic and especially the double metal cyanide (DMC) catalyzed ROP of epoxides as well as cyclic siloxanes is presented. Different polymerization techniques enable the synthesis of tailored microstructures depending on the utilized monomers and conditions. Therefore, the established models for evaluation of *in situ* copolymerization kinetics are described as well. Finally, this chapter characterizes the exceptional biocompatibility of poly(ethylene glycol) and its usage in bioconjugation for drug delivery systems.

In a detailed manner, chapter 1.2 gives a comprehensive overview of the synthesis of poly(short-chain alkyl glycidyl ethers) and their thermoresponsive nature in aqueous solution, which enables a wide range of applications from hydrogels to bioengineering.

RING-OPENING POLYMERIZATION OF CYCLIC MONOMERS

Synthesis of Polyethers by Anionic Ring-Opening Polymerization

Ever since the first polymerization of ethylene oxide (EO) in 18631 by Wurtz[1] and its first systematic study by Staudinger and Schweitzer,[2] later established as anionic ring-opening polymerization (AROP) introduced the controlled synthesis of a myriad of polymer architectures.[3] The simplest of all epoxide monomers EO, permits the synthesis of the industrially as well as academically most significant polyether: poly(ethylene glycol), also referred to as poly(ethylene oxide) (PEG and PEO, respectively). Generally, low molecular weight PEG (200 to $600 \, \text{g mol}^{-1}$) is a viscous liquid at room temperature, whereas high molecular weights result in a (semi-)crystalline material with a melting point T_m of up to $65 \, °C$.[4] Due to its high water-solubility and excellent biocompatibility, PEG represents the gold-standard of polymers for biomedical and pharmaceutical applications which will be more thoroughly discussed in the last section as well as in chapter 1.2.

A crucial requirement for medical purposes is the highly defined nature of the respective polymeric materials, which is fully accessible by AROP. In absence of impurities, in particular water and protic components, the living oxyanionic polymerization of epoxide monomers leads to polymers of narrow Poisson-type molecular weight distributions ($Đ$) and a high end-group fidelity.[5] Herein, the use of purified monomers, dry solvents and carefully chosen ambient reaction conditions is crucial.

The propagation of the AROP polymerization is achieved via a S_N2 reaction and ring-opening of the epoxide, initiated by strong nucleophiles like for instance alkali metal alkoxides (sodium, potassium or cesium) (Scheme 1). Merely partial deprotonation of the alkoxide is required due

to a rapid proton exchange between alkoxide and alcohol, leading to an equilibrium of active and a dormant chains ($k_{\text{proton exchange}} \gg k_{\text{propagation}}$).[6]
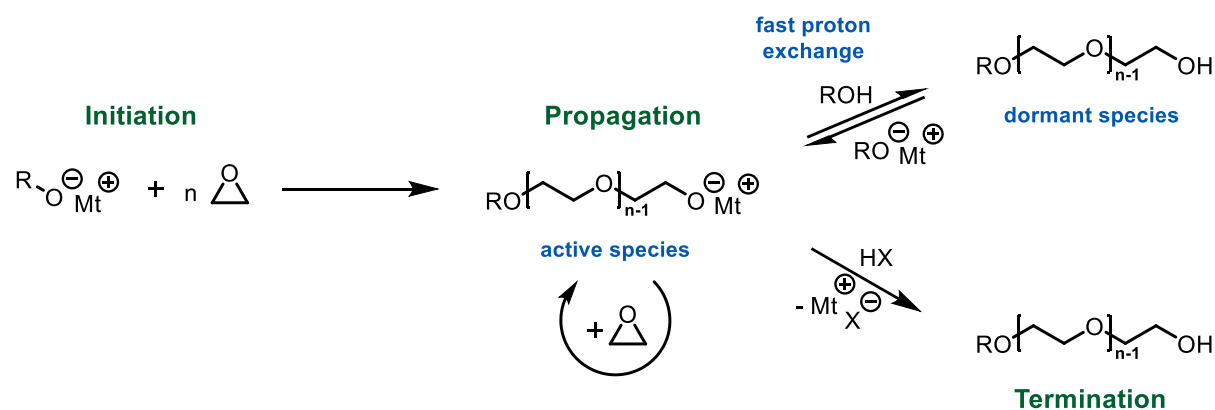
Scheme 1. Pathway of AROP of EO including the partial initiator deprotonation which leads to an active and dormant species.

The AROP of epoxides in solution requires aprotic, polar solvents, thus ethers like tetrahydrofuran (THF) and 1,2-dimethoxyethane (DME)[7,8] or dimethyl sulfoxide (DMSO)[9,10] and hexamethylphosphoramide (HMPA)[11] are commonly used. Depending on the nature of the solvent as well as the counterion, the alkoxide chain ends are present as aggregates, ion pairs or free ions (Scheme 2). Generally, the Pearson[12] "hard" alkali metal lithium forms strong aggregates with the hard oxygen, consequently decelerating or impeding propagation, while Pearson soft alkali metals (potassium and cesium) enable a fast polymerization rate.[13]
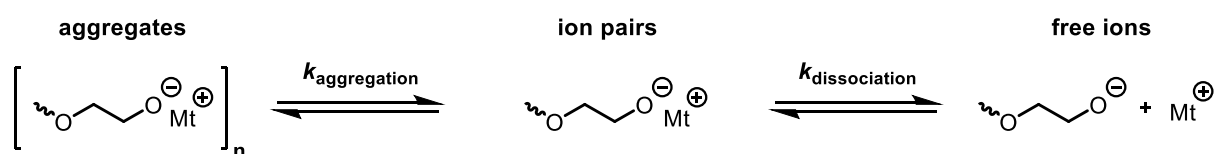
Scheme 2. Different conformations of alkoxide chain end in solution.

In recent years, a toolbox of mono-substituted epoxide monomers has been introduced for the synthesis of a multitude of polyether structures. In these works, the rather simple PEG backbone can be altered and functionalized, i.e. by introducing enhanced hydrophilicity due to hydroxymethylene groups via linear polyglycerol units (*lin*PG),[14] the addition of hydrophobicity by long-chain alkyl ether side chains[15] as well as the incorporation of varying functional groups, i.e. allyl or vinyl ethers (Scheme 3).[6]
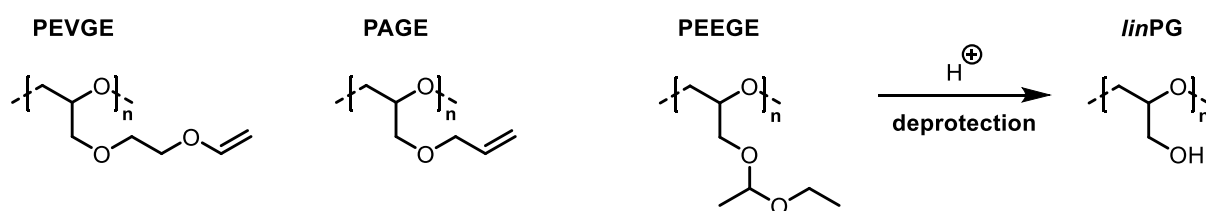
**Scheme 3.** Selection of common functional poly(glycidyl ethers): poly(ethoxy vinyl glycidyl ether) PEVGE, poly(allyl glycidyl ether) PAGE and poly(ethoxy ethyl glycidyl ether) PEEGE as well as linear poly(glycerol) *lin*PG after deprotection.

DMC Catalysis and Its Most Prominent Product: Poly(Propylene Oxide)

Poly(propylene oxide) (PPO) is synthesized by polymerization of the mono-methyl substituted derivative of EO: propylene oxide (PO) (Scheme 4). Whereas the main industrial use of EO is hydrolysis to generate ethylene glycol, $\sim 60\%$ of PO are used for the synthesis of PPO.[16] In contrast to PEG, use of racemic PO leads to the formation of an atactic and therefore amorphous polymer with a low glass transition temperature T_g of around -73 °C.[17] Semi-crystalline PPO is accessible by polymerization of enantiomerically pure PO, but unlike its highly established, aliphatic relative isotactic poly propylene, isotactic PPO is merely of academic interest.[18]

Concerning chemical properties, the additional methyl group per PO unit drastically lowers aqueous solubility compared to PEG, as the additional substituents hinder the interaction of water molecules at the hydrophilic polyether backbone.[19] Oligomeric PPO exhibits a lower critical solution temperature (LCST) in water above room temperature, while the water-solubility decreases drastically with increasing M_n.[20] The amorphous and simultaneously hydrophobic properties render PPO an excellent candidate for soft components in polyurethane foaming[21,22] and for application as a lubricant.[23]
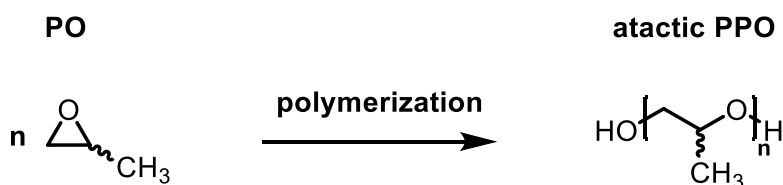
Scheme 4. Structure of racemic PO as well as the resulting atactic PPO obtained after polymerization.

However despite its many advantages, the aforementioned classical AROP is limited in the case of PO as well as longer alkyl oxides, which is due to chain-transfer reactions of the monomers under highly basic conditions.[24,25] This undesired side-reaction will be more thoroughly discussed in chapter 1.2, as it is equally observed for short-chain alkyl glycidyl ethers. Generally, the formation of undesired unsaturated species results in limited molecular weight M_n for PPO of 8000 g mol^{-1} when prepared by AROP. This limitation correlates with the polymerization rate constant k_{poly}

and the rate constant of chain transfer from the PO monomer k_{TrPO} (k_{poly}/k_{TrPO}).[6,26] Careful choice of reaction conditions in regard to the applied solvent, counterion and temperature as well as the addition of crown-ethers[27] enables the suppression of side-reactions to a certain extent, but full elimination is not feasible by classical AROP.

Yet, for PPO polyols in polyurethane foaming, a very low unsaturation level is crucial. The industrial production of polyurethanes (PU) relies on the condensation reaction of isocyanates with multifunctional alcohols like PPO-polyols. The step-growth reaction and PU network formation is hampered by unreactive allyl species. This must be prevented to reach a high degree of polymerization.[22] Hence, several alternative polymerization procedures have been developed in the past to overcome this obstacle. In academic research, techniques like the phosphazene base-catalyzed AROP,[28] the monomer-activated ROP (MAROP)[29] or the usage of *N*-heterocyclic carbenes (NHCs) and *N*-heterocyclic olefins (NHOs)[30,31] enable the polymerization of ultra-high molecular weight PPO ($M_n > 106 \, \mathrm{g \, mol^{-1}}$). In an industrial context however, the double metal cyanide (DMC) catalyst represents the most established method facilitating the production of PPO on a megaton scale at present.[32] Depending on the desired application, small amounts of EO and butylene oxide (BO) are additionally considered in industrial DMC catalysis. In addition to linear PPO, the synthesis of hyperbranched PPO by DMC catalysis was investigated in academic research.[33]

The heterogenous catalyst with the general formular $Zn_3[Co(CN)_6]_2 {}^* ZnCl_2 {}^* xLigand {}^* yH_2O$ was introduced by General Tire and Rubber in 1963[34] (Figure 1).[35,36] Although other catalysts[37] as well as varying active centers for the DMC catalyst containing Fe, Ni, Pd, or Pt, have been reported, the catalyst based on Co and Zn constitutes the most relevant structure to date.[38–41]
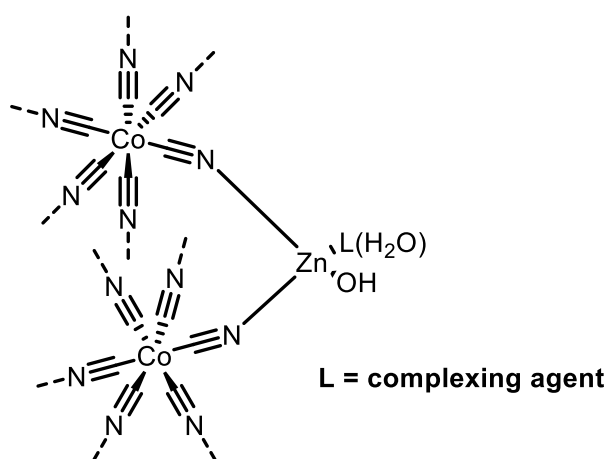

Figure 1. Proposed structure of the active site of Zn-Co(III) DMC catalyst.[42]

Apart from the choice of transition metal, the catalytic activity is substantially defined by the applied complexing agent (Figure 2). Several candidates have been proposed in literature; low molecular structures like dimethoxyethane, diglyme, ethylene glycol mono-tert-butyl ether,

propylene glycol mono-methyl ether or dicarbonyl components but also oligomeric PPO, PEG and poly(tetrahydrofuran) (PTHF).[43–46] Among these, tert-butanol represents the most frequently applied complexing agent.
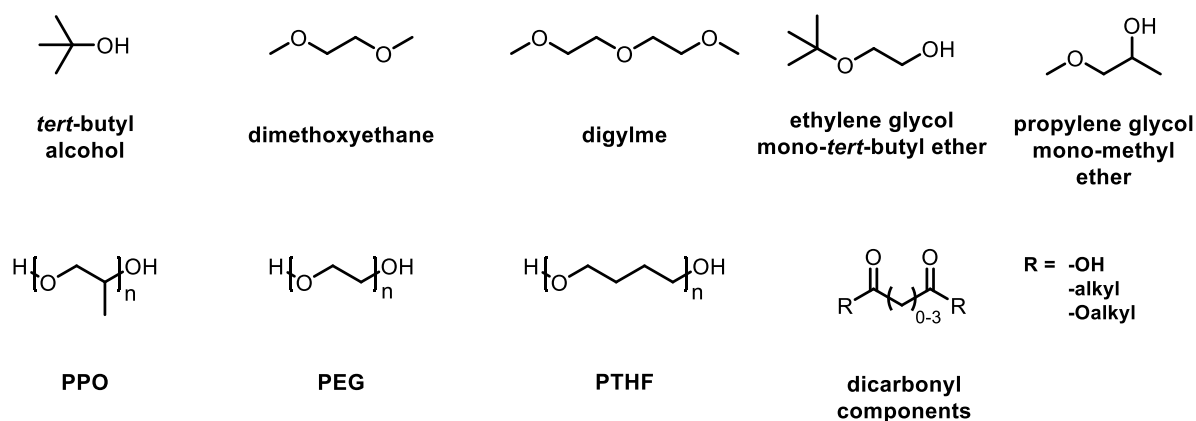

Figure 2. Electron donating complexing agents utilized in the DMC catalysis of cyclic monomers.

Several benefits substantiate the widespread utilization of the DMC catalyst over the conventional catalysis by KOH. PPO polymers synthesized by DMC catalysis not merely possess a very low unsaturation level (0.001 meq g^{-1}),[22] but additionally require very low amounts of catalyst (≥ 13 ppm),[47] which remain finely suspended in the resulting viscous material for subsequent use.[48,49] The polymerization is commonly performed in bulk with varying hydrophobic hydroxyl-containing initiators, therefore requiring no further purification steps.[50] Polymerization of PO is generally feasible with or without addition of an initiator, although the control of M_n and narrow dispersities are merely achievable in presence of an initiator.

Despite its heterogeneous nature, the DMC catalyst yields polymers of narrow dispersities ($Đ$ down to < 1.10), which are usually exclusively known for living polymerization techniques. The mechanism enabling this unusually controlled catalytic polymerization has not been fully understood to date, nevertheless an overview over the hitherto published findings is given in the following paragraph. One must consider that each catalyst sample varies to some extent, depending on the preparation procedure, transition metal and the complexing agent in use. The following paragraph therefore summarizes findings for each specific catalyst, enabling further understanding, but is not capable of providing a universal conclusion valid for each case of DMC catalyzed polymerization.

Mechanistic Insights of DMC Catalyzed Polymerization of Propylene Oxide

The mechanism of DMC catalyzed polymerization of PO is fundamentally described as a cationic coordination-insertion mechanism proceeding on the surface of the catalyst particle with exposed Zn^{2+} species.[22] In 2019, Kim et al. investigated the mechanistic specification of DMC catalysis in

through detail based on experimental investigations as well as density-functional theory (DFT) calculations (Figure 3).[40]
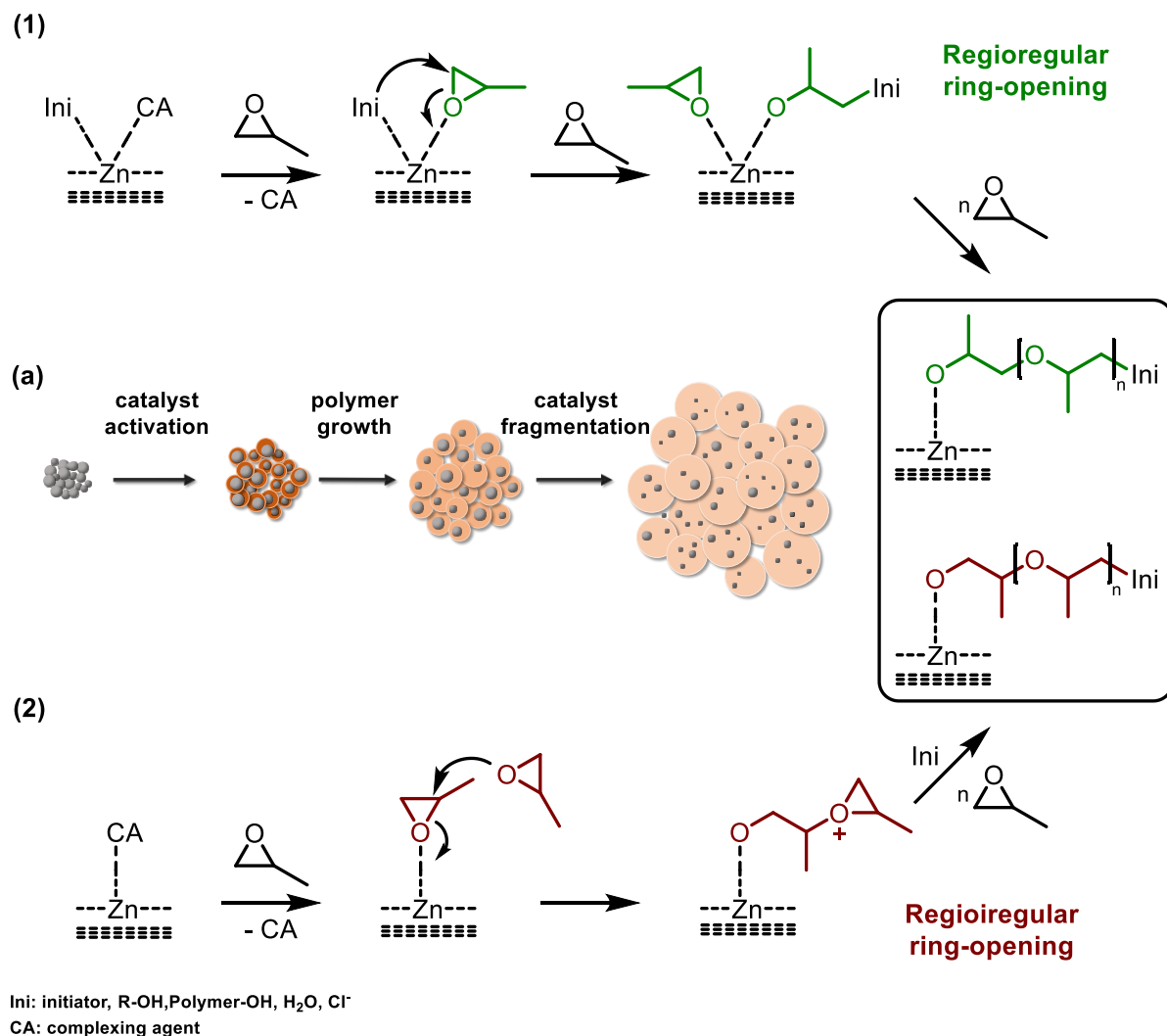
Figure 3. Proposed mechanistic pathways simultaneously occurring during DMC catalyst polymerization of PO. (a) Catalyst activation resulting in a fragmentation of particles while (1) regioregular ring-opening and (2) regioirregular ring-opening by an active-chain end (ACE) mechanism is proceeding.[40]

As described before, the Zn^{2+} sites are complexed by electron donating agents prior to polymerization which are considered as pre-activators of DMC catalysis. Initially, these complexing agents are exchanged with PO when the epoxide together with the initiator is added to the pre-catalyst, resulting in a transformation of dormant to active Zn^{2+} sites. The pre-activation of the catalyst by PO is followed by the reaction of the nucleophilic initiator with the highly activated monomer by ring-opening of the epoxide. The activation leads to a fragmentation of catalyst particles, resulting in an explosively increased propagation rate which is described more closely in the following paragraph. After initiation, chain propagation is continued at

the activated chain at the Zn^{2+} surface until full monomer conversion is reached (Figure 3.1). According to Kim et al., the resulting polymer contains a strict 'head-to-tail' regiosequence since the described mechanism proceeds at the catalyst surface where the complexing agents are located. Supplementary, a small amount of PO molecules is absorbed by the internal Zn^{2+} sites (Figure 3.2). This generates a carbocation intermediate stabilized by additional epoxides which is followed by an iterative addition of PO to the activated chain end (ACE). This pathway yields minor defects of 'head-to-head' and 'tail-to-tail' defects while it proceeds until the growing species is exposed to the external initiator.

Pressure Progression Accompanying DMC Catalysis

Looking at physical aspects of the polymerization process (Figure 3a), initially the catalyst activation by PO leads to polymer chains growing around the particles ($\sim 600\,nm$). Activation of the catalyst subsequently results in the fragmentation of the resulting, finely suspended particles within the amorphous polymer ($\sim 200\,nm$). During polymerization, a sharp reaction acceleration accompanied by an increase of pressure is observed which is ascribed to two aspects: (i) catalyst fragmentation and (ii) ring-opening of PO. Both processes are exothermic reactions leading to an increase in temperature and consequently pressure. The current literature hereby largely focusses on the evaluation of pressure as an indicator of the polymerization rate. Hence, the strong pressure increase symbolizes the strongly accelerated propagation. The time range at the beginning of the polymerization where a low epoxide conversion rate is observed is often referred to as the induction period t_i. The interval till maximum pressure is observed, indicating the maximum conversion rate of PO, is referred to as activation period t_a (Figure 4).
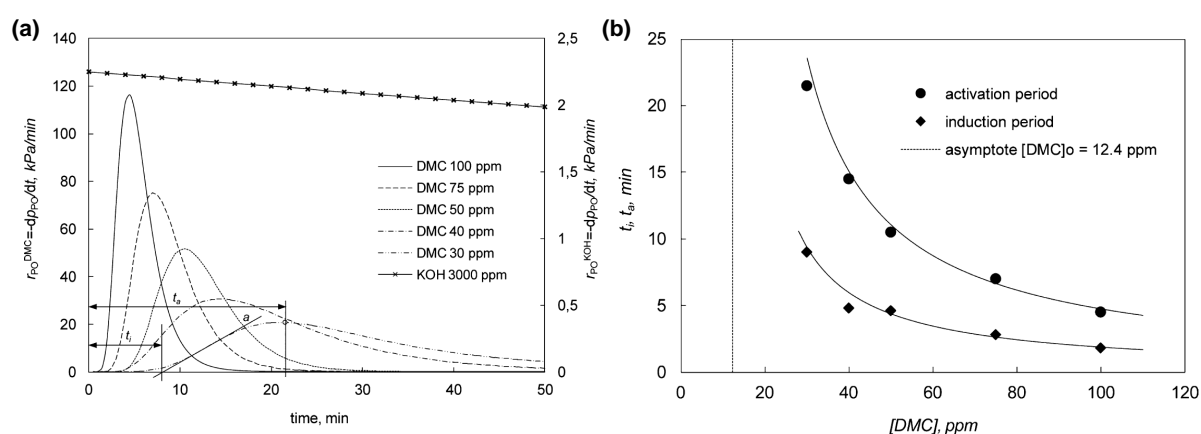
Figure 4. (a) Monitoring of pressure $r_{PO}^{DMC} = -\mathrm{d}p_{PO}\,\mathrm{dt}^{-1}$, kPa min^{-1} by variation of catalyst concentration. (b) Comparison of induction and activation time at 130 °C vs. catalyst concentration.[47]

The activation period itself is poorly understood to date, as different experiments revealed a wide range from minutes up to several hours.[44,47,51–55] Generally, an increase in catalyst loading decreases the activation as well as induction period significantly. However, the impact of monomers other than PO on the pressure progression has not been investigated to date.

Catch-Up Kinetics and High Molecular Weight Tailing of DMC Catalysis

A unique and rather unusual feature observed for DMC-catalyzed polymerization of epoxides is the so-called "catch-up kinetics" (Figure 5). This phenomenon relates to the preferential growth of shorter chains rather than longer ones in mixtures of polymers with varying molecular weights but the same species. Thermodynamic models and mathematical predictions by Pazos and Brown56 and just recently by Bachmann et al.[57] enabled a hypothetical explanation. Hereby, a rapid, reversible complexation of hydroxyl-groups at the Zn^{2+} center was proposed. Low molecular weight chains possess a higher density of hydroxyl groups, which enthalpically favors the monomer insertion at shorter rather than longer polyether chains.

<center>chains after initiation   chains during propagation   chains after full conversion</center>

Figure 5. Schematic illustration of the catch-up kinetics observed for DMC catalysis. Grey: initial monomer units after initiation, blue: added monomer units.
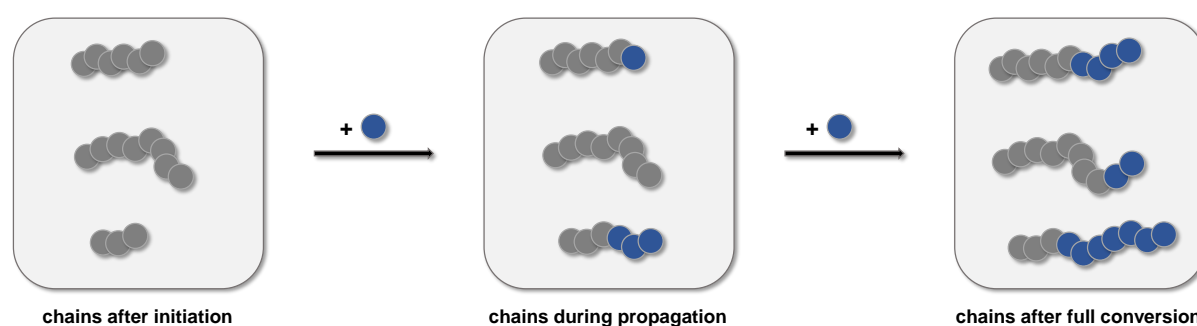
This phenomenon provides a possible explanation on how a heterogenous catalyst enables the synthesis of narrowly dispersed polymers, leading to highly defined polymers as known only from living polymerization techniques.

Apart from the catch-up kinetics, high molecular weight tailing (HMWT) represents a known drawback of polyethers synthesized by DMC catalysis. This translates to chains of $100 \, kg \, mol^{-1}$ and higher observed after polymerization.[58] The inhibition of HMWT is crucial for homogenous foaming of polyurethanes, as high molecular weight chains trigger foam collapse.[22] Several plausible explanations have been given in literature, although full prevention of HMWT remains elusive to this date. The aforementioned mechanistic investigations by Tran et al.[40] suspect the formation of HMWT is due to the delayed initiator insertion during the ACE pathway. López and co-workers describe the possibility of a single chain propagating at multiple Zn^{2+} sites, which therefore leads to an uneven chain growth.[58] The authors further propose a possible solution to the problem based on a patent by Faraj et al..[59] The addition of protic acids to the polymerization mixture potentially leads to cleavage of the redundant OH groups among Zn^{2+} centers while promoting the fragmentation process, therefore yielding a uniform initiation process.

In summary, DMC catalysis represents a highly valuable tool for the controlled synthesis of PPO on an industrial scale. Nevertheless, the mechanistic specifications as well as the origin of the

catch-up kinetics and HMWT remain poorly understood which necessitates detailed future studies in industrial and academic research.

Polymerization and Properties of Polysiloxanes

Besides epoxide polymerization, AROP further enables the synthesis of polysiloxanes with its most prominent representative poly(dimethylsiloxane) (PDMS). The class of polysiloxanes was first reported in 1904,[60,61] however, the industrial production of PDMS was only initiated in 1940 by introduction of the 'direct process' by Müller and Rochow rendering the synthesis of chlorosilanes on large scales possible.[62] The combination of organic (oxygen, methyl) with inorganic (silicon) components results in a unique and widely applied property profile. Compared to its ether analog, the Si-O-Si bond exhibits a larger bond angle (147°, C-O-C: 112°), while simultaneously an enlarged hyperconjugation effect is observed. These features result in a rotation barrier near $0\,\mathrm{kcal\,mol^{-1}}$ which yield highly flexible, amorphous polymer chains with an exceptionally low glass transition temperature of -120 °C.[63–65] The Si-O bond exhibits a high bond-dissociation energy of $460\,\mathrm{kJ\,mol^{-1}}$ (C-O: $345\,\mathrm{kJ\,mol^{-1}}$) which was attributed to a partial double bond character (55 %) (Scheme 5a).[66] However, recent re-investigation regarding the nature of the Si-O-Si bond either prosed a rather ionic bond[67] or a mixture of covalent and strong ionic bonding which resulted in the description as an "elusive bond".[68,69]
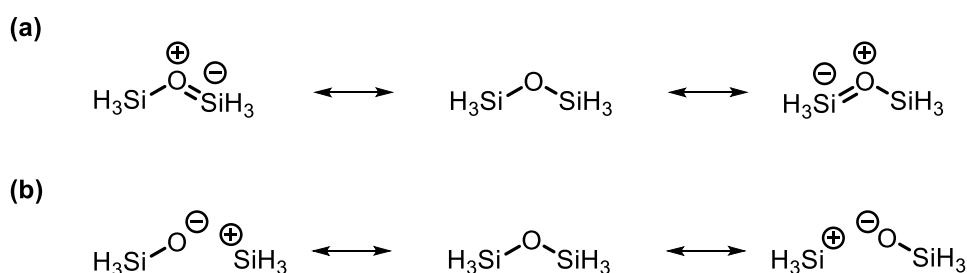
Scheme 5. Display of the Si-O-Si via (a) the obsolete back-bonding model and (b) the currently discussed ionic bond model.[68]

Regardless of its origin, the high bond-dissociation energy of $450\,\mathrm{kJ\,mol^{-1}}$ causes the high stability of PDMS against temperature and UV-light, still permitting excellent permeability regarding O_2. PDMS is widely known for its high hydrophobicity, despite the highly polarized Si-O bond, which is induced by the nonpolar methyl substituents shielding the polar backbone.[70] The transparent, non-flammable PDMS is widely utilized in biomedical applications due to its inert character but is equally established for the fabrication of surfactants, coating materials and sealants.[71–74] Especially highly amphiphilic block copolymers combining the hydrophobic PDMS with hydrophilic polyethers like PEG play a key role for the stabilization of PU foams. Coupling of both homopolymers is achieved by either hydrosilylation or thiol-ene click chemistry.[75–78]

The controlled synthesis of PDMS with narrow molecular weight distributions is commonly achieved by AROP of hexamethylcyclotrisiloxane (D_3) or octamethylcyclotetrasiloxane (D_4).[79,80]

The initiation is feasible by the utilization of strong carbanionic nucleophiles like *n*-butyl lithium (Scheme 6 left). In contrast to epoxide polymerization, propagation of siloxanes is viable with a lithium counterion as the highly flexible siloxane backbone enables a crown-ether-like complexation of the alkali metal.[81] AROP of cyclic siloxanes initiated by alkoxides is not possible, and consequently the copolymerization with epoxides has not been reported to date. Merely the utilization of harsh reaction conditions, high temperat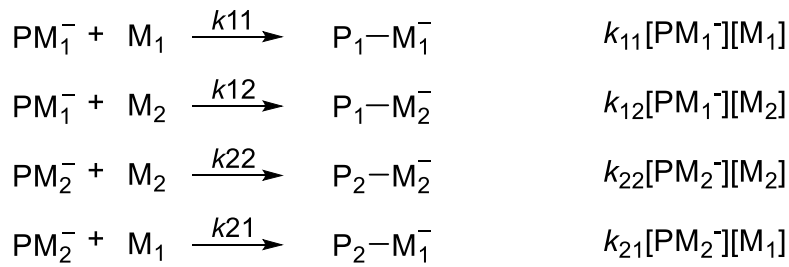ure or catalysts like phosphazene bases[82,83] and NHCs[84] enabled the initiation with alkoxides like methoxide.[82,83] In 2018, Fuchise et al. reported the organocatalytic ROP of D_3 initiated by water yielding polymers of high molecular weights (> 100 kg mol^{-1}) and narrow dispersities ($Đ < 1.16$).[85–87] Utilization of strong organic bases like for instance amidines, guanidines or phosphazene bases were used to catalyze the controlled ring-opening of D_3 (Scheme 6 right).
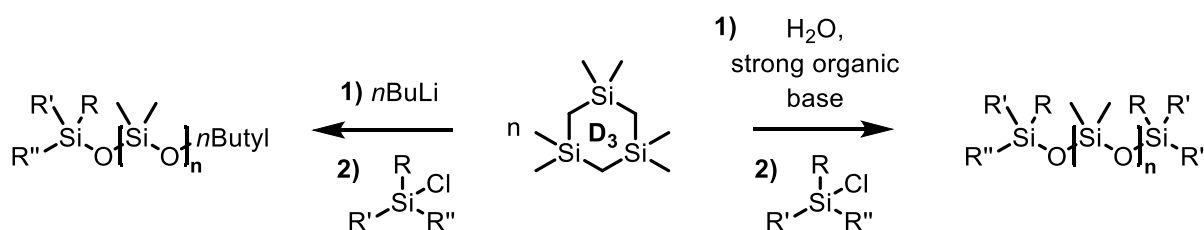
Scheme 6. Synthesis of PDMS by polymerization of D_3 by *n*-butyl lithium initiated AROP (left) and water initiated organic base catalyst polymerization (right).

Copolymerization Kinetics: Gaining Insight in Polymer Microstructures

The copolymerization of different monomers facilitates the combination of diverse characteristics within one material.[6] However, not only the nature of the monomer unit determines the material properties but also the consequent microstructure. Already in 1944, Mayo and Lewis,[88] Alfrey and Goldfinger[89] as well as Wall[90] independently developed a terminal model to describe the copolymerization of two monomers. The model was initially developed for radical polymerizations but is equally applicable for ionic polymerizations described during this introduction, as the model does not include the nature of the chain-end.[91] Fundamentally, the formation of a copolymer is described by four reactions and their respective reaction rates (Scheme 7). Here, the model differentiates between two active chain ends PM_1^- and PM_2^- as well as the addition of two monomers M_1 and M_2.

$$PM_1^- \ + \ M_1 \ \xrightarrow{k11} \ P_1{-}M_1^- \qquad\qquad k_{11}[PM_1^-][M_1]$$

$$PM_1^- \ + \ M_2 \ \xrightarrow{k12} \ P_1{-}M_2^- \qquad\qquad k_{12}[PM_1^-][M_2]$$

$$PM_2^- \ + \ M_2 \ \xrightarrow{k22} \ P_2{-}M_2^- \qquad\qquad k_{22}[PM_2^-][M_2]$$

$$PM_2^- \ + \ M_1 \ \xrightarrow{k21} \ P_2{-}M_1^- \qquad\qquad k_{21}[PM_2^-][M_1]$$

Scheme 7. Fundamental reactions and the respective rates during living anionic copolymerization of M_1 and M_2.

Monitoring of the monomer consumption during the chain-growth reactions over time can be described as follows:

$$\frac{d[M_1]}{dt} = -k_{11}[PM_1^-][M_1] - k_{21}[PM_2^-][M_1] \tag{0.1}$$

$$\frac{d[M_2]}{dt} = -k_{22}[PM_2^-][M_2] - k_{21}[PM_1^-][M_2] \tag{0.2}$$

A time independent expression (0.3) is obtained by division of (0.1) and (0.2):

$$\frac{d[M_1]}{d[M_2]} = \frac{[M_1]}{[M_2]} \frac{k_{11}[PM_1^-] + k_{21}[PM_2^-]}{k_{22}[PM_2^-] + k_{12}[PM_1^-]} \tag{0.3}$$

For living ionic polymerizations, a steady-state assumption is postulated, comprising the numbers of chain-ends remaining constant during the copolymerization. The assumption yields in equation (0.4) with the reactivity ratios $r_1 = k_{11}/k_{12}$ and $r_2 = k_{22}/k_{21}$.

$$\frac{d[M_1]}{d[M_2]} = \frac{[M_1]}{[M_2]} \frac{r_1[M_1] + [M_2]}{r_2[M_2] + [M_1]} \tag{0.4}$$

Despite the almost simultaneous publication by the three above mentioned manuscripts, the equation is nowadays referred to as the "Mayo-Lewis equation". Considering this equation, a description of the behavior of two comonomers is feasible by the resulting reactivity ratios. Equal reactivity ratios ($r_1 = r_2$) result in an ideally random distribution of monomer units along the polymer backbone, while differential ratios ($r_1 < r_2$ or $r_1 > r_2$) describe the preferential polymerization of M_1 or M_2, respectively, yielding gradient microstructures.

$$r_1 = 0 \qquad \text{no homopolymerisation, only cross-over}$$
$$r_1 < 0 \qquad \text{preference of cross-over}$$
$$r_1 = 1 \qquad \text{equal reactivity of } M_1 \text{ and } M_2$$
$$r_1 > 1 \qquad \text{preference of homopolymerisation}$$

Scheme 8. Description of copolymerization behavior by reactivity ratios.

Different models for the determination of reactivity ratios have been postulated since the proposal of the initial equation (0.4). In the context of epoxide polymerizations, non-terminal copolymerization models are commonly applied. Generally, non-terminal models are valid if the rate of monomer incorporation shows a strong dependence on the nature of the reacting monomer rather than the identity of the terminal unit. In 1972, Jaacks[92] introduced a non-terminal model relying on the linearization of the non-terminal Meyer-Lowry equation introduced in 1965.[93] Herein, the Jaacks model enabled the determination by only one reactivity ratio, if a large excess of one comonomer is utilized.[92] This model therefore represents an ideal copolymerization equation, which originates in the simplification $r_1 = r_2^{-1}$.

Nowadays, the Jaacks model is still widely used for the analysis of epoxide copolymerizations by AROP or MAROP.[94–96] In 2015, Lynd and co-workers[97] exploited the knowledge of non-terminal copolymerization models by postulating an integrated model applicable for epoxide copolymerizations as an alternative to traditional linearized models like i.e., Jaacks.[98,99] In 2019, the ideal integrated equation for the non-terminal model similar to the Meyer-Lowry equation further enabled the recognition and suppression of overfitting of the experimental data.[100]

At first, the experimental investigation of epoxide copolymerizations relied on the analysis of prematurely terminated copolymerization. Large errors were observed due to e.g., operator-induced terminations and insufficient removal of residual monomers. During the last decade, *in situ* techniques have been established to enable the precise online monitoring of monomer consumption over time. Currently ^{1}H NMR spectroscopy kinetics represents the most frequently applied technique for epoxide copolymerizations, enabling to map monomer gradients along the polymer chains.[101,102] In addition to the fundamental principles described throughout this section, chapter 1.2 provides an overview regarding the copolymerization kinetics of short-chain alkyl glycidyl ethers with each other and further epoxides.

PEG – The Gold Standard of Stealth Polymers

The outstanding characteristics of PEG have substantiated its leading role for biomedically applied polymers in modern pharmaceutical technologies.[103] The strategy of covalent attachment of PEG to proteins, surfaces or nanocarriers is commonly referred to as "PEGylation". Historically, the concept of PEGylation was described in the late 1970s by Davis, Abuchowski et al.[104,105] for the first time, but merely achieved widespread attention for application in drug delivery systems in the 1990s.[106–108] Nowadays, more than 30 PEGylated drugs are approved by the U.S. Food and Drug Administration (FDA) while several others are in Phase II and III of clinical

trials.[109,110] Especially chronic diseases like hepatitis B and C, hemophilia, different types of cancer or rheumatic disorders are treated. Additionally, PEGylation is utilized for stabilization of fragile structures like mRNA via PEGylated lipids. This currently plays a crucial role in mRNA-based vaccines for the containment of the global SARS-CoV-2 pandemic as well as in development of personalized vaccines for cancer immunotherapy.[111–113]

Generally, the covalent conjugation of polymeric structures to molecules and macromolecules such as drugs, peptides, proteins and nanocarriers comprises several benefits (Figure 6).
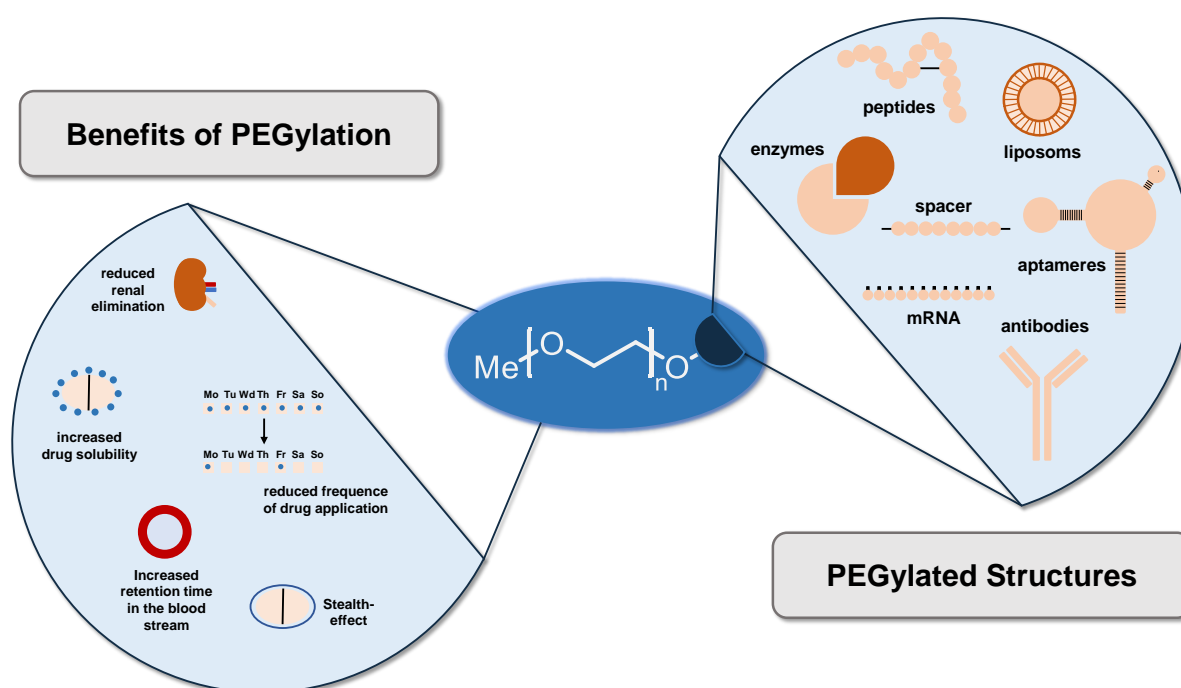
Figure 6. Overview of advantages of PEGylation as well as a selection of PEGylated structures for biomedical applications.

The increased molar mass of drug conjugates results in an strongly prolonged blood circulation times, as it significantly reduces renal excretion. Patients treated with PEG-conjugated drugs therefore require a reduced number of drug administrations. Among other polymers, the utilization of PEG further adds "stealth" properties to such conjugates. The shielding of drug conjugates and carriers by the hydrophilic, non-ionic polyether impedes fast recognition by the immune system. This feature is commonly referred to as the 'stealth effect'. PEG hereby suppresses non-specific protein adsorption and cell uptake while further prolonging the blood half-life of PEGylated drugs.[114–116] The polyether´s highly hydrophilic properties increase the hydrodynamic radius of conjugates, which also imparts solubility of otherwise water-insoluble drugs.[117,118]

In 2016, Wurm, Landfester and co-workers expanded this knowledge by revealing the protein absorption of clusterin (also referred to as apolipoprotein J) as a requirement for the stealth

effect of PEGylated substances.[119,120] In addition to its peculiar properties, PEG offers terminal α- and ω-hydroxy substituents, enabling a vast spectrum of conjugation chemistry. For this purpose, monomethylated PEG (mPEG) is preferentially utilized to avoid undesired coupling reactions during the functionalization and the following conjugation reactions. Modification of the terminal hydroxyl group capitalizing on activated derivatives like active esters or amines subsequently enables covalent attachment of PEG to proteins. The final bioconjugation is achieved via amino acids containing nucleophilic substituents (amino, hydroxyl, thiol) like i.e. lysine, serin, cysteine, tyrosine or histidine.[121,122]

Anti-PEG Antibodies (APA) and Alternatives to PEG

For many years, PEG was considered an inert and physiologically harmless polymer, somewhat invisible to the human immune system. The absence of functional groups and the lack of a fixed conformation as known from proteins indicated no immunological response mechanism. However, the first evidence for the existence of antibodies directed against the polyether structure was reported by Richter and Akerblom already in 1983.[123] The induction of anti-PEG antibodies (APA) and therefore recognition of PEG by the immune system limits its beneficial properties due to the ABC (Advanced Blood Clearance) effect.[124,125] Conversely, an accelerated blood clearance of PEGylated drugs and nanoparticles is observed.[126] In very rare cases, after application of PEGylated drugs allergic reactions up to anaphylaxis attributed to a PEG triggered immune response, were documented.[127,128]

The incidence of APAs in the population has drastically increased over the last decades.[129] The analysis of serum samples from healthy subjects collected during 1970 to 1999 by Lai and co-workers showed a current prevalence for APAs of 56 % in the population. Pursuing analysis of samples from 2016 during the same study revealed an increase of up to 72 %.[130] As stated by the authors, these results dempnstrate the occurrence of APAs in blood samples of patients that never received treatment with PEGylated drugs. Consequently, the induction of APAs by food and cosmetics containing PEG is presumed, supported by the increase of APA prevalence correlating with the increasing use of PEG in this area over the last decades.

Recently, the same group unveiled the mechanism of PEG recognition by APAs.[131] X-ray crystal-lography demonstrated the initial binding of PEG by the anti-PEG Fab via a symmetrical dimer complex. Subsequently, the anti-PEG Fab paratope tightly immobilizes PEG by an open ring structure with tryptophan (Trp96) as a key residue (Figure 7a). After capture of the chain, the polyether is stabilized via Van der Waals interactions along the interior and exterior ring paratope surface (Figure 7b).
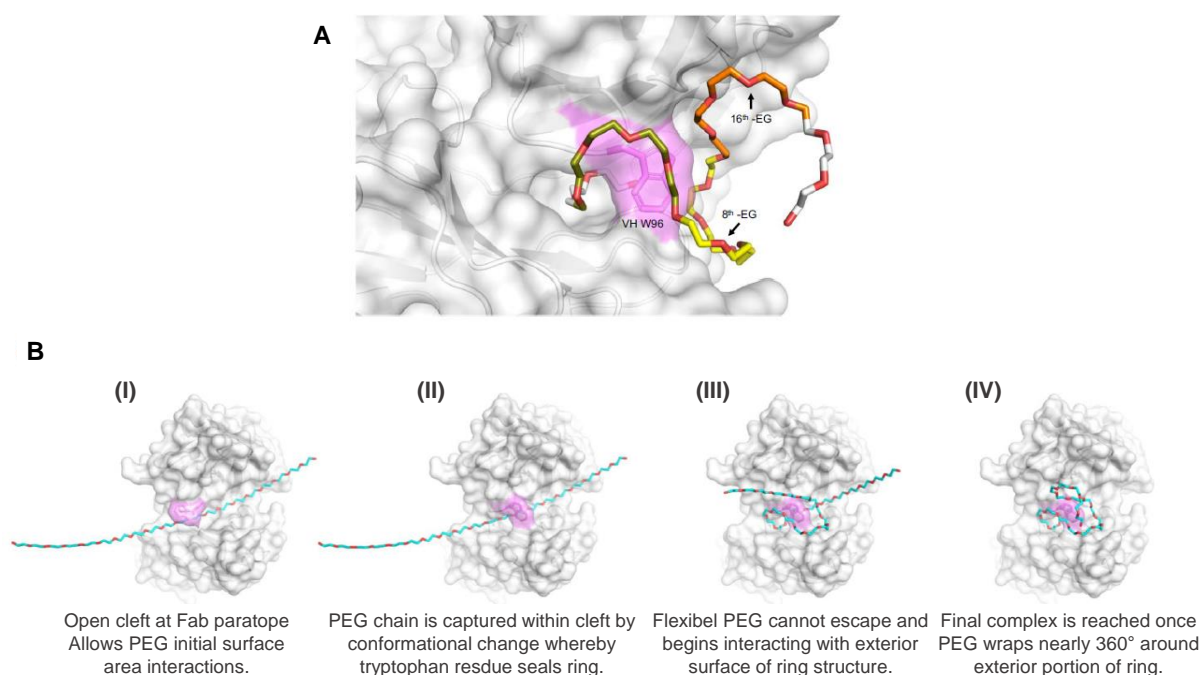
Figure 7. (A) Tightly bound PEG in open ring structure created by Anti-PEG Fab paratope. (B) Theoretical model illustrating the dynamic processes of anti-PEG Fab binding to the PEG antigen.[131]

The rising concerns related to PEG have promoted the development of polymeric alternatives (Figure 8).[103,132,133] An evident solution was the modification of PEG itself by functionalization of its termini. Sherman and co-workers examined mPEG and PEG by immunosorbent assays and found a reduced recognition by APAs for the dihydroxyl-functional PEG compared to the monomethylated polyether.[134,135]

Further, the introduction of methylene hydroxy substituents to PEG backbone is frequently reported as a promising strategy.[136] Linear PG synthesized from P(EEGE) as well as hyperbranched PG are discussed as PEG alternatives but disadvantages are already postulated. PG demonstrated high blood circulation times but accumulation of the sterically demanding polymer was observed in liver and kidneys.[137] *Lin*PG on the other hand, introduces primary hydroxyl-groups at each monomer unit, which enables manifold functionalization possibilities[14] but simultaneously reduces the chemically inert character of the polyether-conjugates in the human body.

Chilkoti and co-workers presented the incorporation of PEG into bottlebrush architectures i.e., poly(oligo(ethylene glycol) methyl ether methacrylate) (P(OEGMA)) as alternatives synthesized by surface-initiated atom transfer radical polymerization (SI ATRP).[138–140] Herein, OEGMA monomers containing short PEG oligomers with two to three ethylene glycol units exhibited the best results concerning inhibition of APA interaction. Nevertheless, the presence of Cu traces in polymers synthesized by ATRP prevent FDA-approval necessary for a widespread pharmaceutical application of such materials.
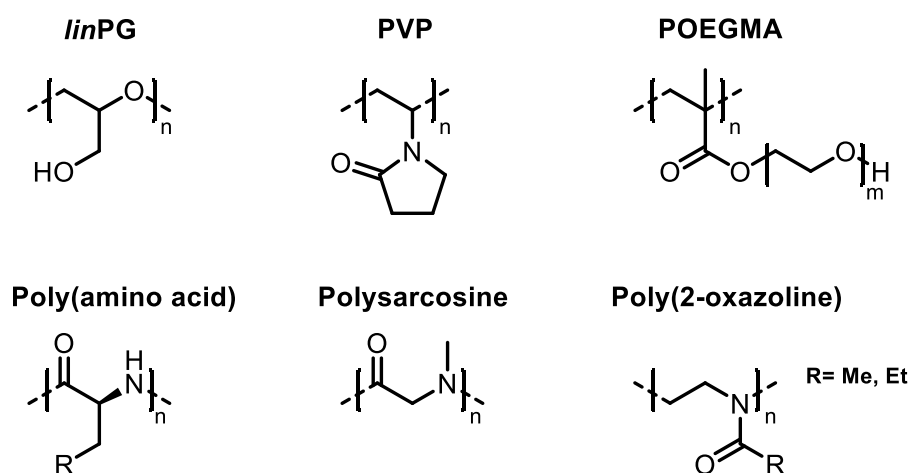
linPG **PVP** **POEGMA**

Poly(amino acid) **Polysarcosine** **Poly(2-oxazoline)**

R= Me, Et

Figure 8. Exemplary illustration of structures proposed as alternatives for PEG in PEGylation.

A prominent and equally promising PEG alternative are poly(2-oxazolines) with short side chains, (POx).[141] These thermoresponsive polymers exhibit high biocompatibility, good stealth properties and show no bioaccumulation. Nevertheless, the high-cost synthesis and lack of FDA-approval currently limit the widespread utilization of POx.[142]

Poly(vinyl pyrrolidone) (PVP) shares many advantages with PEG like its high hydrophilicity and general biocompatibility in addition to the lack of recognition by APAs. However, numerous studies question the non-toxicity of PVP due to the probability of bioaccumulation, carcinogenicity of free monomers and its unclear immunological behavior in the blood stream.[142] Additionally, zwitterionic polymers such as poly(carboxybetaine) and poly(sulfobetaine) are currently considered as PEG alternatives, due to their strong hydration and their high resistance to nonspecific protein interaction.[143,144]

A different approach is represented by the utilization of synthetic polypeptides by polymerization of amino acids, yielding poly(glutamic acid), poly(hydroxyethyl-L-asparagine) and poly(hydroxyethyl-L-glutamine).[145,146] In contrast to non-biodegradable PEG, poly(amino acids) are degraded in vivo to the respective amino acids, which are metabolized via physiological pathways. Especially the non-proteinogenic amino acid sarcosine has recently been discussed as a promising PEG alternative e.g. in the preparation of lipid nanoparticles for mRNA delivery.[147] Ring-opening polymerization of *N*-carboxyanhydride facilitates the controlled synthesis of polysarcosine, albeit to date this has not been adapted to industrial scales.[148]

Collectively, all presented alternatives entail their own synthetic, physiological and economical challenges but equally provide different advantages. Nevertheless, to date PEG maintains its position as the 'gold standard' of polymers for bioconjugation and drug delivery systems (DDS), due to long standing FDA approval and high availability of medical grade PEG, enabled by the low cost and industrially established production under GMP conditions.

REFERENCES

(1) Wurtz, A. Memoire sur l'oxyde d'éthylène et les alcools polyéthyléniques, **1863**.

(2) Staudinger, H.; Schweitzer, O. Über hochpolymere Verbindungen, 20. Mitteil.: Über die Poly-äthylenoxyde. *Ber. dtsch. Chem. Ges. A/B* **1929***, 62*, 2395–2405.

(3) Henderson, J. F.; SZWARC, M. The use of living polymers in the preparation of polymer structures of controlled architecture. *J. Polym. Sci. Macromol. Rev.* **1968***, 3*, 317–401.

(4) Craig, D. Q. A review of thermal methods used for the analysis of the crystal form, solution thermodynamics and glass transition behaviour of polyethylene glycols. *Thermochimica Acta* **1995***, 248*, 189–203.

(5) Flory, P. J. Molecular Size Distribution in Ethylene Oxide Polymers. *J. Am. Chem. Soc.* **1940***, 62*, 1561–1565.

(6) Herzberger, J.; Niederer, K.; Pohlit, H.; Seiwert, J.; Worm, M.; Wurm, F. R.; Frey, H. Polymerization of Ethylene Oxide, Propylene Oxide, and Other Alkylene Oxides: Synthesis, Novel Polymer Architectures, and Bioconjugation. *Chemical reviews* **2016***, 116*, 2170–2243.

(7) Kazanskii, K. S.; Solovyanov, A. A.; Entelis, S. G. Polymerization of ethylene oxide by alkali metal-naphthalene complexes in tetrahydrofuran. *European Polymer Journal* **1971***, 7*, 1421–1433.

(8) Solov'yanov, A. A.; Kazanskii, K. S. The kinetics and mechanism of anionic polymerization of ethylene oxide in ether solvents. *Polymer Science U.S.S.R.* **1972***, 14*, 1186–1195.

(9) Bawn, C.; Ledwith, A.; McFarlane, N. Anionic polymerization of ethylene oxide in dimethyl sulphoxide. *Polymer* **1969***, 10*, 653–659.

(10) Bawn, C.; Ledwith, A.; McFarlane, N. R. Anionic polymerization in dimethyl sulphoxide. *Polymer* **1967***, 8*, 484–487.

(11) Price, C. C.; Akkapeddi, M. K. Kinetics of base-catalyzed polymerization of epoxides in dimethyl sulfoxide and hexamethylphosphoric triamide. *Journal of the American Chemical Society* **1972***, 94*, 3972–3975.

(12) Pearson, R. G. Hard and Soft Acids and Bases. *J. Am. Chem. Soc.* **1963***, 85*, 3533–3539.

(13) Penczek, S.; Cypryk, M.; Duda, A.; Kubisa, P.; Slomokowski, S. Living ring-opening polymerizations of heterocyclic monomers. *Progress in Polymer Science* **2007***, 32*, 247–282.

(14) Thomas, A.; Müller, S. S.; Frey, H. Beyond poly(ethylene glycol): linear polyglycerol as a multifunctional polyether for biomedical and pharmaceutical applications. *Biomacromolecules* **2014***, 15*, 1935–1954.

(15) Verkoyen, P.; Frey, H. Long-Chain Alkyl Epoxides and Glycidyl Ethers: An Underrated Class of Monomers. *Macromol. Rapid Commun.* **2020***, 41*, e2000225.

(16) Bernhard, M.; Anton, J.; Schmidt, F.; Sandkaulen, F.; Pascaly, M. Über den Technologiewandel in der Propylenoxid-Herstellung. *Chemie in unserer Zeit,* **2017** *51 (3)*, 198-209 [Online early access]. DOI: 10.1002/CIUZ.201700764.

(17) Johari, G. P.; Hallbrucker, A.; Mayer, E. Calorimetric relaxation and glass transition in poly(propylene glycols) and its monomer. *J. Polym. Sci. B Polym. Phys.* **1988**, *26*, 1923–1930.

(18) Childers, M. I.; Longo, J. M.; van Zee, N. J.; LaPointe, A. M.; Coates, G. W. Stereoselective epoxide polymerization and copolymerization. *Chemical reviews* **2014**, *114*, 8129–8152.

(19) Malcolm, G. N.; Rowlinson, J. S. The thermodynamic properties of aqueous solutions of polyethylene glycol, polypropylene glycol and dioxane. *Trans. Faraday Soc.* **1957**, *53*, 921.

(20) Saito, S. Cloud points of poly(propylene oxide) and poly(vinyl methylether) in the presence of polymeric acids. *Colloids and Surfaces* **1986**, *19*, 351–357.

(21) Engels, H.-W.; Pirkl, H.-G.; Albers, R.; Albach, R. W.; Krause, J.; Hoffmann, A.; Casselmann, H.; Dormish, J. Polyurethanes: versatile materials and sustainable problem solvers for today's challenges. *Angewandte Chemie (International ed. in English)* **2013**, *52*, 9422–9441.

(22) Ionescu, M. Chemistry and technology of polyols for polyurethanes; Rapra Technology Ltd: *Shawbury, U.K*, **2005**.

(23) Paredes, X.; Pensado, A. S.; Comuñas, M. J. P.; Fernández, J. How Pressure Affects the Dynamic Viscosities of Two Poly(propylene glycol) Dimethyl Ether Lubricants. *J. Chem. Eng. Data* **2010**, *55*, 4088–4094.

(24) Yu, G.-E.; Heatley, F.; Booth, C.; Blease, T. G. Anionic polymerization of propylene oxide: Isomerization of allyl ether to propenyl ether end groups. *J. Polym. Sci. Part A: Polym. Chem.* **1994**, *32*, 1131–1135.

(25) Yu, G.-E.; Masters, A. J.; Heatley, F.; Booth, C.; Blease, T. G. Anionic polymerisation of propylene oxide. Investigation of double-bond and head-to-head content by NMR spectroscopy. *Macromol. Chem. Phys.* **1994**, *195*, 1517–1538.

(26) Price, C. C.; Carmelite, D. D. Reactions of Epoxides in Dimethyl Sulfoxide Catalyzed by Potassium t-Butoxide. *Journal of the American Chemical Society* **1966**, *88*, 4039–4044.

(27) Ding, J.; Heatley, F.; Price, C.; Booth, C. Use of crown ether in the anionic polymerization of propylene oxide—2. Molecular weight and molecular weight distribution. *European Polymer Journal* **1991**, *27*, 895–899.

(28) Isono, T. Synthesis of functional and architectural polyethers via the anionic ring-opening polymerization of epoxide monomers using a phosphazene base catalyst. *Polym J* **2021**, [Online early access]. DOI: 10.1038/s41428-021-00481-3.

(29) Billouard, C.; Carlotti, S.; Desbois, P.; Deffieux, A. "Controlled" High-Speed Anionic Polymerization of Propylene Oxide Initiated by Alkali Metal Alkoxide/Trialkylaluminum Systems. *Macromolecules* **2004**, *37*, 4038–4043.

(30) Walther, P.; Vogler, C.; Naumann, S. Ultrahigh-Molecular-Weight Poly(propylene oxide): Preparation and Perspectives. *Synlett* **2020**, *31*, 641–647.

(31) Naumann, S.; Thomas, A. W.; Dove, A. P. N-Heterocyclic Olefins as Organocatalysts for Polymerization: Preparation of Well-Defined Poly(propylene oxide). *Angewandte Chemie (International ed. in English)* **2015***, 54*, 9550–9554.

(32) Peretti, K. L.; Ajiro, H.; Cohen, C. T.; Lobkovsky, E. B.; Coates, G. W. A highly active, isospecific cobalt catalyst for propylene oxide polymerization. *Journal of the American Chemical Society* **2005***, 127*, 11566–11567.

(33) Tran, C. H.; Lee, M. W.; Kim, S. A.; Jang, H. B.; Kim, I. Kinetic and Mechanistic Study of Heterogeneous Double Metal Cyanide-Catalyzed Ring-Opening Multibranching Polymerization of Glycidol. *Macromolecules,* **2020** [Online early access]. DOI: 10.1021/acs.macromol.9b02373.

(34) Jack Milgrom. Method of Making a Polyether using a Double Metal Cyanide Complex Compound. US 3,278,457, **1963**.

(35) Lawniczak-Jablonska, K.; Dynowska, E.; Lisowski, W.; Sobczak, J. W.; Chruściel, A.; Hreczuch, W.; Libera, J.; Reszka, A. Structural properties and chemical bonds in double metal cyanide catalysts. *X-Ray Spectrom.* **2015***, 44*, 330–338.

(36) Chruściel, A.; Hreczuch, W.; Czaja, K.; Sacher-Majewska, B. On thermal behaviour of DMC catalysts for ring opening polymerization of epoxides. Thermochimica Acta 2016, 630, 78–89. (37) Walsh, D. J.; Hyatt, M. G.; Miller, S. A.; Guironnet, D. Recent Trends in Catalytic Polymerizations. *ACS Catal.* **2019**, 11153–11188.

(38) Chen, S.; Zhang, P.; Chen, L. Fe/Zn double metal cyanide (DMC) catalyzed ring-opening polymerization of propylene oxide. *Progress in Organic Coatings* **2004***, 50*, 269–272.

(39) Robertson, N. J.; Qin, Z.; Dallinger, G. C.; Lobkovsky, E. B.; Lee, S.; Coates, G. W. Two-dimensional double metal cyanide complexes: highly active catalysts for the homopolymerization of propylene oxide and copolymerization of propylene oxide and carbon dioxide. *Dalton transactions* (Cambridge, England : 2003) **2006**, 5390–5395.

(40) Tran, C. H.; Pham, L. T. T.; Lee, Y.; Jang, H. B.; Kim, S.; Kim, I. Mechanistic insights on Zn(II)−Co(III) double metal cyanide-catalyzed ring-opening polymerization of epoxides. *Journal of Catalysis* **2019***, 372*, 86–102.

(41) Chen, S.; Xu, N.; Shi, J. Structure and properties of polyether polyols catalyzed by Fe/Zn double metal cyanide complex catalyst. *Progress in Organic Coatings* **2004***, 49*, 125–129.

(42) Wei, R.-J.; Zhang, Y.-Y.; Zhang, X.-H.; Du, B.-Y.; Fan, Z.-Q. Regio-selective synthesis of polyepichlorohydrin diol using Zn–Co(iii) double metal cyanide complex. *RSC Adv* **2014***, 4*, 21765–21771.

(43) Tran, C. H.; Kim, S. A.; Moon, Y.; Lee, Y.; Ryu, H. M.; Baik, J. H.; Hong, S. C.; Kim, I. Effect of dicarbonyl complexing agents on double metal cyanide catalysts toward copolymerization of CO2 and propylene oxide. *Catalysis Today* **2020** [Online early access]. DOI: 10.1016/j.cattod.2020.01.008.

(44) Lee, S. H.; Lee, I. K.; Ha, J. Y.; Jo, J. K.; Park, I.; Ha, C.-S.; Suh, H.; Kim, I. Tuning of the Activity and Induction Period of the Polymerization of Propylene Oxide Catalyzed by Double Metal Cyanide Complexes Bearing β-Alkoxy Alcohols as Complexing Agents. *Ind. Eng. Chem. Res.* **2010**, *49*, 4107–4116.

(45) Kim, I.; Ahn, J.-T.; Ha, C. S.; Yang, C. S.; Park, I. Polymerization of propylene oxide by using double metal cyanide catalysts and the application to polyurethane elastomer. *Polymer* **2003**, *44*, 3417–3428.

(46) Tran, C. H.; Pham, L. T. T.; Jang, H. B.; Kim, S. A.; Kim, I. Effect of α-,β-,γ-, and δ-dicarbonyl complexing agents on the double metal cyanide-catalyzed ring-opening polymerization of propylene oxide. *Catalysis Today* **2021**, *375*, 429–440.

(47) Chruściel, A.; Hreczuch, W.; Janik, J.; Czaja, K.; Dziubek, K.; Flisak, Z.; Swinarew, A. Characterization of a Double Metal Cyanide (DMC)-Type Catalyst in the Polyoxypropylation Process: Effects of Catalyst Concentration. *Ind. Eng. Chem. Res.* **2014**, *53*, 6636–6646.

(48) Jörg Hofmann, Pieter Ooms, Pramod Gupta, Walter Schäfer, John Lohrenz. Double metal cyanide catalysts for producing polyether polyols, **2000**, US6586566B1.

(49) Eric P. Wassermann, Richard A. Galley, Woo Min Song, Abhijit Ghosh-Dastidar. Polyoxiranes, process and catalysts for making them, **2008**, WO2008048399A1.

(50) Zhang, X.-H.; Wei, R.-J.; Zhang, Y.; Du, B.-Y.; Fan, Z.-Q. Carbon Dioxide/Epoxide Copolymerization via a Nanosized Zinc–Cobalt(III) Double Metal Cyanide Complex: Substituent Effects of Epoxides on Polycarbonate Selectivity, Regioselectivity and Glass Transition Temperatures. *Macromolecules* **2015**, *48*, 536–544.

(51) Huang, Y. J.; Qi, G. R.; Chen, L. S. Effects of morphology and composition on catalytic performance of double metal cyanide complex catalyst. *Applied Catalysis A: General* **2003**, *240*, 263–271.

(52) Huang, Y.-J.; Zhang, X.-H.; Hua, Z.-J.; Chen, S.-L.; Qi, G.-R. Ring-Opening Polymerization of Propylene Oxide Catalyzed by a Calcium-Chloride-Modified Zinc-Cobalt Double Metal-Cyanide Complex. *Macromol. Chem. Phys.* **2010**, *211*, 1229–1237.

(53) Kim, I.; Anas, K.; Lee, S.; Ha, C.-S.; Park, D.-W. Tuning of the activity and induction period of double metal cyanide catalyzed ring-opening polymerizations of propylene oxide by using ionic liquids. *Catalysis Today* ***2008, 131***, 541–547.

(54) Lee, S. H.; Ha, C.-S.; Kim, I. Modified montmorillonite as a tuner of propylene oxide polymerization behavior catalyzed by double metal cyanide compound. *Macromol. Res.* **2007**, *15*, 202–204.

(55) Lee, S.; Baek, S. T.; Anas, K.; Ha, C.-S.; Park, D.-W.; Lee, J. W.; Kim, I. Tuning of activity, induction period and polymer properties of double metal cyanide catalyzed ring-opening polymerizations of propylene oxide by using quaternary ammonium salts. *Polymer* **2007**, *48*, 4361–4367.

(56) Pazos, J.; Browne, E. Catch-Up Kinetics: Selectivity based on equivalent weight in the polymerization of alkylene oxides by double metal cyanide catalysts. *Polymer Preprints* **2008**, *2008*, 434.

(57) Bachmann, R.; Klinger, M.; Jupke, A. Molcular Weight Distribution in Di Metal Cyanide Catalyzed Polymerization 1: Fundamental Distribution for Length Dependent Propagation Constant and Segments. *Macromol. Theory Simul.* **2021**, 2100012.

(58) Almora-Barrios, N.; Pogodin, S.; Bellarosa, L.; García-Melchor, M.; Revilla-López, G.; García-Ratés, M.; Vázquez-García, A. B.; Hernández-Ariznavarreta, P.; López, N. Structure, Activity, and Deactivation Mechanisms in Double Metal Cyanide Catalysts for the Production of Polyols. *ChemCatChem* **2015**, *7*, 928–935.

(59) Mahmoud K. Faraj, Newton Square, all of PA. Silylated Double Metal Cyanide Complex Catalysts. US6,051,680, **2000**

(60) Thomas, N. R. Frederic Stanley Kipping—Pioneer in Silicon Chemistry: His Life & Legacy. *Silicon* **2010**, *2*, 187–193.

(61) Dilthey, W. Ueber Diphenyl-silicon und Benzylsiliciumverbindungen. *Ber. Dtsch. Chem. Ges.* **1905**, *38*, 4132–4136.

(62) Rochow, E. G. The Direct Synthesis of Organosilicon Compounds. *J. Am. Chem. Soc.* **1945**, *67*, 963–965.

(63) Shambayati, S.; Schreiber, S. L.; Blake, J. F.; Wierschke, S. G.; Jorgensen, W. L. Structure and basicity of silyl ethers: a crystallographic and ab initio inquiry into the nature of silicon-oxygen interactions. *J. Am. Chem. Soc.* **1990**, *112*, 697–703.

(64) Weinhold, F.; West, R. The Nature of the Silicon–Oxygen Bond. *Organometallics* **2011**, *30*, 5815–5824.

(65) Guerra-Contreras, A.; Villegas, A.; Ramírez-Oliva, E.; Cervantes, J. Characterization and Study of Properties in a Polar Solvent of a Functionalized and Quaternized Poly(dimethylsiloxane-co-methyl-hydridosiloxane). *Silicon* **2017**, *9*, 525–533.

(66) Haynes, W. M. CRC Handbook of Chemistry and Physics, 95th Edition, 95th ed.; *CRC Press: Hoboken*, **2015**.

(67) Gibbs, G.; Rosso, K.; Teter, D.; Boisen, M.; Bukowinski, M. Model structures and properties of the electron density distribution for low quartz at pressure: a study of the SiO bond. *Journal of Molecular Structure* **1999**, *485-486*, 13–25.

(68) Grabowsky, S.; Hesse, M. F.; Paulmann, C.; Luger, P.; Beckmann, J. How to make the ionic Si-O bond more covalent and the Si-O-Si linkage a better acceptor for hydrogen bonding. *Inorganic chemistry* **2009**, *48*, 4384–4393.

(69) Binggeli; Troullier; Martins; Chelikowsky. Electronic properties of alpha -quartz under pressure. *Physical review. B, Condensed matter* **1991**, *44*, 4771–4777.

(70) Elif Hamurcu, E.; Baysal, B. M. Solubility parameter of a poly(dimethylsiloxane) network. *J. Polym. Sci. Part B: Polym. Phys.* **1994***, 32*, 591–594.

(71) Eduok, U.; Faye, O.; Szpunar, J. Recent developments and applications of protective silicone coatings: A review of PDMS functional materials. *Progress in Organic Coatings* **2017***, 111*, 124–163.

(72) Galli, G.; Martinelli, E. Amphiphilic Polymer Platforms: Surface Engineering of Films for Marine Antibiofouling. *Macromol. Rapid Commun.* **2017***, 38*.

(73) Ackermann, J.; Damrath, V. Chemie und Technologie der Silicone II. Herstellung und Verwendung von Siliconpolymeren. *Chem. Unserer Zeit* **1989***, 23*, 86–99.

(74) Schliebs, R.; Ackermann, J. Chemie und Technologie der Silicone I. *Chem. Unserer Zeit* **1987***, 21*, 121–127.

(75) Galin, M.; Mathis, A. Structural and thermodynamic study of dimethylsiloxane-ethylene oxide PDMS-PEO-PDMS triblock copolymers. *Macromolecules* *1981, 14*, 677–683.

(76) Haesslin, H.-W. Dimethylsiloxane-ethylene oxide block copolymers, 2. Preliminary results on dilute solution properties. *Makromol. Chem.* **1985***, 186*, 357–366.

(77) Haesslin, H. W.; Eicke, H. F.; Riess, G. Dimethylsiloxane-ethylene oxide block copolymers, 1. Microphase separation of low segment mass copolymers and their compatibility with water and oil. *Makromol. Chem.* **1984***, 185*, 2625–2645.

(78) Maassen, H.-P.; Yang, J. L.; Wegner, G. The structure of poly(ethylene oxide)-poly(dimethyl-siloxane) triblock copolymers in solution. Makromolekulare Chemie. *Macromolecular Symposia* **1990***, 39*, 215–228.

(79) Boehm, P.; Mondeshki, M.; Frey, H. Polysiloxane-backbone block copolymers in a one-pot synthesis: a silicone platform for facile functionalization. *Macromolecular rapid communications* **2012***, 33*, 1861–1867.

(80) Yilgör, İ.; McGrath, J. E. Polysiloxane containing copolymers: A survey of recent developments. In Polysiloxane copolymers/anionic polymerization; van Beylen, M., Ed.; *Advances in Polymer Science 86; Springer: Berlin*, **1988**; pp 1–86.

(81) Mazurek, M.; Chojnowski, J. Internal multifunctional assistance of siloxane system to the siloxane bond cleavage by alkali metal silanolates. *Makromol. Chem.* **1977***, 178*, 1005–1017.

(82) Molenberg, A.; Möller, M. A fast catalyst system for the ring-opening polymerization of cyclosiloxanes. *Macromol. Rapid Commun.* **1995***, 16*, 449–453.

(83) Eßwein, B.; Molenberg, A.; Möller, M. Use of polyiminophosphazene bases for ring-opening polymerizations. *Macromol. Symp.* **1996***, 107*, 331–340.

(84) Rodriguez, M.; Marrot, S.; Kato, T.; Stérin, S.; Fleury, E.; Baceiredo, A. Catalytic activity of N-heterocyclic carbenes in ring opening polymerization of cyclic siloxanes. *Journal of Organometallic Chemistry* **2007***, 692*, 705–708.

(85) Fuchise, K.; Igarashi, M.; Sato, K.; Shimada, S. Organocatalytic controlled/living ring-opening polymerization of cyclotrisiloxanes initiated by water with strong organic base catalysts. *Chemical science* **2018**, *9*, 2879–2891.

(86) Fuchise, K.; Sato, K.; Igarashi, M. Precise Synthesis of Linear Polysiloxanes End-Functionalized with Alkynylsilyl Groups by Organocatalytic Ring-Opening Polymerization of Cyclotrisiloxanes. *Macromolecules* **2021** [Online early access]. DOI: 10.1021/acs.macromol.1c00495.

(87) Kawatsu, T.; Fuchise, K.; Takeuchi, K.; Choi, J.-C.; Sato, K.; Matsumoto, K. Well-defined hydrogen and organofunctional polysiloxanes with spiro-fused siloxane backbones. *Polym. Chem.* **2021**, *12*, 2222–2227.

(88) Mayo, F. R.; Lewis, F. M. Copolymerization. I. A Basis for Comparing the Behavior of Monomers in Copolymerization; The Copolymerization of Styrene and Methyl Methacrylate. *J. Am. Chem. Soc.* **1944**, *66*, 1594–1601.

(89) Alfrey, T.; Goldfinger, G. The Mechanism of Copolymerization. *The Journal of Chemical Physics* **1944**, *12*, 205–209.

(90) Wall, F. T. The Structure of Copolymers. II 1. J. Am. Chem. Soc. 1944, 66, 2050–2057. (91) Mayo, F. R.; Walling, C. Copolymerization. *Chem. Rev.* **1950**, *46*, 191–287.

(92) Jaacks, V. A Novel Method of Determination of Reactivity Ratios in Binary and Ternary Copolymerizations. *Makromol. Chem.* **1972**, *161*, 161–172.

(93) Meyer, V. E.; Lowry, G. G. Integral and differential binary copolymerization equations. *J. Polym. Sci. A Gen. Pap.* **1965**, *3*, 2843–2851.

(94) Herzberger, J.; Leibig, D.; Liermann, J. C.; Frey, H. Conventional Oxyanionic versus Monomer-Activated Anionic Copolymerization of Ethylene Oxide with Glycidyl Ethers: Striking Differences in Reactivity Ratios. *ACS Macro Lett.* **2016**, *5*, 1206–1211.

(95) Linker, O.; Blankenburg, J.; Maciol, K.; Bros, M.; Frey, H. Ester Functional Epoxide Monomers for Random and Gradient Poly(ethylene glycol) Polyelectrolytes with Multiple Carboxylic Acid Moieties. *Macromolecules* **2020**, *53*, 3524–3534.

(96) Blankenburg, J.; Maciol, K.; Hahn, C.; Frey, H. Poly(ethylene glycol) with Multiple Aldehyde Functionalities Opens up a Rich and Versatile Post-Polymerization Chemistry. *Macromolecules* **2019**, *52*, 1785–1793.

(97) Beckingham, B. S.; Sanoja, G. E.; Lynd, N. A. Simple and Accurate Determination of Reactivity Ratios Using a Nonterminal Model of Chain Copolymerization. *Macromolecules* **2015**, *48*, 6922–6930.

(98) Herzberger, J.; Fischer, K.; Leibig, D.; Bros, M.; Thiermann, R.; Frey, H. Oxidation-Responsive and "Clickable" Poly(ethylene glycol) via Copolymerization of 2-(Methylthio)ethyl Glycidyl Ether. *Journal of the American Chemical Society* **2016**, *138*, 9212–9223.

(99) Herzberger, J.; Leibig, D.; Langhanki, J.; Moers, C.; Opatz, T.; Frey, H. "Clickable PEG" via anionic copolymerization of ethylene oxide and glycidyl propargyl ether. *Polym. Chem.* **2017**, *8*, 1882–1887.

(100) Blankenburg, J.; Kersten, E.; Maciol, K.; Wagner, M.; Zarbakhsh, S.; Frey, H. The poly(propylene oxide- co -ethylene oxide) gradient is controlled by the polymerization method: determination of reactivity ratios by direct comparison of different copolymerization models. *Polym. Chem.* **2019**, *116*, 2170.

(101) Obermeier, B.; Wurm, F.; Frey, H. Amino Functional Poly(ethylene glycol) Copolymers via Protected Amino Glycidol. *Macromolecules* **2010**, *43*, 2244–2251.

(102) Natalello, A.; Werre, M.; Alkan, A.; Frey, H. Monomer Sequence Distribution Monitoring in Living Carbanionic Copolymerization by Real-Time 1 H NMR Spectroscopy. *Macromolecules* **2013**, *46*, 8467–8471.

(103) Knop, K.; Hoogenboom, R.; Fischer, D.; Schubert, U. S. Poly(ethylene glycol) in drug delivery: pros and cons as well as potential alternatives. *Angewandte Chemie International Edition* **2010**, *49*, 6288–6308.

(104) Abuchowski, A.; McCoy, J. R.; Palczuk, N. C.; van Es, T.; Davis, F. F. Effect of covalent attachment of polyethylene glycol on immunogenicity and circulating life of bovine liver catalase. *Journal of Biological Chemistry* **1977**, *252*, 3582–3586.

(105) Abuchowski, A.; van Es, T.; Palczuk, N. C.; Davis, F. F. Alteration of immunological properties of bovine serum albumin by covalent attachment of polyethylene glycol. *Journal of Biological Chemistry* **1977**, *252*, 3578–3581.

(106) Monfardini, C.; Veronese, F. M. Stabilization of substances in circulation. *Bioconjugate chemistry* **1998**, *9*, 418–450.

(107) Bhadra, D.; Bhadra, S.; Jain, P.; Jain, N. K. Pegnology: a review of PEG-ylated systems. *Die Pharmazie* **2002**, *57*, 5–29.

(108) Pasut, G.; Veronese, F. M. Polymer–drug conjugation, recent achievements and general strategies. *Progress in Polymer Science* **2007**, *32*, 933–961.

(109) Zalipsky, S.; Pasut, G. Evolution of polymer conjugation to proteins. In Polymer-Protein Conjugates; Pasut G., Z. S., *Ed.; Elsevier,* **2020**; pp 3–22.

(110) Pasut G., Z. S., Ed. Polymer-Protein Conjugates; *Elsevier,* **2020**.

(111) Pardi, N.; Hogan, M. J.; Porter, F. W.; Weissman, D. mRNA vaccines - a new era in vaccinology. Nature reviews. *Drug discovery* **2018**, *17*, 261–279.

(112) Schoenmaker, L.; Witzigmann, D.; Kulkarni, J. A.; Verbeke, R.; Kersten, G.; Jiskoot, W.; Crommelin, D. J. A. mRNA-lipid nanoparticle COVID-19 vaccines: Structure and stability. *International Journal of Pharmaceutics* **2021**, *601*, 120586.

(113) Sahin, U.; Türeci, Ö. Personalized vaccines for cancer immunotherapy. *Science (New York, N.Y.)* **2018**, *359*, 1355–1360.

(114) Wörz, A.; Berchtold, B.; Moosmann, K.; Prucker, O.; Rühe, J. Protein-resistant polymer surfaces. *J. Mater. Chem.* **2012**, *22*, 19547.

(115) Otsuka, H.; Nagasaki, Y.; Kataoka, K. PEGylated nanoparticles for biological and pharmaceutical applications. *Advanced drug delivery reviews* **2003**, *55*, 403–419.

(116) Pasut, G.; Veronese, F. M. State of the art in PEGylation: the great versatility achieved after forty years of research. *Journal of controlled release : official journal of the Controlled Release Society* **2012**, *161*, 461–472.

(117) Lee, H.; Venable, R. M.; Mackerell, A. D.; Pastor, R. W. Molecular dynamics studies of polyethylene oxide and polyethylene glycol: hydrodynamic radius and shape anisotropy. *Biophysical journal* **2008**, *95*, 1590–1599.

(118) Pelegri-O'Day, E. M.; Lin, E.-W.; Maynard, H. D. Therapeutic protein-polymer conjugates: advancing beyond PEGylation. *Journal of the American Chemical Society* **2014**, *136*, 14323–14332.

(119) Schöttler, S.; Becker, G.; Winzen, S.; Steinbach, T.; Mohr, K.; Landfester, K.; Mailänder, V.; Wurm, F. R. Protein adsorption is required for stealth effect of poly(ethylene glycol)- and poly(phosphoester)-coated nanocarriers. *Nature nanotechnology* **2016**, *11*, 372–377.

(120) Butcher, N. J.; Mortimer, G. M.; Minchin, R. F. Drug delivery: Unravelling the stealth effect. *Nature nanotechnology* **2016**, *11*, 310–311.

(121) Roberts, M. J.; Bentley, M. D.; Harris, J. M. Chemistry for peptide and protein PEGylation. *Advanced drug delivery reviews* **2012**, *64*, 116–127.

(122) Zalipsky, S. Functionalized poly(ethylene glycol) for preparation of biologically relevant conjugates. *Bioconjugate chemistry* **1995**, *6*, 150–165.

(123) Richter, A. W.; Akerblom, E. Antibodies against polyethylene glycol produced in animals by immunization with monomethoxy polyethylene glycol modified proteins. *International archives of allergy and applied immunology* **1983**, *70*, 124–131.

(124) Kozma, G. T.; Shimizu, T.; Ishida, T.; Szebeni, J. Anti-PEG antibodies: Properties, formation, testing and role in adverse immune reactions to PEGylated nano-biopharmaceuticals. *Advanced drug delivery reviews* **2020**, *154-155*, 163–175.

(125) Schellekens, H.; Hennink, W. E.; Brinks, V. The immunogenicity of polyethylene glycol: facts and fiction. *Pharmaceutical research* **2013**, *30*, 1729–1734.

(126) Yang, Q.; Lai, S. K. Anti-PEG immunity: emergence, characteristics, and unaddressed questions. Wiley interdisciplinary reviews. *Nanomedicine and nanobiotechnology* **2015**, *7*, 655–677.

(127) Rutkowski, K.; Mirakian, R.; Till, S.; Rutkowski, R.; Wagner, A. Adverse reactions to COVID-19 vaccines: A practical approach. *Clinical and experimental allergy : journal of the British*

Society for Allergy and Clinical Immunology [Online early access]. DOI: 10.1111/cea.13880. Published Online: Apr. 4, **2021**.

(128) Sellaturay, P.; Nasser, S.; Islam, S.; Gurugama, P.; Ewan, P. W. Polyethylene glycol (PEG) is a cause of anaphylaxis to the Pfizer/BioNTech mRNA COVID-19 vaccine. *Clinical and experimental allergy : journal of the British Society for Allergy and Clinical Immunology* [Online early access]. DOI: 10.1111/cea.13874. Published Online: Apr. 6, **2021**.

(129) Armstrong, J. K. The occurrence, induction, specificity and potential effect of antibodies against poly(ethylene glycol). In PEGylated Protein Drugs: Basic Science and Clinical Applications; Veronese, F. M., Ed.; Birkhäuser Basel: Basel, **2009**; pp 147–168.

(130) Yang, Q.; Jacobs, T. M.; McCallen, J. D.; Moore, D. T.; Huckaby, J. T.; Edelstein, J. N.; Lai, S. K. Analysis of Pre-existing IgG and IgM Antibodies against Polyethylene Glycol (PEG) in the General Population. *Analytical chemistry* **2016**, *88*, 11804–11812.

(131) Huckaby, J. T.; Jacobs, T. M.; Li, Z.; Perna, R. J.; Wang, A.; Nicely, N. I.; Lai, S. K. Structure of an anti-PEG antibody reveals an open ring that captures highly flexible PEG polymers. *Commun Chem* **2020**, *3*.

(132) Hoang Thi, T. T.; Pilkington, E. H.; Nguyen, D. H.; Lee, J. S.; Park, K. D.; Truong, N. P. The Importance of Poly(ethylene glycol) Alternatives for Overcoming PEG Immunogenicity in Drug Delivery and Bioconjugation. *Polymers* **2020**, *12*.

(133) Qi, Y.; Chilkoti, A. Protein-polymer conjugation-moving beyond PEGylation. *Current opinion in chemical biology* **2015**, *28*, 181–193.

(134) Sherman, M. R.; Williams, L. D.; Sobczyk, M. A.; Michaels, S. J.; Saifer, M. G. P. Role of the methoxy group in immune responses to mPEG-protein conjugates. *Bioconjugate chemistry* **2012**, *23*, 485–499.

(135) Alexa L Martinez, Merry R Sherman, Mark G. P. Saifer, L David Williams. Polymer conjugates with decreased antigenicity, methods of preparation and uses thereof. US8129330B2, **2004**.

(136) Tully, M.; Dimde, M.; Weise, C.; Pouyan, P.; Licha, K.; Schirner, M.; Haag, R. Polyglycerol for Half-Life Extension of Proteins-Alternative to PEGylation? *Biomacromolecules* [Online early access]. DOI: 10.1021/acs.biomac.0c01627. Published Online: Apr. 1, **2021**.

(137) Abbina, S.; Parambath, A. 14 - PEGylation and its alternatives: A summary. In Engineering of biomaterials for drug delivery systems: Beyond polyethylene glycol; Parambath, A., Ed.; Woodhead publishing series in biomaterials; Woodhead Publishing an imprint of Elsevier: Duxford, Cambridge, MA, Kidlington, **2018**; pp 363–376.

(138) Chilkoti, A. e. a. Polymer conjugates having reduced antigenicity and methods of using the same. US20190015520A1, **2019**.

(139) Ashutosh Chilkoti, I. O. Stimuli-Responsive PEG-like Polymer-based Drug Delivery Platform. US 2021/0128734 A1, **2021**.

(140) Joh, D. Y.; Zimmers, Z.; Avlani, M.; Heggestad, J. T.; Aydin, H. B.; Ganson, N.; Kumar, S.; Fontes, C. M.; Achar, R. K.; Hershfield, M. S.; et al. Architectural Modification of Conformal PEG-Bottlebrush Coatings Minimizes Anti-PEG Antigenicity While Preserving Stealth Properties. *Advanced healthcare materials* **2019**, *8*, e1801177.

(141) Adams, N.; Schubert, U. S. Poly(2-oxazolines) in biological and biomedical application contexts. *Advanced drug delivery reviews* **2007**, *59*, 1504–1520.

(142) Hadjesfandiari, N.; Parambath, A. Stealth coatings for nanoparticles. In Engineering of biomaterials for drug delivery systems: Beyond polyethylene glycol; Parambath, A., Ed.; Woodhead publishing series in biomaterials; Woodhead Publishing an imprint of Elsevier: Duxford, Cambridge, MA, Kidlington, **2018**; pp 345–361.

(143) Yang, W.; Zhang, L.; Wang, S.; White, A. D.; Jiang, S. Functionalizable and ultra stable nanoparticles coated with zwitterionic poly(carboxybetaine) in undiluted blood serum. *Biomaterials* **2009**, *30*, 5617–5621.

(144) Jiang, S.; Cao, Z. Ultralow-fouling, functionalizable, and hydrolyzable zwitterionic materials and their derivatives for biological applications. *Advanced materials (Deerfield Beach, Fla.)* **2010**, *22*, 920–932.

(145) Romberg, B.; Metselaar, J. M.; Baranyi, L.; Snel, C. J.; Bünger, R.; Hennink, W. E.; Szebeni, J.; Storm, G. Poly(amino acid)s: promising enzymatically degradable stealth coatings for liposomes. *International Journal of Pharmaceutics* **2007**, *331*, 186–189.

(146) Li, C.; Wallace, S. Polymer-drug conjugates: recent development in clinical oncology. *Advanced drug delivery reviews* **2008**, *60*, 886–898.

(147) Nogueira, S. S.; Schlegel, A.; Maxeiner, K.; Weber, B.; Barz, M.; Schroer, M. A.; Blanchet, C. E.; Svergun, D. I.; Ramishetti, S.; Peer, D.; et al. Polysarcosine-Functionalized Lipid Nanoparticles for Therapeutic mRNA Delivery. *ACS Appl. Nano Mater.* **2020**, *3*, 10634–10645.

(148) Hu, Y.; Hou, Y.; Wang, H.; Lu, H. Polysarcosine as an Alternative to PEG for Therapeutic Protein Conjugation. *Bioconjugate chemistry* **2018**, *29*, 2232–2238.

Chapter 1.2

Polyethers based on Short-Chain Alkyl Glycidyl Ethers: From Thermoresponsive to Highly Biocompatible Materials

The polymerization of short-chain alkyl glycidyl ethers enables the synthesis of polyethers with a finely tunable hydrophilicity. Polyethers, most prominently poly(ethylene glycol) (PEG), are utilized in manifold biomedical applications due to their high biocompatibility. By incorporation of short hydrophobic side-chains
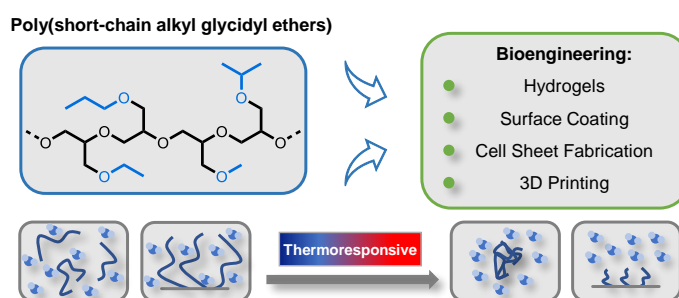
at linear polyglycerol, control of their solubility and lower critical solution temperature (LCST) in aqueous solution is feasible. Concurrently, the inert character in analogy to PEG is maintained, as no further functional groups are introduced at the polyether structure. Adjustment of the hydrophilicity of the resulting poly(glycidyl ether)s in a broad temperature range is achieved by the combination of the different short-chain alkyl glycidyl ethers. The use of diverse ring-opening polymerization techniques allows for the controlled synthesis of these polyethers, while simultaneously determining the resulting microstructures. Further, atactic as well as isotactic polymers are feasible by utilization of the respective racemic or enantiomerically pure monomers. Polymer architectures varying from statistic copolymers, di- and triblock to star-shaped copolymers in combination with PEG are applied in various thermoresponsive hydrogel formulations or polymeric surface coatings for cell sheet engineering. Materials responding to triggered stimuli are of increasing importance for "smart" bioengineering, making thermoresponsive polyethers containing short-alkyl ether side chains promising candidates for future perspectives.

INTRODUCTON

Polymers play a key role in modern nanomedicine, bioconjugated therapeutics as well as tissue engineering. In this context, poly(ethylene glycol) (PEG) represents the most widely established polymer for biomedical and pharmaceutical applications.[1] This polyether exhibits an exceptional hydrophilicity and therefore high aqueous solubility due to the ideal ether oxygen distances within the chain structure, which permit efficient interaction with water molecules in aqueous solution.[2,3] The stable ether linkages give PEG its inert character and also result in a remarkably high biocompatibility.

However, on the other hand excellent aqueous solubility of PEG limits its application, if thermoresponsive properties are required. The precise control of the behavior of polymers in solution is crucial for the design of stimuli-responsive, often called "smart" materials.[4–6] Especially the solution behavior triggered by temperature, known as lower (LCST) and upper critical solution temperature (UCST) offer opportunities in areas such as bioactive surfaces, protein absorption, drug delivery and regenerative medicine.[7] Several water-soluble alternatives to PEG have been introduced in the past. The most prominent representatives among others are poly(*N*-isopropyacrylamide) (PNIPAM), which was examined with regard to its thermoresponsive behavior already in 1968[8] after its introduction one year earlier,[9] poly(2-oxazolines)[10] and poly(oligoethylene glycol methacrylates) (POEGMA)[11].[12] However, one has to consider that the biocompatibility of these polymers is not as widely evaluated as for PEG over the last decades.

The combination of the hydrophobic poly(propylene oxide) (PPO) with PEG in thermosensitive PEG-*b*-PPO-*b*-PEG triblock copolymers is known as poloxamers or commercialized as Pluronics®️ by BASF.[13,14] Nevertheless, the simple structure of PEG limits modification possibilities to the α- and ϖ-end group functionalities. To overcome this limitation, functional glycidyl ethers were established in the recent decade to incorporate in-chain functionalities, i.e., aromatic, allyl, or protected hydroxyl side groups at the PEG chain.[15] The polyether with hydroxy methylene substituents at each repeating unit is commonly referred to as linear polyglycerol (*lin*PG). This biocompatible polymer with high number of hydroxyl groups enables a variety of functionalization strategies.[16] The hydroxyl groups in *lin*PG result in an even increased water-solubility compared to PEG. Incorporation of functional glycidyl ethers in either *lin*PG or PEG via copolymerization can induce LCST behavior.[17]

Systematic alkylation of *lin*PG facilitates two factors: (i) introduction of slightly hydrophobic side chains, thus lowering the hydrophilicity and (ii) the concomitant protection of functional groups. Unfortunately, post-polymerization modifications possess several disadvantages. Consequently , the direct polymerization of short-chain alkyl glycidyl ethers (GE) represents the most promising method for the controlled introduction of hydrophobicity to nonetheless water-soluble PEG-based polyethers. In this topical review, polymers synthesized from the 4 common short-chain alkyl GE (P(sAlkGE)) are outlined: glycidyl methyl ether (GME) as well as ethyl (EGE), propyl (PGE) and *iso*-propyl GE (*i*PGE) (Figure 1).
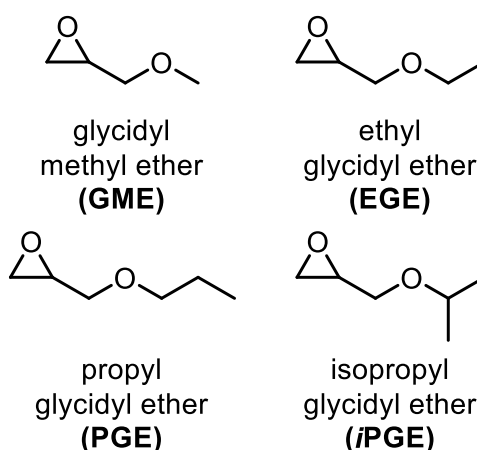
glycidyl
methyl ether
(**GME**)

ethyl
glycidyl ether
(**EGE**)

propyl
glycidyl ether
(**PGE**)

isopropyl
glycidyl ether
(***i*PGE**)

Figure 1. Shot-chain alkyl glycidyl ethers utilized in synthesis of P(GE)s.

SYNTHESIS AND POLYMERIZATION OF SHORT-CHAIN ALKYL GLYCIDYL ETHERS

Glycidyl ether monomers with short alkyl chains are generally accessible by common epoxide synthesis methods. Mechanistic insights regarding the hydrolysis of epoxides like GME in water under neutral and acidic conditions were obtained already in 1965 by Addy and Parker.[18] Hereby, rate constants regarding the attack of chloride ions at the phrased as "normal" and "abnormal" position of the respective epoxides are determined. Generally , the racemic mixtures of GME, EGE as well as *i*PGE are commercially available, low cost liquids.

The technical synthesis of such monomers is achieved by an established two-step reaction introduced by Mouzin et al. in 1983,[19,20] in a similar manner as known for long-chain alkyl glycidyl ethers.[21] Firstly, an alkoxide is generated by addition of the respective alcohol (methanol, ethanol, isopropanol) under basic conditions, typically sodium or potassium hydroxide. Thereafter, the epoxide ring of epichlorohydrin (ECH) is opened by nucleophilic attack of the alkoxide. In a second step, an intramolecular nucleophilic attack under ring-closure occurs, generating the respective glycidyl ether driven by precipitation of the formed alkali metal chloride. The reaction is performed in the presence of a phase-transfer catalyst, for instance tetrabutylammonium hydrogen sulfate, since ECH is not soluble in water (Scheme 1a). Equally, the reaction is feasible with solid sodium or potassium hydroxide without solvent and therefore without the use of a phase-transfer catalyst.[22]

(a)

R = -alkyl

racemic mixture

(b)

enantiomer
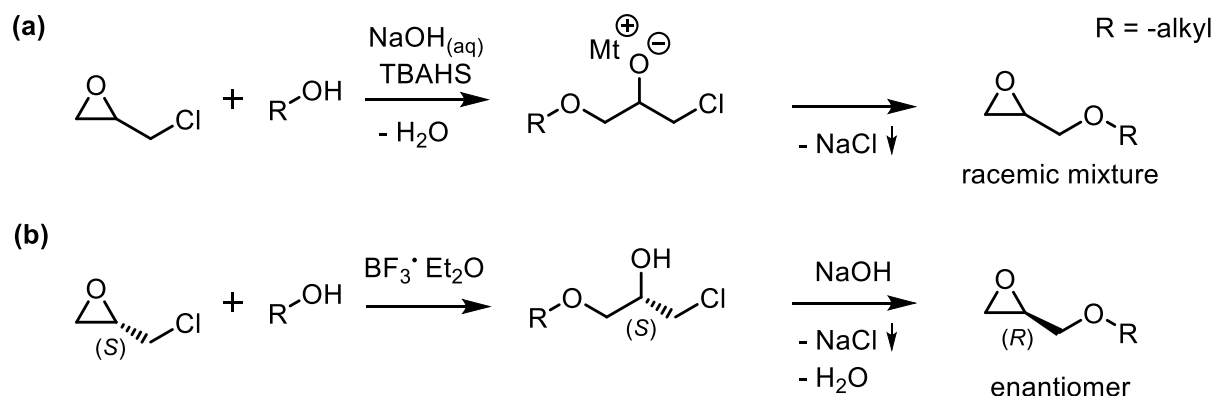
Scheme 1. (a) Synthesis of short-chain alkyl GE monomers by reaction of ECH with the respective alkoxide under basic conditions and utilization of a tetrabutylammonium hydrogen sulfate as phase-transfer agent. (b) Route to optically pure short-chain alkyl GEs by reaction of the respective alcohol with (S)-epichlorohydrin catalyst by BF$_3$·Et$_2$O yielding the corresponding chlorohydrins, followed by ring closure under basic conditions.

Unlike the above-described monomers GME and EGE, propyl glycidyl ether (PGE) is not commercially available although the synthesis via ECH is equally applicable. Alternatively, polymers bearing *n*-propyl ether side groups are synthesized by post-polymerization reaction based on linear poly allyl glycidyl ether (PAGE). Polyethers bearing allyl ether side groups synthesized by polymerization of allyl glycidyl ether (AGE) are hydrogenated (H$_2$, Pd/C), yielding the desired propyl side chains at the polyether.[23]

The synthesis of enantiomerically pure alkyl GEs is conducted in a related procedure.[24] In a first step, the chlorohydrin is formed by nucleophilic attack of the respective alcohol at the (S) or (R) isomer of ECH in presence of the Lewis acid BF$_3$·Et$_2$O, while preserving its stereo information. Subsequently, stereo inversion of the chiral center is achieved by nucleophilic ring-closure under basic conditions (Scheme 1b).

Throughout the last decades, several techniques have been established to polymerize alkyl glycidyl ethers, which were already discussed in reviews by our group.[15,21,25,26] The "classical" approach, the oxyanionic ring-opening polymerization (AROP) enables the synthesis of well-defined polyethers with narrow dispersities and high end-group fidelity due to its living character.
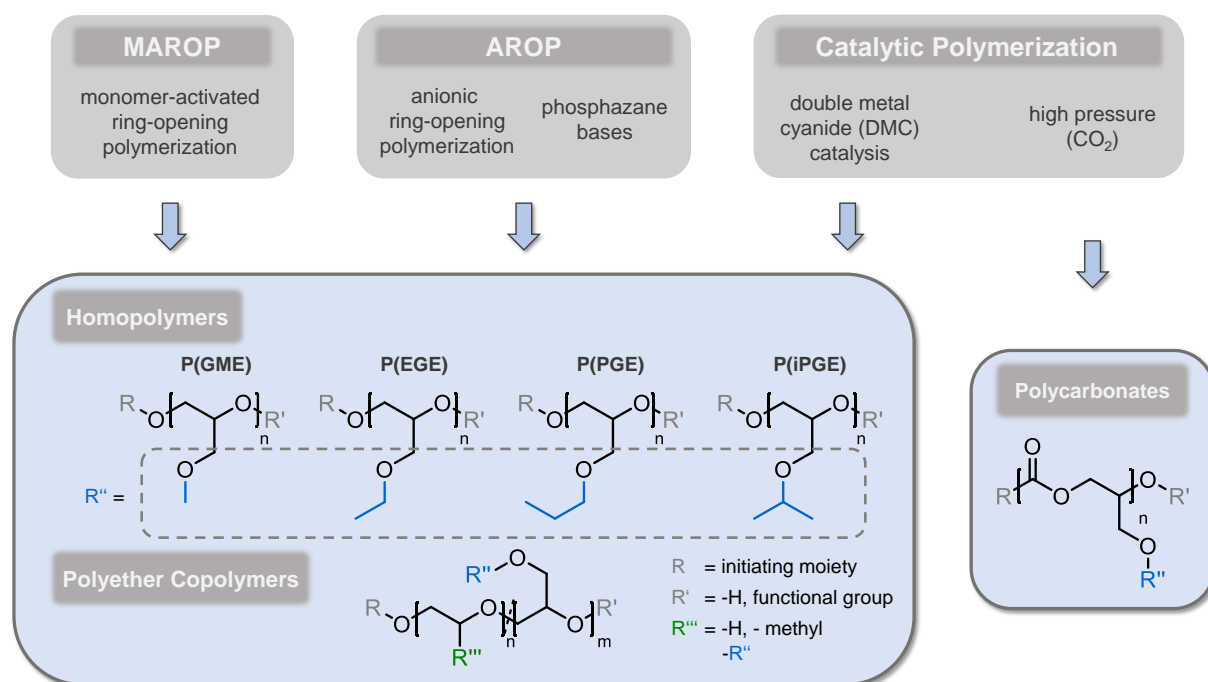
Figure 2. Overview of commonly utilized polymerization techniques for the synthesis of polyethers based on short-chain alkyl GE monomers.

The first polymerization of a short-chain alkyl glycidyl ether was published in 1970 by Ponomarenko et al., who presented the anionic copolymerization of GME and propylene oxide (PO) with a molecular weight of 3.1 kg mol^{-1}.[27] In 2002, Aoki et al. were the first to present the homopolymerization of short-chain alkyl glycidyl ethers, namely PGME (M_n = 3.0 kg mol^{-1}) and PEGE (M_n = 3.1 kg mol^{-1}), achieving moderate dispersities ($Đ$ > 1.19).[28] Adachi and co-workers presented the anionic polymerization of high molecular weight PiPGE (22 kg mol^{-1}), however, rather polydisperse polymers ($Đ$ = 1.55) were obtained.[29,30]

Some years later, Haag and co-workers further developed the results of Aoki et al. by synthesis of low molecular weight PGME (M_n < 1.5 kg mol^{-1}) and PEGE (M_n < 1.9 kg mol^{-1}), reporting narrow dispersities ($Đ$ < 1.10) under anionic conditions.[31–33] The polymerizations were performed in 1,2-dimethoxyethane (T_b = 85 °C) at very high temperatures (110 °C). Unfortunately, no further characterization concerning the formation of allylic species caused by the common proton abstraction (discussed later in Scheme 2) was conducted. The polymerizations were initiated by a dibenzyl amino alkyl alkoxide, which allows for the synthesis of α, ϖ-telechelic polyethers.[34,35] After the polymerization, the benzyl protective groups of the initiator are removed by hydrogenation (H$_2$, Pd/C), yielding an amine in α-position of the polymer chain, permitting subsequent reactions, which will be discussed below. In 2009 Schmalz and co-workers[36] as well as in several publications since 2011 by Haag, Weinhart and co-workers the copolymerization of GME and EGE by AROP was exploited extensively to control aqueous solubility and the corresponding LCST.[37–44] Copolymers of varying comonomer ratios with M_n of up to 4.9 kg mol^{-1} and narrow dispersities were successfully synthesized.

In a publication from 2014, Kamata et al. demonstrated the synthesis of star-shaped P(EGE$_{190}$-*co*-GME$_{47}$) copolymers with an 8:2 molar ratio (incorporation of 190 EGE and 47 GME units) under anionic conditions.[45] By utilization of a multifunctional initiator, namely pentaerythritol, a tetra-armed polyether copolymer of 22 kg mol^{-1} was prepared ($Đ = 1.02$). In 2018, Fellin et al. published an elaborate study of homopolymers synthesized from methyl, ethyl, *n*-propyl as well as *iso*-propyl glycidyl ether.[46] Using AROP, low molecular weight polymers ($M_n < 3.3$ kg mol^{-1}) of all 4 herein discussed GEs with narrow molecular weight distributions ($Đ < 1.10$) were obtained. Further, they were able to realize the synthesis of PEGE and PIGE with higher molecular weights (24.5 and 16.0 kg mol^{-1}, respectively) with still low dispersities (1.14 and 1.22, respectively).

Just recently, Brennecke, Lynd and co-workers synthesized PEGE and P*i*PGE ($M_n = 5.1$ and 7.0 kg mol^{-1}, respectively) by AROP, albeit with higher dispersities (1.98 for PEGE). The respective polymers were further investigated in regard to their interaction in binary blends with ionic liquids as well as their CO$_2$ solubility.[47,48]

In addition to low molecular weight alkoxide initiators, PEG is also a suitable macroinitiator for AROP of short-chain alkyl glycidyl ethers due to its primary hydroxyl termini. Different research groups reported the synthesis of triblock copolymers by the polymerization of *i*PGE as well as the copolymerization of EGE and *i*PGE initiated by PEG, affording P*i*PGE-*b*-PEG-*b*-P*i*PGE[49] and P(EGE-*co*-*i*PGE)-*b*-PEG-*b*-P(EGE-*co*-*i*PGE),[50–52] respectively. PPGE-*b*-PEG-*b*-PPGE triblock copolymers were obtained via similar polymerization procedures by bifunctional initiation of allyl glycidyl ether (AGE) and subsequent hydrogenation of the resulting polymer.[23] In a reverse manner, Watanabe and co-workers synthesized PEGE that was further used as a macroinitiator for the anionic polymerization of EO, yielding PEGE-*b*-PEG.[53–55]

Despite the many advantages like highly controlled polymerization, high end-group fidelity as well as a large variety of mono- and multifunctional nucleophilic initiators, AROP has one major drawback when applied to the polymerization of glycidyl ethers. Under anionic conditions, the weakly acidic methylene protons in α-position to the epoxide ring are easily abstracted by the nucleophilic polyether chain end, resulting in a chain-transfer reaction. This side reaction leads to the undesired, aforementioned allylic initiator (Scheme 2) and consequently a loss of control over molecular weights. The side reaction, which is likewise observed for alkylene oxide monomers and has been discussed in a detailed manner for propylene oxide, can generally be reduced by utilization of crown-ethers[56], ambient or at least low polymerization temperature[57] and the use of Pearson soft (HSAB)[58] counterions.[59–61]
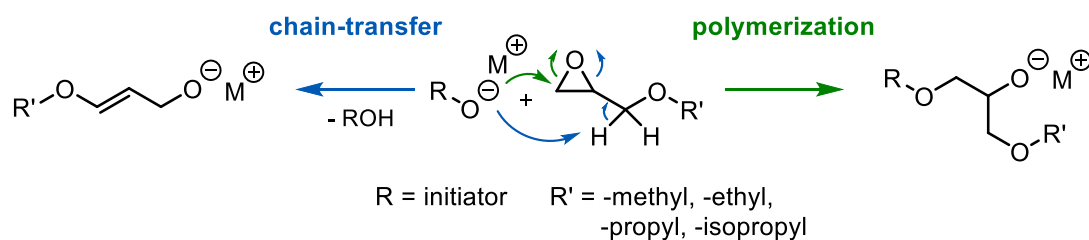
Scheme 2. Mechanism of chain transfer to monomer by proton abstraction in the polymerization of short-chain alkyl GEs, which leads to broadening of the distribution and lowered molecular weights.

In the past, the introduction of phosphazene base[62,63] assisted AROP and the monomer-activated ring-opening polymerization (MAROP)[64], first presented in 2004[65], have been established to fully overcome this obstacle. The utilization of *t*-Bu-P$_4$ as a catalyst enables a significant decrease of reaction time without the need of elevated temperatures, which thereby prevents undesired chain-transfer reactions. In a comparative study, Isono et al. demonstrated not only the phosphazene base catalyzed anionic synthesis of well-defined ($Đ < 1.08$) PGME, PEGE and P*i*PGE (M_n = 2.3 to 8.9 kg mol^{-1}) but also the polymerization of enantiomerically pure GME and EGE yielding isotactic P[(*R*)GME] and P[(*R*)EGE].[24,62] In contrast to the otherwise atactic, amorphous poly(glycidyl ether)s, the isotactic polymers exhibited melting points T_m at 23.0 and 31.7 °C, respectively. However, the polymerization of enantiomerically pure short-chain alkyl glycidyl ethers has not been investigated in regard to EGE, *i*PGE or copolymerizations of sAlkGe. Nevertheless, the crystalline properties of these thermoresponsive, isotactic polymers offer promising future possibilities.

In 2011, Schmalz and co-workers synthesized ABC block copolymers by use of phosphazene bases while incorporating a copolymer block containing of GME and EGE.[66] In contrast to classic AROP of epoxides where oxyanion and lithium form strong ionic aggregates,[15] catalysis by phosphazene bases enables polymerization despite the presence of lithium counterions. Schmalz and co-workers nicely exploited this feature to combine carbanionic with oxyanionic ROP in a one-pot synthesis route. Firstly, 2-vinyl pyridine (2VP) was polymerized by initiation of *sec*-butyl lithium, subsequently a PEG block was added by phosphazene base catalyzed polymerization of EO. Finally, GME and EGE were added in an equal molar ratio, ultimately yielding a P2VP$_{62}$-*b*-PEG$_{452}$-*b*-P(GME$_{36}$-*co*-EGE$_{36}$) copolymer. In 2015, polyether based P*i*PGE-*b*-PEG-*b*-P*i*PGE triblock copolymers were synthesized by phosphazene base catalysis, similar to the aforementioned approach by AROP, encouraging the versatile applicability of such bases in polymerization of epoxides.[67] Despite the many advantages offered by utilization of phosphazene bases, their high cytotoxicity and the required rigorous removal after polymerization is prohibitive, if polymers for bioapplication are desired.[68]

Similar to phosphazene bases, polymerization of short-chain alkyl glycidyl ethers by MAROP enables the suppression of undesired proton abstraction from the methylene group. This technique relies on the interaction of the epoxide with a Lewis acid (trialkyl aluminum), which reduces the

electron density of the epoxide ring and consequently enables ring-opening by weak nucleophiles, for instance bromide or azide. The activation of the epoxide monomer therefore enables the suppression of side reactions and concurrently the synthesis of high molecular weight polyethers. Deffieux, Carlotti and co-workers presented the first synthesis of very high molecular weight PGME ($87.1\,\mathrm{kg\,mol^{-1}}$) in 2007 as well as the copolymerization of GME with glycidyl methacrylate (GMA) in 2011 by MAROP.[69,70]

Weinhart and co-workers studied the copolymerization of GME and EGE in great detail, employing MAROP in several publications.[38,39,71–76] Copolymers of varying molar ratios were synthesized in a molecular weight range of 1.8 to $26\,\mathrm{kg\,mol^{-1}}$ with narrow to moderate dispersities ($Đ < 1.13$). Similarly, Calderon and co-workers synthesized P(GME-*co*-EGE) copolymers by MAROP for nanogel applications which will be discussed in ensuing sections.[77–84] In 2014, our group utilized the MAROP technique to present the first copolymerization of GME with EO, yielding P(GME-*co*-EO) copolymers of varying monomer compositions.[85] PGME as well as copolymers of molecular weights ranging from 3.2 to $16\,\mathrm{kg\,mol^{-1}}$ with low to moderate dispersities (1.21 to 1.68) were obtained.

The copolymerization of GME with ethoxy ethyl glycidyl ether (EEGE) was presented in 2015[86] and was further exploited by our group to synthesize linear polyglycerols with tailored degree of methylation by MAROP in 2017.[87] Nevertheless, one has to note that MAROP of epoxides lacks the high end-group fidelity of conventional AROP, therefore impeding complete end-functionalization of these polymers and block copolymer synthesis. Additionally, if a biomedical application is considered, residual aluminum salts must be thoroughly removed.

Apart from anionic methods, catalytic polymerization of short-chain alkyl glycidyl ethers has been realized, especially in combination with CO_2, yielding polyether carbonates. Listoś and co-workers were the first to demonstrate the incorporation of short-chain alkyl glycidyl ethers to polycarbonates with pendant allyl groups by catalytic copolymerization of CO_2 and *i*PGE with CO_2 with ultra-high molecular weights ($> 600\,\mathrm{kg\,mol^{-1}}$) and large dispersities in 2001.[88] Further developing these results, Nakamura et al. prepared polycarbonates by copolymerization of CO_2 with EGE and *i*PGE, respectively.[89] In 2014 and 2015 our group reported the copolymerization of CO_2 and GME with furfuryl glycidyl ether, enabling cross-linking by Diels-Alder-Reaction after polymerization.[90] Additionally, the copolymerization with benzyl glycidyl ether andCO_2 was studied, yielding polycarbonates with tailored hydroxyl groups after deprotection.[91] Herein, GME was utilized as a polar but easier and safer to handle alternative to EO. Recently, our group further employed the aqueous solubility of GME in copolymerization with PO by catalytic copolymerization, using the industrially highly established double metal cyanide (DMC) catalyst.[92]

COPOLYMIZERATION KINETICS OF SHORT-CHAIN ALKYL GLYICDYL ETHERS AND OTHER EPOXIDES

The above-described techniques illustrate the diversity of polymerization techniques for glycidyl ethers in general and short-chain alkyl GEs in particular. Apart from the specific reagents and conditions, the different approaches exhibit differential monomer reactivities, which is crucial regarding copolymerization kinetics. By choosing a specific technique for copolymerization of epoxide monomers, one simultaneously selects a certain microstructure within the resulting polymer chains, which in turn defines possible subsequent applications. For instance, statistical AROP copolymerization of EO and GEs like EEGE usually results in almost ideally random copolymers, while MAROP of the same monomer combination affords a strong gradient microstructure.[93] Thus, investigations of copolymerization kinetics are indispensable for an in-depth understanding and consequently have been conducted for several copolymerizations of short-chain alkyl GEs and further epoxides (Table 1). Generally, the reactivity of monomers in copolymerizations of two monomers can be described by reactivity ratios r_1 and r_2 (eq. 0.5 and 0.6). These r-parameters are defined as the ratio of the varying rate constants k_{11}, k_{12}, k_{21} and k_{22}. In a non-terminal model, the copolymerization behavior can be described by a single r-parameter as r_1 equals $1/r_2$.

$$r_1 = \frac{k_{11}}{k_{12}} \tag{0.5}$$

$$r_2 = \frac{k_{22}}{k_{21}} \tag{0.6}$$

In 1971, Ponomarenko et al. were the first to investigate the copolymerization behavior of a short-chain alkyl GE, namely GME, by evaluation of reactivity ratios.[27] The copolymerization with PO under AROP conditions was investigated by the terminal model established by Fineman and Ross,[94] a linearized form of the Mayo-Lewis equation.[95] Taking samples at low conversions ($< 12\,\%$) revealed the highly preferred incorporation of GME ($r_{GME} = 3.15$, $r_{PO} = 0.305$), yielding gradient P(GME-*co*-PO) copolymers. As confirmed later by implementation of the Mayo-Lewis model, ethylene oxide (EO) equally exhibits a higher reactivity than the less polar epoxide PO ($r_{EO} = 2.8$, $r_{PO} = 0.25$) under anionic conditions.[96]

Table 1. Reactivity ratios of varying copolymerizations of short-chain alkyl glycidyl ethers and epoxides by different polymerization techniques and evaluation methods.

technique	method	comonomer		r_x	r_y	r_x*r_y	lit.
		x	y				
AROP	Finemann-Ross	GME	PO	3.15	0.305	0.96	[27]
AROP	Finemann-Ross	GME	EGE	1.31	0.55	0.72	[36]
MAROP	Kelen-Tüdös	GME	EGE	0.98	0.95	0.93	[71]
MAROP	Kelen-Tüdös	GME	GMA	0.37	1.24	0.46	[70]
MAROP	Jaacks	GME	EEGE	1.11	0.90	1.00	[87]
MAROP	^{13}C triad analysis	GME	EO	EO-preferred			[85]
DMC	Jaacks	GME	PO	0.71	1.40	1.00	[92]

The copolymerization of P(GME-*co*-EGE) was investigated under AROP as well as MAROP conditions, illustrating the impact of polymerization technique on the microstructure. The implementation of the Finemann-Ross model revealed a slight gradient microstructure when employing AROP ($r_{GME} = 1.31$, $r_{EGE} = 0.55$),[36] whereas MAROP afforded random copolymers ($r_{GME} \approx r_{EGE}$),[71] determined by the Kelen-Tüdös model.[97,98] The MAROP of GME with ethoxy ethyl glycidyl ether (EEGE) evaluated by the non-terminal Jaacks[99] model equally showed a random-like copolymerization behavior.[87] Noteworthy, these are the only results evaluated by *in situ* ^{1}H NMR kinetics, enabling to obtain a precise understanding of the monomer sequence statistics along the polyether chains. Interestingly, the polymerization of GME with glycidyl methacrylate (GMA) revealed a higher reactivity of the glycidyl ester compared to the glycidyl ether under MAROP conditions ($r_{GME} = 0.37$, $r_{GMA} = 1.24$).[70] Investigations of the MAROP of GME with EO demonstrated a preference of EO over GME.[85] A number of P(GME-*co*-EO) copolymers were examined by ^{13}C NMR triad analysis, revealing the preferred incorporation of ethylene glycol units throughout the copolymerization. Explorations concerning the copolymerizations of GME with PO catalyzed by the industrially established double metal cyanide (DMC) catalyst resulted in slight gradient microstructures ($r_{GME} = 0.71$, $r_{PO} = 1.40$, Jaacks). To visualize the impact of reactivity ratios on the polymer microstructure, simulated molar composition plots for the different copolymers are shown in Figure 3.
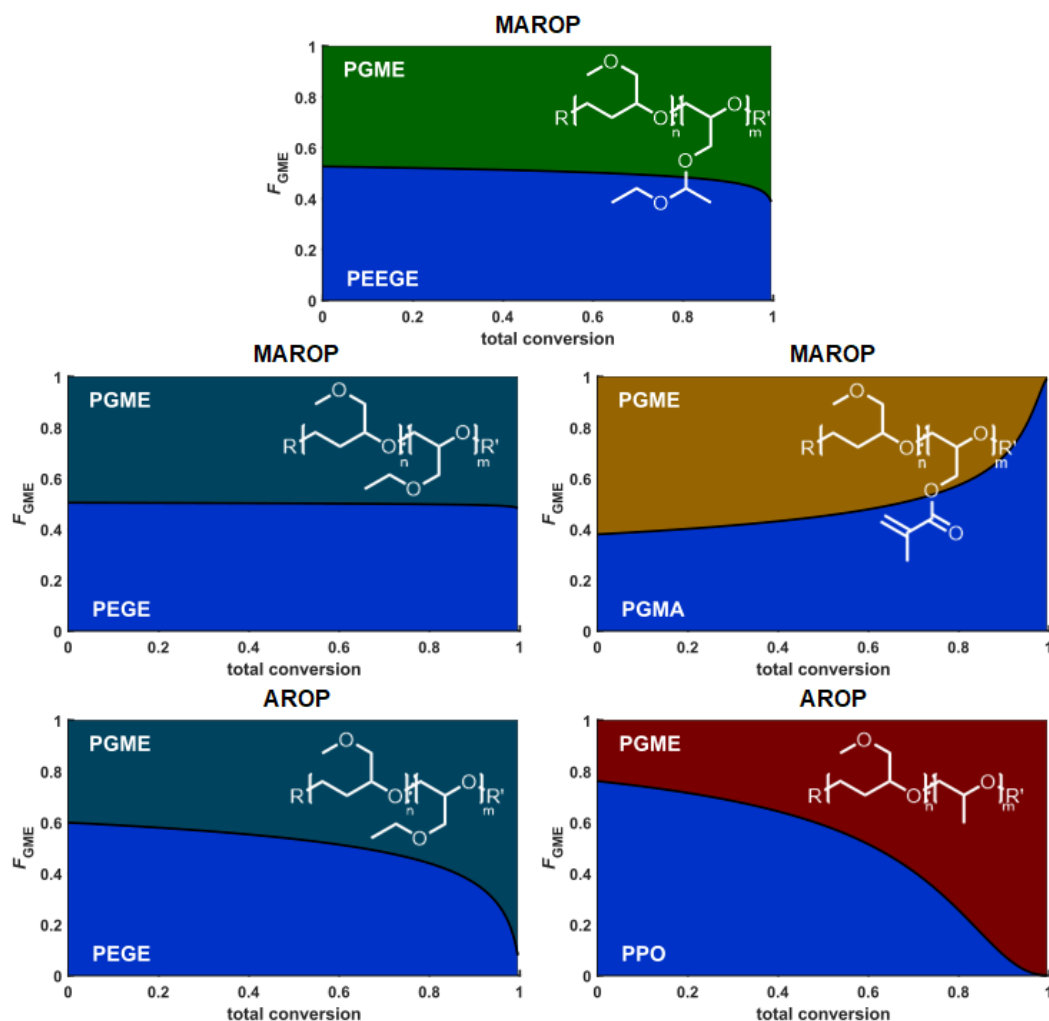
Figure 3. Simulated molar composition plots illustrating the microstructure of GME copolymers synthesized by copolymerization with initial equimolar ratios of GME with EEGE, EGE, GMA or PO by AROP and MAROP, respectively. F_{GME} = GME incorporation. The simulations were conducted by using NIREVAL software from Johann, Steube and Frey.[100]

The computed plots (Figure 3) illustrate the almost exclusive accumulation of the respective comonomers EGE and PO at the chain end in the anionic copolymerization with GME. The reverse gradient is observed for copolymerization with GMA under MAROP conditions, were the chain ends almost exclusively consist of GME units.

THERMOSPONSIV BEHAVIOR OF P(sAlkGE)s

One of the major and most commonly exploited characteristic of polyethers with short-chain alkyl side-groups is their thermoresponsive nature. The specific temperature above which a mixture becomes immiscible is described as the lower critical solution temperature (LCST), indicating the behavior in dependence of temperature.[7,12,101] The thermodynamics of LCST can be described by the Gibbs-Helmholtz equation (eq. 0.7).[102]

$$\Delta G_{mix} = \Delta H_{mix} - T \Delta S_{mix} \tag{0.7}$$

Fundamentally, the dissolution of a substance in solution results in a negative Gibbs free energy ΔG_{mix}. More specifically, a polymer in aqueos solution evinces a LCST if the entropic term ΔS_{mix} as well as the entalphic term ΔH_{mix} of mixing are negative. The occurence of a negative Smix in case of polymers is caused by solvent molecules forming an ordered layer around the macromolecular chains in solution. When ΔG_{mix} becomes positive at a specific temperature, a two-phase-system is obtained, as the dissolution of the polymer in water is no longer favored.[103] At this point, the polymer chains perform a transition from a hydrated coil to a collapsed structure (Figure 4, left), resulting in a turbid solution, which is defined as the cloud point temperature T_{cp}. During this temperature-induced collapse, a nanoscopic spatial inhomogeneity is observed which can be considered as a nanoscoppic cluster of polymer sgements.[104,105]

The Flory-Huggins theory with its simplified lattice model takes the molecular differences of solvent and polymer into account, facilitating interpretation of the obtained experimetal results. By means of the mixing paramter χ, the theory enables the inclusion of polymer-solvent interactions for the calculation of ΔG_{mix}.[12,106]

The widely utilized method for investigation of thermoresponsive behaviour of polyethers bearing short-chain alkyl groups is the determination of the phase transition temperature T_{cp} by turbidimetric measurements. In general, dynamic light scattering (DLS), calorimetry and 1NMR spectroscopy in D_2O are alternative methods for the examination of LCST behaviour, however, turbidimetry is mostly prefered due to its simplicity. Determination of the T_{cp} by turbidimetry is influenced not only by the copolymer composition, but multiple other factors like concentration, molecular weight, wavelength, heating and stirring rate as well as the cuvette and temperature sensor in use. The following fundamentals have to be taken into account when comparing values from different experiments a hypothetical, schematic plot of transmission versus temperature is shown in Figure 4 (right).
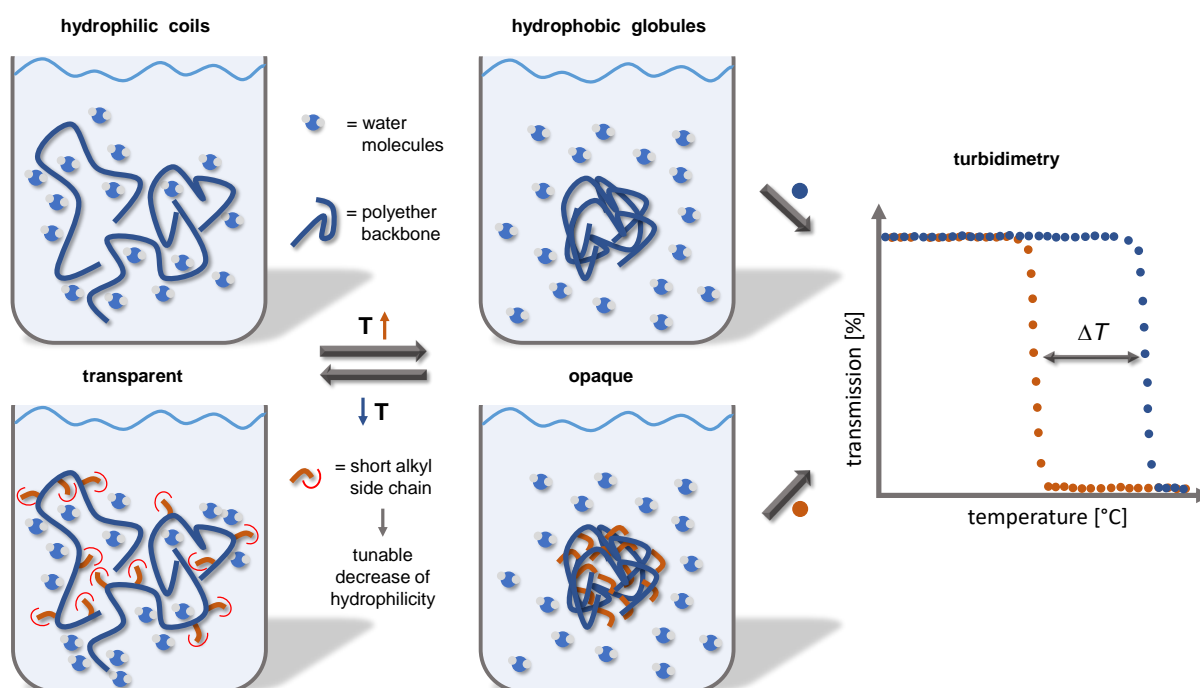
Figure 4. Behavior of polyethers bearing short-alkyl side chains (bottom) compared to PEG (top) in aqueous solution with change of temperature, illustrating the tunable thermoresponsivity and its detection by turbidimetric measurements.

PEG, as the most prominent polyether, exhibits a LCST above 100 °C, which emphasizes its strong water solubility but prevents its application as a thermoresponsive polymer in aqueous solution.[3,107] Incorporation of segments with hydrophobic characteristic results in lowering of the LCST, leading to useful thermoresponsive behavior. As indicated in Figure 4 (bottom), the short alkyl side chains of the herein discussed glycidyl ethers represent slightly hydrophobic substituents, which weaken the interaction of the hydrophilic backbone with the hydration shell.

Homopolymerization of the less hydrophilic short-chain alkyl GEs leads to polyethers with lower LCST than PEG. However, adjustment of the thermoresponsive behavior is feasible by combination of different monomers by copolymerization as well as by combination of PEG with short-chain alkyl GE blocks within statistical or block copolymer structures. A classification of the different short-chain alkyl glycidyl ethers according to their cloud points (T_{cp}) values determined by turbidimetry is summarized in Table 2.

The reported cloud point of PGME varies between 45.0 and 63.4 °C with different molecular weights in the respective studies and depends on polymerization methods and sample concentration. The isotactic homopolymer P[(*R*)GME] shows a T_{cp} within that range (62.7 °C), indicating the expected indifference of tacticity with regard to thermoresponsive behavior in aqueous solution . With longer alkyl ether side chains, the T_{cp} significantly decreases in accordance to the increase hydrophobicity. PEGE as well as P[(*R*)EGE] exhibit low cloud points between 10.0 to 14.6 °C, while P*i*PGE and PPGE show no solubility in aqueous solution at all temperatures with

respective molecular weights above 4.0 and 3.2 kg mol^{-1}.

Short-chain alkyl GEs enable to introduce thermoresponsive behavior in two ways: (**i**) by lowering the polarity of highly hydrophilic polymers i.e., PEG and P(*lin*G) or (**ii**) by increasing the polarity of water-insoluble polymers like PPO. In this regard, the thermorheological behavior of linear polyglycerol with a tailored degree of methylation in P(*lin*G-*co*-GME) copolymers was investigated by our group in 2017.[87] It is worth mentioning that the incorporation of 69 mol% GME units was necessary to enable a T_{cp} below 100 °C (91 °C), due to the high hydrophilicity induced by H-bond formation of linear glycerol units. Incorporation of 90 mol% GME lowered the T_{cp} to 61 °C. Additionally, the incorporation of GME was used in reverse to increase the hydrophilicity of otherwise non-soluble PPO in aqueous solution, resulting in a T_{cp} of 35 °C in random P(PO-*co*-GME) copolymers.[92]

Table 2. Cloud points (T_{cp}) of homopolymers containing short-chain alkyl ether side chains determined by turbidimetric measurements. Molecular weights were calculated from ^{1}H NMR, unless noted otherwise. All samples were evaluated in a 1 wt% aqueous solution, unless noted otherwise.

polymers	M_n [kg mol^{-1}]	Đ	T_{cp} [°C]	lit.
	2.1	1.14	45.0	[46]
	3.0	1.19	57.7	[28]
	5.2[a]	1.50	55[c]	[85]
PGME	9.0	1.04	63.6	[24]
	10.9[b]	1.06	60.5	[69]
	43.6[b]	1.10	56.5	[69]
	87.0[b]	1.16	56.5	[69]
P[(*R*)GME]	9.0	1.04	63.5	[24]
	3.1	1.20	14.6	[28]
	3.0	1.09	10.0	[46]
PEGE	5.3	1.04	12.3	[24]
	9.5	1.12	11.1	[46]
	24.5	1.14	10.8	[46]
P[(*R*)EGE]	5.4	1.04	10.3	[24]
P*i*PGE	4.0 - 16.0	1.08 - 1.22	-	[46]
PPGE	3.2 - 8.0	1.16	-	[46]

^{a} Molecular weight determined by SEC (PEG calibration)

^{b} Molecular weight determined by SEC (polystyrene calibration)

^{c} Cloud point determined in a 5 wt% aqueous solution

BIOAPPLICATION OF THERMORESPONSIVE P(sAlkGE)s

Based on the LCST of the poly(alkGE) homopolymers, copolymerization of P(GME-*co*-EGE) enables the precise adjustment of the LCST around body temperature of 37 °C, which represents one of the main features Haag, Weinhart and co-workers eploited in various publications mentioned throughout this review.[71,76] In several studies, P(GME-*co*-EGE) was utilized for surface engineering as coatings for gold, polystyrene (PS) or glass surfaces (Figure 5a,b). Surface-attached brushes of these copolymers on PS culture substrates were employed for the fabrication of human dermal fibroblast cell (HDF), human aortic smooth muscle cell (HAoSMC) and human umbilical vein endothelial cell (HUVEC) sheets.[73] The copolymers provide excellent biocompatibility[44] and inhibition of nonspecific protein interaction in analogy to PEG, but additionally offer a thermal switchability of these materials e.g for thermally-triggered cell detachment in tissue cultures (Figure 5c).[38,74] Recently, Schulze-Tanzil and co-workers used this knowledge for fabrication of anterior cruciate ligament cell (ACL) sheets, which were utlized for colonization of embroidered scaffolds.[43] Herein, the thermoresponsive P(GME-*co*-EGE) copolymers enable the thermal, enzyme-free detachment of cell sheets.

Beyond surface modification, the copolymerization of short-chain alkyl GEs was utilized in a number of studies concerning thermoresponsive and therefore stimuli-responsive, physically cross-linkable nanogels.[108] A recently published review from Jabbari and co-workers summarizes the general concept of thermoresponsive, polymeric nanogels for biomedical applications.[109] Schmalz and co-workers investigated the temperature-dependent gelation behaviour of double responsive $P2VP_{62}$-*b*-PEG_{452}-*b*-$P(GME_{36}$-*co*-$EGE_{36})$ terpolymers while the 2VP units introduced pH responsivity. Hydrogel formation is observed, if one of the end blocks was insoluble and further indicated a temperature induced gel-sol-gel transition.[36,66] These block copolymers were part of a review from Manners and co-workers in 2012, presenting functional block copolymers utilized as nanostructured materials.[110] In 2014, Kamata et al. demonstrated the synthesis of "nonswellable" hydrogels without mechanical hysteresis, capitalizing on star-shaped four-arm P(GME-*co*-EGE) copolymers.[45]

As these polyethers are known for their high biocompatibility, hydrogels were implemented in several medical and pharmaceutical applications. In studies concerning the treatment of severe dermatological diseases, Caldéron, Kleuser and co-workers utilized P(GME-*co*-EGE) for the fabrication of thermoresponsive nanogels i.e. for hydration of the stratum corneum, the outermost layer of the epidermis.[77–79,81] Further investigations showed a temperature dependent uptake mechanism of the polyether nanogels as a result of phase transition[80,81] as well as their intracellular localization in epidermal keratinocytes.[81] Following publications exploited this knowledge by investigation of the dermal delivery ability of these copolymer nanogels for the drugs dexamethasone[82], etanercept[83] and tacrolimus.[84]
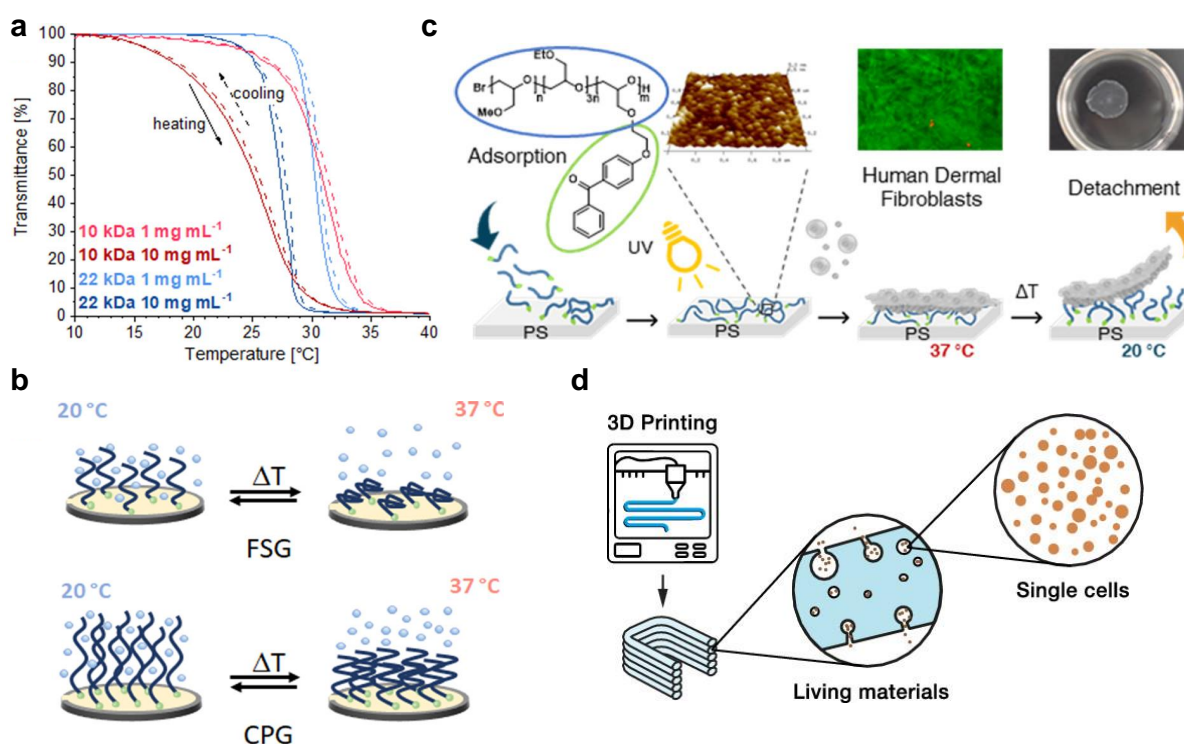
Figure 5. (a) Turbidimetric measurements and (b) quartz crystal microbalance with dissipation monitoring (QCM-D) monitoring of P(GME$_{0.5}$-*co*-EGE$_{0.5}$) (10 and 22 kg mol^{-1}) coated on gold.[76] (c) Temperature-triggered human dermal fibrolast sheet fabrication of PS coated with P(GME-*co*-EGE).[74] (d) 3D printed hydrogels of P(EGE-*co-i*PGE)-*b*-PEG-*b*-(EGE-*co-i*PGE) for investigation of cellular phenotypes within living materials.[50]

Hydrogels based on P*i*PGE-*b*-PEG-*b*-P*i*PGE triblock copolymers published by Nelson and co-workers in 2015 revealed a dual-responsive behavior both with respect to temperature as well as shear response.[67] In 2018, they further refined this concept by urea-termination of these triblock copolymers, enabling self-assembly through noncovalent interactions.[49] As the authors state, these polymers might serve as valuable materials in biomaterial applications like e.g. biomimetic and tissue engineering scaffolds.

In 2018, Fellin et al. demonstrated the 3D-printing of P(EGE-*co-i*PGE)-*b*-PEG-*b*-P(EGE-*co-i*PGE) triblock copolymer hydrogels via temperature as well as shear-responsivity.[46] This idea was further developed in a follow-up work by end functionalization of these block copolymers with α, ω-methacrylate functionalities. The photo-cross-linkable polymer was immobilized with budding yeast Saccharomyces cerevisiae to enable characterization of the cellular phenotype within living materials (Figure 5d).[46,50] Additionally, the 3D printable hydrogel was laden with yeast for immobilized whole-cell catalysis.[51] The crosslinking of pendant methacrylate functions in P(GME-*co*-GMA) copolymers equally enabled the fabrication of thermoresponsive hydrogels, as shown by Labbé et al. already in 2011.[70]

Recently, Choi and co-workers examined the relaxation dynamics of self-assembled P(EGE-*co-i*PGE)-*b*-PEG-*b*-P(EGE-*co-i*PGE) triblock copolymers in dependence of temperature as well as end-block hydrophobicity by adjustment of the EGE/*i*PGE ratio and respective degree of polymerization.[52] As expected, the sol-gel transition occured at higher temperatures and concentrations with increasing ratio of the more hydrophilic comonomer EGE. Additional characterization of PEGE-*b*-PEG-*b*-PEGE based hydrogels demonstrated the self-healing abilities as well as the injectability of these polymers.[23] Supporting cell toxicity tests for both type of ABA triblock copolymers illustrated their non-toxicity.

FURTHER BIOAPPLICATION AND OTHER PURPOSES

Statistical copolymers of GME with the protected glycerol monomer EEGE enabled the fabrication of transparent hydrogel based spray coating for the reduction of marine biofouling.[86] After deprotection of the acetal protection group, the P(GME-*co-lin*G) copolymer was further functionalized with 3-(triethoxysilyl)propyl isocyanate as the silyl substituent enabling the covalent immobilization on glass surfaces.

Haag and co-workers further utilized PGME as an alternative to PEG in biocompatible surfactants by synthesis of perfluoropolyether based PTFE-*b*-PGME-*b*-PTFE triblock copolymers.[32] The triblock copolymers were analyzed in regard to their application in cell encapsulation and in vitro gene expression in droplet-based microfluidics.[31] Besides the versatile utilization in bioapplications, other studies concerning short-chain alkyl glycidyl ether bearing polyethers and their possible applications were conducted.[29,30] For instance, block copolymers consisting of PEGE-*b*-PEG and PPGE-*b*-PEG were examined with respect to the formation of micellar structures in water as well as in ionic liquids.[54] Additionally, phenothiazine-labeled PEGE-*b*-PEG facilitated reversible redox properties by core-shell micelle formation.[55] The thermoresponsivity of the discussed homopolymers PGME and PEGE was systematically investigated in comparison to PEG and PPO concerning their liquid-liquid phase separation behavior in ionic liquids by Watanabe and co-workers in 2008 and 2011.[111,112]

Another field of application was investigated by Nakamura et al. in 2011, as polycarbonates containing EGE and *i*PGE were considered as ion-conductive polymers.[89] The ion transport of PEGE and P*i*PGE was similarly evaluated by Ganesan, Lynd and co-workers by all-atom molecular dynamic simulations. Hereby, the influence of the dielectric constant on the transport of lithium bis-(trifluoromethylsulfonyl)imide (LiTFSI) doped polyethers was examined.[113–115] Recently, this knowledge was expanded for investigations on binary blends of P*i*PGE and other polyglycidyl ethers with imidazolium TFSI ionic liquids.[47] In a recent study from 2021, amorphous PEGE and P*i*PGE among other polyethers were compared to semi-crystalline PEG by examination in regard to the effect of structure and ether oxygen placement on CO_2 solubility.[48]

CONCLUSION & OUTLOOK

Poly(ethylene glycol) (PEG) is widely considered the gold-standard of biocompatible polymers in a vast variety of medical and pharmaceutical applications due to its high solubility in aqueous solution and chemical inertness. Nonetheless, modification of the chain structure of PEG is a synthetically demanding task, requiring rigorous safety precautions and synthetic expertise to handle the toxic, flammable and gaseous monomer ethylene oxide (EO). The polymerization of short-chain alkyl glycidyl ethers (GE) on the contrary, enables variation of the degree of hydrophilicity in polymers consisting of a PEG backbone while, liquid alkyl glycidyl ether monomers facilitate a saver handling compared to EO. Polymers derived from the set of four herein described monomers glycidyl methyl ether (GME), ethyl (EGE), propyl (PGE) and *iso*-propyl glycidyl ether (*i*PGE) can be considered as alkylated linear polyglycerols P(*lin*G). Polymerization of these monomers further enables the combination with CO_2 by the catalytic synthesis of polycarbonates with increased hydrophilicity, using GME units. The manifold copolymerization methods from classical or phosphazene base-catalyzed anionic (AROP) and monomer-activated ring-opening polymerization (MAROP), as well as the use of inorganic catalyst systems allow for the synthesis of random as well as gradient copolymer microstructures. While preserving the high biocompatibility, the incorporation of short alkyl ether side chains adds a valuable feature to the simple structure of PEG: thermoresponsivity. While PEG exhibits a LCST behavior above 100 °C, utilization of short-chain alkyl GEs facilitates a tailorable LCST. Homopolymers containing methyl and ethyl substituted side-chains show high hydrophilicity, while propyl as well as *iso*-propyl ethers in the side-chains are no longer water soluble. Hence, the monomer-activated copolymerization of P(GME-*co*-EGE) has been widely examined, as the LCST in this copolymer is tunable within the range of body temperature. Additionally, the rather hydrophobic side-chains of P(*i*PGE) and P(EGE-*co*-*i*PGE) introduced in ABA triblock copolymers with PEG result in thermoresponsive hydrogels. Prospectively, a wide range of future studies is imaginable, considering the huge scope these 4 monomers offer, especially in PEG-based block copolymers of varying molecular weights. The finely tunable hydrophilicity of these polymers enables bioapplications ranging from dermatologically utilized hydrogels and micellar structures to switchable coatings for cell sheet engineering. In summary, introducing short-chain alkyl ether side chains at the polyglycerol backbone by polymerization of the respective GEs represents an immensely versatile tool kit. The precise control of the LCST facilitates the excellent future perspective for these highly biocompatible polyethers in manifold medical and pharmaceutical applications.

REFERENCES

(1) Knop, K.; Hoogenboom, R.; Fischer, D.; Schubert, U. S. Poly(ethylene glycol) in drug delivery: pros and cons as well as potential alternatives. *Angewandte Chemie International Edition* **2010**, *49*, 6288–6308.

(2) Dormidontova, E. E. Role of Competitive PEO−Water and Water−Water Hydrogen Bonding in Aqueous Solution PEO Behavior. *Macromolecules* **2002**, *35*, 987–1001.

(3) Malcolm, G. N.; Rowlinson, J. S. The thermodynamic properties of aqueous solutions of polyethylene glycol, polypropylene glycol and dioxane. *Trans. Faraday Soc*. **1957**, *53*, 921.

(4) Hu, J.; Liu, S. Responsive Polymers for Detection and Sensing Applications: Current Status and Future Developments. *Macromolecules* **2010**, *43*, 8315–8330.

(5) Mendes, P. M. Stimuli-responsive surfaces for bio-applications. *Chemical Society reviews* **2008**, *37*, 2512–2529.

(6) Roy, D.; Brooks, W. L. A.; Sumerlin, B. S. New directions in thermoresponsive polymers. *Chemical Society reviews* **2013**, *42*, 7214–7243.

(7) Weber, C.; Hoogenboom, R.; Schubert, U. S. Temperature responsive bio-compatible polymers based on poly(ethylene oxide) and poly(2-oxazoline)s. *Progress in Polymer Science* **2012**, *37*, 686–714.

(8) Heskins, M.; Guillet, J. E. Solution Properties of Poly(N-isopropylacrylamide). *Journal of Macromolecular Science: Part A - Chemistry* **1968**, *2*, 1441–1455.

(9) Scarpa, J. S.; Mueller, D. D.; Klotz, I. M. Slow hydrogen-deuterium exchange in a non-.alpha.-helical polyamide. *J. Am. Chem. Soc.* **1967**, *89*, 6024–6030.

(10) Adams, N.; Schubert, U. S. Poly(2-oxazolines) in biological and biomedical application contexts. *Advanced drug delivery reviews* **2007***, 59*, 1504–1520.

(11) Lutz, J.-F.; Akdemir, O.; Hoth, A. Point by point comparison of two thermosensitive polymers exhibiting a similar LCST: is the age of poly(NIPAM) over? *J. Am. Chem. Soc.* **2006***, 128*, 13046–13047.

(12) Cook, M. T.; Haddow, P.; Kirton, S. B.; McAuley, W. J. Polymers Exhibiting Lower Critical Solution Temperatures as a Route to Thermoreversible Gelators for Healthcare. *Adv. Funct. Mater.* **2021***, 31*, 2008123.

(13) Dumortier, G.; Grossiord, J. L.; Agnely, F.; Chaumeil, J. C. A review of poloxamer 407 pharmaceutical and pharmacological characteristics. *Pharmaceutical research* **2006***, 23*, 2709–2728.

(14) Batrakova, E. V.; Kabanov, A. V. Pluronic block copolymers: evolution of drug delivery concept from inert nanocarriers to biological response modifiers. *Journal of controlled release : official journal of the Controlled Release Society* **2008***, 130*, 98–106.

(15) Herzberger, J.; Niederer, K.; Pohlit, H.; Seiwert, J.; Worm, M.; Wurm, F. R.; Frey, H. Polymerization of Ethylene Oxide, Propylene Oxide, and Other Alkylene Oxides: Synthesis, Novel Polymer Architectures, and Bioconjugation. *Chemical reviews* **2016***, 116*, 2170–2243.

(16) Thomas, A.; Müller, S. S.; Frey, H. Beyond poly(ethylene glycol): linear polyglycerol as a multifunctional polyether for biomedical and pharmaceutical applications. *Biomacromolecules* **2014***, 15*, 1935–1954.

(17) Mangold, C.; Obermeier, B.; Wurm, F.; Frey, H. From an epoxide monomer toolkit to functional PEG copolymers with adjustable LCST behavior. *Macromol. Rapid Commun.* **2011***, 32*, 1930–1934.

(18) Addy, J. K.; Parker, R. E. 104. The mechanism of epoxide reactions. Part VII. The reactions of 1,2-epoxybutane, 3,4-epoxybut-1-ene, 1,2-epoxy-3-chloropropane, and 1,2-epoxy-3-methoxypropane with chloride ion in water under neutral and acidic conditions. *J. Chem. Soc.* **1965***, 644*.

(19) Mouzin, G.; Cousse, H.; Rieu, J.-P.; Duflos, A. A Convenient One-Step Synthesis of Glycidyl Ethers. *Synthesis* **1983***, 1983*, 117–119.

(20) Singh, G. S.; Mollet, K.; D'hooghe, M.; Kimpe, N. de. Epihalohydrins in organic synthesis. *Chemical reviews* **2013***, 113*, 1441–1498.

(21) Verkoyen, P.; Frey, H. Long-Chain Alkyl Epoxides and Glycidyl Ethers: An Underrated Class of Monomers. *Macromol. Rapid Commun.* **2020***, 41*, e2000225.

(22) Lee, A.; Lundberg, P.; Klinger, D.; Lee, B. F.; Hawker, C. J.; Lynd, N. A. Physiologically relevant, pH-responsive PEG-based block and statistical copolymers with N,N-diisopropylamine units. *Polym. Chem.* **2013***, 4*, 5735–5742.

(23) Hong, Y.; Kim, J.-M.; Jung, H.; Park, K.; Hong, J.; Choi, S.-H.; Kim, B.-S. Facile Synthesis of Poly(ethylene oxide)-Based Self-Healable Dynamic Triblock Copolymer Hydrogels. *Biomacromolecules* **2020***, 21*, 4913–4922.

(24) Isono, T.; Miyachi, K.; Satoh, Y.; Sato, S.; Kakuchi, T.; Satoh, T. Design and synthesis of thermoresponsive aliphatic polyethers with a tunable phase transition temperature. *Polym. Chem.* **2017***, 8*, 5698–5707.

(25) Mangold, C.; Wurm, F.; Frey, H. Functional PEG-based polymers with reactive groups via anionic ROP of tailor-made epoxides. *Polym. Chem.* **2012***, 3*, 1714.

(26) Klein, R.; Wurm, F. R. Aliphatic Polyethers: Classical Polymers for the 21st Century. *Macromolecular rapid communications 2015,* **36**, 1147–1165.

(27) Ponomarenko, V. A.; Khomutov, A. M.; Il'chenko, S. I.; Ignatenko, A. V. The effect of substituents of the anionic polymerization of α-oxides. *Polymer Science U.S.S.R.* **1971***, 13*, 1735–1740.

(28) Aoki, S.; Koide, A.; Imabayashi, S.; Watanabe, M. Novel Thermosensitive Polyethers Prepared by Anionic Ring-Opening Polymerization of Glycidyl Ether Derivatives. *Chem. Lett.* **2002**, *31*, 1128–1129.

(29) Hirose, Y.; Adachi, K. Dielectric Study of Dynamic Heterogeneity in Miscible Blends of Polyethers and Poly(vinylethylene). *Macromolecules* **2006**, *39*, 1779–1789.

(30) Yamane, M.; Hirose, Y.; Adachi, K. Dielectric Study of Terminal Chain Dynamics, Segmental Motion, and Rotation of Side Groups in Polyethers of Type ABC. *Macromolecules* **2005**, *38*, 10686–10693.

(31) Wagner, O.; Thiele, J.; Weinhart, M.; Mazutis, L.; Weitz, D. A.; Huck, W. T. S.; Haag, R. Biocompatible fluorinated polyglycerols for droplet microfluidics as an alternative to PEG-based copolymer surfactants. *Lab on a chip* **2016**, *16*, 65–69.

(32) Wagner, O.; Thota, B. N. S.; Schade, B.; Neumann, F.; Cuellar, J. L.; Böttcher, C.; Haag, R. Perfluoroalkylated linear polyglycerols and their supramolecular assemblies in aqueous solution. *Polym. Chem.* **2016**, *7*, 2222–2229.

(33) Rainer Haag, Heidemarie Weinhart, Monika Wyszogrodzka. Verfahren zur Herstellung von linearen, methylierten Polyglycerolderivaten und ihre Verwendung zur Funktionalisierung von Oberflächen. **2007**, WO2007141248A1.

(34) Wurm, F.; Klos, J.; Räder, H. J.; Frey, H. Synthesis and noncovalent protein conjugation of linear-hyperbranched PEG-poly(glycerol) alpha,omega(n)-telechelics. *Journal of the American Chemical Society* **2009**, *131*, 7954–7955.

(35) Almiento, G. M.; Balducci, D.; Bottoni, A.; Calvaresi, M.; Porzi, G. Stereoselective synthesis and conformational analysis of unnatural tetrapeptides. *Part 2. Tetrahedron: Asymmetry* **2007**, *18*, 2695–2711.

(36) Reinicke, S.; Schmelz, J.; Lapp, A.; Karg, M.; Hellweg, T.; Schmalz, H. Smart hydrogels based on double responsive triblock terpolymers. *Soft Matter* **2009**, *5*, 2648–2657.

(37) Becherer, T.; Heinen, S.; Wei, Q.; Haag, R.; Weinhart, M. In-depth analysis of switchable glycerol based polymeric coatings for cell sheet engineering. *Acta biomaterialia* **2015**, *25*, 43–55.

(38) Heinen, S.; Cuéllar-Camacho, J. L.; Weinhart, M. Thermoresponsive poly(glycidyl ether) brushes on gold: Surface engineering parameters and their implication for cell sheet fabrication. *Acta biomaterialia* **2017**, *59*, 117–128.

(39) Heinen, S.; Weinhart, M. Poly(glycidyl ether)-Based Monolayers on Gold Surfaces: Control of Grafting Density and Chain Conformation by Grafting Procedure, Surface Anchor, and Molecular Weight. *Langmuir : the ACS journal of surfaces and colloids* **2017**, *33*, 2076–2086.

(40) Stöbener, D. D.; Donath, D.; Weinhart, M. Fast and solvent-free microwave-assisted synthesis of thermoresponsive oligo(glycidyl ether)s. *J. Polym. Sci. Part A: Polym. Chem.* **2018**, *56*, 2496–2504.

(41) Stöbener, D. D.; Scholz, J.; Schedler, U.; Weinhart, M. Switchable Oligo(glycidyl ether) Acrylate Bottlebrushes "Grafted-from" Polystyrene Surfaces: A Versatile Strategy toward Functional Cell Culture Substrates. *Biomacromolecules* **2018**, *19*, 4207–4218.

(42) Weinhart, M.; Becherer, T.; Haag, R. Switchable, biocompatible surfaces based on glycerol copolymers. *Chemical communications* **2011**, *47*, 1553–1555.

(43) Zahn, I.; Stöbener, D. D.; Weinhart, M.; Gögele, C.; Breier, A.; Hahn, J.; Schröpfer, M.; Meyer, M.; Schulze-Tanzil, G. Cruciate Ligament Cell Sheets Can Be Rapidly Produced on Thermoresponsive poly(glycidyl ether) Coating and Successfully Used for Colonization of Embroidered Scaffolds. *Cells* **2021**, *10*.

(44) Weinhart, M.; Grunwald, I.; Wyszogrodzka, M.; Gaetjen, L.; Hartwig, A.; Haag, R. Linear poly(methyl glycerol) and linear polyglycerol as potent protein and cell resistant alternatives to poly(ethylene glycol). *Chemistry, an Asian journal* **2010**, *5*, 1992–2000.

(45) Kamata, H.; Akagi, Y.; Kayasuga-Kariya, Y.; Chung, U.; Sakai, T. "Nonswellable" hydrogel without mechanical hysteresis. *Science (New York, N.Y.)* **2014**, *343*, 873–875.

(46) Fellin, C. R.; Adelmund, S. M.; Karis, D. G.; Shafranek, R. T.; Ono, R. J.; Martin, C. G.; Johnston, T. G.; DeForest, C. A.; Nelson, A. Tunable temperature- and shear-responsive hydrogels based on poly(alkyl glycidyl ether)s. *Polym. Int.* **2018**, *68*, 1238–1246.

(47) Bentley, C. L.; Chwatko, M.; Wheatle, B. K.; Burkey, A. A.; Helenic, A.; Morales-Collazo, O.; Ganesan, V.; Lynd, N. A.; Brennecke, J. F. Modes of Interaction in Binary Blends of Hydrophobic Polyethers and Imidazolium Bis(trifluoromethylsulfonyl)imide Ionic Liquids. *Macromolecules* **2020**, *53*, 6519–6528.

(48) Bentley, C. L.; Song, T.; Pedretti, B. J.; Lubben, M. J.; Lynd, N. A.; Brennecke, J. F. Effects of Poly(glycidyl ether) Structure and Ether Oxygen Placement on CO 2 Solubility. *J. Chem. Eng. Data* [Online early access]. DOI: 10.1021/acs.jced.1c00219.

(49) Shafranek, R. T.; Leger, J. D.; Zhang, S.; Khalil, M.; Gu, X.; Nelson, A. Sticky ends in a self-assembling ABA triblock copolymer: the role of ureas in stimuli-responsive hydrogels. *Mol. Syst. Des. Eng.* **2019**, *4*, 91–102.

(50) Priks, H.; Butelmann, T.; Illarionov, A.; Johnston, T. G.; Fellin, C.; Tamm, T.; Nelson, A.; Kumar, R.; Lahtvee, P.-J. Physical Confinement Impacts Cellular Phenotypes within Living Materials. *ACS Appl. Bio Mater.* **2020**, *3*, 4273–4281.

(51) Johnston, T. G.; Fellin, C. R.; Carignano, A.; Nelson, A. Poly(alkyl glycidyl ether) hydrogels for harnessing the bioactivity of engineered microbes. *Faraday discussions* **2019**, *219*, 58–72.

(52) Jung, H.; Gang, S.-E.; Kim, J.-M.; Heo, T.-Y.; Lee, S.; Shin, E.; Kim, B.-S.; Choi, S.-H. Regulating Dynamics of Polyether-Based Triblock Copolymer Hydrogels by End-Block Hydrophobicity. *Macromolecules* **2020**, *53*, 10339–10348.

(53) Ogura, M.; Tokuda, H.; Imabayashi, S.; Watanabe, M. Preparation and solution behavior of a thermoresponsive diblock copolymer of poly(ethyl glycidyl ether) and poly(ethylene oxide). *Langmuir: the ACS journal of surfaces and colloids* **2007***, 23*, 9429–9434.

(54) Chen, Z.; FitzGerald, P. A.; Kobayashi, Y.; Ueno, K.; Watanabe, M.; Warr, G. G.; Atkin, R. Micelle Structure of Novel Diblock Polyethers in Water and Two Protic Ionic Liquids (EAN and PAN). *Macromolecules* ***2015***, 48*, 1843–1851.

(55) Tsuda, R.; Kaino, S.; Kokubo, H.; Imabayashi, S.; Watanabe, M. Effect of core-shell micelle formation on the redox properties of phenothiazine-labeled poly(ethyl glycidy ether)-block-poly(ethylene oxide). *Colloids and surfaces. B, Biointerfaces* **2007***, 56*, 255–259.

(56) Grobelny, Z.; Golba, S.; Jurek-Suliga, J. Characterization of new polyether-diols with different molar masses and modality prepared by ring opening polymerization of oxiranes initiated with anhydrous potassium hydroxide. *J Polym Res* **2019***, 26*.

(57) Hans, M.; Keul, H.; Moeller, M. Chain transfer reactions limit the molecular weight of polyglycidol prepared via alkali metal based initiating systems. *Polymer* **2009***, 50*, 1103–1108.

(58) Pearson, R. G. Hard and Soft Acids and Bases. *J. Am. Chem. Soc.* **1963***, 85*, 3533–3539.

(59) Allgaier, J.; Willbold, S.; Chang, T. Synthesis of Hydrophobic Poly(alkylene oxide)s and Amphiphilic Poly(alkylene oxide) Block Copolymers. *Macromolecules* **2007***, 40*, 518–525.

(60) Becker, H.; Wagner, G.; Stolarzewicz, A. Zur Übertragungsreaktion bei der anionischen Polymerisation von Oxiranen. III. Zur Dynamik der Doppelbindungsbildung bei der Propylenoxid-polymerisation. Acta Polym. 1982, 33, 34–37.

(61) Grobelny, Z.; Jurek-Suliga, J.; Golba, S. Application of cesium hydroxide monohydrate for ring opening polymerization of monosubstituted oxiranes: characterization of synthesized polyether-diols. Polymer Bulletin [Online early access]. DOI: 10.1007/s00289-020-03480-1.

(62) Isono, T. Synthesis of functional and architectural polyethers via the anionic ring-opening polymerization of epoxide monomers using a phosphazene base catalyst. *Polym J* **2021***, 53*, 753–764.

(63) Boileau, S.; Illy, N. Activation in anionic polymerization: Why phosphazene bases are very exciting promoters. *Progress in Polymer Science* **2011***, 36*, 1132–1151.

(64) Brocas, A.-L.; Mantzaridis, C.; Tunc, D.; Carlotti, S. Polyether synthesis: From activated or metal-free anionic ring-opening polymerization of epoxides to functionalization. *Progress in Polymer Science* **2013***, 38*, 845–873.

(65) Billouard, C.; Carlotti, S.; Desbois, P.; Deffieux, A. "Controlled" High-Speed Anionic Polymerization of Propylene Oxide Initiated by Alkali Metal Alkoxide/Trialkylaluminum Systems. *Macromolecules* **2004***, 37*, 4038–4043.

(66) Karg, M.; Reinicke, S.; Lapp, A.; Hellweg, T.; Schmalz, H. Temperature-Dependent Gelation Behaviour of Double Responsive P2VP-b-PEO-b-P(GME-co-EGE) Triblock Terpolymers: A SANS Study. *Macromol. Symp.* **2011***, 306-307*, 77–88.

(67) Zhang, M.; Vora, A.; Han, W.; Wojtecki, R. J.; Maune, H.; Le, A. B. A.; Thompson, L. E.; McClelland, G. M.; Ribet, F.; Engler, A. C.; et al. Dual-Responsive Hydrogels for Direct-Write 3D Printing. *Macromolecules* **2015**, *48*, 6482–6488.

(68) Xia, Y.; Shen, J.; Alamri, H.; Hadjichristidis, N.; Zhao, J.; Wang, Y.; Zhang, G. Revealing the Cytotoxicity of Residues of Phosphazene Catalysts Used for the Synthesis of Poly(ethylene oxide). *Biomacromolecules* **2017**, *18*, 3233–3237.

(69) Labbé, A.; Carlotti, S.; Deffieux, A.; Hirao, A. Controlled Polymerization of Glycidyl Methyl Ether Initiated by Onium Salt/Triisobutylaluminum and Investigation of the Polymer LCST. *Macromol. Symp.* **2007**, *249-250*, 392–397.

(70) Labbé, A.; Brocas, A.-L.; Ibarboure, E.; Ishizone, T.; Hirao, A.; Deffieux, A.; Carlotti, S. Selective Ring-Opening Polymerization of Glycidyl Methacrylate: Toward the Synthesis of Cross-Linked (Co)polyethers with Thermoresponsive Properties. *Macromolecules* **2011**, *44*, 6356–6364.

(71) Heinen, S.; Rackow, S.; Schäfer, A.; Weinhart, M. A Perfect Match: Fast and Truly Random Copolymerization of Glycidyl Ether Monomers to Thermoresponsive Copolymers. *Macromolecules* **2017**, *50*, 44–53.

(72) Heinen, S.; Rackow, S.; Cuellar-Camacho, J. L.; Donskyi, I. S.; Unger, W. E. S.; Weinhart, M. Transfer of functional thermoresponsive poly(glycidyl ether) coatings for cell sheet fabrication from gold to glass surfaces. *Journal of materials chemistry. B* **2018**, *6*, 1489–1500.

(73) Stöbener, D. D.; Hoppensack, A.; Scholz, J.; Weinhart, M. Endothelial, smooth muscle and fibroblast cell sheet fabrication from self-assembled thermoresponsive poly(glycidyl ether) brushes. *Soft Matter* **2018**, *14*, 8333–8343.

(74) Stöbener, D. D.; Uckert, M.; Cuellar-Camacho, J. L.; Hoppensack, A.; Weinhart, M. Ultrathin Poly(glycidyl ether) Coatings on Polystyrene for Temperature-Triggered Human Dermal Fibroblast Sheet Fabrication. *ACS Biomater. Sci. Eng.* **2017**, *3*, 2155–2165.

(75) Stöbener, D. D.; Weinhart, M. Thermoresponsive Poly(glycidyl ether) Brush Coatings on Various Tissue Culture Substrates-How Block Copolymer Design and Substrate Material Govern Self-Assembly and Phase Transition. *Polymers* **2020**, *12*.

(76) Schweigerdt, A.; Heinen, S.; Stöbener, D. D.; Weinhart, M. Grafting Density-Dependent Phase Transition Mechanism of Thermoresponsive Poly(glycidyl ether) Brushes: A Comprehensive QCM-D Study. *Langmuir* **2021**, *37*, 7087-7096

(77) Giulbudagian, M.; Asadian-Birjand, M.; Steinhilber, D.; Achazi, K.; Molina, M.; Calderón, M. Fabrication of thermoresponsive nanogels by thermo-nanoprecipitation and in situ encapsulation of bioactives. *Polym. Chem.* **2014**, *5*, 6909–6913.

(78) Giulbudagian, M.; Rancan, F.; Klossek, A.; Yamamoto, K.; Jurisch, J.; Neto, V. C.; Schrade, P.; Bachmann, S.; Rühl, E.; Blume-Peytavi, U.; et al. Correlation between the chemical composition of thermoresponsive nanogels and their interaction with the skin barrier. *Journal of controlled release : official journal of the Controlled Release Society* **2016**, *243*, 323–332.

(79) Rancan, F.; Giulbudagian, M.; Jurisch, J.; Blume-Peytavi, U.; Calderón, M.; Vogt, A. Drug delivery across intact and disrupted skin barrier: Identification of cell populations interacting with penetrated thermoresponsive nanogels. *European journal of pharmaceutics and biopharmaceutics : official journal of Arbeitsgemeinschaft fur Pharmazeutische Verfahrenstechnik e.V* **2017***, 116*, 4–11.

(80) Edlich, A.; Gerecke, C.; Giulbudagian, M.; Neumann, F.; Hedtrich, S.; Schäfer-Korting, M.; Ma, N.; Calderon, M.; Kleuser, B. Specific uptake mechanisms of well-tolerated thermoresponsive polyglycerol-based nanogels in antigen-presenting cells of the skin. *European journal of pharmaceutics and biopharmaceutics : official journal of Arbeitsgemeinschaft fur Pharmazeutische Verfahrenstechnik e.V* **2017***, 116*, 155–163.

(81) Gerecke, C.; Edlich, A.; Giulbudagian, M.; Schumacher, F.; Zhang, N.; Said, A.; Yealland, G.; Lohan, S. B.; Neumann, F.; Meinke, M. C.; et al. Biocompatibility and characterization of polyglycerol-based thermoresponsive nanogels designed as novel drug-delivery systems and their intracellular localization in keratinocytes. *Nanotoxicology* **2017***, 11*, 267–277.

(82) Giulbudagian, M.; Hönzke, S.; Bergueiro, J.; Işık, D.; Schumacher, F.; Saeidpour, S.; Lohan, S. B.; Meinke, M. C.; Teutloff, C.; Schäfer-Korting, M.; et al. Enhanced topical delivery of dexamethasone by *β*-cyclodextrin decorated thermoresponsive nanogels. *Nanoscale* **2017***, 10*, 469–479.

(83) Giulbudagian, M.; Yealland, G.; Hönzke, S.; Edlich, A.; Geisendörfer, B.; Kleuser, B.; Hedtrich, S.; Calderón, M. Breaking the Barrier - Potent Anti-Inflammatory Activity following Efficient Topical Delivery of Etanercept using Thermoresponsive Nanogels. *Theranostics* **2018***, 8*, 450–463.

(84) Rancan, F.; Volkmann, H.; Giulbudagian, M.; Schumacher, F.; Stanko, J. I.; Kleuser, B.; Blume-Peytavi, U.; Calderón, M.; Vogt, A. Dermal Delivery of the High-Molecular-Weight Drug Tacrolimus by Means of Polyglycerol-Based Nanogels. *Pharmaceutics* **2019***, 11*.

(85) Müller, S. S.; Moers, C.; Frey, H. A Challenging Comonomer Pair: Copolymerization of Ethylene Oxide and Glycidyl Methyl Ether to Thermoresponsive Polyethers. *Macromolecules* **2014***, 47*, 5492–5500.

(86) Becherer, T.; Vieira Nascimento, M.; Sindram, J.; Noeske, P.-L. M.; Wei, Q.; Haag, R.; Grunwald, I. Fast and easily applicable glycerol-based spray coating. *Progress in Organic Coatings* **2015***, 87*, 146–154.

(87) Schubert, C.; Dreier, P.; Nguyen, T.; Maciol, K.; Blankenburg, J.; Friedrich, C.; Frey, H. Synthesis of linear polyglycerols with tailored degree of methylation by copolymerization and the effect on thermorheological behavior. *Polymer* **2017***, 121*, 328–339.

(88) Łukaszczyk, J.; Jaszcz, K.; Kuran, W.; Listoś, T. Synthesis and Modification of Functional Polycarbonates with Pendant Allyl Groups. *Macromol. Biosci.* **2001***, 1*, 282–289.

(89) Nakamura, M.; Tominaga, Y. Utilization of carbon dioxide for polymer electrolytes [II]: Synthesis of alternating copolymers with glycidyl ethers as novel ion-conductive polymers. *Electrochimica Acta* **2011***, 57*, 36–39.

(90) Hilf, J.; Scharfenberg, M.; Poon, J.; Moers, C.; Frey, H. Aliphatic polycarbonates based on carbon dioxide, furfuryl glycidyl ether, and glycidyl methyl ether: reversible functionalization and cross-linking. *Macromolecular rapid communications* **2015**, *36*, 174–179.

(91) Hilf, J.; Phillips, A.; Frey, H. Poly(carbonate) copolymers with a tailored number of hydroxyl groups from glycidyl ethers and CO 2. *Polym. Chem.* **2014**, *5*, 814–818.

(92) R. Matthes, C. Bapp, M. Wagner, S. Zarbakhsh, H. Frey. Introducing Hydrophilicity to Polypropylene Oxide: DMC Catalyzed Copolymerization of Propylene Oxide with Glycidyl Methyl Ether **2021**, to be submitted.

(93) Herzberger, J.; Leibig, D.; Liermann, J. C.; Frey, H. Conventional Oxyanionic versus Monomer-Activated Anionic Copolymerization of Ethylene Oxide with Glycidyl Ethers: Striking Differences in Reactivity Ratios. *ACS Macro Lett.* **2016**, *5*, 1206–1211.

(94) Fineman, M.; Ross, S. D. Linear method for determining monomer reactivity ratios in copolymerization. *J. Polym. Sci.* **1950**, *5*, 259–262.

(95) Mayo, F. R.; Lewis, F. M. Copolymerization. I. A Basis for Comparing the Behavior of Monomers in Copolymerization; The Copolymerization of Styrene and Methyl Methacrylate. *J. Am. Chem. Soc.* **1944**, *66*, 1594–1601.

(96) Heatley, F.; Yu, G.-E.; Booth, C.; Blease, T. G. Determination of reactivity ratios for the anionic copolymerization of ethylene oxide and propylene oxide in bulk. European Polymer Journal 1991, 27, 573–579.

(97) Tüdos, F.; Kelen, T.; Földes-berezsnich, T.; Turcsányi, B. Analysis of Linear Methods for Determining Copolymerization Reactivity Ratios. III. Linear Graphic Method for Evaluating Data Obtained at High Conversion Levels. *Journal of Macromolecular Science: Part A - Chemistry* **1976**, *10*, 1513–1540.

(98) Kelen, T.; TÜds, F. Analysis of the Linear Methods for Determining Copolymerization Reactivity Ratios. I. A New Improved Linear Graphic Method. *Journal of Macromolecular Science: Part A - Chemistry* **1975**, *9*, 1–27.

(99) Jaacks, V. A Novel Method of Determination of Reactivity Ratios in Binary and Ternary Copolymerizations. *Makromol. Chem.* **1972**, *161*, 161–172.

(100) Steube, M.; Johann, T.; Plank, M.; Tjaberings, S.; Gröschel, A. H.; Gallei, M.; Frey, H.; Müller, A. H. E. Kinetics of Anionic Living Copolymerization of Isoprene and Styrene Using in Situ NIR Spectroscopy: Temperature Effects on Monomer Sequence and Morphology. *Macromolecules* **2019**, *52*, 9299–9310.

(101) Zhang, Q.; Weber, C.; Schubert, U. S.; Hoogenboom, R. Thermoresponsive polymers with lower critical solution temperature: from fundamental aspects and measuring techniques to recommended turbidimetry conditions. *Mater. Horiz.* **2017**, *4*, 109–116.

(102) Gibbs, J. W. A Method of Geomtrical Representation of the Thermodynamic Properties of Substances by Means of Surfaces. *Transaction of the Connecticut Academy,* **1873**, 382–404.

(103) Heyda, J.; Soll, S.; Yuan, J.; Dzubiella, J. Thermodynamic Description of the LCST of Charged Thermoresponsive Copolymers. *Macromolecules* **2014**, *47*, 2096–2102.

(104) Kurzbach, D.; Junk, M. J. N.; Hinderberger, D. Nanoscale inhomogeneities in thermoresponsive polymers. *Macromol. Rapid Commun.* **2013**, *34*, 119–134.

(105) Kurzbach, D.; Schömer, M.; Wilms, V. S.; Frey, H.; Hinderberger, D. How Structure-Related Collapse Mechanisms Determine Nanoscale Inhomogeneities in Thermoresponsive Polymers. *Macromolecules* **2012**, *45*, 7535–7548.

(106) Flory, P. J. Thermodynamics of High Polymer Solutions. *The Journal of Chemical Physics* **1942**, *10*, 51–61.

(107) Saeki, S.; Kuwahara, N.; Nakata, M.; Kaneko, M. Upper and lower critical solution temperatures in poly (ethylene glycol) solutions. *Polymer* **1976**, *17*, 685–689.

(108) Abdollahiyan, P.; Baradaran, B.; La Guardia, M. de; Oroojalian, F.; Mokhtarzadeh, A. Cutting-edge progress and challenges in stimuli responsive hydrogel microenvironment for success in tissue engineering today. *Journal of controlled release : official journal of the Controlled Release Society* **2020**, *328*, 514–531.

(109) Ghaeini-Hesaroeiye, S.; Razmi Bagtash, H.; Boddohi, S.; Vasheghani-Farahani, E.; Jabbari, E. Thermoresponsive Nanogels Based on Different Polymeric Moieties for Biomedical Applications. *Gels* **2020**, *6*.

(110) Schacher, F. H.; Rupar, P. A.; Manners, I. Functional block copolymers: nanostructured materials with emerging applications. *Angewandte Chemie International Edition* **2012**, *51*, 7898–7921.

(111) Kodama, K.; Tsuda, R.; Niitsuma, K.; Tamura, T.; Ueki, T.; Kokubo, H.; Watanabe, M. Structural effects of polyethers and ionic liquids in their binary mixtures on lower critical solution temperature liquid-liquid phase separation. *Polym J* **2011**, *43*, 242–248.

(112) Tsuda, R.; Kodama, K.; Ueki, T.; Kokubo, H.; Imabayashi, S.; Watanabe, M. LCST-type liquid-liquid phase separation behaviour of poly(ethylene oxide) derivatives in an ionic liquid. *Chemical communications (Cambridge, England)* **2008**, 4939–4941.

(113) Wheatle, B. K.; Keith, J. R.; Mogurampelly, S.; Lynd, N. A.; Ganesan, V. Influence of Dielectric Constant on Ionic Transport in Polyether-Based Electrolytes. *ACS Macro Lett.* **2017**, *6*, 1362–1367.

(114) Nathaniel A. Lynd, Glenn H. Fredrickson, Craig J. Hawker, Edward J. Kramer, Kate Barteau. Polymer electrolytes based on poly(gylcidyl ether)s. US 8,911,639 B2, **2012**.

(115) Barteau, K. P. Poly(Glycidyl Ether)-Based Battery Electrolytes: Correlating Polymer Properties to Ion Transport. Dissertation, University of California, Santa Barbara, [Santa Barbara, Calif.], **2015**.

Chapter 2

Polymerization Kinetics and Concepts for Bioapplicaton of Polyether Copolymers

Questioning a Paradigm: Random PEG Copolymers for a Better PEGylation?

PEGylation, the conjugation of poly(ethylene glycol) (PEG) to bioactive peptide drugs or nanocarriers, is an important tool to increase the blood stream circulation time of therapeutics due to the "stealth" effect of PEG. However, anti-PEG antibodies (APA) are becoming increasingly widespread in the population, leading to a pronounced immune-responses after drug application and advanced blood clearance of PEGylated drugs due to a loss of the stealth-effect. By introduction of statistically distributed, hydrophilic side chains at the polyether backbone in copolymers of ethylene oxide (EO) and glycidyl methyl ether (GME), the antigen recognition by the APA is effectively disturbed or prevented. Ideally random anionic ring-opening copolymerization of EO and GME is demonstrated by *in situ* ^{1}H NMR kinetics, while highly defined copolymers ($Đ < 1.09$) of $M_\mathrm{n} = 4.2$ to $10.9\,\mathrm{kg\,mol^{-1}}$ and up to 49 mol% GME content are obtained. A competitive enzyme-linked immunosorbent assay (ELISA) of several copolymers revealed reduced (< 24 mol% GME) or fully suppressed recognition of the copolymers by APAs in comparison to the PEG homopolymer. Kinetic Monte Carlo (kMC) simulations illustrate the microstructure of the resulting copolymer chains and allow an in-depth understanding regarding the required GME amount from a theoretical point of view. Cell viability tests confirmed full biocompatibility, as known for the established PEG. Excellent aqueous solubility of P(EG-*co*-GME) copolymers is confirmed by determination of the lower critical solution temperature (LCST) of copolymer with 50% GME (> 94.5 °C). Model reactions with bovine serum albumin evidence the application of P(EG-*co*-GME) for protein bioconjugation. P(EG-*co*-GME) copolymers promise the full preservation of the excellent characteristics of PEG, while eliminating the adverse immune response.
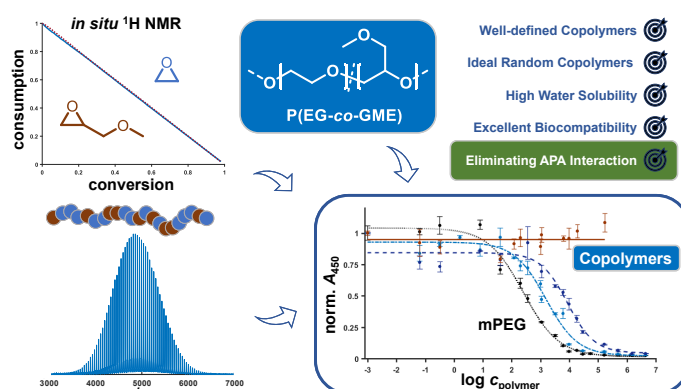
INTRODUCTION

Polymer conjugation with polyethylene glycol (PEG, sometimes also designated "polyethylene oxide", PEO) currently plays an eminent and still growing role for numerous medical therapeutics. In the "PEGylation" strategy introduced in the late 1970ies,[1–5] the polyether "polyethylene glycol" (PEG, or more commonly monofunctional methoxy-PEG, "mPEG") is covalently linked to a drug. This is usually achieved via its end group, leading to considerably prolonged circulation times in the blood stream with a half-life on the order of 1-2 weeks. This consequence of PEG attachment is based on the so-called "stealth-effect", which means that the immune system fails to recognize and eliminate the respective pharmaceuticals from the blood stream. It is commonly attributed to the highly hydrated PEG, forming a hydrophilic corona around the drug molecule or nanocarrier. The non-ionic, hydrophilic PEG thereby provides a steric shield that protects from recognition by the patient's immune system and effectively increases the size of the biomolecule,[6] consequently reducing clearance from the bloodstream. Investigations of coated nanocarriers additionally revealed the effect of PEG on the composition of protein corona formed around the particles which is necessary to prevent non-specific cellular uptake.[7]

Depending on the procedure employed, several PEG chains or in some cases a single PEG chain are attached to the respective drug molecule, which can be a peptide or polypeptide, a protein or any type of medical nanocarrier (liposomes, micelles, degradable nanoparticles, etc.).[8–11] By increasing the half-life of protein drugs, the dosage frequency is strongly reduced. Since PEGylated therapeutics are injected and often have to be applied for extended periods, this feature is significant. Increased duration of pharmacological activity, reduction of toxic side effects, and increased quality of life due to controlled, timed release are the main effects attributed to PEGylation of therapeutics.

PEGylated drugs, such as e.g. PEGASYS (peginterferon alfa-2a) and Krystexxa (pegloticase) play a key role for the treatment of numerous chronic diseases. such as e.g. Hepatitis C or gout, requiring regular and repeated injections of the respective PEGylated therapeutic for extended periods, often for many years.[12–14] PEGylated drugs further include products such as Adynovate® and Esperoct® for the treatment of chronic haemophilia.[15] The recently approved mRNA vaccines from Moderna and Pfizer-BioNTech also require PEGylated lipids to ensure the stability of the mRNA in the lipid-based nanoparticle.[16,17] In summary, PEGylation is a crucial strategy for peptide and protein drugs, for liposomal formulations, but also for PEGylated lipids as solubilizing components of lipid nanoparticles used for the SARS-CoV-2 vaccine, enabling to disperse the respective lipid nanoparticles in aqueous solution.[18,19] It is appropriate to state that PEGylation represents the key technology of current nanomedicine. Currently, more than 40 PEGylated therapeutics are on the market or in clinical phase III, market introduction pending.[13]

PEG is a non-biodegradable polymer and must be eliminated from the body through the kidneys, which limits the molecular weight of PEG for medical therapeutics to the renal cutoff size, which for globular proteins is approximately 50 to 60 kDa.

Whereas it was initially believed that PEG is immunologically inert, it has become obvious in recent decades that an increasing number of patients possess anti-PEG antibodies. The induction of anti-PEG antibodies in humans does not only stem from PEGylated therapeutics, but also from food, cosmetics, and other sources, where PEG is abundant. Several reports have stated that PEGylated proteins can elicit antibody responses against PEG that adversely affect their pharmacokinetics and therapeutic efficacy.[20,21] The potential antigenicity of PEG has even been confirmed by the existence of anti-PEG antibodies (APA) in individuals who have never received PEGylated therapeutics systemically.[22] A phase III clinical study regarding anti-coagulation factor IXa RNA PEG-conjugated aptamer had to be interrupted as anaphylactic reactions in 0.6% of the patients were observed which was most likely caused by the pre-existence of APAs in the blood stream.[23]

The incidence of anti-PEG antibodies observed in healthy blood donors has grown from around 1% in 1984 to more than 42%.[22] The presence of APA-Fabs leads to undesired accelerated blood clearance (ABC) i.e., lowered half-life times of PEGylated therapeutics and rapid clearance from the blood stream. This effect lowers or even disables therapeutic activity. In other cases allergic reactions and in extreme cases anaphylactic shocks were observed.[24]

The mechanism of the antibody interaction with PEG was recently studied by Lai et al., who explained the recognition capability of the binding center of the antibody with an open ring structure of the flexible PEG chain bound by the anti-PEG antibody.[25] The interaction with the antibody is stabilized via multiple, unspecific polar and Van der Waals interactions at the surface of the ring. By counting the number of monomer repeats interacting with the interior and exterior paratope of the Fab, these authors found the size of the PEG antigen epitope to be ~700 Da, equivalent to 16 monomer subunits. Other works suggest that also shorter regular chain segments of PEG as well as the methoxy end group of mPEG structure play a key role for the recognition. Sherman et al. used competitive enzyme-linked immunosorbent assays (ELISA) and reported that antibodies elicited by PEG-OH have similar affinity to both mPEG and PEG-OH, while antibodies induced by mPEG recognize mPEG more effectively than PEG-OH. These results imply that the anti-PEG antibodies elicited by PEG-OH-proteins are directed against the backbone of the PEG (backbone-specific), while antibodies induced by mPEG-protein conjugates are methoxy group specific.[26,27] It can be concluded that regular segments of at least 4-5 to 16 regularly arranged ethylene glycol units are required to achieve recognition and immunogenic reaction by APA-Fabs. Recent clinical works regarding Pegasparagase have shown that the presence of antibodies against PEG permits to predict allergic reactions and failure of rechallenge, emphasizing the clinical relevance of APA-Fabs for the success of the treatment of leukemia in this case.[28]

In the light of constantly increasing numbers of individuals with anti-PEG antibodies, mainly two solutions briefly summarized in the following have been suggested to lower antibody interaction by altering the PEG structure. Sherman et al.[26] introduced methods for the preparation of PEG conjugates that are based on end group modification of the PEG chains, aiming at minimizing interaction with anti-PEG Abs. The authors disclosed conjugates, wherein a hydroxyl group

is present on all of the distal polyalkylene glycol termini. They showed that these conjugates exhibited reduced antigenicity compared to mPEG-protein conjugates.[29] Chilkoti et al. used methacrylate monomers bearing oligoethylene oxide side chains and radical polymerization, resulting in POEGMA brushes with sidechain lengths of two and three EG repeats. These structures were identified as the optimal polymer architecture to minimize binding of anti-PEG antibodies (APAs).[30,31]

The strategy described in this work enables to prevent immune reactions due to APA-Fabs against PEGylated therapeutics by random incorporation of polar methoxymethyl side chains into PEG by statistical copolymerization. The increased spatial requirements of the PEG copolymers and their random distribution impede or even disable interaction with APA-Fabs according to the specific "lock and key principle". Besides the steric impact, we believe that the random distribution of the alkyl groups over the polymer chains additionally disables the development and formation of specific anti-polymer Fabs. In this context, it is vital that the dispersity M_w/M_n ($Đ$) of the random copolymers is as low as for the established PEG. Further, a high end-group fidelity of the resulting polymers is crucial for subsequent utilization in bioconjugations. Thus, the anionic ring-opening copolymerization (AROP) was employed to prepare the respective copolymers of ethylene oxide (EO) and the glycidyl methyl ether (GME).

RESULTS AND DISCUSSION

Synthesis of Copolymers of Ethylene Oxide (EO) and Glycidyl Methyl Ether (GME)

Poly(ethylene glycol) (PEG) is the key polymer for bioconjugation and a cornerstone of nanomedicine in general. Poly(glycidyl methyl ether) (PGME) represents a biocompatible structural isomer of PEG, consequently showing the very same ratio of carbon and oxygen and therefore high hydrophilicity. PGME has been observed to possess high biocompatibility in cell viability tests.[32] Combining EO and GME in a copolymer leads to polyethers with sterically more demanding structures, due to the incorporation of polar GME repeating units in the polyether backbone.

However, to date copolymerization of EO with GME as an isomer of two EO-units has rarely been investigated, due to synthetic challenges. Homopolymers of PGME were either synthesized as oligomers[32,33] or with a high dispersity of 1.5.[34] Copolymers of EO and GME, namely P(EG-co-GME) were merely accessible using an activated monomer approach,[34] resulting likewise in ill-defined materials contaminated with toxic aluminum impurities.[35] Here we present the first successful synthesis of well-defined P(EG-co-GME) copolymers under common anionic ring-opening polymerization (AROP) conditions (Figure 1a). This was accomplished by the utilization of pure GME (>99 %). The required degree of purity of GME is not available in commercial products, because traces of epichlorohydrin (ECH) remain in the product, even after fractional distillation (Figure 1b). The presence of ECH in AROP results in ill-defined oligomeric polyether structures due to side-reactions between the active chain end and ECH, necessitating an ECH-free synthesis route for GME (SI, Scheme S1). In the current work GME has been synthesized via

two approaches: Prilezhaev-epoxidation of allyl methyl ether with *meta*-chloroperbenzoic acid (*m*-CPBA) and ring-closure of 1-chloro-3-methoxy-propan-1-ol.
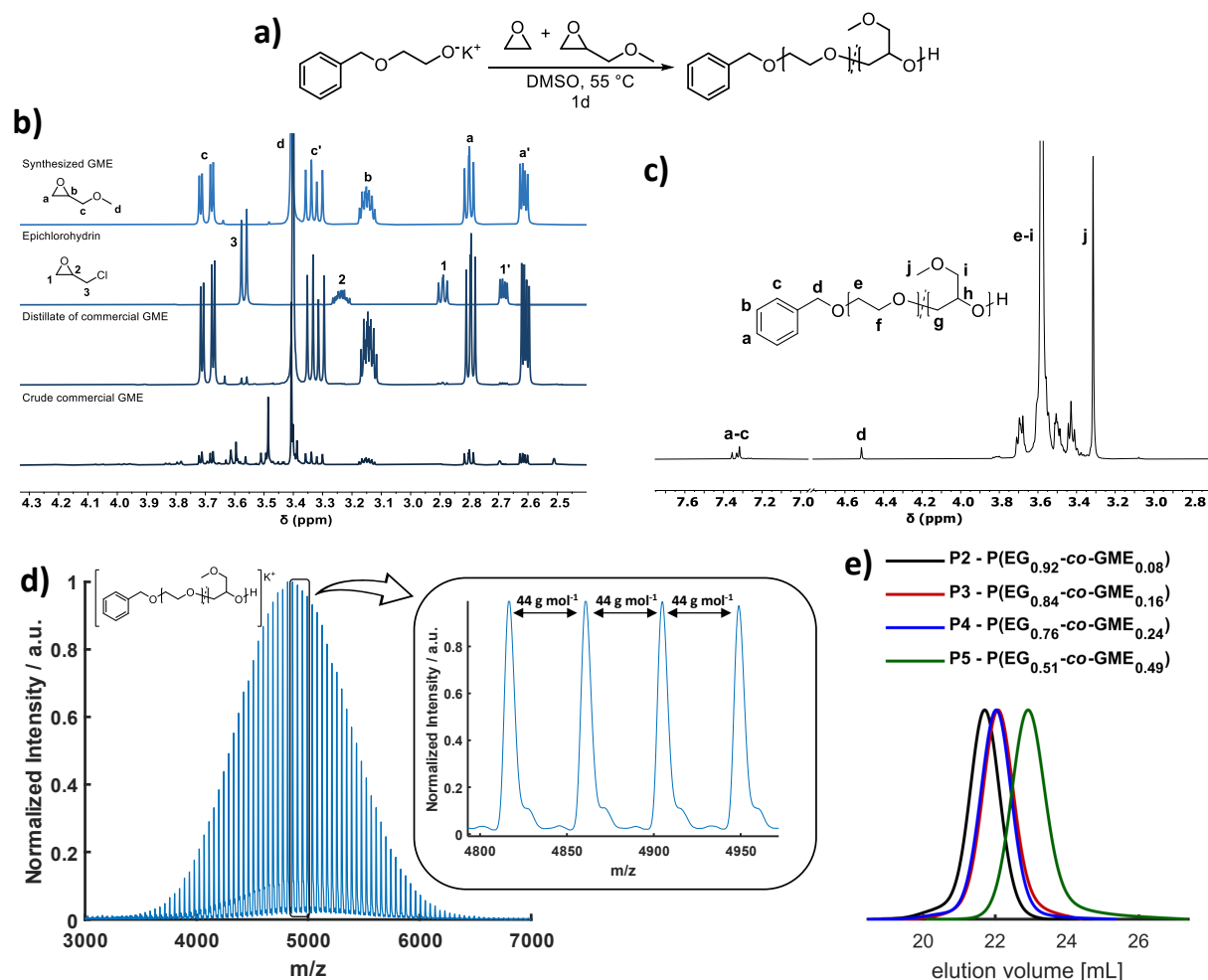

Figure 1. a) Synthesis of P(EG-*co*-GME); b) Comparison of commercial and synthesized GME; c) ^{1}H NMR spectrum of P(EG-*co*-GME); d) MALDI ToF mass spectrum of P(EG-*co*-GME); e) SEC traces of P(EG-*co*-GME).

Both routes yielded highly pure GME (> 99%), enabling the utilization in AROP (full NMR analysis, see SI section 3). Copolymerizations of EO and GME were carried out in DMSO at 55 °C under established AROP conditions, utilizing potassium or cesium 2-benzyloxy ethoxide as an initiator system. Resulting ^{1}H NMR spectra (Figure 1c) of the prepared copolymers show the expected signals of the polyether backbone and the methyl groups of the GME repeating units as well as the absence of any other undesired side-products (full NMR analysis, see SI section 4). Further monitoring of the copolymerization via size exclusion chromatography (SEC) (Figure 1e, SI, Figure S9 and S11) confirms well-defined copolymers with monomodal distributions and low dispersities (1.04-1.09) in the range of 4 to 9 kg mol^{-1} (Table 1). The molar amount of incorporated GME repeating units (mol%$_{GME}$) was varied from 4 to 100 %. Matrix-assisted laser desorption/ionization time of flight mass spectroscopy (MALDI ToF MS) of the synthesized

copolymers (Figure 1d) further support the monomodal distributions, showing mass differences of 44 g mol^{-1} in the desired m/z ratio and a single molecular weight distribution.

Table 1. Overview of synthesized P(EG-*co*-GME) copolymers and PGME homopolymer.

No.	Sample	EG ratio[a] [mol%]	GME ratio[a] [mol%]	M_n[a] [kg mol^{-1}]	M_n[b] [kg mol^{-1}]	M_n[c] [kg mol^{-1}]	$Đ$[c]
P1	P(EG$_{0.96}$-*co*-GME$_{0.04}$)	96	4	5.3	4.8	3.9	1.04
P2	P(EG$_{0.92}$-*co*-GME$_{0.08}$)	92	8	5.2	5.3	4.5	1.05
P3	P(EG$_{0.84}$-*co*-GME$_{0.16}$)	84	16	6.9	4.9	3.7	1.05
P4	P(EG$_{0.76}$-*co*-GME$_{0.24}$)	76	24	6.0	5.2	3.8	1.06
P5	P(EG$_{0.51}$-*co*-GME$_{0.49}$)	51	49	4.2	3.8	2.4	1.09
P6	P(EG$_{0.96}$-*co*-GME$_{0.04}$)	96	4	10.9	8.5	7.5	1.08
P7	P(EG$_{0.93}$-*co*-GME$_{0.07}$)	93	7	9.0	8.5	7.3	1.05
P8	PGME	-	100	4.2	4.0	2.7	1.05

a) Determined by ^{1}H NMR spectroscopy

b) Determined by MALDI-TOF MS

c) Determined by SEC.

Noteworthy, these statistical copolymers yield unusually clean MALDI ToF mass spectra, which is a result of GME, representing the molecular weight of two EG repeating units (M_{GME} = 2 x M_{EO} = 88.08 g mol^{-1}). The copolymerization procedure is further adaptable to other alkoxide initiators known for AROP, e.g., potassium 2-(2-methoxyethoxy) ethoxide and potassium *N,N*-dibenzylamino ethoxide, showing that methoxy, amino and multiple other functionalities are accessible at the α-functionality of P(EG-*co*-GME) via the presented approach (SI, Figure S10). MALDI-ToF mass spectra of the synthesized copolymers evidence an end group fidelity of > 99% for all synthesized copolymers (Figure 1d). The latter is a unique feature of AROP and an indispensable aspect for the sufficient conjugation of polymers to proteins, nanocarriers or surfaces. In comparison, this end group control cannot be achieved via the monomer activated method previously employed for the copolymerization of EO and GME by our group,[34] due to different and unreactive end-groups present at the chain end as well as aluminum impurities.[35]

Investigations of the Microstructure and the Introduction of 'Synthetic Point Mutations' to the Polyether Backbone

Recently, the hitherto elusive binding mechanism of anti-PEG antibodies (APA) with PEG was elucidated. The polyether chain interacts as an open ring structure with the APA paratope.[25] The APA relies on the flexible PEG conformation to capture the rather inert PEG chain and trap the polyether via Van-der-Waals interactions. The respective epitope is believed to consist of 16 monomer units. In order to suppress APA interaction, we propose incorporation of GME repeating units to disrupt the regular PEG chain structure, which may be viewed as introducing 'synthetic

point mutations' to PEG. Both the steric demand and the random distribution of side chains are capable of inhibiting the interaction of the APAs with the polyether antigen.

We conducted *in situ* ^{1}H NMR measurements to elucidate the incorporation of GME into the copolymer during the living anionic copolymerization process, permitting to follow the mean composition at all chain positions. The almost linear decrease of the consumption vs. total conversion plot clearly demonstrates that the introduction of EO and GME repeating units occurs in an ideally random manner (Figure 2a+b, SI, section 6). Evaluation of the kinetic data via the non-terminal Jaacks model ($R^2 = 0.9998$) confirms the visible trend with reactivity ratios of $r_{\text{EO}} = r_{\text{GME}} = 1 \pm 0.0005$ (Figure 2c). Based on the determined reactivity ratios, kinetic Monte Carlo (kMC) simulations (SI, section 7) were performed to further illustrate the random distribution of the "synthetic point mutations" along the PEG copolymer chains (Figure 2d). The chemical heterogeneity within the polymer sample is evident, as each distinct chain possesses different sequence of repeating units. The GME units as 'point mutations' are randomly introduced into the polyether backbone, but the statistical diversity within each chain within one sample is tremendously high. As an example, for a copolymer with 50 monomer units, among which 10 monomer units are GME (20%), the number of possible chain isomers with different structure is 10,272,278,170, which illustrates that the induction of polymer-specific antibodies targeting a regular chain segment will be impossible.

Figure 2. a) Stacked spectra of *in situ* ^{1}H NMR measurement, showing the decrease of monomer resonances over time due to monomer consumption; b) Consumption plot versus total conversion; c) Jaacks fit of the copolymerization of EO and GME; d) Section of a 65 repeating units sequence from 10 out of 1000 chains calculated by Monte-Carlo simulations for 25 and 50 mol% GME (blue dots: EG repeating units, red dots: GME repeating units).

Influence of Synthetic Point Mutations on the Interaction of APAs with Random Copolymers

The effect of a varied concentration of synthetic point mutations (16, 24 and 49 mol%$_{GME}$) on the binding capability of PEG backbone-specific APAs was investigated via competitive enzyme-linked immunosorbent assay (competitive ELISA) at different polymer concentrations. Herein, the concentration-dependent interaction between the APA and PEG homo- and copolymers is observed by a decrease of the fluorescence intensity. An explicit trend is observed: Compared to mPEG (5 kg mol^{-1}), the synthesized copolymers with GME contents > 16 mol% show strongly reduced interaction with APAs. A clear shift of the ELISA curves of 16 and 24 mol% GME to higher polymer concentrations relative to mPEG is manifest in the plot (Figure 3a). Remarkably, with an incorporation of 49 mol% GME, no recognition of the copolymer by APAs is observed. We assume that this translates to full disappearance of the undesired effects, such as ABC and allergic reactions caused by PEG.
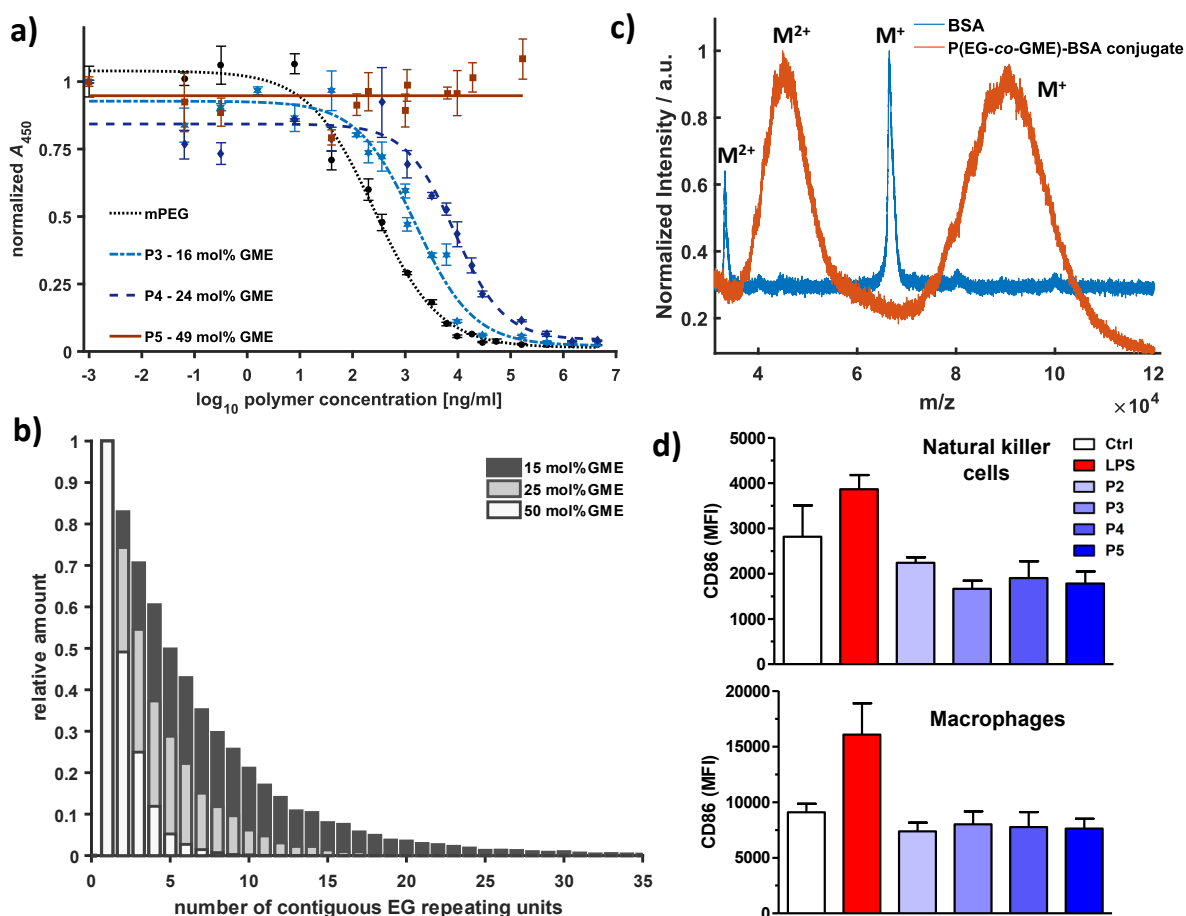
Figure 3. a) Competitive ELISA for mPEG and 16, 24 and 49 mol% GME-containing copolymers; b) Visualization of distribution of EG repeating units in the copolymers with 15, 25 and 50 mol% GME determined via Monte-Carlo-Simulations: Relative amounts of segments with a number of contiguous EG repeating units; c) Overlay of MALDI ToF mass spectra of BSA (blue) and P(EG-*co*-GME)-BSA conjugate (orange) (Matrix: Sinapinic acid); d) PEG derivatives exert no stimulatory effects on immune cells.

In their publication, Lai and co-workers[25] presented the interaction mechanism of PEG and APAs, showing that 16 sequential EG units interact with the interior and exterior paratope of the APA-Fab, regular PEG-segments of this type constitute the epitope. Quantitative analysis of the results generated by kMC simulations allow for the determination of proportional occurrences of sequential EG units in P(EG-*co*-GME) copolymers in dependence of the respective GME ratio. As shown in Figure 3b, in the case of 15 mol% GME, still segments containing > 35 EG-exclusive contiguous repeating units are observed, permitting sufficient interaction of the APA-Fab with the polyether.

This is equally applicable for the copolymer with 24 mol% GME, even though the probability to find these PEG segments in the polymer chains decreases dramatically. With incorporation of 49 mol% GME, the probability of finding longer EG-segments in the polyether almost approaches zero, and the APA-Fab is no longer capable of recognizing the polymeric antigen. Considering

these statistical findings in combination with the herein presented experimental results, one may conclude that the APA binds to chain segments exceeding 10 EG subunits. Chain segments below this value are no longer recognized by the APA-Fab. This conclusion further supports the crucial importance of a random distribution of GME repeating units along the polyether chains. On the contrary, a gradient structure would result in an accumulation of contiguous EG repeating units at the beginning or end of the polymer chain, resulting in enhanced APA recognition.

Suitability of P(EG-*co*-GME) Copolymers for Medical Applications

The hydrophilicity of PEG and the resulting accumulation of water molecules in combination with protein interaction[7] play an essential role for the reduced protein adsorption of PEGylated drugs and the stealth effect.[6] To examine the solubility of the presented copolymers in aqueous solution with regard to temperature, we conducted turbidimetric experiments (SI, section 5, Figure S13). All herein prepared copolymers exhibit excellent water solubility with an LCST of 94.5 °C for 49 mol% GME and are therefore comparable with PEG with respect to their hydrophilicity. In addition to the already mentioned features, the incorporation of GME units into the polyether backbone leads to the inhibition of crystallization of the EG units, yielding amorphous materials (SI, section 10). The indispensable non-toxicity for biomedical application of the synthesized copolymers was investigated by flow cytometry of murine spleen cells. All immune cell types showed the same cell viability after treatment with P(EO-*co*-GME) (c = 0.1 to 10 mg ml^{-1}) compared to untreated cells (SI, section 11). Subsequent screening of the copolymers (c = 1 mg ml^{-1}) (Figure 3d) demonstrated no stimulatory effect on immune cells compared to untreated cells, while the utilized positive control (lipopolysaccharide, LPS) exhibited high stimulation. These results show full biocompatibility, as commonly known for the PEG homopolymer. Finally, a model bioconjugation of a P(EG-*co*-GME) copolymer to bovine serum albumin (BSA) was performed to demonstrate the chemical suitability of these copolymers for protein conjugation as an alternative to PEGylation (SI, section 8). Figure 3c shows the corresponding MALDI ToF MS of BSA and a conjugate with P3 (16 mol% GME). The absence of unfunctionalized BSA in the spectra confirms quantitative functionalization of BSA with P(EG-*co*-GME). The broadening of the P(EG-*co*-GME)-BSA conjugate signal compared to the unfunctionalized BSA is explained by multiple conjugation with different numbers of P(EG-*co*-GME) chains. The successful conjugation was conducted using an established procedure for PEG, relying on NHS activation of the ω-chain end (SI, section 8). The results demonstrate the suitability of P(EG-*co*-GME) copolymers for protein bioconjugation, relying on procedures established for PEG.

CONCLUSION

The increasing abundance of anti-PEG antibodies (APA) in the population leads to undesired immune-responses to PEGylated drugs. This has become an increasingly severe concern over the years since it renders the stealth effect ineffective. Recently, its topicality has drastically increased, as the containment of the global COVID-19 pandemic partly relies on PEGylated lipids for the transport of the RNA vaccines. We introduce the concept of random polyether copolymers containing chemical 'point mutations' as a novel alternative to the established PEGylation. The immediately obvious advantage of the strategy described in this work lies in the fact that existing PEG technology in all steps is equally applicable. Unlike in the case of recently discussed PEG alternatives, such as polyoxazolines[8,36] or polysarcosine,[37] completely new GMP manufacturing strategies and supply chains are not required. Highly defined poly(ethylene glycol-*co*-glycidyl methyl ether) (P(EG-*co*-GME)) copolymers (Đ < 1.09, mostly < 1.05; end-group fidelity of > 99 %) of up to 9.4 kg mol^{-1} have been synthesized by anionic ring-opening copolymerization of ethylene oxide (EO) and glycidyl methyl ether (GME). Detailed *in situ* ^{1}H NMR kinetic experiments revealed an ideally random copolymerization of both monomers, enabling a random incorporation of chemical 'point mutations' into the PEG backbone. The highly hydrophilic copolymers demonstrate dramatically reduced recognition by APAs (< 24 mol% GME) in a competitive enzyme-linked immunosorbent assay (ELISA). while incorporation of 49 mol% of GME lead to a full suppression of any APA interaction, which is crucial for PEGylation type bioconjugation. Kinetic Monte Carlo (kMC) simulations regarding the microstructure of such copolymers further supported the experimental ELISA results. A wide range of structural diversity of the P(EG-*co*-GME) copolymers, determined by statistics, is present in the copolymers, despite the highly controlled chain length due to the living synthesis method. A further adjustment of GME ratios enables further variation possibilities. Versatile conjugation chemistry has been established for PEG for more than 3 decades and is fully transferrable to the GME-PEG copolymers, as demonstrated in this study by a model conjugation with bovine serum albumin (BSA). Further architectural variation may include different bi- to multifunctional initiators, block copolymers as well as the utilization of varied alkyl side chains by incorporation of ethyl, propyl or *iso*-propyl glycidyl ether units. On the other hand, the possibility of segregating the medical and pharmaceutical application by use of GME-PEGs may aid to avoid antibody induction.

We firmly believe that PEGylation with random copolymers as outlined here bears immense potential for the treatment of chronic diseases. One can for instance imagine giving drugs that are GME-PEGylated with different contents upon repeated administration, thereby disabling the immune system from developing an antibody response. Hence, "Beyond PEG" – as it was mentioned in the title of recent critical reviews, may simply mean randomizing the PEG structure by the introduction of suitable comonomers.

REFERENCES

(1) Harris, J. M.; Chess, R. B. Effect of pegylation on pharmaceuticals. Nature reviews. *Drug discovery* **2003**, *2*, 214–221.

(2) Kolate, A.; Baradia, D.; Patil, S.; Vhora, I.; Kore, G.; Misra, A. PEG - a versatile conjugating ligand for drugs and drug delivery systems. *Journal of controlled release: official journal of the Controlled Release Society* **2014**, *192*, 67–81.

(3) Mishra, P.; Nayak, B.; Dey, R. K. PEGylation in anti-cancer therapy: An overview. *Asian Journal of Pharmaceutical Sciences* **2016**, *11*, 337–348.

(4) Hoffman, A. S. The early days of PEG and PEGylation (1970s-1990s). *Acta biomaterialia* **2016**, *40*, 1–5.

(5) Ostuni, E.; Chapman, R. G.; Holmlin, R. E.; Takayama, S.; Whitesides, G. M. A Survey of Structure−Property Relationships of Surfaces that Resist the Adsorption of Protein. *Langmuir* **2001**, *17*, 5605–5620.

(6) Pelegri-O'Day, E. M.; Lin, E.-W.; Maynard, H. D. Therapeutic protein-polymer conjugates: advancing beyond PEGylation. *Journal of the American Chemical Society* **2014**, *136*, 14323–14332.

(7) Schöttler, S.; Becker, G.; Winzen, S.; Steinbach, T.; Mohr, K.; Landfester, K.; Mailänder, V.; Wurm, F. R. Protein adsorption is required for stealth effect of poly(ethylene glycol)- and poly(phosphoester)-coated nanocarriers. *Nature nanotechnology* **2016**, *11*, 372–377.

(8) Knop, K.; Hoogenboom, R.; Fischer, D.; Schubert, U. S. Poly(ethylene glycol) in drug delivery: pros and cons as well as potential alternatives. *Angewandte Chemie International Edition* **2010**, *49*, 6288–6308.

(9) Alconcel, S. N. S.; Baas, A. S.; Maynard, H. D. FDA-approved poly(ethylene glycol)–protein conjugate drugs. *Polym. Chem.* **2011**, *2*, 1442.

(10) D'souza, A. A.; Shegokar, R. Polyethylene glycol (PEG): a versatile polymer for pharmaceutical applications. *Expert opinion on drug delivery* **2016**, *13*, 1257–1275.

(11) Roberts, M. J.; Bentley, M. D.; Harris, J. M. Chemistry for peptide and protein PEGylation. *Advanced drug delivery reviews* **2012**, *64*, 116–127.

(12) Heredia, K. L.; Maynard, H. D. Synthesis of protein-polymer conjugates. *Organic & biomolecular chemistry* **2007**, *5*, 45–53.

(13) Zalipsky, S.; Pasut, G. Evolution of polymer conjugation to proteins. *Polymer-Protein Conjugates; Elsevier*, **2020**; 3–22.

(14) Irizarry Rovira, A. R.; Bennet, B. M.; Bolon, B.; Braendli-Baiocco, A.; Chandra, S.; Fleurance, R.; Garman, R.; Hutto, D.; Lane, J.; Romeike, A.; et al. Scientific and Regulatory Policy Committee Points to Consider: Histopathologic Evaluation in Safety Assessment Studies for PEGylated Pharmaceutical Products. *Toxicologic pathology* **2018**, *46*, 616–635.

(15) Valentino, L. A.; Cong, L.; Enockson, C.; Song, X.; Scheiflinger, F.; Muchitsch, E. M.; Turecek, P. L.; Hakobyan, N. The biological efficacy profile of BAX 855, a PEGylated recombinant factor VIII molecule. *Haemophilia : the official journal of the World Federation of Hemophilia* **2015**, *21*, 58–63.

(16) Michael McCoy. Lipids, the unsung COVID-19 vaccine component, get investment: Several specialty chemical companies are adding capacity to supply Moderna and Pfizer-BioNTech. *American Chemical Society*, **2021**.

(17) Pastor, F.; Berraondo, P.; Etxeberria, I.; Frederick, J.; Sahin, U.; Gilboa, E.; Melero, I. An RNA toolbox for cancer immunotherapy. *Nature reviews. Drug discovery* **2018**, *17*, 751–767.

(18) Pardi, N.; Hogan, M. J.; Porter, F. W.; Weissman, D. mRNA vaccines - a new era in vaccinology. *Nature reviews. Drug discovery* **2018**, *17*, 261–279.

(19) Schoenmaker, L.; Witzigmann, D.; Kulkarni, J. A.; Verbeke, R.; Kersten, G.; Jiskoot, W.; Crommelin, D. J. A. mRNA-lipid nanoparticle COVID-19 vaccines: Structure and stability. *International Journal of Pharmaceutics* **2021**, *601*, 120586.

(20) d'Avanzo, N.; Celia, C.; Barone, A.; Carafa, M.; Di Marzio, L.; Santos, H. A.; Fresta, M. Immunogenicity of Polyethylene Glycol Based Nanomedicines: Mechanisms, Clinical Implications and Systematic Approach. *Adv. Therap.* **2020**, *3*, 1900170.

(21) Barz, M.; Luxenhofer, R.; Zentel, R.; Vicent, M. J. Overcoming the PEG-addiction: well-defined alternatives to PEG, from structure–property relationships to better defined therapeutics. *Polym. Chem.* **2011**, *2*, 1900.

(22) Yang, Q.; Jacobs, T. M.; McCallen, J. D.; Moore, D. T.; Huckaby, J. T.; Edelstein, J. N.; Lai, S. K. Analysis of Pre-existing IgG and IgM Antibodies against Polyethylene Glycol (PEG) in the General Population. *Analytical chemistry* **2016**, *88*, 11804–11812.

(23) Lincoff, A. M.; Mehran, R.; Povsic, T. J.; Zelenkofske, S. L.; Huang, Z.; Armstrong, P. W.; Steg, P. G.; Bode, C.; Cohen, M. G.; Buller, C.; et al. Effect of the REG1 anticoagulation system versus bivalirudin on outcomes after percutaneous coronary intervention (REGULATE-PCI): a randomised clinical trial. *The Lancet* **2016**, *387*, 349–356.

(24) Sellaturay, P.; Nasser, S.; Islam, S.; Gurugama, P.; Ewan, P. W. Polyethylene glycol (PEG) is a cause of anaphylaxis to the Pfizer/BioNTech mRNA COVID-19 vaccine. *Clin Exp Allergy.* **2021**, *51*, 861-863.

(25) Huckaby, J. T.; Jacobs, T. M.; Li, Z.; Perna, R. J.; Wang, A.; Nicely, N. I.; Lai, S. K. Structure of an anti-PEG antibody reveals an open ring that captures highly flexible PEG polymers. *Commun Chem* **2020**, 3.

(26) Sherman, M. R.; Williams, L. D.; Sobczyk, M. A.; Michaels, S. J.; Saifer, M. G. P. Role of the methoxy group in immune responses to mPEG-protein conjugates. *Bioconjugate chemistry* **2012**, *23*, 485–499.

(27) Saifer, M. G. P.; Williams, L. D.; Sobczyk, M. A.; Michaels, S. J.; Sherman, M. R. Selectivity of binding of PEGs and PEG-like oligomers to anti-PEG antibodies induced by methoxyPEG-proteins. *Molecular immunology* **2014**, *57*, 236–246.

(28) Liu, Y.; Smith, C. A.; Panetta, J. C.; Yang, W.; Thompson, L. E.; Counts, J. P.; Molinelli, A. R.; Pei, D.; Kornegay, N. M.; Crews, K. R.; et al. Antibodies Predict Pegaspargase Allergic Reactions and Failure of Rechallenge. *Journal of Clinical Oncology* **2019**, *37*, 2051–2061.

(29) Alexa L Martinez, Merry R Sherman, Mark G. P. Saifer, L David Williams. Polymer conjugates with decreased antigenicity, methods of preparation and uses thereof.

(30) Joh, D. Y.; Zimmers, Z.; Avlani, M.; Heggestad, J. T.; Aydin, H. B.; Ganson, N.; Kumar, S.; Fontes, C. M.; Achar, R. K.; Hershfield, M. S.; et al. Architectural Modification of Conformal PEG-Bottlebrush Coatings Minimizes Anti-PEG Antigenicity While Preserving Stealth Properties. *Advanced healthcare materials* **2019**, *8*, e1801177.

(31) Chilkoti, A. e. a. Polymer conjugates having reduced antigenicity and methods of using the same.

(32) Weinhart, M.; Grunwald, I.; Wyszogrodzka, M.; Gaetjen, L.; Hartwig, A.; Haag, R. Linear poly(methyl glycerol) and linear polyglycerol as potent protein and cell resistant alternatives to poly(ethylene glycol). *Chemistry, an Asian journal* **2010**, *5*, 1992–2000.

(33) Isono, T.; Miyachi, K.; Satoh, Y.; Sato, S.; Kakuchi, T.; Satoh, T. Design and synthesis of thermoresponsive aliphatic polyethers with a tunable phase transition temperature. *Polym. Chem.* **2017**, *8*, 5698–5707.

(34) Müller, S. S.; Moers, C.; Frey, H. A Challenging Comonomer Pair: Copolymerization of Ethylene Oxide and Glycidyl Methyl Ether to Thermoresponsive Polyethers. *Macromolecules* **2014**, *47*, 5492–5500.

(35) Sakakibara, K.; Nakano, K.; Nozaki, K. Regio-controlled ring-opening polymerization of perfluoroalkyl-substituted epoxides. *Chemical communications* **2006**, 3334–3336.

(36) Lorson, T.; Lübtow, M. M.; Wegener, E.; Haider, M. S.; Borova, S.; Nahm, D.; Jordan, R.; Sokolski-Papkov, M.; Kabanov, A. V.; Luxenhofer, R. Poly(2-oxazoline)s based biomaterials: A comprehensive and critical update. *Biomaterials* **2018**, *178*, 204–280.

(37) Nogueira, S. S.; Schlegel, A.; Maxeiner, K.; Weber, B.; Barz, M.; Schroer, M. A.; Blanchet, C. E.; Svergun, D. I.; Ramishetti, S.; Peer, D.; et al. Polysarcosine-Functionalized Lipid Nanoparticles for Therapeutic mRNA Delivery. *ACS Appl. Nano Mater.* **2020**, *3*, 10634–10645.

SUPPORTING INFORMATION

Materials and Instrumentation

Reagents and Equipment

All chemicals and solvents were purchased from *Acros Organics*, *Roth*, *TCI*, *Sigma-Aldrich*, *Fisher Scientific* and *Fluka*, unless noted otherwise. Deuterated solvents were received from *Deutero GmbH*. Ethylene Oxide was acquired from *Air Liquide*. THF was flashed over basic aluminum oxide before usage. Glycidyl methyl ether was dried over CaH_2 and cryo-transferred before the polymerizations.

Size Exlcusion Chromatography

Size exclusion chromatography (SEC) measurements were performed in dimethylformamide (DMF) with 1 g L^{-1} lithium bromide as an eluent at 50 °C. An *Agilent 1100 Series* was used, equipped with HEMA 300/100/40 columns, and calibration was carried out using polyethylene glycol (PEG) standards, both provided by *Polymer Standard Service* (PSS), Mainz.

Differential Scanning Calorimetry

DSC measurements were carried out in the temperature range of -100 to 100 °C with a heating rate of 10 K min^{-1} at a *PerkinElmer DSC 8500*. The thermal history of the samples was excluded via two cooling and two heating cycles. For each sample, the glass transition and the melting temperatures were obtained from the second heating curve.

MALDI-ToF Mass Spectrometry (MS)

MALDI-ToF MS measurements were carried out at a *Bruker autoflex maX* MALDI-TOF/TOF. For copolymers, the potassium salt of triflouroacetic acid and DCTB were utilized as ionization salt and matrix, respectively. For conjugates, sinapinic acid was utilized as matrix.

NMR Spectroscopy and *in situ* ^{1}H NMR Kinetic Experiments

^{1}H and ^{13}C NMR spectra were recorded on a *Bruker Avance III HD 300* spectrometer with 300 MHz and 75 MHz, respectively, and referenced internally to residual proton signals of the deuterated solvent. The herein performed online ^{1}H NMR kinetic study was conducted according to a protocol by Herzberger et al. in a *Norell S-500-VT-7* NMR tube.[1] The monomer consumption over time was recorded by online ^{1}H NMR spectra with a Bruker Avance III HD 400 MHz spectrometer which was equipped with a 5 mm BFFO SmartProbe. Prior to the experiment, KO*t*Bu (19.2 mg, 172 μmol) was dissolved in a THF/water mixture and transferred to a septum and stop cock-equipped flame-dried Schlenk flask. Benzyl alcohol (29.0 mg, 191 μmol) was dissolved in benzene and added to the base solution. The initiator salt was dried under high vacuum at 60 °C after the solvent was slowly evaporated under high vacuo. The dry initiator salt was dissolved in dry DMSO-d_6 (1 mL) and stirred for 30 min. Simultaneously, EO (96 mg, 100 μL, 2.2 μmol) was cryo-transferred under static vacuum at -50 °C with an acetone/nitrogen bath to

the evacuated NMR tube which was attached to the Schlenk-line. Following, GME (95 mg, 95 μL, 1.1 μmol) and 200 μL initiator solution were transferred under inert argon-atmosphere to the NMR tube. Subsequently, the solution was cooled by liquid nitrogen, evacuated and sealed with a Teflon stop cock. After warming to room temperature, the reaction mixture was shaken vigorously to ensure a homogenous mixture and then paced in the preheated (55 °C) NMR spectrometer. After the temperature was stable ($T = 0.1$ K), one spectrum was recorded every 30 sec with 1 scan. The experimental data was analyzed by help of NIREVAL software from Johann, Steube and Frey.[2]

Regarding ethylene oxide: EO is a toxic, highly flammable gas. Therefore, careful handling and specific precautions are necessary. The addition of EO to the NMR tube was carried out in a reproducible procedure. Hence, a very small amount was utilized (< 0.1 ml) which might cause small deviations in the measured volumes. The targeted monomer ratios might therefore differ from the actual monomer ratios to a small extent.

Turbidimetric Measurements

Turbidimetry measurements were performed with a UV/VIS-spectrometer V-630 by *JASCO* for determination of the cloud point T_{cp}. Samples were measured at a wavelength of 600 nm and with a heating rate of 1 K min^{-1}. Samples were prepared in Milli-Q® water, which was utilized as reference prior to each experiment. The sample concentration was 2.5 mg ml^{-1} while the T_{cp} was determined at a transmission of 50 %.

Competitive Enzyme-linked Immunsorbent Assay (ELISA)

The interaction of the copolymers with APA was evaluated by a competitive PEG ELISA kit using a murine monoclonal, horseradish peroxidase conjugated anti PEG antibody (HRP anti-PEG) (*Life diagnostics*, West Chester, PA, USA). Samples of concentrations ranging from 0 to 4600 μg mL^{-1} were prepared in dilution buffer. Additionally, mPEG with a molecular weight of 5 kg mol^{-1} was utilized as an internal standard for comparison. 50 μL of each prepared sample was dispensed to a PEG pre-coated 96-well plate and 50 μL of HRP anti-PEG was added to each well. The solutions were incubated for 1 h at 25 °C with a micro-plate shaker and then washed six times with 400 μL of wash buffer per each well. After removal of residual droplets, 100 μL of 3,3′,5,5′-tetramethylbiphenyl-4,4'-diamine (TMB) was added to each well and the solutions were mixed on a micro-plate shaker for 20 min. The reaction was stopped by addition of 100 μL of stop solution and the absorbance at 450 nm was read within 5 min.

The determined absorbance values were normalized to visualize the percent of maximal binding. The sample concentrations were transformed to a function of $\log_{10}$. Sigmoidal fits were calculated using the following equation with a representing the upper limit b the lower limit c the inflection point and d the hill slope.

$$y = \frac{a+(b-a)}{1+10^{(c-x)d}}$$

Flow cytometry

Potential cytotoxic and stimulatory effects of the various copolymers on primary immune cell populations were assessed using mouse spleen cells. For this purpose, spleens retrieved from C57BL/6 mice were mechanically dissected, and erythrocytes were lysed using a hypotonic lysis buffer. Spleen cells were resuspended in IMDM culture medium (107 mL) and aliquots (200 μL) were transferred into sterile FACS tubes. Then, the different PEG derivatives were applied at the concentrations indicated (0.1-10 mg mL^{-1}). In some experiments, lipopolysaccharide (LPS; Sigma-Aldrich, Deisenhofen, Germany) was applied as a positive control for immune cell activation (1 μg mL^{-1}). On the next day, samples were washed and preincubated (20 min, 4 °C) with a Fcγ receptor-blocking antibody (clone 2.4G2) to prevent unspecific binding of receptor-specific antibodies. Then, samples were incubated (20 min, 4 °C) with antibodies specific for CD3 (labeled with eFl500), CD11b (SB600), CD11c (BV421), CD19 (SB702), NK1.1 (PE), Ly6G (PE-eFl610), and CD86 (FITC) was added (20 min at 4 °C. Cell viability was assessed by applying Fixable viability dye (FVD)-eFl780 (30 min, 4° C). Subsequently, samples were fixed (0.7% paraformaldehyde) and subjected to flow cytometric analysis using an Attune NxT flow cytometer (Thermo Fisher) equipped with Attune Nxt Software v3.1.1. The different spleen cell populations were identified by sequential gating as described.[3] Polymers were dialyzed against deionized water before incubation.

EXPERIMENTAL PROCDURES

Synthesis of Glycidyl Methyl ether
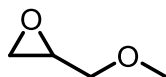
The monomer glycidyl methyl ether (GME) is commercially available with a purity rate of 85 % including high amounts of epichlorohydrin (ECH). The contamination of ECH leads to undesired termination reactions, shown in Scheme S1. The potassium alkoxide of either the initiator or the living chain end leads to nucleophilic ring opening of ECH, followed by ring closure under precipitation of potassium chloride, while either the chain end is terminated by epoxidation or the respective glycidyl ether is formed.
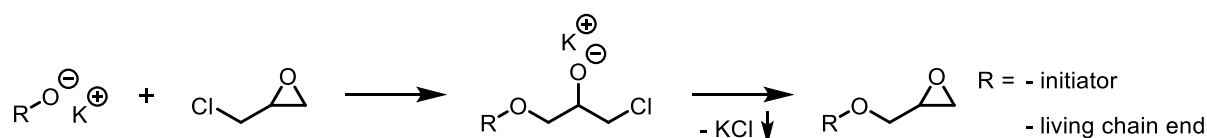
Scheme S1. Side reaction during anionic ring-opening polymerization of epoxides with epichlorohydrin impurities present.

Route (a). Synthesis of GME by Prileschajew epoxidation.[4] Allyl methyl ether (10.0 g, 139 mmol) was dissolved in 274 mL dichloromethane (DCM) and *m*-chloroperoxybenzoic acid (*m*-CPBA) (70%, 37.6 g, 153 mmol (based on *m*-CPBA)) was added to the solution. After stirring overnight, the solution was filtrated and slowly concentrated under reduced pressure. Crude glycidyl methyl ether was separated from solid impurities via cryo-transfer. Slow evaporation of residual dichloromethane in vacuo gave pure glycidyl methyl ether as a colorless liquid; Yield 41%.

Route (b). Synthesis of GME by ring-closure. 1-Chloro-3-methoxy-propan-2-ol (3.00 g, 2.56 mL, 24.1 mmol) and anhydrous sodium sulfate (1.02 g, 7.23 mmol) were added to a flask equipped with a magnetic stirrer and cooled with a water bath. Finely grounded sodium hydroxide (1.25 g, 31.3 mmol) was added under stirring. After complete reaction (TLC control) the crude product was cryo-transferred in vacuo from the reaction flask and dried over CaH$_2$ under cooling. After an additional cryo-transfer, GME was obtained as a colorless liquid with a yield of 93%.

^{1}H NMR (CDCl$_3$) δ [ppm]: 3.72-3.67 (dd, 1H, C*H*$_2$-O-CH-), 3.41 (s, 3H, -C*H*$_3$), 3.36-3.30 (dd, 1H, C*H*$_2$-O-CH-), 3.17-3.12 (m, 1H, CH$_2$-O-C*H*-),), 2.82-2.79 (dd, 1H, -C*H*$_2$-CH$_3$), 2.63-2.60 (dd, 1H, -C*H*$_2$-CH$_3$).

Synthesis of PGME
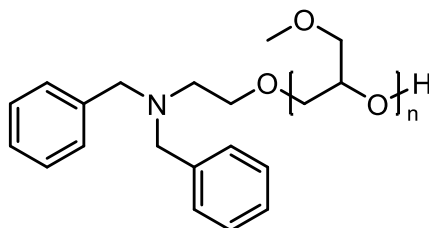
Cesium hydroxide monohydrate (25.0 mg, 149 μmol) was dissolved in a THF/water mixture and transferred to a flame-dried reaction flask, equipped with a septum and a Teflon stopcock. The initiator salt was produced by dissolving *N*,*N*-dibenzyl-2-aminoethanol (40.0 mg, 166 μmol) in benzene and addition to the reaction flask. After slow evaporation of the solvent, the resulting solid was dried at 60 °C under high vacuum overnight. Subsequently, the salt was dissolved in dry DMSO (5 mL) and the mixture was cooled to -78 °C. After addition of GME (660 mg, 670 μL, 7.46 mmol) via syringe, the solution was stirred for 48 h at room temperature under vacuum. After polymerization, the reaction solution was dissolved in excess chloroform and extracted against water (3 times) and brine, dried over MgSO$_4$ and filtrated. Poly(glycidyl methyl ether) (PGME) was obtained in quantitative yield as a viscous liquid after evaporation of the solvent and drying under high vacuo.

^{1}H NMR (DMSO-*d*$_6$) δ [ppm]: 7.38-7.21 (m, 10H, Ar-*H*), 3.75-3.40 (m, polyether backbone, Ar-C*H*$_2$-N), 3.31 (OC*H*$_3$), 2.54 (t, 2H, N-C*H*$_2$-CH$_2$-O).

Synthesis of P(EG-*co*-GME)
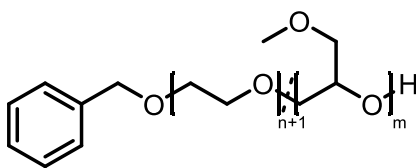
An exemplary procedure for the synthesis of random P(EG-*co*-GME) copolymers is given in the following. Additional polymers were synthesized with the same procedure. Potassium *tert*-butoxide (13.0 mg, 118 μmol) was dissolved in a THF/water mixture and transferred to a flame-dried reaction flask, equipped with a septum and a Teflon stopcock. The initiator, 2-benzyloxy-ethanol (20.0 mg, 18.7 μL, 131 μmol) was dissolved in benzene and added to the flame-dried reaction flask. After slow evaporation of the solvent, the resulting solid was dried at 60 °C under high vacuum overnight. Subsequently, the salt was dissolved in dry DMSO (5 mL) and the mixture was cooled to -78 °C. GME (119 mg, 122 μL, 1.35 mmol) was added via syringe and ethylene oxide (537 mg, 553 μL, 12.2 mmol) was cryo-transferred into the reaction flask. The solution was heated to 55 °C and stirred for 24 h under vacuum. After polymerization, the reaction solution was dissolved in excess chloroform and extracted against water (3 times) and brine, dried over MgSO$_4$ and filtrated. α-BzO-P(EG$_{0.92}$-*co*-GME$_{0.08}$) was obtained in quantitative yield as a colorless solid after evaporation of the solvent and drying under high vacuo.

^{1}H NMR (CDCl$_3$) δ [ppm]: 7.35-7.27 (m, 5H, Ar-*H*), 4.56 (s, 2H, Ph-C*H*$_2$), 3.75-3.40 (m, polyether backbone), 3.31 (s, GME-OC*H*$_3$).

Synthesis of mPEG-*b*-PGME
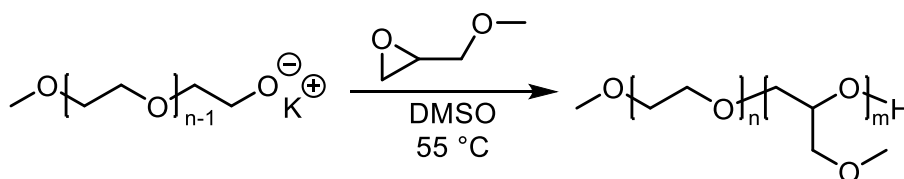
mPEG-*b*-PGME was synthesized in a similar procedure as the random copolymers. The initiator mPEG (M_n = 2 kg mol^{-1}; 250 mg, 125 μmol) was utilized for this purpose. mPEG-*b*-PGME 4k was obtained as a colorless solid after precipitation in ice-cold diethyl ether with quantitative yield.

^{1}H NMR (CDCl$_3$) δ [ppm]: 3.75-3.40 (m, polyether backbone), 3.31 (s, GME-OC*H*$_3$ + PEG-O-C*H*$_3$).

Synthesis of α-BzO-ω-N-succinimidyl carbonate-P(EG-*co*-GME)

R = -H, -CH$_2$OCH$_3$
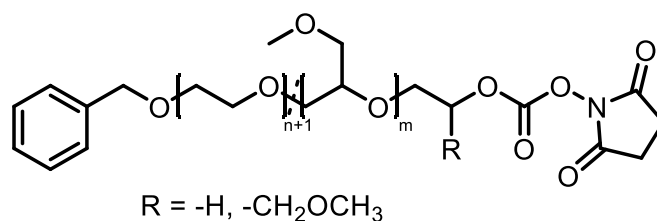
N,N'-disuccinimidyl carbonate (3.5 mg, 13.8 μmol) was added to a stirred solution of α-BzO-P(EG-*co*-GME) (50.0 mg, 4.6 μmol) in dry CH$_3$CN (1 mL) at room temperature for 18 h. The reaction mixture was dissolved in dichloromethane, extracted with a saturated NaHCO$_3$, water and brine, dried over MgSO$_4$ and filtered. The solvent was removed under reduced pressure and the polymer dried under vacuum. The product was obtained as a white solid in quantitative yield.

^{1}H NMR (CDCl$_3$) δ [ppm]: 7.35-7.27 (m, 5H, Ar-*H*), 4.56 (s, 2H, Ph-C*H*$_2$), 4.49-4.45 (t, 2H, C*H*$_2$-OCOO-succinimidyl), 3.86-3.27 (m, polyether backbone), 3.36 (s, GME-OC*H*$_3$), 2.86 (s, 4H, OCC*H*$_2$C*H*$_2$CO).

Conjugation of α-BzO-ω-N-succinimidyl carbonate-P(EG-*co*-GME) to bovine serum albumin (BSA)

R = -H, -CH$_2$OCH$_3$
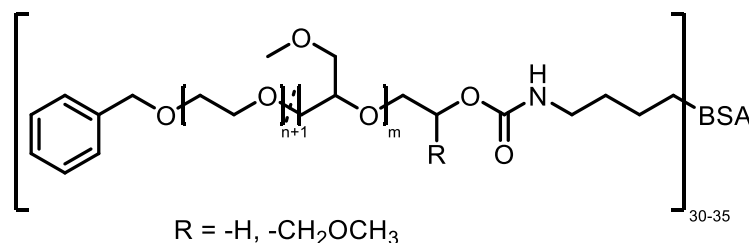
For conjugation of P(EG-*co*-GME) copolymers to BSA, the surface-accessible lysine groups (30-35) were targeted for conjugation. For this purpose, BSA (5.00 mg, 0.07 μmol) and α-BzO-ω-N-succinimidyl carbonate-P(EG-*co*-GME) (16.9 mg, 2.6 μmol) were stirred in PBS buffer for 1 h. The unreacted polymer was removed by dialysis in deionized water with a 25 kDa membrane filter. The conjugate was then dried by lyophilization and obtained in quantitative yield.

Additional Spectra of GME
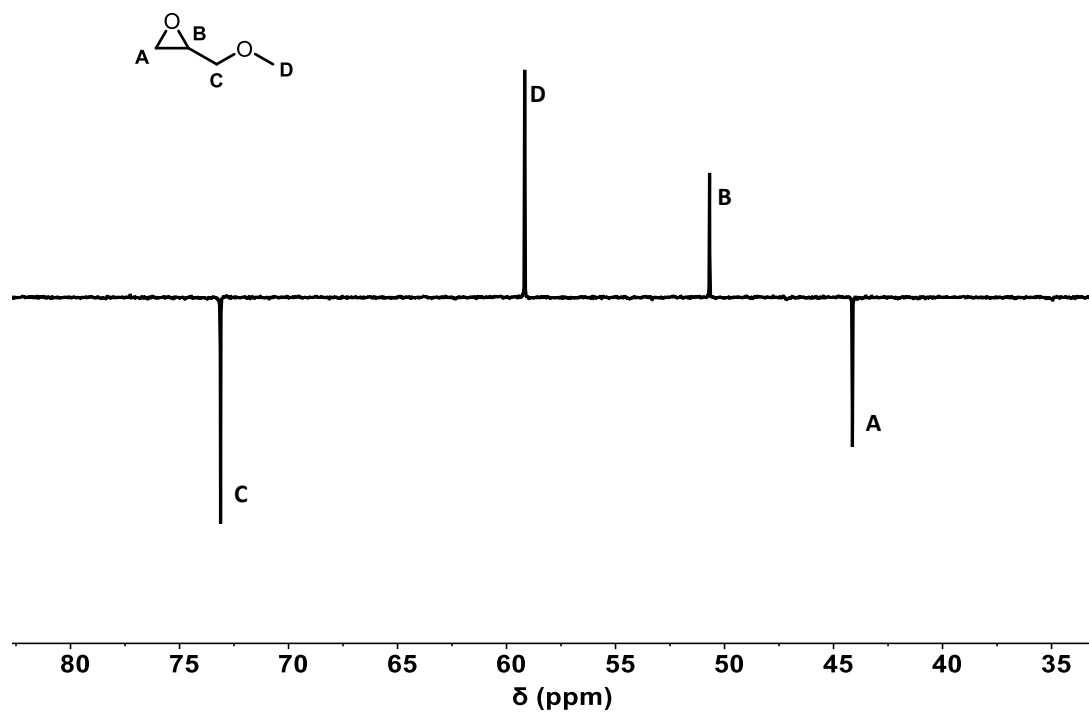
Figure S1. ^{13}C DEPT NMR spectrum (CDCl$_3$) of GME.
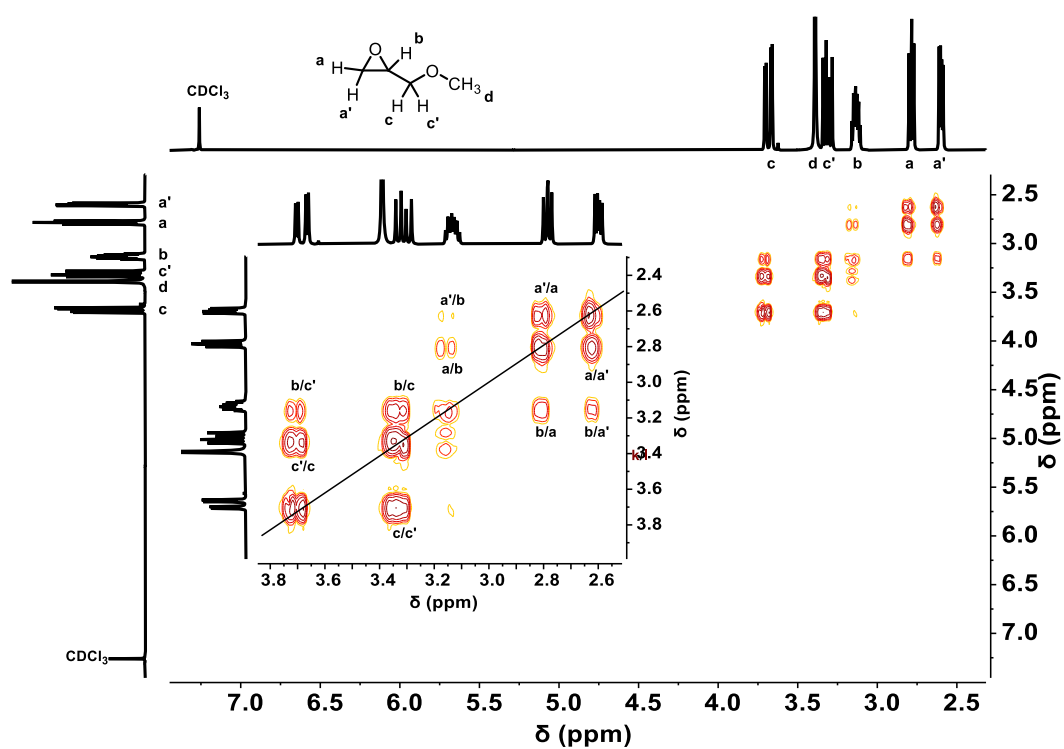
Figure S2. ^{1}H,^{1}H COSY NMR spectrum (CDCl$_3$) of GME.
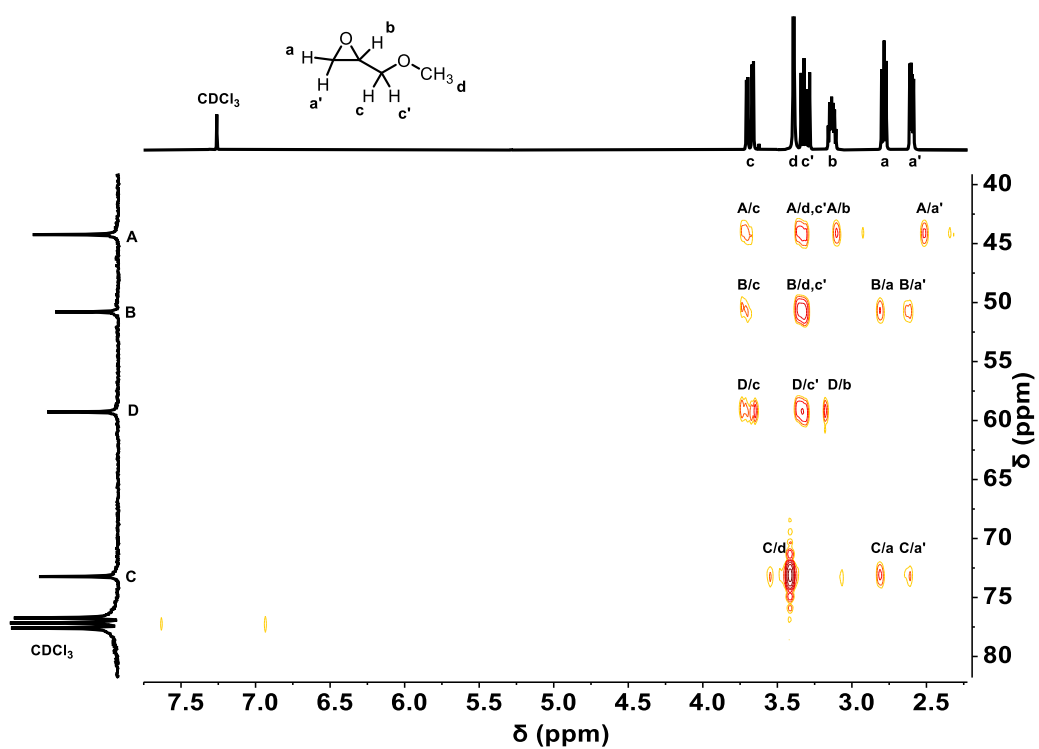
Figure S3. ^{1}H,^{13}C HMBC NMR spectrum (CDCl$_3$) of GME.
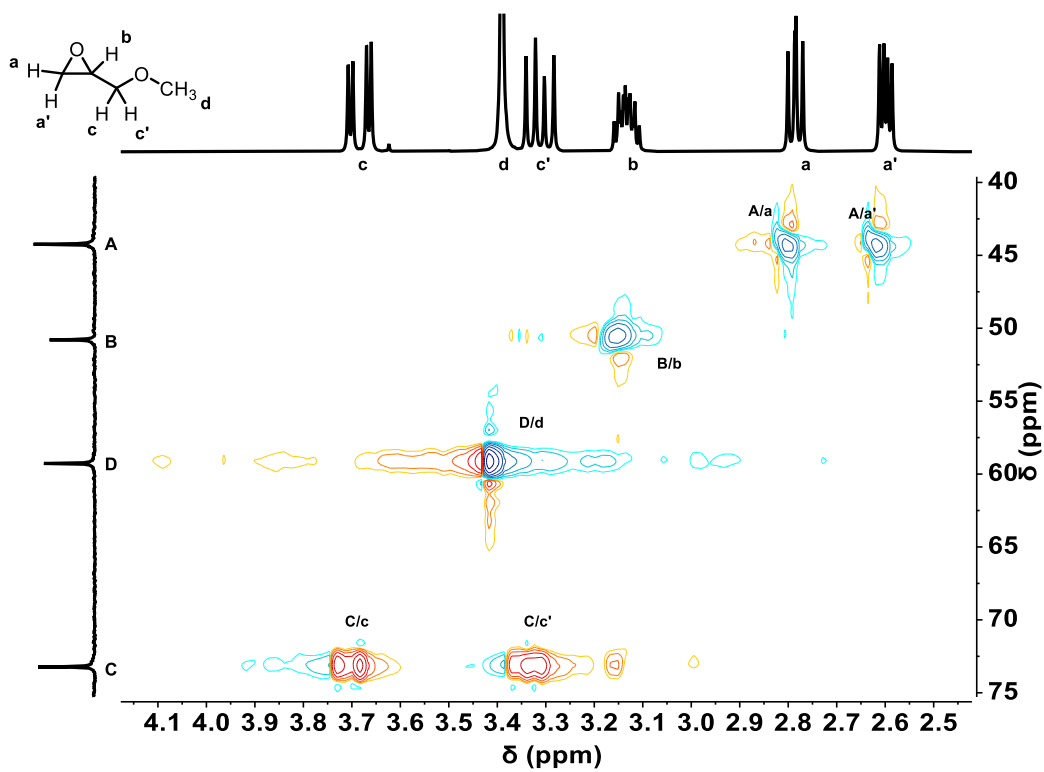
Figure S4. ^{1}H,^{13}C HSQC NMR spectrum (CDCl$_3$) of GME.

Additional Spectra and Plots of P(EG-*co*-GME) and PGME
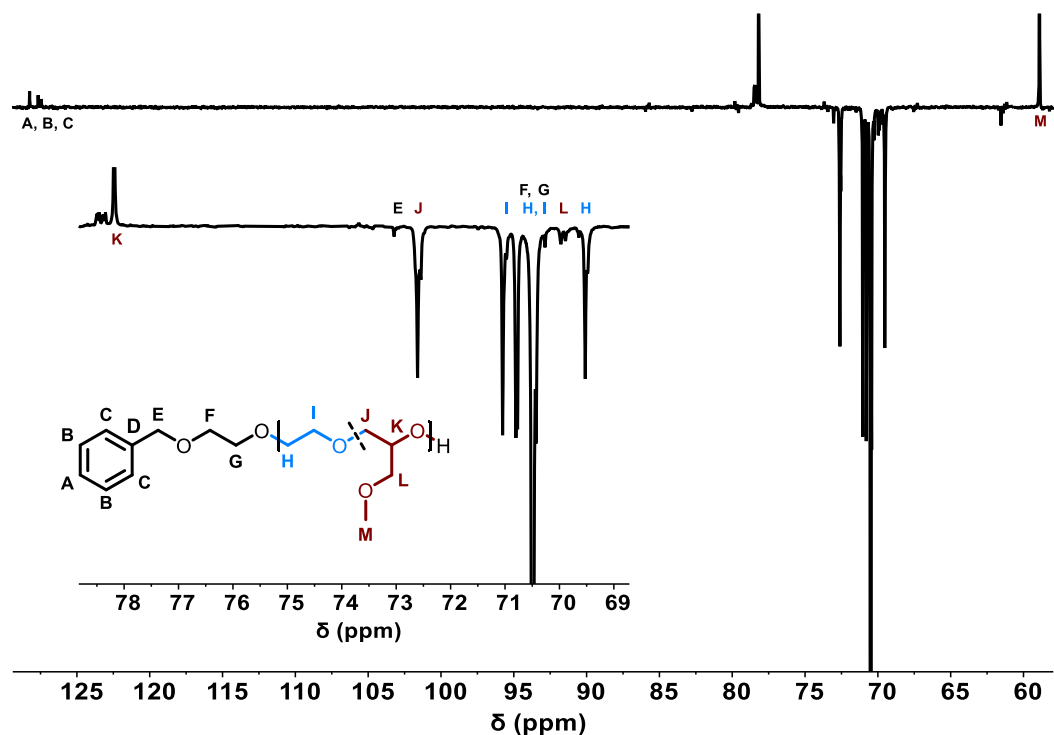
Figure S5. ^{13}C DEPT NMR spectrum (CD$_2$Cl$_2$) of P(EG-*co*-GME).
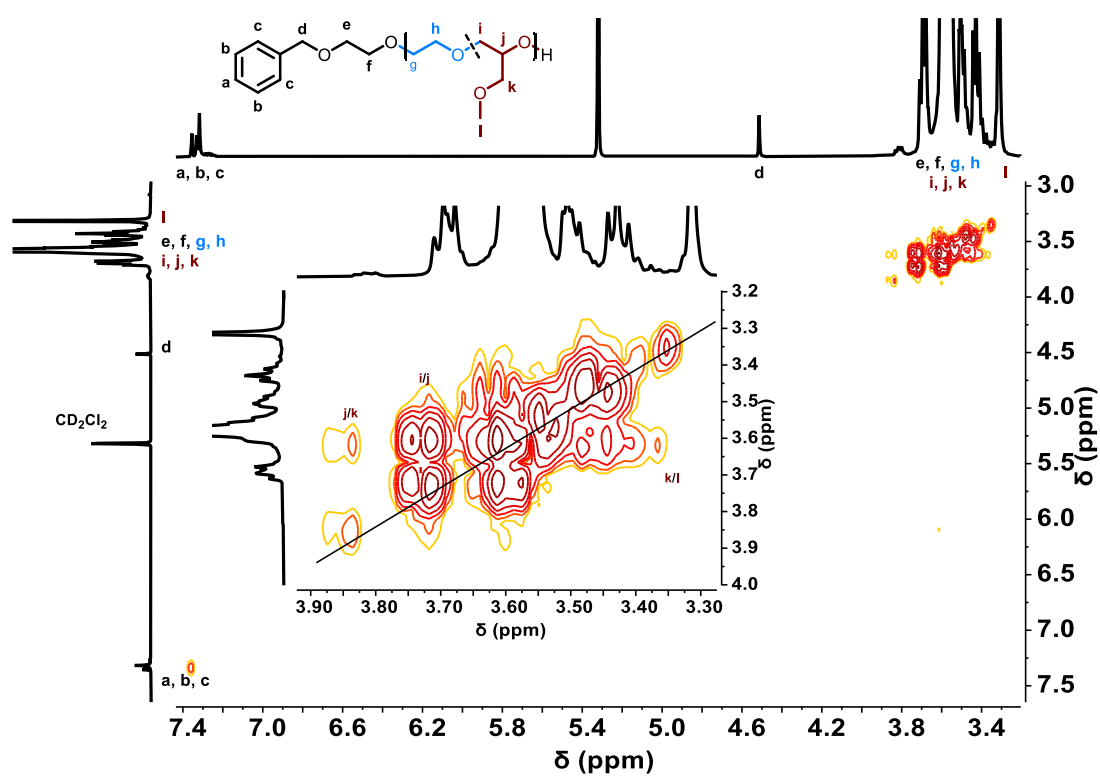
Figure S6. ^{1}H,^{1}H COSY NMR spectrum (CD$_2$Cl$_2$) of P(EG-*co*-GME).
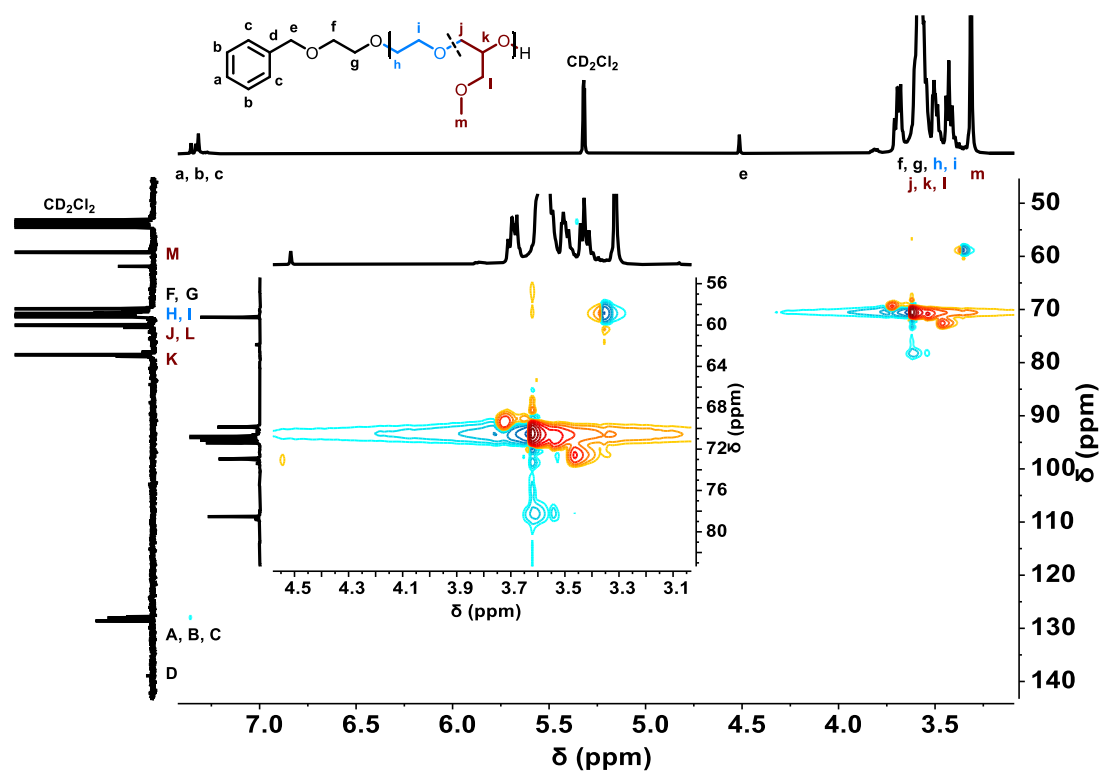
Figure S7. ^{1}H,^{13}C HSQC NMR spectrum CD$_2$Cl$_2$) of P(EG-*co*-GME).
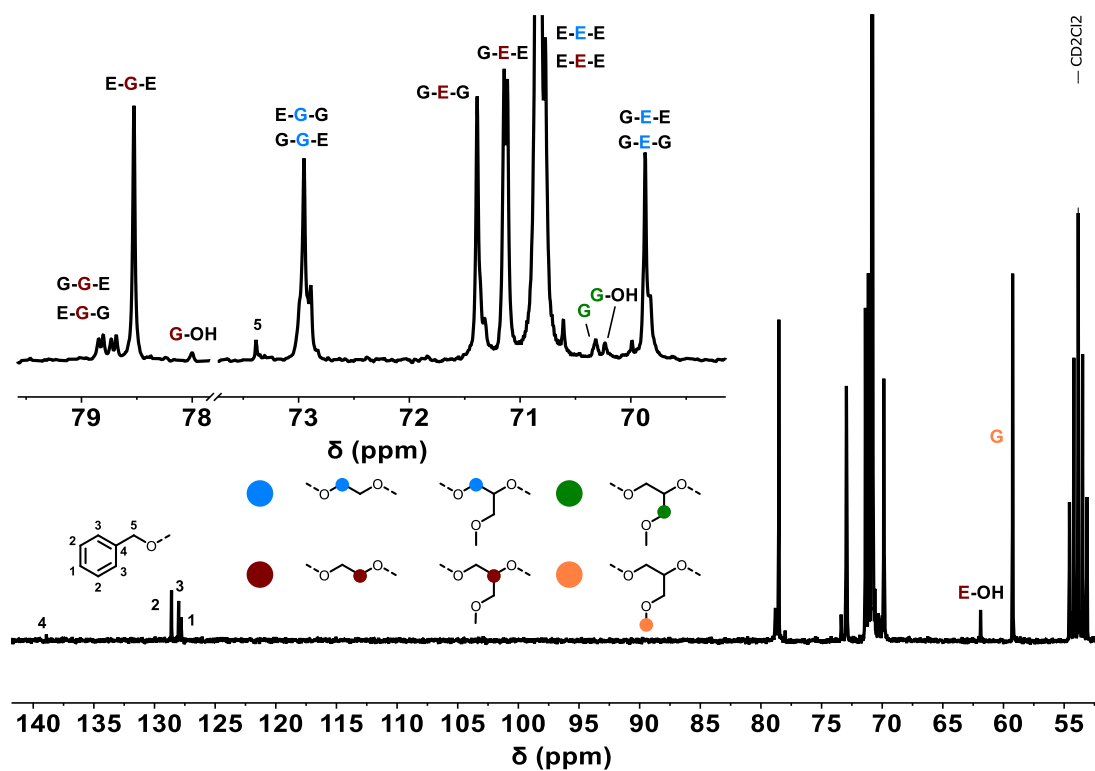
Figure S8. ^{13}C IG NMR spectrum (CD$_2$Cl$_2$, 75 MHz) of P(EG-*co*-GME).
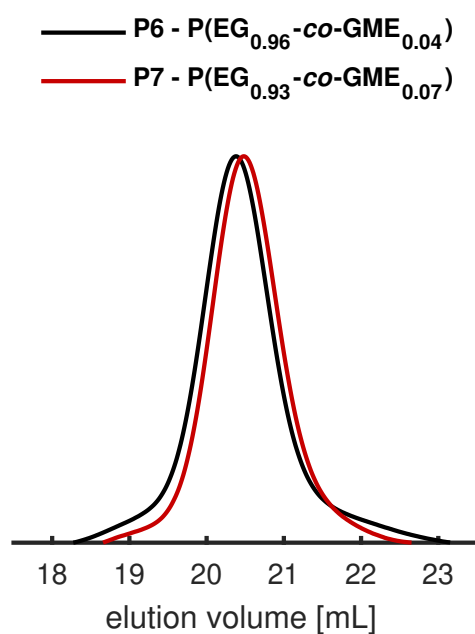
Figure S9. SEC (DMF, PEG calibration) of P6 and P7.
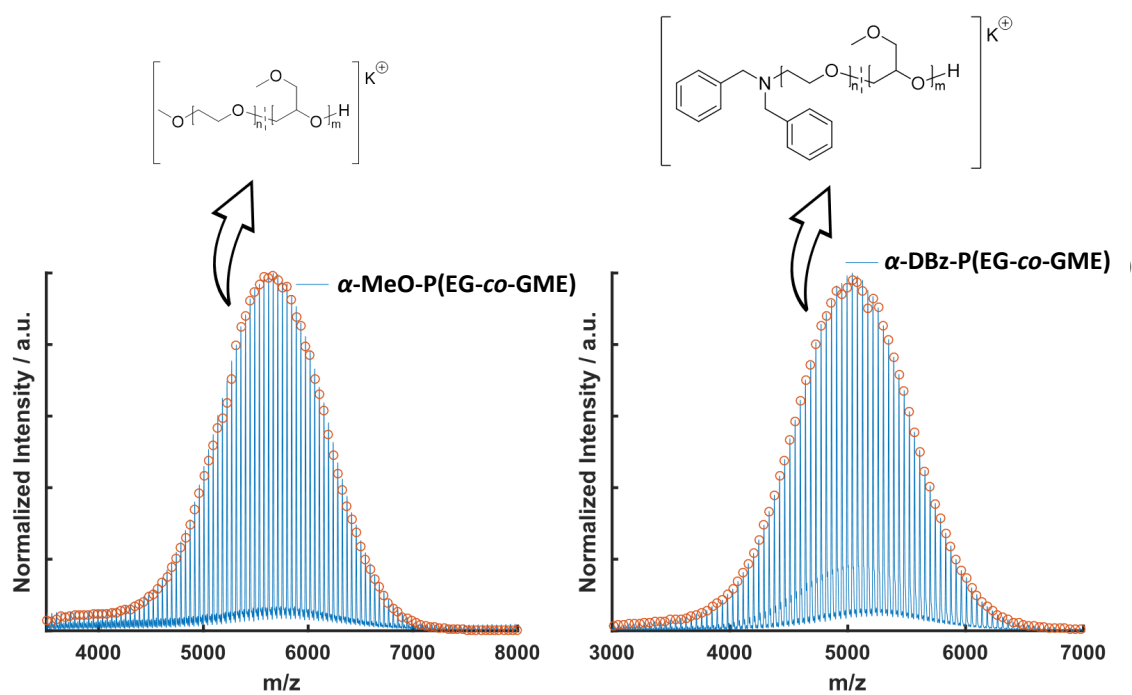
Figure S10. MALDI ToF mass spectra of α-methoxy (left) and α-*N,N*-dibenzylamino-P(EG-*co*-GME) (right).

PGME (M_n: 2670 g/mol; Đ: 1.05)

elution volume [mL]
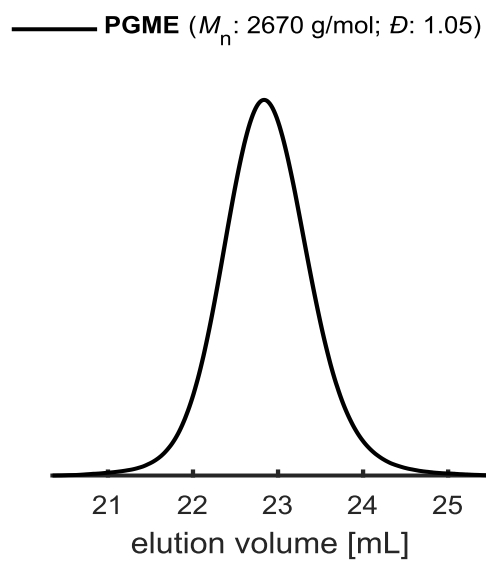
Figure S11. SEC (DMF, PEG calibration) of PGME (P8).
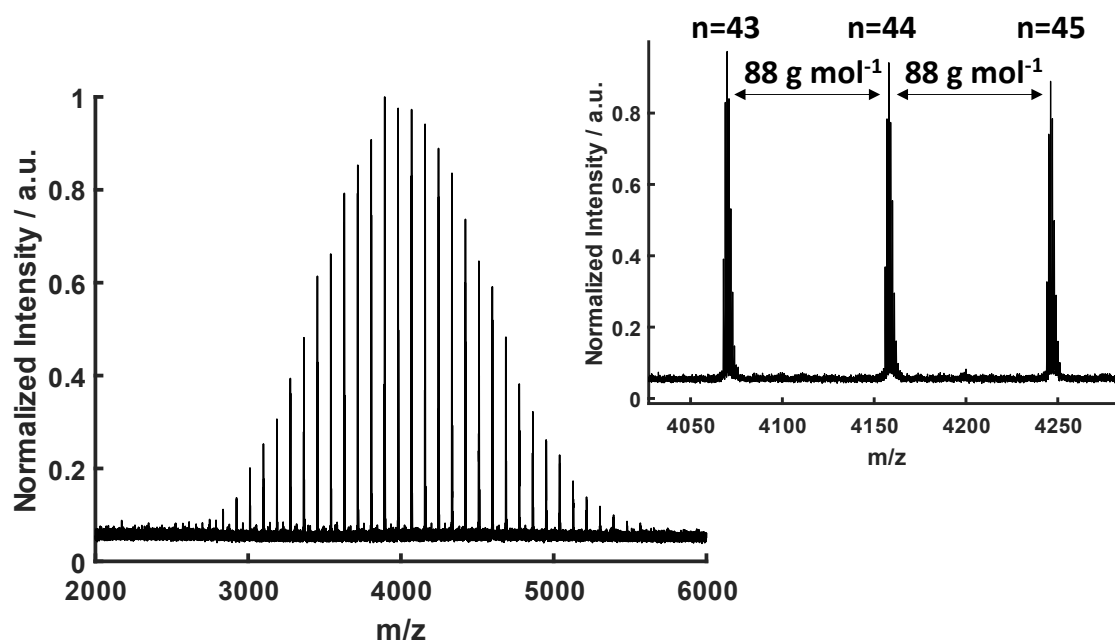
Figure S12. MALDI ToF MS of PGME (P8).

Investigation of Thermoresponsivity

Investigations concerning the LCST of P(EG-*co*-GME) copolymers was conducted by turbidimetric measurements for calculation of the cloud point T_{cp}. The highly hydrophilic PEG exhibits a LCST above 100 °C, underlining its excellent aqueous solubility.[9] The LCST of PGME was investigated in several papers, showing a T_{cp} between 45 to 64 °C depending on factors like M_n and concentration.[10-12] However, the herein investigated random P(EG-*co*-GME) copolymers with GME amounts < 49 mol% exhibited no thermoresponsive behavior, while a 49 mol% of GME incorporation lead to a T_{cp} of 94.5 °C. These results strongly support the high hydrophilicity of the random copolymers as well as their possible bioapplication at body temperature of 37 °C without formation of aggregates and subsequent precipitation.
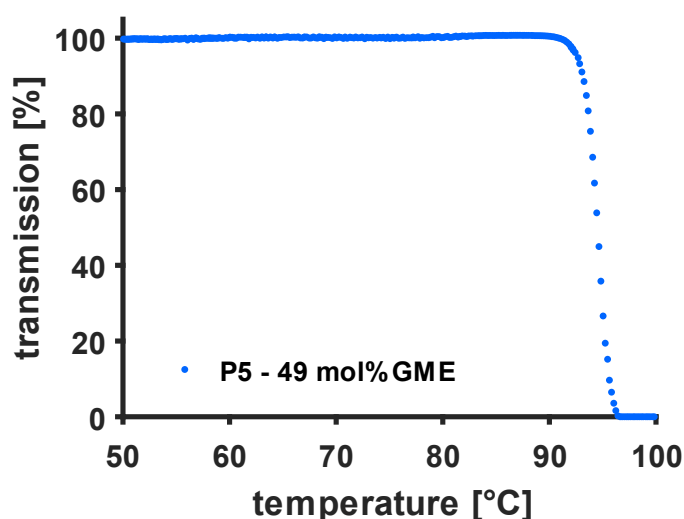
Figure S13. Determination of the cloud point T_{cp} by turbidimetry in 2.5 mg mL^{-1} for copolymer with 49% GME in aqueous solution. The heat rate was 1 °C min^{-1} while the T_{cp} was determined at 50% transmission.

Additional Plots *in situ* Kinetics
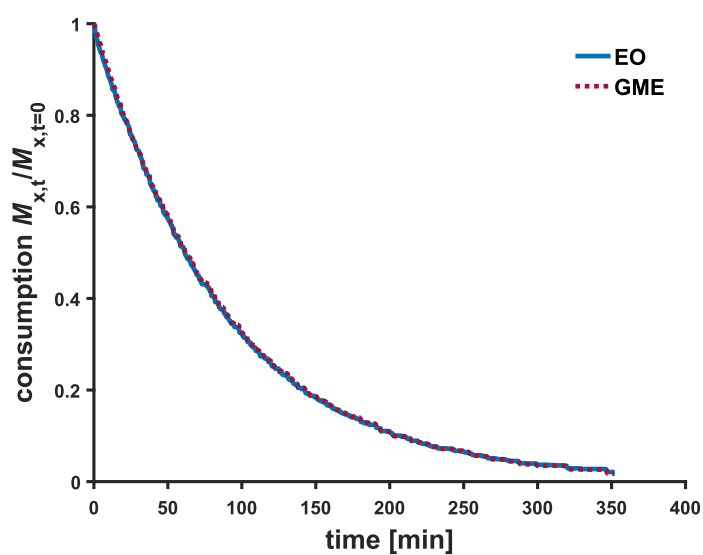
Figure S14. Consumption $M_{x,t}/M_{x,t=0}$ vs. time plot of the copolymerization of EO and GME determined by *in situ* ^{1}H NMR kinetics.
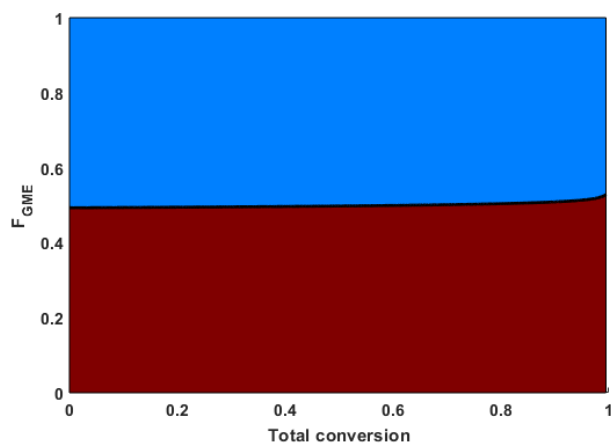
Figure S15. Visualization of the polymer microstructure of P(EG-*co*-GME) by plotting the molar mean incorporation of GME (F_{GME}) (red) as a function of total conversion.

Analysis of Microstructure Based on DFT Calculations

As recently shown by Lai and co-workers[9] the anti-PEG antibody (APA) captures around 16 ethylene glycol units within its paratope. Based on these findings, the P(EG-*co*-GME) copolymers are examined regarding the occurrence of 16 sequential EG units, so called hektakaidekads. In this manner, the interaction of the APA with the herein presented copolymers can be quantified on a theoretical level. To enable the analysis of the P(EG-*co*-GME) copolymers with respect to their microstructure, kinetic Monte-Carlo (kMC) simulations were conducted. The model of the kMC simulation originates in the stochastic simulation algorithm by Gillespie and relies on the conversion of the continuum-based reaction rates into number-based probabilities.[10-12] In order to provide an insight into chemical composition distribution, more precisely the distribution of consecutive EG repeating units in EO/GME copolymers, kMC simulations represent a versatile tool and hence eight polymerizations were performed *in silico*. For this purpose, the rationale of a living anionic polymerization was taken as a basis, what implies the absence of chain termination or chain transfer reactions. The copolymerization reaction can simply be described by the four rate constants: the homopropagation rate constants k_{11} and k_{22} aa well as the cross-propagation rate constants k_{12} and k_{21}. These rate constants are transformed into number-based probabilities, where A_i denotes the corresponding aggregation number of the chain ends ($A_i = 2 \rightarrow$ dimers, $A_i = 4 \rightarrow$ tetramers, etc.) and concentrations are converted by multiplying with the Avogadro's number N and the simulation volume V.

$$kMC_{11} = \frac{k_{11}}{(NV)^{1/A_1}}$$

$$kMC_{22} = \frac{k_{22}}{(NV)^{1/A_2}}$$

$$kMC_{12} = \frac{k_{12}}{(NV)^{1/A_1}}$$

$$kMC_{21} = \frac{k_{21}}{(NV)^{1/A_2}}$$

The copolymerization is then determined based on the cumulative probabilities P_v by a uniformly distributed random number $rn_1 = [0 \dots 1]$.

$$P_v = \frac{R_v}{\sum_{M}^{v=1} R_v}$$

$$\sum_{v=1}^{\mu=1} P_v < rn_1 < \sum_{v}^{\mu} P_v$$

The copolymerization kinetics was assumed to be perfectly random, implying $k_{11} = k_{22} = k_{12} = k_{21} = 1$. Furthermore, no aggregated chain ends ($A_1 = A_2 = 1$) were supposed. For each polymerization, 1000 chains were simulated. The simulations were run with the listed degrees of polymerizations of the individual monomers, a targeted conversion of 99.9%, initiator concentrations of $1 \, \text{mmol L}^{-1}$ and polymerization volumes of $1.66 \, 10^{-18} \, \text{L}$. For every polymerization, an overall molecular weight of $5 \, \text{kg mol}^{-1}$ was targeted, leading to the listed degrees of polymerization with molar ratios of 20 up to 50% of GME with a stepwise increase by 5 mol%. In Table S1 the seven simulated polymerizations and the respective proportional occurrence of hektakaidekads are listed.

Table S1. Analysis concerning the occurrence of hektakaidekads (16 EG units) within the P(EG-*co*-GME) copolymers with varying GME ratios (20 to 50 mol%$_{\text{GME}}$). Results were obtained by DFT calculations which were performed based on the estimated reactivity ratios of the copolymerization of EO and GME.

Polymer	mol%$_{\text{GME}}$ [%]	hektakaidekad analysis (16 EG units) [%]	number of chains (16 EG units) [%]
P(EG$_{0.80}$-*co*-GME$_{0.20}$)	20	44.4	38.5
P(EG$_{0.75}$-*co*-GME$_{0.25}$)	25	19.6	17.7
P(EG$_{0.70}$-*co*-GME$_{0.30}$)	30	7.2	6.9
P(EG$_{0.65}$-*co*-GME$_{0.35}$)	35	2.9	2.9
P(EG$_{0.60}$-*co*-GME$_{0.40}$)	40	0.5	0.5
P(EG$_{0.55}$-*co*-GME$_{0.45}$)	45	0.4	0.4
P(EG$_{0.50}$-*co*-GME$_{0.50}$)	50	0	0

The investigations regarding the recognition of P(EG-*co*-GME) by APAs revealed a decrease (< 24 mol% GME) up to the full prevention (49 mol% GME) of recognition with increasing GME content. This observation is supported by the theoretical consideration revealing the full exclusion of 16 sequential EG units if 50 mol% of GME are incorporated to the polyether. On the contrary, polymers containing 25 mol% of GME still 17.7% of 1000 simulated chains possess at least one EG-hektakaidekad. To graphically transfer the results of kMC simulations, ten exemplary chains for each respective GME ratio are shown in Figure S16. As the GME units are statistically distributed throughout the polyether, the occurrence of EG-rich regions consequently decreases with increasing GME ratio.
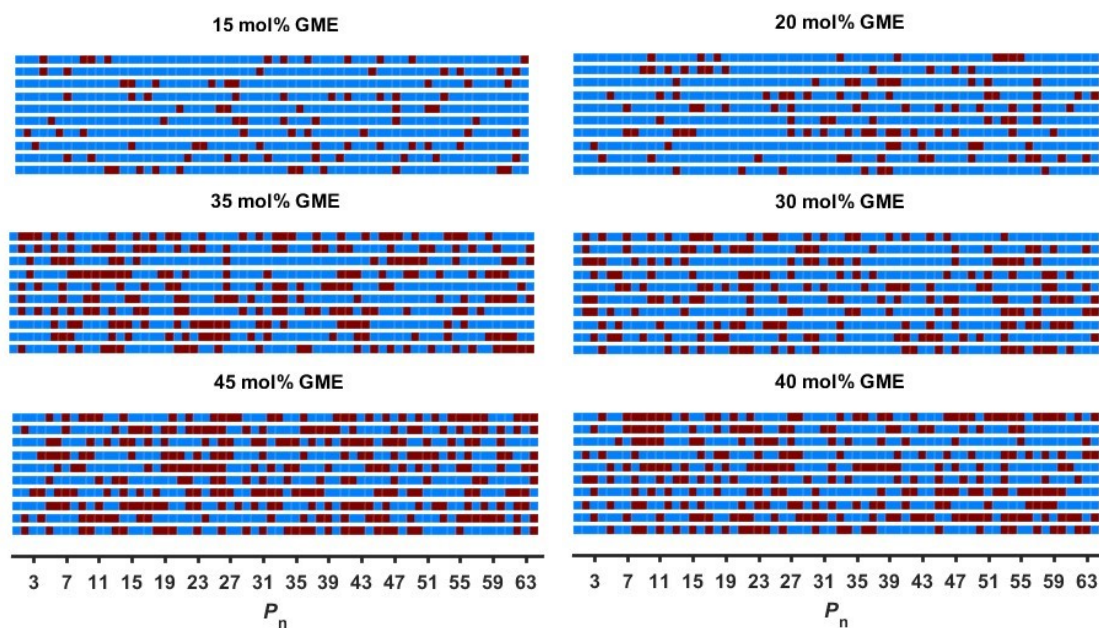
Figure S16. Graphical illustration of individual chains of P(EG-*co*-GME) copolymers with varying GME ratio calculated by DFT calculations (EG = blue, GME = red).

Conjugation of BSA with P(EG-*co*-GME)

Figure S17 shows the ^{1}H NMR spectrum of α-BzO-ω-*N*-succinimidyl carbonate-P(EG-*co*-GME). The copolymer was synthesized with a GME content of 16 mol%. Considering the random copolymerization demonstrated by the described *in situ* ^{1}H NMR kinetics, statistically 84% of *N,N'*-disuccinimidyl carbonate is attached to an EO chain end. The overall degree of functionalization for terminal EG as well as GME units is calculated by the integral of the methylene protons m and n at 2.86 ppm of the succinimidyl-substituent in comparison to the benzylic initiator protons at 4.58 ppm. The calculation reveals a successful functionalization of 68%. Integration of the corresponding methylene protons l at 4.45 to 4.49 ppm shows 88% of functionalized EG units which consequently results in 12% terminal GME units, which is a similar value compared to the determined 16 mol% of the precursor.
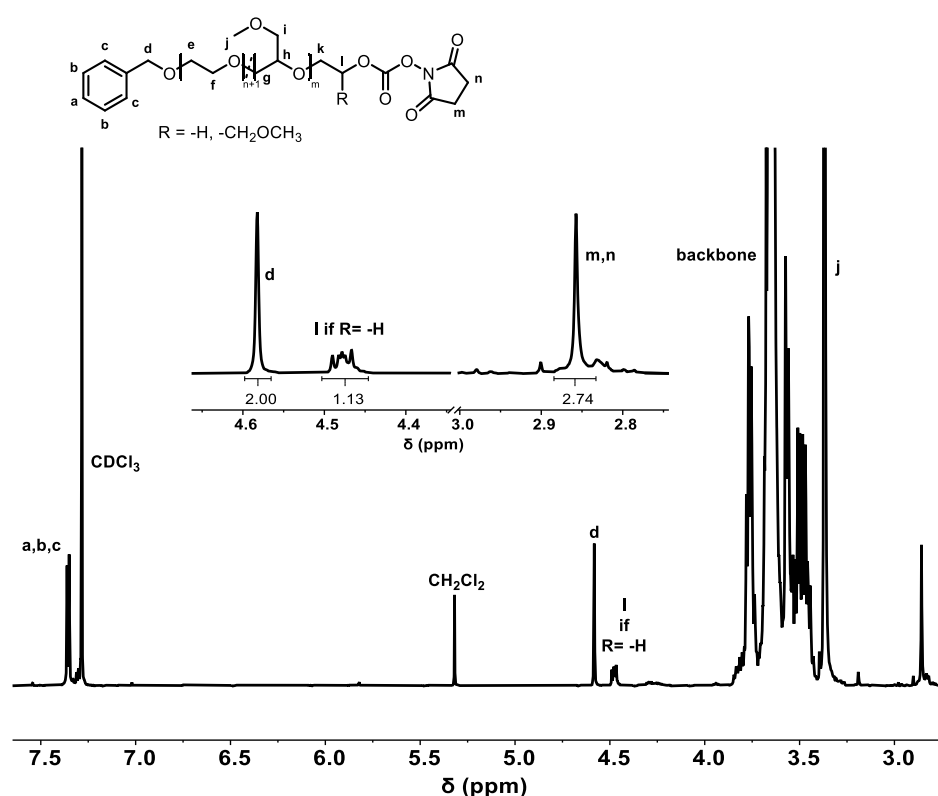
Figure S17. ^{1}H NMR spectrum of α-BzO-ω-*N*-succinimidyl carbonate-P(EG-*co*-GME).

Block Copolymer Synthesis

Besides random copolymers, the synthesis of mPEG-*b*-PGME is achieved by the utilization of mPEG as macroinitiator.
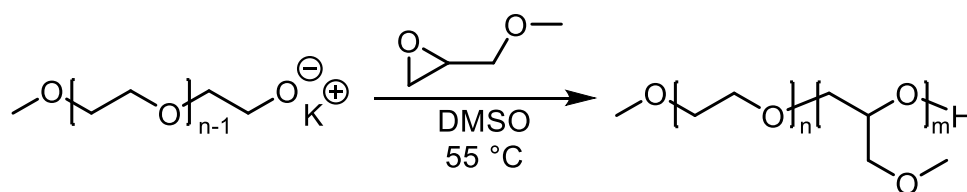
Scheme S2. Synthesis of mPEG-*b*-PGME.

The corresponding SEC (Figure S18) and MALDI-ToF mass spectra (Figure S19) show a clear shift to lower elution volume and higher molecular weights, respectively, of the block copolymer relative to the precursor mPEG and the absence of homopolymer traces. Additionally, the molecular weight distribution of mPEG-*b*-PGME exhibits a 44 g mol^{-1} difference between the signals in the MALDI-ToF MS, showing successful block copolymer formation.
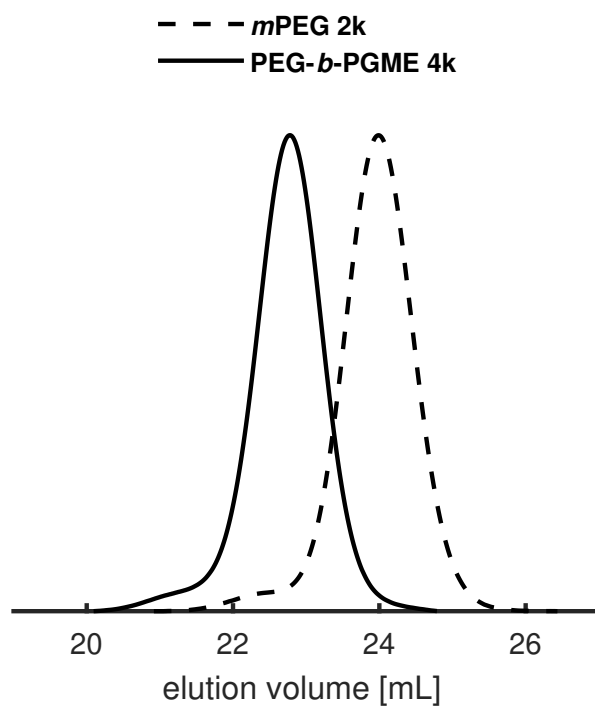
Figure S18. SEC (DMF, PEG calibration) of mPEG and mPEG-*b*-PGME.
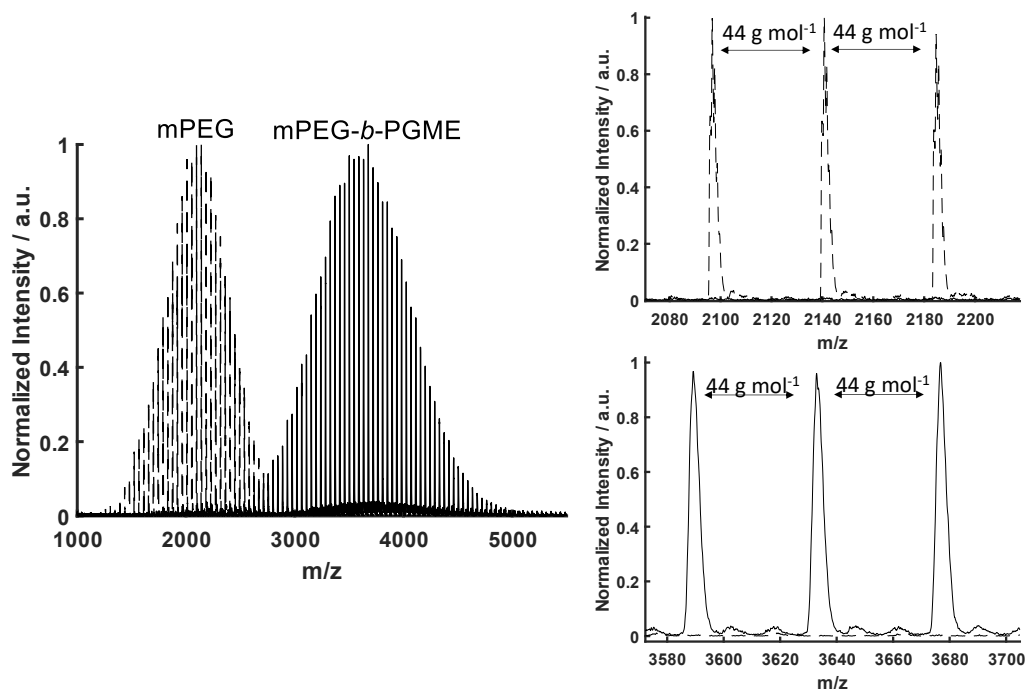
Figure S19. Overlay MALDI ToF mass spectra of mPEG and mPEG-*b*-PGME (Matrix: DCTB, KTFA).

Thermal Properties of Random and Block Copolymers

The melting temperature and degree of crystallinity of the random copolymers strongly depends on the molar amount of incorporated GME. With increasing GME content, the melting temperature and melting enthalpy of the copolymers decreases, independent of molecular weight (Table S2). In the case of mPEG-*b*-PGME only a minor influence of the PGME block on crystallinity of PEG is observed compared to random copolymers with similar molar amounts of GME. These results are in accordance with the literature[13] and support the ideal random incorporation of GME in the polyether during the copolymerization.

Table S2. Thermal Properties of Random and Block Copolymers; Determined via DSC ($10 \, \text{K min}^{-1}$) (xk = x kg mol^{-1}).

Sample	mol%$_{\text{GME}}$ [%]	T_g [°C]	T_m [°C]	ΔH_{PEG} [J g^{-1}]	$X_{\text{c,PEG}}$
P(EG$_{0.96}$-*co*-GME$_{0.04}$) 5k	4	-56	46	88.63	0.45
P(EG$_{0.92}$-*co*-GME$_{0.08}$) 5k	8	-59	35	58.22	0.30
P(EG$_{0.85}$-*co*-GME$_{0.15}$) 6k	15	-61	7	32.62	0.16
P(EG$_{0.96}$-*co*-GME$_{0.04}$) 10k	4	-56	45	76.79	0.39
P(EG$_{0.93}$-*co*-GME$_{0.07}$) 10k	7	-59	37	56.26	0.28
PEG-*b*-PGME 4k	22	-59	45	80.16	0.41
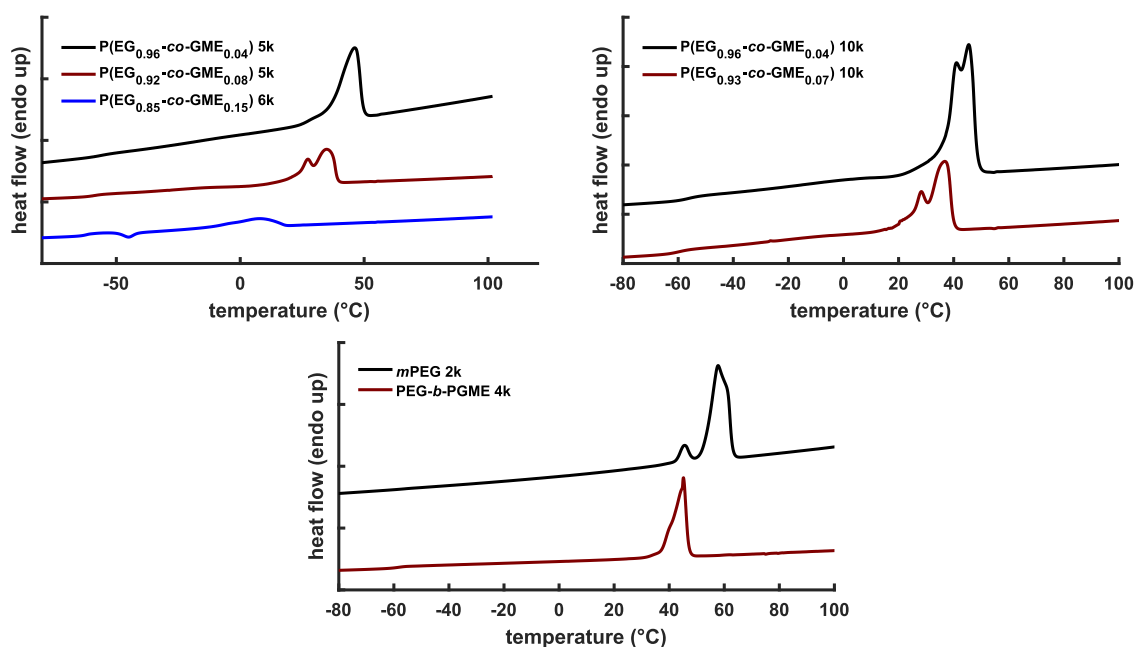
Figure S20. 2$^{\text{nd}}$ DSC heating curves ($10 \, \text{K min}^{-1}$) of random and block copolymers.

Cell Viability Tests
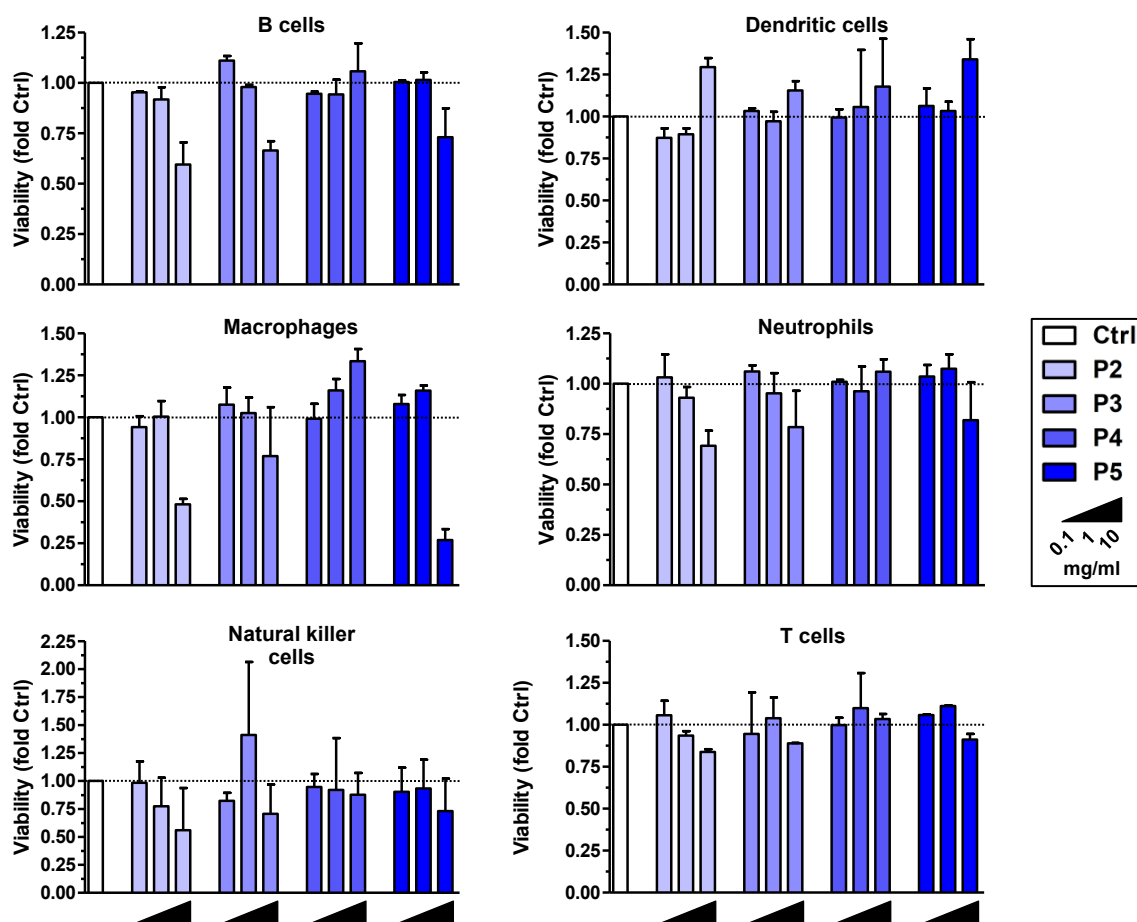
Figure S21. PEG derivatives influence the viability of immune cells in a formulation- and cell type-specific manner at high concentrations. Murine spleen cells were incubated over-night with different PEG derivatives at various concentrations as indicated (0.1-10 mg mL^{-1}). Graphs show the viability of the various leukocyte populations in response to treatment given relative to the viability of untreated cells (Ctrl). Data denote the mean ± SD of two independent experiments.
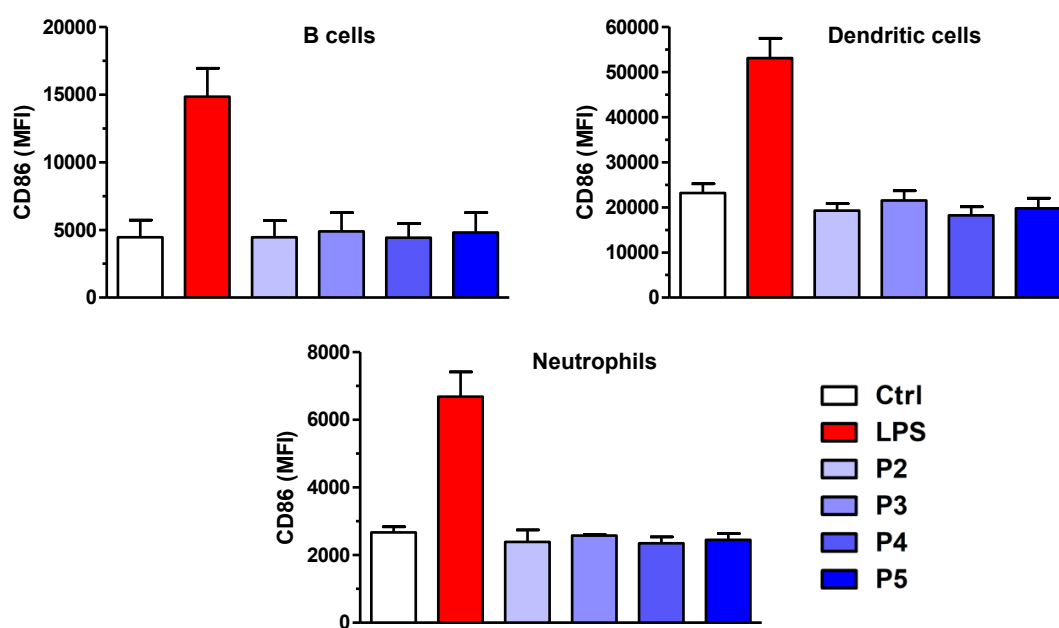
Figure S22. PEG derivatives exert no stimulatory effects on immune cells. Murine spleen cells were incubated over-night with different PEG derivatives at subtoxic concentration ($1\,mg\,mL^{-1}$) and LPS ($1\,\mu g\,mL^{-1}$) as a positive control. On the next day, expression of the costimulatory receptor CD86 was assessed for the different leukocyte populations. Data denote the mean fluorescence intensity (MFI) ± SEM of three independent experiments.

REFERENCES

(1) Herzberger, J.; Leibig, D.; Liermann, J. C.; Frey, H. Conventional Oxyanionic versus Monomer-Activated Anionic Copolymerization of Ethylene Oxide with Glycidyl Ethers: Striking Differences in Reactivity Ratios. *ACS Macro Lett.* **2016**, *5*, 1206–1211.

(2) Steube, M.; Johann, T.; Plank, M.; Tjaberings, S.; Gröschel, A. H.; Gallei, M.; Frey, H.; Müller, A. H. E. Kinetics of Anionic Living Copolymerization of Isoprene and Styrene Using in Situ NIR Spectroscopy: Temperature Effects on Monomer Sequence and Morphology. *Macromolecules* **2019**, *52*, 9299–9310.

(3) Wagener, K.; Bros, M.; Krumb, M.; Langhanki, J.; Pektor, S.; Worm, M.; Schinnerer, M.; Montermann, E.; Miederer, M.; Frey, H.; et al. Targeting of Immune Cells with Trimannosylated Liposomes. *Adv. Therap.* **2020**, *3*, 1900185.

(4) Prileschajew, N. Oxydation ungesättigter Verbindungen mittels organischer Superoxyde. *Ber. Dtsch. Chem. Ges.* **1909**, *42*, 4811–4815.

(5) Saeki, S.; Kuwahara, N.; Nakata, M.; Kaneko, M. Upper and lower critical solution temperatures in poly (ethylene glycol) solutions. *Polymer* **1976**, *17*, 685–689.

(6) Fellin, C. R.; Adelmund, S. M.; Karis, D. G.; Shafranek, R. T.; Ono, R. J.; Martin, C. G.; Johnston, T. G.; DeForest, C. A.; Nelson, A. Tunable temperature- and shear-responsive hydrogels based on poly(alkyl glycidyl ether)s. *Polym. Int.* **2019**, *68*, 1238–1246.

(7) Müller, S. S.; Moers, C.; Frey, H. A Challenging Comonomer Pair: Copolymerization of Ethylene Oxide and Glycidyl Methyl Ether to Thermoresponsive Polyethers. *Macromolecules* **2014**, *47*, 5492–5500.

(8) Isono, T.; Miyachi, K.; Satoh, Y.; Sato, S.-i.; Kakuchi, T.; Satoh, T. Design and synthesis of thermoresponsive aliphatic polyethers with a tunable phase transition temperature. *Polym. Chem.* **2017**, *8*, 5698–5707.

(9) Huckaby, J. T.; Jacobs, T. M.; Li, Z.; Perna, R. J.; Wang, A.; Nicely, N. I.; Lai, S. K. Structure of an anti-PEG antibody reveals an open ring that captures highly flexible PEG polymers. *Commun Chem* **2020**, 3.

(10) Gillespie, D. T. Exact stochastic simulation of coupled chemical reactions. *J. Phys. Chem.* **1977**, *81*, 2340–2361.

(11) Gillespie, D. T. A general method for numerically simulating the stochastic time evolution of coupled chemical reactions. *Journal of Computational Physics* **1976**, *22*, 403–434.

(12) Steube, M.; Johann, T.; Galanos, E.; Appold, M.; Rüttiger, C.; Mezger, M.; Gallei, M.; Müller, A. H. E.; Floudas, G.; Frey, H. Isoprene/Styrene Tapered Multiblock Copolymers with up to Ten Blocks: Synthesis, Phase Behavior, Order, and Mechanical Properties. *Macromolecules* **2018**, *51*, 10246–10258.

(13) Mangold, C.; Wurm, F.; Obermeier, B.; Frey, H. Hetero-Multifunctional Poly(ethylene glycol) Copolymers with Multiple Hydroxyl Groups and a Single Terminal Functionality. *Macromolecular rapid communications* **2010**, *31*, 258–264.

Chapter 2.2

In situ Kinetics is Indispensable: Influence of Solvents and Monomers on Anionic Ring-Opening Copolymerization of Epoxides

In-depth understanding of copolymerization kinetics and the resulting polymer microstructure is crucial for the design of materials with well-defined properties. *In situ* ^{1}H NMR spectroscopy enables precise monitoring of the living anionic ring-opening copolymerization (AROP) of ethylene oxide (EO) with the glycidyl

ethers allyl glycidyl ether (AGE) and ethoxy vinyl glycidyl ether (EVGE), respectively. Determination of reactivity ratios revealed slightly higher reactivity of both glycidyl ethers compared to EO, emphasizing a pronounced counterion chelation effect by glycidyl ethers in AROP. Implementation of density functional theory (DFT) calculations further illustrated the complexation capability of ether-containing side groups in glycidyl ethers, in analogy to crown ethers ("crown ether effect"). Investigation of the copolymerization both in THF-d_8 and DMSO-d_6 showed the increasing reactivity disparity of both glycidyl ethers compared to EO with decreasing solvent polarity. Furthermore, a comparison of the determined reactivity ratios via the herein utilized *in situ* ^{1}H NMR spectroscopy and the end-group-dyad (EGD) analysis introduced by Lynd, Hawker et al. was conducted, showing significant differences with respect to the reactivity ratios. Hence, supporting DFT calculations were implemented, illustrating the different preferential incorporation at the initiator and in the course of the further growth of the polymer chains. The results evidence the crucial importance of detailed *in situ* studies by initiator-independent methods in the living copolymerization, encompassing the entire monomer consumption range for the evaluation of copolymerization kinetics. Information derived merely from the initiating dyad provides only insufficient tendencies rather than accurate reactivity ratios.
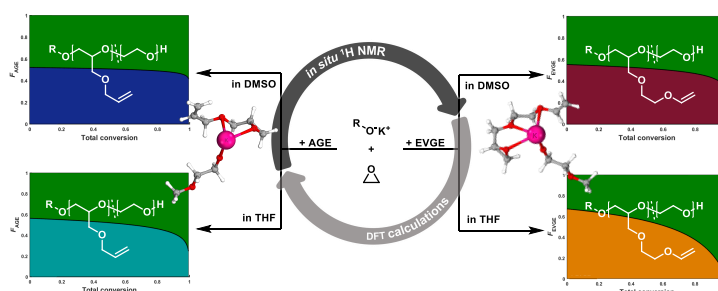
INTRODUCTION

In depth kinetic studies of the statistical copolymerization of different monomers, have received renewed interest in recent years, particularly for living polymerization (LP) techniques. Besides the controlled radical polymerization, the anionic LP remains the most efficient method for the synthesis of well-defined copolymers with narrow molecular weight distribution and controlled monomer gradients. Detailed knowledge regarding the compositional profile of the comonomers along the polymer chains is of key importance in gradient or tapered copolymers to adjust the thermal properties in bulk[1–6] and solution and consequently to control the morphology[1,4,7] of the resulting materials.

In the past, common methods for the evaluation of the reactivity ratios and the corresponding comonomer gradient in the copolymer chains formed were determination of the comonomer content at different stages of the copolymerization after precise termination[8,9] and subsequent gas chromatographic analysis of the residual monomers.[10] These monitoring techniques are time-consuming, often rather difficult to implement and may hold uncertainties due to missing reproducibility, since the data have to be obtained from different polymerization experiments. In comparison, triad analysis via ^{13}C inverse gated (IG) spectroscopy[11–13] is a more reliable method for determination of the microstructure, but a large variety of samples must be synthesized for correct assignment and evaluation of the corresponding triads. More recently, *in situ* monitoring via near infrared (NIR) spectroscopy[7,14,15] was established as a feasible analytical set-up to directly correlate the polymerization kinetics with the copolymer microstructure for carbanionic copolymerization. The *in situ* methods advantageously permit to follow the mean composition over the whole conversion range, i.e. at all given chain positions, resulting in a complete compositional profile of the copolymers.[7,16] For instance, the influence of temperature[7] and polar additives[14,15] on the compositional drift and steepness of the gradient in isoprene/styrene-based tapered block copolymers, synthesized via carbanionic copolymerization, was recently investigated in great detail via NIR spectroscopy.

In comparison to the living carbanionic polymerization, the relatively slow polymerization kinetics of the anionic ring-opening polymerization (AROP) in polar aprotic solvents facilitates monitoring. This has been exploited to follow the monomer consumption of epoxides[13,17–24] as well as activated aziridines[25–28] via *in situ* ^{1}H NMR spectroscopy. Depending on the comonomer employed, the copolymerization of EO with monosubstituted epoxides may result in rather different polymer microstructures. For example, preferred addition of EO over alkylene oxides[20] and glycidyl amines[17,19] to the active chain end has been observed. In contrast, the copolymerization of EO with various glycidyl ethers (GE) generally revealed an almost ideally random distribution of the comonomer units along the polyether backbone.[18,21,22,29] Considering the underlying reactivity ratios, r, and rate constants, k ($r_{EO} = k_{EO,EO}/k_{EO,GE}$, $r_{EO} = k_{GE,GE}/k_{GE,EO}$), this copolymerization behavior necessitates $k_{EO,EO} = k_{GE,EO}$ as well as $k_{GE,GE} = k_{EO,GE}$ and thus

strictly results in the product $r_{EO} \cdot r_{GE}$ being unity. Consequently , non-terminal models, e.g., the Jaacks method[30] can be employed to investigate the underlying copolymerization kinetics in AROP.[18,24,29]

In 2012, Lynd, Hawker and coworkers reported a novel initiator-based method for the calculation of the reactivity ratios in the AROP copolymerization of EO and monosubstituted epoxides based on ^{1}H NMR spectroscopy. This method relies solely on evaluating the dyad containing the benzylic alkoxide initiator and the following two monomer units (end-group-dyad (EGD) analysis). Surprisingly, a dramatically preferred incorporation of ethoxy vinyl glycidyl ether (EVGE) relative to EO and consequently a gradient microstructure was observed by the authors in THF, relying on the EGD method.[31,32] These findings contradict the current knowledge regarding EO/glycidyl ether copolymerizations under AROP conditions in THF and are inconsistent with the results obtained in our group via ^{13}C inverse gated spectroscopy in a preceding publication. For the statistical copolymerization of ethoxy vinyl glycidyl ether (EVGE) and EO a random distribution of the EVGE units along the polymer backbone was obtained by comparison of the triad distribution.[12] In addition to the chemical nature of the monomers, the polarity of the solvent and its potential interaction with the counterion affect the kinetics of AROP copolymerization. EO or substituted epoxides have been investigated with regard to polymerization kinetics in different aprotic polar solvents ranging from linear and cyclic ethers[33–36] to polar solvents like dimethyl sulfoxide (DMSO)[37–41] and hexamethylphosphoramide (HMPA).[39,42] Depending on the polarity of the solvents, ion pairs were observed as reactive species in ethers,[34,36] whereas free ions were found to be present in the case of the more polar DMSO[43] and HMPA.[42] Nevertheless, although the homopolymerization kinetics in these solvents is well understood, the influence of the solvent on the copolymerization kinetics of EO with monosubstituted epoxides remains largely unexplored. To the best of our knowledge, only the variation of the reactivity ratios in the presence of electron donors has been investigated in detail for the copolymerization of epoxides to date.[10]
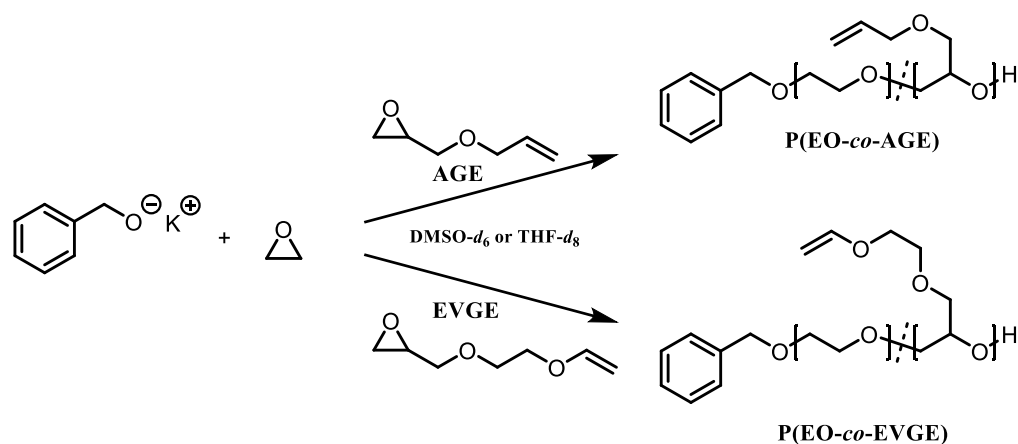
Scheme 1. Synthesis route of P(EO-*co*-AGE) and P(EO-*co*-EVGE) initiated by potassium phenylmethanolate in DMSO-d_6 and THF-d_8.

In the current work we utilize *in situ* ^{1}H NMR kinetics monitoring to evaluate and compare the reactivity ratios of the copolymerization of EO with EVGE and AGE, respectively, both in the presence of tetrahydrofuran-d_8 (THF-d_8) and DMSO-d_6 (Scheme 1). DFT calculations were employed, leading to an in-depth understanding of the copolymerization kinetics. Additionally, the values obtained from *in situ* monitoring are directly compared to the reactivity ratios reported by Lynd, Hawker et al. via ^{1}H NMR end group dyad (EGD) analysis, where only the first two chain units are considered.

RESULTS AND DISCUSSION

Impact of Solvents on AROP Copolymerization Kinetics of EO and Glycidyl Ethers

The anionic ring-opening polymerization (AROP) of epoxides is commonly performed in polar solvents to sufficiently dissolve the involved ionic species. DMSO with a dipole moment of 3.96 D is the solvent with the highest polarity that can be utilized in AROP apart from HMPA, which was not used in this study for safety reasons. Thus, DMSO can be considered as the ideal polar system with a high extent of ion dissociation and free ions as the active species.[43] On the contrary, THF exhibits a lower dipole moment of 1.63 D and accordingly is a less polar solvent implemented in AROP, permitting only partial dissociation of alkali metal alkoxides.[44] The reactive species of the alkoxide chain ends in THF can be characterized as ion pairs, which are in equilibrium with unreactive aggregates,[34] and most likely mimics the behavior in bulk polymerizations of epoxides. Therefore, the outlined solvents represent the upper and lower limit of polarity for AROP. Although several studies targeted at the copolymerization of EO with substituted epoxides have been conducted in either THF, DMSO or mixtures of both, their influence on the copolymerization kinetics has not been compared in a detailed manner to date. Based on this lack of data, we elucidated the impact of solvent polarity on the incorporation of different epoxides in the polyether during the copolymerization of EO with monosubstituted epoxides via *in situ* ^{1}H NMR kinetics. To this end, model copolymerizations of EO with the two glycidyl ethers AGE and EVGE were performed, initiated by potassium phenylmethanolate at 45 °C in DMSO-d_6 and THF-d_8, respectively.

As shown in Figure 1, in DMSO, the copolymerization of EO with AGE and EVGE exhibits high propagation rates, with a half-life (50 % conversion) of the respective glycidyl ether of 13 (AGE) and 20 min (EVGE), respectively. By recording one spectrum every 30 s, the monomer consumption was monitored over time (Figure S1), enabling the determination of the comonomer consumption versus total conversion, as shown in Figure 1 (bottom). The data show that in both cases the glycidyl ether is incorporated slightly faster than EO. Implementation of the Jaacks equation[30] enabled the calculation of reactivity ratios for both copolymerizations with a coefficient of determination (R^2) of 0.9995 (AGE) and 0.998 (EVGE), respectively (Figure S2). The Jaacks model is a non-terminal, integrated model for ideal copolymerizations that originates in the simplification $r_1 = r_2^{-1}$ and relies on the linearization of the Meyer-Lowry equation.
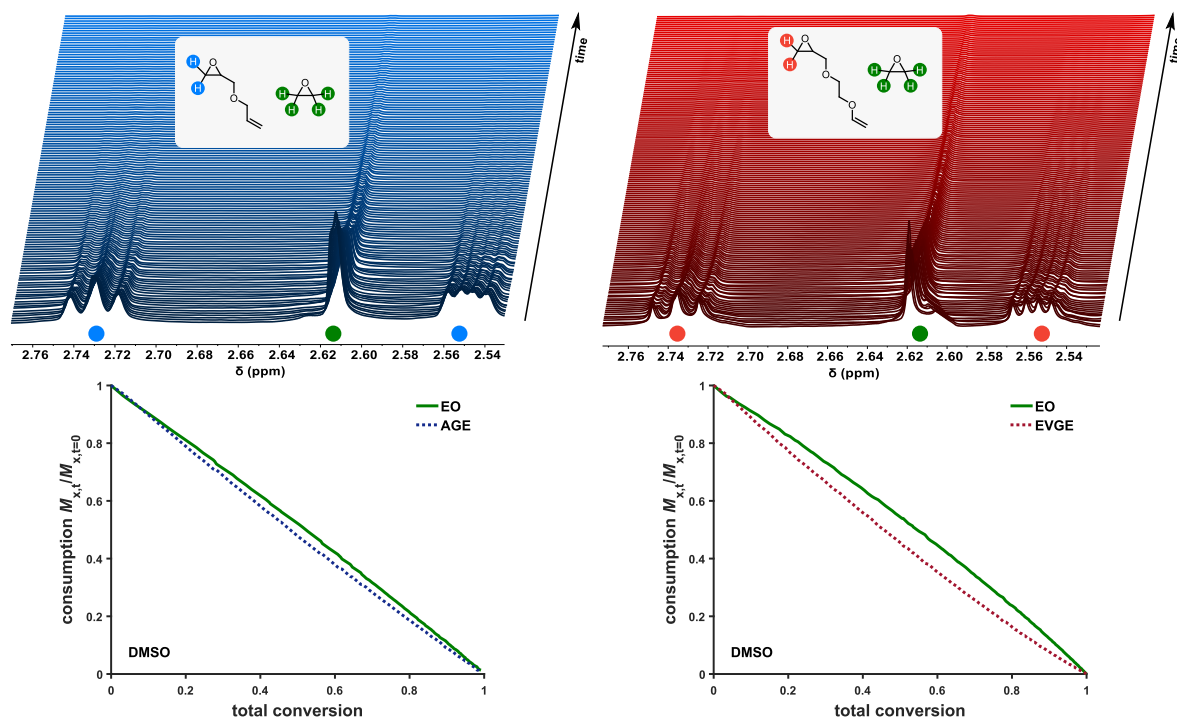
Figure 1. top: *in situ* ^{1}H NMR kinetics of the anionic copolymerization of EO with AGE in DMSO-d_6 (left) and with EVGE (right), initiated by potassium phenylmethanolate at 45 °C; bottom: conversion of both comonomers vs. total conversion.

The latter is applicable, if the rate of monomer incorporation does not show a strong dependence on the identity of the terminal unit, but on the nature of the reacting monomers. Its strength lies in the reduction of potential errors caused by overfitting. The implementation of the non-terminal model is further justified by DFT calculations, as discussed in a later section. Note that reactivity ratios are defined as $r_1 = k_{1,1}/k_{1,2}$ and $r_2 = k_{2,2}/k_{2,1}$ with index 1 representing EO and 2 the respective glycidyl ether. Both glycidyl ethers demonstrate rate constants of $k_{\text{AGE,AGE}} > k_{\text{AGE,EO}}$ and $k_{\text{EVGE,EVGE}} > k_{\text{EVGE,EO}}$, resulting in the preferential incorporation of AGE and EVGE in the early stages of the copolymerization compared to EO. The herein performed *in situ* kinetic experiments in DMSO consequently revealed reactivity ratios of $r_{\text{EO}}^{\text{DMSO}} = 0.92 \pm 0.002$ and $r_{\text{AGE}}^{\text{DMSO}} = 1.08 \pm 0.002$ as well as $r_{\text{EO}}^{\text{DMSO}} = 0.81 \pm 0.001$ and $r_{\text{EVGE}}^{\text{DMSO}} = 1.23 \pm 0.002$. Collectively, the copolymerization of EO and AGE in DMSO shows a nearly ideally random character, whereas the copolymerization with EVGE results in a very slight gradient microstructure. Based on the obtained reactivity ratios, the molar composition diagrams FGE versus total conversion illustrate the close to random (AGE) and slight gradient (EVGE) structure (Figure S3).

Subsequently, similar *in situ* ^{1}H NMR kinetic experiments were performed in THF to determine the polymerization kinetics of ion pairs in equilibrium with unreactive aggregates. As expected, both copolymerizations revealed significantly decreased propagation rates compared to DMSO, leading to a half-life of 17.3 h (AGE) and 7.6 h (EVGE), respectively (Figure S4). The experiment was not carried out to full conversion due to limited measurement time. Nevertheless, the amount

of data points reaching > 70 % conversion ensures a reliable evaluation of reactivity ratios by the Jaacks equation (R^2 of 0.997 (AGE) and 0.992 (EVGE)) (Figure S5). The differences in reactivity between EO and both glycidyl ethers are notably increased in THF in comparison to the polar DMSO system, albeit without affecting the overall trend.
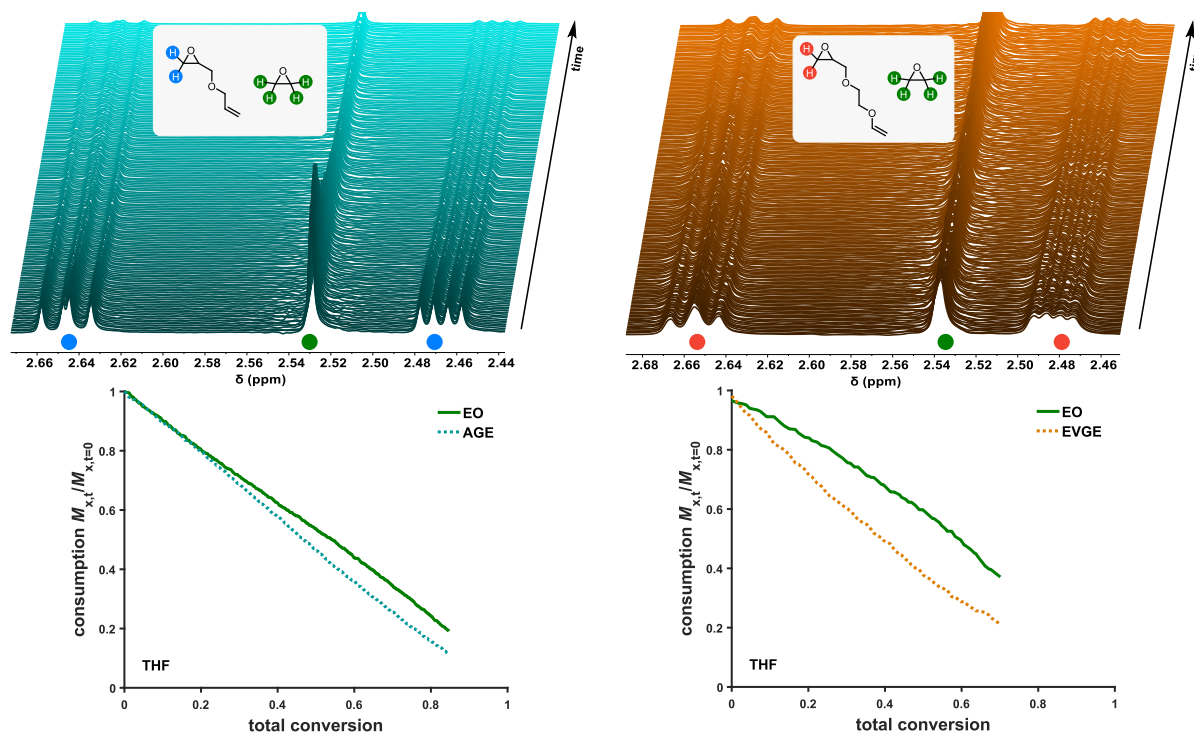

Figure 2. top: *in situ* ^{1}H NMR kinetics in THF-d_8 investigating the anionic copolymerization of P(EO-*co*-AGE) (blue) and P(EO-*co*-EVGE) (red) initiated by potassium phenylmethanolateat 45 °C; bottom: consumption $M_{x,t}/M_{x,t=0}$ versus total conversion of P(EO-*co*-AGE) (blue) and P(EO-*co*-EVGE) (red).

Accordingly, reactivity ratios were determined as $r_{EO}^{THF} = 0.78 \pm 0.001$ and $r_{AGE}^{THF} = 1.29 \pm 0.002$ as well as $r_{EO}^{THF} = 0.48 \pm 0.004$ and $r_{EVGE}^{THF} = 2.05 \pm 0.015$. In THF, both copolymerizations exhibit soft gradient microstructures, illustrated in the molar composition diagrams (Figure S6). In the case of of P(EO-*co*-EVGE) the gradient determines the nature of the terminal units, consisting almost exclusively of EO repeating units. The investigated polymerizations in DMSO as well as THF resulted in polymers of narrow dispersities ($Đ < 1.19$) (Figure S9). A summary of the evaluated reactivity ratios compared to the values reported by Lynd, Hawker et al.[31] (based on the EGD method) is given in Table 1. Comparison of the herein presented results with the reactivity ratios evaluated by the EGD method show a strong discrepancy between the different methods. The end-group dyad (EGD) analysis yields a more pronounced reactivity of the respective glycidyl ethers compared to the established *in situ* methods. These findings are discussed in the following.

Table 1. Reactivity ratios evaluated by *in situ* ^{1}H NMR experiments using the Jaacks method[30] and EGD analysis.[31]

Comonomer	Method	Solvent	r_{EO}	$r_{EO}{}^{err}$	r_{GE}	$r_{GE}{}^{err}$	$r_{EO}*r_{GE}$	R^2
	Jaacks	DMSO	0.92	0.002	1.08	0.002	1.00	0.9995
AGE	Jaacks	THF	0.78	0.001	1.29	0.002	1.00	0.997
	EGD	THF	0.54	0.03	1.31	0.26	0.71	-
	Jaacks	DMSO	0.81	0.001	1.23	0.002	1.00	0.998
EVGE	Jaacks	THF	0.48	0.004	2.05	0.015	1.00	0.992
	EGD	THF	0.32	0.10	3.50	0.90	1.12	-

In addition to the Jaacks equation,[30] the reactivity ratios were evaluated by ideal integrated equation of Meyer-Lowry[20] as well as the Beckingham-Sanoja-Lynd (BSL)[45] method (Table S1 and Figures S7 and S8).

Impact of transition state on monomer reactivity

The described results demonstrate that the influence of cation complexation on monomer reactivities during the polymerization is more pronounced in THF rather than DMSO. Following these findings, we postulate the transient "crown ether-effect" of the investigated glycidyl ethers causing the enhanced reactivity of both glycidyl ethers compared to EO in THF. It is a known phenomenon that the addition of 18 crown-6, a cyclic oligo(ethylene glycol) consisting of six EO repeating units, strongly complexes potassium cations in THF.[46] The distance of two methylene units between the oxygens of 18-crown-6 is similarly found for the three oxygens in EVGE. Based on this rationale, a preferential combined complexation of the potassium cation with EVGE monomer and the alkoxide of the propagating chain via chelation can be hypothesized and investigated by quantum chemistry methods, namely density functional theory (DFT) (Figure 3, right). In contrast, EO exhibits only one coordination site per monomer and therefore a lower complex coordination constant with potassium cations. Consequently, this results in a higher probability to find EVGE rather than EO in the chain segments close to the initiator, explaining the preferential incorporation of EVGE ($r_{EVGE} > r_{EO}$) during chain propagation. The chelation of potassium cations is less pronounced for AGE, as only two possible coordination sites are present in each AGE monomer (Figure 3, center). Therefore, the stability constant of AGE complexes is lower than that of EVGE, but still somewhat higher than for EO, resulting in a merely slightly preferred addition of AGE to the chain end in THF ($r_{AGE} > r_{EO}$). DFT calculations further provide information concerning the geometry of the precursor complexes of the chain ends with the different monomers. The enhanced coordination of the potassium counterion by the monomer going from EO and AGE to EVGE was observed as a local energy minimum. Hence, the inherent entropic benefit is a determining factor for the preferred chelation of the potassium cation.
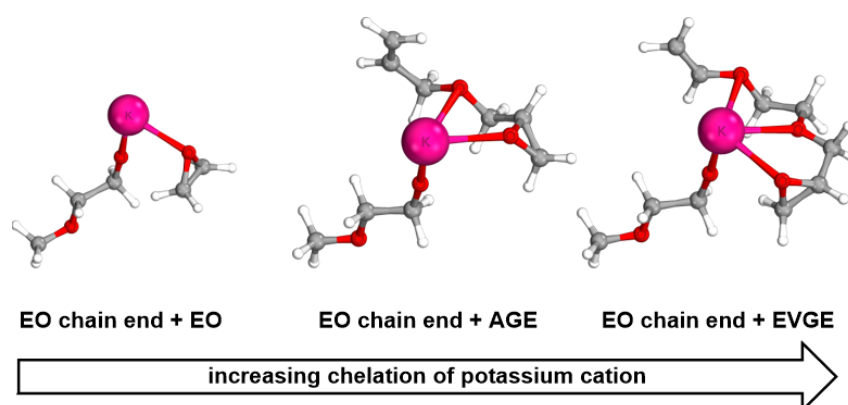
Figure 3. Complexation of potassium by EO chain end with EO, AGE and EVGE calculated by DFT.

Furthermore, we compared the electron densities of the electrophilic methylene groups of the epoxides calculated by DFT, which are attacked by the alkoxide during polymerization. Since the bond angles of the different epoxides and hence the ring strain of the monomers are comparable, the electron density is the pivotal parameter for the monomer reactivity. In Table 2, the partial charges of the three monomers simulated in vacuum as well as in THF and DMSO are given, using the implicit solvation model CPCM.

Table 2. Partial charges of the unsubstituted methylene carbon of the epoxide moiety of the monomers ethylene oxide (EO), allyl glycidyl ether (AGE) and ethoxy vinyl glycidyl ether (EVGE) calculated by DFT without taking solvation into account or rather in THF and DMSO using CPCM.

System	EO	AGE	EVGE
vacuum	-0.285 e	-0.251 e	-0.251 e
THF	-0.275 e	-0.242 e	-0.249 e
DMSO	-0.273 e	-0.240 e	-0.243 e

Both investigated glycidyl ethers exhibit lower electron density at their electrophilic carbon relative to EO. The trend is further decreased for all epoxides with increasing dipole moment of the respective solvent. Consequently, the partial charges give a first indication for preferential incorporation of the glycidyl ethers at the chain end compared to EO. This is in accordance with the observed trend from the *in situ* ^{1}H NMR kinetic experiments. Surprisingly, the unsubstituted methylene carbon of AGE exhibits a higher electrophilicity than the respective carbon of EVGE in all solvents. Considering the afore described reactivity ratios, the potassium complexation of glycidyl ethers appears to be the major contributing factor to the copolymerization kinetics in THF, rather than the electrophilicity itself. These findings suggest that the monomer, but not the respective chain, primarily affects the incorporation with its specific complexation behavior. This further supports the implementation of the non-terminal model for the determination of reactivity ratios by *in situ* ^{1}H NMR measurements.

Additional considerations are required to understand the impact of solvent polarity on the differences of the reactivity ratios in THF and DMSO (r_{GE}^{DMSO} and r_{GE}^{THF}). Compared to THF, DMSO is a solvent with a high dipole moment. The resulting high polarity of the solvent allows an excellent dissolution of ions. Therefore, free ions are the primary active species, which mainly contribute to propagation.[43] The strong solvation effect of DMSO has a documented impact on complexes, e.g. it is known to decrease the stability constants of crown ether complexes.[47] This influence is clearly visible when comparing the reactivity ratios obtained via *in situ* ^{1}H NMR measurements in the different solvents. In DMSO, only a slightly preferred incorporation of EVGE over EO is observed. Therefore, the previously proposed crown ether-effect of EVGE in THF (Figure 3) is less pronounced in the case of DMSO. This is additionally confirmed by the increasing r_{EO} values from THF (0.57) to DMSO (0.81) and the increasing similarity of r_{EVGE}^{DMSO} (1.23) and r_{AGE}^{DMSO} (1.08). The described influence of DMSO is equally observed in the copolymerization of EO with AGE, resulting in an almost ideally random copolymerization with $r_{EO} \approx r_{AGE}$. Similar values of the reactivity ratios were previously reported by our group for the copolymerization of ethoxyethyl glycidyl ether (EEGE) with EO in DMSO under AROP conditions.[18]

In summary, variation of the chemical structure of a glycidyl ether, e.g., the addition of an ethylene glycol spacer at the monomer side chain, has a distinct influence on the behavior of epoxide monomers in copolymerizations with EO and consequently the microstructure of the resulting copolymers. In this context, the choice of solvent thus has a pronounced effect on the copolymerization reaction kinetics.

Comparison of *in situ* kinetics and end-group dyad (EGD) analysis

The presented results describe the reactivities of the epoxide monomers throughout the copolymerization process. When *in situ* kinetic experiments are utilized to monitor the AROP, monomer consumption is observed over time and translated to reactivity ratios by non-terminal evaluation methods, such as the herein applied Jaacks[30] or the Beckingham-Sanoja-Lynd (BSL)[45] method or alternatively the ideal integrated copolymerization equation.[20,48] On the contrary, the ^{1}H NMR EGD analysis by Lynd, Hawker and coworkers relies on the splitting of the benzylic proton signals based on the dyads formed directly upon initiation of the polymer chain. In this manner, the reactivity of the initiator towards the first monomer and the following initiator-monomer adduct towards the second monomer can be quantified via ^{1}H NMR EGD analysis in a simple manner. However, the reactivity ratio r_{EVGE}^{THF} determined via EGD analysis (3.50) significantly differs from r_{EVGE}^{THF} obtained via our *in situ* ^{1}H NMR spectroscopy measurements (2.05). Furthermore, the product of r_{EVGE} and r_{EO} deviates from unity in the case of the EGD method (Table 1) and therefore contradicts the assumption of a non-terminal model. The latter is surprising, as non-terminal-based methods were successfully implemented for various copolymerizations of EO and glycidyl ethers.[18,24,29] To explain these contradictory results, the presence of chain end-dependent polymerization kinetics can be emphasized at the beginning of the copolymerization process. As mentioned by Kazanskii et al., an auto-acceleration of the EO homopolymerization kinetics in THF is observed at low monomer conversion, until a critical number of repeating units is

reached. At this point, the polymerization process becomes stationary. These peculiar kinetics are explained by the poor solubility of alkoxides in THF: A sufficient chain length must be reached to permit the abovementioned multidentate chelation of the potassium cation via the backbone ether oxygens and the subsequent full dissolution of the oligo-PEO.[34] A similar behavior is highly probable for the copolymerization of EVGE and EO. The nucleophilic attack of the initiator at an EVGE monomer (I-EVGE) results in a product with four ether oxygens. Therefore, the coordination sites of the potassium cation can be saturated by at least three oxygens of the EVGE chain end, increasing the solubility of I-EVGE. Multidentate chelation of I-EVGE is supported by the implemented DFT calculations of the initiator-monomer adducts (Figure 4) and suggests a preferred addition of EVGE over EO to the initiator. A similar rationale can be considered for the AGE adduct, even though only two oxygens (chain end and side chain ether oxygen) coordinate the potassium cation, as observed via DFT calculations (Figure 4). Therefore, the additional oxygen of EVGE compared to AGE results in an enhanced complexation behavior and supports the preferred incorporation of EVGE. In the case of the initiator-EO adduct, due to the lack of side-chain ether oxygens, only weak coordination with the oxygen of the initiator is present. The overestimation of the reactivity gap of EO and AGE by the EGD method compared to our findings support the conclusion that the side-chain ether oxygens of glycidyl ethers result in an enhanced crown ether-effect compared to the single oxygen of the initiator.

Initiator-AGE Adduct

Initiator-EO Adduct   **Initiator-EVGE Adduct**
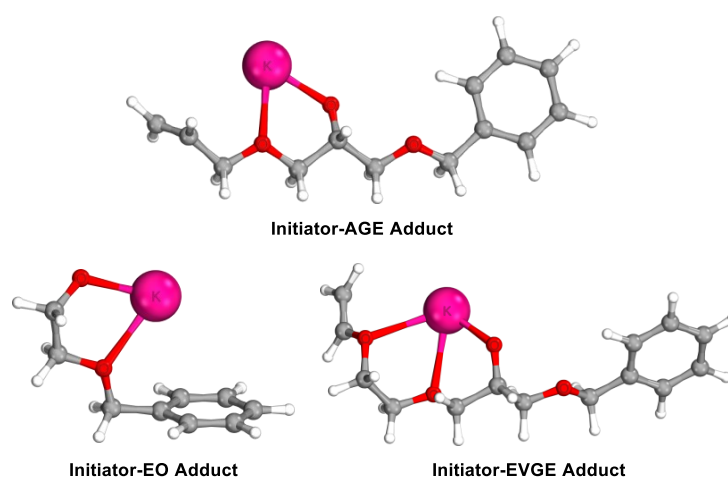
Figure 4. Complexation of potassium cation by initiator-monomer adducts calculated by DFT.

Following this line of thought, the coordination of the addition product and an additional EVGE monomer further saturates the complexation sites of the potassium cation, independent of an EO or EVGE chain end. In both cases, the addition of the second EVGE monomer would allow for a better solubility of the chain due the multidentate chelation observed by Kazanskii et al..[34]

Having reached a critical conversion, the polymer chains are solubilized, because the polyether chain possesses a sufficient length, and subsequent multidentate chelation with the potassium cation occurs (Figure 5 and Figure S10).[34] At this point, the copolymerization becomes merely

monomer-dependent, resulting in the non-terminal polymerization kinetics discussed above. These considerations are supported by the aforementioned successful implementation of the Jaacks method. A similar behavior is observed for copolymerizations in DMSO, although the enhanced ion dissolution in the more polar solvent reduces the proposed crown ether-effect, resulting in less pronounced reactivity disparity between EO and both glycidyl ethers. Based on this explanation, it is important to note that the complexation of the cation by the monomer remains in equilibrium with the coordination of the backbone. However, r_{GE} determined via *in situ* ^{1}H NMR spectroscopy in THF shows a slightly preferred complexation by the monomer rather than the polyether backbone, underlined by the observation that r_{EO} and r_{GE} are not approaching equality ($r_{EO} \neq r_{GE}$).

Initiator-EVGE Adduct + EVGE   **Initiator-(EO)$_3$ Adduct + EVGE**
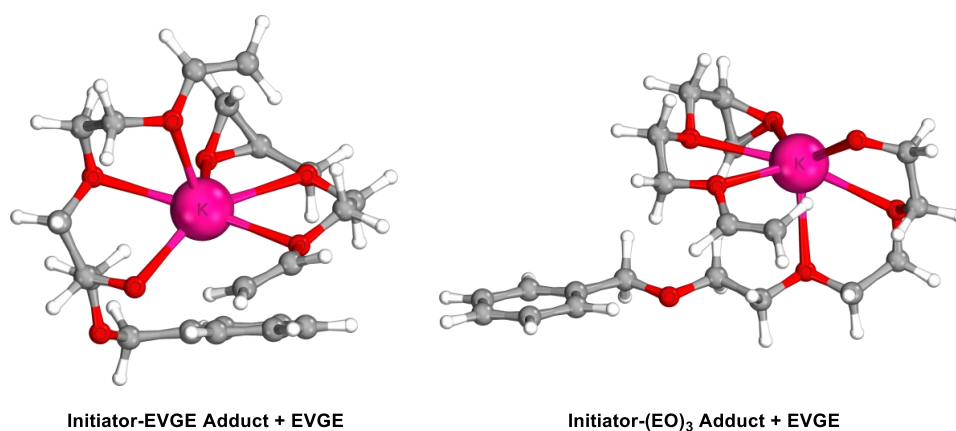
Figure 5. Complexation of potassium cation via EVGE chain end and EVGE monomer (left) and polyether backbone and EVGE monomer (right).

These considerations underline the observation of the pronounced presence of EVGE repeating units near the initiator compared to the residual polymer chain, resulting in differing reactivity ratios observed via EGD and *in situ* ^{1}H NMR analysis. As a result, EGD analysis is exclusively applicable in the beginning of the copolymerization. Vice versa, determination of the compositional drift is not feasible by the employed EGD method.

Only a single *in situ* experiment is necessary to obtain reliable and reproducible reactivity ratios in case of *in situ* ^{1}H NMR spectroscopy. The integration of the overlapping signals of the benzylic protons in the EGD analysis is prone to errors as it relies on a user-dependent estimation. *In situ* ^{1}H NMR monitoring ultimately provides normalized data determined by a constant integration area, which eliminates possible errors.

CONCLUSION

With this study we aim at a general understanding of the anionic ring-opening copolymerization kinetics of ethylene oxide (EO) with glycidyl ethers (GE) via online ^{1}H NMR measurements. Allyl glycidyl ether (AGE) and ethoxy vinyl glycidyl ether (EVGE) were chosen as typical and synthetically valuable representatives of glycidyl ether monomers, and copolymerization was carried out either in THF or DMSO. Online ^{1}H NMR kinetics enables *in situ* monitoring of monomer consumption, leading to precise and reliable determination of reactivity ratios by common non-terminal models. Both investigated glycidyl ethers exhibited slightly higher reactivity ratios than EO in DMSO as well as in THF, while the difference increased with reduced solvent polarity. These results emphasize the crown ether-effect and the underlying multidentate cation complexation as the driving force for the enhanced reactivity of glycidyl ethers compared to EO in the anionic copolymerization. The impact of the crown ether-like complexation consequently increased with reduced cation dissociation in less polar media on going from DMSO to THF. Supplementary calculations by density functional theory (DFT) support the presented crown ether-effect, showing the stronger complexation with increasing number of oxygen atoms comparing EO with ethylene glycol spacer containing GEs (EO < AGE < EVGE). Furthermore, the superiority of *in situ* ^{1}H NMR kinetics over end-group dyad (EGD) analysis for the evaluation of reactivity ratios with non-terminal models has been demonstrated. In general, the EGD analysis is strongly affected by the limited solubility of the initiator and the respective first comonomer pair. Consequently, this method enables the exclusive investigation of the reactivity of the applied monomers at the beginning of polymerization rather than the determination of true reactivity ratios of the considered copolymerization process at any given time.

Overall, the results disclose the underlying effects of the slightly preferred glycidyl ether incorporation over EO. This is crucial for the design of glycidyl ether-based copolymerizations, since the resulting microstructure is tunable by choice of solvent as well as the introduction of ethylene glycol spacers in the monomer structures. The monomer gradient governs the behavior of the resulting materials in bulk or solution. In summary, our results manifest the importance of *in situ* experiments for in-depth analysis of epoxide copolymerizations and demonstrate that there is no simple shortcut to determine reactivity ratios.

REFERENCES

(1) Steube, M.; Johann, T.; Galanos, E.; Appold, M.; Rüttiger, C.; Mezger, M.; Gallei, M.; Müller, A. H. E.; Floudas, G.; Frey, H. Isoprene/Styrene Tapered Multiblock Copolymers with up to Ten Blocks: Synthesis, Phase Behavior, Order, and Mechanical Properties. *Macromolecules* **2018**, *51*, 10246–10258.

(2) Grune, E.; Johann, T.; Appold, M.; Wahlen, C.; Blankenburg, J.; Leibig, D.; Müller, A. H. E.; Gallei, M.; Frey, H. One-Step Block Copolymer Synthesis versus Sequential Monomer Addition: A Fundamental Study Reveals That One Methyl Group Makes a Difference. *Macromolecules* **2018**, *51*, 3527–3537.

(3) Hodrokoukes, P.; Floudas, G.; Pispas, S.; Hadjichristidis, N. Microphase Separation in Normal and Inverse Tapered Block Copolymers of Polystyrene and Polyisoprene. 1. Phase State. *Macromolecules* **2001**, *34*, 650–657.

(4) Lach, R.; Weidisch, R.; Knoll, K. Morphology and mechanical properties of binary triblock copolymer blends. *J. Polym. Sci. B Polym. Phys.* **2005**, *43*, 429–438.

(5) Singh, N.; Tureau, M. S.; Epps, T. H. Manipulating ordering transitions in interfacially modified block copolymers. *Soft Matter* **2009**, *5*, 4757.

(6) Thunga, M.; Staudinger, U.; Satapathy, B. K.; Weidisch, R.; Abdel-Goad, M.; Janke, A.; Knoll, K. Influence of molecular architecture of S-S/B-S triblock copolymers on rheological properties. *J. Polym. Sci. B Polym. Phys.* **2006**, *44*, 2776–2788.

(7) Steube, M.; Johann, T.; Plank, M.; Tjaberings, S.; Gröschel, A. H.; Gallei, M.; Frey, H.; Müller, A. H. E. Kinetics of Anionic Living Copolymerization of Isoprene and Styrene Using *in Situ* NIR Spectroscopy: Temperature Effects on Monomer Sequence and Morphology. *Macromolecules* **2019**, *52*, 9299–9310.

(8) Korotkov, A. A.; Rakova, G. V. The copolymerization of isoprene and styrene with butyllithium as catalyst. *Polymer Science U.S.S.R.* **1962**, *3*, 990–1000.

(9) Price, C. C.; Atarashi, Y.; Yamamoto, R. Polymerization and copolymerization of some epoxides by potassium tert-butoxide in DMSO. *J. Polym. Sci. A-1 Polym. Chem.* **1969**, *7*, 569–574.

(10) Stolarzewicz, A.; Becker, H.; Wagner, G. Zum Einfluß von Elektronendonatoren auf die anionische Copolymerisation von Oxiranen. *Acta Polym.* **1980**, *31*, 743–745.

(11) Heatley, F.; Yu, G.-e.; Booth, C.; Blease, T. G. Determination of reactivity ratios for the anionic copolymerization of ethylene oxide and propylene oxide in bulk. *European Polymer Journal* **1991**, *27*, 573–579.

(12) Mangold, C.; Dingels, C.; Obermeier, B.; Frey, H.; Wurm, F. PEG-based Multifunctional Polyethers with Highly Reactive Vinyl-Ether Side Chains for Click-Type Functionalization. *Macromolecules* **2011**, *44*, 6326–6334.

(13) Reuss, V. S.; Obermeier, B.; Dingels, C.; Frey, H. *N,N*-Diallylglycidylamine: A Key Monomer for Amino-Functional Poly(ethylene glycol) Architectures. *Macromolecules* **2012**, *45*, 4581–4589.

(14) Steube, M.; Johann, T.; Hübner, H.; Koch, M.; Dinh, T.; Gallei, M.; Floudas, G.; Frey, H.; Müller, A. H. E. Tetrahydrofuran: More than a "Randomizer" in the Living Anionic Copolymerization of Styrene and Isoprene: Kinetics, Microstructures, Morphologies, and Mechanical Properties. *Macromolecules* **2020**, *53*, 5512–5527.

(15) Kim, J. M.; Chakrapani, S. B.; Beckingham, B. S. Tuning Compositional Drift in the Anionic Copolymerization of Styrene and Isoprene. *Macromolecules* **2020**, *53*, 3814–3821.

(16) Natalello, A.; Werre, M.; Alkan, A.; Frey, H. Monomer Sequence Distribution Monitoring in Living Carbanionic Copolymerization by Real-Time ^{1}H NMR Spectroscopy. *Macromolecules* **2013**, *46*, 8467–8471.

(17) Obermeier, B.; Wurm, F.; Frey, H. Amino Functional Poly(ethylene glycol) Copolymers via Protected Amino Glycidol. *Macromolecules* **2010**, *43*, 2244–2251.

(18) Herzberger, J.; Leibig, D.; Liermann, J. C.; Frey, H. Conventional Oxyanionic versus Monomer-Activated Anionic Copolymerization of Ethylene Oxide with Glycidyl Ethers: Striking Differences in Reactivity Ratios. *ACS Macro Lett.* **2016**, *5*, 1206–1211.

(19) Herzberger, J.; Kurzbach, D.; Werre, M.; Fischer, K.; Hinderberger, D.; Frey, H. Stimuli-Responsive Tertiary Amine Functional PEGs Based on *N,N*-Dialkylglycidylamines. *Macromolecules* **2014**, *47*, 7679–7690.

(20) Blankenburg, J.; Kersten, E.; Maciol, K.; Wagner, M.; Zarbakhsh, S.; Frey, H. The poly(propylene oxide-*co*-ethylene oxide) gradient is controlled by the polymerization method: determination of reactivity ratios by direct comparison of different copolymerization models. *Polymer chemistry* **2019**, *10*, 2863–2871.

(21) Blankenburg, J.; Maciol, K.; Hahn, C.; Frey, H. Poly(ethylene glycol) with Multiple Aldehyde Functionalities Opens up a Rich and Versatile Post-Polymerization Chemistry. *Macromolecules* **2019**, *52*, 1785–1793.

(22) Niederer, K.; Schüll, C.; Leibig, D.; Johann, T.; Frey, H. Catechol Acetonide Glycidyl Ether (CAGE): A Functional Epoxide Monomer for Linear and Hyperbranched Multi-Catechol Functional Polyether Architectures. *Macromolecules* **2016**, *49*, 1655–1665.

(23) Zhang, W.; Allgaier, J.; Zorn, R.; Willbold, S. Determination of the Compositional Profile for Tapered Copolymers of Ethylene Oxide and 1,2-Butylene Oxide by *in situ*-NMR. *Macromolecules* **2013**, *46*, 3931–3938.

(24) Verkoyen, P.; Dreier, P.; Bros, M.; Hils, C.; Schmalz, H.; Seiffert, S.; Frey, H. "Dumb" pH-Independent and Biocompatible Hydrogels Formed by Copolymers of Long-Chain Alkyl Glycidyl Ethers and Ethylene Oxide. *Biomacromolecules* **2020**, *21*, 3152–3162.

(25) Homann-Müller, T.; Rieger, E.; Alkan, A.; Wurm, F. R. *N*-Ferrocenylsulfonyl-2-methylaziridine: the first ferrocene monomer for the anionic (co)polymerization of aziridines. *Polymer chemistry* **2016**, *7*, 5501–5506.

(26) Rieger, E.; Alkan, A.; Manhart, A.; Wagner, M.; Wurm, F. R. Sequence-Controlled Polymers via Simultaneous Living Anionic Copolymerization of Competing Monomers. *Macromolecular rapid communications* **2016**, *37*, 833–839.

(27) Rieger, E.; Blankenburg, J.; Grune, E.; Wagner, M.; Landfester, K.; Wurm, F. R. Controlling the Polymer Microstructure in Anionic Polymerization by Compartmentalization. *Angewandte Chemie (International ed. in English)* **2018**, *57*, 2483–2487.

(28) Gleede, T.; Markwart, J. C.; Huber, N.; Rieger, E.; Wurm, F. R. Competitive Copolymerization: Access to Aziridine Copolymers with Adjustable Gradient Strengths. *Macromolecules* **2019**, *52*, 9703–9714.

(29) Herzberger, J.; Fischer, K.; Leibig, D.; Bros, M.; Thiermann, R.; Frey, H. Oxidation-Responsive and "Clickable" Poly(ethylene glycol) via Copolymerization of 2-(Methylthio)ethyl Glycidyl Ether. *Journal of the American Chemical Society* **2016**, *138*, 9212–9223.

(30) Jaacks, V. A Novel Method of Determination of Reactivity Ratios in Binary and Ternary Copolymerizations. *Makromol. Chem.* **1972**, *161*, 161–172.

(31) Lee, B. F.; Wolffs, M.; Delaney, K. T.; Sprafke, J. K.; Leibfarth, F. A.; Hawker, C. J.; Lynd, N. A. Reactivity ratios, and mechanistic insight for anionic ring-opening copolymerization of epoxides. *Macromolecules* **2012**, *45*, 3722–3731.

(32) Lee, A.; Lundberg, P.; Klinger, D.; Lee, B. F.; Hawker, C. J.; Lynd, N. A. Physiologically relevant, pH-responsive PEG-based block and statistical copolymers with N,N-diisopropylamine units. *Polymer chemistry* **2013**, *4*, 5735–5742.

(33) Majdanski, T. C.; Vitz, J.; Meier, A.; Brunzel, M.; Schubert, S.; Nischang, I.; Schubert, U. S. "Green" ethers as solvent alternatives for anionic ring-opening polymerizations of ethylene oxide (EO): *In-situ* kinetic and advanced characterization studies. *Polymer* **2018**, *159*, 86-94.

(34) Kazanskii, K. S.; Solovyanov, A. A.; Entelis, S. G. Polymerization of ethylene oxide by alkali metal-naphthalene complexes in tetrahydrofuran. *European Polymer Journal* **1971**, *7*, 1421–1433.

(35) Ptitsyna, N.V.; Kazakevich, V.K.; Kazanskii, K.S. Conductometric study of "live" polyethylene oxide and its models. *Polymer Science U.S.S.R.* **1977**, *19*, 3218–3224.

(36) Solov'yanov, A. A.; Kazanskii, K. S. The kinetics and mechanism of anionic polymerization of ethylene oxide in ether solvents. *Polymer Science U.S.S.R.* **1972**, *14*, 1186–1195.

(37) Bawn, C.E.H.; Ledwith, A.; McFarlane, N. R. Anionic polymerization in dimethyl sulphoxide. *Polymer* **1967**, *8*, 484–487.

(38) Bawn, C.E.H.; Ledwith, A.; McFarlane, N. Anionic polymerization of ethylene oxide in dimethyl sulphoxide. *Polymer* **1969**, *10*, 653–659.

(39) Price, C. C.; Akkapeddi, M. K. Kinetics of base-catalyzed polymerization of epoxides in dimethyl sulfoxide and hexamethylphosphoric triamide. *J. Am. Chem. Soc.* **1972**, *94*, 3972–3975.

(40) Price, C. C.; Carmelite, D. D. Reactions of Epoxides in Dimethyl Sulfoxide Catalyzed by Potassium *t*-Butoxide. *J. Am. Chem. Soc.* **1966**, *88*, 4039–4044.

(41) Solov'yanov, A. A.; Kazanskii, K. S. Polymerization of ethylene oxide in dimethyl sulphoxide (DMS). *Polymer Science U.S.S.R.* **1972**, *14*, 1196–1206.

(42) Figueruelo, J. E.; Worsfold, D. J. The anionic polymerization of ethylene oxide in hexamethyl phosphoramide. *European Polymer Journal* **1968**, *4*, 439–444.

(43) Kazanskii, K. S.; Solovyanov, A. A.; Dubrovsky, S. A. Some Remarks to the Kinetics of Anionic Polymerization of Ethylene Oxide in Dimethyl Sulfoxide. *Makromol. Chem.* **1978**, *179*, 969–973.

(44) Penczek, S.; Cypryk, M.; Duda, A.; Kubisa, P.; Slomkowski, S. Living ring-opening polymerizations of heterocyclic monomers. *Progress in Polymer Science* **2007**, *32*, 247–282.

(45) Beckingham, B. S.; Sanoja, G. E.; Lynd, N. A. Simple and Accurate Determination of Reactivity Ratios Using a Nonterminal Model of Chain Copolymerization. *Macromolecules* **2015**, *48*, 6922–6930.

(46) Ding, J.; Heatley, F.; Price, C.; Booth, C. Use of crown ether in the anionic polymerization of propylene oxide—2. Molecular weight and molecular weight distribution. *European Polymer Journal* **1991**, *27*, 895–899.

(47) Solov'ev, V. P.; Strakhova, N. N.; Raevsky, O. A.; Rüdiger, V.; Schneider, H.-J. Solvent Effects on Crown Ether Complexations. *J. Org. Chem.* **1996**, *61*, 5221–5226.

(48) Meyer, V. E.; Lowry, G. G. Integral and differential binary copolymerization equations. *J. Polym. Sci. A Gen. Pap.* **1965**, *3*, 2843–2851.

SUPPORTING INFORMATION

Materials and Experimental Procedures

Reagent and Equipment

All chemicals and solvents were purchased from *Acros Organics*, *TCI*, *Sigma-Aldrich* and *Fluka*. Deuterated solvents were received from *Deutero GmbH*. Ethyl vinyl glycidyl ether (EVGE) was synthesized according to the procedure established by our group in 2011.[1] Allyl glycidyl ether (AGE) was purchased from *TCI* and purified before use by fractional distillation. Both glycidyl ethers were dried prior to the experiments by cryo-transfer after stirring over CaH_2 for 30 min.

In situ ^{1}H NMR Kinetic Experiments

Online ^{1}H NMR kinetic measurements were performed according to a protocol by Herzberger et al.[2] in a *Norell S-500-VT-7* NMR tube. The *in situ* ^{1}H NMR spectra were recorded on a Bruker Avance III HD 400 MHz spectrometer equipped with a 5 mm BBFO SmartProbe. An exemplary protocol for P(EO-*co*-AGE) in DMSO-d_6 is described in the following, other experiments were performed equivalently. KO*t*Bu (24.6 mg, 219 μmol) was dissolved in a THF/water mixture and transferred in a flame-dried Schlenk flask equipped with a septum and stop cock. Benzyl alcohol (24.9 mg, 23.9 μl, 230 μmol) was dissolved in benzene and added to the base solution. After slow evaporation of the solvent under high vacuo, the initiator salt was dried at 60 °C under high vacuum. The dried initiator salt was then dissolved in 1.12 ml DMSO-d_6 and stirred for 30 min. Concurrently, EO (0.05 ml, 23 eq) was cryo-transferred to the evacuated NMR tube attached to the Schlenk-line under static vacuum at -50 °C with an acetone/nitrogen bath. Subsequently, 0.21 ml of the initiator solution and AGE (0.11 ml, 20 eq) were transferred to the NMR tube under an inert argon-atmosphere. The reaction mixture was then cooled by liquid nitrogen, evacuated and finally sealed with a Teflon stop cock. The reaction mixture was warmed to room temperature, shaken vigorously to ensure a homogenous solution and placed in the preheated (45 °C) NMR spectrometer. One spectrum every 30 sec. was recorded in DMSO-d_6 with one scan after the temperature was stable ($T = \pm 0.1$ K). In THF, spectra were recorded in a 10 min interval. The experimental data was analyzed by using NIREVAL software from Johann, Steube and Frey.[3]

Note regarding ethylene oxide: EO is a highly flammable and toxic gas. It therefore has to be handled with care and the necessary precautions. The addition of EO throughout this study was carried out in a reproducible procedure. Yet, small deviations in the measured volumes are possible considering the very small amounts utilized (< 0.1 ml). The evaluated reaction times depend on the overall concentration, which may therefore vary with each measurement. The targeted monomer ratios might differ to a small extent as well.

DFT Calculations

DFT calculations were performed on MOGON II at the high-performance computing center of the Johannes Gutenberg University Mainz using ORCA 4.2.1. software.[4,5] The B3LYP hybrid density functionals[6,7] were used as the calculation of the analytical Hessian matrix is available. Furthermore, the D3BJ[8,9] atom-pairwise dispersion correction to the DFT energy with Becke-Johnson damping was enabled. The def2-TZVP valence triple-zeta basis set[10,11] was selected and for an accurate single point energy TightSCF was chosen together with a Grid6 integration grid. The RIJCOSX approximation[12] was implemented together with a GridX8 for accurate geometry optimization, as it offers large accelerations. Finally, geometrical Counterpoise Corrections (gCP)[13] were enabled to prevent artificial overbinding effects. To take solvation into account, the implicit solvation model of the conductor-like polarizable continuum (CPCM)[14] simulating the solvate in a solvent cavity was utilized where appropriate. Furthermore, the maximum amount of memory to be used for integral buffering was defined by %maxcore and parallel jobs were invoked by %pal nprocs. The number of parallel jobs was set to the threefold of the number of atoms. The SCF calculations were specified in terms of their integral direct integration, by a maximal number of iterations and by a very tight convergence as threshold. An exemplary ORCA inputfile allowing the calculation of a local energy minimum is shown below:

!B3LYP D3BJ def2-TZVP CPCM(*solvent*) TightSCF RIJCOSX Opt Grid6 NoFinalGrid GridX8 FREQ NORMALPRINT GCP(DFT/TZ)

%maxcore *8000*

%PAL NPROCS 64 END

%scf MaxIter *2000*

SCFMode Direct

Convergence VeryTight

End

* xyzfile *Charge Multiplicity 3d_coordinates.xyz*

Size Exclusion Chromatography

Size exclusion chromatography (SEC) measurements were performed in dimethylformamide (DMF) with 1 g L^{-1} lithium bromide as an eluent at 50 °C. An Agilent 1100 Series was used, equipped with HEMA 300/100/40 columns, and calibration was carried out using polyethylene glycol (PEG) standards, both provided by *Polymer Standard Service* (PSS), Mainz.

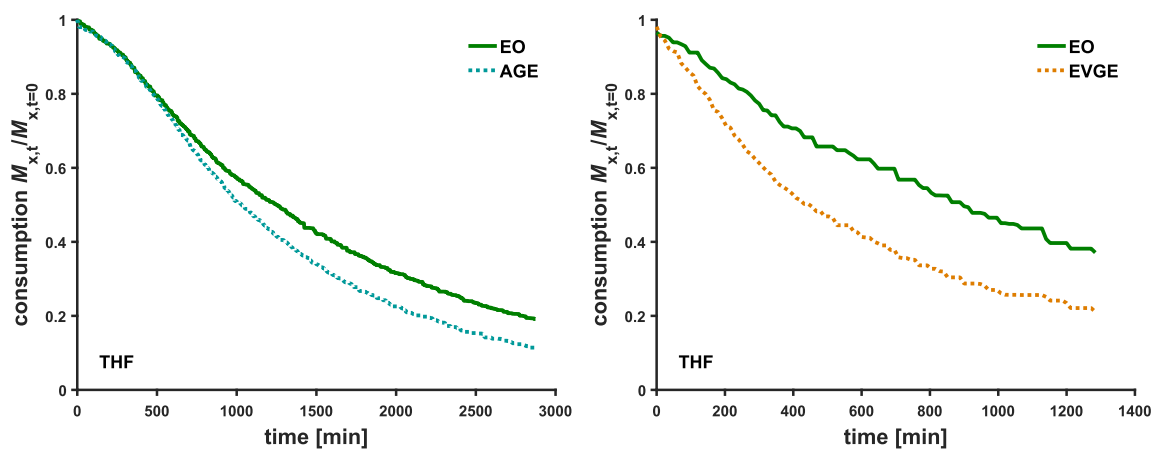**Results of *in situ* ^{1}H NMR Kinetic Experiments**
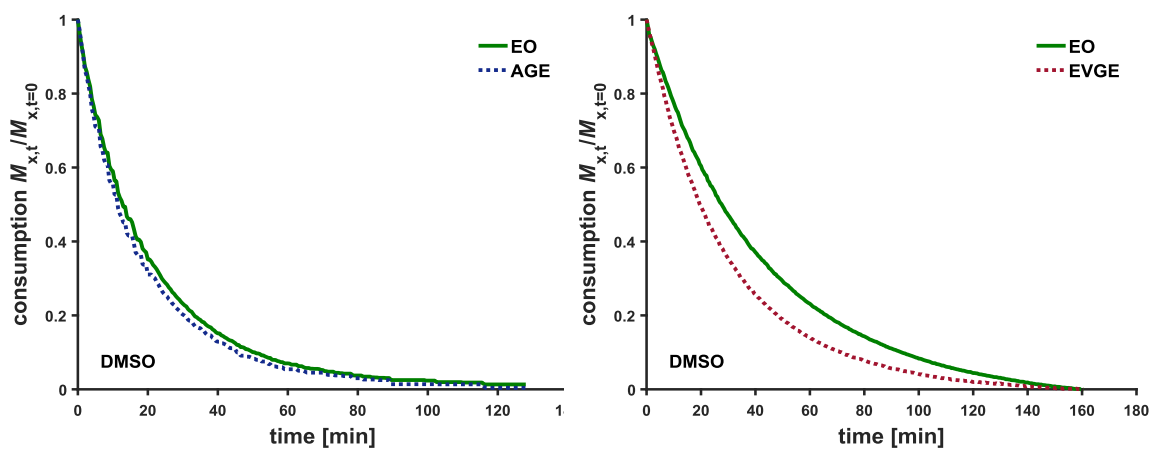
Figure S1. Time-conversion plot of of the copolymerization of EO with AGE (left) and with-EVGE (right) determined via *in situ* ^{1}H NMR kinetics in DMSO-d_6 at 45 °C.
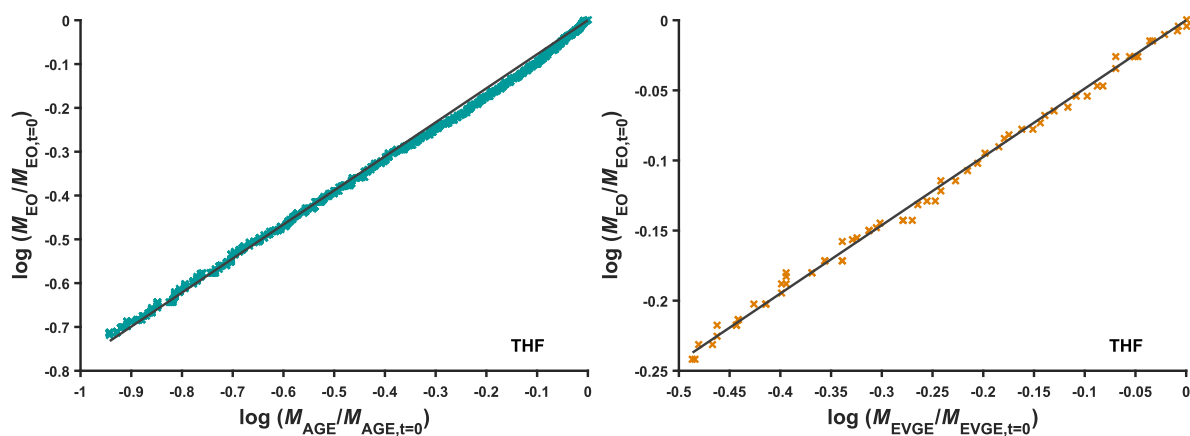

Figure S2. Jaacks plot for the copolymerization of EO with AGE (left, R^2 = 0.99) and with EVGE (right, R^2 = 0.99) determined via *in situ* ^{1}H NMR kinetics in DMSO-d_6 at 45 °C.
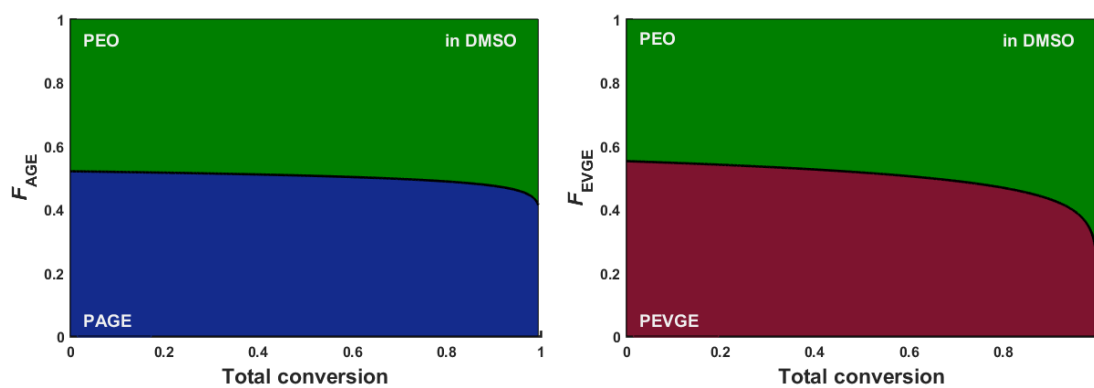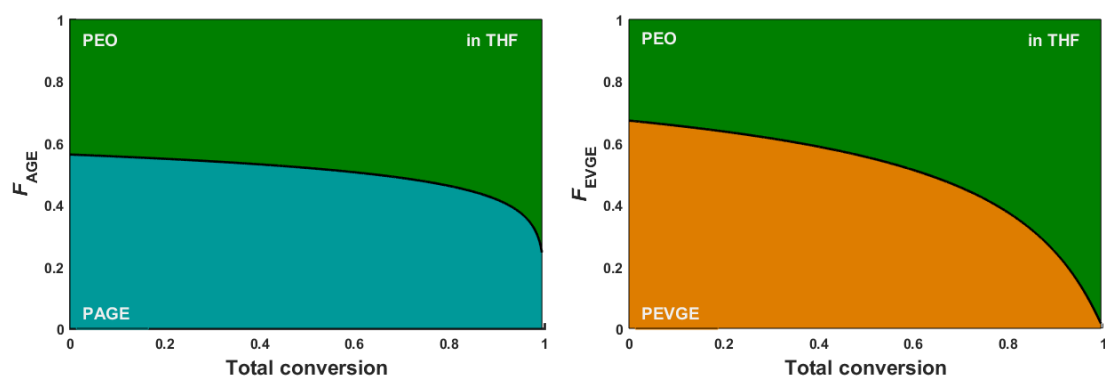
Figure S3. Molar-based composition diagram of P(EO-*co*-AGE) (left) and P(EO-*co*-EVGE) (right) in DMSO-d_6 with an initial equimolar ratio; F_{AGE} = AGE incorporation, F_{EVGE} = EVGE incorporation.

Figure S4. Time-conversion plot of the copolymerization of EO with AGE (left) and with-EVGE (right), determined via *in situ* ^{1}H NMR kinetics in THF-d_8 at 45 °C.

Figure S5. Jaacks plot for the copolymerization of EO with AGE (left, $R^2 = 0.99$) and with EVGE (right, $R^2 = 0.99$) determined via *in situ* ^{1}H NMR kinetics in THF-d_8 at 45 °C.

Figure S6. Molar-based composition diagram of P(EO-*co*-AGE) (left) and P(EO-*co*-EVGE) (right) in THF-d_8 with an initial equimolar monomer ratio; F_{AGE} = AGE incorporation, F_{EVGE} = EVGE incorporation.

Table S1. Reactivity ratios r_{EO} and r_{GE} from *in situ* ^{1}H NMR spectroscopy of the copolymerization of EO with AGE and EVGE evaluated by implementation of Jaacks,[15] Meyer-Lowry ideal integrated,[16] Beckingham-Sanoja-Lynd (BSL)[17] and end group dyad analysis (EGD).[18]

Method	Comonomer	Solvent	r_{EO}	r_{EO}^{err}	r_{GE}	r_{GE}^{err}	$r_{EO}*r_{GE}$
Jaacks			0.92	0.002	1.08	0.002	1.000
Meyer-Lowry ideal	AGE	DMSO	0.91	0.003	1.09	0.004	1.000
BSL			0.91	0.003	1.10	0.003	1.002
Jaacks			0.78	0.001	1.29	0.002	1.000
Meyer-Lowry ideal	AGE	THF	0.76	0.002	1.31	0.004	1.000
BSL			0.79	0.002	1.25	0.004	0.990
EGD			0.54	0.03	1.31	0.26	0.71
Jaacks			0.81	0.001	1.23	0.002	1.00
Meyer-Lowry ideal	EVGE	DMSO	0.80	0.003	1.25	0.007	1.00
BSL			0.79	0.002	1.27	0.002	1.01
Jaacks			0.48	0.004	2.05	0.015	1.00
Meyer-Lowry ideal	EVGE	THF	0.48	0.01	2.08	0.03	1.00
BSL			0.49	0.002	2.04	0.02	1.00
EGD			0.32	0.10	3.50	0.90	1.12
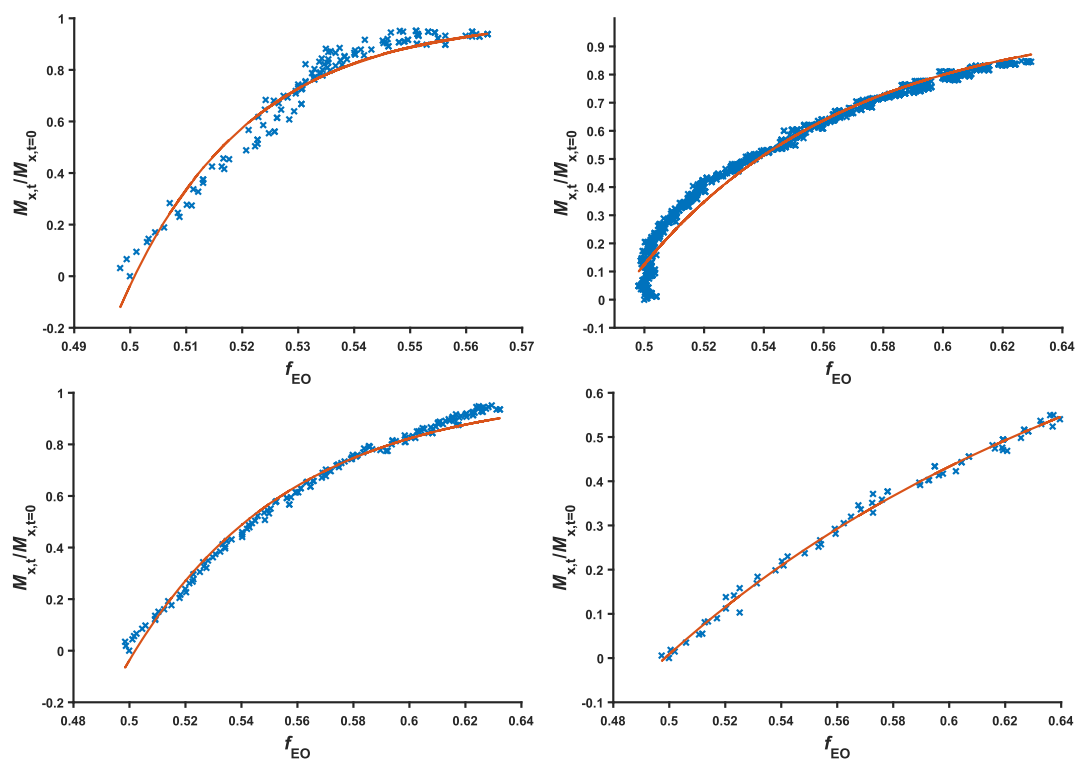
Figure S7. Ideal integrated equation fits of P(EO-*co*-AGE) (top) and P(EO-*co*-EVGE) (bottom) in DMSO (left) and THF (right) determined via *in situ* ^{1}H NMR kinetics at 45 °C.
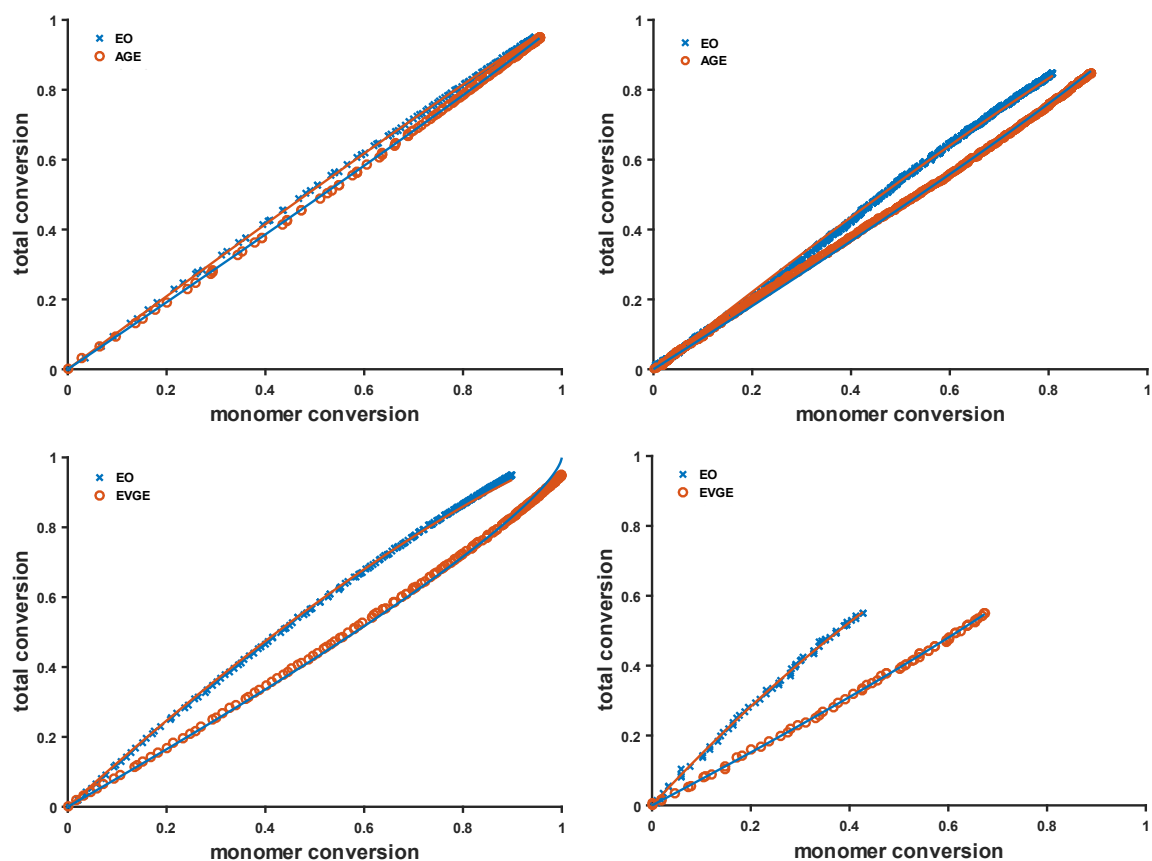
Figure S8. Beckingham-Sanoja-Lynd (BSL) fits of P(EO-*co*-AGE) (top) and P(EO-*co*-EVGE) (bottom) in DMSO (left) and THF (right) determined via *in situ* ^{1}H NMR kinetics at 45 °C.

Molecular Weight Distribution of Copolymers Prepared

The SEC traces of the *in situ* ^{1}H NMR kinetic show molecular weight distribution from 3000 to 3700 g mol^{-1} with dispersities ranging from 1.08 to 1.19 (Figure S9). Please note that the samples were formed in the NMR tube. In the case of the THF samples, high molecular weight shoulders can be observed, which can be explained by the presence of traces of water in the polymerization process. However, the presence of water has no influence on the concentration of active chain-ends and the monomer consumption. Therefore, online monitoring results regarding monomer consumption via *in situ* ^{1}H NMR measurements are independent of the dispersity of the samples.
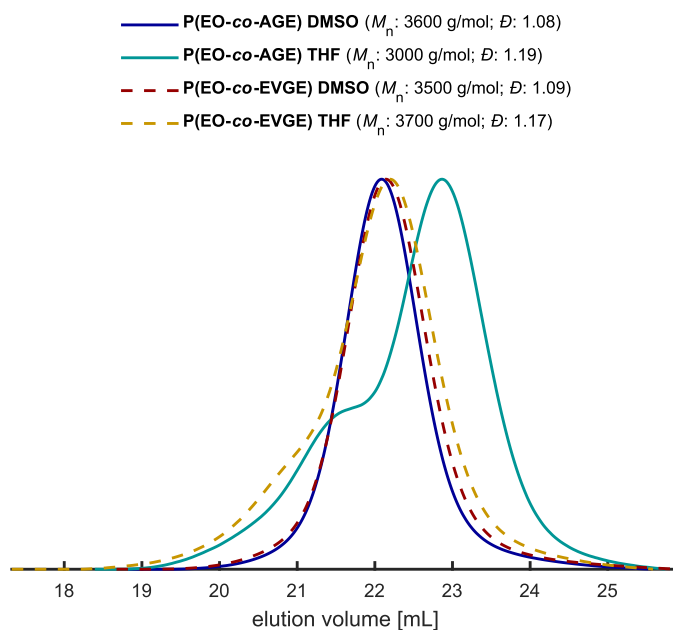
Figure S9. SEC traces of P(EO-*co*-AGE) and P(EO-*co*-EVGE) copolymers synthesized in DMSO-d_6 und THF-d_8 at 45 °C (solvent: DMF, standard: PEG).

Supplementary DFT Calculations
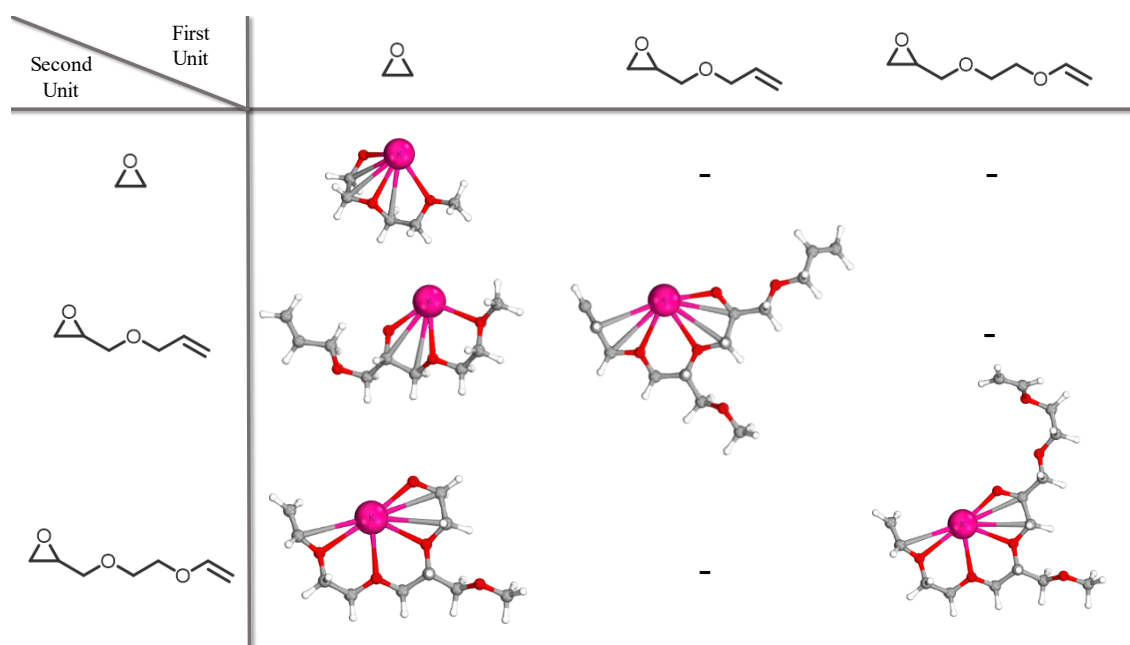
Figure S10. Complexation of the potassium counterion within the two penultimate monomer units. Potassium methanolate was utilized as a model initiator for this simulation. The multidentate chelation with the potassium counterion is shown for combined incorporated monomer units, visualizing the comparably poor complexation by solely EO repeating units.

REFERENCES

(1) Mangold, C.; Dingels, C.; Obermeier, B.; Frey, H.; Wurm, F. PEG-based Multifunctional Polyethers with Highly Reactive Vinyl-Ether Side Chains for Click-Type Functionalization. *Macromolecules* **2011**, *44*, 6326–6334.

(2) Herzberger, J.; Leibig, D.; Liermann, J. C.; Frey, H. Conventional Oxyanionic versus Monomer-Activated Anionic Copolymerization of Ethylene Oxide with Glycidyl Ethers: Striking Differences in Reactivity Ratios. *ACS Macro Lett.* **2016**, *5*, 1206–1211.

(3) Steube, M.; Johann, T.; Plank, M.; Tjaberings, S.; Gröschel, A. H.; Gallei, M.; Frey, H.; Müller, A. H. E. Kinetics of Anionic Living Copolymerization of Isoprene and Styrene Using *in Situ* NIR Spectroscopy: Temperature Effects on Monomer Sequence and Morphology. *Macromolecules* **2019**, *52*, 9299–9310.

(4) Neese, F. Software update: the ORCA program system, version 4.0. *WIREs Comput Mol Sci* **2018**, 8.

(5) Neese, F. The ORCA program system. WIREs *Comput Mol Sci* **2012**, *2*, 73–78.

(6) Lee; Yang; Parr. Development of the Colle-Salvetti correlation-energy formula into a functional of the electron density. *Phys. Rev. B* **1988**, *37*, 785–789.

(7) Becke, A. D. A new mixing of Hartree–Fock and local density-functional theories. *The Journal of chemical physics* **1993**, *98*, 1372–1377.

(8) Grimme, S.; Antony, J.; Ehrlich, S.; Krieg, H. A consistent and accurate ab initio parametrization of density functional dispersion correction (DFT-D) for the 94 elements H-Pu. *The Journal of chemical physics* **2010**, *132*, 154104.

(9) Grimme, S.; Ehrlich, S.; Goerigk, L. Effect of the damping function in dispersion corrected density functional theory. *Journal of computational chemistry* **2011**, *32*, 1456–1465.

(10) Schäfer, A.; Horn, H.; Ahlrichs, R. Fully optimized contracted Gaussian basis sets for atoms Li to Kr. *The Journal of chemical physics* **1992**, *97*, 2571–2577.

(11) Weigend, F.; Ahlrichs, R. Balanced basis sets of split valence, triple zeta valence and quadruple zeta valence quality for H to Rn: Design and assessment of accuracy. *Physical chemistry chemical physics: PCCP* **2005**, *7*, 3297–3305.

(12) Neese, F.; Wennmohs, F.; Hansen, A.; Becker, U. Efficient, approximate and parallel Hartree–Fock and hybrid DFT calculations. A 'chain-of-spheres' algorithm for the Hartree–Fock exchange. *Chemical Physics* **2009**, 356, 98–109.

(13) Kruse, H.; Grimme, S. A geometrical correction for the inter- and intra-molecular basis set superposition error in Hartree-Fock and density functional theory calculations for large systems. *The Journal of chemical physics* **2012**, *136*, 154101.

(14) Barone, V.; Cossi, M. Quantum Calculation of Molecular Energies and Energy Gradients in Solution by a Conductor Solvent Model. *J. Phys. Chem. A* **1998**, *102,* 1995–2001.

(15) Jaacks, V. A Novel Method of Determination of Reactivity Ratios in Binary and Ternary Copolymerizations. *Makromol. Chem.* **1972**, *161*, 161–172.

(16) Blankenburg, J.; Kersten, E.; Maciol, K.; Wagner, M.; Zarbakhsh, S.; Frey, H. The poly(propylene oxide-*co*-ethylene oxide) gradient is controlled by the polymerization method: determination of reactivity ratios by direct comparison of different copolymerization models. *Polym. Chem.* **2019**, *116*, 2170.

(17) Beckingham, B. S.; Sanoja, G. E.; Lynd, N. A. Simple and Accurate Determination of Reactivity Ratios Using a Nonterminal Model of Chain Copolymerization. *Macromolecules* **2015**, *48*, 6922–6930.

(18) Lee, B. F.; Wolffs, M.; Delaney, K. T.; Sprafke, J. K.; Leibfarth, F. A.; Hawker, C. J.; Lynd, N. A. Reactivity ratios, and mechanistic insight for anionic ring-opening copolymerization of epoxides. *Macromolecules* **2012**, *45*, 3722–3731.

Chapter 3

Exploiting the Potential of DMC Catalysis

Chapter 3.1

Tailorable Introduction of Hydrophilicity to Polypropylene Oxide via DMC Catalyzed Copolymerization

The synthesis of amorphous, polar polyether polyols based on propylene oxide (PO) and glycidyl methyl ether (GME) is described. Copolymers with M_n of 1.9 to 4.5 kg mol^{-1}, with low dispersities ($Đ < 1.29$) and up to 45 mol% GME content were synthesized via double metal cyanide (DMC) catalysis. An in-depth investigation of the solvent-free copolymerization was conducted by pressure monitoring, *in situ* ^{1}H NMR spectroscopy and ^{13}C NMR triad analysis. Surprisingly, the results reveal an almost random copolymerization of both epoxides ($r_{PO} = 1.40 \pm 0.01$ and $r_{GME} = 0.71 \pm 0.00$). This observation is in pronounced contrast to the well-known preferential incorporation and generally high reactivity of PO in DMC catalysis in comparison to other epoxide monomers as well as the lower reactivity of PO in the anionic ring-opening polymerization compared to glycidyl ethers. The reactivity ratios were evaluated at 60 °C and 80 °C, demonstrating the reproducibility of the utilized solvent-free *in situ* measurement, showing the temperature independence within this range. Supplementary ^{13}C NMR triad analysis further supports the almost random copolymerization, ensuring an evenly distributed incorporation of polar GME units in the hydrophobic PPO backbone. Turbidimetric measurements demonstrate tunable thermoresponsive behavior and hydrophilicity of the synthesized copolymers with lower critical solution temperatures (LCST) between 19 °C and 35 °C. Furthermore, the increase of hydrophilicity is illustrated by contact angle measurements. This first account of an almost ideally random copolymerization of PO by DMC catalysis shows that the resulting amorphous polyethers are an alternative to established ethylene oxide/PO copolymers for soft components in polyurethane foams.
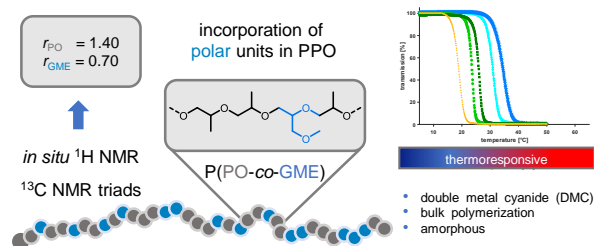
INTRODUCTION

The amorphous polyether poly(propylene oxide) (PPO) is the most commonly utilized polyol as soft component in polyurethane formulations.[1–4] PPO is industrially produced on a megaton scale by polymerization of propylene oxide (PO)[5], yielding highly flexible atactic polyethers with a low glass transition temperature (T_g) of - 73 °C.[5,6] The atactic microstructure prevents the crystallization of the polymer chains, which results in an amorphous polyether

On industrial scales, PPO and its respective copolymers with ethylene oxide (EO) and butylene oxide (BO) are commonly synthesized via DMC catalysis, developed by *General Tire & Rubber* in 1963.[7–11] The high industrial relevance of the DMC catalyst is based on several benefits concerning the resulting polyols.[12] Primarily, the catalyst enables the suppression of chain-transfer reactions inevitable for conventional anionic ring-opening polymerization (AROP) of PO catalyzed by KOH, namely proton abstraction.[13,14] This leads to polyols of an exceptionally low unsaturation level (0.001 meq g^{-1}),[15,16] a crucial criterion for application in polyurethane foaming. Additionally, as the catalyst is inactive after exposure to air once the initiation-fragmentation process has occurred, the small required amount of DMC catalyst (≥ 13 ppm) remains finely suspended in the resulting polymer upon subsequent use.[17]

Nevertheless, mechanistic details of the heterogeneous DMC catalysis are not fully understood to this date. Multiple investigations proposed a cationic coordination-insertion mechanism proceeding at the Zn^{2+}-sites of the catalyst particles.[8,15,18] A rather unique phenomenon known for DMC catalysis is the so called catch-up kinetics,[19] which was recently described from a theoretical point of view.[20] The term outlines the preferential propagation of shorter polymer chains in a mixture of polyethers with varying molecular weights. In addition to the unknown cause of high molecular weight tailing (HMWT)[21–24] commonly observed in polyols synthesized by DMC catalysis, the exact catalysis mechanism remains unidentified. This necessitates deeper kinetic investigations of DMC catalyzed ring-opening polymerization of epoxides.[25]

Considering the polymer properties, the methyl substituent of PO induces the hydrophobic character of PPO, which is in strong contrast to the structurally related, but highly hydrophilic poly(ethylene glycol) (PEG).[26,27] Hence, the copolymerization of PO with ethylene oxide (EO) is employed industrially to tune the hydrophilicity of the resulting soft components.[28] In 1970, Ponomarenko et al. were the first to demonstrate the copolymerization of PO and GME by AROP. Studies regarding the copolymerization kinetics of P(GME-*co*-PO) showed a strongly preferred incorporation of GME over PO, resulting in gradient structures. Alternatively, the anionic copolymerization of PO with the acetal protected glycerol monomer EEGE (ethoxy ethyl glycidyl ether) allows the incorporation of polar units to the PPO backbone after acidic deprotection.[29] However, kinetic investigations revealed a gradient structure which leads to the increased incorporation of polar units near the chain-end.

Recently, our group[30] investigated the copolymerization behavior of PO and EO under DMC catalysis in benzene. In comparative *in situ* ^{1}H NMR spectroscopy studies investigating different

polymerization methods,[31,32] a surprisingly strong preference of PO over EO in DMC catalysis was revealed, resulting in reverse gradient copolymers compared to polymers obtained by AROP. Generally, the copolymerization with EO via DMC catalysis introduces hydrophilicity to the polyether segments near the chain. Nevertheless, depending on the initial molar ratio, with higher molecular weights semi-crystalline segments are added to the PPO backbone, reducing its beneficial viscous character for utilization as amorphous soft component in polyurethane foaming.[33] PPO exhibits a lower critical solution temperature (LCST) in water. Already in 1957, Malcolm and Rowlinson found a LCST of oligomeric PPO (400 g mol^{-1}) at around 50 °C[34,35] which drops below 0 °C with increasing molecular weight.[27,36] PGME on the other hand, shows LCST behavior between 55 and 64 °C at higher molecular weights, representing a thermoresponsive polymer in aqueous solution. Thus, the introduction of substituted epoxides into the PPO backbone is an established tool in tuning thermoresponsive behavior in water.[37–41]

Herein, we present the DMC catalyzed copolymerization of PO with glycidyl methyl ether (GME), the sterically least demanding of all glycidyl ethers. GME is sometimes considered as a liquid alternative to EO, which is true, considering two aspects.[42,43] First, in comparison to the gaseous EO, GME possess a T_b of 112 °C[44] and therefore requires less stringent safety precautions. On the other hand, GME represents an isomer of dimeric EO, resulting in comparable properties regarding the respective polyethers. The polymerization of racemic GME leads to the formation of an amorphous, viscous oil, while the incorporation of higher amount of EO units results in the formation of semi-crystalline segments. Thus, in this study, by replacing EO with GME for the DMC-catalyzed copolymerization with PO, the hydrophilicity of the resulting polyols is enhanced, while preserving their desired amorphous nature. By employing *in situ* ^{1}H NMR investigations, ^{13}C triad analysis and pressure monitoring, we examine the reactivity ratios of PO and GME copolymerization as well as the resulting microstructure of P(PO-*co*-GME). Further, the material properties are analyzed by differential scanning calorimetry (DSC) and turbidimetry as well as contact angle measurements for aqueous solutions of the copolymers.

RESULTS AND DISCUSSION

Polymerization Kinetics

The high affinity and preference of the DMC catalyst towards propylene oxide (PO) is well known in literature, although the cause for this phenomenon remains unidentified. Noteworthy, PO also exhibits a higher reactivity in DMC catalysis than EO, the sterically least demanding of all epoxides.[30] To date, neither the herein used monomer glycidyl methyl ether (GME) nor any other representative of the class of alkyl glycidyl ethers has been examined in bulk by *in situ* techniques regarding their reactivity in DMC catalyzed copolymerizations.
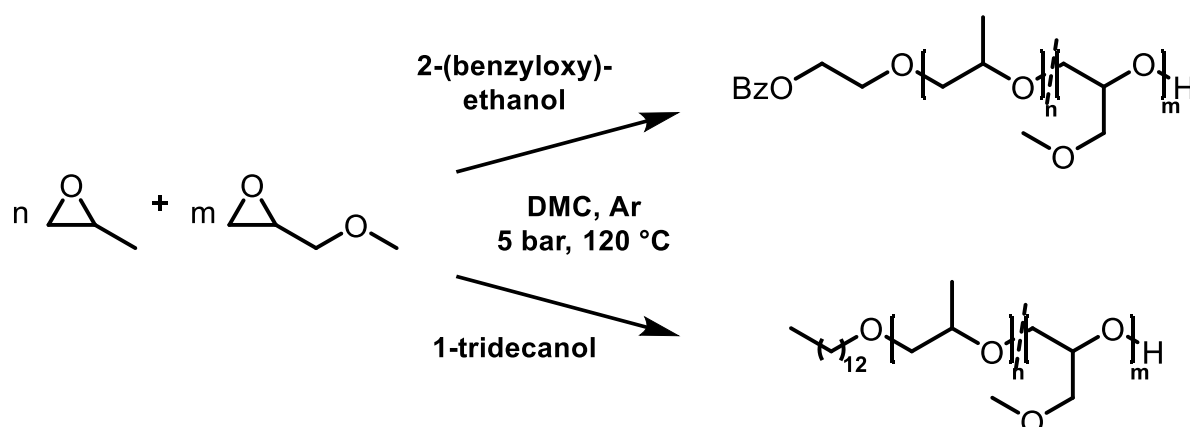
Scheme 1. Synthesis route of P(PO-*co*-GME) copolymers initiated by 2-(benzyloxy)ethanol and 1-tridecanol, respectively.

Initially, we investigated the pressure progression of the DMC catalyzed copolymerization of PO and GME initiated by 2-(benzyloxy)ethanol. *In situ* pressure monitoring enabled to obtain one data point per 100 ms. Fast data collection is crucial, taking the explosive pressure increase during DMC catalysis known in literature into account.[17,45] All polymerizations were performed at 120 °C, using the same amount of the volatile PO for all polymerizations. This procedure enabled the use of a constant reaction volume, which ensures comparability of all pressure curves. In advance of the reaction, a pressure of 5 bar at room temperature was applied to the autoclave. While the temperature increases to ultimately 120 °C, the pressure increases steadily to approx. 10 bar before the initiation of polymerization occurs, which is accompanied by an explosive pressure increase (Figure 1). At 10 bar pressure, both monomers exhibit a liquid state of matter with T_b of 117 °C (PO) and 216 °C (GME) (calculation of T_b at different pressures, see Supporting Information, section 2.1.1.). Consequently, the explosive pressure increase can primarily be ascribed to the fragmentation of the DMC catalyst particles as well as exothermic ring-opening of the monomers, but not to evaporation of the epoxide monomers.

In Figure 1, copolymerizations of PO and GME with 10 and 24 mol% GME are compared. Additionally, homopolymerization of PPO (**P0.1**) was conducted as a reference. The polymerizations exhibited the expected curve progression, with an induction period showing a steady increase of pressure due to temperature elevation, followed by an explosive pressure increase.
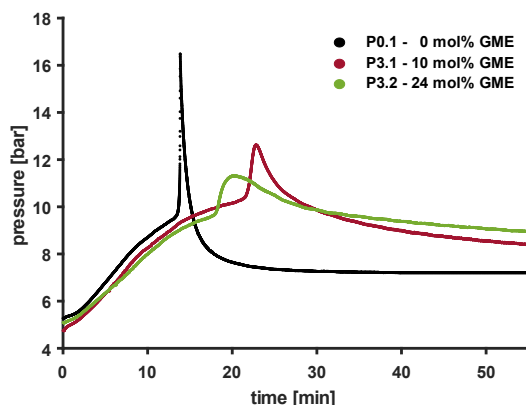
Figure 1. Pressure-time diagram monitoring the homopolymerization of PPO P0.1 and the copolymerization of P(PO-*co*-GME) P3.1 and P3.2 by DMC catalysis with varied monomer ratios.

The induction periods were determined to be between 14 and 23 min. Nevertheless, one has to keep in mind that induction periods in DMC catalyzed polymerizations are time-independent to some extent. Additionally, they depend on several factors and therefore have been observed to vary extensively from 5 min up to 1 hour.[45] Induction times of polymerizations can be decreased by increase of temperature and catalyst level but also by the fragmentation rate of the catalyst particles.[9,15,17] Hence, the polymerizations were analyzed by their curve progression, maximum pressure pmax, the rate of pressure increase after the turning point tind and the slope of the pressure decrease m rather than the induction time t_{max} (Table 1). With increasing incorporation of GME, t_{ind} (0.4 to 2.2 min) increases in accordance with the decrease of p_{max} (16.5 to 11.3 bar). Equally, the value m (- 2.7 to - 0.2 bar min^{-1}) increases from 0 to 24 mol% of GME, indicating a slower pressure normalization after initiation with higher amounts of glycidyl ether present.

Table 1. Pressure monitoring of the homopolymerization of PPO and selected copolymerizations of P(PO-*co*-GME) with evaluation of the induction time t_{max}, maximum pressure p_{max} and the slope m of the pressure decrease.

sample	$GME_{mol\%}$ [%]	t_{max} [min]	Δt_{ind} [min]	p_{max} [bar]	m [bar min^{-1}]
P0.1	0	13.9	0.4	16.5	- 2.7
P2.1	10	22.8	1.5	12.6	- 0.6
P2.3	24	20.1	2.2	11.3	- 0.2

The results reveal a strong influence of the comonomer GME on the initiation process, which leads to the mechanistic hypothesis illustrated in Scheme 2. As previously published, the methyl substituent, PO exhibits a higher reactivity in DMC catalyzed copolymerization than EO, demonstrating that steric effects alone are not a sufficient explanation.[30] In the case of glycidyl ethers, in particular for the sterically least hindered example GME, another aspect needs to be considered.

During the polymerization process, the oxygens of the oxirane ring and the methyl ether of the monomer side chain can coordinate to the zinc center of the DMC catalyst. Therefore, the non-polymerizable ether oxygen blocks the binding site at the active metal center for further monomer consumption. To continue propagation, the GME molecule has to either rotate to coordinate the epoxide oxygen or has to be replaced by another GME monomer. Both processes decelerate the propagation rate and lower the pressure increase, as seen in Figure 1. This hypothesis provides an explanation for the discussed results, showing an inhibited polymerization initiation process in the presence of GME as a comonomer.
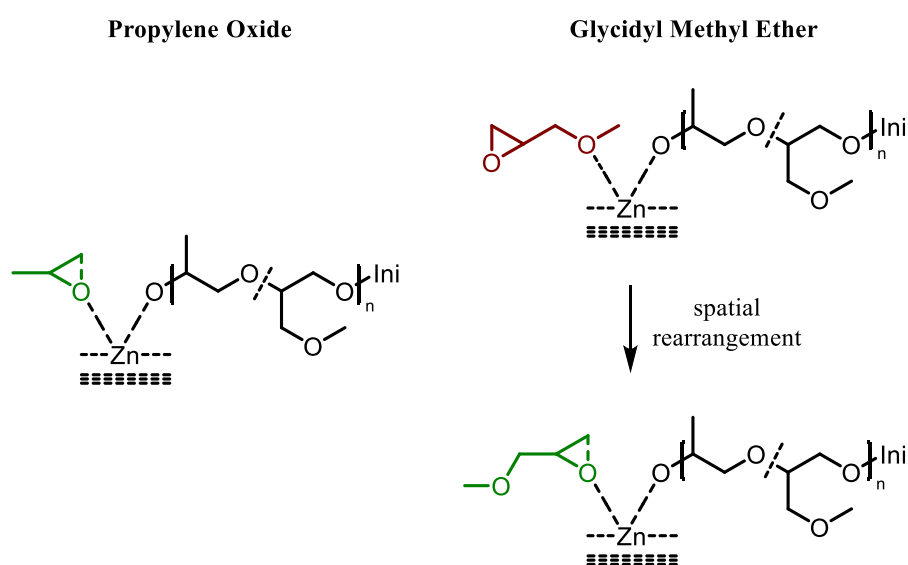
Scheme 2. Coordination site of the active Zn^{2+} center coordinating the respective monomer PO (left) or GME (right) as well as the propagating chain.

In situ ^{1}H NMR kinetic experiments

Pressure monitoring provides valuable insight regarding the polymerization mechanism but is insufficient regarding the polymerization kinetics of the individual monomers. To follow monomer consumption, *in situ* ^{1}H NMR kinetic experiments regarding the formation of P(PO-*co*-GME) in bulk with 20 mol% of GME were conducted to evaluate the respective reactivity ratios. After a shimming process of approximately 5 minutes, one spectrum was recorded every 20 sec (Supporting Information, 80 °C: Figure S1, 60 °C: Figure S3). The experiment was performed at 60 and additionally 80 °C to investigate the temperature influence on the copolymerization parameters. The monomer consumption $M_{x,t}/M_{x,t=0}$ was tracked over time (Supporting Information, Figure S2) and plotted vs. total conversion, revealing a conversion of > 70 % (Figure 2, left). Higher conversions were not accessible in this experiment, due to an increase of the viscosity throughout the propagation in bulk as well as the usage of a special high pressure NMR tube with reduced diameter.

Reactivity ratios were calculated via implementation of the non-terminal Jaacks model[46] with a coefficient of determination (R^2) of 0.99 for both experiments (temperature: 80 °C; Figure 2 right, 60 °C: Supporting Information, Figure S4). The calculated r-parameters are defined as follows: $r_1 = k_{11}/k_{12}$ and $r_2 = k_{22}/k_{21}$ with the rate constant k, 1 representing PO and 2 representing GME.
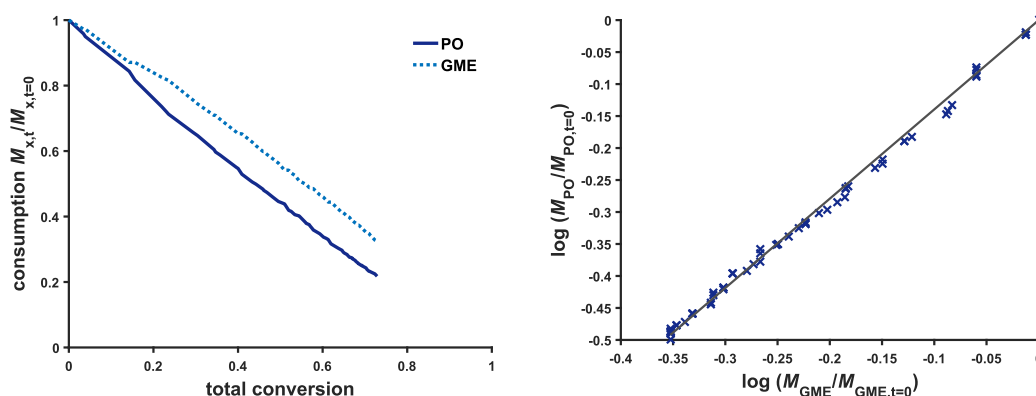

Figure 2. (left) Monomer consumption $M_{x,t}/M_{x,t=0}$ versus total conversion of P(PO-*co*-GME) evaluated by *in situ* ^{1}H NMR kinetic experiments. (right) Linear fit of data calculated by the Jaacks equation for evaluation of reactivity ratios at 80 °C. Reactivity ratios: $r_{PO} = 1.40 \pm 0.01$, $r_{GME} = 0.71 \pm 0.00$ with a coefficient of determination $R^2 = 0.997$.

The results show that the copolymerization of PO and GME at 80 °C displays a slightly preferred propagation of PO over GME under DMC catalysis conditions, manifest in *r*-parameters of $r_{PO} = 1.40 \pm 0.01$ and $r_{GME} = 0.71 \pm 0.00$. Surprisingly, the experiment at 60 °C showed the same parameters ($r_{PO} = 1.41 \pm 0.02$ and $r_{GME} = 0.71 \pm 0.01$), demonstrating the independence of copolymerization kinetics within the examined temperature range (Supporting Information, Figure S4). Both copolymerizations yielded an equally low polydispersity of 1.10 in the NMR tube, proving the reproducibility of the investigated system as well as the absence of undesired side reactions (Supporting Information, Figure S6).

At large, the herein investigated copolymerization by DMC catalysis shows an almost random character with a slight preference for incorporation of PO over GME. Previous studies of our group revealed a gradient structure for the DMC catalyzed copolymerization of PO and EO in benzene-d_6.[30] In absence of a solvent, the reactivity ratios of PO and the respective comonomer appear to be either converging, or GME simply exhibits a higher reactivity than EO. The random copolymerization is somewhat surprising, but represents a remarkable feature, as it allows for the incorporation of evenly distributed polar segments along the rather hydrophobic PPO backbone. In contrast, copolymerization of PO with EO by (i) DMC catalysis[30] ($r_{PO} = 2.4$ and $r_{EO} = 0.42$), (ii) monomer-activated ROP[30] ($r_{PO} = 0.16$ and $r_{EO} = 6.4$) or (iii) conventional AROP[31] ($r_{PO} = 0.26$ and $r_{EO} = 2.8$) is known to lead to gradient polymers with hydrophobic as well as hydrophilic segments.

The current observation differs from the AROP of PO and GME, which likewise results in a gradient structure (r_{PO} = 0.305 and r_{GME} = 3.15).[47] Altogether, with regard to monomer reactivity, the presented copolymerization of PO and GME via DMC catalysis seems to be comparable to known copolymerizations of EO and various glycidyl ethers[48–50] rather than the commonly observed high reactivity of PO in DMC catalysis.

Synthesis of P(PO-*co*-GME) with varying GME ratios

The bulk polymerization of P(PO-*co*-GME) was initiated by the sterically hindered 2-(benzyloxy)ethanol, as it enables precise analysis by NMR spectroscopy and prevents poisoning of the heterogeneous DMC catalyst (Scheme 1). Additionally, **P2.1** was initiated by 1-tridecanol as an example of initiator variation. As listed in Table 2, the theoretical M_n are in good agreement with molecular weights determined via ^{1}H NMR spectroscopy M_n^{NMR} which ranged from 1,900 to 4,500 g mol^{-1}, while the GME content was varied from 12 up to 45 % (Figure 3, SI; Figure S12). The synthesis of copolymers without side products (e.g. homopolymer) was confirmed by ^{1}H diffusion-ordered spectroscopy (DOSY) NMR (Figure S8, section 4, SI). Narrow dispersities ($Đ$ < 1.29) were obtained, however significant broadening was observed for higher molecular weights (> 5,000 g mol^{-1}) with a GME content exceeding 50 % (SI, Figure S7). A plausible explanation for the dispersity broadening is the aforementioned dual coordination of the glycidyl ether GME at the active Zn^{2+} center as well as the generally observed HMWT in DMC catalysis.
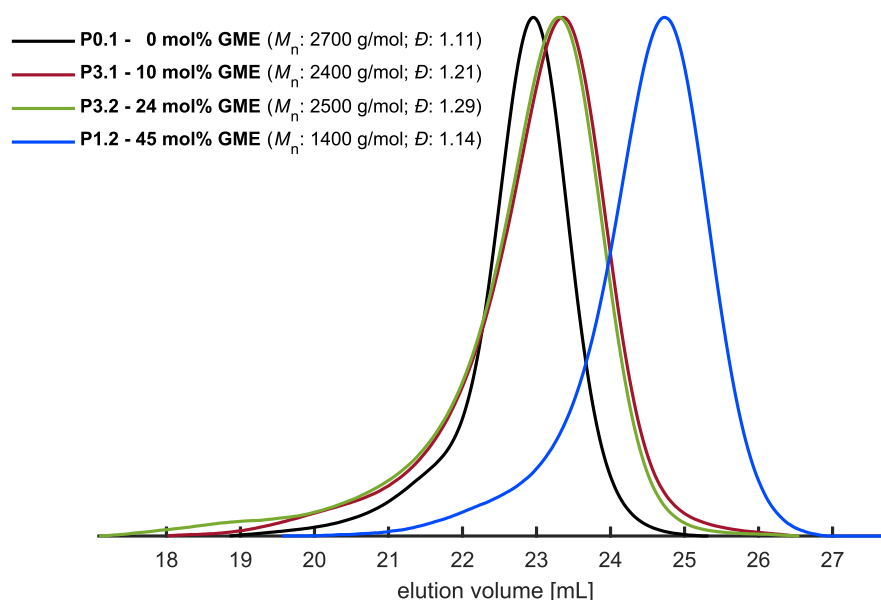
Figure 3. SEC diagrams of selected P(PO-*co*-GME) copolymers and PPO homopolymer (solvent: DMF, standard: PEG, detector: RI).

Additionally, the molecular weights as well as the incorporation of both monomers have been confirmed by matrix-assisted laser desorption/ionization time-of-flight mass spectroscopy (MALDI-

TOF MS). The monomodal and narrow distributions of the presented SEC measurements are in good agreement with the obtained mass spectrum (Figure 4). The M_n^{SEC} evaluated by PEG standard shows a significant underestimation compared to M_n evaluated by ^{1}H NMR integration, referenced to the benzylic initiator protons. GME but especially PO units are less water soluble then ethylene glycol units in PEG. Accordingly, PPO as well es P(PO-*co*-GME) exhibit a lower hydrodynamic radius than the standard and therefore lower elution volumes in SEC measurements.
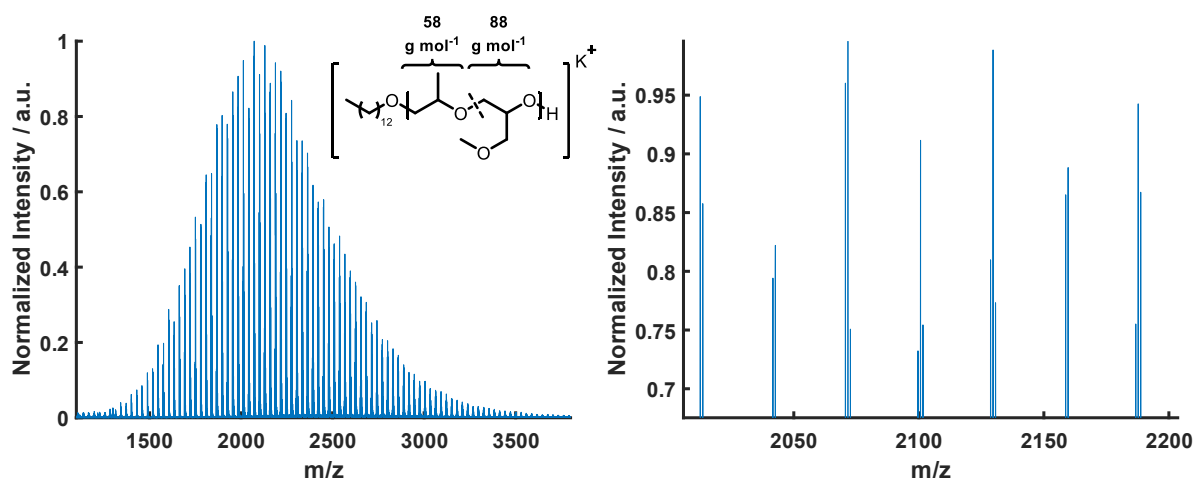
Figure 4. Exemplary MALDI-TOF mass spectrum of the copolymer P2.1 α-tridecanO-P(PO-*co*-GME).

Purification of the resulting polymer could be avoided due to the low demand of catalyst (300 ppm) required during polymerization. As proposed by Tran et al.[15] the catalyst particles (600 nm) rupture into small fragments (250 nm) during the polymerization initiation process. The chains of the polymer grow around the catalyst fragments, which therefore remain finely suspended within the amorphous polymer. Removal of the in organic solvents highly insoluble catalyst is feasible though unnecessary as the catalyst is inactivated after polymerization and exposure to air.[16,51]

Table 2. Overview of the P(PO-*co*-GME) copolymers P1.1-P3.2. The sample P0.1 represents a PPO homopolymer for comparison. The polymerization was initiated by 2-(benzyloxy)ethanol with the exception of P2.1 which was initiated by 1-tridecanol.

type	$P_n^{PO,th.}$	$P_n^{PO,a)}$	$P_n^{GME,th.}$	$P_n^{GME,a)}$	$GME^{a)}$ [%]	$M_n^{th.}$ [g mol^{-1}]	$M_n^{a)}$ [g mol^{-1}]	$M_n^{b)}$ [g mol^{-1}]	conv.$^{a)}$ [%]	$Đ$
P0.1	71	71	-	-	-	4,300	4,300	2,700	100	1.11
P1.1	17	17	9	9	32	1,900	2,000	1,600	100	1.11
P1.2	14	13	11	11	45	2,000	1,900	1,400	96	1.19
P2.1	37	37	4	5	12	2,800	2,700	2,200	100	1.18
P2.2	34	28	7	6	18	2,700	2,400	1,700	83	1.12
P2.3	30	24	9	8	25	2,700	2,300	1,600	82	1.10
P3.1	61	61	8	7	10	4,400	4,300	2,400	99	1.21
P3.2	51	51	16	16	24	4,500	4,500	2,500	100	1.29

a) Estimated via ^{1}H NMR spectroscopy (300 MHz, CDCl$_3$)

b) Estimated by SEC (solvent: DMF, standard: PEG)

Triad-Analysis of P(PO-*co*-GME)

The ^{1}H NMR kinetic results provide important insight regarding the monomer reactivity during DMC catalysis. Using the evaluated reactivity ratios to assess the polymer microstructure however is somewhat error-prone and therefore challenging. Polymers synthesized by DMC catalysis show similarities to polymers prepared by living anionic techniques like narrow distribution and a precise control of M_n. However, to date the cationic coordination-insertion mechanism of DMC catalysis is not understood in detail. The heterogeneous mechanism offers different, currently partly unknown simultaneous reaction pathways. The diversity of mechanistic pathways therefore contradicts ideal living conditions necessary to draw directly link reactivity ratios to the microstructure of the resulting polymer.

Hence, the P(PO-*co*-GME) copolymers were examined by ^{13}C NMR triad analysis, since this method offers additional details concerning the polymer microstructure.[52] Figure 5 shows the stacked inverse gated (IG) ^{13}C NMR spectra of the synthesized P(PO-*co*-GME) copolymers and the PPO homopolymer **P0.1** as reference. The carbon atoms considered during the following ^{13}C NMR triad analysis are shown in Scheme 3. The detailed assignment of the relevant triads is provided in Figure S7, section 4 in the Supporting Information. The GGG and PPP triads of the homopolymers were identified by comparison to literature reports.[42,53] The individual triads were determined by 2D NMR spectroscopy, namely ^{1}H, ^{1}H correlation (COSY), ^{1}H ^{13}C heteronuclear single quantum correlation (HSQC) and ^{1}H, ^{13}C heteronuclear multiple-bond correlation (HMBC) NMR spectroscopy (Figure S9-S11, section 4 SI).
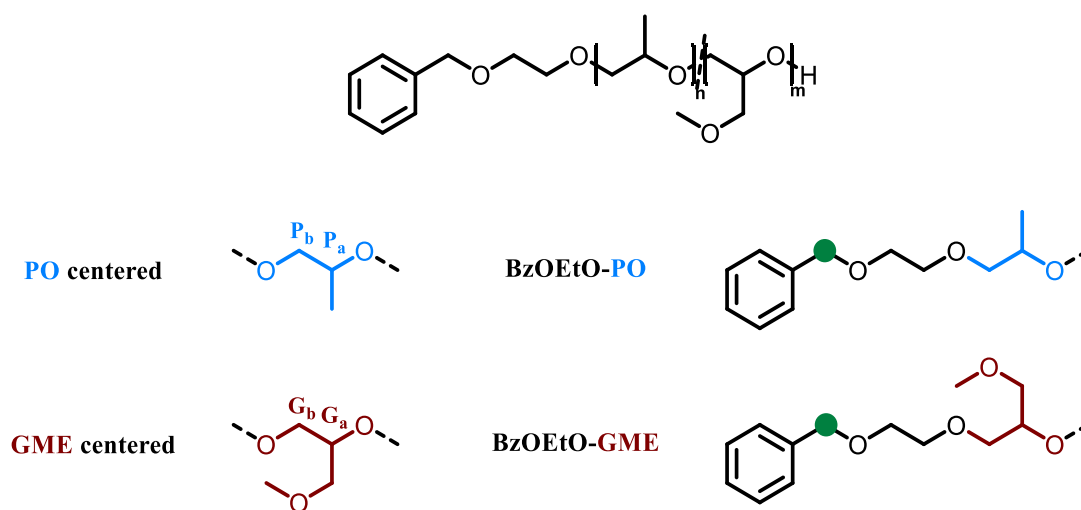
Scheme 3. Assignment of the relevant carbon atoms examined during ^{13}C NMR triad analysis.

The spectra shown in Figure 4 generally mirror the findings from the *in situ* ^{1}H NMR kinetics. The intensity of GME-centered triads (78.5 ppm) increases with increasing amount of GME in the copolymers. Noteworthy, GG$_a$G-triads at 78.3 ppm rarely increase with higher GME content, which verifies a nearly random copolymerization without a pronounced gradient. Further, the GP$_b$G and GP$_b$P triads (74.5 ppm) accordingly increase with higher GME ratios.
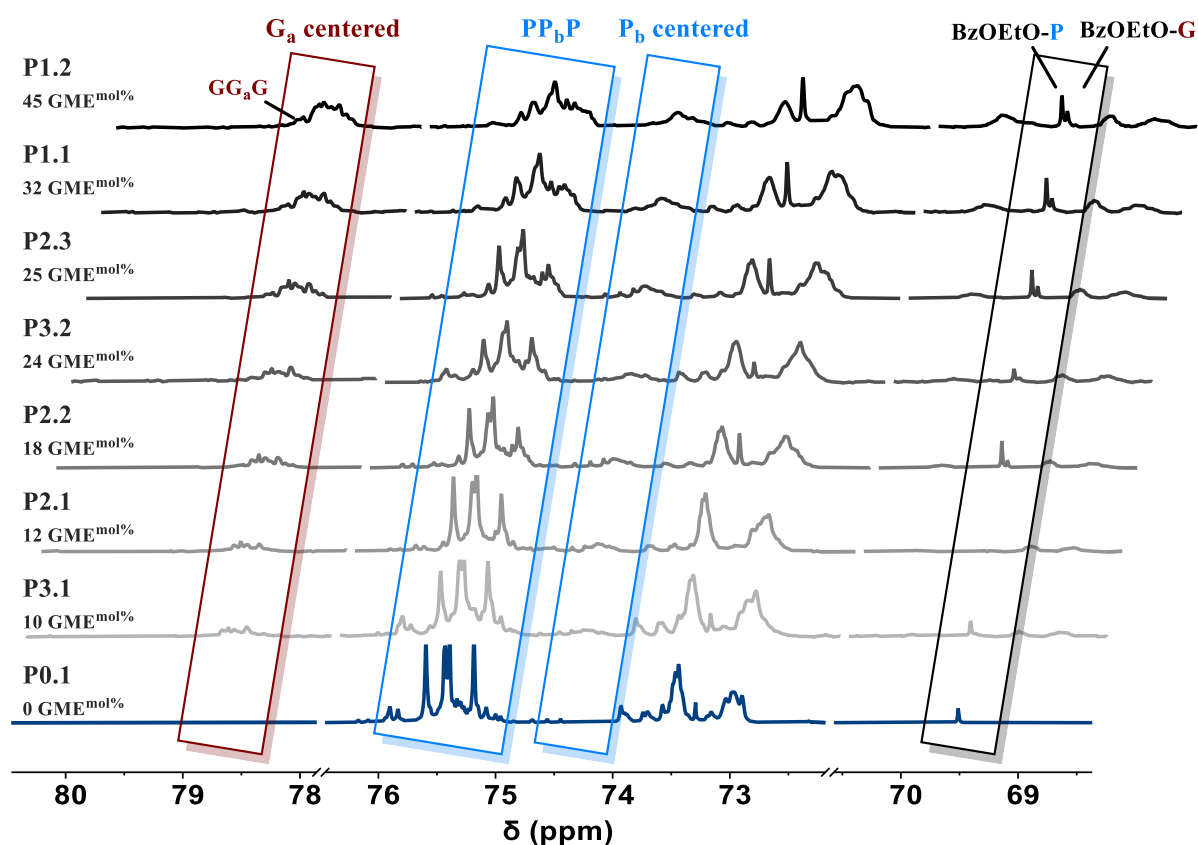
Figure 5. Stacked Inverse Gated (IG, named zgig30) ^{13}C NMR spectra of P(PO-*co*-GME) copolymers P1.1 to P3.2 (grey) and PPO homopolymer P0.1 (blue) in ascending order from bottom to top in regard to the GME content. Polymer P2.1 was initiated by 1-tridecanol and hence shows no peak at 69.5 ppm representing the benzylic carbon. Exact assignment of triads observed in ^{13}C NMR spectra of P(PO-*co*-GME) is illustrated in Figure S7, section 4 in the Supporting Information.

Interestingly, the benzylic carbon of all polymers initiated by 2-(benzyloxy)ethanol exhibits two signals in 13C NMR spectra. The addition of a GME monomer to the initiator instead of a PO molecule causes a slight high field shift of the respective carbon signal, yielding two individual signals (Scheme 3, Figure 5: 69.52 to 69.48 ppm). Integration of the initiator peaks and comparison with monomer resonances permits the calculation of the GME content GME^{Ini} for all copolymers. Comparison of these values with the GME content $GME^{\text{mol\%}}$ evaluated by ^{1}H NMR spectroscopy shows good agreement within the expected error margin (Table 3). In case of a gradient structure by preferential incorporation of PO, solely the signal generated by the initiator-PO adduct would be observed. These findings therefore validate the almost ideally random copolymerization of PO and GME by DMC catalysis.

Table 3. Comparison of GME content $GME^{mol\%}$ to GME^{Ini}. The first value was obtained by recalculation of the backbone integral (3.79-3.09 ppm) to the methyl-substituent of the PO units (1.38-0.79 ppm) in the respective ^{1}H NMR spectra. GME^{Ini} was calculated from dyads produced by the benzylic carbon next to a PO or GME (right) unit in IG ^{13}C NMR spectra.

type	$GME^{mol\%}$ [%]	GME^{Ini} [%]
P0.1	-	-
P3.1	10	11
P2.2	18	23
P3.2	24	30
P2.3	25	31
P1.1	32	33
P1.2	45	40

Investigation of P(PO-*co*-GME) thermal properties in bulk and solution

As shown in a previous work of our group from 2014[42], P(EO-*co*-GME) copolymers synthesized by the monomer-activated ring-opening polymerization (MAROP) exhibit cloud points T_{cp} in the range of 55 to 98 °C, depending on the incorporated GME content. The cloud point decreases with increasing ratio of GME, as the glycidyl ethers lowers to polarity of the polyether copolymer for this monomer combination. As listed in Table 4, for P(PO-*co*-GME) the reverse trend is obtained, as the water-soluble GME units increase the polarity of the PPO-backbone (Figure 6).
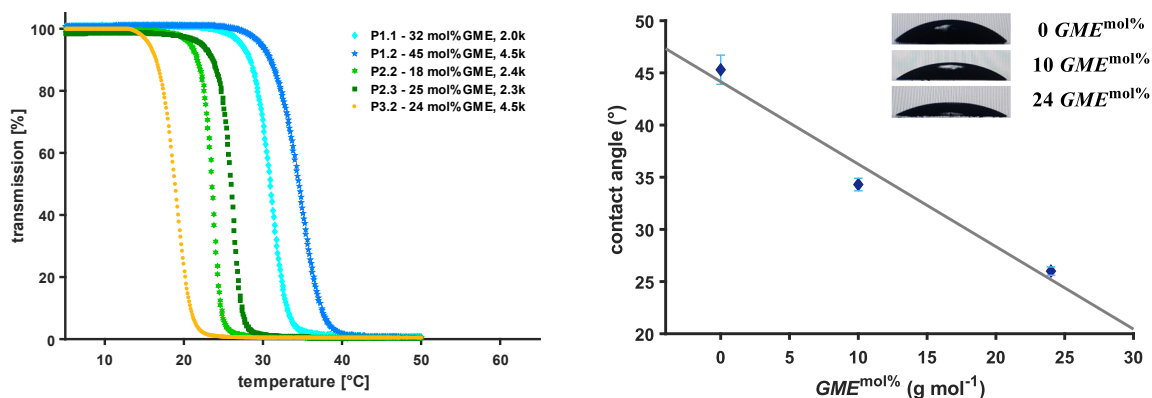
Figure 6. (left) Turbidimetric measurements of P(PO-*co*-GME) copolymers with a GME ratio of > 18 mol% for evaluation of T_{cp} (c = 2.5 mg ml^{-1}). (right) Linear increase in hydrophilicity illustrated exemplary by contact angle versus $GME^{mol\%}$ of P(PO-*co*-GME) copolymers P1.1 and P1.2 as well as PPO homopolymer P0.1 (Glass surface (SiO$_2$), contact angle = 70.6°, M_n^{NMR} = 4.3 to 4.5 kg mol^{-1}).

Accordingly, the polymers exhibit cloud points from 19 to 35 °C with a GME content > 18 mol%. This LCST behavior demonstrates the temperature tunability of the copolymers, enabling water

solubility above as well as below room temperature. Noteworthy, all samples exhibit a steeply decreasing slope within the respective temperature range, further lending further support to the close to random distribution of GME along the polymer backbone.

The tunable polarity of the P(PO-*co*-GME) copolymers is further demonstrated by contact angle measurements (Figure 6, Table S3, section 5 in SI). The contact angle of the PPO homopolymer P0.1 of 45° is decreased to 34° (10 $GME^{mol\%}$) and 26° (24 $GME^{mol\%}$) respectively, verifying the enhanced polarity with increasing GME content.

The synthesized polymers are obtained as fully amorphous materials with low glass transition temperatures T_g, a known result for atactic polyethers with short alkyl side chains (Table 4).[42] As expected, the P(PO-*co*-GME) copolymers show merely slightly increased T_g values with increasing mol% GME (67 to 65 °C) compared to PPO (68 °C), evidencing unchanged chain flexibility upon incorporation of GME. The second heating curves of the DSC measurements are given in Figures S8-S10, Supporting Information.

Table 4. Results of DSC and turbidimetric measurements of P(PO-*co*-GME) copolymers P1.1 to P3.2 and PPO homopolymer P0.1 evaluating the glass transition temperature T_g and the cloud point T_{cp}.

type	M_n^{NMR} [g mol^{-1}]	$GME^{mol\%}$ [%]	T_g [°C]	T_{cp} [°C]
P0.1	4,300	-	- 68	n.d.*
P1.1	2,000	32	- 66	31
P1.2	1,900	45	- 66	35
P2.1	2,700	12	- 65	n.d.*
P2.2	2,400	18	- 66	24
P2.3	2,300	25	- 66	26
P3.1	4,300	10	- 67	n.d.*
P3.2	4,500	24	- 65	19

* not detected as the polymer was not water-soluble at any temperature

Industrially, the widely established and convenient method of introducing polarity to PPO is copolymerization with EO. For polyols utilized as soft components in polyurethanes, an increased polarity is desirable, as the hydrophilicity allows increased dissolution of small amounts of water needed during the blowing process.[16,28] Nevertheless, one major drawback of utilization of ethylene oxide in PPO polyols for certain applications is the semi-crystallinity of the resulting PEG segments at higher ratios of ethylene oxide. The flexibility and simultaneous amorphous character are crucial and inevitable features for application as soft components in polyurethane foaming. In contrast to EO, the herein investigated racemic GME, is randomly distributed throughout the PPO backbone, increasing copolymer polarity without the formation of undesired semi-crystalline segments . The highly flexible chain properties of PPO are preserved, despite the incorporation of

the glycidyl ether and additionally extended by a tunable polarity of the copolymers. The benefit of using GME as a water soluble, thermoresponsive monomer alternative to EO is obvious.

CONCLUSION

We have studied the formation kinetics as well as the materials properties of copolymers of propylene oxide (PO) and glycidyl methyl ether (GME), synthesized by DMC catalysis. The glycidyl ether GME represents a water soluble and thermoresponsive monomer alternative to ethylene oxide (EO) with significant advantages. GME is an easy to handle, commercially gopavailable, liquid epoxide, which does not require the stringent safety precautions necessary for handling gaseous EO. As demonstrated by the first example of *in situ* ^{1}H NMR kinetics of a DMC catalyzed epoxide copolymerization in the absence of a solvent, PO and GME exhibit close to random polymerization kinetics, with reactivity ratios of r_{PO} = 1.40 ± 0.01 and r_{GME} = 0.71 ± 0.00 (60 °C). Interestingly, the monomer reactivity was fully reproducible at 80 °C, therefore showed no temperature dependence between 60 and 80 °C. Further experiments are required to determine the solvent effect on copolymerization kinetics as well as the reactivity of different epoxide monomers in DMC catalysis. Further, the random copolymerization of P(PO-*co*-GME) was substantiated by an in-depth microstructure investigation via ^{13}C NMR triad analysis of copolymers with a GME content of up to 45 %. Pressure monitoring of the copolymerization revealed a significantly decelerating effect of GME on the initiation process. Nevertheless, P(PO-*co*-GME) copolymers of narrow dispersity (Đ < 1.29) in the range of 1.9 to 4.5 kg mol^{-1} were obtained. The investigation of thermal properties in bulk and solution revealed the expected increased polarity due to GME units, resulting in a decrease of contact angles of the homopolymer PPO from 45° to 26° for a copolymer containing 24 mol% of GME. The copolymers with > 18 % GME incorporation exhibited cloud points T_{cp} in the range of 19 °C to 35 °C, demonstrating thermoresponsive behavior and additionally confirming the random distribution of GME along the polymer backbone. As expected, the highly flexible nature of the polyether chain was preserved despite GME incorporation, yielding glass transition temperatures T_g between - 67 to - 65 °C. To sum up our data, the P(PO-*co*-GME) copolymers obtained by DMC catalyzed copolymerization are highly suitable, polar alternatives to the established P(PO-*co*-EO) copolymers as soft-components, e.g. in polyurethane foams.

REFERENCES

(1) Engels, H.-W.; Pirkl, H.-G.; Albers, R.; Albach, R. W.; Krause, J.; Hoffmann, A.; Casselmann, H.; Dormish, J. Polyurethanes: versatile materials and sustainable problem solvers for today's challenges. *Angewandte Chemie (International ed. in English)* **2013**, *52*, 9422–9441.

(2) Wegener, G.; Brandt, M.; Duda, L.; Hofmann, J.; Klesczewski, B.; Koch, D.; Kumpf, R.-J.; Orzesek, H.; Pirkl, H.-G.; Six, C.; et al. Trends in industrial catalysis in the polyurethane industry. *Applied Catalysis A: General* **2001**, *221*, 303–335.

(3) Szycher, M. Szycher's handbook of polyurethanes, 2. ed.; *CRC Press / Taylor & Francis: Boca Raton*, Fla., **2013**.

(4) Król, P. Synthesis methods, chemical structures and phase structures of linear polyurethanes. Properties and applications of linear polyurethanes in polyurethane elastomers, copolymers and ionomers. *Progress in Materials Science* **2007**, *52*, 915–1015.

(5) Peretti, K. L.; Ajiro, H.; Cohen, C. T.; Lobkovsky, E. B.; Coates, G. W. A highly active, isospecific cobalt catalyst for propylene oxide polymerization. *J. Am.Chem. Soc.***2005**, *127*, 11566–11567.

(6) Johari, G. P.; Hallbrucker, A.; Mayer, E. Calorimetric relaxation and glass transition in poly(propylene glycols) and its monomer. *J. Polym. Sci. B Polym. Phys.* **1988**, *26*, 1923–1930.

(7) Jack Milgrom. US Patent, US3278457, Method of Making a Polyether using a Double Metal Cyanide Complex Compound, **1963**.

(8) Kim, I.; Ahn, J.-T.; Ha, C. S.; Yang, C. S.; Park, I. Polymerization of propylene oxide by using double metal cyanide catalysts and the application to polyurethane elastomer. *Polymer* **2003**, *44*, 3417–3428.

(9) Kim, I.; Byun, S. H.; Ha, C.-S. Ring-opening polymerizations of propylene oxide by double metal cyanide catalysts prepared with ZnX2 (X = F, Cl, Br, or I). *J. Polym. Sci. Part A: Polym. Chem.* **2005**, *43*, 4393–4404.

(10) Huang, Y.-J.; Qi, G.-R.; Wang, Y.-H. Controlled ring-opening polymerization of propylene oxide catalyzed by double metal-cyanide complex. *J. Polym. Sci. Part A: Polym. Chem.* **2002**, *40*, 1142–1150.

(11) Walsh, D. J.; Hyatt, M. G.; Miller, S. A.; Guironnet, D. Recent Trends in Catalytic Polymerizations. *ACS Catal.* **2019,** 11153–11188.

(12) Tran, C. H.; Lee, M. W.; Kim, S. A.; Jang, H. B.; Kim, I. Kinetic and Mechanistic Study of Heterogeneous Double Metal Cyanide-Catalyzed Ring-Opening Multibranching Polymerization of Glycidol. *Macromolecules* **2020.**

(13) Price, C. C.; Atarashi, Y.; Yamamoto, R. Polymerization and copolymerization of some epoxides by potassium tert-butoxide in DMSO. *J. Polym. Sci. A-1 Polym. Chem.* **1969**, *7*, 569–574.

(14) Hans, M.; Keul, H.; Moeller, M. Chain transfer reactions limit the molecular weight of polyglycidol prepared via alkali metal based initiating systems. *Polymer* **2009**, *50*, 1103–1108.

(15) Tran, C. H.; Pham, L. T. T.; Lee, Y.; Jang, H. B.; Kim, S.; Kim, I. Mechanistic insights on Zn(II)−Co(III) double metal cyanide-catalyzed ring-opening polymerization of epoxides. *Journal of Catalysis* **2019**, *372*, 86–102.

(16) Ionescu, M. Chemistry and technology of polyols for polyurethanes; *Rapra Technology Ltd: Shawbury, U.K,* **2005**.

(17) Chruściel, A.; Hreczuch, W.; Janik, J.; Czaja, K.; Dziubek, K.; Flisak, Z.; Swinarew, A. Characterization of a Double Metal Cyanide (DMC)-Type Catalyst in the Polyoxypropylation Process: Effects of Catalyst Concentration. *Ind. Eng. Chem. Res.* **2014**, *53*, 6636–6646.

(18) Zhang, X.-H.; Hua, Z.-J.; Chen, S.; Liu, F.; Sun, X.-K.; Qi, G.-R. Role of zinc chloride and complexing agents in highly active double metal cyanide catalysts for ring-opening polymerization of propylene oxide. *Applied Catalysis A: General* **2007**, *325*, 91–98.

(19) Pazos, J.; Browne, E. Catch-Up Kinetics: Selectivity based on equivalent weight in the polymerization of alkylene oxides by double metal cyanide catalysts. *Polymer Preprints* **2008**, *434*.

(20) Bachmann, R.; Klinger, M.; Jupke, A. Molcular Weight Distribution in Di Metal Cyanide Catalyzed Polymerization 1: Fundamental Distribution for Length Dependent Propagation Constant and Segments. *Macromol. Theory Simul.* **2021**, *2100012*.

(21) Zhao, J.; Li, B.-G.; Fan, H. Molecular Weight Distribution in Ring-Opening Polymerization of Propylene Oxide Catalyzed by Double Metal Complex: A Model Simulation. *Macromol. Theory Simul.* **2021**, *2000101*.

(22) Almora-Barrios, N.; Pogodin, S.; Bellarosa, L.; García-Melchor, M.; Revilla-López, G.; García-Ratés, M.; Vázquez-García, A. B.; Hernández-Ariznavarreta, P.; López, N. Structure, Activity, and Deactivation Mechanisms in Double Metal Cyanide Catalysts for the Production of Polyols. *Chem. Cat. Chem.* **2015**, *7*, 928–935.

(23) Bi Le-Khac, W. C.; Wei Wang, U. D.; Mahmoud K. Faraj, Newton Square, all of PA. US Patent, 6,051,680, Acid-Treated Double Metal Cyanide Complex Catalysts, **2000**.

(24) Jeffrey J. Lear, Oliver D. Sloan, Jose F. Pazos., US Patent, US6083420A, Method for decreasing the propensity for phase-out of the high molecular weight component of double metal cyanide-catalyzed high secondary hydroxyl polyoxypropylene polyols, **2000**.

(25) Böhm, K.; Maerten, S. G.; Liauw, M. A.; Müller, T. E. Exploring the Sequence of Comonomer Insertion into Growing Poly(ether carbonate) Chains with Monte Carlo Methods. *Macromolecules,* **2020**.

(26) Dormidontova, E. E. Influence of End Groups on Phase Behavior and Properties of PEO in Aqueous Solutions, *Macromolecules,* **2004**, *37*, 7747-7761

(27) Kjellander, R.; Florin, E. Water structure and changes in thermal stability of the system poly(ethylene oxide)–water. *J. Chem. Soc., Faraday Trans. 1* **1981**, *77*, 2053.

(28) Kwon, O.-J.; Oh, S.-T.; Lee, S.-D.; Lee, N.-R.; Shin, C.-H.; Park, J.-S. Hydrophilic and flexible polyurethane foams using sodium alginate as polyol: Effects of PEG molecular weight and cross-linking agent content on water absorbency. *Fibers Polym* **2007**, *8*, 347–355.

(29) Schömer, M.; Frey, H. Water-Soluble "Poly(propylene oxide)" by Random Copolymerization of Propylene Oxide with a Protected Glycidol Monomer. *Macromolecules* **2012**, *45*, 3039–3046.

(30) Blankenburg, J.; Kersten, E.; Maciol, K.; Wagner, M.; Zarbakhsh, S.; Frey, H. The poly(propylene oxide- co -ethylene oxide) gradient is controlled by the polymerization method: determination of reactivity ratios by direct comparison of different copolymerization models. *Polym. Chem.* **2019**, *116*, 2170.

(31) Heatley, F.; Yu, G.-E.; Booth, C.; Blease, T. G. Determination of reactivity ratios for the anionic copolymerization of ethylene oxide and propylene oxide in bulk. *European Polymer Journal* **1991**, *27*, 573–579.

(32) Rejsek, V.; Sauvanier, D.; Billouard, C.; Desbois, P.; Deffieux, A.; Carlotti, S. Controlled Anionic Homo- and Copolymerization of Ethylene Oxide and Propylene Oxide by Monomer Activation. *Macromolecules* **2007**, *40*, 6510–6514.

(33) Powell, D. G.; Puig, J. E.; van Leuwen, B. G. Polyols and Requirements for Ambient Cure Foams. *Journal of Cellular Plastics* **1972**, *8*, 90–99.

(34) Malcolm, G. N.; Rowlinson, J. S. The thermodynamic properties of aqueous solutions of polyethylene glycol, polypropylene glycol and dioxane. *Trans. Faraday Soc.* **1957**, *53*, 921.

(35) Weber, C.; Hoogenboom, R.; Schubert, U. S. Temperature responsive bio-compatible polymers based on poly(ethylene oxide) and poly(2-oxazoline)s. *Progress in Polymer Science* **2012**, *37*, 686–714.

(36) Saito, S. Cloud points of poly(propylene oxide) and poly(vinyl methylether) in the presence of polymeric acids. *Colloids and Surfaces* **1986**, *19*, 351–357.

(37) Blankenburg, J.; Wagner, M.; Frey, H. Well-Defined Multi-Amino-Functional and Stimuli-Responsive Poly(propylene oxide) by Crown Ether Assisted Anionic Ring-Opening Polymerization. *Macromolecules* **2017**, *50*, 8885–8893.

(38) Dimitrov, P.; Rangelov, S.; Dworak, A.; Tsvetanov, C. B. Synthesis and Associating Properties of Poly(ethoxyethyl glycidyl ether)/Poly(propylene oxide) Triblock Copolymers. *Macromolecules* **2004**, *37*, 1000–1008.

(39) Mangold, C.; Obermeier, B.; Wurm, F.; Frey, H. From an epoxide monomer toolkit to functional PEG copolymers with adjustable LCST behavior. *Macromol. Rapid Commun.* **2011**, *32*, 1930–1934.

(40) Labbé, A.; Carlotti, S.; Deffieux, A.; Hirao, A. Controlled Polymerization of Glycidyl Methyl Ether Initiated by Onium Salt/Triisobutylaluminum and Investigation of the Polymer LCST. *Macromol. Symp.* **2007**, 249-250, 392–397.

(41) Aoki, S.; Koide, A.; Imabayashi, S.; Watanabe, M. Novel Thermosensitive Polyethers Prepared by Anionic Ring-Opening Polymerization of Glycidyl Ether Derivatives. *Chem. Lett.* **2002**, *31*, 1128–1129.

(42) Müller, S. S.; Moers, C.; Frey, H. A Challenging Comonomer Pair: Copolymerization of Ethylene Oxide and Glycidyl Methyl Ether to Thermoresponsive Polyethers. *Macromolecules* **2014,** *47*, 5492–5500.

(43) Herzberger, J.; Niederer, K.; Pohlit, H.; Seiwert, J.; Worm, M.; Wurm, F. R.; Frey, H. Polymerization of Ethylene Oxide, Propylene Oxide, and Other Alkylene Oxides: Synthesis, Novel Polymer Architectures, and Bioconjugation. *Chemical reviews* **2016**, *116*, 2170–2243.

(44) Addy, J. K.; Parker, R. E. 104. The mechanism of epoxide reactions. Part VII. The reactions of 1,2-epoxybutane, 3,4-epoxybut-1-ene, 1,2-epoxy-3-chloropropane, and 1,2-epoxy-3-methoxypropane with chloride ion in water under neutral and acidic conditions. *J. Chem. Soc.* **1965**, *644*.

(45) Mohr, R.; Wagner, M.; Zarbakhsh, S.; Frey, H. The Unique Versatility of the Double Metal Cyanide (DMC) Catalyst: Introducing Siloxane Segments to Polypropylene Oxide by Ring-Opening Copolymerization. *Macromol. Rapid Commun.* **2020**, *2000542*.

(46) Jaacks, V. A Novel Method of Determination of Reactivity Ratios in Binary and Ternary Copolymerizations. *Makromol. Chem.* **1972**, *161*, 161–172.

(47) Ponomarenko, V. A.; Khomutov, A. M.; Il'chenko, S. I.; Ignatenko, A. V. The effect of substituents of the anionic polymerization of α-oxides. *Polymer Science U.S.S.R.* **1971**, *13*, 1735–1740.

(48) Herzberger, J.; Fischer, K.; Leibig, D.; Bros, M.; Thiermann, R.; Frey, H. Oxidation-Responsive and "Clickable" Poly(ethylene glycol) via Copolymerization of 2-(Methylthio)ethyl Glycidyl Ether. *J. Am. Chem. Soc.* **2016**, *138, 9212–9223*.

(49) Verkoyen, P.; Dreier, P.; Bros, M.; Hils, C.; Schmalz, H.; Seiffert, S.; Frey, H. "Dumb" pH-Independent and Biocompatible Hydrogels Formed by Copolymers of Long-Chain Alkyl Glycidyl Ethers and Ethylene Oxide. *Biomacromolecules* **2020**, *21*, 3152–3162.

(50) Herzberger, J.; Leibig, D.; Liermann, J. C.; Frey, H. Conventional Oxyanionic versus Monomer-Activated Anionic Copolymerization of Ethylene Oxide with Glycidyl Ethers: Striking Differences in Reactivity Ratios. *ACS Macro Lett.* **2016**, *5*, 1206–1211.

(51) Jonathan L. Schuchardt., US Patent, US5010047, Recovery of double metal cyanide complex catalyst from a polymer. **1991**.

(52) Mangold, C.; Dingels, C.; Obermeier, B.; Frey, H.; Wurm, F. PEG-based Multifunctional Polyethers with Highly Reactive Vinyl-Ether Side Chains for Click-Type Functionalization. *Macromolecules* **2011**, *44*, 6326–6334.

(53) Schilling, F. C.; Tonelli, A. E. Carbon-13 NMR determination of poly(propylene oxide) microstructure. *Macromolecules*, **1986**, *19(5)*, 1337-1343

SUPPORTING INFORMATION

Materials and Experimental Procedures

Reagent and Equipment

All chemicals and solvents were purchased from *Acros Organics*, *TCI*, *Sigma-Aldrich* and *Fluka*. Deuterated solvents were received from *Deutero GmbH*. The DMC catalyst was provided by BASF SE. Glycidyl methyl ether was purified before use by fractionated distillation. Propylene oxide (PO) and the predistilled GME were dried by addition of *n*-Butyllithium (2.5 M, 0.025 eq.) while stirring and cryotransferred to a Schlenk flask. 2-(Benzyloxy)ethanol was dissolved in benzene and dried by azeotropic distillation. Polymerizations were performed in 100 ml high-pressure autoclaves purchased by *Carl Roth GmbH*.

Polymerization Procedure

An exemplary synthesis protocol is described in the following. Other copolymerization were performed accordingly. The dried monomers, initiator, the DMC catalyst and an autoclave were transferred to the glovebox to carry out the ensuing reaction under strict argon atmosphere. PO, GME, 2-(benzyloxy)ethanol (1 eq) and DMC catalyst (300 ppm) were added to the autoclave. Then a pressure of 5 bar was applied to the autoclave. The reactions mixture was stirred and heated to 120 °C overnight. After evaporation of possibly unreacted monomers at reduced pressure, the resulting polymers were used without further purification. Polymers with varied amounts of GME were synthesized analogously.

^{1}H NMR (300 MHz, CDCl$_3$, δ): 7.35-7.27 (m, 5H, Ar H), 4.56 (s, 2H, Ph-CH$_2$), 3.79-3.09 (m, polyether backbone), 3.35 (s, 3H, -OCH$_3$), 1.38-0.79 (m, propylene oxide -CH$_3$)

Instrumentation

Pressure Monitoring

Pressure Monitoring was performed by use of MEAS M5600 Wireless Pressure Transducer by *TE*. The Bluetooth sensor was attached to the autoclave under continuous argon flow outside the glovebox. Pressure values were measured every 100 ms.

Calculation of *T*b for PO and GME for varying pressure

The state of matter for both epoxide monomers PO and GME was calculated for the utilized reaction conditions. The boiling points T_b at atmospheric pressure, 5 and 10 bar were evaluated by the integrated form of the Clausius-Clapeyron relation (equation 0.9), the August equation (equation 0.2). PO possess an enthalpy of vaporization vapm = 27.735 kJ mol⁻¹.[1] The vapm of GME was approximated by Trouton's rule as no reliable source was available (equation 0.8).[2] The estimated values are listed in Table S1.

$$\Delta_{vap}H_m = 88\frac{J}{molK}T_b \tag{0.8}$$

$$\ln(\frac{p(T_2)}{p(T_1)}) = -\frac{\Delta_{vap}H_m}{R}(\frac{1}{T_2} - \frac{1}{T_1}) \tag{0.9}$$

Table S1. Calculated values of the enthalpy of vaporization $\triangle_{vap}H_m$ and boiling temperatures T_b at atmospheric pressure, 5 and 10 bar for the monomers PO and GME.

monomer	$\triangle_{vap}H_m$ [J mol⁻¹]	T_b [°C]	$T_{b,5}$ [°C]	$T_{b,10}$ [°C]
PO	27735	34	87	117
GME	33704	110	178	216

In situ ¹H NMR kinetic experiments

NMR-Kinetic Experiments were performed in a special high-pressure NMR tube (*Norell S-5-500-HW-HPV-7*) due to the increase of temperature and therefore pressure during polymerization. Equally to polymerizations in the autoclave, all reagents were dried and transferred to the glovebox. A stock solution of PO (0.024 mmol, 25 eq), GME (0.006 mmol, 6 eq), 2-(benzyloxy)ethanol (0.001 mmol, 1 eq) and DMC catalyst (0.7 mg, 300 ppm) was prepared and stirred for 10 min before further use. 0.1 ml of the suspension was transferred to the NMR tube. The *in situ* ¹H NMR spectroscopy was performed at 60 °C and 80 °C respectively with a *Bruker Avance III BR 500/51* (500 MHz), recording a spectrum every 30 sec with one scan. The synthesized polymer was removed from the NMR tube by use of acetone, dried and analyzed by SEC. The data was evaluated by using NIREVAL software from Johann, Steube and Frey.[3]

Size Exclusion Chromatography

Size Exclusion Chromatography (SEC) measurements were performed in dimethylformamide (DMF) with 1 g L^{-1} lithium bromide as an eluent at 50 °C. An *Agilent 1100 Series* was used, equipped with HEMA 300/100/40 columns, and calibration was carried out using polyethylene glycol (PEG) standards, both provided by *Polymer Standard Service* (PSS), Mainz.

Differential Scanning Calorimetry

Differential Scanning Calorimetry (DSC) of P(PO-*co*-GME) polymers was studied with a *Perkin-Elmer Thermal Analysis Controller TAC7/DX* differential scanning calorimeter (DSC). By using indium as a standard (H = 28.71 J g^{-1}, T_m = 155.6 °C) for baseline correction, calibration of the instrument was performed. At a rate of 20 °C min^{-1}, two cooling and heating cycles were applied in a temperature range of - 100 °C to 40 °C. The glass transition temperature T_g was determined in the second cycle.

Contact Angle Measurements

Contact angle measurements were performed on glass slides (SiO$_2$). Prior to use, the slides were cleaned in acetone by sonification for 2 h. The slides were placed in polymer solutions in DCM (5 mg mL^{-1}) and incubated at room temperature overnight. After the solvent evaporated under air, the slides were cleaned with *MilliQ* water for removal of non-adhered particles. For evaluation of contact angles, the sessile drop method was used. One drop of *MilliQ* water was applied to the surface, so the according angle between solid and liquid phase could be recorded. All samples were measured 6 times to minimize systematic errors.

Turbidimetry

Turbidimetry measurements were performed for determination of the cloud point T_{cp} with the UV/VIS spectrometer V-630 by *JASCO*. The heating rate was 1 K min^{-1} with a wavelength of 600 nm. The samples were prepared with a concentration of 2.5 mg ml^{-1} in *Milli-Q* water which was additionally used as reference. The cloud points T_{cp} were determined at a transmission of 50 %.

Mass Spectroscopy (MS) MALDI-TOF

Mass spectrometry (MS) MALDI-TOF was performed with a *Shimadzu Axima CFR* MALDI-ToF-Mass spectrometer. The samples were prepared in methanol (1 g L^{-1}) with 1 μl in potassium trifluoroacetate and a trans-2-[3-(4-tert-Butylphenyl)-2-methyl-2-propenylidene]malononitrile (DCTB) matrix.

Temperature Impact on Reactivity Ratios in DMC Catalysis of PO and GME

Both copolymerizations were performed in a special high pressure NMR tube with a reinforced glass wall which reduces the overall diameter. The viscosity of the polymerization mixture increased steadily with ongoing conversion which simultaneously increased the solution viscosity. Correspondingly, no full conversion was observed as the monomer motion in the highly viscos solution in the tight NMR tube was strongly restrained. Nevertheless, both copolymerizations exceeded 70 % conversion which enabled the reliable determination of reactivity ratios.
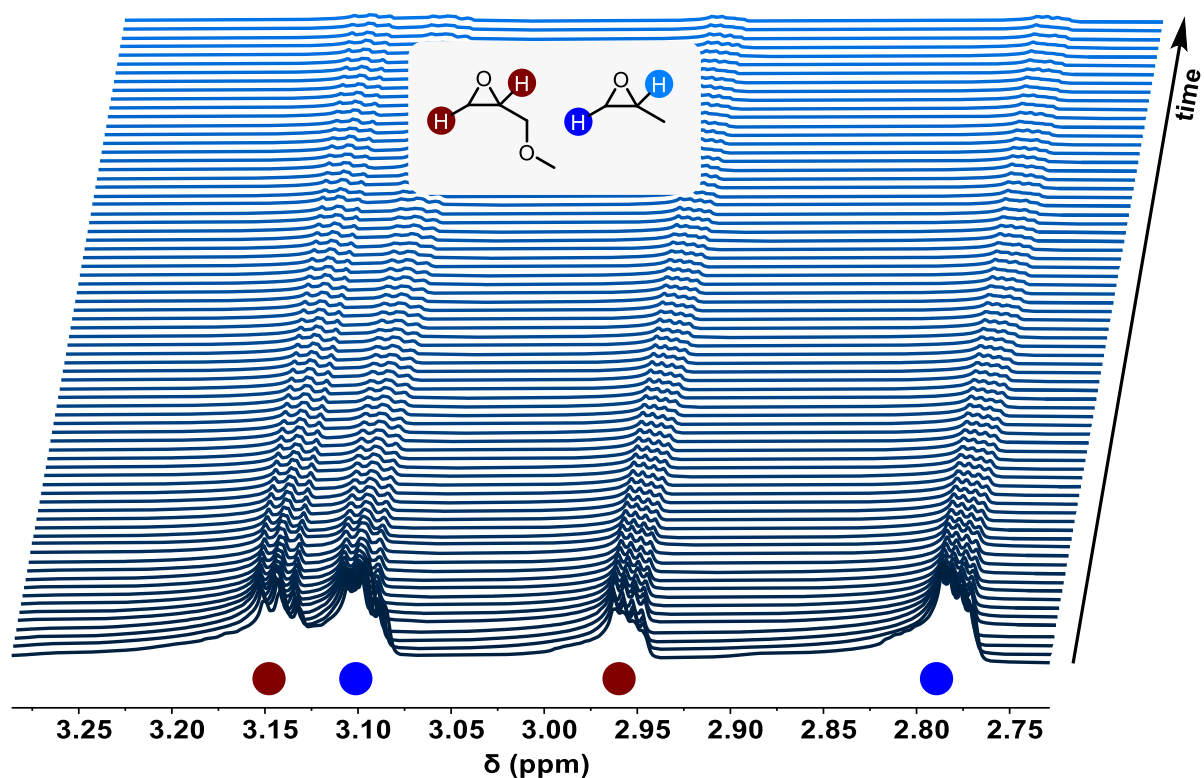
Figure S1. Stacked ^{1}H NMR spectra of *in situ* bulk kinetic of P(PO$_{0.8}$-*co*-GME$_{0.2}$) at 60 °C. As no deuterated solvent was present, each spectrum was referred to the aromatic signals of the initiator 2-(benzyloxy)ethanol at 7.81 ppm. One spectrum every 30 s was recorded (500 MHz).
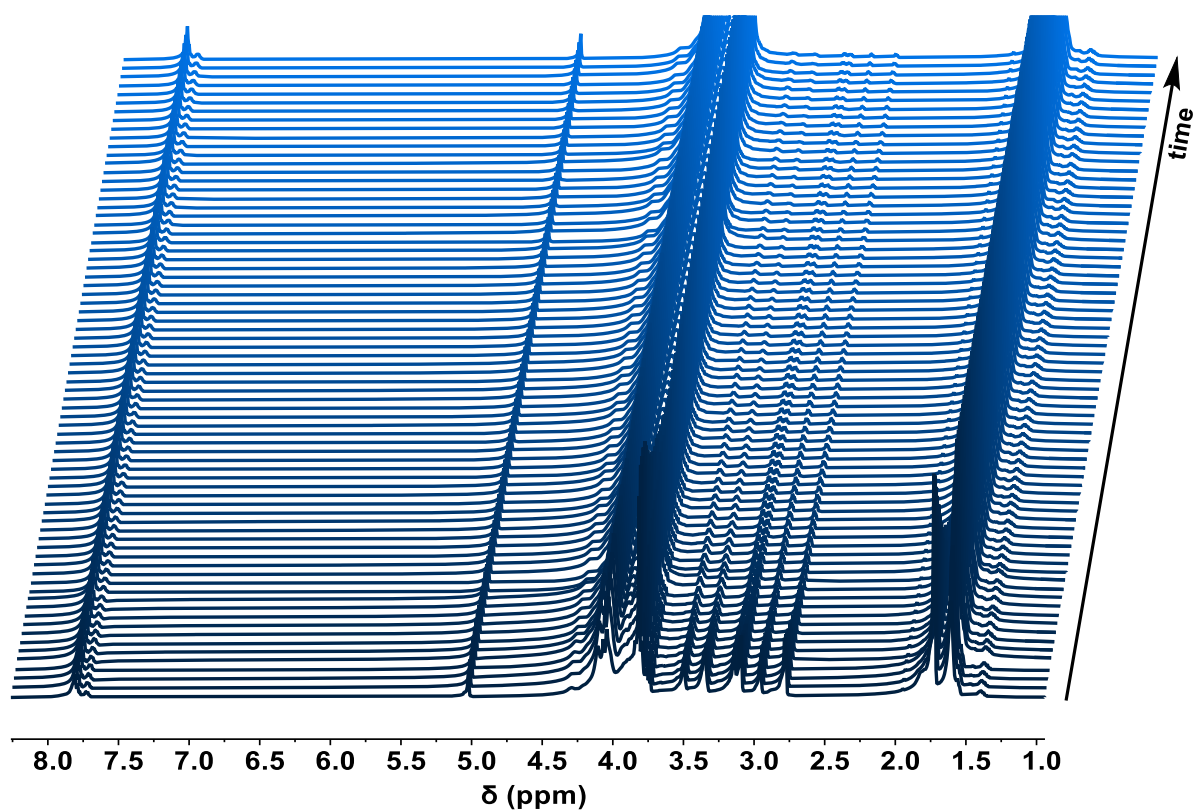
Figure S2. Full stacked ^{1}H NMR spectra of *in situ* bulk kinetic of P(PO$_{0.8}$-*co*-GME$_{0.2}$) at 60 °C.
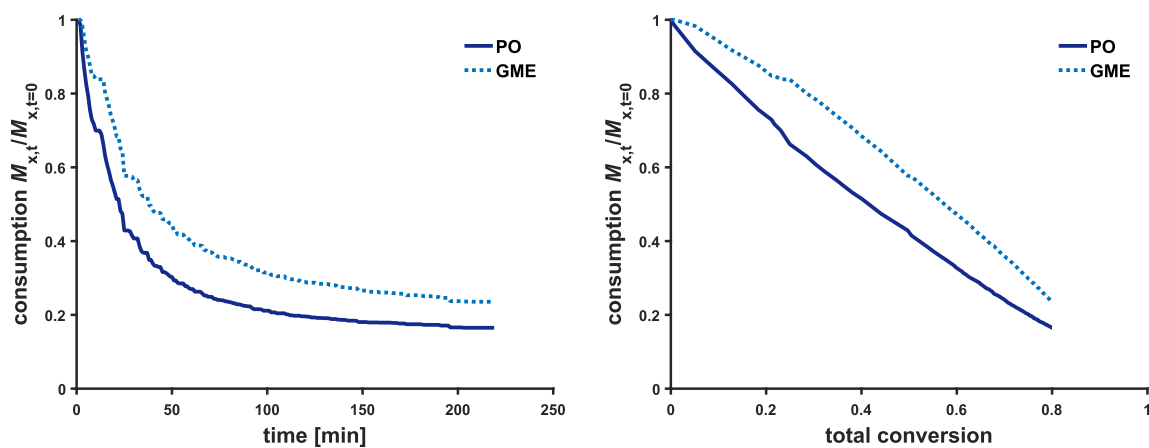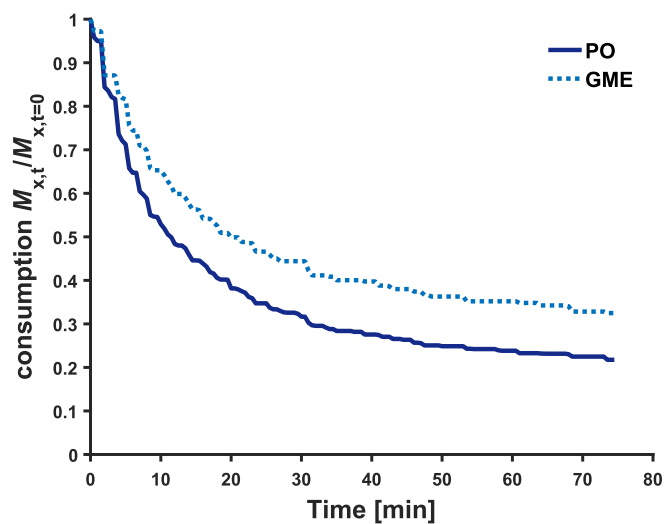

Figure S3. Consumption $M_{x,t}/M_{x,t=0}$ versus time (left) and consumption $M_{x,t}/M_{x,t=0}$ versus total conversion (right) of P(PO-*co*-GME) evaluated by *in situ* ^{1}H NMR kinetic experiments at 60 °C.
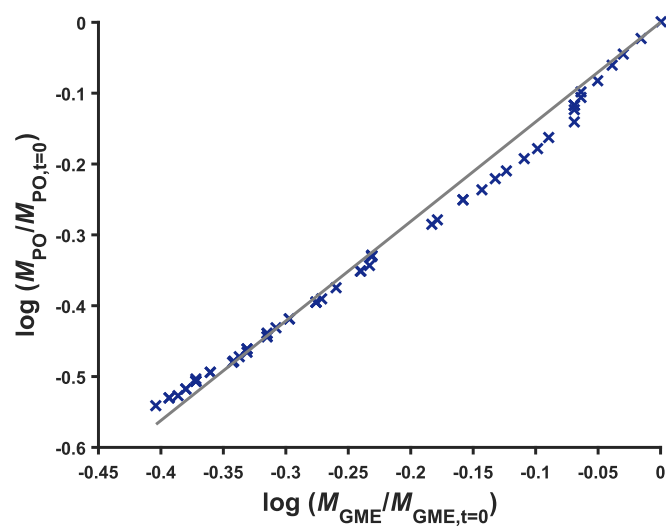
Figure S4. Linear fit of plot calculated by the Jaacks equation for evaluation of reactivity ratios r_{PO} and r_{GME} at 60 °C. Reactivity ratios: $r_{PO} = 1.41 \pm 0.02$, $r_{GME} = 0.71 \pm 0.01$ with a coefficient of determination $R^2 = 0.98$.

The ^{1}H NMR kinetic experiments within this study were conducted in bulk at 60 and 80 °C respectively. The reaction solution of propylene oxide (PO), glycidyl methyl ether (GME), 2(benzyloxy)-ethanol and DMC catalyst possesses 67 wt% of the highly volatile PO (T_b = 34 °C). Hence, boiling retardations occurred during the NMR experiment at 80 °C which induced the rapid decrease of the shown epoxide signals displayed in Figure S 4. Therefore, all relevant proton signals (2.10 and 2.30 ppm) were normalized to the benzylic protons of the initiator 2(benzyloxy)-ethanol which offsets the systematic error.
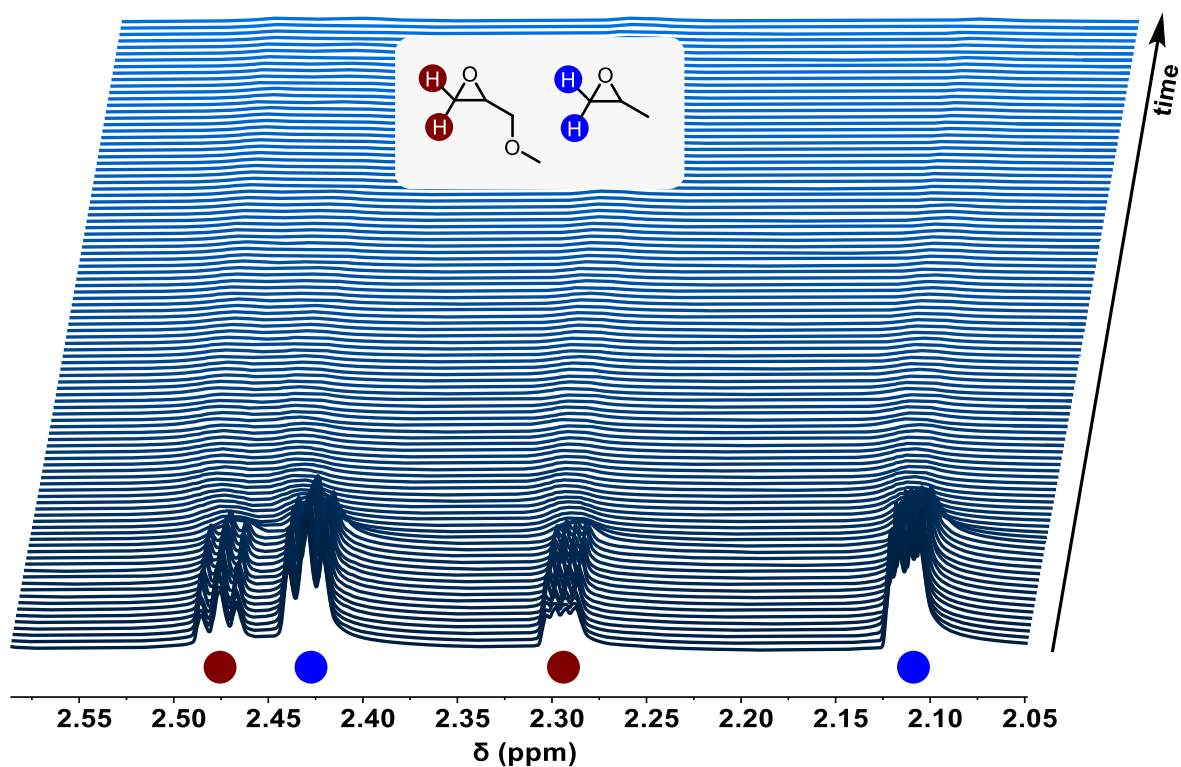
Figure S5. Stacked ^{1}H NMR spectra of *in situ* bulk kinetic of P(PO$_{0.8}$-*co*-GME$_{0.2}$) at 80 °C. As no deuterated solvent was present, each spectrum was referred to the aromatic signals of the initiator 2-(benzyloxy)ethanol considered as benzene-d_6 at 7.16 ppm. One spectrum every 30 s was recorded (500 MHz).
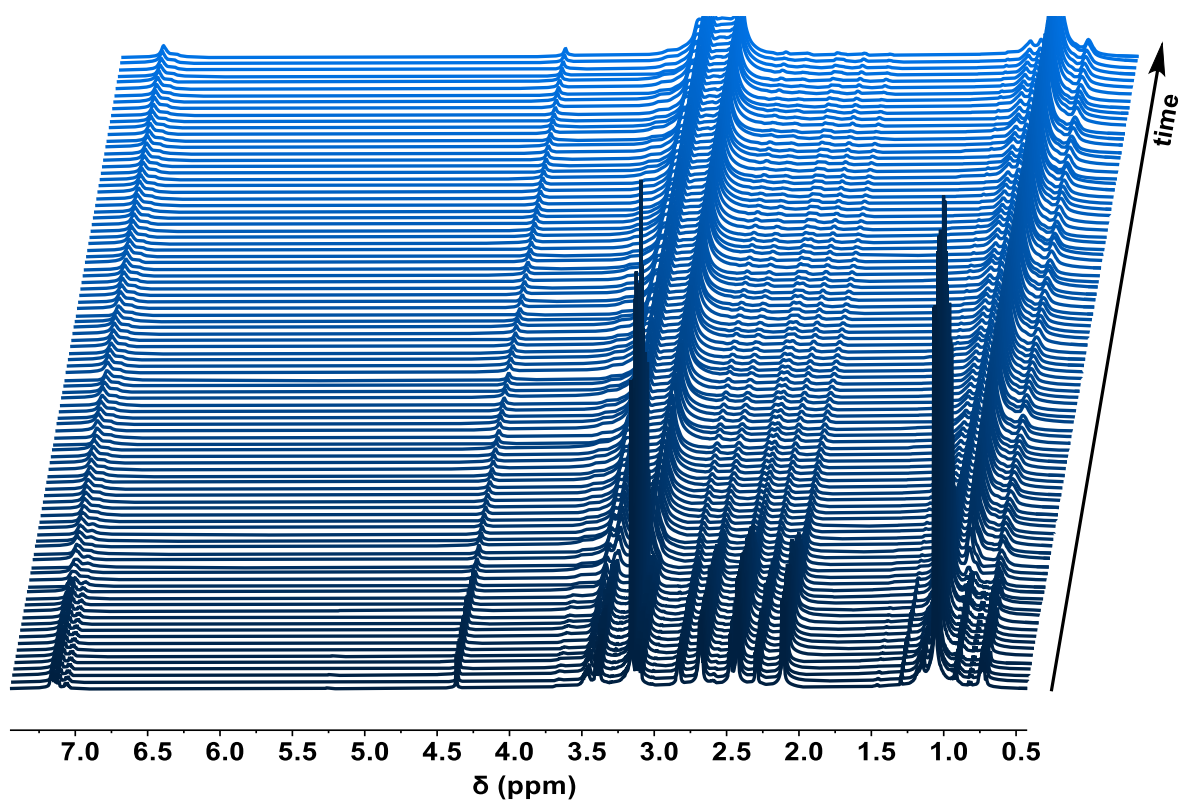
Figure S6. Full stacked ^{1}H NMR spectra of *in situ* bulk kinetic of P(PO$_{0.8}$-*co*-GME$_{0.2}$) at 80 °C

Figure S7. Consumption $M_{x,t}/M_{x,t=0}$ versus time of P(PO-*co*-GME) evaluated by *in situ* ^{1}H NMR kinetic experiments at 80 °C.
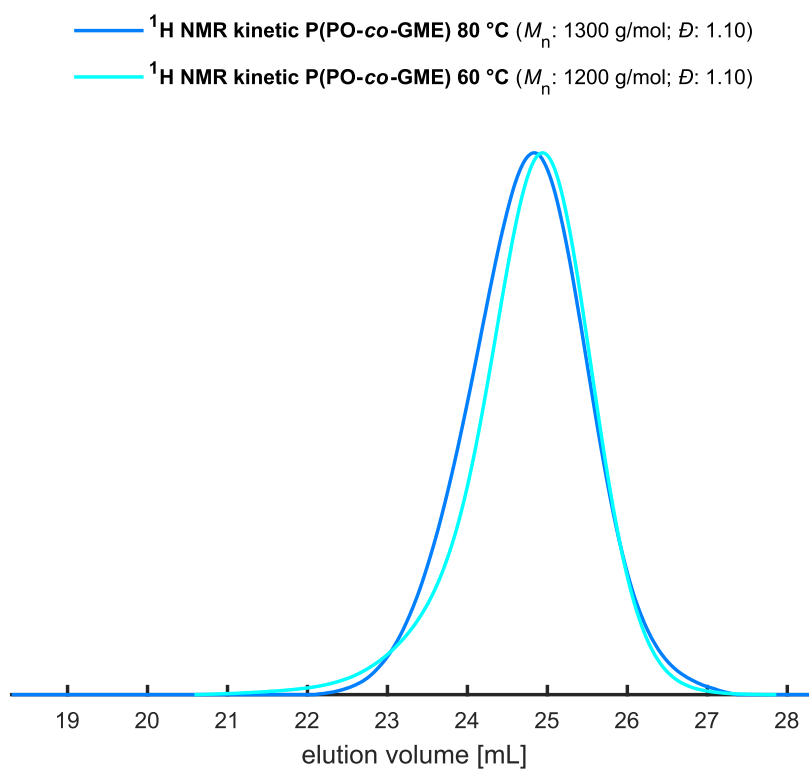
Figure S8. SEC diagrams of P(PO-*co*-GME) of polymers studied by *in situ* ^{1}H NMR kinetic experiments at 60 and 80 °C respectively with PO to GME ratio of 80/20 (solvent: DMF, standard: PEG, detector: RI).

NMR Analysis of P(PO-*co*-GME) Copolymers

Note, that the dyad exhibited by the benzylic carbon and the first added monomer is influenced by the initiator reactivity to the respective monomer. It is hence not suitable for the evaluation of reactivity ratios but nevertheless enables a trend estimation. Head-to-head and tail-to-tail triads as well as tacticity were no suspect of this observation and were therefore not further investigated.
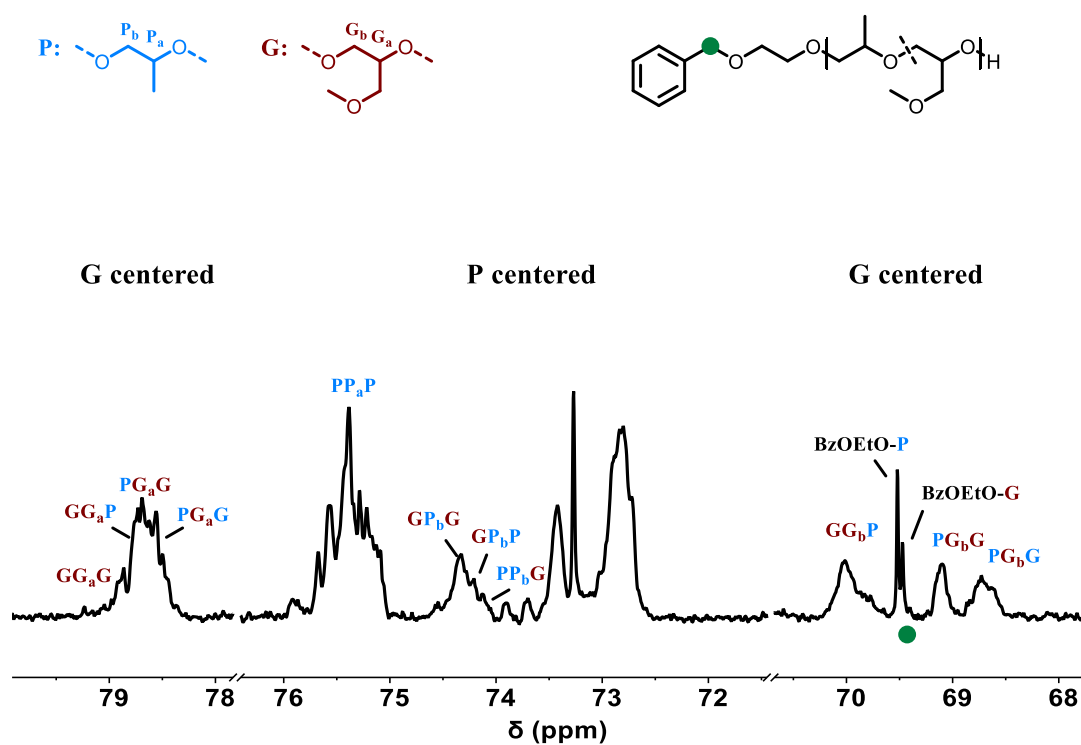
Figure S9. Inverse Gated (IG) ^{13}C NMR spectrum of P1.2 containing 45 mol% GME (400 MHz, CDCl$_3$) with assigned triads observed in P(PO-*co*-GME) copolymers.
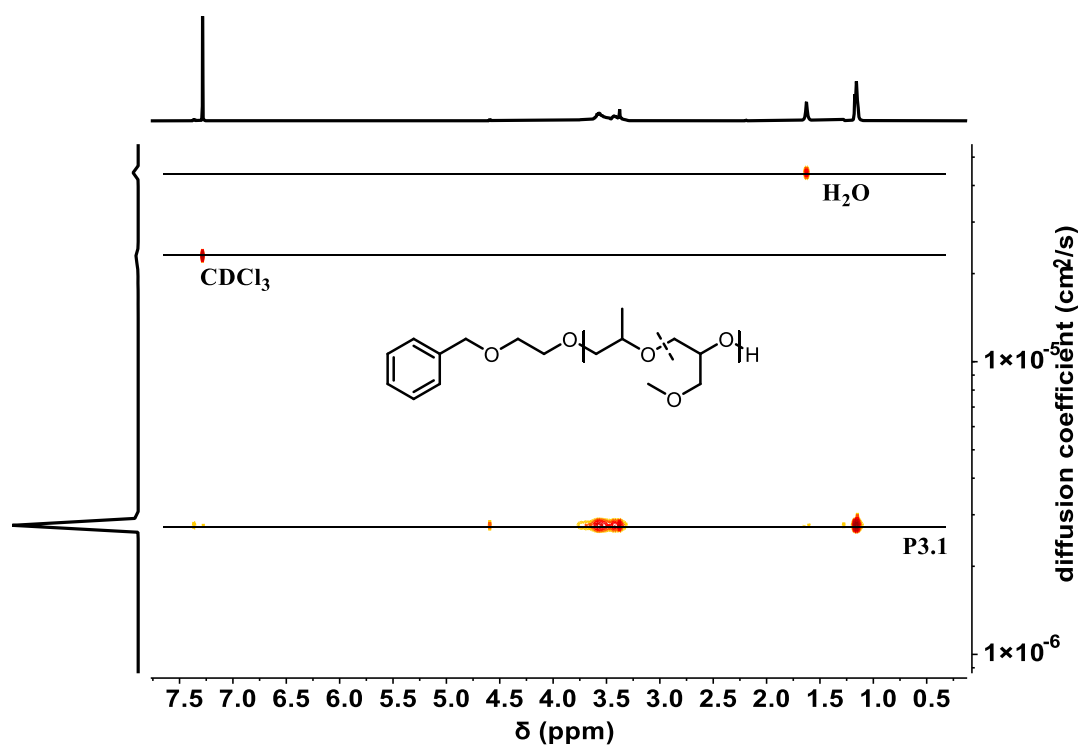
Figure S10. ^{1}H DOSY NMR spectrum (CDCl$_3$, 400 MHz) of the P(PO-*co*-GME) copolymer P3.1.
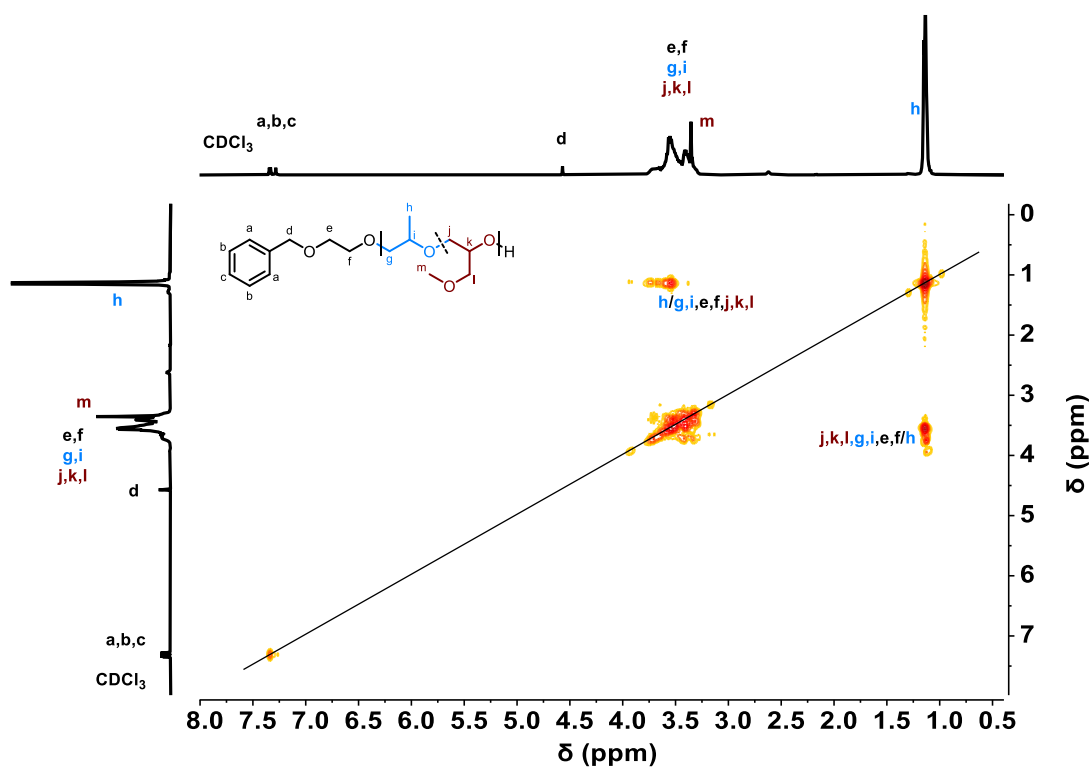
Figure S11. ^{1}H ^{1}H COSY NMR spectrum (CDCl$_3$, 400 MHz) of the P(PO-*co*-GME) copolymer P3.1.
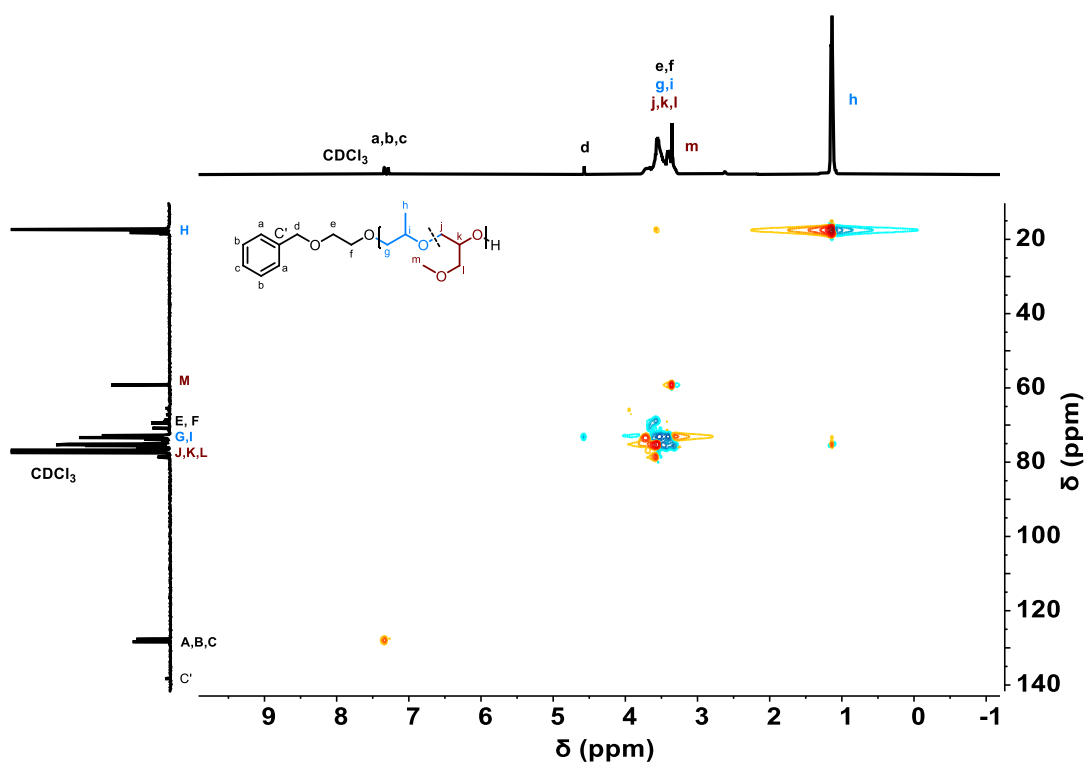
Figure S12. ^{1}H ^{13}C HSQC NMR spectrum (CDCl$_3$, 400 MHz) of the P(PO-*co*-GME) copolymer P3.1.
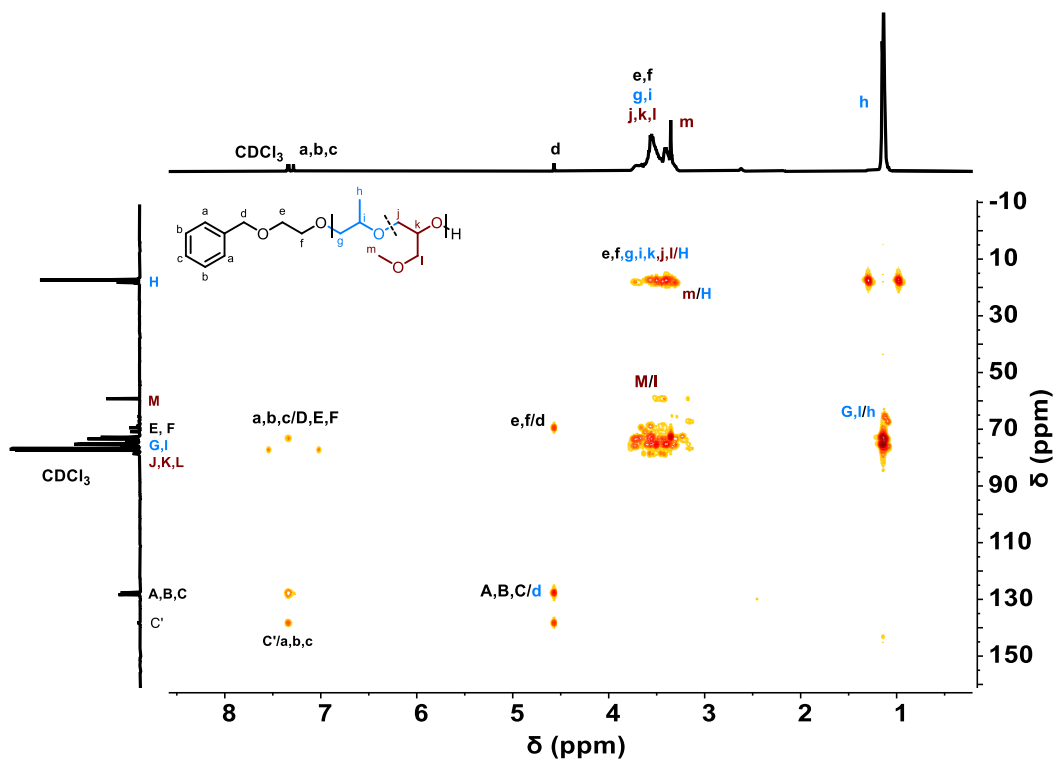
Figure S13. ^{1}H ^{13}C HMBC NMR spectrum (CDCl$_3$, 400 MHz) of the P(PO-*co*-GME) copolymer P3.1.

Characterization of P(PO-*co*-GME) Copolymers
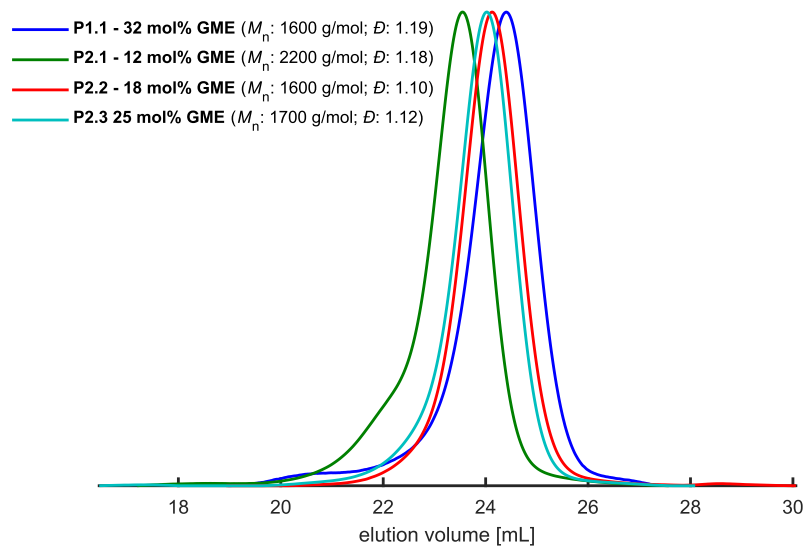
Figure S14. SEC diagrams of selected P(PO-*co*-GME) copolymers (solvent: DMF, standard: PEG, detector: RI).
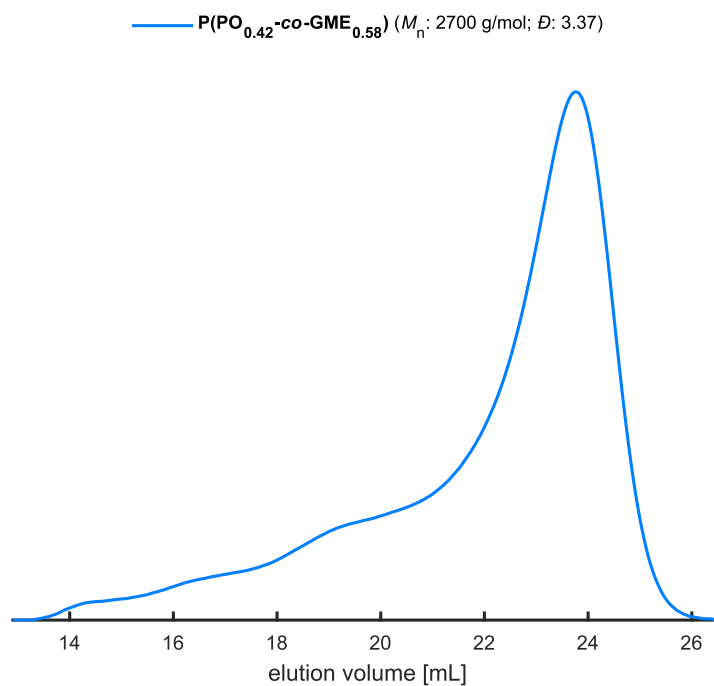
Figure S15. SEC diagrams of P(PO$_{0.42}$-*co*-GME$_{0.58}$) copolymer showing significant tailing towards high molecular weights (solvent: DMF, standard: PEG, detector: RI). $M_\text{n}^\text{NMR} = 5.200\,\text{g}\,\text{mol}^{-1}$.
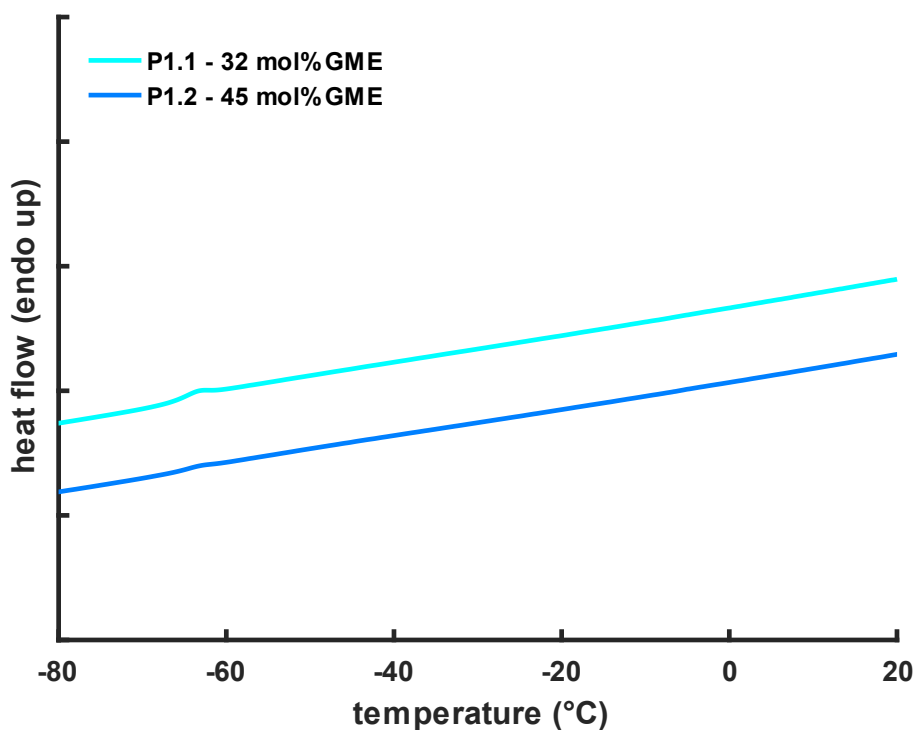
Figure S16. Thermal analysis of P(PO-*co*-GME) copolymers P1.1 and P1.2 by DSC measurements. Temperature range from - 100 to 30 °C, 20 °C min^{-1} (endo up).
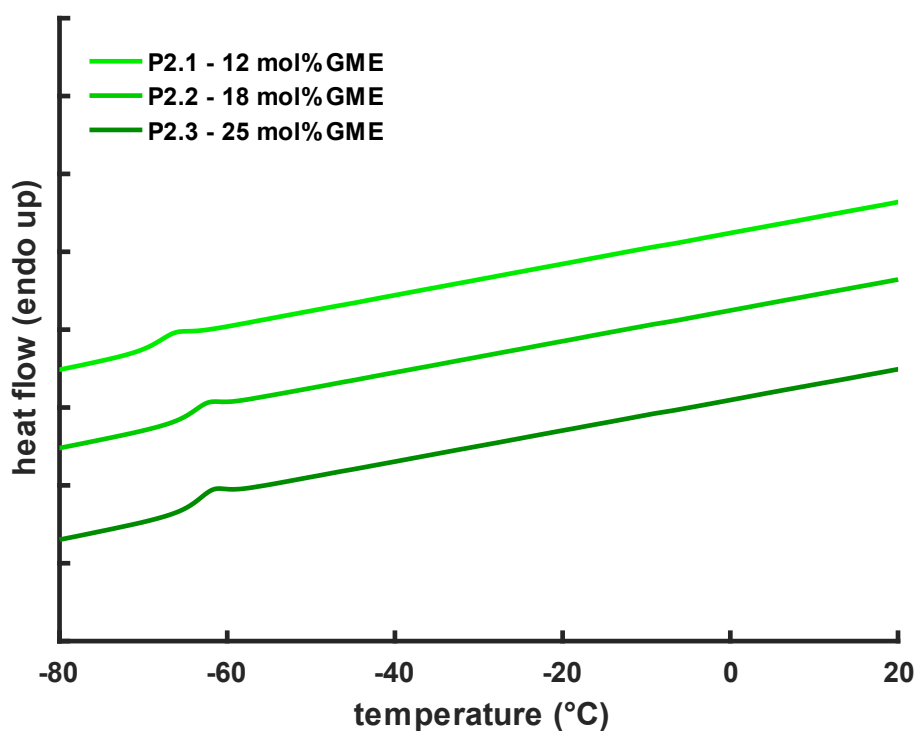
Figure S17. Thermal analysis of P(PO-*co*-GME) copolymers P2.1, P2.2 and P2.3 by DSC measurements. Temperature range from - 100 to 30 °C, 20 °C min^{-1} (endo up).
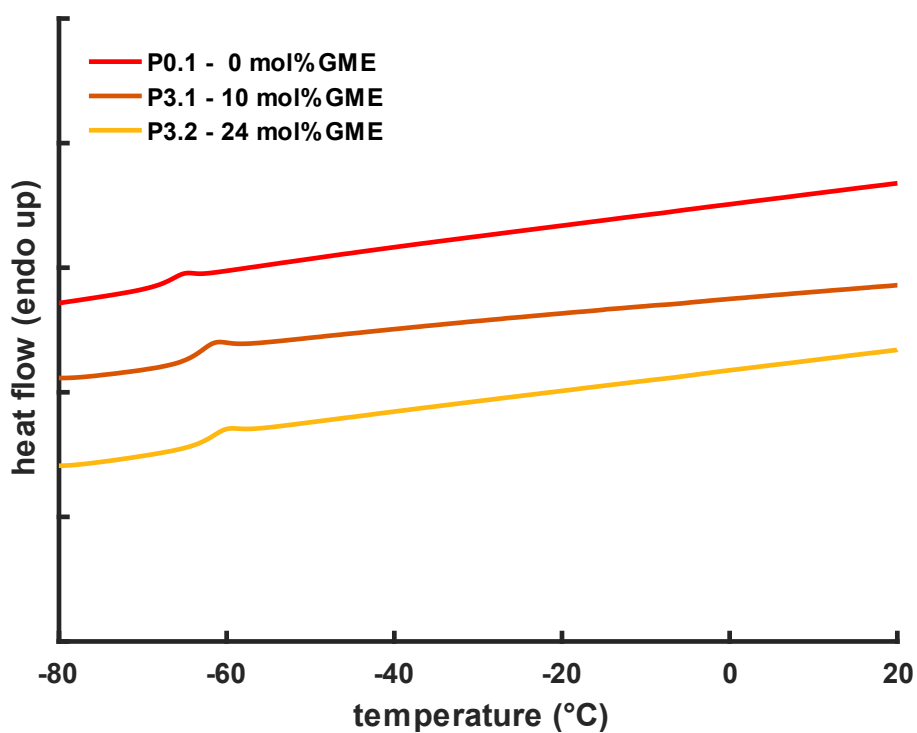
Figure S18. Thermal analysis of P(PO-*co*-GME) copolymers P3.1 and P3.2 as well as P(PO) homopolymer P0.1 by DSC measurements. Temperature range from - 100 to 30 °C, 20 °C min^{-1} (endo up).

Table S2. Results of contact angle measurement of P(PO) homopolymer P0.1 and P(PO-*co*-GME) copolymers P3.1 and P3.2 illustrating the increasing hydrophilicity with higher GME content.

type	M_n^{NMR} [g mol^{-1}]	$GME^{mol\%}$ [%]	contact angle [°]	σ [°]
P0.1	4,300	0	45.3	1.4
P3.1	4,400	10	34.3	0.6
P3.2	4,500	24	36.0	0.4
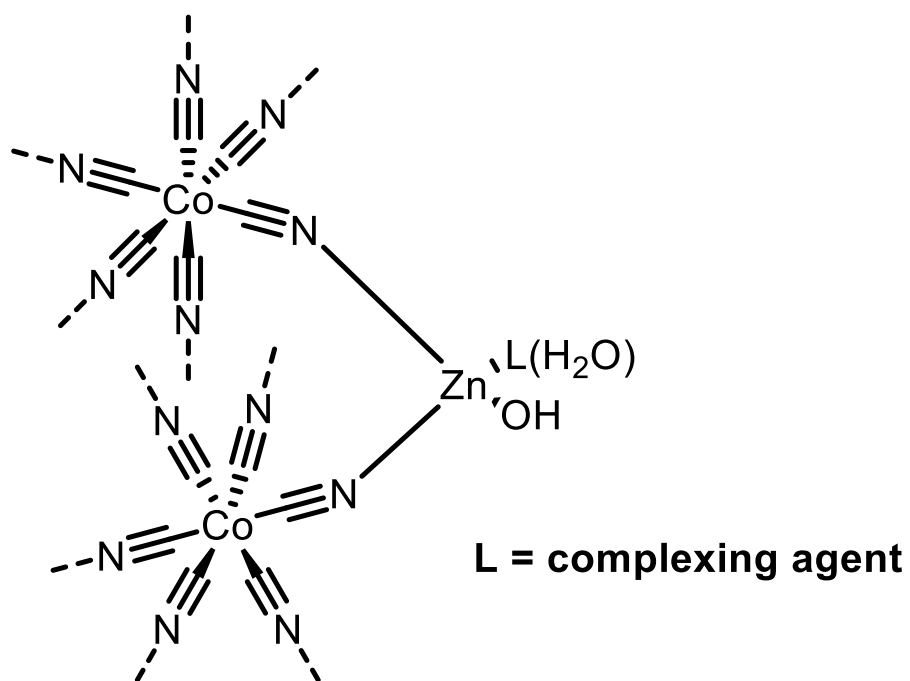
Figure S19. Proposed structure of the active site of Zn-Co(III) DMC catalyst.[4]

REFERENCES

(1) Yaws, C. L.; Banadur, P. Enthalpy of vaporization at boiling point—Organic compounds. In Thermophysical properties of chemicals and hydrocarbons; Yaws, C. L., Ed.; Andrew: Norwich, NY, **2008**; pp 409–546.

(2) Wisniak, J. Frederick Thomas Trouton: The Man, the Rule, and the Ratio. *Chem. Educator* **2001**, *6*, 55–61.

(3) Steube, M.; Johann, T.; Plank, M.; Tjaberings, S.; Gröschel, A. H.; Gallei, M.; Frey, H.; Müller, A. H. E. Kinetics of Anionic Living Copolymerization of Isoprene and Styrene Using in Situ NIR Spectroscopy: Temperature Effects on Monomer Sequence and Morphology. *Macromolecules* **2019**, *52*, 9299–9310.

(4) Wei, R.-J.; Zhang, Y.-Y.; Zhang, X.-H.; Du, B.-Y.; Fan, Z.-Q. Regio-selective synthesis of polyepichlorohydrin diol using Zn–Co(iii) double metal cyanide complex. *RSC Adv* **2014**, *4*, 21765–21771.

Chapter 3.2

The Unique Versatility of the Double Metal Cyanide (DMC) Catalyst: Introducing Siloxane segments to Polypropylene Oxide by Ring-Opening Copolymerization

The combination of hydrophobic polydimethyl-siloxane (PDMS) blocks with hydrophilic polyether segments plays a key role for silicone surfactants. Capitalizing on the double metal cyanide (DMC) catalyst, the direct (i.e. statistical) copolymerization of cyclic siloxanes and epoxides is shown to be feasible. The solvent-free one-pot copolymerization of hexamethyl-cyclotrisiloxane and propylene oxide results in the formation of gradient PPO-PDMS copolymers. Copolymers with up to 46 % siloxane content with low dispersities ($Đ < 1.2$) are obtained in the molecular weight range of 2.100 to 2.900 g mol^{-1}. The polymerization kinetics was investigated by pressure monitoring and *in situ* ^{1}H and *in situ* ^{29}Si NMR spectroscopy. Contact angle measurements reveal the impact of siloxane incorporation, manifest in strongly increased hydrophobicity of PPO-PDMS copolymers and a glass transition of - 95 °C for 46 % SiO content. This unusual copolymerization offers promise for the synthesis of silicone/polyether polyols.

182
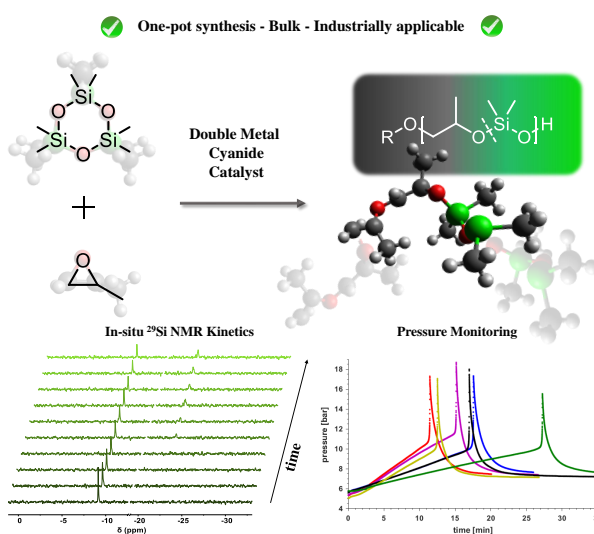
INTRODUCTON

Polydimethylsiloxane (PDMS) represents a versatile and highly relevant commodity polymer due to its unique range of properties.[1] The viscoelastic material shows excellent thermal and oxidative stability combined with a remarkably low T_g (-120 °C). Especially the extreme hydrophobicity of polysiloxanes is widely used both in industry and academic research for the synthesis of surfactants, coating materials and sealants.[2] For the synthesis of such amphiphilic materials, PDMS is often covalently linked to water-soluble polyethers.[3] One of the first and by now widely established applications for linear polysiloxane-polyether block copolymers is their use as foam stabilizers in polyurethane foaming.[4] Epoxides and cyclic siloxanes, in particular hexamethylcyclotrisiloxane (D_3), are commonly polymerized by the living anionic ring-opening polymerization (AROP) due to the precise control of molecular weights and narrow molecular weight distributions. Highly nucleophilic carbanions e.g. alkyl lithium reagents are generally utilized to initiate the ring-opening polymerization of D_3, whereas epoxides are commonly initiated by alkoxides.[3,5,6] Coupling of the two components is achievable by hydrosilylation or thiol-ene click chemistry of the homopolymer segments.[7–11] However, direct (i.e. statistical) copolymerization of cyclic siloxane monomers with epoxides like propylene oxide is not feasible via common AROP and has not been reported to the best of our knowledge. The partial double-bond character (55 %) of the silicon-oxygen bond results in an exceptional dissociation energy of 460 kJ mol^{-1}.[12,13] Copolymerization of D_3 and epoxides by living AROP is therefore impeded because of the insufficient nucleophilicity of the active alkoxide chain end of polyethers with respect to the cleavage of a Si-O bond. Hence, alkoxide initiated ROP of D_3 is only achievable under harsh reaction conditions. Strong basic alkoxides like potassium and caesium hydroxide as well as potassium amide are described to polymerize cyclic dimethylsiloxanes (DMS) at high temperatures.[14] Ring-opening of D_3 by alcohols like methanol was realized by use of strong organic catalysts like phosphazene bases and α-electron-donating N-heterocyclic carbenes in the past.[15,16] Both methods are powerful, but limited by the toxicity of the catalysts used and difficult applicability on industrial scale due to demanding handling and high cost. Recently, Fuchise et al. presented an organocatalytic route to polymerize various cyclic siloxanes, initiated by water.[17] To the best of our knowledge, fluorocarbon-organosilicon copolymer films synthesized by hot filament chemical vapor deposition to this date represent the only example of statistical polyether-polysiloxane copolymers.[18] However, a detailed investigation of the structures of these polymer films was not carried out. We present the direct, i.e. statistical copolymerization of D_3 and propylene oxide. The DMC catalyst developed by *General Tire & Rubber* in 1963 represents an established system for the industrial synthesis of polyether polyols based on propylene oxide as the key monomer and ethylene oxide (EO) (structure see Fig. S2, Supporting Information).[19–22] The catalyst´s capability to suppress side reactions like proton abstraction known for conventional AROP, results in polymers of a very low unsaturation level (0.001 meq g^{-1}).[23] The low amount of catalyst remains in the resulting polymer upon subsequent use, as it is inactive after exposure to air once the initiation-fragmentation step has occurred.[24]

RESULTS & DISCUSSION

Here we introduce a catalytic copolymerization route of D_3 and PO in a solvent-free statistical copolymerization. For the DMC-catalyst, an initiation period of several minutes is typical. As Tran et al. reported in 2019, during the initiation process fragmentation of the catalyst particles occurs, which leads to the exposure of further active sites.[25] The sudden multiplication of active sites at this point results in an increase of catalyst activity, which also enables the ring-opening of monomers that are less reactive than PO. The active center of the catalyst coordinates cyclic monomers via interaction of zinc and the substrates´ oxygen atoms. D_3 is therefore a potential substrate of the DMC catalyst, its significant ring strain enabling the ring-opening polymerization (3-4 kcal mol^{-1}).[26] Initiated by 2-(benzyloxy)ethanol, the copolymerization of PO and D_3 was followed by pressure monitoring, as the activation and initiation process is typically accompanied by a characteristic, explosive pressure increase (Figure 1).[24]
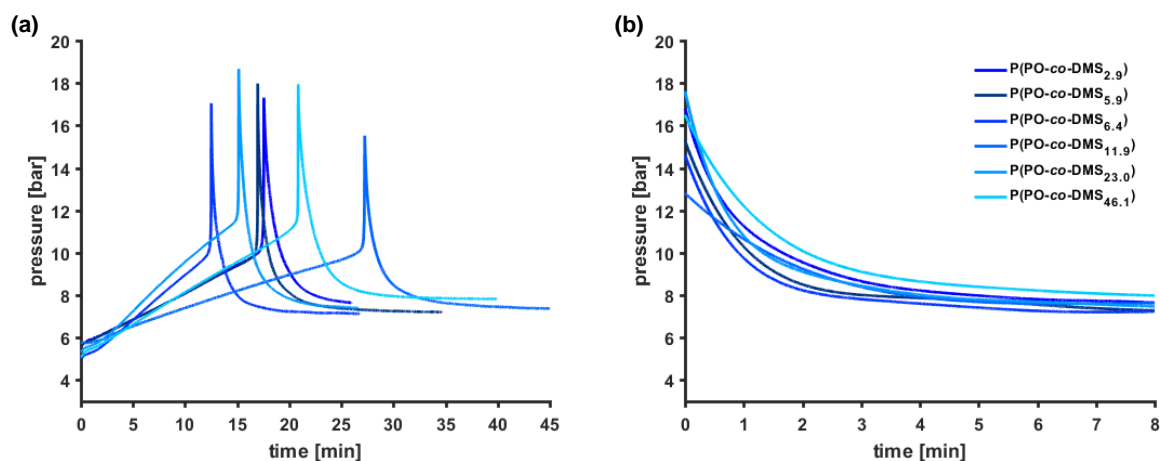

Figure 1. (a) Pressure-time graph of the copolymerization of PO and D_3 by DMC catalysis. Monitoring of induction period occurring during polymerization process. (b) Linear regression of the pressure decrease after p_{max}.

The synthesis is performed at a pressure of 5 bar argon, applied to the autoclave containing the reaction mixture. The pressure is elevated up to 11 bar, caused by heating the reactor to 120 °C. The subsequent explosive pressure increase followed by a fast pressure decrease indicates the catalyst activation due to ring-opening of PO. All polymerizations showed a similar curve progression even though the time to actual initiation varied from 11.5 to 27.2 min, as well as the maximum pressure increase ranging from 15.5 to 18.6 bar. Linear regression of the sigmoidal pressure decrease after p_{max} can give further insight regarding the polymerization kinetics (Figure 1b). For all pressure-time curves an accurate fit of $R^2 > 0.99$ was calculated. Although pressure increase as well as the extent of pressure decrease varied for all runs, no clear correlation with respect to $t_{ini.}$ as well as p_{max} between the polymerizations with varied amounts of D_3 was obtained (Figure 1a, Table S1, Supporting Information). These findings lead to the

conclusion that D_3 has no impact on the catalyst initiation process, which is exclusively ascribed to the ring-opening of PO with its much higher ring strain. The results further permit the assumption that the ring-opening of D_3 is promoted by the temperature and pressure increase due to the catalyst activation caused by PO. This assumption is further supported by *in situ* NMR kinetics. The ^{29}Si *in situ* NMR kinetics measurements of the copolymerization of PO and D_3 confirm polymerization of D_3 to form PDMS (-23 ppm), evident from the constant decrease of the D_3 peak at -8 ppm (Figure 2c). NMR analysis reveals that even after 19 h of heating polymerization of D_3 still continues. In prior research of our group, *in situ* ^{1}H NMR studies of the copolymerization of PO and EO in DMC catalysis showed rapid PO consumption in DMC catalysis after the induction period.[27] In comparison, consumption of D_3 is remarkably slower than PO polymerization, which is typically complete within an hour, in agreement with *in situ* ^{1}H NMR kinetic studies performed in the course of this work (Figure S4, Supporting Information).[25] A variety of NMR experiments was carried out to confirm copolymerisation of D_3 und PO. ^{1}H, ^{1}H nuclear Overhauser effect spectroscopy (NOESY) NMR reveals cross-relaxation in space between the proton attached to the tertiary carbon of PO units close to the methyl protons of the siloxane units (Figure S12, Supporting Information). ^{1}H Diffusion-ordered spectroscopy (DOSY) NMR additionally confirmed the formation of a copolymer containing PO as well as siloxane units (Figure S10, Supporting Information). NMR studies consisting of ^{13}C spin echo attached proton test (APT), ^{29}Si Insensitive nuclei enhancement by polarization transfer (INEPT), ^{1}H, ^{1}H correlation spectroscopy (COSY), ^{1}H, ^{29}Si heteronuclear multiple-bond correlation spectroscopy (HMBC), ^{1}H, ^{13}C heteronuclear single-quantum correlation spectroscopy (HSQC) as well as HMBC further support these findings (Figure S11 and S13-S16, Supporting Information). To investigate the microstructure of the resulting copolymers, ^{13}C NMR spectroscopy experiments were performed, which were compared to ^{13}C NMR spectra of a PDMS as well as a PPO homopolymer (Figure S3, Supporting Information). Other than the homopolymers, the copolymer **P2.1** shows multiple peaks in the range of 0 to -1.2 ppm. These peaks demonstrate the ring-opening of D_3 by PO due to the formation of a C-O-Si bond, which results in a high-field shifting of the corresponding carbon of the polyether next to the cross-over region of the microstructure. The variety of peaks additionally indicates that in spite of the rapid consumption of PO the copolymerization results in gradient microstructures within the copolymer.
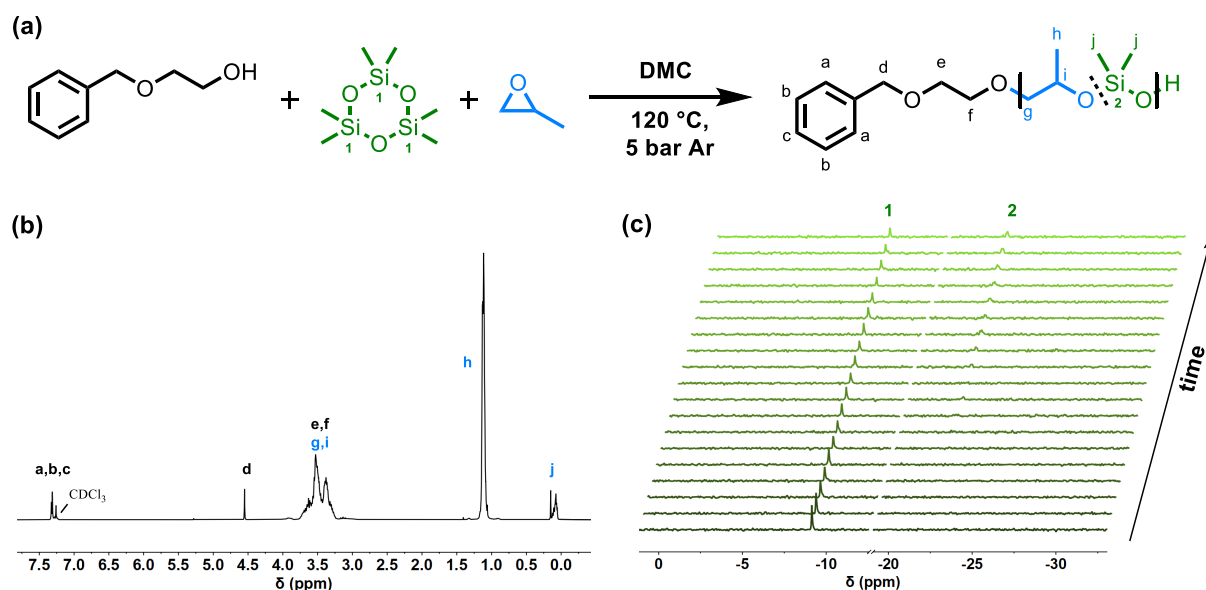
Figure 2. (a) Copolymerization of D_3 and PO; (b) ^{1}H NMR (300 MHz, CDCl$_3$) of P1.1 (c) *In situ* ^{29}Si NMR kinetics (500 MHz, bulk, 120 °C) of copolymerization of PO and D_3, recording one spectrum per h for 19 h reaction time.

The ^{1}H NMR spectrum shows the typical polyether backbone from 3.3 to 3.8 ppm as well as the methyl group of propylene oxide at 1.15 ppm (Figure 2b). The PDMS content was calculated by integration of the methyl substituents attached to the Si atom in the signal range of 0.06 to 0.2 ppm. Molecular weights were evaluated by normalization on the benzylic CH$_2$ group of the initiator 2-(benzyloxy)ethanol at 4.57 ppm. P(PO-*co*-DMS) copolymers with low dispersity ranging from 1.07 to 1.20 and molecular weights up to 2.900 g mol^{-1} were obtained (Table 1, Figure S5-S10, Supporting Information). Aiming at an increased content of D_3 resulted in a constant conversion of PO (> 90 %) while the conversion of D_3 decreased, which afforded lower molecular weights (**P1.1** to **P1.4**). An increase of the reaction time from 24 to 72 h and 144 h, respectively, lead to a significant improvement of D_3 conversion during the copolymerization (97 % for **P2.1** and 67 % for **P3.1**). The conversion of PO decreased to 83 and 80 %, respectively.

Table 1. Overview of the P(PO-*co*-DMS) copolymers P1.1-P3.1.

type	t [h]	$M_n^{th.}$ [g mol^{-1}]	PDMS$^{th.}$ [mol%]	PDMS[a] [mol%]	Conv. D_3[a] [%]	M_n[a] [g mol^{-1}]	M_n[b] [g mol^{-1}]	Conv.[a] [%]	$Đ$	T_g [°C]
P1.1	24	3.000	10	2.9	27	2900	2100	97	1.08	-67
P1.2	24	3.000	20	5.9	23	2500	2000	83	1.09	-69
P1.3	24	3.000	30	6.4	14	2200	1700	73	1.14	-69
P1.4	24	3.000	40	11.9	18	2100	1500	70	1.12	- 71
P2.1	72	3.000	20	23.0	97	2800	1800	93	1.14	-76
P3.1	144	3.000	50	46.1	67	2300	1400	77	1.20	-95

[a] Determined via ^{1}H NMR (300 MHz, CDCl$_3$)

[b] Determined via SEC (PEG calibration)

Thermal analysis revealed a decreasing glass temperature T_g (-67 to -95 °C) with increasing amount of siloxane units within the copolymer (Figure S18 and S19, Supporting Information). PDMS is known for its exceptionally low T_g at - 120 °C due to the highly flexible backbone, characterized by a very low rotation energy barrier of the Si-O bond.[28] Therefore, the flexible siloxane units incorporated in the copolymers show a remarkable impact on the T_g values of P(PO-*co*-DMS) ($T_g^{homoPPO}$ = -67 °C, Figure S14, Supporting Information) copolymers, even with low siloxane content. To further investigate the effect of the incorporation of siloxanes into PPO, the copolymers were analyzed by surface tension measurements (Figure 3). Linear PDMS represents a strongly hydrophobic liquid due to its methyl substituents attached to silicon, which shield the polar Si-O bonds of the polymer.[29] PPO in comparison is not water soluble due to its methyl groups, but shows a lower critical solution temperature (LCST) in water at lower molecular weights at around 15 °C.[30] Evaluation of the contact angles of the P(PO-*co*-DMS) samples revealed a significant impact of the siloxane units incorporated to the copolymers. The contact angle measurements were performed at room temperature using glass (SiO$_2$) surfaces coated with the copolymers (Experimental Section, Supporting Information). The contact angle increased from 39.7° of PPO to 53.6° of **P3.1** containing 46.1 mol% of siloxane units (Table S2, Supporting Information). The hydrophobicity was enhanced with increasing PDMS content, and the effect even for low amounts of siloxane units is remarkable.
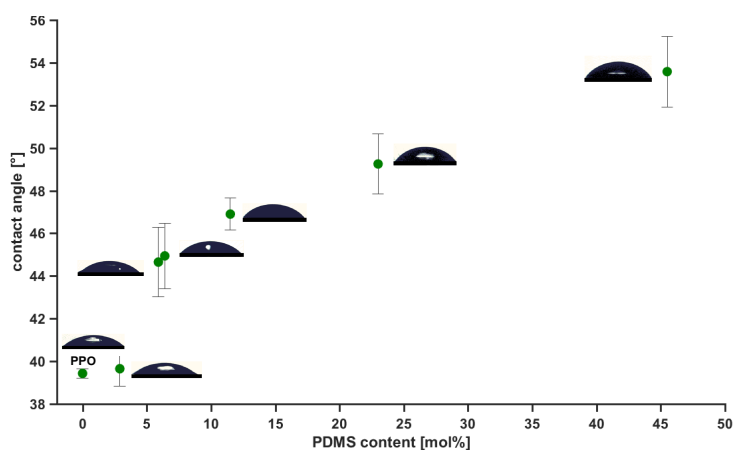
Figure 3. Effect of increasing siloxane content on hydrophobicity of P(PO-*co*-DMS) manifested by contact angles. Measurements were performed on a glass surface (SiO$_2$) (contact angle: 75.4°). Measured contact angle of PDMS: 81.2°.

CONCLUSION

In conclusion, statistical P(PO-*co*-DMS) copolymers with varied amounts of siloxane units were successfully synthesized using DMC catalysis for the first time. Pressure monitoring of the catalyst activation revealed fast consumption of PO during the initiation step, whereas ring-opening of D$_3$ occurs in the following, indicating a strong composition gradient in the copolymers. *In situ* [1]H and [29]Si kinetics support these results, as the polymerization of D$_3$ occurs when the epoxide is consumed to nearly full conversion. Further kinetic studies of the DMC-catalyzed copolymerization of PO and D$_3$ are in progress to gain a better mechanistic understanding. The incorporation of siloxane units in PPO leads to an increase in polymer backbone flexibility, which results in a decrease of the T_g from -67 °C to -95 °C. Furthermore, the hydrophobic nature of PDMS altered the polyether, as demonstrated by contact angle measurements on glass surfaces, showing an increase by 14° from PPO homopolymer to 46 % incorporation of D$_3$ within the copolymer P3.1. Amphiphilic PDMS copolymers are known as foam stabilizers in polyurethane foaming.[31] The DMC catalysis provides polymers of exceptionally low unsaturation levels. The P(PO-*co*-DMS) copolymers are promising components for polyurethane foams, and further studies regarding the copolymerization other epoxide monomers with D$_3$ is in progress.

REFERENCES

(1) Eduok, U.; Faye, O.; Szpunar, J. Recent developments and applications of protective silicone coatings: A review of PDMS functional materials. *Progress in Organic Coatings* **2017**, *111*, 124–163.

(2) Galli, G.; Martinelli, E. Amphiphilic Polymer Platforms: Surface Engineering of Films for Marine Antibiofouling. *Macromol. Rapid Commun.* **2017**, *38*.

(3) Boehm, P.; Mondeshki, M.; Frey, H. Polysiloxane-backbone block copolymers in a one-pot synthesis: a silicone platform for facile functionalization. *Macromol. Rapid Commun.* **2012**, *33*, 1861–1867.

(4) Yilgör, İ.; McGrath, J. E. Polysiloxane containing copolymers: A survey of recent developments. In Polysiloxane copolymers/anionic polymerization; van Beylen, M., Ed.; *Advances in Polymer Science 86; Springer: Berlin*, **1988**; pp 1–86.

(5) Herzberger, J.; Niederer, K.; Pohlit, H.; Seiwert, J.; Worm, M.; Wurm, F. R.; Frey, H. Polymerization of Ethylene Oxide, Propylene Oxide, and Other Alkylene Oxides: Synthesis, Novel Polymer Architectures, and Bioconjugation. *Chemi. Rev.* **2016**, *116*, 2170–2243.

(6) Frye, C. L.; Salinger, R. M.; Fearon, F. W. G.; Klosowski, J. M.; DeYoung, T. Reactions of organolithium reagents with siloxane substrates. *J. Org. Chem.* **1970**, *35*, 1308–1314.

(7) Galin, M.; Mathis, A. Structural and thermodynamic study of dimethylsiloxane-ethylene oxide PDMS-PEO-PDMS triblock copolymers. *Macromolecules* **1981**, *14*, 677–683.

(8) Haesslin, H. W.; Eicke, H. F.; Riess, G. Dimethylsiloxane-ethylene oxide block copolymers, 1. Microphase separation of low segment mass copolymers and their compatibility with water and oil. *Makromol. Chem.* **1984**, *185*, 2625–2645.

(9) Haesslin, H.-W. Dimethylsiloxane-ethylene oxide block copolymers, 2. Preliminary results on dilute solution properties. *Makromol. Chem.* **1985**, *186*, 357–366.

(10) Maassen, H.-P.; Yang, J. L.; Wegner, G. The structure of poly(ethylene oxide)-poly(dimethyl-siloxane) triblock copolymers in solution. *Makromolekulare Chemie. Macromolecular Symposia* **1990**, *39*, 215–228.

(11) Reijerkerk, S. R.; Knoef, M. H.; Nijmeijer, K.; Wessling, M. Poly(ethylene glycol) and poly(dimethyl siloxane): Combining their advantages into efficient CO2 gas separation membranes. *Journal of Membrane Science* **2010**, *352*, 126–135.

(12) Linus Pauling. The nature of silicon-oxygen bonds. *American Mineralogist*, **1980**, *65*, p. 321-323 .

(13) Haynes, W. M. CRC Handbook of Chemistry and Physics, 95th Edition, 95th ed.; *CRC Press: Hoboken*, **2015**.

(14) Hurd, D. T.; Osthoff, R. C.; Corrin, M. L. The Mechanism of the Base-catalyzed Rearrangement of Organopolysiloxanes 1. *J. Am. Chemi. Soc.* **1954**, *76*, 249–252.

(15) Molenberg, A.; Möller, M. A fast catalyst system for the ring-opening polymerization of cyclosiloxanes. *Macromol. Rapid Commun.* **1995**, *16*, 449–453.

(16) Rodriguez, M.; Marrot, S.; Kato, T.; Stérin, S.; Fleury, E.; Baceiredo, A. Catalytic activity of N-heterocyclic carbenes in ring opening polymerization of cyclic siloxanes. *Journal of Organometallic Chemistry* **2007**, *692*, 705–708.

(17) Fuchise, K.; Igarashi, M.; Sato, K.; Shimada, S. Organocatalytic controlled/living ring-opening polymerization of cyclotrisiloxanes initiated by water with strong organic base catalysts. *Chemical science* **2018**, *9*, 2879–2891.

(18) Murthy, S. K.; Gleason, K. K. Fluorocarbon−Organosilicon Copolymer Synthesis by Hot Filament Chemical Vapor Deposition. *Macromolecules* **2002**, *35*, 1967–1972.

(19) Jack Milgrom. US Patent US3278457, Method of Making a Polyether using a Double Metal Cyanide Complex Compound, **1963**.

(20) Kim, I.; Ahn, J.-T.; Ha, C. S.; Yang, C. S.; Park, I. Polymerization of propylene oxide by using double metal cyanide catalysts and the application to polyurethane elastomer. *Polymer* **2003**, *44*, 3417–3428.

(21) Kim, I.; Byun, S. H.; Ha, C.-S. Ring-opening polymerizations of propylene oxide by double metal cyanide catalysts prepared with ZnX2 (X = F, Cl, Br, or I). *J. Polym. Sci. Part A: Polym. Chem.* **2005**, *43*, 4393–4404.

(22) Huang, Y.-J.; Qi, G.-R.; Wang, Y.-H. Controlled ring-opening polymerization of propylene oxide catalyzed by double metal-cyanide complex. *J. Polym. Sci. Part A: Polym. Chem.* **2002**, *40*, 1142–1150.

(23) Ionescu, M. Chemistry and technology of polyols for polyurethanes; Rapra Technology Ltd: *Shawbury, U.K*, **2005**.

(24) Chruściel, A.; Hreczuch, W.; Janik, J.; Czaja, K.; Dziubek, K.; Flisak, Z.; Swinarew, A. Characterization of a Double Metal Cyanide (DMC)-Type Catalyst in the Polyoxypropylation Process: Effects of Catalyst Concentration. *Ind. Eng. Chem. Res*. **2014**, *53*, 6636–6646.

(25) Tran, C. H.; Pham, L. T. T.; Lee, Y.; Jang, H. B.; Kim, S.; Kim, I. Mechanistic insights on Zn(II)−Co(III) double metal cyanide-catalyzed ring-opening polymerization of epoxides. *Journal of Catalysis* **2019**, *372*, 86–102.

(26) Chawla, A. S.; St.-Pierre, L. E. The chemically initiated solid-state polymerization of hexamethylcyclotrisiloxane. *J. Appl. Polym. Sci.* **1975**, *19*, 353–359.

(27) Blankenburg, J.; Kersten, E.; Maciol, K.; Wagner, M.; Zarbakhsh, S.; Frey, H. The poly(propylene oxide- co -ethylene oxide) gradient is controlled by the polymerization method: determination of reactivity ratios by direct comparison of different copolymerization models. *Polym. Chem.* **2019**, *116*, 2170.

(28) Shambayati, S.; Schreiber, S. L.; Blake, J. F.; Wierschke, S. G.; Jorgensen, W. L. Structure and basicity of silyl ethers: a crystallographic and ab initio inquiry into the nature of silicon-oxygen interactions. *J. Am. Chem. Soc.* **1990**, *112*, 697–703.

(29) Elif Hamurcu, E.; Baysal, B. M. Solubility parameter of a poly(dimethylsiloxane) network. *J. Polym. Sci. Part B: Polym. Phys.* **1994**, *32*, 591–594.

(30) Dai, S.; Tam, K. C. Isothermal titration calorimetric studies on the temperature dependence of binding interactions between poly(propylene glycol)s and sodium dodecyl sulfate. *Langmuir : the ACS journal of surfaces and colloids* **2004**, *20*, 2177–2183.

(31) Zhang; Macosko; Davis; Nikolov; Wasan. Role of Silicone Surfactant in Flexible Polyurethane Foam. *Journal of colloid and interface science* **1999**, *215*, 270–279.

(32) Zhang, W.; Allgaier, J.; Zorn, R.; Willbold, S. Determination of the Compositional Profile for Tapered Copolymers of Ethylene Oxide and 1,2-Butylene Oxide by In-situ-NMR. *Macromolecules* **2013**, *46*, 3931–3938.

(33) Wei, R.-J.; Zhang, Y.-Y.; Zhang, X.-H.; Du, B.-Y.; Fan, Z.-Q. Regio-selective synthesis of polyepichlorohydrin diol using Zn–Co(iii) double metal cyanide complex. *RSC Adv* **2014**, *4*, 21765–21771.

SUPPORTING INFORMATION

Experimental Section

Reagents and Equipment

All chemicals and solvents were purchased from *Acros Organics*, *TCI*, *Sigma-Aldrich* and *Fluka*. Deuterated solvents were received from *Deutero GmbH*. The DMC catalyst was provided by *BASF SE*. Hexamethylcyclotrisiloxane (D_3) was stirred over calcium hydride overnight and cryotransferred to a Schlenk flask. Propylene oxide (PO) was dried by addition of *n*-Butyllithium while stirring and cryo-transferred to a Schlenk flask. 2-(benzyloxy)ethanol was dissolved in benzene and dried by azeotropic distillation. Polymerizations were performed in 100 ml high-pressure autoclaves purchased from *Carl Roth GmbH*. Pressure was monitored by a wireless pressure transducer (MEAS) received from the company *TE connectivity*.

Polymerization Procedure

An exemplary synthesis protocol is described in the following. The DMC catalyst as well as the initiator 2-(benzyloxy)ethanol were dried under high vacuum (10^{-3} mbar) by azeotropic distillation with benzene. PO (addition of *n*-butyl lithium (in hexane, 2.5 molar) and D_3, (stirring with CaH_2) were dried via cryotransfer before use. The dried monomers, initiator, the DMC catalyst and an autoclave were transferred to the glovebox to carry out the ensuing reaction under strict argon atmosphere. PO, D_3, 2-(benzyloxy)ethanol (1 eq) and DMC catalyst (300 ppm) were added to the autoclave. Then an Ar pressure of 5 bar was applied to the autoclave. The reaction mixture was stirred and heated at 120 °C overnight. To prevent sublimation of D_3 to the top of the autoclave, a high temperature headband was attached and heated to 180 °C. After evaporation of possibly unreacted monomers at reduced pressure, the resulting polymers were used without further purification. Polymers with varied amounts of D_3 were synthesized analogously.

^{1}H NMR (300 MHz, $CDCl_3$, δ): 7.35-7.27 (m, 5H, Ar H), 4.56 (s, 2H, Ph-CH_2), 3.79-3.09 (m, polyether backbone), 1.38-0.79 (m, propylene oxide -CH_3), 0.24-0.03 (m, Siloxane -CH_3)

Size Exclusion Chromatography (SEC)

SEC measurements were performed in dimethylformamide (DMF) with $1\,g\,L^{-1}$ lithium bromide as an eluent at 50 °C. An Agilent 1100 Series was used, equipped with HEMA 300/100/40 columns, and calibration was carried out using polyethylene glycol (PEG) standards, both provided by *Polymer Standard Service* (PSS), Mainz.

NMR-Kinetic Experiments

Online NMR kinetic measurements were performed in a special high-pressure NMR tube (Norell S-5-500-HW-HPV-7) due to the increase of temperature and pressure during polymerization. Similar to polymerizations in the autoclave, all reagents were dried and transferred to the glovebox. PO (0.015 mg, 0.26 mmol, 26 eq), D_3 (0.005 mg, 0.065 mmol, 7 eq), 2-(benzyloxy)ethanol

(0.0015 mg, 0.01 mmol, 1 eq) and DMC catalyst (300 ppm) were used for the reaction. A special Schlenk-ampule was designed for polymerizations in bulk, filled with the required components, evacuated and sealed by melting (Figure S1).[32] Undesired sublimation of D_3 could be prevented by this procedure. The contents of the ampule were transferred to the NMR tube, which was filled with toluene-d_8. *In situ* ^{1}H and ^{29}Si NMR spectroscopy was performed at 120 °C with a *Bruker Avance III BR 500/51* (500 MHz) and a 5 mm BBFO [1]H-^{19}F/BB z-gradient probe, recording one ^{1}H NMR spectrum per minute and one ^{29}Si NMR spectrum per hour, respectively.

Figure S1. Special designed Schlenk-ampule for *in situ* NMR kinetic measurement of polymerization of PO and D_3 in DMC catalysis.

Differential Scanning Calorimetry (DSC)

Thermal properties of P(PO-*co*-DMS) polymers were studied with a *Perkin-Elmer Thermal Analysis Controller TAC7/DX* differential scanning calorimeter (DSC). By using indium as a standard (H = 28.71 J g^{-1}, T_m=155.6 °C) for baseline correction, calibration of the instrument was performed. Two cooling and heating cycles were applied at a rate of 20 °C min^{-1} in a temperature range of - 100 to 30 °C. Thermal analysis of the sample P(PO-*co*-DMS$_{46.1}$) was performed with a *Mettler Toledo DSC 823*. Two cooling and heating cycles were applied at a rate of 10 K min^{-1} in a temperature range of - 140 to 30 °C. The glass transition temperature T_g was determined in the second cycle for both devices.

Contact Angle Measurements

Prior to use, the glass slides were cleaned in acetone by sonification for 2 h. The slides were placed in polymer solutions in DCM (5 mg ml^{-1}) and incubated at room temperature overnight. After the solvent had evaporated under air, the slides were cleaned with *MilliQ* water for removal of non-adhered particles. For evaluation of contact angles, the sessile drop method was used. One

drop of *MilliQ* water was applied to the surface, so the according angle between solid and liquid phase could be recorded. All samples were measured 6 times to minimize systematic errors.
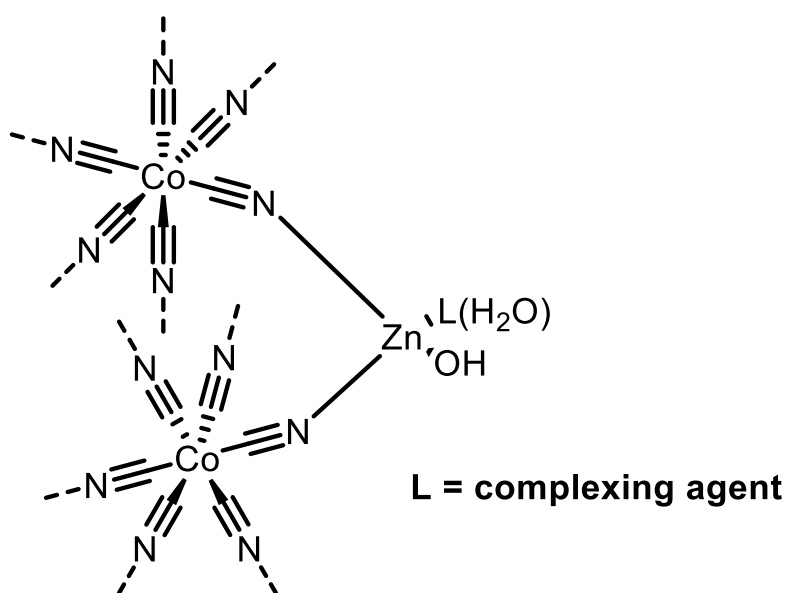
Figure S2. Proposed structure of the active site of Zn-Co(III) DMC catalyst.[33]

Table S1. Induction time t_{ini} and maximum pressure p_{max} of polymerization of PO and D_3 in DMC catalysis.

type	polymer	PDMS [g mol^{-1}]	p_{max} [bar]	$t_{ini.}$ [min]
P1.1	P(PO-*co*-DMS$_{2.9}$)	2.9	17.31	17.57
P1.2	P(PO-*co*-DMS$_{5.9}$)	5.9	17.98	16.97
P1.3	P(PO-*co*-DMS$_{6.4}$)	6.4	17.05	12.51
P1.4	P(PO-*co*-DMS$_{11.9}$)	11.9	15.52	27.24
P2.1	P(PO-*co*-DMS$_{23.0}$)	23.0	18.67	15.15
P2.2	P(PO-*co*-DMS$_{46.1}$)	46.1	17.95	20.86

a) Determined via ^{1}H NMR (300 MHz, CDCl$_3$)

b) Determined via SEC (PEG calibration)
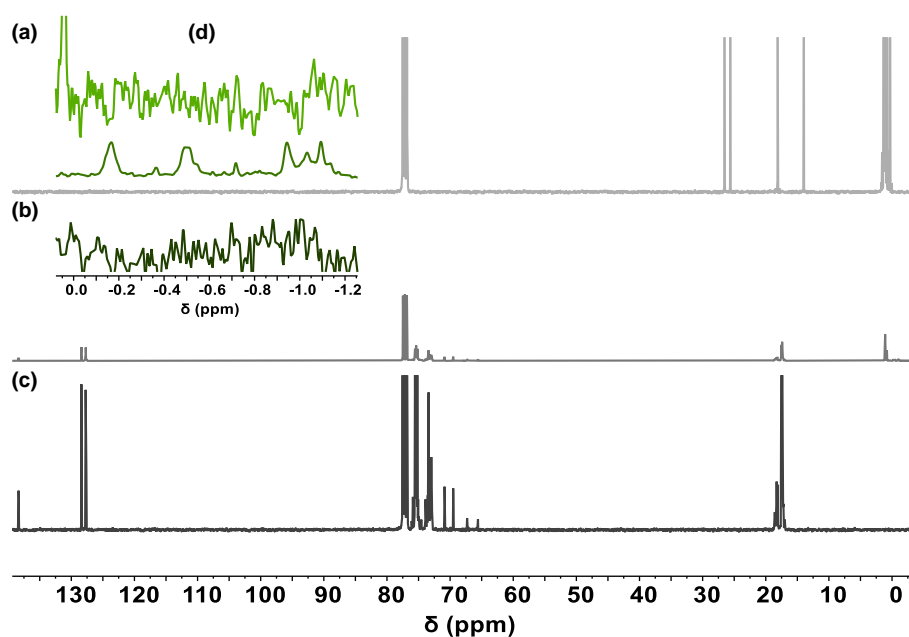
Figure S3. ^{13}C NMR spectrum, Inverse Gated (CDCl$_3$, 300 MHz, 25 °C) of (a) PDMS, via AROP initiated by *n*-butyllithium, (b) P2.1 (c) PPO, synthesized by DMC catalysis initiated by 2-(benzyloxy)ethanol, (d) spectral region of 0.0 to -1.2 ppm of 13C spectra a-c.
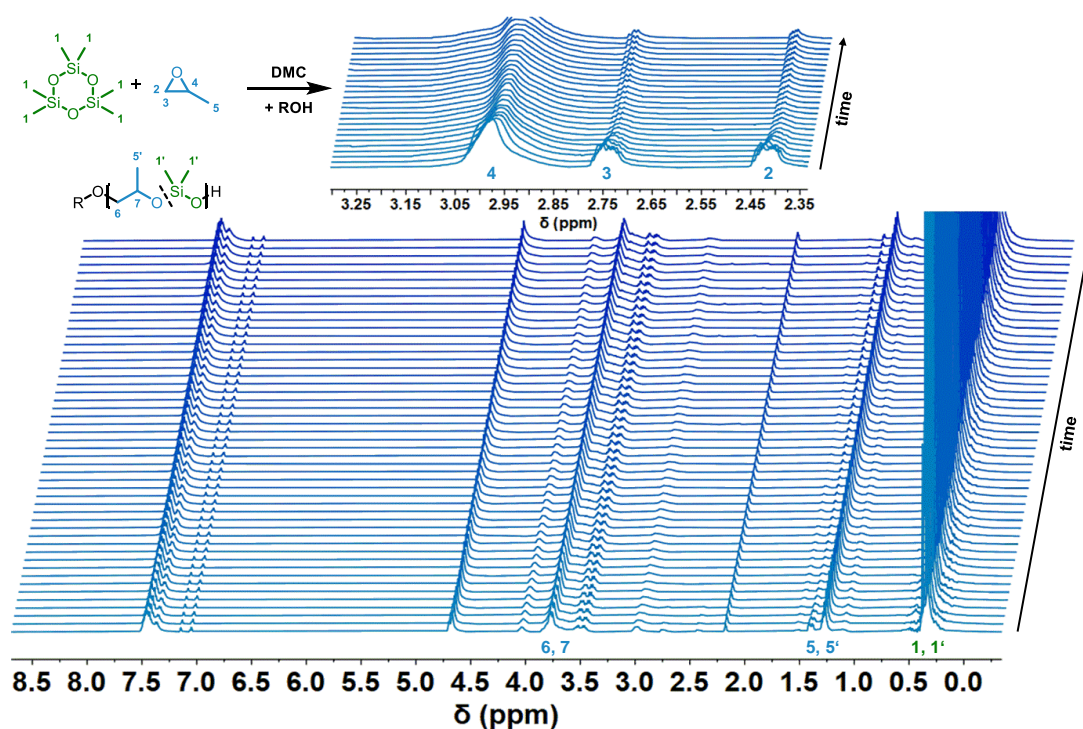
Figure S4. *In situ* ^{1}H NMR kinetic measurement with one spectrum min^{-1}: decrease of epoxide signals (3.0-2.4 ppm) and increase of polyether backbone signals (4.1-3.5 ppm), respectively.
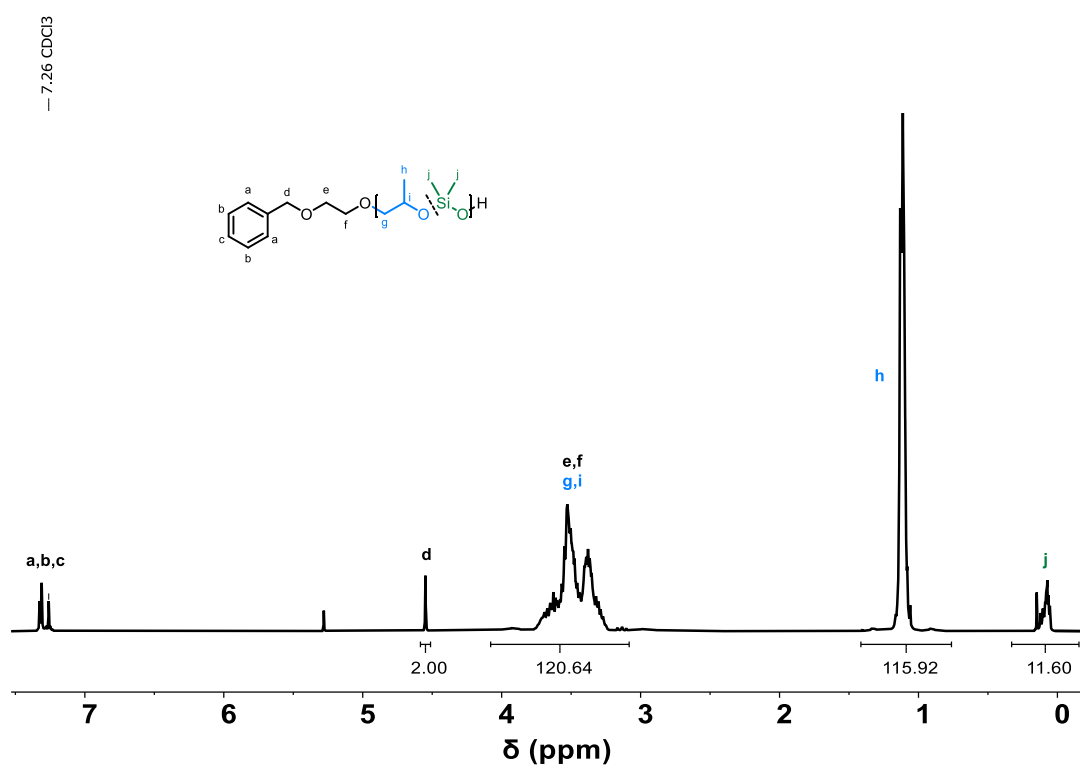
Figure S5. ^{1}H NMR spectrum (CDCl$_3$, 300 MHz, 25 °C) of P1.2. Evaluation of molecular weights by normalization to Bz-CH$_2$ at 4.55 ppm.
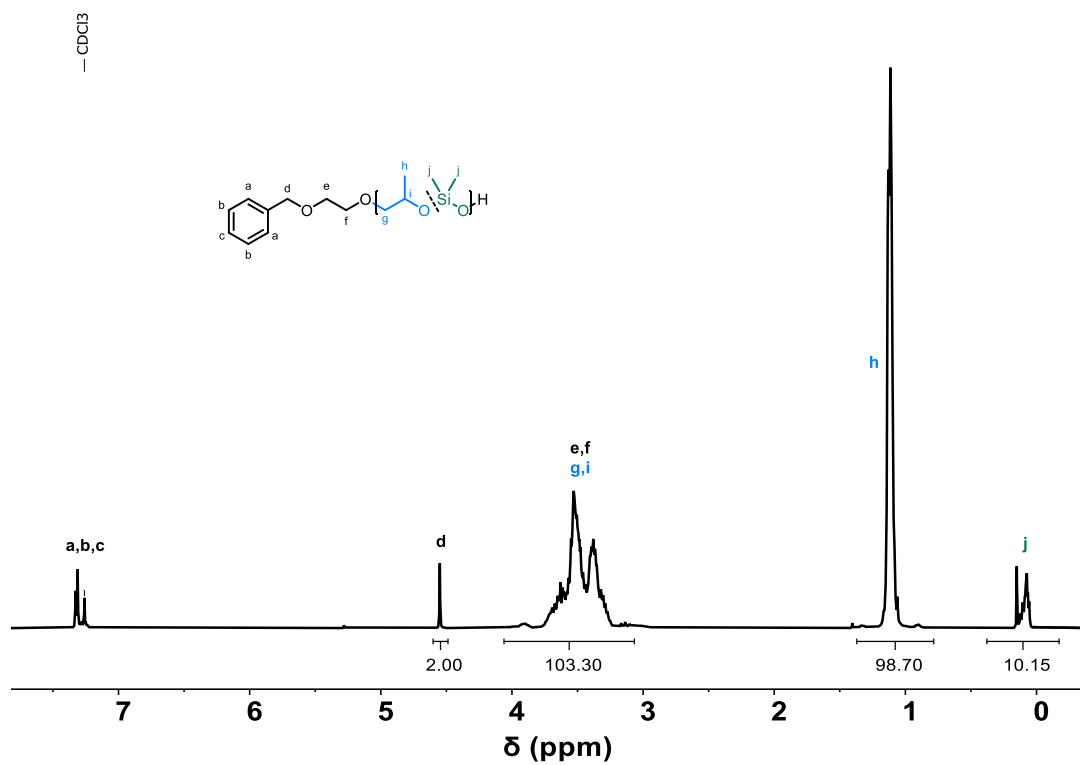

Figure S6. ^{1}H NMR spectrum (CDCl$_3$, 300 MHz, 25 °C) of P1.3. Evaluation of molecular weights by normalization to Bz-CH$_2$ at 4.55 ppm.
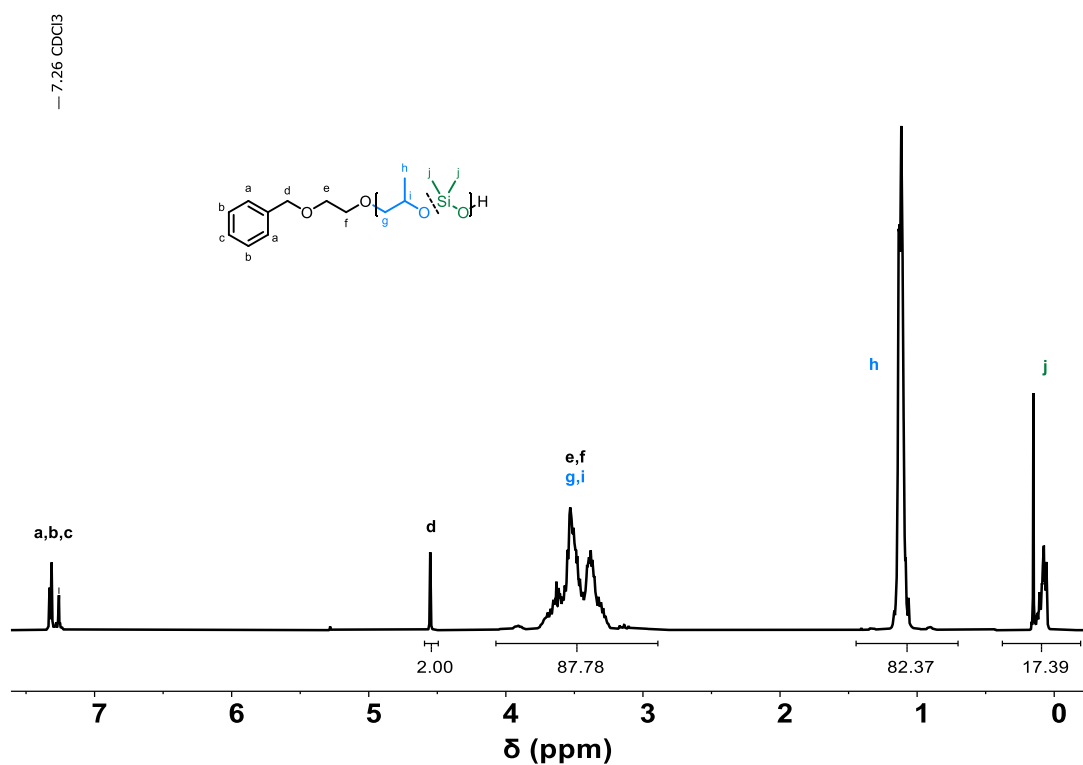
Figure S7. ^{1}H NMR spectrum (CDCl$_3$, 300 MHz, 25 °C) of P1.4. Evaluation of molecular weights by normalization on Bz-CH$_2$ at 4.55 ppm.
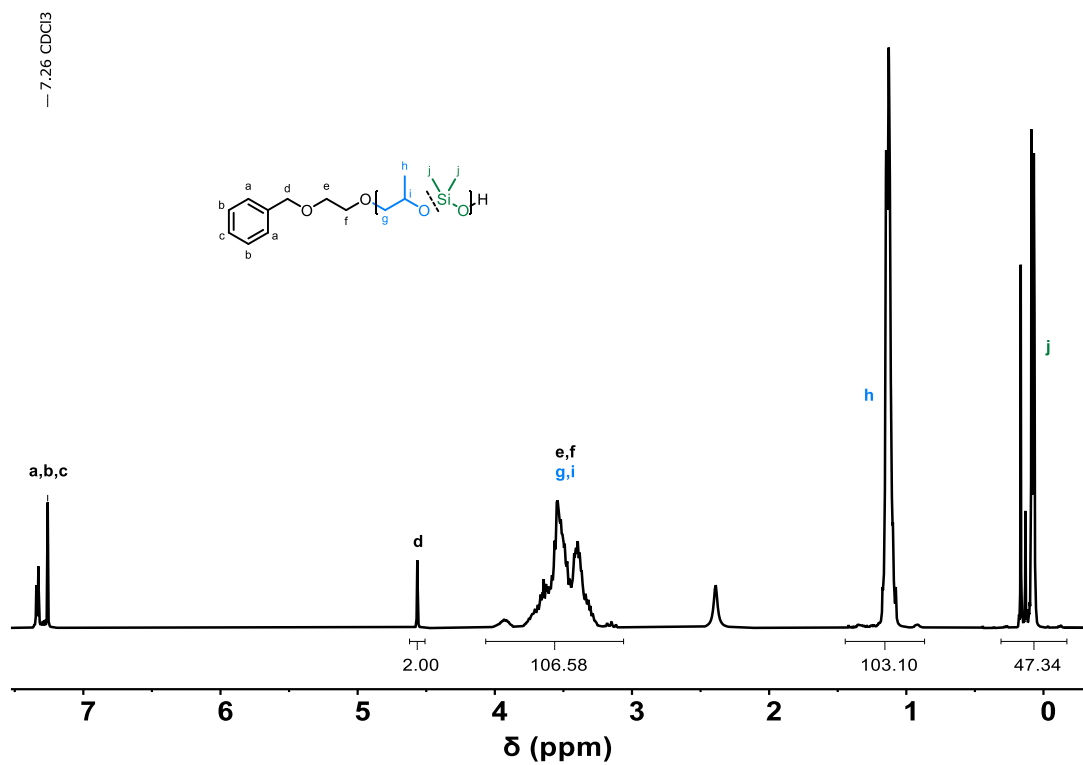
Figure S8. ^{1}H NMR spectrum (CDCl$_3$, 300 MHz, 25 °C) of P2.1. Evaluation of molecular weights by normalization on Bz-CH$_2$ at 4.55 ppm.
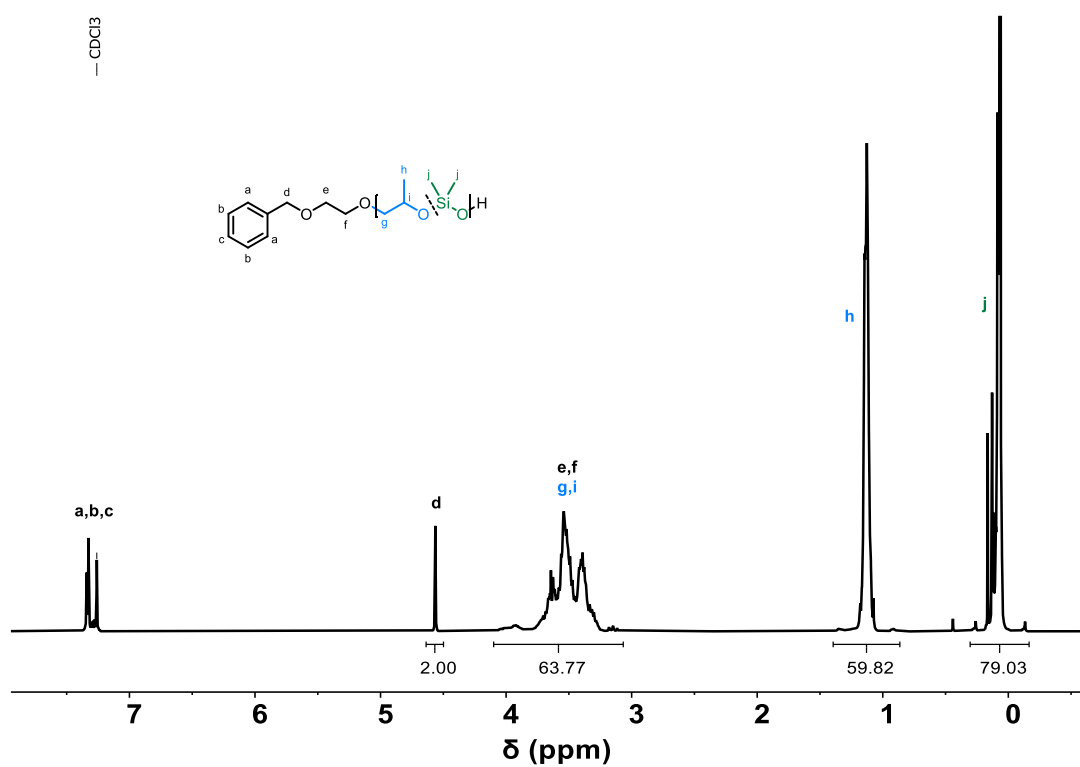
Figure S9. ^{1}H NMR spectrum (CDCl$_3$, 300 MHz, 25 °C) of P3.1. Evaluation of molecular weights by normalization to Bz-CH$_2$ at 4.55 ppm.
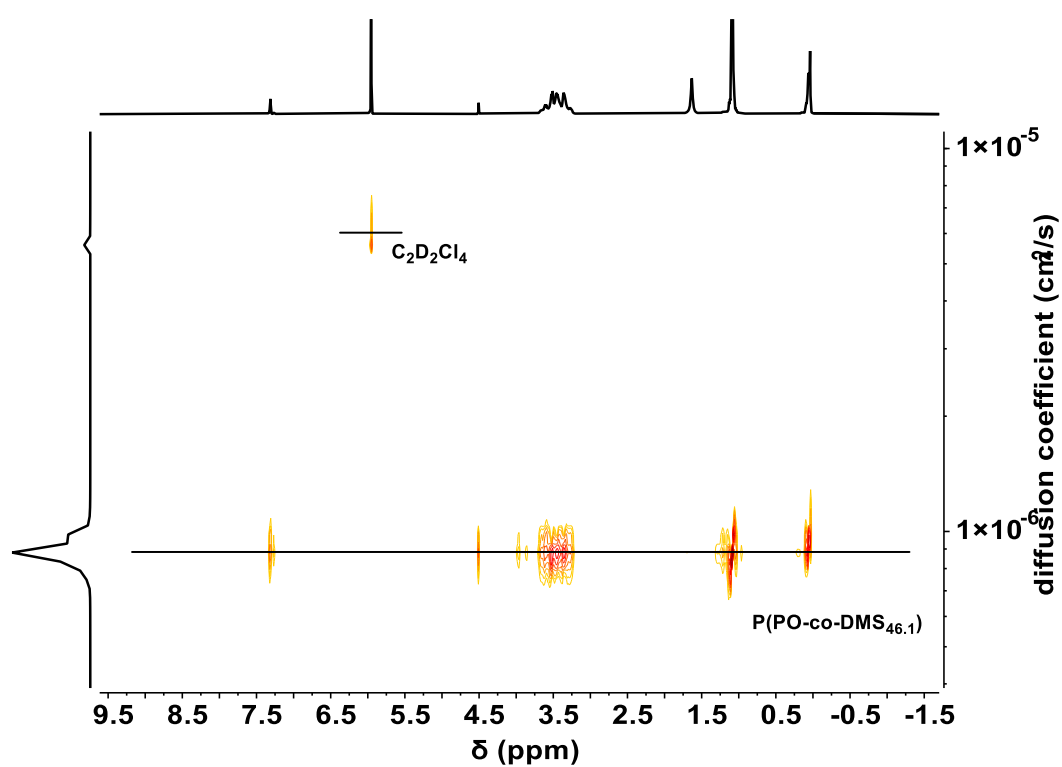
Figure S10. ^{1}H DOSY NMR spectrum (C$_2$D$_2$Cl$_4$, 500 MHz, 25 °C) of P3.1.
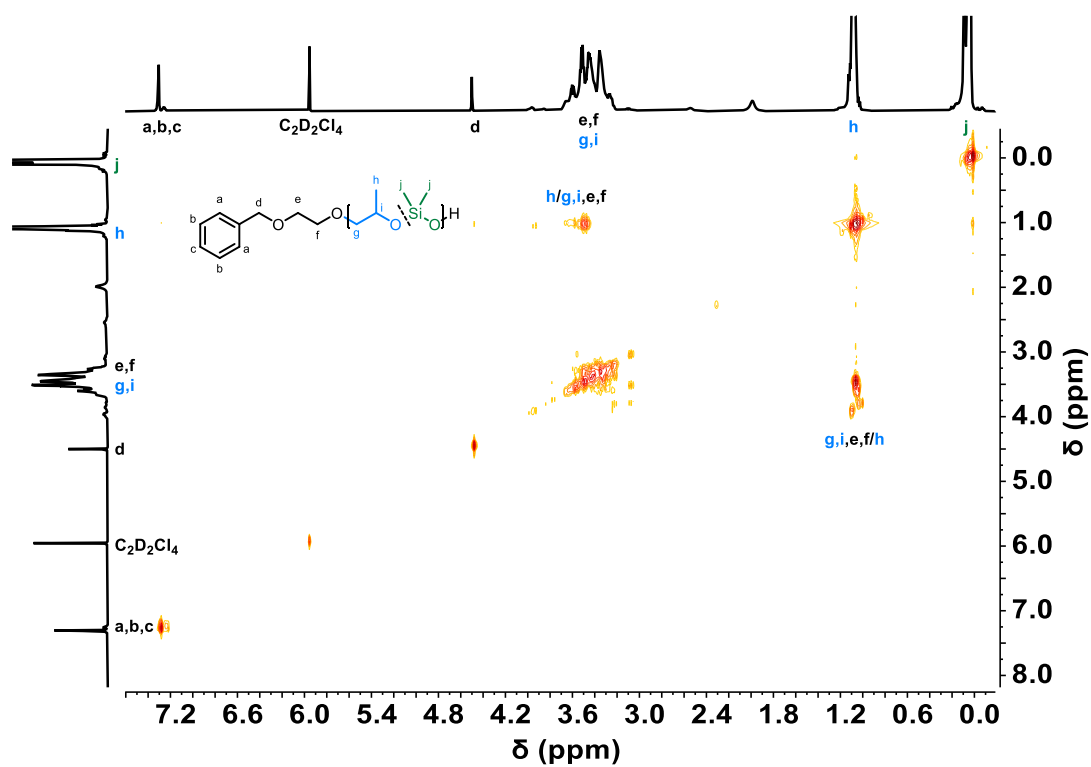
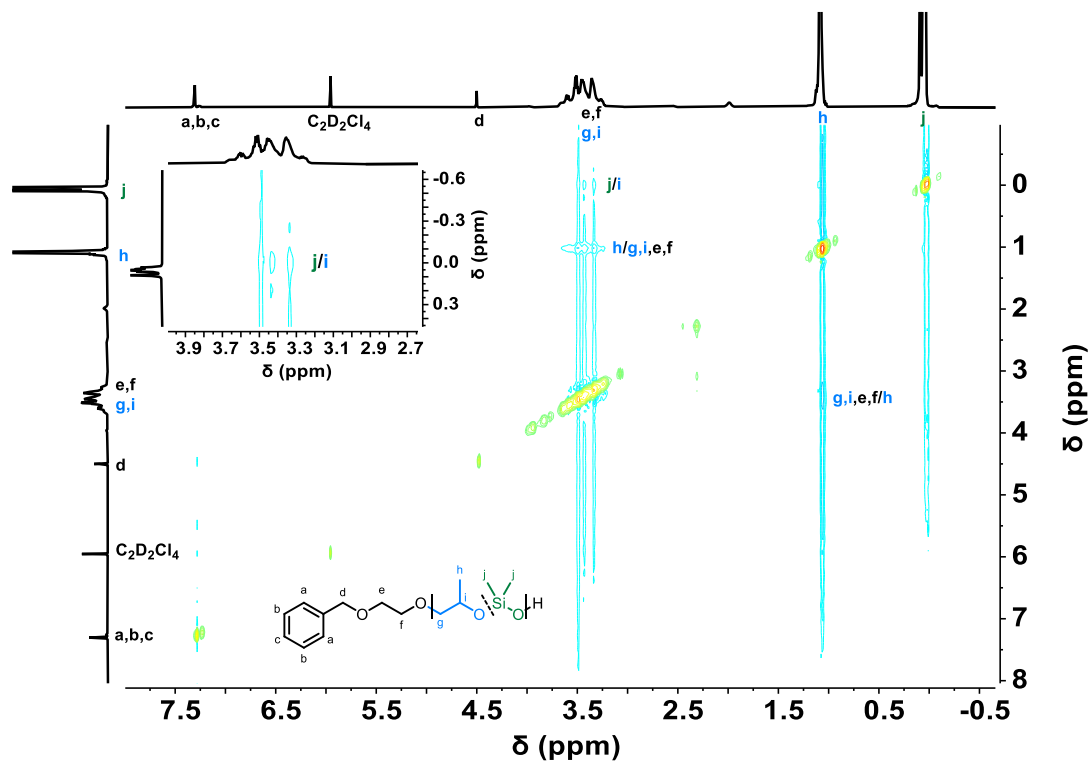**Figure S11.** ^{1}H ^{1}H COSY NMR spectrum (C$_2$D$_2$Cl$_4$, 500 MHz, 25 °C) of P3.1.

Figure S12. ^{1}H ^{1}H NOESY NMR spectrum (C$_2$D$_2$Cl$_4$, 500 MHz, 25 °C) of P3.1. Data of 1H spectra on right and left axes were taken from 1D experiments.

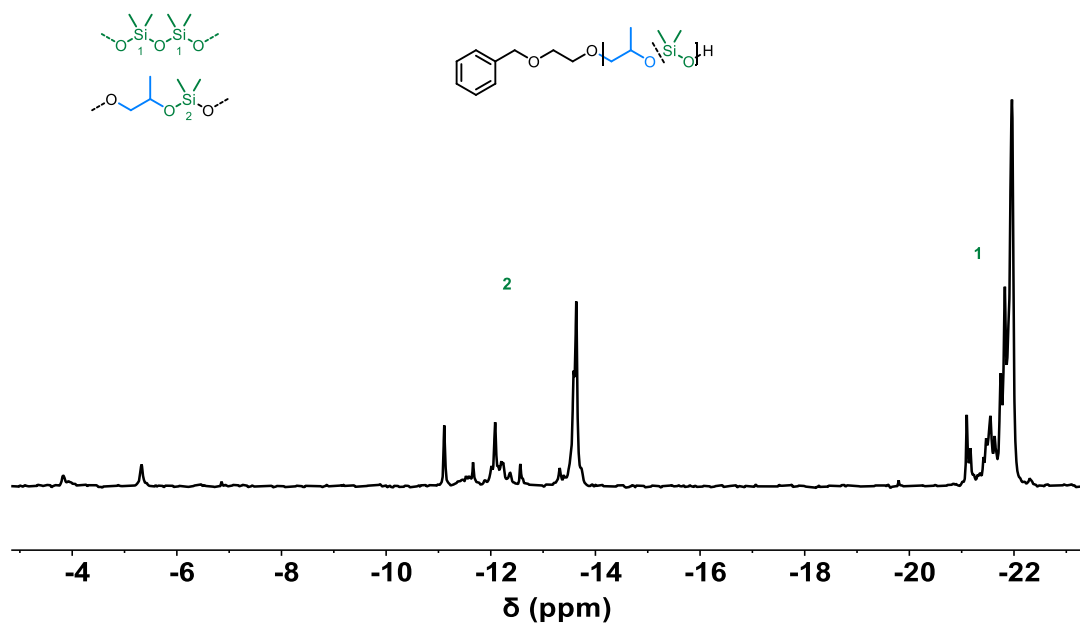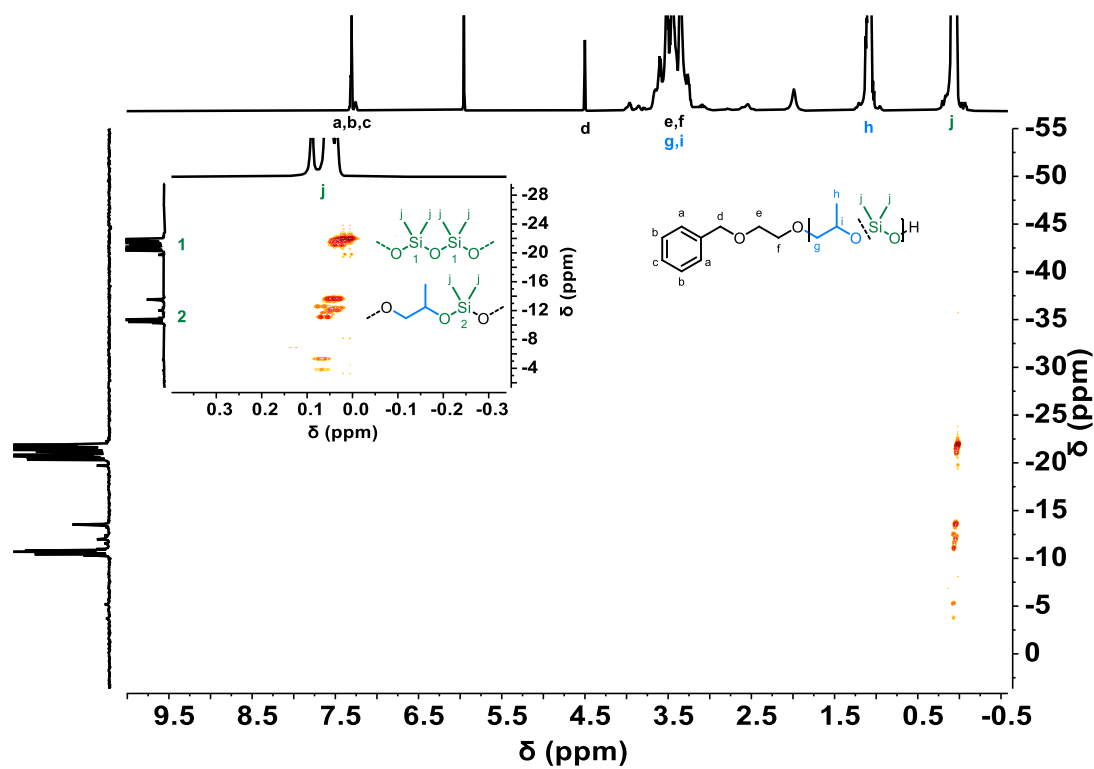**Figure S13.** ^{29}Si INEPT NMR spectrum (C$_2$D$_2$Cl$_4$, 500 MHz, 25 °C) of P3.1.

Figure S14. ^{1}H ^{29}Si HMBC NMR spectrum (C$_2$D$_2$Cl$_4$, 500 MHz, 25 °C) of P3.1.
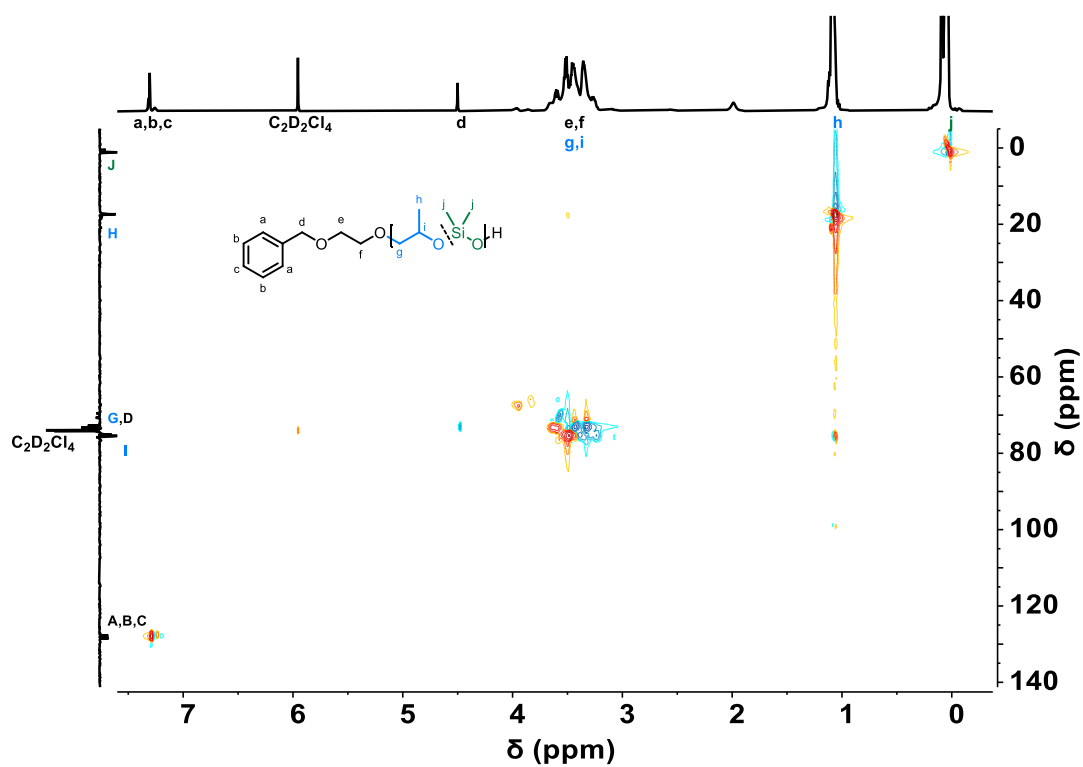
Figure S15. ^{1}H ^{13}C HSQC NMR spectrum (C$_2$D$_2$Cl$_4$, 500 MHz, 25 °C) of P3.1. Plotted carbon on the left axes was 1D 13C-NMR spin echo APT (attached proton test) experiment.
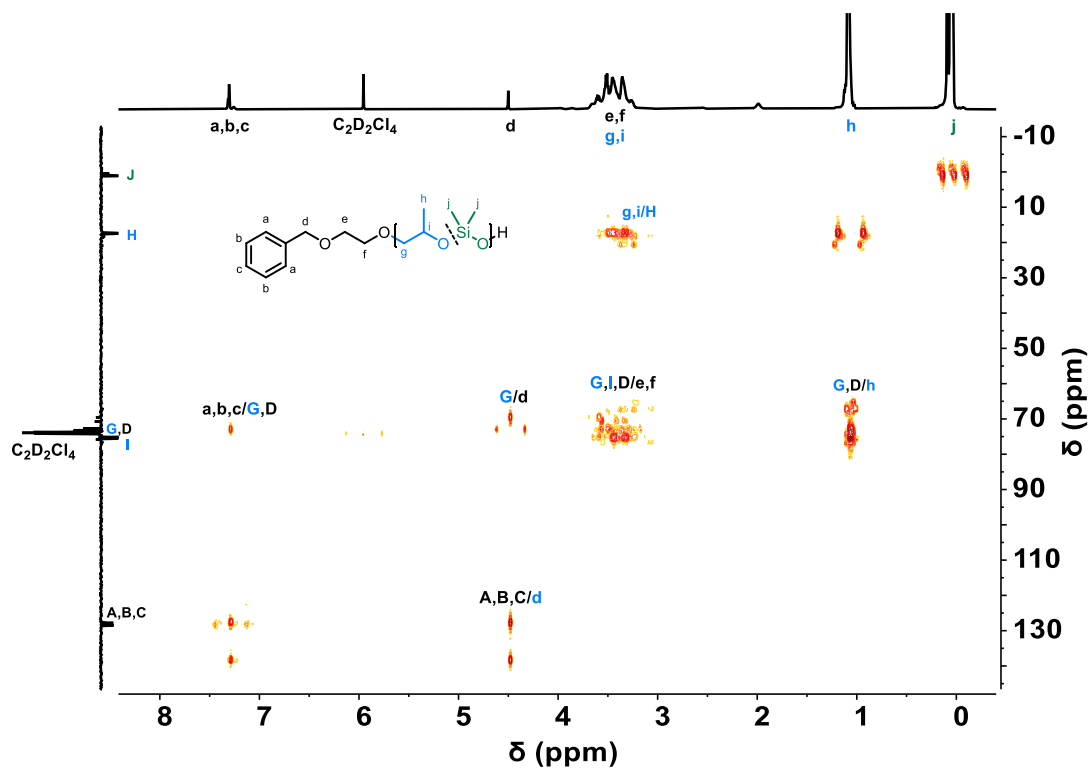

Figure S16. ^{1}H ^{13}C HMBC NMR spectrum (C$_2$D$_2$Cl$_4$, 500 MHz, 25 °C) of P3.1. Plotted carbon on the left axes was 1D 13C-NMR spin echo APT experiment.
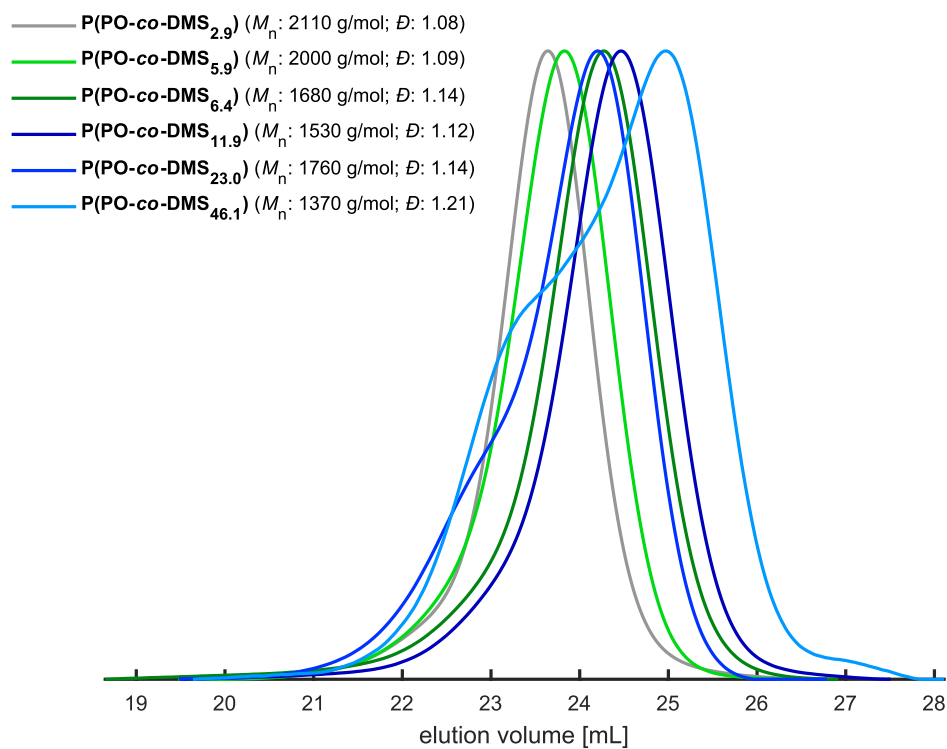
Figure S17. SEC diagrams of P(PO-*co*-DMS) copolymers (solvent: DMF, standard: PEG).
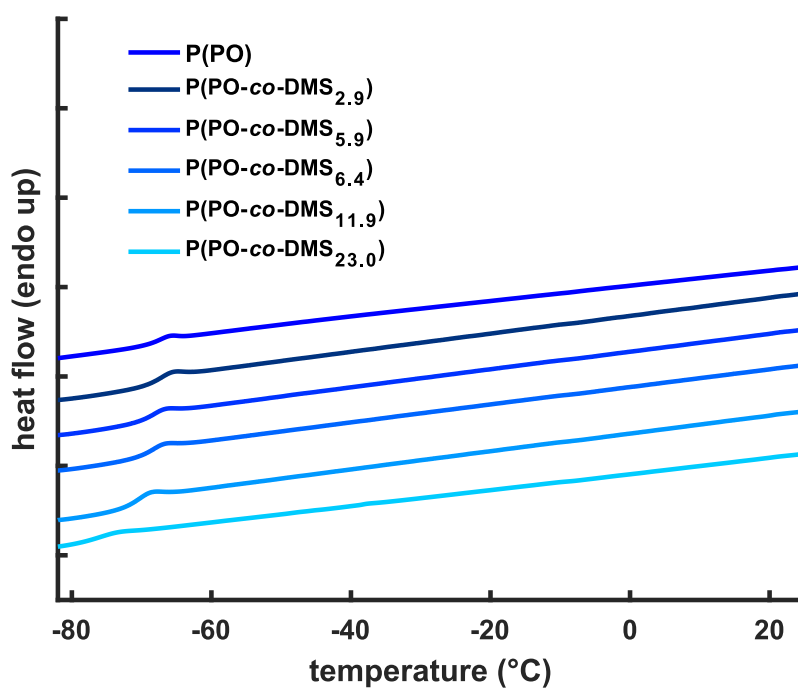

Figure S18. Thermal analysis of P(PO-*co*-DMS) by DSC measurements. Temperature range from -100 to 30 °C, 20 °C min^{-1} (endotherm: up).
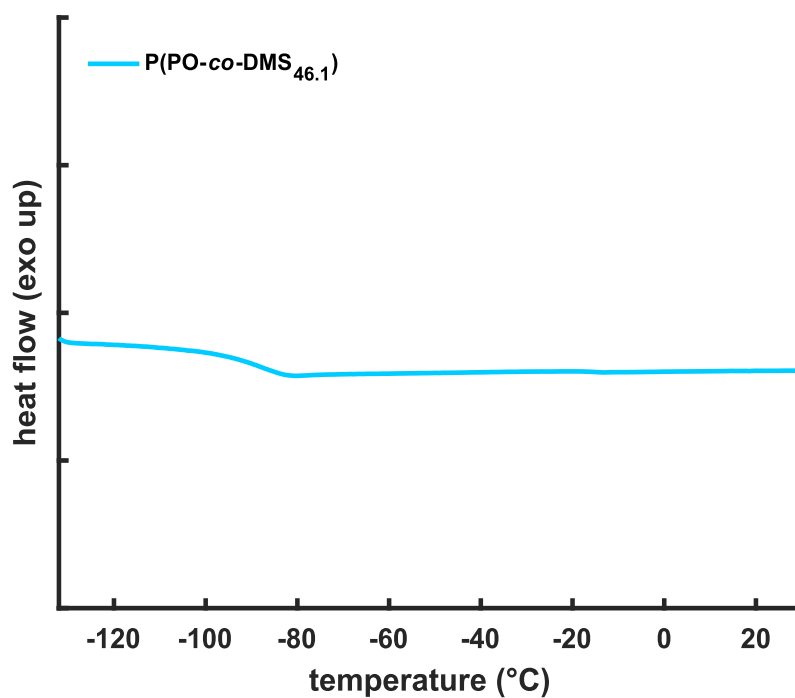
Figure S19. Thermal analysis of P3.1 by DSC measurements. Temperature range from -140 to 30 °C, 10 °C min^{-1}, exo up.

Table S2. Results of contact angle measurements to evaluate the PDMS impact to the hydrophobicity of P(PO-*co*-DMS) copolymers.

type	PDMS content [mol%]	contact angle [°]	σ [°]
PPO	0	39.4	0.2
P1.1	2.9	39.7	0.8
P1.2	5.9	44.7	1.6
P1.3	6.4	45.7	1.5
P1.4	11.9	45.7	0.8
P2.1	23.0	49.3	1.4
P3.1	46.1	53.9	1.7

Chapter 3.3

Toolbox DMC Catalysis: Synthesis and Modification of Multifunctional Polyether-Polysiloxane Copolymers

Materials possessing both polyether and polysiloxane segments possess a highly valuable property profile, which is widely utilized in silicone surfactants. Herein, polyether-polysiloxane based copolymers possessing functional side chains are introduced via DMC catalyzed statistical copolymerization. The established functional epoxide monomers allyl glycidyl ether (AGE), ethoxy ethyl glycidyl ether (EEGE) and the rarely investigated glycidyl trimethylsilane (GlyTMS) are utilized in the unusual copolymerization with propylene oxide (PO) and hexamethylcyclotrisiloxane (D_3). Amorphous copolymers of 1.8 to 2.5 kg mol^{-1}, with dispersities of 1.10 to 1.43 are obtained with varied amounts of functional groups and up to 25 mol% siloxane content. Exemplary post-polymerization experiments were conducted, proving the versatile application possibilities offered by these structures. Thiol-ene click chemistry is presented for the introduction of carboxylic acid functions to AGE containing copolymers. Further, the incorporation of methacrylic esters at linear glycerol units is performed via Steglich esterification after acidic deprotection of the EEGE containing copolymers. Radical cross-linking experiments demonstrate the formation of polymer networks. Additionally, a deprotection study regarding polyether-polysiloxane copolymers bearing GlyTMS units was conducted. Hereby, the deprotection of the TMS protection groups and the behavior under acidic treatment of C-O-Si bonds of the polymeric backbone is investigated. The introduction of functional groups further expands the application scope of amorphous and amphiphilic statistical polyether-polysiloxane copolymers. The acid sensitivity of C-O-Si bonds in the functional polyether-polysiloxane copolymers containing polar substituents offers promise for pH-responsive, degradable surfactants.

INTRODUCTION

Multifunctional polymers enable the customized design of materials for manifold applications. The anionic ring-opening polymerization (AROP) represents a versatile platform for preparation of multifunctional polyethers via epoxides as well as polysiloxanes via cyclic siloxanes.[1,2] The introduction of monomers bearing functional groups enables the controlled synthesis of copolymers that can undergo versatile post-modification.[3,4] In the past, numerous glycidyl ethers possessing side-chains like acetal-protected hydroxyl-groups or allyl, vinyl and aromatic substituents have been introduced as epoxide monomers and successfully polymerized by AROP.[5–8] Such functional groups allow the protection of hydroxyl-functionalities to avoid the formation of hyperbranched polyethers. Several protected monomers enabling the synthesis of linear polyglycerol (*lin*PG) are widely used due to the wide functionalization possibilities offered by primary hydroxyl-groups, but also due to the high polarity of *lin*PG.[9,10] At present, the most prominent of these monomers is the acetal protected glycerol derivative, ethoxy ethyl glycidyl ether (EEGE).[11] Already in 1968 Tsuruta et al.[12] investigated the AROP of another alternative to generate *lin*G units, glycidyl trimethylsilane (GlyTMS), which was patented one year later by Vandenberg.[13] However, primarily oligomeric structures were obtained for the polymerization of GlyTMS initiated by alkali metal alkoxides. Besides the epoxide ring-opening, a transesterification-like reaction, termination reactions as well as the formation of hyperbranched structures were observed.[14,15]

In contrast to functional polyethers, the most prominent polysiloxane, polydimethylsiloxane (PDMS) is widely applied as a commodity polymer due to its viscoelastic properties as well as its excellent thermal and oxidative stability.[16] The highly hydrophobic, amorphous polymer with its exceptionally low T_g (-120 °C) is widely used for the synthesis of surfactants, coating materials and sealants.[17] Particularly the highly hydrophobic properties are exploited for the synthesis of amphiphilic structures, mostly in combination with water-soluble polyethers i.e. as block copolymers in foam stabilizers for polyurethane foaming.[18] Polyether-polysiloxane based copolymers are generally achieved via coupling reactions of both homopolymer segments by hydrosilylation or thiol-ene click chemistry.[19–22]

Yet, the statistical copolymerization of epoxides and cyclic siloxanes is not possible by AROP due to the insufficient nucleophilicity of the alkoxide chain end in regard to the ring-opening of cyclic siloxanes. Recently, our group presented the first controlled synthesis of statistical P(PO-*co*-DMS) copolymers by use of the double metal cyanide (DMC) catalyst for polymerization of propylene oxide (PO) and hexamthylcyclotrisiloxane D_3.[23] *In situ* ^{29}Si NMR spectroscopy revealed the formation of gradient copolymers. The cationic coordination-insertion mechanism[24] permits to overcome the obstacles observed for AROP regarding the ring-opening of D_3 by the alkoxide chain end.

Due to the suppression of proton abstraction at the methyl group of PO, polymers of very low unsaturation levels are obtained (0.001 meq g^{-1})[25] via DMC-based ring-opening polymerization.[26–29] Elaborate work up for polymers synthesized via bulk DMC catalysis is redundant, as the inactive

catalyst remains finely suspended in the respective product, once the initiation-fragmentation mechanism is completed.[30–32]

Throughout this work, we further elaborate the scope and limitations of DMC catalyzed statistical copolymerization of PO and D_3, focusing on the implementation of different epoxides which contain functional groups (*f*Gly). For this purpose, the two established glycidyl ether monomers ethoxy ethyl glycidyl ether (EEGE) and allyl glycidyl ether (AGE) as well as the rarely investigated monomer glycidyl trimethylsilane (GlyTMS) are utilized. Various post-polymerization reactions are employed to demonstrate the introduction of polar groups as well as the formation of polymer networks based on polyether-polysiloxane copolymers.

RESULTS & DISCUSSION

Polymer Synthesis

The copolymerization of P(PO-*co*-*f*Gly-*co*-DMS) was conducted by DMC catalysis (structure catalyst, SI Figure S1) in a solvent-free one-pot synthesis under high pressure (1 or 5 bar argon) and at high temperatures of 120 °C (Scheme 1). 2-(benzyloxy)ethanol was utilized as an initiator, enabling precise characterization of the resulting polymers by ^{1}H NMR spectroscopy (SI, Figure S3 to S5). Supporting 2D NMR spectroscopy analysis enabled the in-depth characterization of the synthesized copolymers. ^{1}H diffusion-ordered (DOSY) NMR spectroscopy confirmed the synthesis of a single polymeric species, excluding a blend of homopolymers (SI, Figure S6 to S9). Additionally, ^{1}H ^{1}H correlation (COSY), ^{1}H ^{13}C heteronuclear single-quantum correlation (HSQC) and multiple-bond correlation (HSQC) spectroscopy permitted full characterization of the obtained products (SI, Figure S10 to S19). Additionally, ^{29}SI INEPT DOSY NMR was performed for a typical P(PO-*co*-GlyTMS-*co*-DMS) copolymer, which indicates the occurrence of siloxane-only, TMS-only as well as polyether-siloxane dyads, supporting the successful synthesis of statistical copolymers (SI, Figure S20).
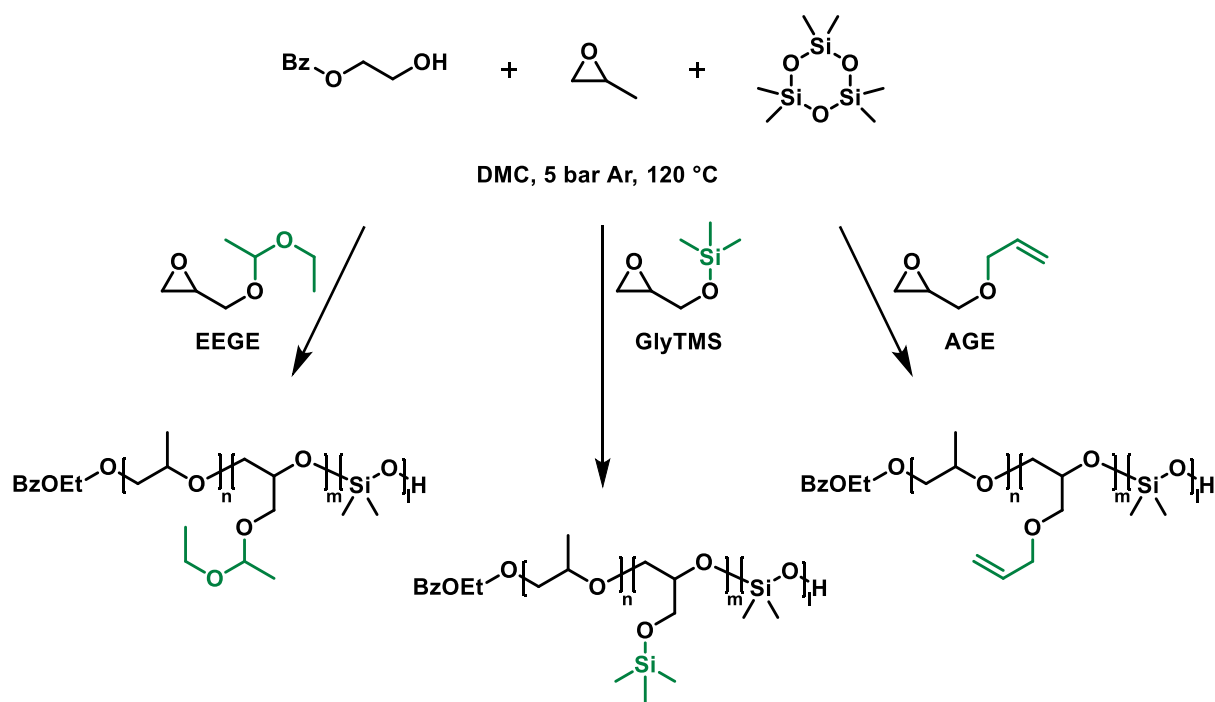
Scheme 1. Pathway for synthesis of P(PO-*co*-EEGE-*co*-DMS), P(PO-*co*-AGE-*co*-DMS) and P(PO-*co*-GlyTMS-*co*-DMS) copolymers via DMC catalysis.

Copolymers with theoretical molecular weights $M_n^{th.}$ of 2.5 to 3.2 kg mol^{-1} with 3 to 4 fGly units were targeted (Table 1). The theoretical content of DMS units was 9 or 10 for sample **P1.1** to **P2.1** and **P3.0**, therefore 3 equivalents of D$_3$ regarding the initiator was utilized. Further, polymers with a theoretical amount of 15 to 25 units of DMS were synthesized (**P2.3**, **P2.4** and **P3.2**). Polymers of low to moderate dispersities ($Đ$ = 1.10 to 1.43) were obtained, as measured by SEC in DMF (PEG standard). Monomodal distributions were observed (SI, Figure S21 and S23). The increase of $M_n^{th.}$ > 3.0 kg mol^{-1} induced tailing to higher molecular weights, which is commonly known for DMC catalyzed polymerizations of epoxides.[33] Full conversion of PO as well as the respective fGly monomer was obtained in all cases. Nevertheless, a low to moderate conversion of D$_3$ (13 to 78 %) was observed after 24 as well as 144 h reaction time. To examine the impact of functional glycidyl ethers to the polymerization efficiency of D$_3$ in the presented copolymerization, a polymerization with merely 1 unit of EEGE (**P2.1**) was performed. Considering polymerization statistics, one can surmise the absence of glycidyl ether units in some polymer chains within this sample. Expectedly, the low amount of fGly lead to a strongly enhanced conversion of D$_3$ (100 %), which is in good agreement with the results recently reported on the copolymerization of PO and D$_3$ under DMC catalysis.[23]

Table 1. Overview of synthesized P(PO-*co*-*f*Gly-*co*-DMS) copolymers.

| No. | Mono. | $P_n^{th.}/P_n$ | | | $M_n^{th.}$ [kg mol^{-1}] | M_n^1 [kg mol^{-1}] | M_n^2 [kg mol^{-1}] | Đ | T_g [°C] |
		PO[1]	*f*Gly[1]	DMS[1]					
P1.1[3]		27/27	2/3	9/7	2.7	2.1	1.4	1.16	-73
P1.2[3]	AGE	26/23	3/2.5	9/2	2.6	1.8	1.4	1.10	-71
P1.3[3]		26/23	3/3	9/5	2.5	2.2	1.4	1.28	-72
P1.4[4]		28/28	4/4	10/4	3.0	2.0	1.6	1.43	-67
P2.1[3]		30/28	1/1	9/10	2.5	2.5	1.2	1.26	-73
P2.2[3]	EEGE	26/25	3/3	9/2	2.7	2.0	1.1	1.31	-70
P2.3[4]		18/18	4/4	25/8	3.2	2.0	1.0	1.26	-75
P2.4[4]		24/23	5/4	15/8	3.1	2.5	1.0	1.35	-74
P3.0[3]		27/27	3/3	-	2.2	2.2	0.9	1.28	-66
P3.1[4]	GlyTMS	27/28	3/3	10/2	2.7	2.3	1.1	1.38	-67
P3.2[4]		27/29	3/3	15/2	3.0	2.4	1.1	1.30	-66

[1] Determined by ^{1}H NMR spectroscopy (CDCl$_3$, 300 MHz)

[2] Determined by SEC (solvent: dimethylformamide (DMF), calibration: PEG)

[3] Reaction time of 24 h

[4]Reaction time of 144 h

To investigate the impact of siloxane units on the thermal properties of the copolymers in bulk, differential scanning calorimetry (DSC) was performed. In general, the glass transition temperatures (T_g) of the respective polyether homopolymers range from -67 °C (PPO[23] and PEEGE[34]) to -77 °C[5] (PAGE), while PDMS possess an exceptionally low T_g (-120 °C) due to its highly flexible polymer backbone.[35] The T_g values of copolymers containing AGE (**P1.1**-**P1.4**) range between 67 to 73 °C, EEGE between 70 to -75 °C and GlyTMS between 66 and 67 °C (Table 1).The impact of siloxane units regarding the glass transition was detected for polymers containing > 7 DMS units. Thus, **P2.2** with merely 2 DMS units exhibits a T_g of 70 °C while 8 to 10 units in **P2.1**, **P2.3** and **P2.4** result in a decrease of the T_g up to 5 °C. Henceforth, P(PO-*co*-*f*Gly-*co*-DMS) samples containing higher incorporation rates of siloxane units show a high impact of PDMS on the thermal properties of the presented copolymer structures, which was similar observed for P(PO-*co*-DMS).

Pressure Monitoring

To gain further insights regarding the polymerization kinetics, analysis of the pressure progression during the DMC catalyzed copolymerizations was monitored. DMC catalyzed polymerization of PO is commonly accompanied by an explosive pressure increase after an induction period indicating the initiation of polymerization, followed by a fast decrease of pressure until a constant pressure plateau is reached.[36]

The recently published copolymerization of PO and D_3 by our group revealed the independence of polymerization initiation from to the ring-opening of D_3.[23] Throughout these studies, the pressure progression during the polymerization of PPO and P(PO-*co*-DMS) exhibited no significant difference, regardless of the concentration of D_3. This observation led to the conclusion that the pressure increase is exclusively due to the fragmentation of catalyst particles and the ensuing ring-opening of PO.

Fundamentally, different studies examined the impact of catalyst concentration on the initiation period t_{ini}.[36–39] An increase of catalyst loading reduced the t_{ini} significantly, however a precise correlation as well as an exact reproducibility has not been achieved to date as t_{ini} ranges from minutes up to several hours. Based upon the above-mentioned observations, the impact of presence of *f*Gly on the pressure progression was investigated.
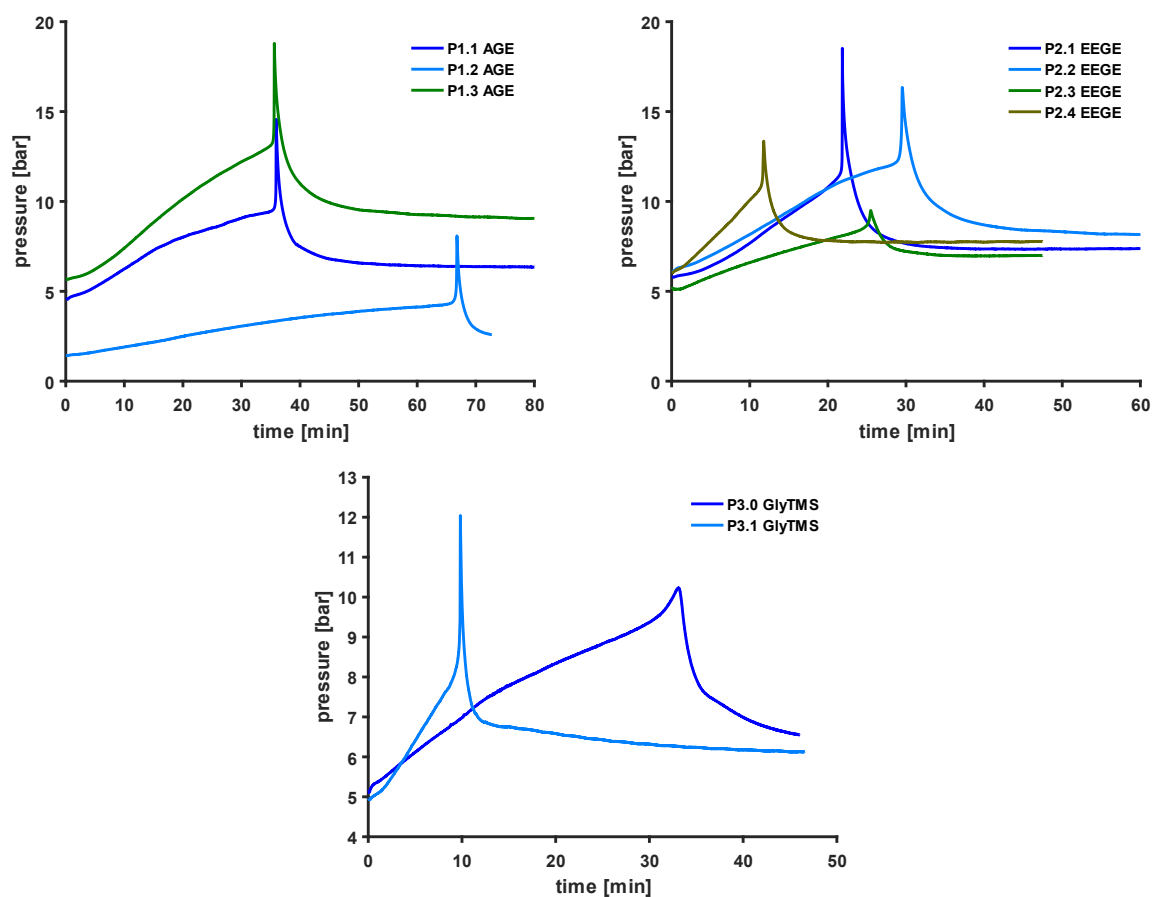

Figure 1. Exemplary pressure-time graph received from the copolymerizations of P(PO-*co*-AGE-*co*-DMS) (top left), P(PO-*co*-EEGE-*co*-DMS) (top right), P(PO-*co*-GlyTMS-*co*-DMS) and P(PO-*co*-GlyTMS) (bottom).

Figure 1 shows the exemplary pressure-time graphs recorded during the copolymerization of PO, D_3 and the respective *f*Gly. To date, several publications investigate the pressure progression occurring during homopolymerisation of PO. However, the investigation of epoxide copolymerization kinetics in relation to pressure during DMC catalysis remained unexplored. Characteristic

pressure progressions are recorded which correlate with the literature reports. Yet, one has to take the low P_n of fGly for the respective copolymerizations into account. Higher ratios of fGly possibly exhibit a stronger impact on the initiation process, therefore lead to a decelerated pressure increase. Further experiments are therefore required to investigate the impact of increasing the fGly content on the initiation process.

Apart from the pressure progression, the herein illustrated results correspond with the described literature findings with a sharp peak. The values of t_{ini} varied between 10 to 35 min which were observed for all polymerizations with a starting pressure of 5 bar. For all copolymerization experiments, no distinct trend between t_{ini} and the comonomer composition was deducible. Noteworthy, the polymerization of **P1.2** conducted at 1 bar showed an exceptionally long tini of 68 min, indicating a prolonged initiation period with lower pressure. However, further experiments are required to confirm this hypothesis.

The maximum pressure pmax recorded for each polymerization at 5 bar varied between 9 to 19 bar while equal to t_{ini}, no distinct trend was apparent. The polymerization of PO and GlyTMS in the absence of D_3 yielding **P3.0** exhibits a conspicuously different pressure progression as no sharp pressure acceleration was recorded. The pressure increase as well as the subsequent decrease is significantly decelerated, indicating a slow initiation process which is supported by the moderate dispersity ($Đ = 1.28$) observed. However, the determination regarding the origin of this observation requires further experiments as the following polymerization of **P3.1** including D_3 exhibited the commonly observed progression (Figure 1, bottom).

Post-polymerization modification of P(PO-*co*-AGE-*co*-DMS)

The incorporation of functional epoxide monomers offers manifold possibilities for post-polymerization modifications. Therefore, allyl ether side-chains of P(PO-*co*-AGE-*co*-DMS) was exemplary addressed by a thiol-ene click reaction (TEC) with thioglycolic acid (Scheme 2). Hereby, the thiol-ene reaction enables to use the C=C bond[40] to introduce carboxylic acid functionalities to the polymeric side-chains, which are not accessible by AROP or DMC catalysis without suitable protection groups.
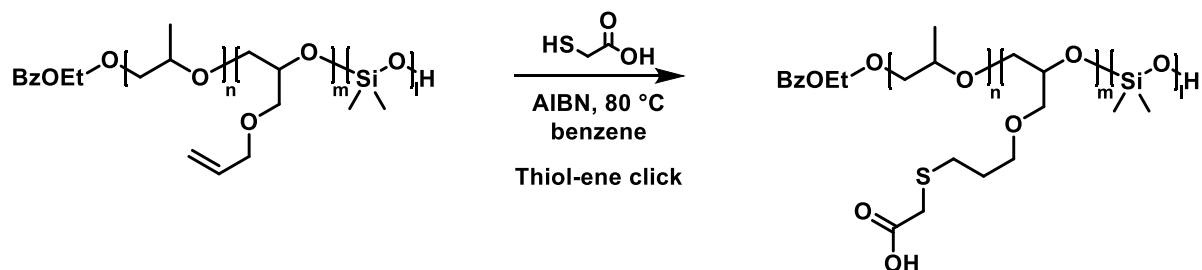
Scheme 2. Introduction of carboxylic acid functionalities to the polyether side chain of P(PO-*co*-AGE-*co*-DMS) by thiol-ene click of allylic substituents with thioglycolic acid.

The radical reaction was performed in benzene at 80 °C with addition of the thermally unstable azobis(isobutyronitril) (AIBN). The full conversion of the double bonds of AGE units was determined via ^{1}H NMR and IR spectroscopy (Figure 2 and Figure 3). Comparison of the IR spectra of **P1.2** (top) with the functionalized product after the thiol-ene click reaction **P1.2** TEC (bottom) illustrate the absence of the double bond valence oscillation (1647 cm^{-1}) and the appearance of the valence oscillation of the carboxylic acid (1730 cm^{-1}).
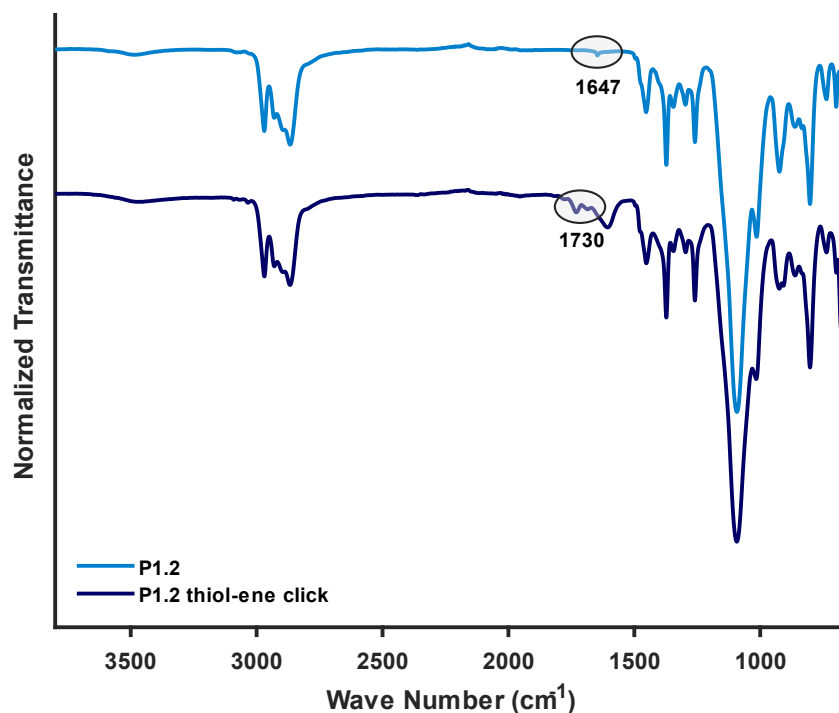

Figure 2. IR spectra of P1.2 P(PO-*co*-AGE-*co*-DMS) and P1.2 TEC after thiol-ene click with thioglycolic acid.

To verify the full consumption of all allylic functionalities, comparative ^{1}H NMR spectra were performed. The signals of both allylic protons, namely the terminal CH$_2$ (5.22 ppm) as well as the CH (5.90 ppm) protons together with the methylene protons (3.98 ppm) are no longer present in the resulting product. Subsequent 2D NMR experiments further confirm the transformation of the unsaturated side-chains to thioether structure with methylene proton signal at 2.73 and 1.86 ppm (Figure 3, bottom) (SI: Figure S27 to S30). The ^{1}H NMR spectrum combined with the ^{1}H DOSY NMR (SI, Figure S21) confirms the preservation of siloxane content within the copolymer. Notably, the splitting pattern of the siloxane protons changes after functionalization. A possible reason for this observation is the change of chemical environment as the introduction of carboxylic acid substituents leads to a significant increase of the polarity. Further, the introduction of statistically 2.5 carboxylic groups to **P1.2** facilitates the water-solubility of the otherwise hydrophobic terpolymer. Thus, water-solubility after thiol-ene click was observed at 4 °C while the hydrophobicity of the starting polymer **P1.2** impeded the solubility in water.
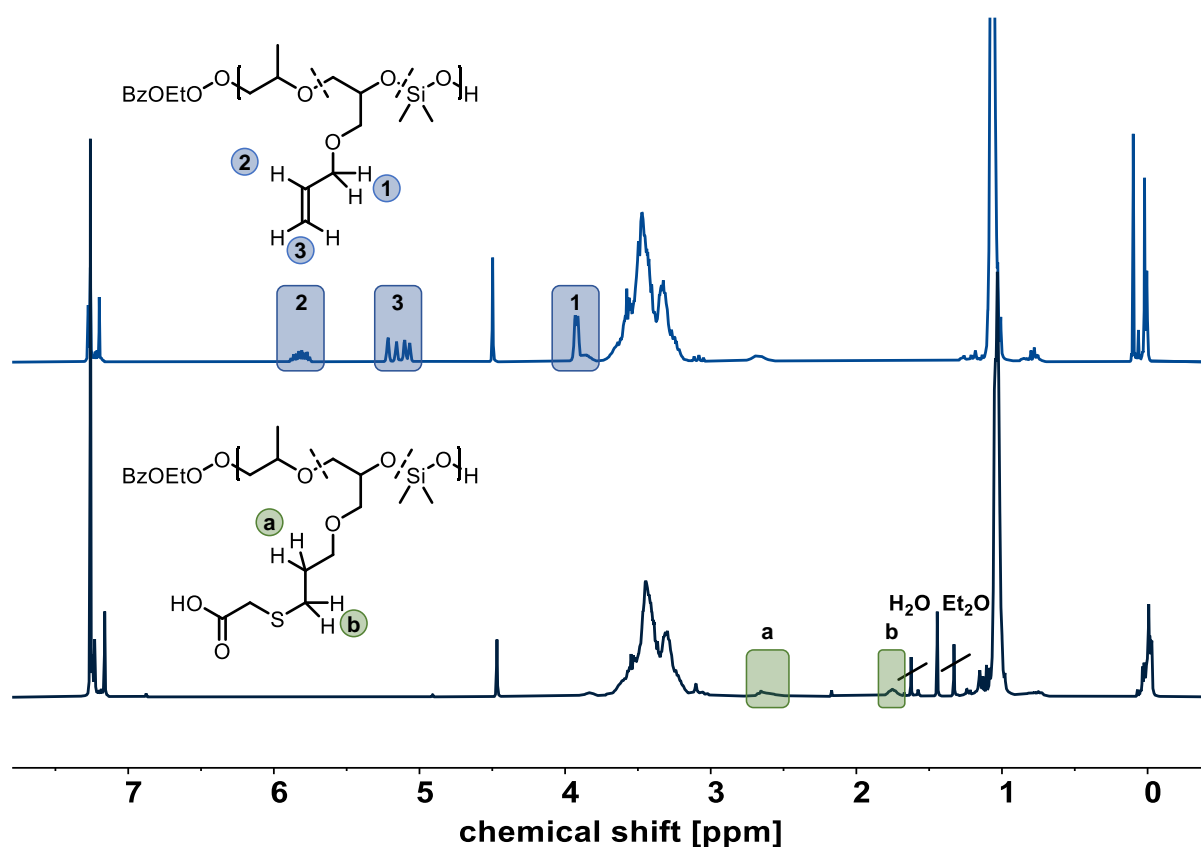
Figure 3. ^{1}H NMR spectra of P1.2 (top) and the subsequent thioether product P1.2 TEC (bottom) after thiol-ene click with thioglycolic acid (300 MHz, CDCl$_3$).

Post-Polymerization Modification of P(PO-*co*-EEGE-*co*-DMS)

EEGE units represent the acetal protected analog of linear polylglycerol (*lin*PG). After acidic deprotection, a variety of modification reactions are possible, capitalizing on the multiple hydroxyl-groups in the side-chains. To outline the capacity of the copolymer to function as modification platform, P(PO-*co-lin*G-*co*-DMS) **P2.1** was functionalized according to the synthesis scheme illustrated in Scheme 3. After acidic deprotection of the acetal protection groups by the acidic ion exchange resin Dowex®, a Steglich esterification of methacrylic acid was conducted. In the final step, the methacrylic functionalities were employed to enable radical crosslinking by addition of AIBN via heat and UV light irradiation. The successful cross-linking was confirmed by the transformation of the amorphous, viscous polymer to a cross-linked gel (Scheme 3, bottom right).
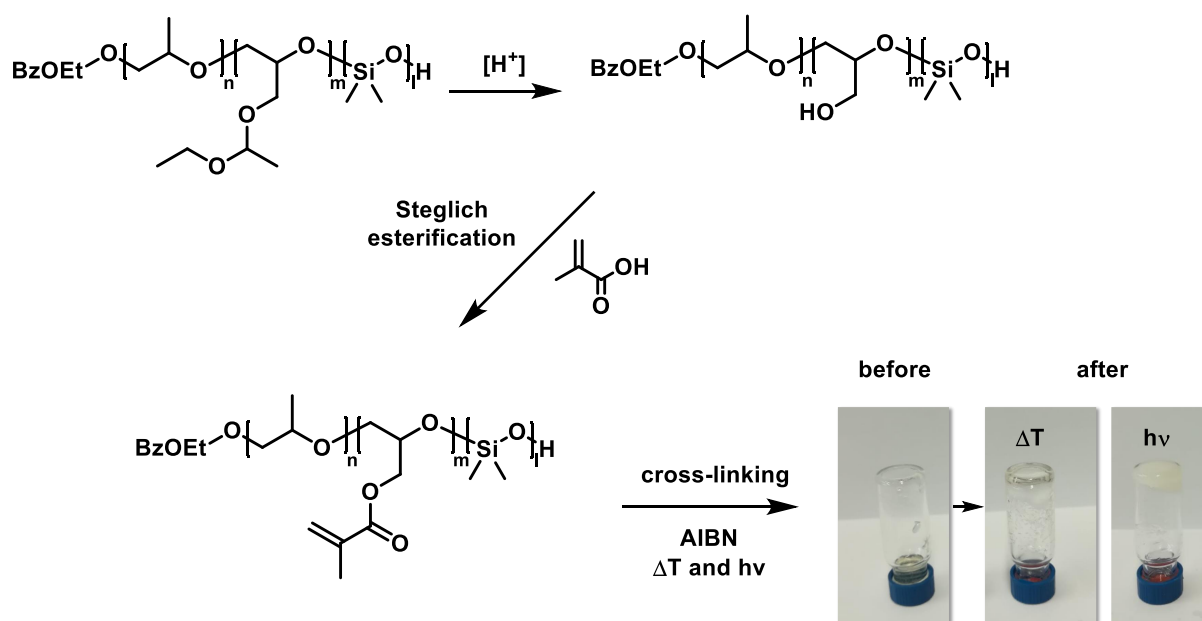
Scheme 3. Synthetic route of (i) acidic deprotection of P(PO-*co*-EEGE-*co*-DMS), (ii) Steglich esterification of *lin*G units with methacrylic acid and (iii) thermic or photochemical induced radical cross-linking.

The products of the different reaction steps were examined by ^{1}H NMR spectroscopy, shown in Figure 4. The full removal of the acetal protection groups is demonstrated by the absence of methine (4.66 ppm) and methyl protons (1.29 ppm) (Figure 4A and B). The deprotection was further indicated by a reduced M_n observed by SEC, shown in Figure S25, SI. The introduction of the desired ester functionalities was apparent from the appearance of protons in the unsaturated region (6.22 and 5.83 ppm) and the methyl group signal (1.98 ppm) of the methacrylate functionality (Figure 4C). In addition, the successfully cross-linking was confirmed by the absence of methacrylic protons and the appearance of methylene protons (1.55 ppm). As expected, the dissolution of the cross-linked polymer in CDCl$_3$ was merely partially feasible. Nevertheless, due to the initial low amount of fGly in **P2.1**, the solvation of polymer fractions with a low cross-linking ratio was successful, enabling the monitoring of the cross-linking efficiency via ^{1}H NMR spectroscopy (Figure 4D).
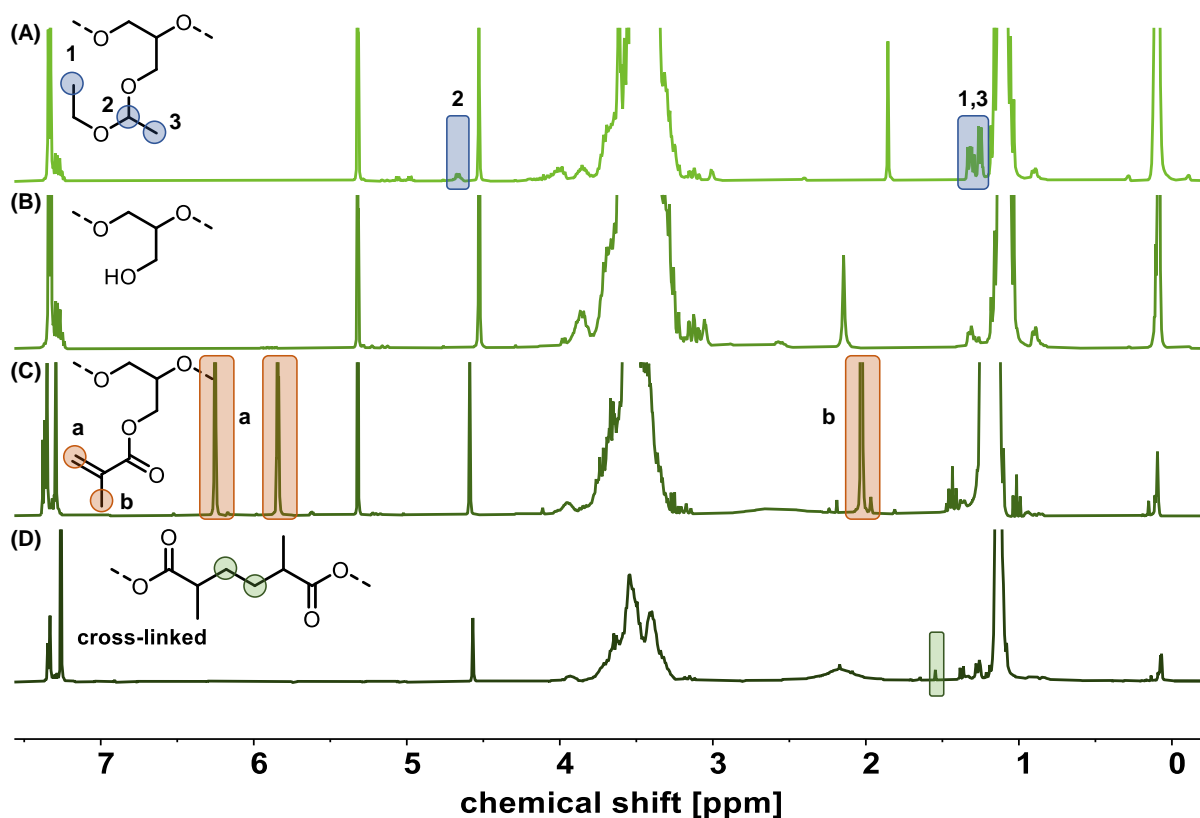
Figure 4. ^{1}H NMR spectra of (A) P2.1, (B) P2.1 after acidic deprotection, (C) product of Steglich esterification with methacrylic acid and (D) the product after cross-linking.

Despite the successful functionalization and cross-linking, an acidic instability regarding the siloxane units was observed. During the acidic treatment of **P2.1** with Dowex® ionic exchange resin not merely the acetal function but also the acid label C-O-Si bonds of PO-DMS or EEGE-DMS were cleaved, which was apparent by a strongly decreased integral of the $Si(Me)_2$ protons at 0 ppm. Calculations based on the specific integral revealed the reduction of 10 siloxane units found for **P2.1** to an average of 1 unit. This observation is further supported by the shift of the SEC elugram to higher elution volumes in Figure S31, SI. In addition to the reduced M_n, the high molecular weight shoulder determined for **P2.1** vanishes for the deprotected polymer which further supports the presumable cleavage of C-O-Si bonds. Such high molecular weight shoulders are equally observed for P(PO-*co*-DMS) copolymers with increasing DMS content. Using DMC catalysis, the polymerization of D_3 is considerably slower than PO, which presumably results in a less controlled polymerization mechanism, which in turn results in a non-uniform chain-growth at higher DMS incorporations.[23] This may account for the decreased dispersity of deprotected **P2.1** compared to the starting polymer.

In summary, the addressability of the hydroxyl group of deprotected P(PO-*co*-EEGE-*co*-DMS) was described, even though the acidic deprotection of acetal side-chains also leads to partial cleavage of C-O-Si bonds, resulting in a strongly decreased PDMS content in the copolymer.

To circumvent this issue, an alternative synthesis route for *lin*G units containing polyether-polysiloxane copolymers was established, which is described in the following paragraph.

Acidic Deprotection Study of P(PO-*co*-GlyTMS-*co*-DMS)

GlyTMS represents an acid labile monomer, yielding *lin*G after removal of the silyl protection group. Nevertheless, its instability under the strongly basic conditions of the AROP, have limited its synthetic applicability in the past. In this study, GlyTMS was successfully polymerized via DMC and investigated as an alternative to EEGE in regard to its behavior under acidic deprotection conditions. Compared to siloxane units incorporated to the polymeric backbone of P(PO-*co*-GlyTMS-*co*-DMS), the TMS substituents are located at the polar polyether segments. The sterically less hindered TMS side-chains in combination with the higher polarity presumably lead to preferential cleavage over the siloxane backbone.

Therefore, a deprotection study under varying concentrations was conducted with **P3.1** to investigate the acidic cleavage of TMS and ether-siloxane units. Solutions of acetic acid in methanol ranging between 0.1 to 1 mol l^{-1} (**P3.1** S8-S2) were prepared and analyzed along with the untreated polymer (**P3.1** S1) via ^{1}H and ^{13}NMR spectroscopy. The stacked ^{1}H NMR spectra of **P3.1** S2 to S5 indicate the general cleavage of C-O-Si bonds based on the occurrence of an additional singlet at -0.04 ppm (SI, Figure S32, SEC Figure S33). This singlet represents the hydrolysis product TMS-OH after cleavage of GlyTMS therefore indicating the successful deprotection. Further, the subsequent dimerization of TMS-OH yielding hexamethyldisiloxane under the applied acidic conditions can be assumed. On the other hand, lower acid concentrations (P3.1 S6-S8) revealed no difference to the untreated polymer. However, the precise analysis of cleaved ether-siloxane units in the backbone is challenging via ^{1}H NMR spectroscopy due to the overlapping of signals.

Therefore, ^{13}C NMR spectra of **P3.1** treated with 0.4 to 0.5 M solutions were recorded (Figure 5) to monitor the deprotection. All acid-treated samples show similar signals but significantly differ from the neat sample. The appearance of a singlet at -1.5 ppm in the ^{13}C equally to the aforementioned ^{1}H NMR spectrum indicates the presence of TMS-OH, therefore confirming successful deprotection. Nevertheless, comparison the spectra of P(PO$_{0.77}$-*co*-DMS$_{0.23}$) as well as untreated P3.1 with the acid treated ones reveals the cleavage of siloxane units in the polymer backbone. Both spectra equally show several signals of Si(Me)$_2$ protons in proximity to PO or EEGE units (0.5 to -1.0 ppm) highfield from the signal of pure PDMS segments. These signals are absent in the spectra of the treated samples, indicating the cleavage of ether-siloxane bonds. Additionally, a sharp singlet at 1.05 ppm appears for all three treated samples which is not present in untreated **P3.1**, possibly indicating free siloxane units.
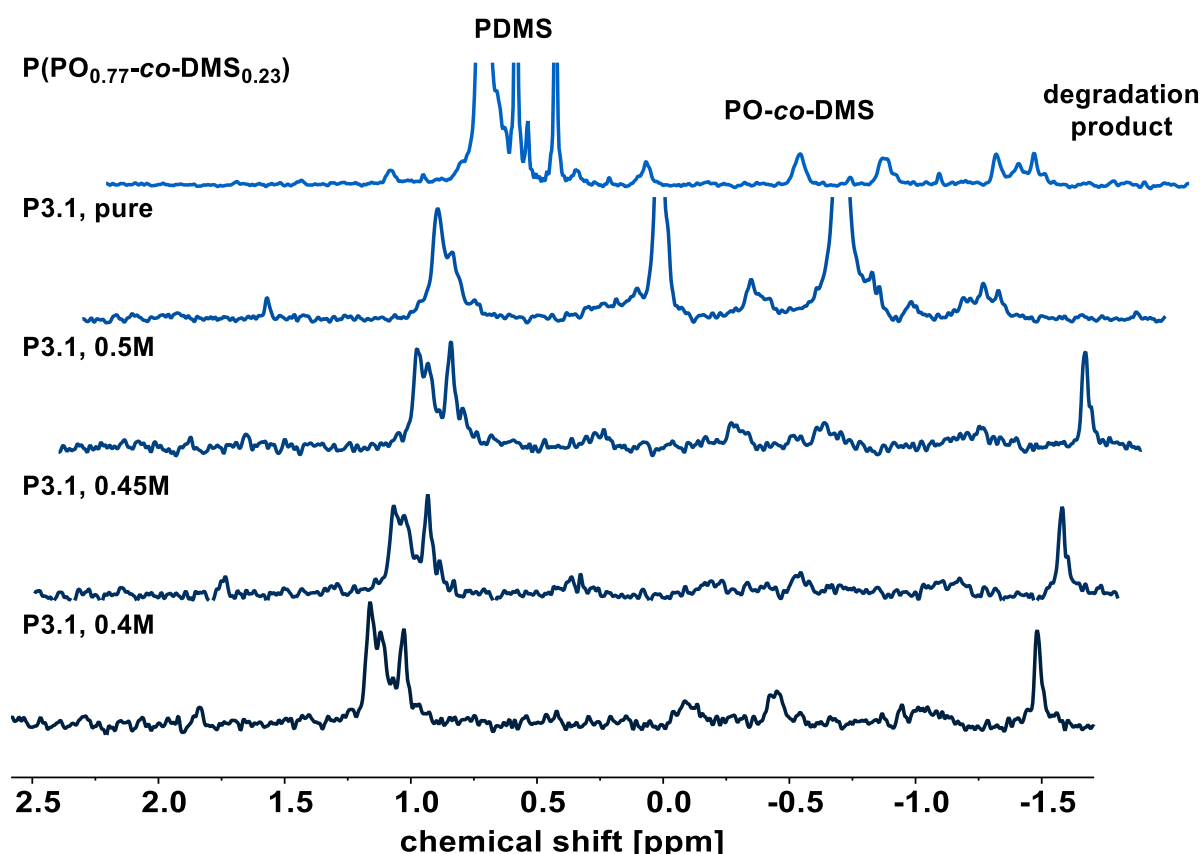
Figure 5. ^{13}C NMR spectra of acidic deprotection of P3.1 in methanol and varying concentrations of acetic acid (400 MHz, CD$_2$Cl$_2$). ^{13}C NMR spectrum of P(PO$_{0.77}$-*co*-DMS$_{0.23}$) for comparison (CDCl$_3$).

The introduction of *lin*G units via both EEGE and GlyTMS generally enables the water-solubility of the investigated terpolymers at 4 °C. Nevertheless, this observation is not surprising considering the aforementioned cleavage of C-O-Si bonds, consequently separating siloxane units from the terpolymer. Fundamentally, P(PO-*co*-*lin*G) copolymers exhibit a lower critical solution temperature (LCST) behavior below as well as above room temperature depending on the respective monomer ratio.[34] Hence, to enable the significant investigation of water-solubility of P(PO-*co*-*lin*G-*co*-DMS) copolymers, a synthesis route without acidic treatment is required, ensuring the preservation of the polymeric C-O-Si bonds.

On the contrary, taking the cleavable C-O-Si bond into account, a worthwhile feature for the herein presented polymers in applications as surfactants comes to mind. Firstly, the introduction of *lin*G units as well as incorporation of carboxylic acid functionalities leads to the increased polarity of the polyether segments, therefore generating highly amphiphilic properties due to the hydrophobic DMS units. The instability of the carbon silicon ethers within the polymeric backbone however enables a pH-triggered degradation of such amphiphilic copolymers, releasing separate polyether and polysiloxane segments in solution. Thus, the DMC catalyzed copolymerization of epoxides and D$_3$ enables the synthesis of copolymers which possess a pH-responsive degradability.

CONCLUSION & OUTLOOK

The statistical copolymerization of epoxides and hexamethylcyclotrisiloxane (D$_3$) is a highly challenging task due to the insufficient capability of alkoxides as initiators for ring-opening of cyclic siloxanes under anionic ring-opening polymerization conditions. Recently, utilization of the double metal cyanide (DMC) catalyst enabled the first copolymerization of an epoxide, namely propylene oxide (PO), and hexamethylcyclotrisiloxane (D$_3$). PO represents the most reactive monomer in DMC catalyzed polymerizations, however, epoxides bearing functional groups have never been investigated regarding the synthesis of statistical polyether-polysiloxane based copolymers.

In this study, we performed the DMC catalyzed terpolymerization of PO, D$_3$ and functional glycidol derivatives (*f*Gly), namely allyl glycidyl ether (AGE), ethoxy ethyl glycidyl ether (EEGE) and glycidyl trimethylsilane (GlyTMS). Polymers with molecular weights of 1.8 to 2.5 kg mol^{-1} with dispersities ranging from 1.10-1.43 and < 5*f*Gly as well as up to 25 mol% dimethylsiloxane (DMS) were synthesized.

The addressability of functional groups was successfully verified by synthesis of cross-linked materials as well as the introduction of carboxyl acid functionalities via thiol-ene click. Subsequently, the capability of these functional polymers regarding the complexation of dicationic metals could be investigated in future studies.

However, the acidic treatment of P(PO-*co*-EGEE-*co*-DMS) simultaneously lead to the cleavage of acid label C-O-Si bonds of PO-DMS and EEGE-DMS segments. Thus, GlyTMS was proposed as an alternative route to gain *lin*G. Hereby, we present the first controlled copolymerization of GlyTMS which is not accessible by classical anionic ring-opening polymerization. A deprotection study of P(PO-*co*-GlyTMS-*co*-DMS) was conducted by addition of varying concentrations of acetic acid/methanol and analysis via ^{1}H and ^{13}C NMR spectroscopy. The successful deprotection of GlyTMS was observed, nevertheless the simultaneous cleavage of ether-siloxane units in the polymeric backbone could not be fully avoided.

Perspectively, different conditions apart from acidic treatment should be considered for successful and exclusive synthesis of *lin*G. For instance, the post-polymerization hydrogenation of AGE[41] or benzyl glycidyl ether supply *lin*G units while possibly preserving the siloxane segments incorporated to the polymer backbone. Additionally, adjustment of the reaction parameters i.e., temperature and especially increase of pressure could lead to an improved conversion rate of D$_3$, therefore enabling the introduction of increased siloxane contents.

Despite the synthetic challenges offered by these polyether-polysiloxane terpolymers, the incorporation of functional groups offers a multitude of possibilities. *Lin*G units facilitate the introduction of polar units to statistical polyether-polysiloxane copolymers, thus leading to strongly amphiphilic properties. Hereby, the utilization of the presented copolymers as degradable surfactants represents a highly interesting future application. The introduction of polar *lin*G or glycidol derivatives (i.e. carboxylic acid substituents) enables the increased hydrophilicity of

the polyether segment whereas the cleavage of apolar siloxane segments can be triggered under acidic conditions.

The polysiloxane segments of the presented copolymers further facilitates the utilization for coating applications while combining valuable properties like high chain flexibility, modifiability and gas permeability in one amorphous material.

REFERENCES

(1) Herzberger, J.; Niederer, K.; Pohlit, H.; Seiwert, J.; Worm, M.; Wurm, F. R.; Frey, H. Polymerization of Ethylene Oxide, Propylene Oxide, and Other Alkylene Oxides: Synthesis, Novel Polymer Architectures, and Bioconjugation. *Chemical reviews* **2016***, 116*, 2170–2243.

(2) Boehm, P.; Mondeshki, M.; Frey, H. Polysiloxane-backbone block copolymers in a one-pot synthesis: a silicone platform for facile functionalization. *Macromolecular rapid communications* **2012***, 33*, 1861–1867.

(3) Mangold, C.; Wurm, F.; Frey, H. Functional PEG-based polymers with reactive groups via anionic ROP of tailor-made epoxides. *Polym. Chem.* **2012***, 3*, 1714.

(4) Brocas, A.-L.; Mantzaridis, C.; Tunc, D.; Carlotti, S. Polyether synthesis: From activated or metal-free anionic ring-opening polymerization of epoxides to functionalization. *Progress in Polymer Science* **2013***, 38*, 845–873.

(5) Obermeier, B.; Frey, H. Poly(ethylene glycol-co-allyl glycidyl ether)s: a PEG-based modular synthetic platform for multiple bioconjugation. *Bioconjugate chemistry* **2011***, 22*, 436–444.

(6) Scharfenberg, M.; Hilf, J.; Frey, H. Functional Polycarbonates from Carbon Dioxide and Tailored Epoxide Monomers: Degradable Materials and Their Application Potential. *Adv. Funct. Mater.* **2018***, 28*, 1704302.

(7) Lee, B. F.; Kade, M. J.; Chute, J. A.; Gupta, N.; Campos, L. M.; Fredrickson, G. H.; Kramer, E. J.; Lynd, N. A.; Hawker, C. J. Poly(allyl glycidyl ether)-A versatile and functional polyether platform. *J. Polym. Sci. Part A: Polym. Chem.* **2011***, 49*, 4498–4504.

(8) Lee, B. F.; Wolffs, M.; Delaney, K. T.; Sprafke, J. K.; Leibfarth, F. A.; Hawker, C. J.; Lynd, N. A. Reactivity ratios, and mechanistic insight for anionic ring-opening copolymerization of epoxides. *Macromolecules* **2012***, 45*, 3722–3731.

(9) Thomas, A.; Müller, S. S.; Frey, H. Beyond poly(ethylene glycol): linear polyglycerol as a multifunctional polyether for biomedical and pharmaceutical applications. *Biomacromolecules* **2014***, 15*, 1935–1954.

(10) Schubert, C.; Dreier, P.; Nguyen, T.; Maciol, K.; Blankenburg, J.; Friedrich, C.; Frey, H. Synthesis of linear polyglycerols with tailored degree of methylation by copolymerization and the effect on thermorheological behavior. *Polymer* **2017***, 121*, 328–339.

(11) Taton, D.; Le Borgne, A.; Sepulchre, M.; Spassky, N. Synthesis of chiral and racemic functional polymers from glycidol and thioglycidol. *Macromol. Chem. Phys.* **1994***, 195*, 139–148.

(12) Tsuruta, T.; Inoue, S.; Koenuma, H. Polymerization of Epoxyorganosilanes. *Makromol. Chem.* **1968***, 112*, 58–65.

(13) Edwin J Vandenberg. High molecular weight hydroxyl-containing polyethers. US3446757A, **1969**.

(14) Vandenberg, E. J. Polymerization of glycidol and its derivatives: A new rearrangement polymerization. *J. Polym. Sci. Polym. Chem. Ed.* **1985**, *23*, 915–949.

(15) Haouet, A.; Sepulchre, M.; Spassky, N. Preparation et proprietes des poly(R)-glycidols. *European Polymer Journal* **1983**, *19*, 1089–1098.

(16) Eduok, U.; Faye, O.; Szpunar, J. Recent developments and applications of protective silicone coatings: A review of PDMS functional materials. *Progress in Organic Coatings* **2017**, *111*, 124–163.

(17) Galli, G.; Martinelli, E. Amphiphilic Polymer Platforms: Surface Engineering of Films for Marine Antibiofouling. *Macromol. Rapid Commun.* **2017**, *38*.

(18) Yilgör, İ.; McGrath, J. E. Polysiloxane containing copolymers: A survey of recent developments. In Polysiloxane copolymers/anionic polymerization; van Beylen, M., Ed.; Advances in Polymer Science 86; *Springer: Berlin*, **1988**; pp 1–86.

(19) Galin, M.; Mathis, A. Structural and thermodynamic study of dimethylsiloxane-ethylene oxide PDMS-PEO-PDMS triblock copolymers. *Macromolecules* **1981**, *14*, 677–683.

(20) Haesslin, H. W.; Eicke, H. F.; Riess, G. Dimethylsiloxane-ethylene oxide block copolymers, 1. Microphase separation of low segment mass copolymers and their compatibility with water and oil. *Makromol. Chem.* **1984**, *185*, 2625–2645.

(21) Haesslin, H.-W. Dimethylsiloxane-ethylene oxide block copolymers, 2. Preliminary results on dilute solution properties. *Makromol. Chem.* **1985**, *186*, 357–366.

(22) Maassen, H.-P.; Yang, J. L.; Wegner, G. The structure of poly(ethylene oxide)-poly(dimethyl-siloxane) triblock copolymers in solution. Makromolekulare Chemie. *Macromolecular Symposia* **1990**, *39*, 215–228.

(23) Mohr, R.; Wagner, M.; Zarbakhsh, S.; Frey, H. The Unique Versatility of the Double Metal Cyanide (DMC) Catalyst: Introducing Siloxane Segments to Polypropylene Oxide by Ring-Opening Copolymerization. *Macromol. Rapid Commun.* **2020**, 2000542.

(24) Tran, C. H.; Pham, L. T. T.; Lee, Y.; Jang, H. B.; Kim, S.; Kim, I. Mechanistic insights on Zn(II)−Co(III) double metal cyanide-catalyzed ring-opening polymerization of epoxides. *Journal of Catalysis* **2019**, *372*, 86–102.

(25) Ionescu, M. Chemistry and technology of polyols for polyurethanes; Rapra Technology Ltd: *Shawbury, U.K*, **2005**.

(26) Jack Milgrom. Method of Making a Polyether using a Double Metal Cyanide Complex Compound. *US Patent US3278457A*, **1963**.

(27) Kim, I.; Ahn, J.-T.; Ha, C. S.; Yang, C. S.; Park, I. Polymerization of propylene oxide by using double metal cyanide catalysts and the application to polyurethane elastomer. *Polymer* **2003**, *44*, 3417–3428.

(28) Kim, I.; Byun, S. H.; Ha, C.-S. Ring-opening polymerizations of propylene oxide by double metal cyanide catalysts prepared with ZnX2 (X = F, Cl, Br, or I). *J. Polym. Sci. Part A: Polym. Chem.* **2005**, *43*, 4393–4404.

(29) Huang, Y.-J.; Qi, G.-R.; Wang, Y.-H. Controlled ring-opening polymerization of propylene oxide catalyzed by double metal-cyanide complex. *J. Polym. Sci. Part A: Polym. Chem.* **2002**, *40*, 1142–1150.

(30) Zhang, X.-H.; Wei, R.-J.; Zhang, Y.; Du, B.-Y.; Fan, Z.-Q. Carbon Dioxide/Epoxide Copolymerization via a Nanosized Zinc–Cobalt(III) Double Metal Cyanide Complex: Substituent Effects of Epoxides on Polycarbonate Selectivity, Regioselectivity and Glass Transition Temperatures. *Macromolecules* **2015**, *48*, 536–544.

(31) Jörg Hofmann, Pieter Ooms, Pramod Gupta, Walter Schäfer, John Lohrenz. Double metal cyanide catalysts for producing polyether polyols, **2000**, US6586566B1.

(32) Eric P. Wassermann, Richard A. Galley, Woo Min Song, Abhijit Ghosh-Dastidar. Polyoxiranes, process and catalysts for making them, **2008**, WO2008048399A1.

(33) Almora-Barrios, N.; Pogodin, S.; Bellarosa, L.; García-Melchor, M.; Revilla-López, G.; García-Ratés, M.; Vázquez-García, A. B.; Hernández-Ariznavarreta, P.; López, N. Structure, Activity, and Deactivation Mechanisms in Double Metal Cyanide Catalysts for the Production of Polyols. *ChemCatChem* **2015**, *7*, 928–935.

(34) Schömer, M.; Frey, H. Water-Soluble "Poly(propylene oxide)" by Random Copolymerization of Propylene Oxide with a Protected Glycidol Monomer. *Macromolecules* **2012**, *45*, 3039–3046.

(35) Shambayati, S.; Schreiber, S. L.; Blake, J. F.; Wierschke, S. G.; Jorgensen, W. L. Structure and basicity of silyl ethers: a crystallographic and ab initio inquiry into the nature of silicon-oxygen interactions. *J. Am. Chem. Soc.* **1990**, *112*, 697–703.

(36) Chruściel, A.; Hreczuch, W.; Janik, J.; Czaja, K.; Dziubek, K.; Flisak, Z.; Swinarew, A. Characterization of a Double Metal Cyanide (DMC)-Type Catalyst in the Polyoxypropylation Process: Effects of Catalyst Concentration. *Ind. Eng. Chem. Res.* **2014**, *53*, 6636–6646.

(37) Lee, S. H.; Lee, I. K.; Ha, J. Y.; Jo, J. K.; Park, I.; Ha, C.-S.; Suh, H.; Kim, I. Tuning of the Activity and Induction Period of the Polymerization of Propylene Oxide Catalyzed by Double Metal Cyanide Complexes Bearing β-Alkoxy Alcohols as Complexing Agents. *Ind. Eng. Chem. Res.* **2010**, *49*, 4107–4116.

(38) Kim, I.; Anas, K.; Lee, S.; Ha, C.-S.; Park, D.-W. Tuning of the activity and induction period of double metal cyanide catalyzed ring-opening polymerizations of propylene oxide by using ionic liquids. *Catalysis Today* **2008**, *131*, 541–547.

(39) Lee, S.; Baek, S. T.; Anas, K.; Ha, C.-S.; Park, D.-W.; Lee, J. W.; Kim, I. Tuning of activity, induction period and polymer properties of double metal cyanide catalyzed ring-opening polymerizations of propylene oxide by using quaternary ammonium salts. *Polymer* **2007**, *48*, 4361–4367.

(40) Lowe, A. B. Thiol-ene "click" reactions and recent applications in polymer and materials synthesis. *Polym. Chem.* **2010**, *1*, 17–36.

(41) Erberich, M.; Keul, H.; Möller, M. Polyglycidols with Two Orthogonal Protective Groups: Preparation, Selective Deprotection, and Functionalization. *Macromolecules* **2007**, *40*, 3070–3079.

SUPPORTING INFORMATION

EXPERIMENTAL SECTION

Reagents and Equipment.

All chemicals and solvents were purchased from *Acros Organics*, *TCI*, *Sigma-Aldrich* and *Fluka*. Deuterated solvents were received from *Deutero GmbH*. The DMC catalyst was provided by *BASF SE*. Ethoxyethyl glycidyl ether (EEGE) was synthesized according to Fitton et al.[1] Hexamethylcyclotrisiloxane (D$_3$), allyloxy glycidyl ether (AGE), EEGE and GlyTMS were stirred over calcium hydride overnight and cryotransferred to a Schlenk flask. Propylene oxide (PO) was dried by addition of *n*-Butyllithium while stirring and cryo-transferred to a Schlenk flask. The DMC catalyst as well as the initiator 2-(benzyloxy)ethanol were dried under high vacuum (10^{-3} mbar) by azeotropic distillation with benzene. Polymerizations were performed in 100 ml high-pressure autoclaves purchased from *Carl Roth GmbH*. ^{1}H NMR spectra were recorded on a *Bruker Avance III HD* (300 MHz) with a 5 mm BBFO-head with z-gradient and ATM BACS 60 sample changer or with a a *Bruker Avance III BR 500/51* (500 MHz) and a 5 mm BBFO[1]H-^{19}F/BB z-gradient probe. Spectra were referenced to the respective solvent CDCl$_3$, CD$_2$Cl$_2$, DMSO-d_6 or 1,4-dioxane-d_8.

Pressure Monitoring

Pressure Monitoring was performed by use of *MEAS M5600 Wireless Pressure Transducer* by *TE*. The Bluetooth sensor was attached to the autoclave under continuous argon flow outside the glovebox. Pressure values were measured every 100 ms.

Size Exclusion Chromatography (SEC)

SEC measurements were performed in dimethylformamide (DMF) with 1 g L^{-1} lithium bromide as an eluent at 50 °C. An Agilent 1100 Series was used, equipped with HEMA 300/100/40 columns, and calibration was carried out using polyethylene glycol (PEG) standards, both provided by *Polymer Standard Service* (PSS), Mainz.

Differential Scanning Calorimetry (DSC)

Thermal properties of P(PO-*co*-*f*Gly-*co*-DMS) polymers were studied with a *Perkin-Elmer Thermal Analysis Controller TAC7/DX* differential scanning calorimeter (DSC). By using indium as a standard ($\Delta H = 28.71$ J g^{-1}, $T_m = 155.6$ °C) for baseline correction, calibration of the instrument was performed. Two cooling and heating cycles were applied at a rate of 20 °C min^{-1} in a temperature range of -100 °C to 30 °C. The glass transition temperature T_g was determined in the second cycle for both devices.

Calculation of Tb for PO, AGE, EEGE and GlyTMS for varying pressure

The state of matter for both epoxide monomers PO and GME was calculated for the utilized reaction conditions. The boiling points T_b at atmospheric pressure, 5 and 10 bar were evaluated by the integrated form of the Clausius-Clapeyron relation, the August equation (equation 0.11).

PO possess an enthalpy of vaporization $\Delta_{vap}H_m$ = 27.735 kJ mol^{-1}.[2] The $\Delta_{vap}H_m$ of AGE; EEGE and GlyTos was approximated by Trouton's rule as no reliable source was available (equation 0.10).[3] The estimated values are listed in Table S1.

$$\Delta_{vap}H_m = 88 \frac{J}{mol \cdot K} \cdot T_b \qquad (0.10)$$

$$ln\left(\frac{p(T_2)}{p(T_1)}\right) = -\frac{\Delta_{vap}H_m}{R} \cdot (\frac{1}{T_2} - \frac{1}{T_2}) \qquad (0.11)$$

Table S1. Calculated values of the enthalpy of vaporization $\Delta_{vap}H_m$ and boiling temperatures T_b at atmospheric pressure, 5 and 10 bar for the utilized monomers.

monomer	$\Delta_{vap}H_m$ [kJ mol^{-1}]	T_b [°C]	$T_{b,5}$ [°C]	$T_{b,10}$ [°C]
PO	27.735[2]	34[2]	87	117
AGE	37.664	155[4]	231	273
EEGE	37.488	153	229	270
GlyTMS	37.941	158	234	276

**Synthesis of Glycidyl trimethylsilane**
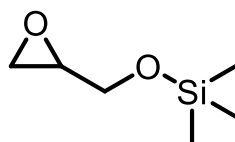
Glycidyl trimethlysilane (GlyTMS) was synthesized adjusted procedure used for synthesis of glycidyl tosylate.[5] Glycidol (17.05 g, 1 eq) was dried prior to use by cryotransfer after stirring for 30 min over CaH$_2$. Dry glycidol was then dissolved in dry DCM and triethylamine (30.27 g, 1.3 eq) was added. The solution was cooled to 0 °C and trimethylsilane chloride (25.00 g, 1 eq) was slowly added dropwise. The mixture was stirred for 1 h at room temperature. The organic layer was then washed by saturated solutions of NH4Cl, NaHCO3 and finally water. The organic phase was dried over MgSO$_4$, the solvent removed under reduced pressure and the product was obtained by fractionated distillation (T_b = 31 °C at 7 mbar). GlyTMS was obtained as a colorless liquid with a yield of 34 %.

^{1}H NMR (300 MHz, CD$_2$Cl$_2$) δ [ppm]: 3.84-3.80 (dd, 1H, CH-CH_2-O), 3.55-3.49 (dd, 1H, CH-CH_2-O), 3.06-3.01 (m, 1H, CH2-CH-CH2), 2.74-2.71 (dd, 1H, O-CH2-CH2), 2.57-2.54 (dd, 1H, O-CH2-CH2), 0.12 (s, 9H, Si-(CH_3)$_3$)

Polymerization Procedure P(PO-*co*-AGE-*co*-DMS)
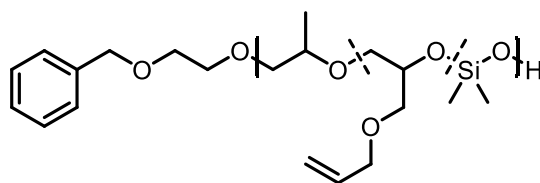
The dried monomers PO, D_3, AGE, the initiator, the DMC catalyst and an autoclave were transferred to the glovebox to carry out the ensuing reaction under strict argon atmosphere. PO, AGE, D_3, 2-(benzyloxy)ethanol (1 eq) and DMC catalyst (300 ppm) were added to the autoclave. Then an Ar pressure of 1 or 5 bar was applied to the autoclave. The reaction mixture was stirred and heated at 120 °C for 24 to 144 h. To prevent sublimation of D_3 to the top of the autoclave, a high temperature headband was attached and heated to 180 °C. After evaporation of possibly unreacted monomers at reduced pressure, the resulting polymers were used without further purification. Polymers with varied amounts of D_3 were synthesized analogously.

^{1}H NMR (300 MHz, CDCl$_3$) δ [ppm]: 7.35-7.27 (m, 5H, Ar-*H*), 4.56 (s, 2H, Ph-C*H$_2$*), 5.93-5.88 (m, CH$_2$=C*H*-), 5.31-5.15 (m, C*H$_2$*=CH-), 4.02-4.00 (d, CH-C*H$_2$*-O), 3.79-3.09 (m, polyether backbone), 1.38-0.79 (m, propylene oxide -C*H$_3$*), 0.24-0.03 (m, Siloxane -C*H$_3$*)

Polymerization Procedure P(PO-*co*-EEGE-*co*-DMS)
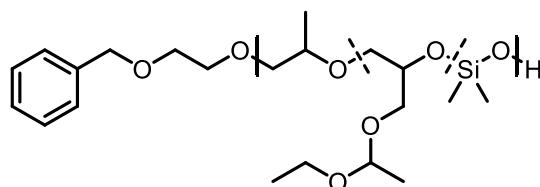
The dried monomers PO, D_3, EEGE, the initiator, the DMC catalyst and an autoclave were transferred to the glovebox to carry out the ensuing reaction under strict argon atmosphere. PO, EEGE, D_3, 2-(benzyloxy)ethanol (1 eq) and DMC catalyst (300 ppm) were added to the autoclave. Then an Ar pressure of 5 bar was applied to the autoclave. The reaction mixture was stirred and heated at 120 °C for 24 to 144 h. To prevent sublimation of D_3 to the top of the autoclave, a high temperature headband was attached and heated to 180 °C. After evaporation of possibly unreacted monomers at reduced pressure, the resulting polymers were used without further purification. Polymers with varied amounts of D_3 were synthesized analogously.

^{1}H NMR (300 MHz, CD$_2$Cl$_2$) δ [ppm]: 7.35-7.27 (m, 5H, Ar-*H*), 4.69-4.53 (m O-C*H*-CH$_3$) 4.56 (s, 2H, Ph-C*H$_2$*), 3.79-3.09 (m, polyether backbone), 1.33-1.25 (s, -CH$_2$-C*H$_3$*) 1.38-0.79 (m, propylene oxide -C*H$_3$* and m, CH-C*H$_3$*), 0.24-0.03 (m, Siloxane -C*H$_3$*)

Polymerization Procedure P(PO-*co*-GlyTMS-*co*-DMS)
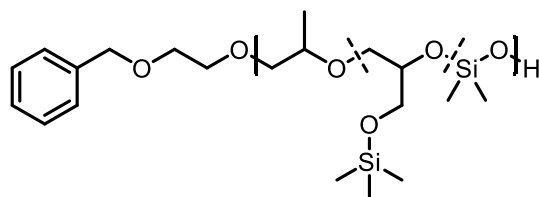
The dried monomers PO, D_3, GlyTMS, the initiator, the DMC catalyst and an autoclave were transferred to the glovebox to carry out the ensuing reaction under strict argon atmosphere. PO, GlyTMS, D_3, 2-(benzyloxy)ethanol (1 eq) and DMC catalyst (300 ppm) were added to the autoclave. Then an Ar pressure of 5 bar was applied to the autoclave. The reaction mixture was stirred and heated at 120 °C for 144 h. To prevent sublimation of D_3 to the top of the autoclave, a high temperature headband was attached and heated to 180 °C. After evaporation of possibly unreacted monomers at reduced pressure, the resulting polymers were used without further purification. Polymers with varied amounts of D_3 were synthesized analogously.

^{1}H NMR (300 MHz, CD_2Cl_2) δ [ppm]: 7.35-7.27 (m, 5H, Ar-*H*), 4.56 (s, 2H, Ph-C*H*$_2$), 3.79-3.09 (m, polyether backbone), 1.38-0.79 (m, propylene oxide -C*H*$_3$), 0.24-0.03 (m, Siloxane -C*H*$_3$ and m, -(C*H*$_3$)$_3$)

Post-polymerization modification Thiol-ene functionalization of P(PO-*co*-AGE-*co*-DMS)
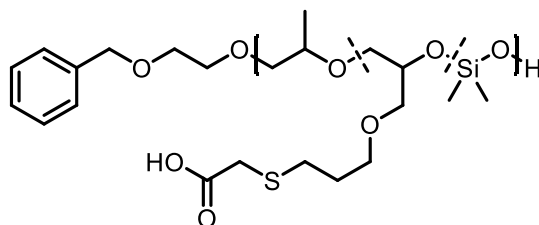
The AGE containing polymer sample P1.2 was dried by azeotropic distillation of benzene in a Schlenk-flask. 2-sulfanylacetic acid (0.42 g,15 eq), azobis(isobutyronitril) (AIBN, 0.04 g; 0.75 eq) and the dried copolymer (0.52 g, 1 eq) was dried in benzene. The solution was degassed by three freeze-pump cycles and heated under reflux at 80 °C for 4 h. Thereafter, the mixture was washed three times with saturated solutions of $NaHCO_3$, NH_4Cl and finally water. The aqueous phase was extracted three times with diethyl ether und dried over $MgSO_4$. After removal of the organic solvent under reduced pressure, the amorphous polymer was dried under vacuum at 60 °C. Acidic deprotection of P(PO-*co*-EEGE-*co*-DMS). First, the acetal protecting group of EEGE units was removed under acidic conditions yielding P(PO-*co*-*lin*G-*co*-DMS). For this purpose, the EEGE containing polymer sample P2.1 was dissolved in methanol, the ion exchange resin Dowex® was added and the dispersion was stirred overnight. Prior to use, Dowex® was washed with conc. hydrochloric acid. The next day, the solution was filtrated and methanol was removed under

reduced pressure. This procedure achieved full deprotection of the acetal protecting group but equally resulted in the acidic cleavage of C-O-Si bonds.

Acidic Deprotection of P(PO-*co*-GlyTMS-*co*-DMS)

For deprotection of TMS protecting groups of polymer P3.1, a study with varying concentrations of acid was performed. Solutions of methanol with varying concentrations of acetic acid were utilized while each sample (50 mg) was dissolved in 0.5 ml (Table S2).

Table S2. Acidic deprotection study of P(PO-*co*-GlyTMS-*co*-DMS) P3.1 in methanol with varying concentrations of acetic acid.

sample	c [mol L^{-1}]
P3.1 S1	untreated
P3.1 S2	1
P3.1 S3	0.8
P3.1 S4	0.6
P3.1 S5	0.5
P3.1 S6	0.4
P3.1 S7	0.2
P3.1 S8	0.1

Steglich esterification of P(PO-*co*-EEGE-*co*-DMS)
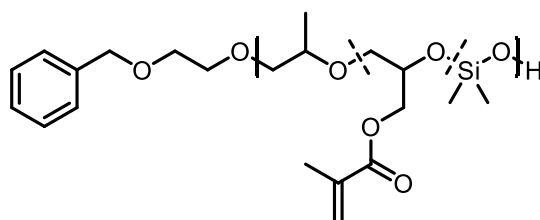
The Steglich esterification was performed following a procedure of Gallei and co-workers.[6] The deprotected polymer (0.82 g, 1 eq) was dissolved in DCM while 4-dimethylaminopyridine (DMAP, 0.03 g, 0.4 eq) and methacrylic acid (0.45 g, 8 eq) were added. The solution was cooled to 0 °C, N,N-diisopropylcarbodiimide (DIC, 0.17 g, 2 eq) was added and the mixture was stirred for 3 h at 0 °C. The mixture was filtrated and the filtrate was washed with saturated solutions of NaHCO$_3$ and NH$_4$Cl. The aqueous phase was extracted with diethyl ether, the organic layers combined and dried over MgSO$_4$. Finally, the organic solvents were removed under reduced pressure.

Cross-linking of methacrylic ester substituents

Two sample of polymer P2.1 containing methacrylic ester substituents (100 mg) were dissolved in THF (0.2 ml). AIBN was added to both vials each. One vail was heated to 60 °C for 24 h, one was irradiated with UV-light for the same time.
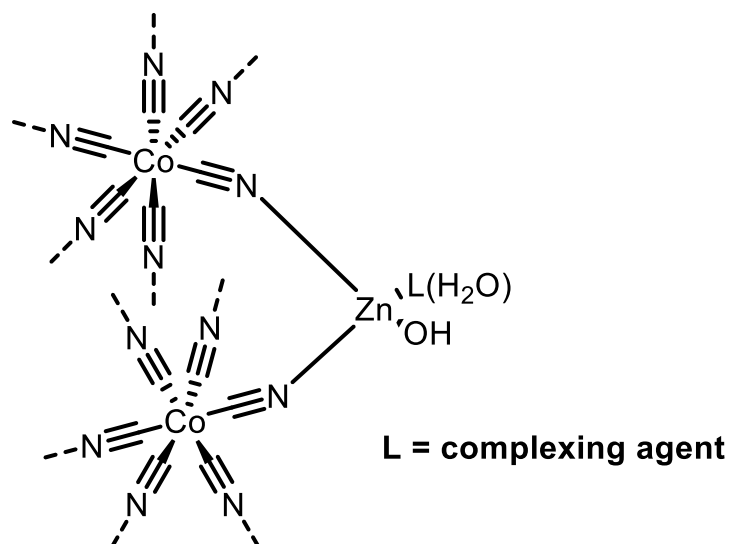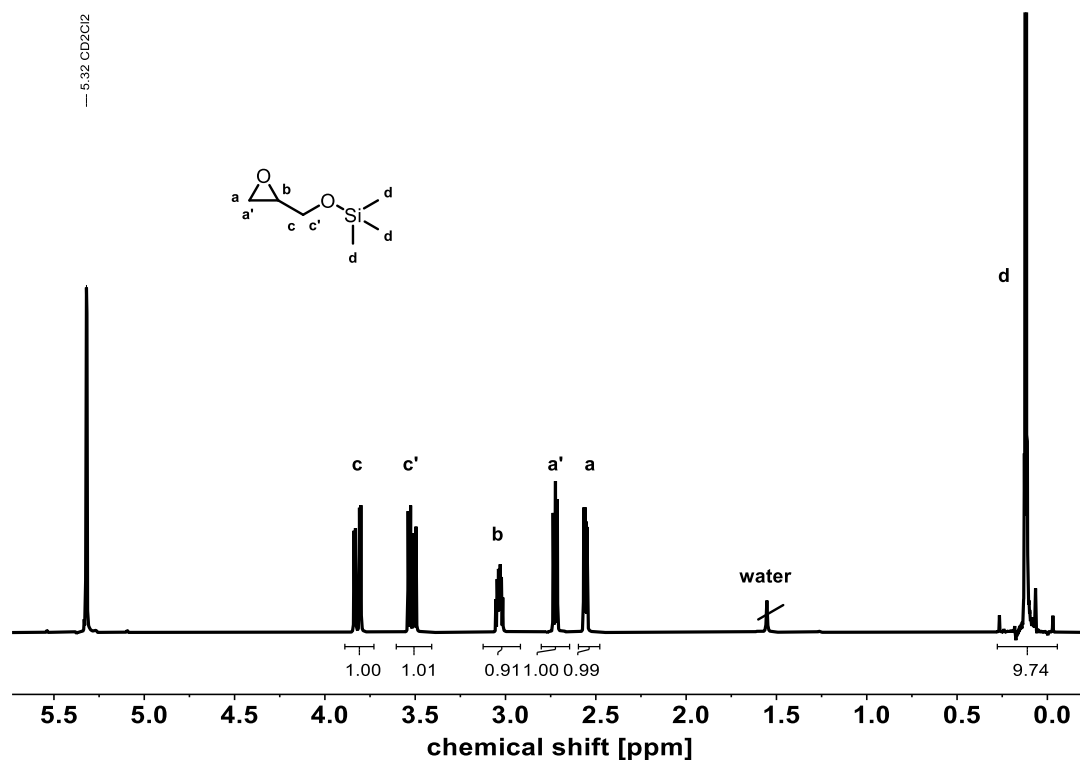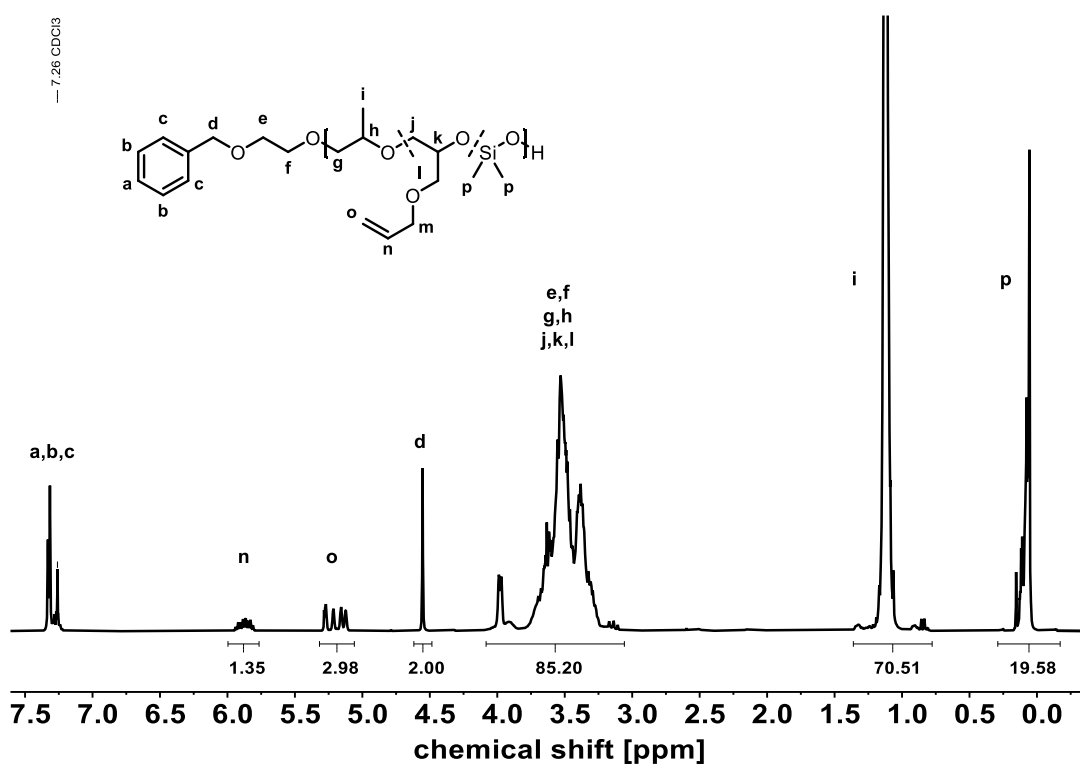
Figure S1. Proposed structure of the active site of Zn-Co(III) DMC catalyst.[7]

Supporting NMR Spectra

Figure S2. ^{1}H NMR glycidyl trimethylsilane (GlyTMS) (300 MHz, CD$_2$Cl$_2$)

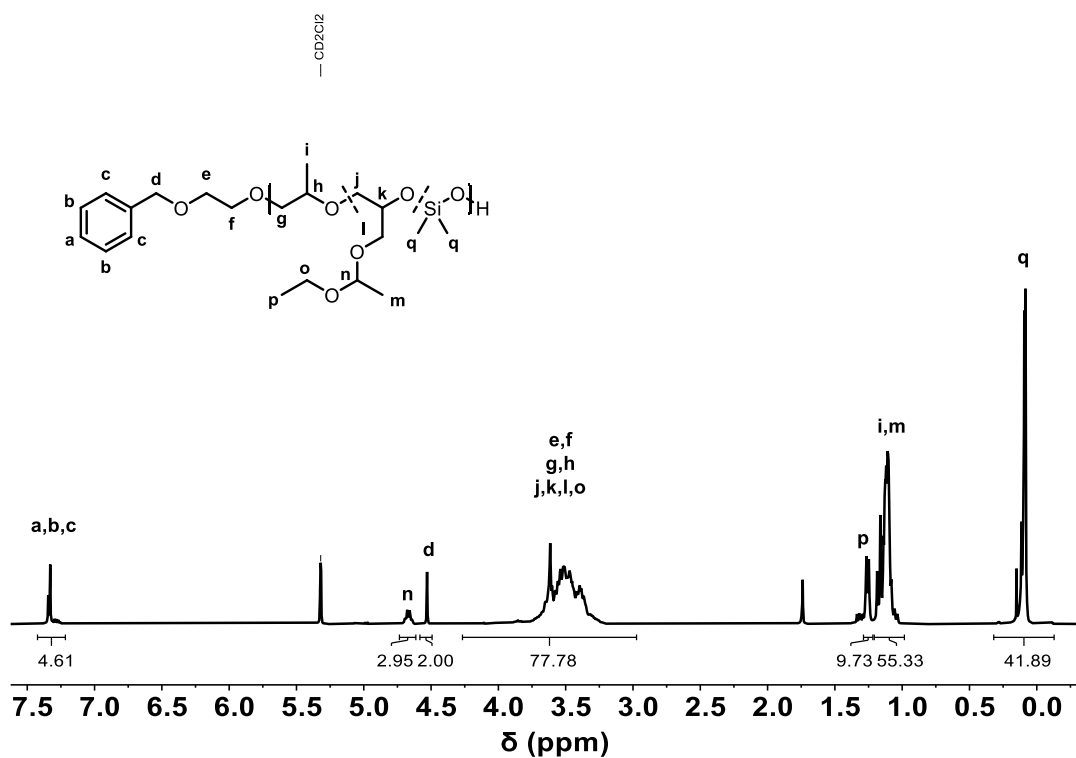**Figure S3.** ^{1}H NMR P(PO-*co*-AGE-*co*-DMS) P1.1 (300 MHz, CDCl$_3$)

Figure S4. ^{1}H NMR P(PO-*co*-EEGE-*co*-DMS) P2.2 (300 MHz, CD$_2$Cl$_2$)
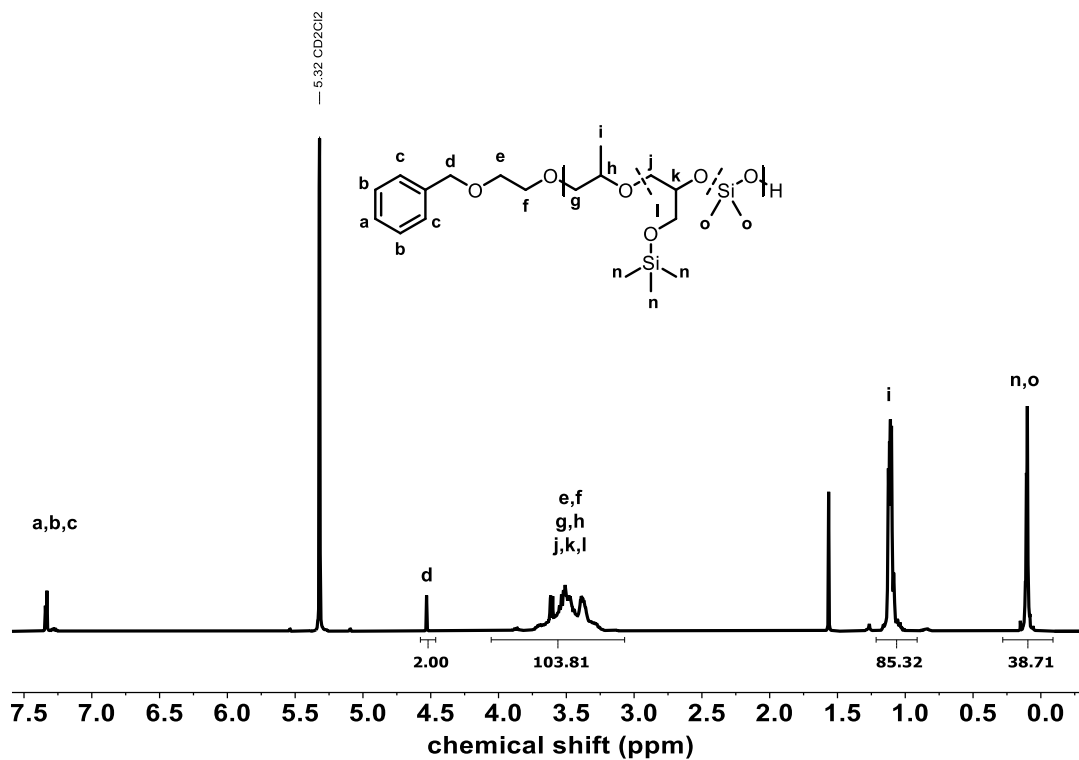
Figure S5. ^{1}H NMR P(PO-*co*-GlyTMS) P3.1 (300 MHz, CD$_2$Cl$_2$)
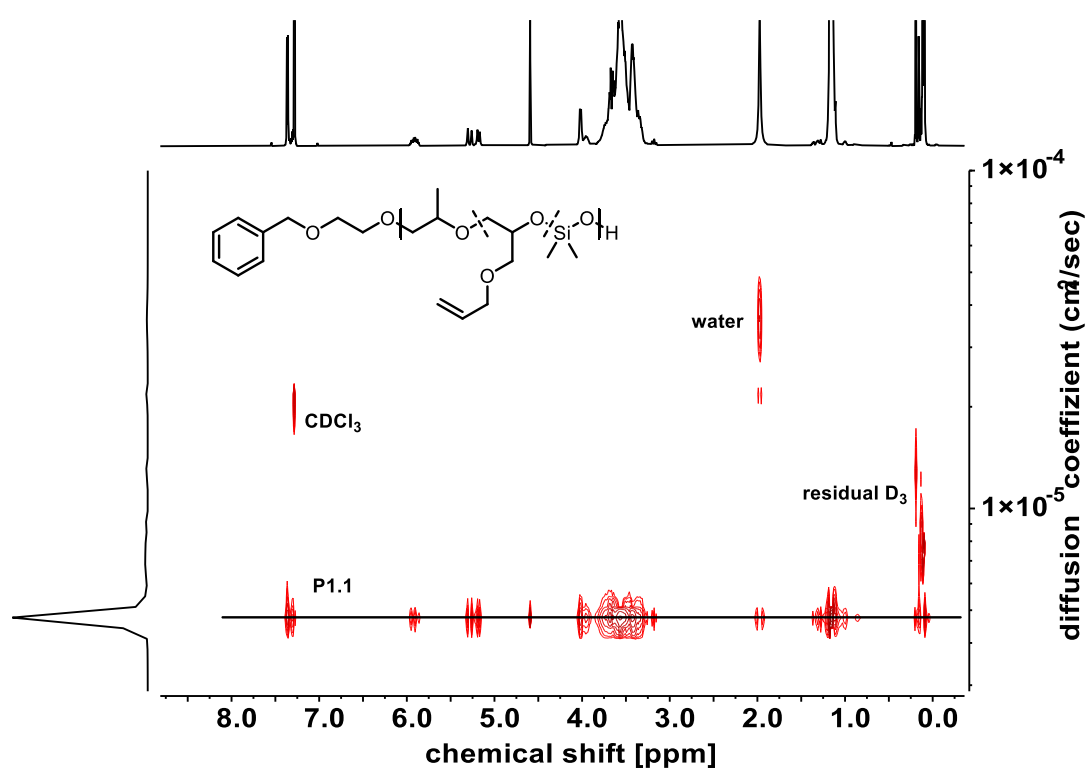
Figure S6. ^{1}H DOSY NMR P1.1 P(PO-*co*-AGE-*co*-DMS) (400 MHz, CDCl$_3$)
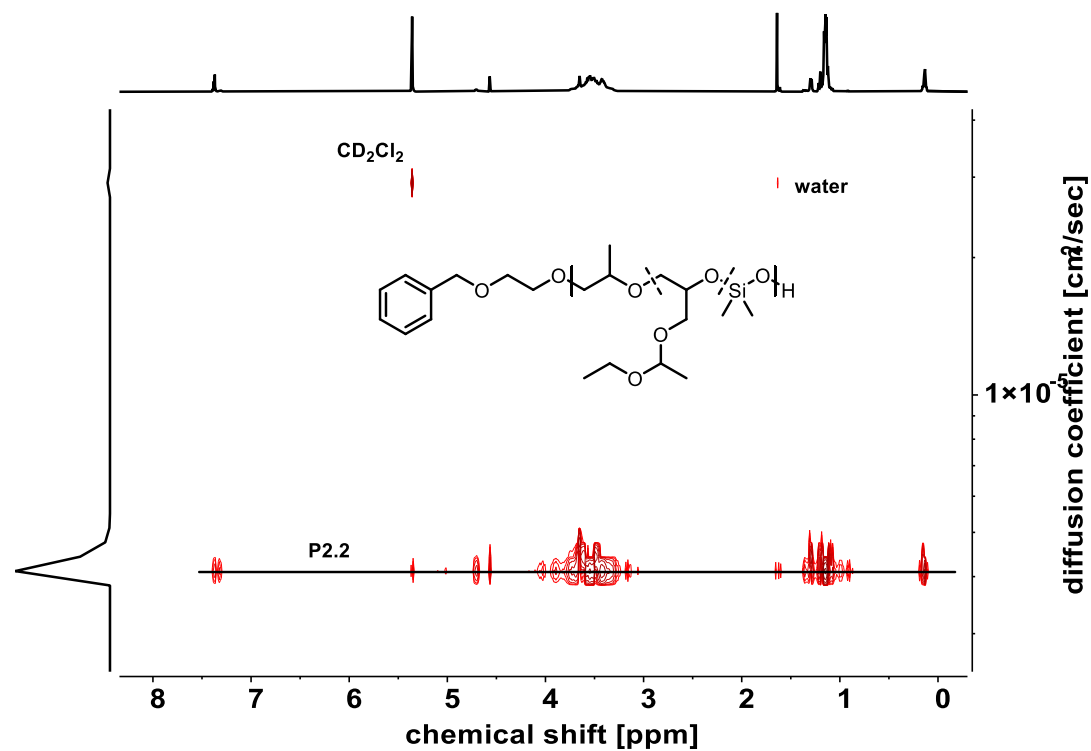
Figure S7. ^{1}H DOSY NMR P2.2 P(PO-*co*-EEGE-*co*-DMS) (400 MHz, CD$_2$Cl$_2$)
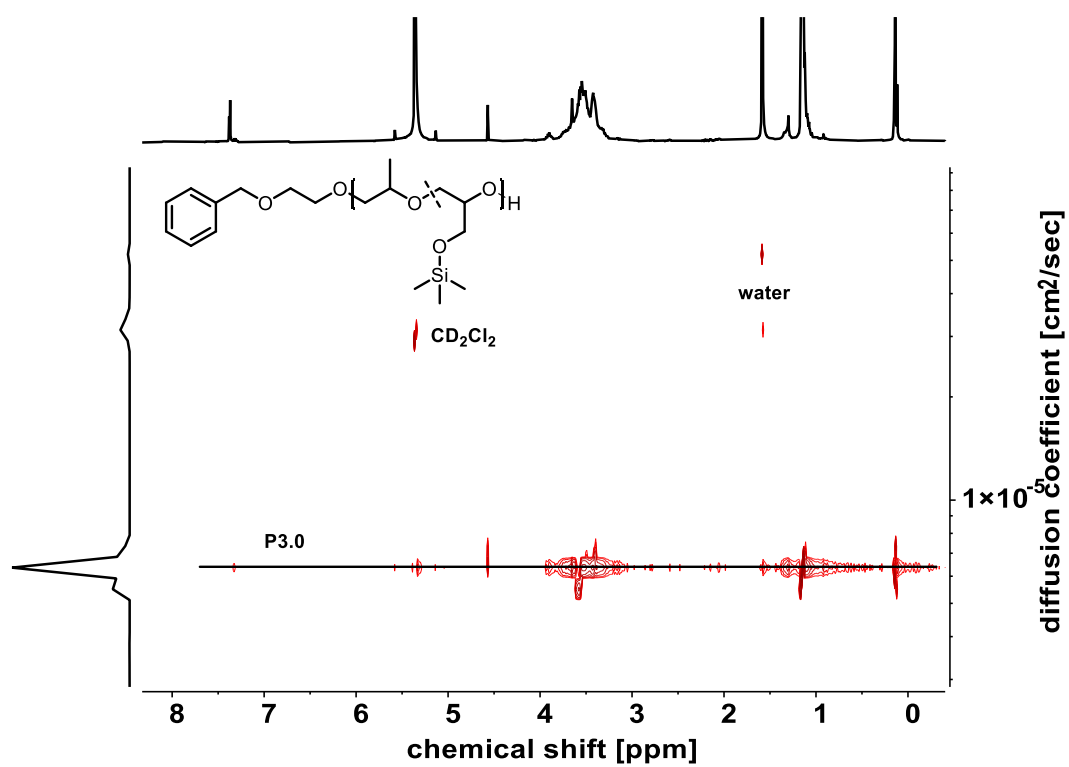
Figure S8. ^{1}H DOSY NMR P3.0 P(PO-*co*-GlyTMS) (400 MHz, CD$_2$Cl$_2$)
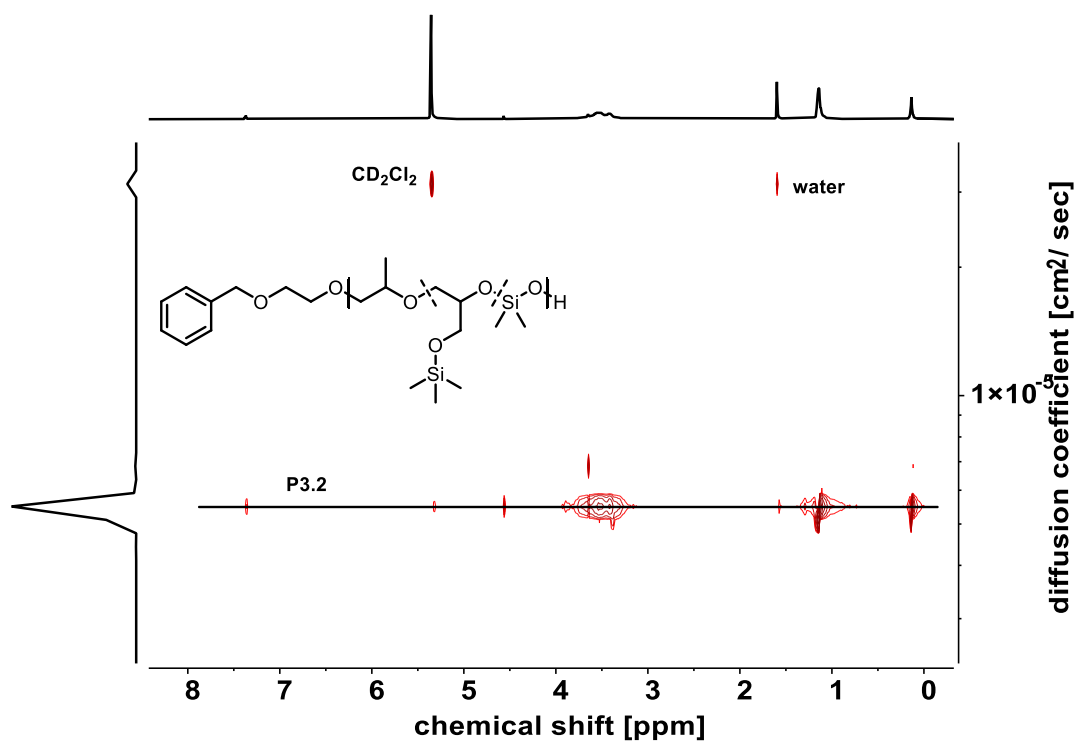
Figure S9. ^{1}H DOSY NMR P3.2 P(PO-*co*-GlyTMS-*co*-DMS) (400 MHz, CD$_2$Cl$_2$)
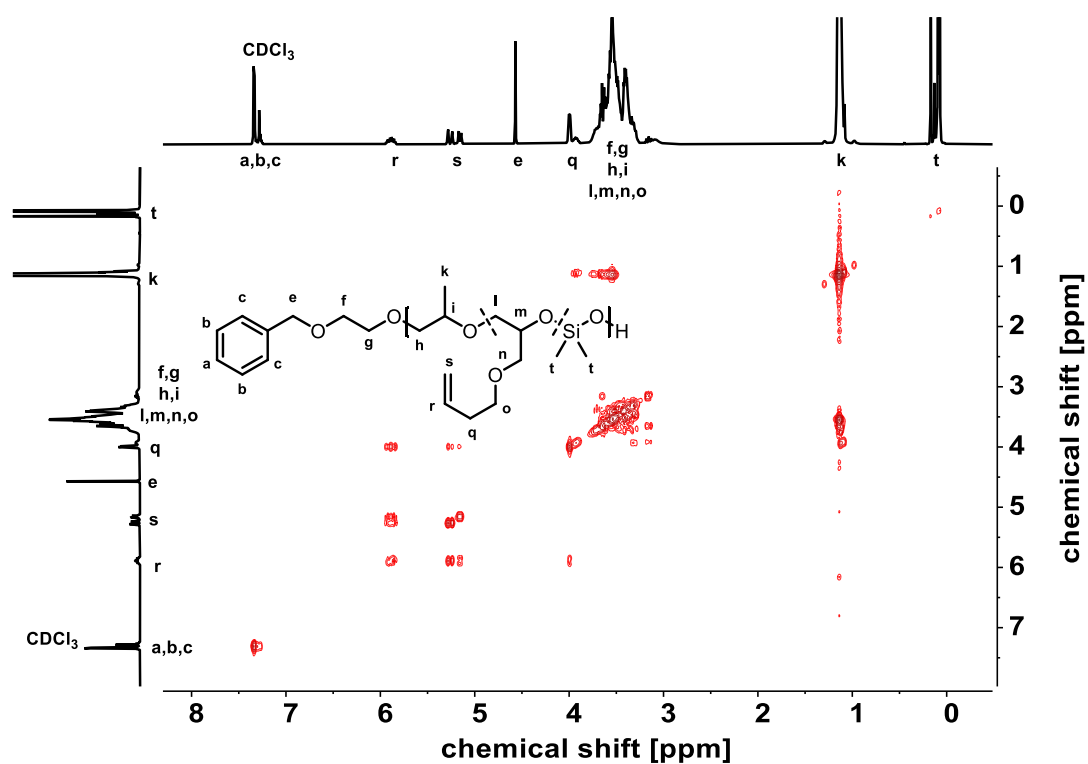
Figure S10. ^{1}H ^{1}H COSY NMR P1.1 P(PO-*co*-AGE-*co*-DMS) (400 MHz, CDCl$_3$)
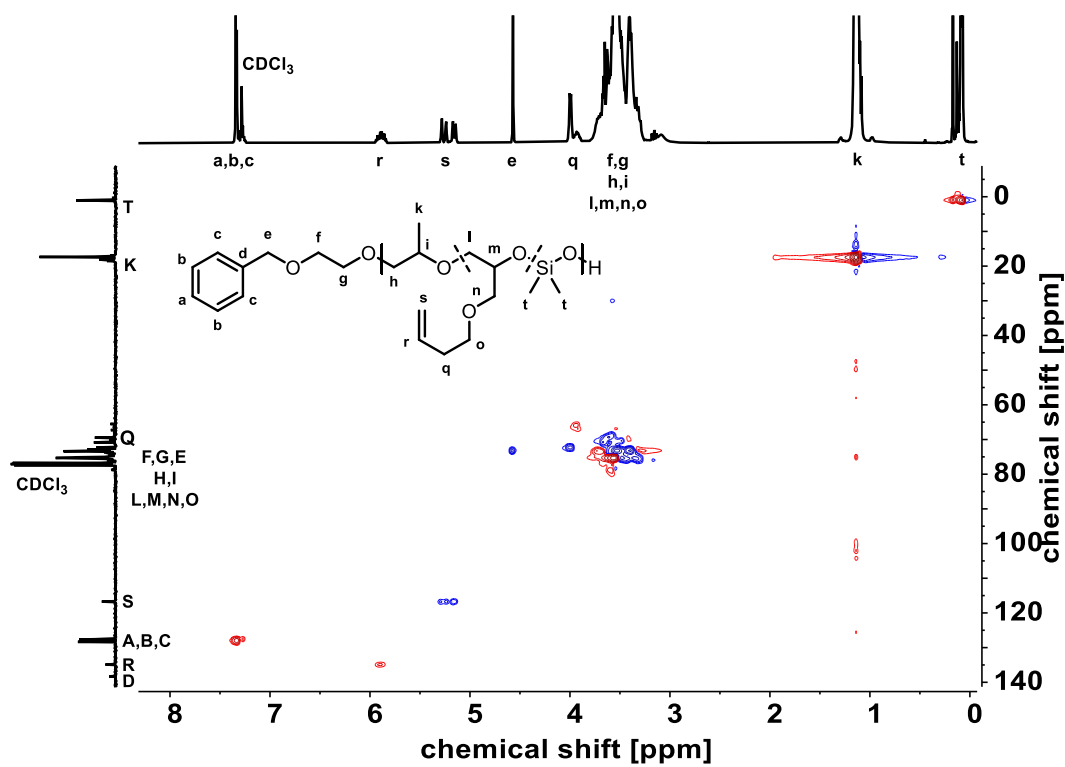
Figure S11. ^{1}H ^{13}C HSQC NMR P1.1 P(PO-*co*-AGE-*co*-DMS) (400 MHz, CDCl$_3$)
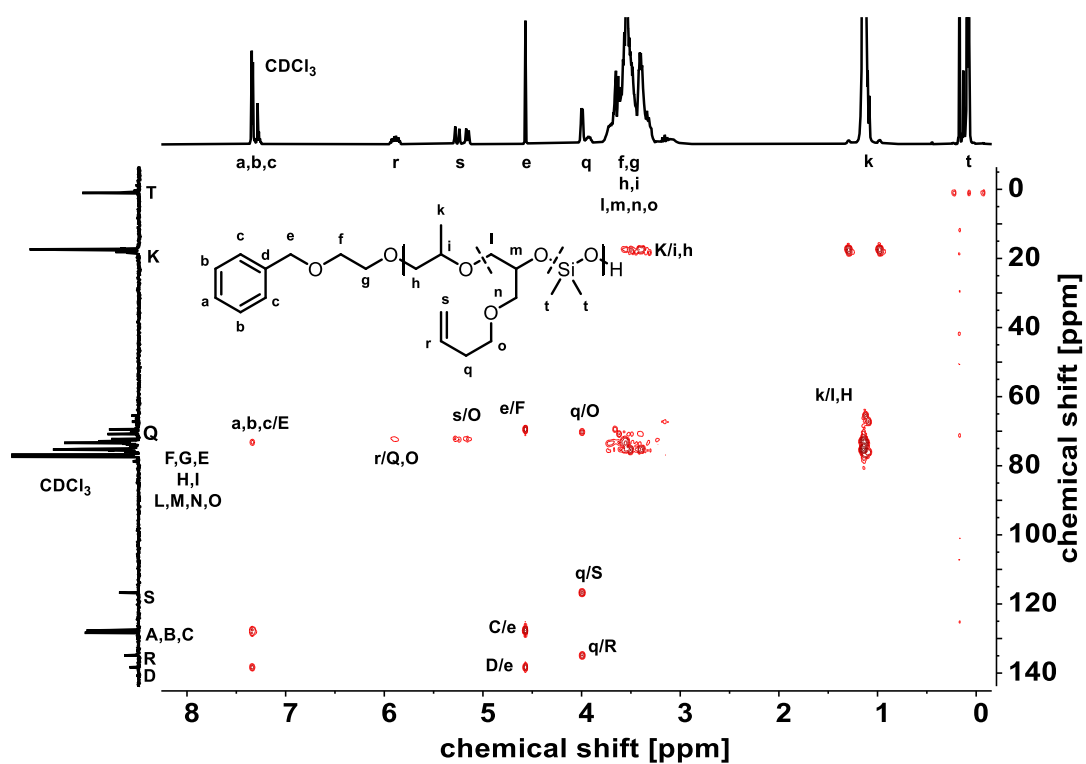
Figure S12. ^{1}H ^{13}C HMBC NMR P1.1 P(PO-*co*-AGE-*co*-DMS) (400 MHz, CDCl$_3$)
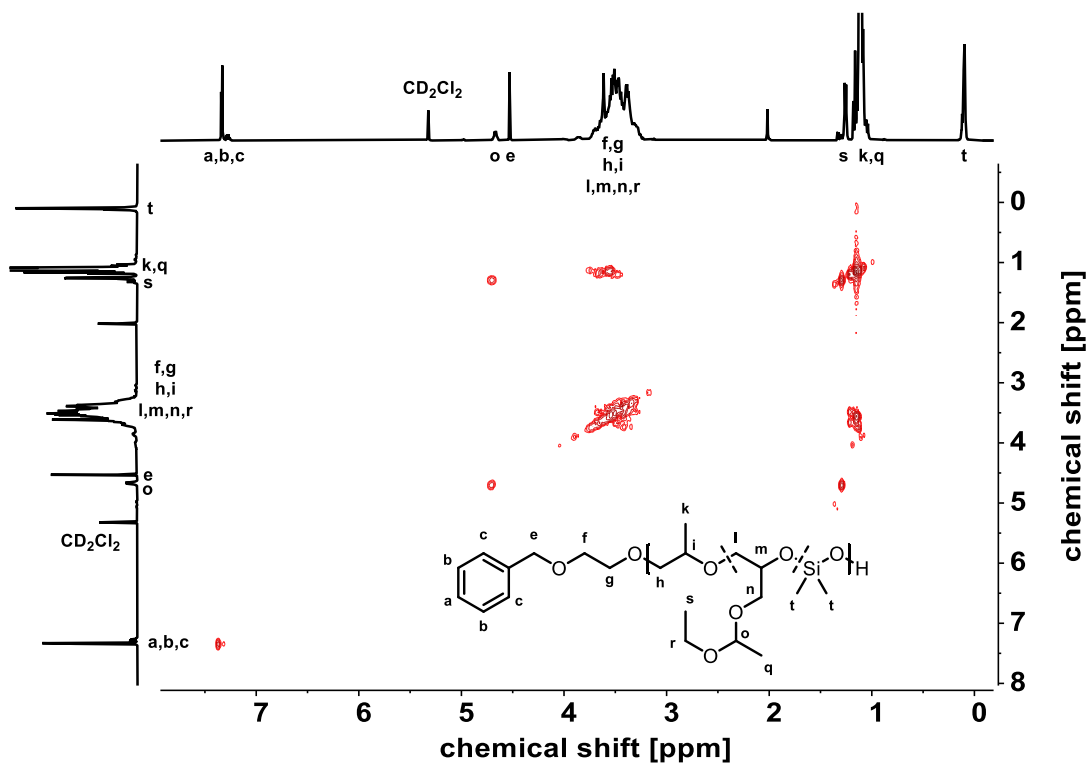
Figure S13. ^{1}H ^{1}H COSY NMR P2.2 P(PO-*co*-EEGE-*co*-DMS) (400 MHz, CD$_2$Cl$_2$)
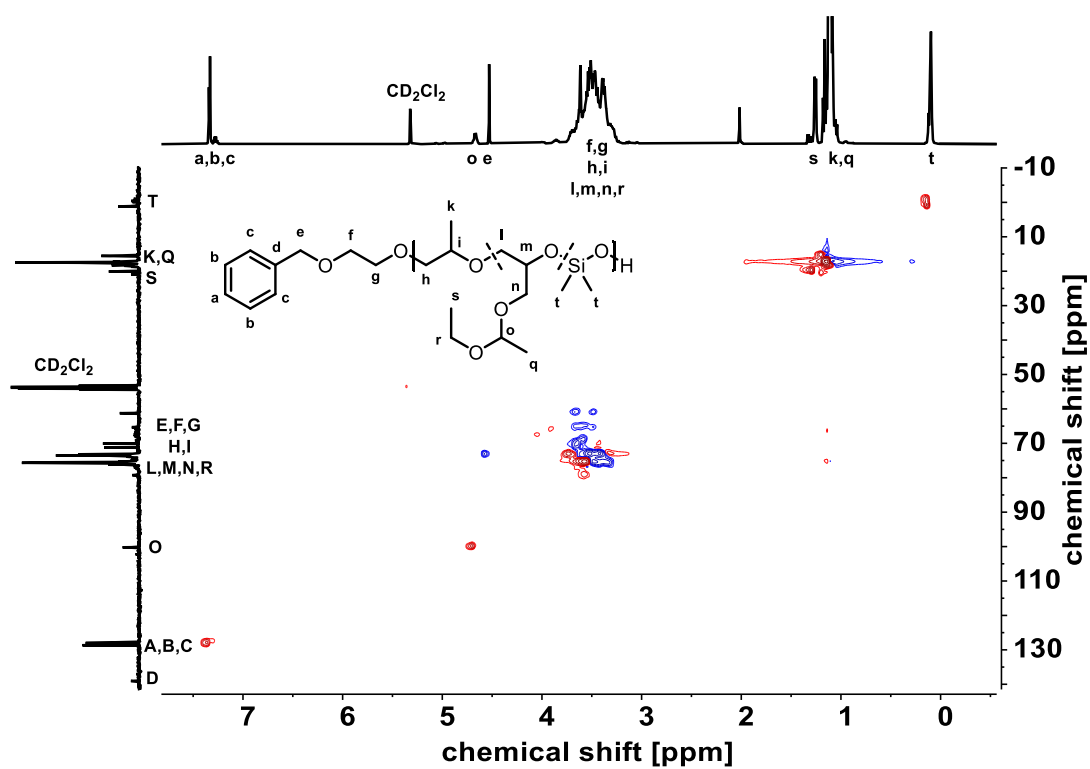
Figure S 14. ^{1}H ^{13}C HSQC NMR P2.2 P(PO-*co*-EEGE-*co*-DMS) (400 MHz, CD$_2$Cl$_2$)
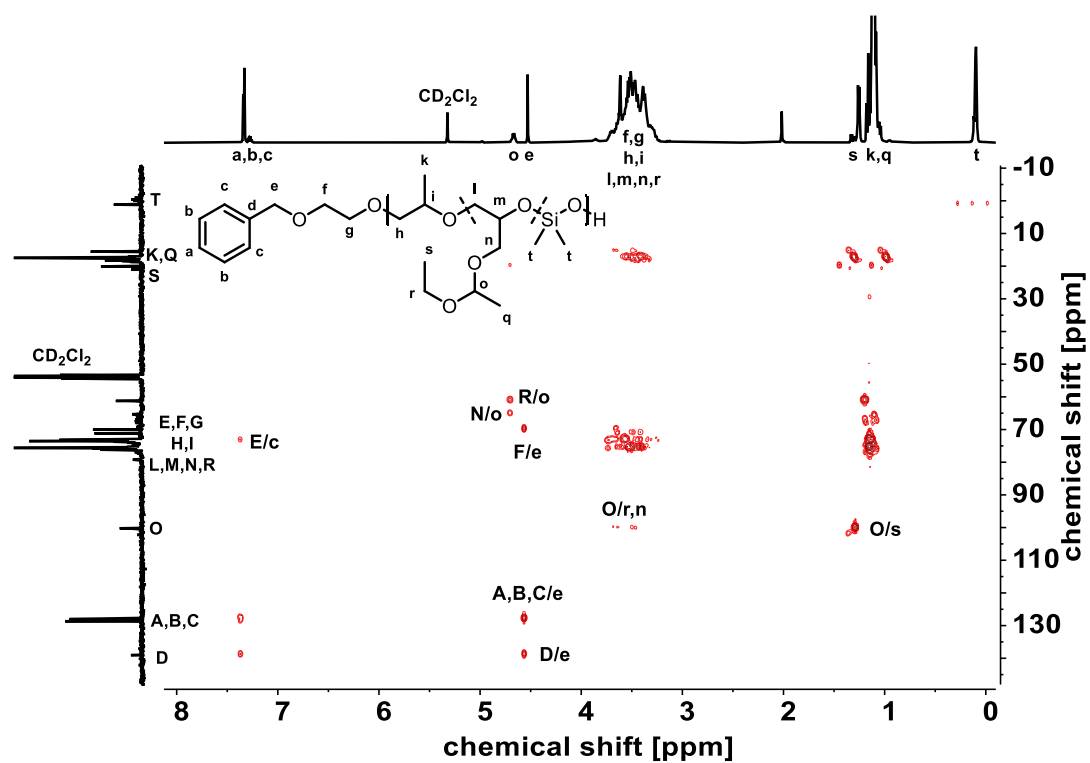
Figure S 15. ^{1}H ^{13}C HMBC NMR P2.2 P(PO-*co*-EEGE-*co*-DMS) (400 MHz, CD$_2$Cl$_2$)
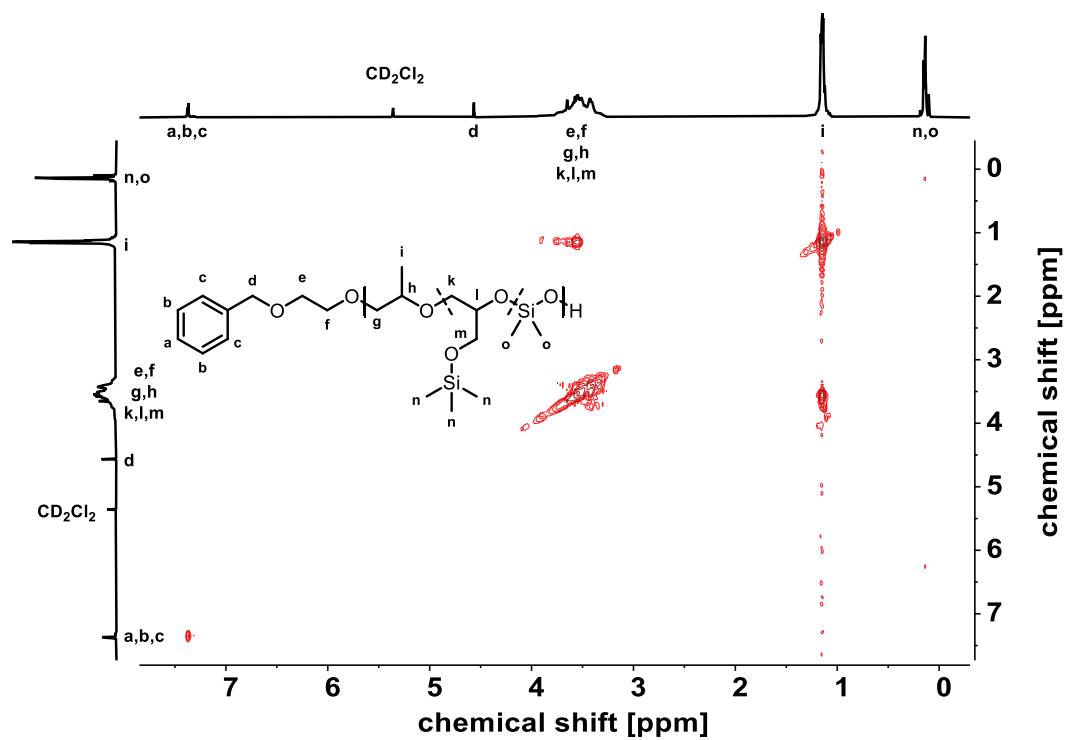
Figure S 16. ^{1}H ^{1}H COSY NMR P3.2 P(PO-*co*-GlyTMS-*co*-DMS) (400 MHz, CD$_2$Cl$_2$)
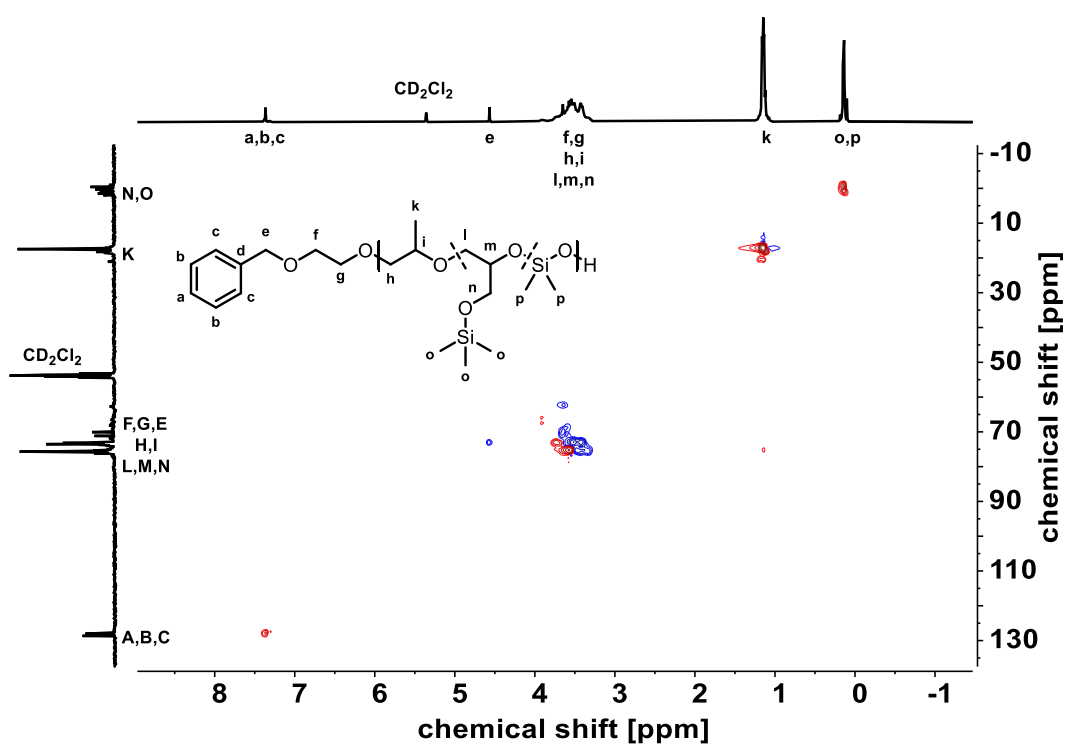
Figure S 17. ^{1}H ^{13}C HSQC P3.2 P(PO-*co*-GlyTMS-*co*-DMS) (400 MHz, CD$_2$Cl$_2$)
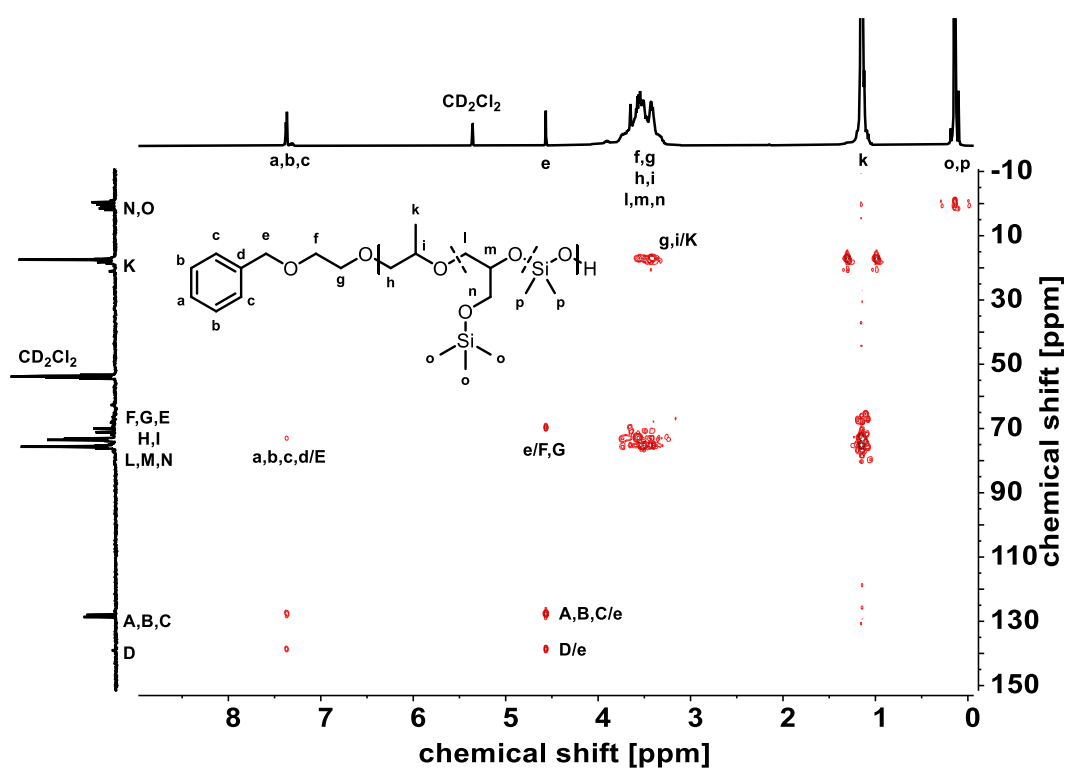
Figure S 18. ^{1}H ^{13}C HMBC P3.2 P(PO-*co*-GlyTMS-*co*-DMS) (400 MHz, CD$_2$Cl$_2$)
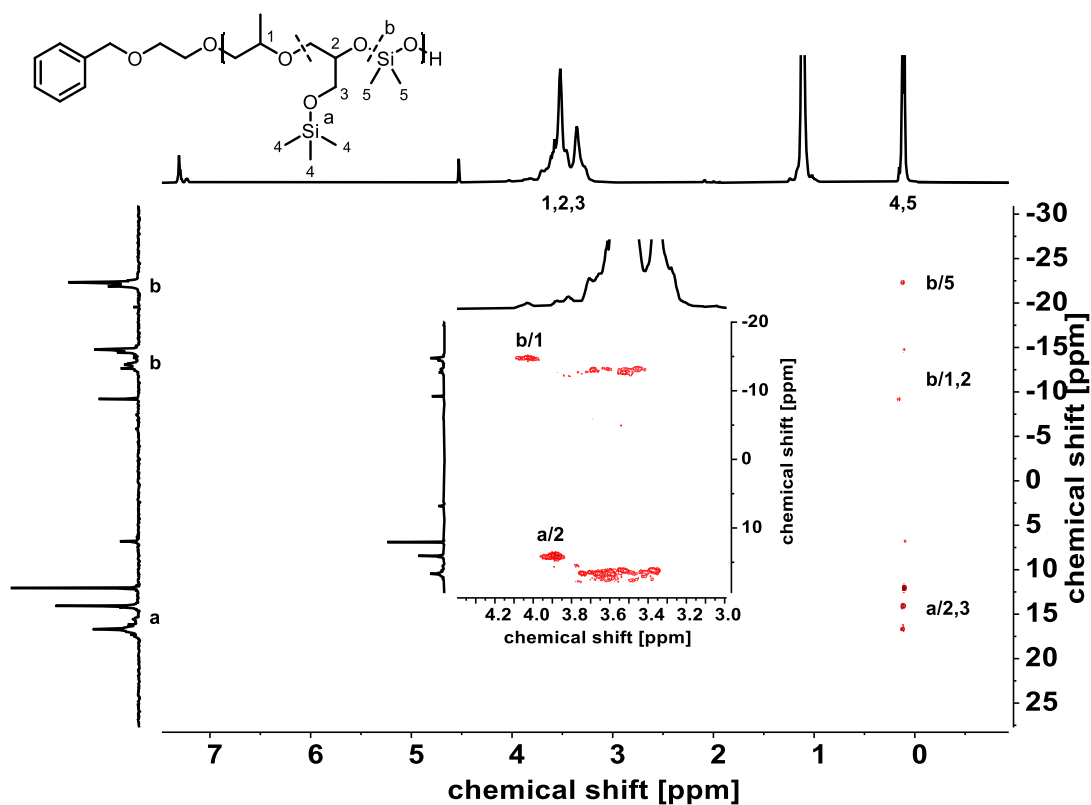
Figure S 19. ^{1}H ^{29}Si HMBC P3.1 P(PO-*co*-GlyTMS-*co*-DMS) (600 MHz, 1,4-dioxane-d_8).
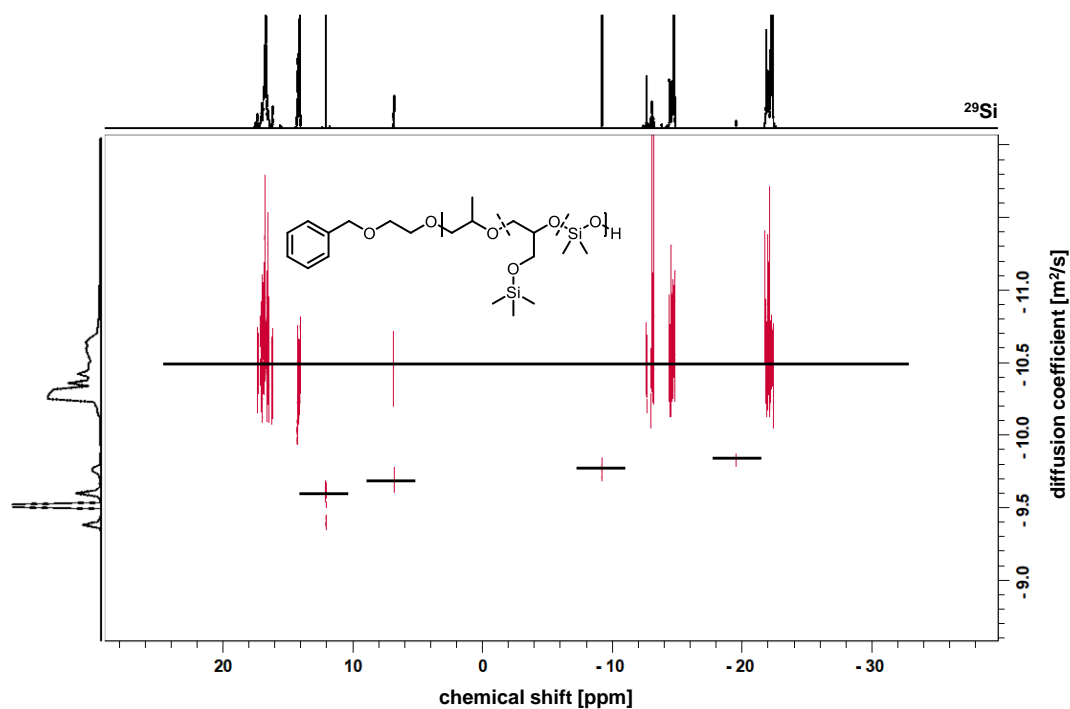
Figure S20. ^{29}Si INEPT DOSY NMR of P3.1 P(PO-*co*-GlyTMS-*co*-DMS) (500 MHz, 1,4-dioxane-d_8).

The ^{29}Si INEPT DOSY NMR was performed using a 9:1 ratio of copolymer sample to 1,4-dioxane-d_8. The very high sample concentration was necessary to achieve a sufficient concentration of ^{29}Si cores for analysis via DOSY NMR. Due to the high concentration and therefore highly viscous solution, the diffusion coefficient is significantly decreased, resulting in the non-uniform diffusion pattern shown at the left y-axes in Figure S20.
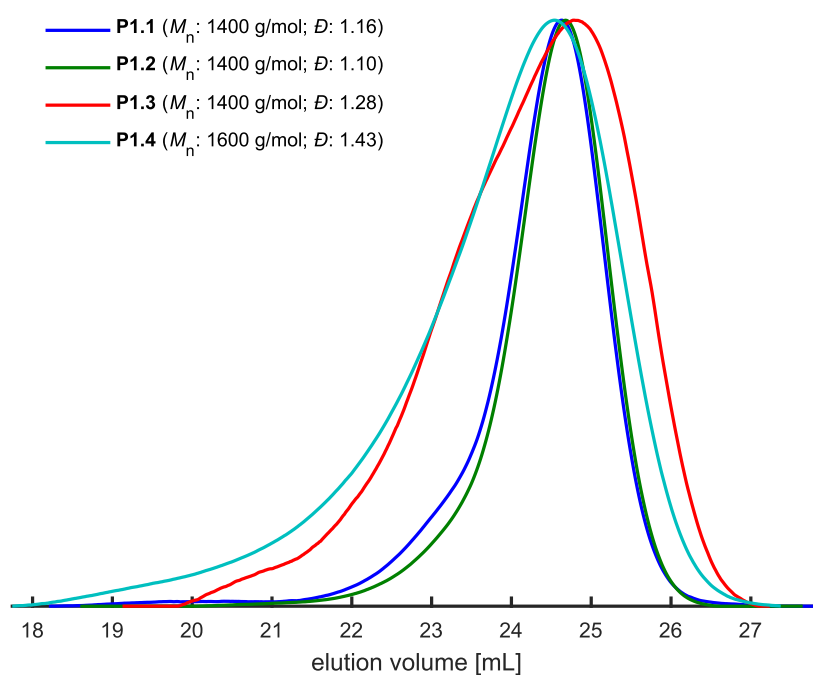
Figure S21. SEC elugrams of P(PO-*co*-AGE-*co*-DMS) (solvent: DMF, calibration: PEG).
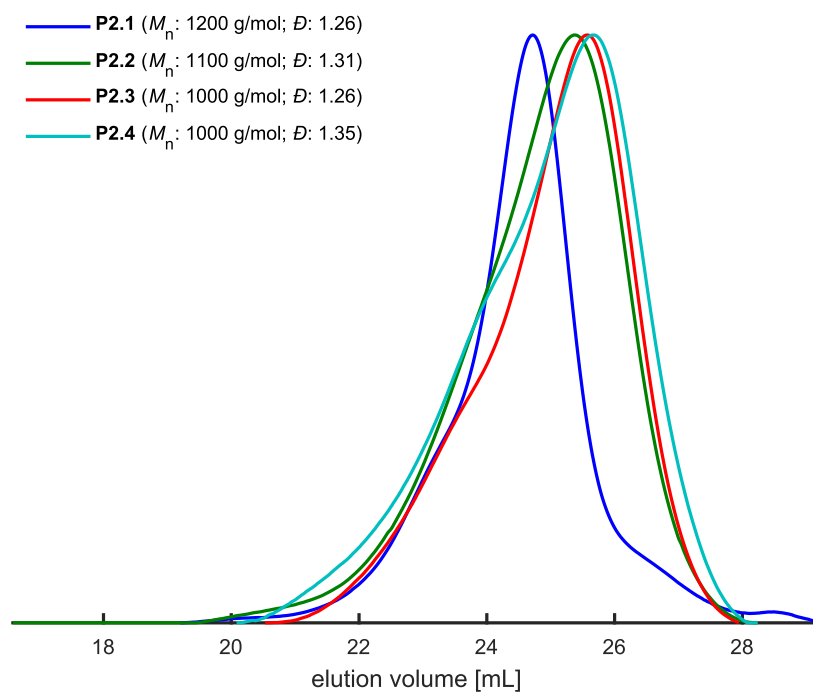
Figure S22. SEC elugrams of P(PO-*co*-EEGE-*co*-DMS) (solvent: DMF, calibration: PEG).
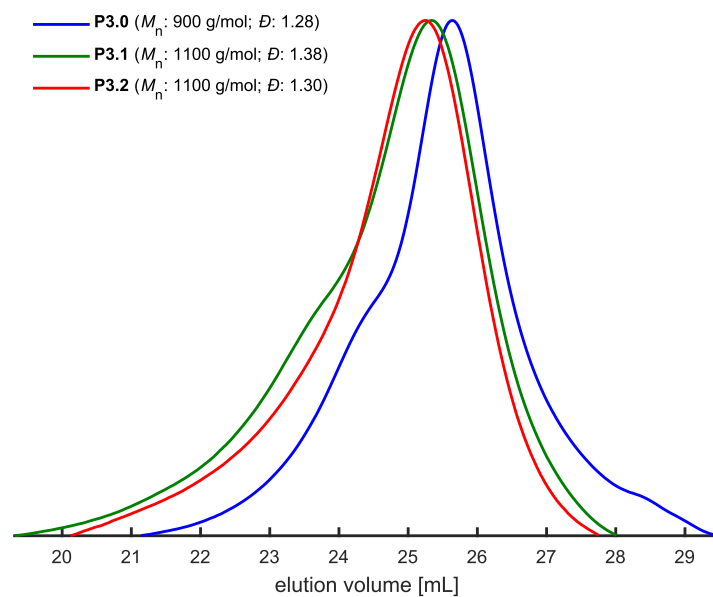
Figure S23. SEC elugrams of P(PO-*co*-GlyTMS) P3.0 as well as P(PO-*co*-GlyTMS-*co*-DMS) P3.1 and P3.2 (solvent: DMF, calibration: PEG).

Determination of Glass Transition Temperature via Differential Scanning Calorimetry
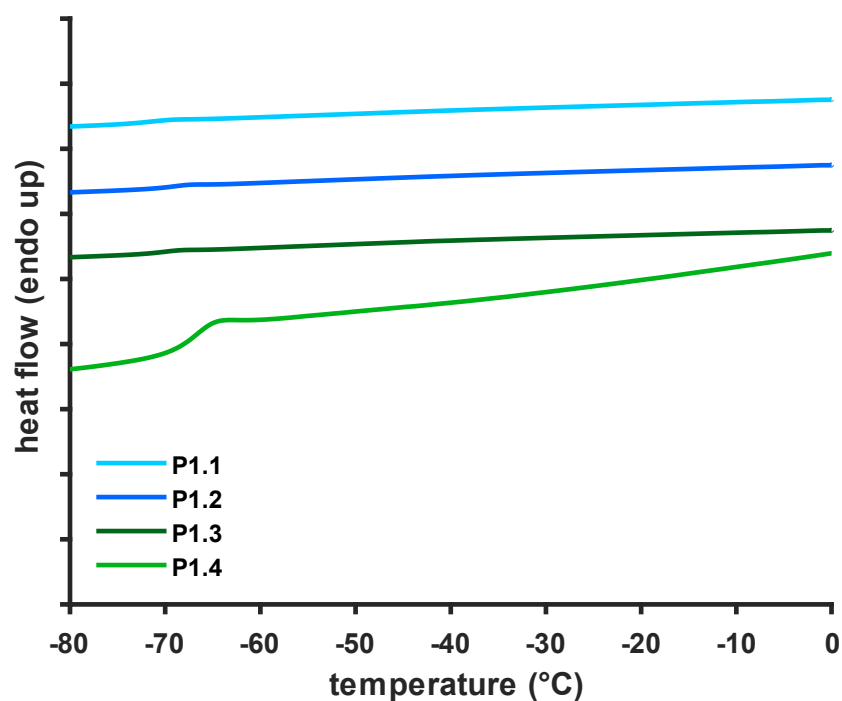
Figure S24. Thermal analysis of P(PO-*co*-AGE-*co*-DMS) via DSC (20 °C min^{-1}, endo up, second heating curve).
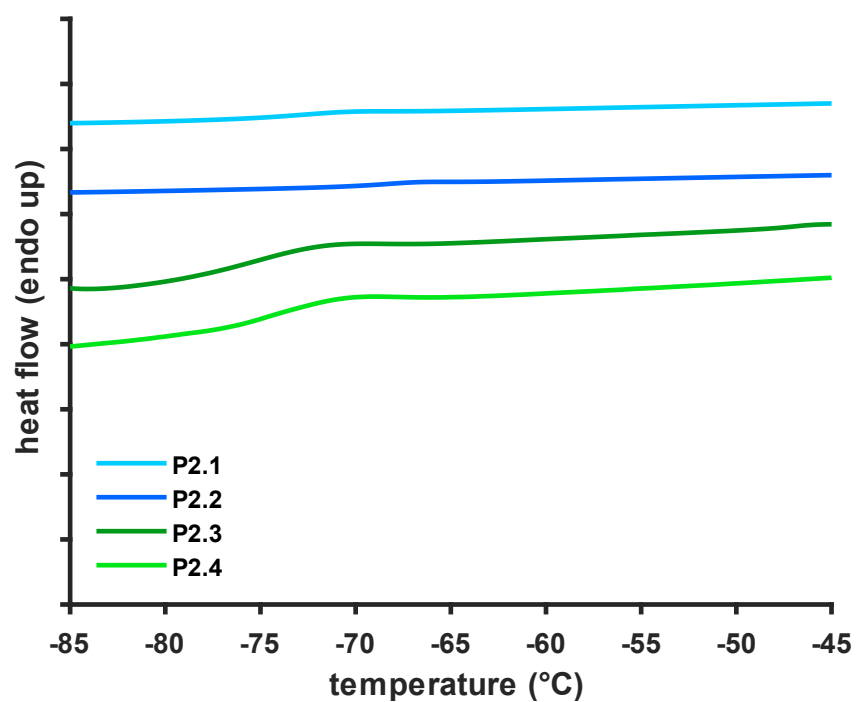
Figure S25. Thermal analysis of P(PO-*co*-EEGE-*co*-DMS) via DSC (20 °C min^{-1}, endo up, second heating curve).
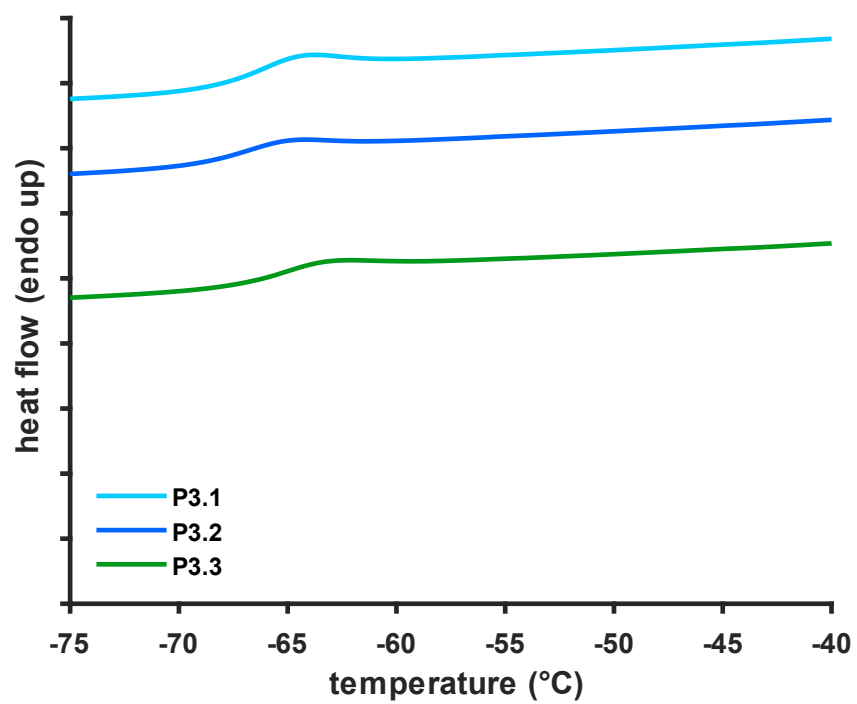
Figure S26. Thermal analysis of P(PO-*co*-GlyTMS-*co*-DMS) via DSC (20 °C min^{-1}, endo up, second heating curve).

Supporting NMR spectra for Post-Polymerization modifications
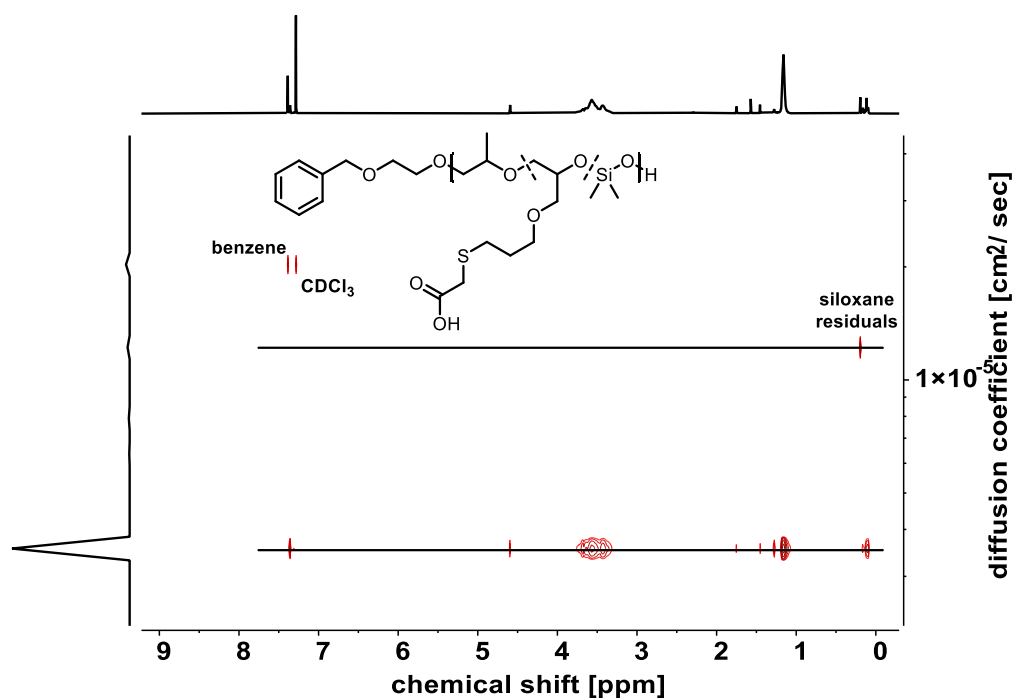
Figure S27. ^{1}H DOSY NMR spectrum showing the product of thiol-ene click reaction of P1.2 P(PO-*co*-AGE-*co*-DMS) and thioglycolic acid (300 MHz, CDCl$_3$).
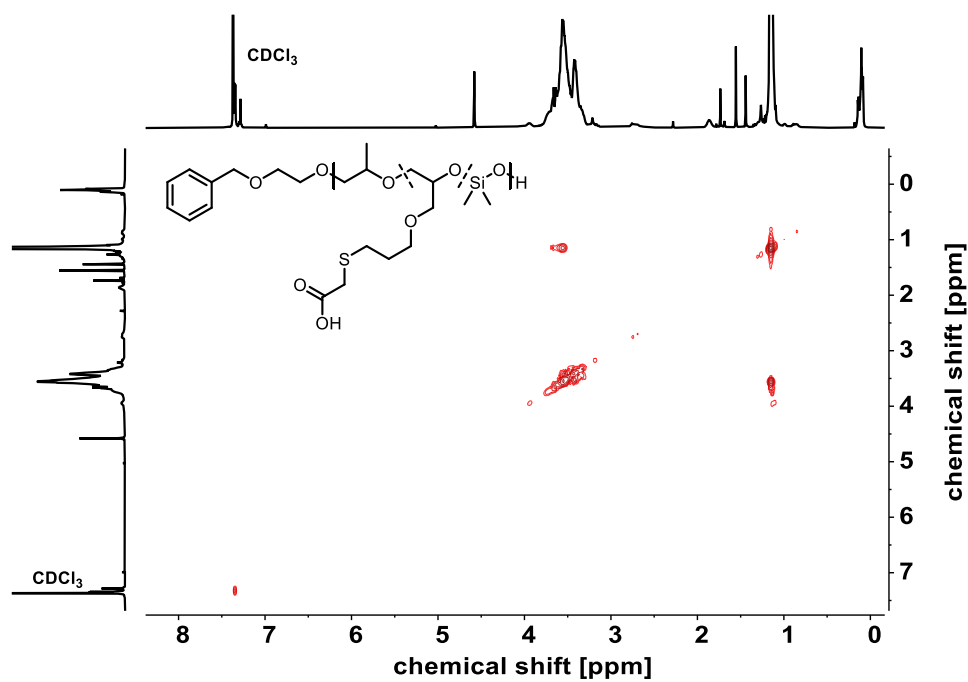
Figure S28. ^{1}H ^{1}H COSY NMR spectrum showing the product of thiol-ene click reaction of P1.2 P(PO-*co*-AGE-*co*-DMS) and thioglycolic acid (300 MHz, CDCl$_3$).
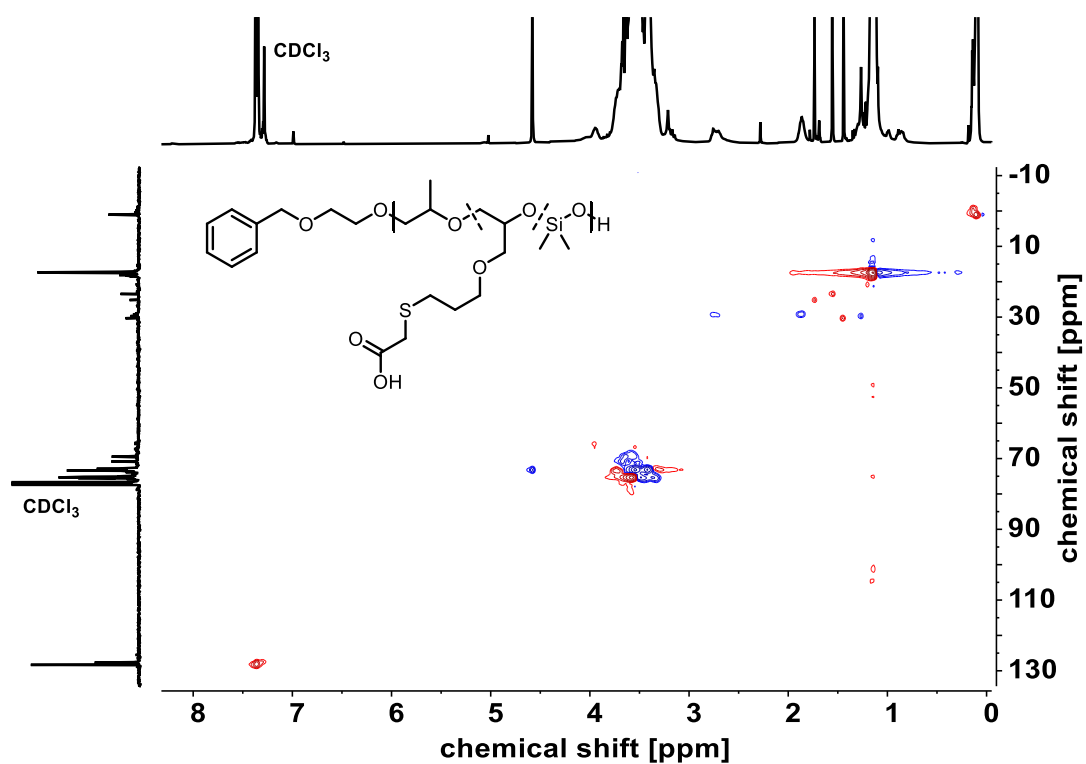
Figure S29. ^{1}H ^{13}C HSQC NMR spectrum showing the product of thiol-ene click reaction of P1.2 P(PO-*co*-AGE-*co*-DMS) and thioglycolic acid (300 MHz, CDCl₃).
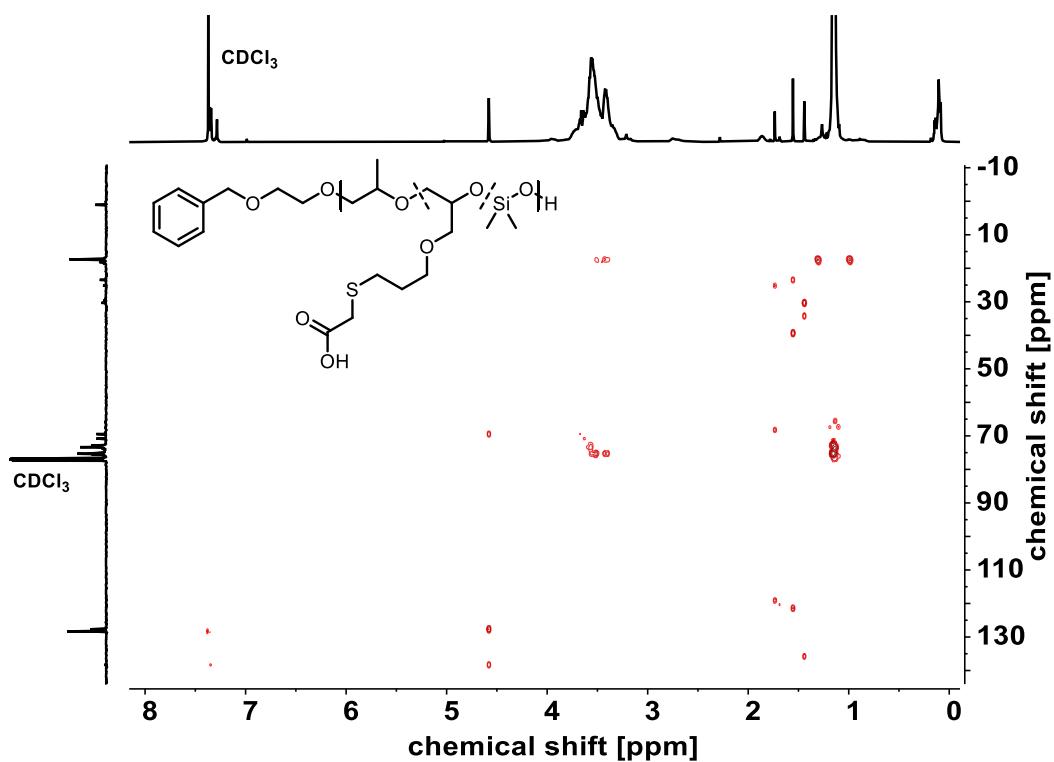
Figure S30. ^{1}H ^{13}C HMBC NMR spectrum showing the product of thiol-ene click reaction of P1.2 P(PO-*co*-AGE-*co*-DMS) and thioglycolic acid (300 MHz, CDCl₃).

P2.1 deprotected (M_n: 1100 g/mol; $Đ$: 1.14)

P2.1 (M_n: 1200 g/mol; $Đ$: 1.26)

elution volume [mL]
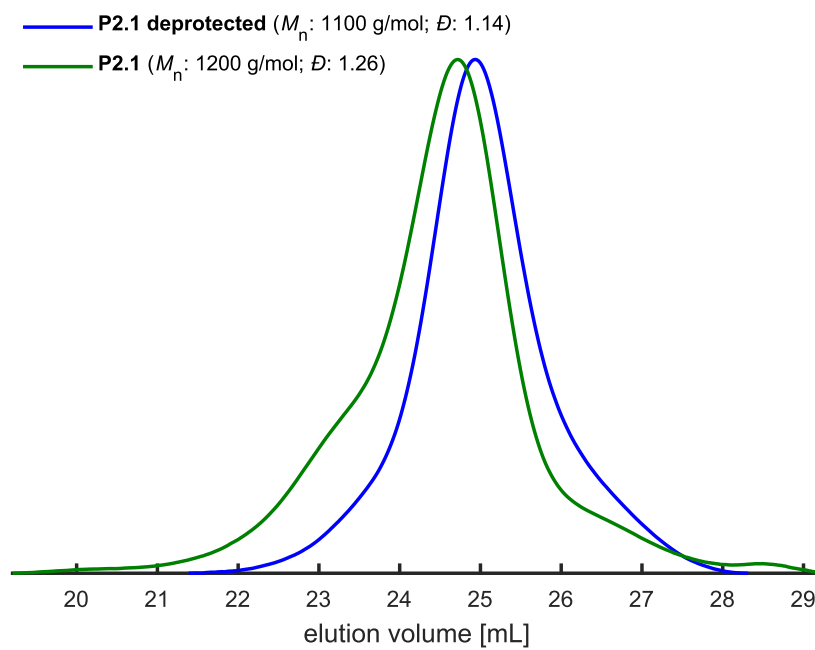
Figure S31. SEC of P2.1 as well as the product P(PO-*co-lin*G-*co*-DMS) after acidic deprotection (solvent: DMF; calibration: PEG).

Study Regarding the deprotection of P(PO-*co*-GlyTMS-*co*-DMS)
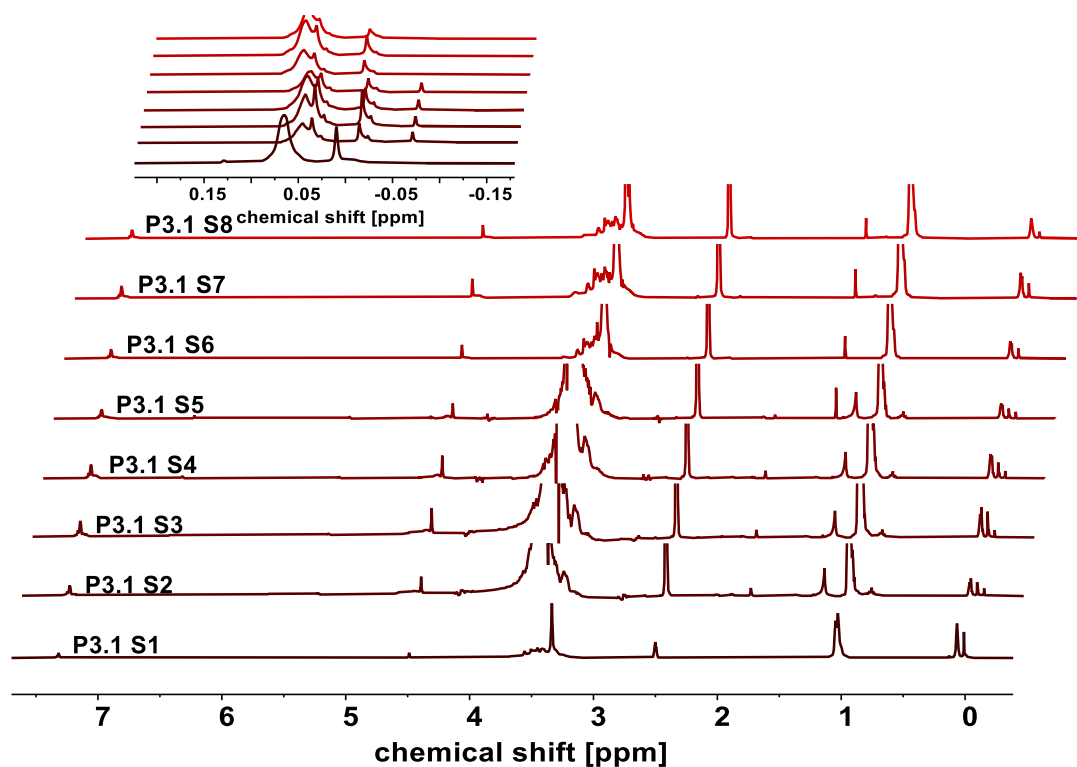
Figure S32. ^{1}H NMR spectra of deprotection study under acidic conditions of P3.1 in DMSO-d_6. Respective concentrations of acetic acid in methanol are listed in Table S2.
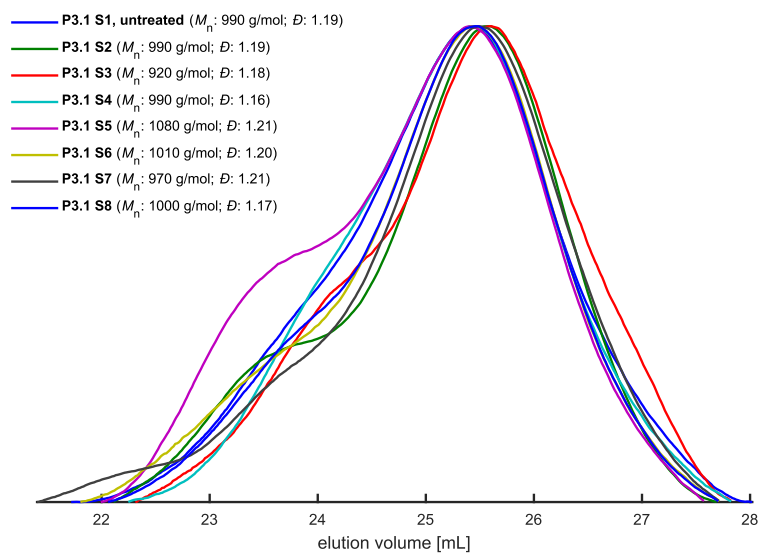
Figure S33. SEC of samples P3.1 S1 to S8 of the deprotection study under acidic conditions (solvent: DMF; calibration: PEG).

REFERENCES

(1) AO Fitton, J Hill, DE Jane, R Millar. Synthesis of simple oxetanes carrying reactive 2-substituents. *Synthesis* **1987**, *1987,* 1140–1142.

(2) Yaws, C. L.; Banadur, P. Enthalpy of vaporization at boiling point—Organic compounds. In Thermophysical properties of chemicals and hydrocarbons; Yaws, C. L., Ed.; Andrew: Norwich, NY, **2008**; pp 409–546.

(3) Wisniak, J. Frederick Thomas Trouton: The Man, the Rule, and the Ratio. *Chem. Educator* **2001**, *6*, 55–61.

(4) Lee, B. F.; Kade, M. J.; Chute, J. A.; Gupta, N.; Campos, L. M.; Fredrickson, G. H.; Kramer, E. J.; Lynd, N. A.; Hawker, C. J. Poly(allyl glycidyl ether)-A versatile and functional polyether platform. *J. Polym. Sci. Part A: Polym. Chem.* **2011**, *49,* 4498–4504.

(5) Marvanova, P.; Padrtova, T.; Pekarek, T.; Brus, J.; Czernek, J.; Mokry, P.; Humpa, O.; Oravec, M.; Jampilek, J. Synthesis and Characterization of New 3-(4-Arylpiperazin-1-yl)-2-hydroxypropyl 4-Propoxybenzoates and Their Hydrochloride Salts. *Molecules* (Basel, Switzerland) **2016**, *21*.

(6) Schöttner, S.; Brodrecht, M.; Uhlein, E.; Dietz, C.; Breitzke, H.; Tietze, A. A.; Buntkowsky, G.; Gallei, M. Amine-Containing Block Copolymers for the Bottom-Up Preparation of Functional Porous Membranes. *Macromolecules* **2019**, *52*, 2631–2641.

(7) Wei, R.-J.; Zhang, Y.-Y.; Zhang, X.-H.; Du, B.-Y.; Fan, Z.-Q. Regio-selective synthesis of polyepichlorohydrin diol using Zn–Co(III) double metal cyanide complex. *RSC Adv* **2014**, *4*, 21765–21771.

(8) Shambayati, S.; Schreiber, S. L.; Blake, J. F.; Wierschke, S. G.; Jorgensen, W. L. Structure and basicity of silyl ethers: a crystallographic and ab initio inquiry into the nature of silicon-oxygen interactions. *J. Am. Chem. Soc.* **1990**, *112*, 697–703.

(9) Mohr, R.; Wagner, M.; Zarbakhsh, S.; Frey, H. The Unique Versatility of the Double Metal Cyanide (DMC) Catalyst: Introducing Siloxane Segments to Polypropylene Oxide by Ring-Opening Copolymerization. *Macromol. Rapid Commun.* **2020**, 2000542.

(10) Obermeier, B.; Frey, H. Poly(ethylene glycol-co-allyl glycidyl ether)s: a PEG-based modular synthetic platform for multiple bioconjugation. *Bioconjugate chemistry* **2011**, *22*, 436–444.

(11) Schömer, M.; Frey, H. Water-Soluble "Poly(propylene oxide)" by Random Copolymerization of Propylene Oxide with a Protected Glycidol Monomer. *Macromolecules* **2012**, *45*, 3039–3046.

Appendix

Chapter A1

Kinetic Investigations on DMC Catalysis of Propylene Oxide by Ring-Opening Polymerization

The control of molecular weight and suppression of unsaturated side products of polyols based on poly(propylene oxide) play a crucial role during foaming of polyurethanes. Key parameters of the ring-opening polymerization of propylene oxide (M_n = 4-8 kg mol^{-1}) were investigated, facilitating a deeper understanding to develop an improved performance of the industrially established DMC catalysis. The catalyst concentration ranging from 100 to 300 ppm, temperatures from 80 to 140 °C as well as varying catalyst polyol suspensions were examined. The concentration screening enabled the evaluation of an ideal mass per *SA:V* ratio of > 0.85 mg cm. The herein determined thermal results show a decrease of initiation time with higher temperatures as well as the enhanced suppression of unsaturated side products for temperatures < 120 °C. Comparing varying polyol suspensions, the results indicate the enhanced control over M_n with lower dispersities ($Đ < 2.0$) for suspension polyols possessing less terminal hydroxy-functionalities. Based on these findings, a mechanistic explanation for the formation of high molecular weight tailing is postulated. These fundamental findings offer promising guidelines for the further optimization of the industrially established polyol synthesis as soft components in polyurethane foaming.
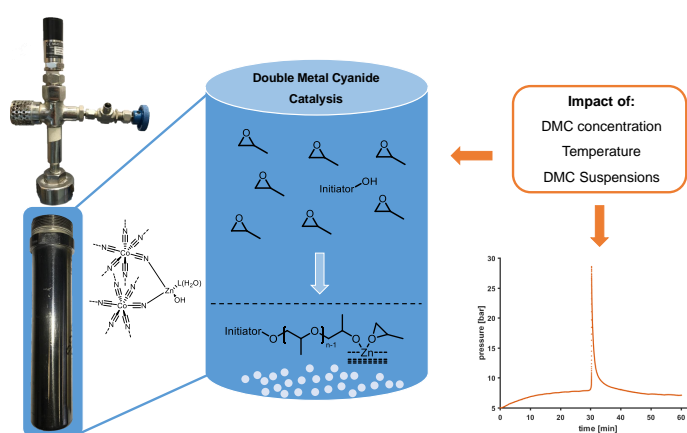
INTRODUCTION

The polyether poly(propylene oxide) (PPO) is the most commonly used polyol as soft component in nowadays polyurethane formulations. In 1963, General Tire & Rubber introduced the double metal cyanide (DMC) catalyst promising the production of polyols with a highly upgraded efficiency compared to the at the time established synthesis catalyzed by KOH.[1–4] Such polyether polyols are mostly produced by catalytic ring-opening polymerization (ROP) of propylene oxide (PO), with low amounts of ethylene oxide (EO) and to some extent higher alkylene oxides.

Several benefits lead to the ongoing industrial relevance of polyols produced by DMC catalysis. The catalyst´s capability to suppress chain-transfer reactions, e.g. proton abstraction known for conventional anionic ring-opening polymerization (AROP), results in polymers with a very low unsaturation level (0,001 meq g^{-1}).[5] The small amount of catalyst (≥ 13 ppm) required is inactive after exposure to air after polymerization has occurred and therefore remains in the resulting polymer upon subsequent use.[6] Additionally, polymerizations are commonly performed in bulk with varying hydroxyl initiators, requiring no further purification steps.[7–10]

Mechanistic specifications of the DMC catalysis are not fully understood to this date. Multiple publications proposed a heterogeneous cationic coordination-insertion mechanism proceeding on the exposed Zn species on the surface of the catalyst particles.[2,11,12] The assumed cationic coordination is capable of suppressing proton abstraction, a known chain-transfer reaction of AROP. This phenomenon results in the aforementioned low level of unsaturations, which is crucial for the application in polyurethane foaming.[5,11]

Kim et al. postulated a possible mechanistic pathway for ring-opening polymerization of racemic propylene oxide by DMC catalysis based on experimental data and DFT calculations in 2019.[11] Initially, the Zn^{2+} sites of the catalyst are preoccupied by the complexing agent which is *tert*-butyl alcohol in the herein presented DMC catalyst. Other complexing agents like diglyme, PPO, poly(ethylene oxide) and poly(tetrahydrofuran) are known alternatives to *t*BuOH. Such ethers are additionally considered as activating ligands in DMC catalysis. However, DMC catalyst suspensions have not been investigated in detail regarding their influence on the polymerization behavior until today.[2,11] During polymerization, addition of PO to the pre-catalyst leads to the exchange of the complexing agents with the epoxides, resulting in the transfer of the dormant sites to active Zn^{2+} sites. Herein, the initiator reacts with the highly activated monomer by ring-opening of the epoxide after an induction period of minutes up to several hours. Simultaneously, a fragmentation of the catalyst particles during the initiation is observed which leads to a highly activated catalyst, resulting in a strongly increased polymerization rate. The polymerization propagates by nucleophilic attack at the activated chain at the Zn^{2+} surface till full monomer consumption is reached (Scheme 1). The described acceleration of the polymerization rate generates a sharp pressure increase which is proportional to the PO pressure within the reaction flask.[6] The described reaction pathway proceeds at the catalyst surface where the complexing agents are located leading to a strict 'head-to-tail' regiosequence of the resulting PPO. According to Kim et al. some PO monomers are supplementary adsorbed by the internal Zn^{2+} site. The

adsorbance leads to formation of a carbocation intermediate stabilized by additional epoxides, followed by the iterative addition of PO to the thus activated chain end (ACE). This mechanism proceeds until the growing species is exposed to the external initiator resulting in minor defects of 'head-to-head' and 'tail-to-tail' irregularities.
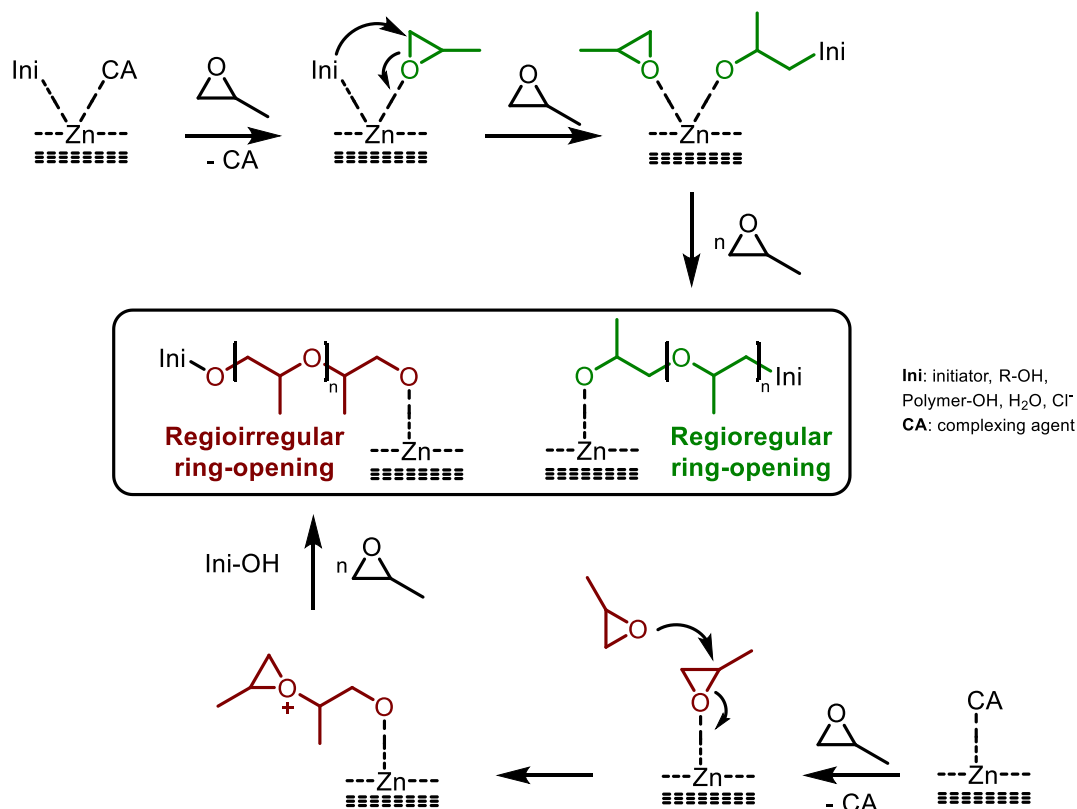
Scheme 1. Postulated cationic insertion mechanism of DMC catalyzed polymerization exemplary illustrated by ring-opening of propylene oxide.[11] (upper, green) Coordinative mechanism at active zinc center resulting in regioregular propylene oxide ring-opening. (lower, red) Active-chain end mechanism resulting in regioirregular propylene oxide ring-opening.

An additional and rather unique phenomenon occurring in DMC catalyzed ring-opening polymerization is the so called catch-up kinetic, which describes the preferential propagation of shorter chains in a mixture of polyethers with varying molecular weights. Pazos and Brown investigated this behavior and developed an hypothetical explanation based on thermodynamic modeling and mathematical predictions.[13] They assumed a rapid and reversible complexation of hydroxy groups at the Zn^{2+} active centers of the catalyst. Polymer chains of lower molecular weights provide a higher density of hydroxy groups and are therefore enthalpically favored to insert monomer units rather than polymer chains of higher molecular weight.

A known disadvantage of DMC catalysis is the occurrence of high molecular weight tailing (HMWT) of 100.000 g mol^{-1} and higher throughout polymerization.[14] During the process of polyurethane foaming, polyether polyols with high amounts of HMWT cause an undesired

collapse of polyurethane foams. Therefore, the clarification and suppression of the mechanism leading to HMWT is of great industrial relevance.[5] Although the reason for this high molecular weight side products has not been fully discovered to this date, several possible causes are postulated in literature. Tran et al. account the formation of high molecular weight products to the delayed insertion of the initiator during the aforementioned ACE mechanism. Theoretical considerations via DFT calculations by López et al. suggested the possibility of propagation of one polymer chain occurring at multiple different active Zn^{2+} centers as a cause of HMWT.[14] Based on a patent by Faraj et al.[15], the authors further proposed the addition of protic acids to cleave the redundant OH groups among Zn^{2+} centers while promoting the fragmentation process. A different angle was considered in a patent by Pazos et al.[16], to compensate the HMWT dilemma by changing the hydrophile/lipophile balance of the high molecular chains. By incorporation of ethylene oxide (EO) in the polyether chain the hydrophobicity of high molecular weight PPG is reduced and the foaming process is therefore less affected by HMWT.

In the past, the different reaction parameters of ring-opening polymerization of PO by DMC catalysis were investigated by a variety of publications. *In situ* ^{1}H NMR kinetics by our group recently revealed the strongly favored incorporation of PO over EO, reinforcing the well-known preference of the DMC catalyst towards PO.[7] A comprehensive publication by Swinarew et al. examined DMC catalysis of PO with differing catalyst concentrations revealing a strong impact of the catalyst amount to reactivity and dispersity of the obtained polyether.[6] Chen et al. investigated the DMC catalysis regarding kinetic factors, revealing a less pronounced induction period with increased reaction temperatures and priorly dried starting materials. However, detailed analysis of the synthesized polymers concerning conversion, dispersities and degree of unsaturations were not part of the performed explorations.[17]

In this work, we present an investigation of several parameters to improve the ring-opening polymerization of PO by DMC catalysis in regard to performance efficiency, HMWT and unsaturation levels. In respect thereof, polymerizations with varying amounts of DMC catalyst (100 to 300 ppm) were performed to evaluate an ideal mass per surface area:volume (SA:V) ratio. Additional analysis of polymerization temperatures ranging from 80 to 140 °C enable an estimation concerning the temperature impact during DMC catalysis. Further, suspensions of the DMC catalyst are examined as suspensions are preferred for handling the catalyst in an industrial scale. Therefore, the influence of catalyst suspensions on the activation of the Zn^{2+} centers are investigated by the utilization of different polyether polyols with varying degrees of terminal OH-functionalities and varying viscosities. Finally, based on the current state of knowledge regarding DMC catalysis a mechanism focusing on the formation of high molecular weight tailing is proposed.

RESULTS & DISCUSSION

Investigations of Catalyst Concentration in DMC catalysis

One of the prominent advantages of ring-opening polymerization of PO to gain poly(propylene oxide) by DMC catalysis is the low amount of catalyst needed (structure see Figure S1, Supporting Information). Additionally, the low ppm of catalyst residues are inactive after polymerization and can therefore remain in the polymer for following applications. Comprehensibly, the amount of catalyst needed is attempted to be kept as low as possible without impairing its many benefits for the resulting polymers: narrow dispersities, low unsaturation levels and good control of molecular weights. Therefore, we investigated the ideal catalyst quantity for ROP of PO initiated by 2-(benzyloxy)ethanol. The reaction parameters were kept constant except for the varying amounts of DMC catalyst c_{DMC} (bulk, $T = 120\,°C$, $M_n^{theo.} = 6.0\,\text{kg mol}^{-1}$). The constant volume of monomer and initiator was crucial as both chemicals determine the pressure progression. All catalyst concentrations were performed three times to reduce statistical errors. The polymerization process was monitored and evaluated by pressure observation. All polymerization showed similar curve progressions with a course commonly known for DMC catalysis (Figure 1).[6,11] One curve progression for each polymerization (100 to 300 ppm DMC catalyst) is shown exemplary.
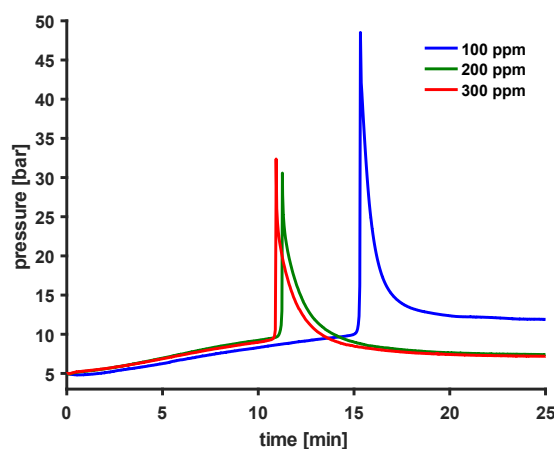
Figure 1. Pressure-time graph of the ring-opening polymerization of propylene oxide with varying amounts of DMC catalyst.

The activation time of the catalyst was determined as t_{max} of the induction period is reached, accompanied with a sharp pressure increase up to a to explosively attain the maximum pressure p_{max} followed by a decrease to a constant pressure value. The duration to reach a constant pressure was denoted as t_{const}, which is considered as an indicator of the completed polymerization of PO. Noteworthy, the parameter t_{const} must be considered as an estimation determined by visual assessment for all polymerizations rather than a definite value. The reaction using 100 ppm of catalyst with the reaction scale equal to the other concentrations showed no catalyst activation and accordingly no polymerization. Therefore, the scale was doubled from 12 to

24 ml volume to explore the polymerization at lower catalyst concentrations. The different polymerizations are analyzed via the average of three runs by comparison of the values p_{max}, t_{max}, t_{const} and the difference Δt of both time variables (Table 1). The full data of all runs, concerning the pressure monitoring, is listed in Table S1 (Supporting Information). Values of t_{max} of the polymerizations **P2** and **P3** are approximately equal with 11 min. The higher catalyst load of **P3** nonetheless results in a value of 32.3 bar which is an increase of 1.5 bar compared to p_{max} of **P2**. In accordance with the pressure increase, t_{const} and consequently Δt are prolongated for a higher concentration of the catalyst in **P3**. The numbers of p_{max}, t_{max} and t_{const} of **P1.2** are elevated by the factors of 1.5, 2 and 1.4 respectively compared to **P2** and **P3** which is in good agreement with the enhanced reaction scale. The difference of Δt of **P1.2** with 18.8 min is slightly prolongated compared to **P2** (14.8 min) and **P3** (17.5 min). An extended Δt could indicate a slower initiation of polymerization which will be discussed in the following paragraphs. By determination of the medium slope m, the speed of polymerization of the individual reactions can be correlated with the variation of c_{DMC}. The slope was calculated from the pressure decrease subsequent to p_{max} and the following pressure progression 3 min after reaching the maximum value. Expectedly, the sample **P1.2** exhibits the lowest value of m with - 11.2 bar min^{-1} which is in good agreement with the highest p_{max} of all compared concentrations. The slopes of **P2** and **P3** reveal factors of - 6.9 and - 7.2 bar min^{-1} respectively. To draw precise conclusions concerning the polymerization speed based on pressure progression, further polymerizations with varying amounts of DMC catalyst are necessary.

Table 1. Average values of pressure monitoring of ring-opening polymerization of propylene oxide by varying amounts of DMC catalyst. The sample P1.2 differs from P1 by a doubled reaction scale by a constant catalyst concentration.

sample	c_{DMC} [ppm]	p_{max} [bar]	t_{max} [min]	t_{const} [min]	Δt^1 [min]	m [bar min^{-1}]
P1	99	-	-	-	-	-
P1.2	98	47.1	20.4	39.2	18.8	- 11.2
P2	199	30.8	11.7	26.5	14.8	- 6.9
P3	313	32.3	11.3	28.8	17.5	- 7.2

^{1} $\Delta t = t_{const} - t_{max}$

SEC analysis was performed for all samples to gain further knowledge regarding the quality of the synthesized polymers. All samples were calibrated with a poly(ethylene glycol) (PEG) standard in DMF. Similar to pressure analysis, the average values for the different concentrations were considered for the following correlations (Table 2). Full data of all runs concerning the molecular weight analysis is listed in Table S2 (Supporting Information). The molecular weight M_n determined by SEC is underestimated for all samples due to the lower hydrodynamic radius of PPO compared to PEG. Therefore, ^{1}H NMR spectroscopy was performed to estimate the precise M_n by calculation of the monomer to initiator ratio via integration of the specific signals.

Furthermore, in ^{1}H NMR spectroscopy the integral ratio between the benzylic protons and the methine proton of allyl end-groups provides a value for the amount of side reactions during the polymerization. The corresponding ^{1}H NMR spectra are presented in Figure S3, Figure S4 and Figure S5 (Supporting Information). A commonly known side reaction in anionic ring-opening polymerization (AROP) of PO is the proton abstraction of the basic chain end at the acidic proton of the methyl group of PO (Scheme 2). This chain transfer reaction leads to the formation of an allyl alkoxide which initiates another polymer chain. Consequently, the dispersity of the resulting polymer is increased and the maximum molecular weight is limited.
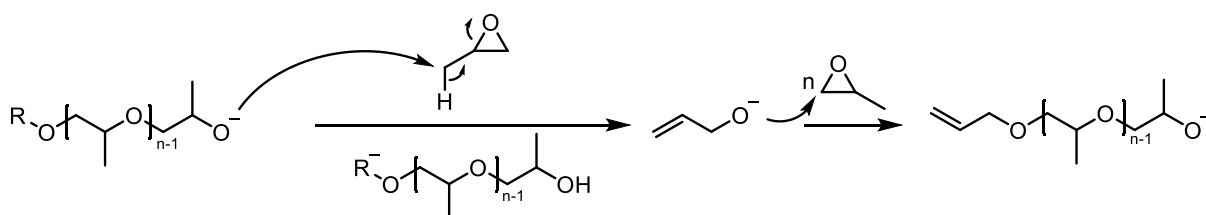
Scheme 2. Exemplary mechanism of proton abstraction and therewith formation of allylic species in anionic ring-opening polymerization.

In comparison to AROP, DMC catalysis proceeds in a cationic coordinative polymerization mechanism. Therefore, basic proton abstraction at PO leading to unsaturated side products is not expected. Although the level of unsaturation is tremendously decreased in DMC catalysis, it is not eliminated.[5,11] The cause of the unsaturations has to this date not been discovered and requires further investigations. Nevertheless, analysis of the unsaturated by-products provides additional information for the implemented concentration screening (Table 2).

Table 2. Average values of molecular weight and HMWT analysis of PPO prepared by varying amounts of DMC catalyst. The sample P1.2 differs from P1 by a doubled reaction scale by a constant catalyst concentration. Theoretical M_n for all samples was $6.0 \, \text{kg mol}^{-1}$.

sample	c_{DMC} [ppm]	HMWT$_{>10k}$[1] [%]	HMWT$_{>20k}$[1] [%]	M_n [kg mol^{-1}]	M_n[2] [kg mol^{-1}]	$Đ$	unsat.[3] [%]	yield [%]
P1	99	-	-	-	-	-	-	-
P1.2	98	12.22	4.59	2.1	3.1	2.73	10.6	46
P2	199	8.83	2.35	3.1	5.2	1.55	5.3	84
P3	313	5.90	1.22	2.8	5.1	1.43	21.6	81

[1] Determined by SEC (DMF, Poly(ethylene glycol) calibration)

[2] Determined by ^{1}H NMR spectroscopy (CDCl$_3$, 300 MHz)

[3] Unsaturation level calculated from the integral ratio (^{1}H NMR spectroscopy, CDCl$_3$, 300 MHz)

   between the CH of the allyl end-groups and the methylene protons of the initiator 2-(benzyloxy)ethanol.

Allylic species were highest in **P3** (21.6 %) followed by **P1.2** (10.6 %) and **P2** (5.3 %). The determined yields and M_n^{NMR} correlate with these findings as **P2** offers the best results (84 %

yield, $5.2\,\mathrm{kg\,mol^{-1}}$) although the difference to **P3** is negligible for these values. Particularly the yields and M_n^{NMR} of **P1.2** are considerably decreased ($46\,\%$, $3.1\,\mathrm{kg\,mol^{-1}}$). Values of *Đ* range from 1.43 to 2.73 concluding that the highest c_{DMC} leads to the lowest dispersities and consequently to the lowest level of high molecular weight tailing (HMWT) > 10 and $> 20\,\mathrm{kg\,mol^{-1}}$. The values of HMWT were calculated as percentage of the elution curve > 10 and $> 20\,\mathrm{kg\,mol^{-1}}$, respectively.

Collectively, these findings indicate that the suppression of HMWT and narrow dispersities are superior for higher catalyst concentrations c_{DMC} (Figure 2). Detection of p_{max} in DMC catalyzed polymerization with an equal reaction scale can be utilized to evaluate the reaction speed. An enlarged p_{max} indicates an accelerated and therefore uniform initiation leading to lower dispersities. Oppositely, a higher c_{DMC} did not result in a lower unsaturation level. Further investigations and an increased number of polymerizations is necessary for more precise evaluations concerning the formation of allylic species.
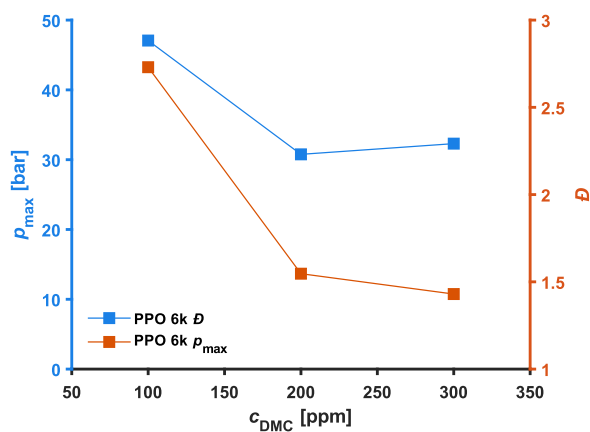
Figure 2. Diagram indicating the impact of catalyst concentration on p_{max} and *Đ* in ring-opening polymerization of PO. Polymerizations using $100\,\mathrm{ppm}$ DMC catalyst were performed with the doubled reaction scale which results in an increase p_{max}.

The described findings are in good agreement with the results presented by Chruściel et al., who observed decreased *Đ* as well as accelerated induction times t_{const} with increasing amounts of catalyst.[6]

Evaluation of mass per SA:V for varying catalyst concentrations

In this study, polymerizations were performed in a scale of 12 and $24\,\mathrm{ml}$ in contrast to industrial synthesis of PPO which is conducted in a multiple ton scale. To enable the comparability of the described findings, a correlation of the surface-area-to-volume ratio *SA:V* of the reactants to the mass of used DMC catalyst mass/*SA:V* is implemented. Figure 3 shows the reaction autoclave, its measurements and the resulting volume (*V*) and surface area (*SA*).
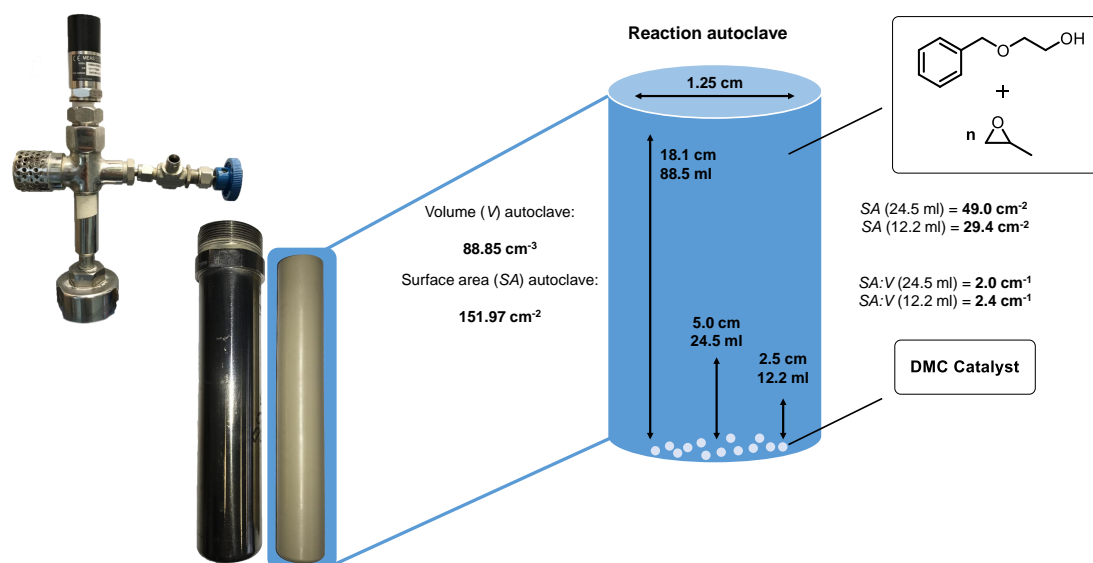
Figure 3. Schematical presentation of volume (*V*) and surface area (*SA*) calculated for the reaction autoclave in use for PO polymerization catalysed by the DMC catalyst. Reaction scales of 24.5 and 12.2 ml are considered.

The determination of mass/*SA:V* was performed by application of the calculated values *SA* and *SA:V* for the specific reaction scales illustrated in Figure 3 and the individual mass of catalyst m_{DMC} for different concentrations (Table 3). Comparison of the calculated mass/*SA:V* shows no PPO formation occurring at a value of 0.43 mg cm (Table 3, red). This finding permits the assumption that below 0.43 mg cm no polymerization of PO in DMC catalysis is feasible. Doubling of the reaction scale to 100 ppm catalyst yielded in an insufficient polymerization of PO (compare with Table 2) with a value of 1.02 (orange). Higher c_{DMC} values of 200 und 300 ppm led to a successful PO polymerization with mass/*SA:V* of 0.85 and 1.28 (green), respectively. Summarizing, the presented results suggest a minimum value of mass/*SA:V* for ring-opening polymerization of PO catalyzed by the DMC catalyst of > 0.85 mg cm. Nevertheless, a value of 1.02 mg cm for 100 ppm of catalyst still led to an insufficient polymerization. Therefore, further investigations of higher reaction scales and an increased number of data points is necessary to obtain a reliable value of mass/*SA:V* applicable for all reaction vessels and scales. Noteworthy, the heat transfer as well as the mixing are parameters which have to be considered by applying the herein presented findings to larger scales.

Table 3. Evaluation of surface-area-to-volume ratio SA:V for varying concentrations of DMC catalyst. Underlying values of *SA* and *SA:V* are illustrated in Figure 3. Red: no polymerization. Orange: insufficient polymerization. Green: polymerization. Values of V_{total} in brackets are theoretical values which were not investigated experimentally.

m_{DMC} [mg]			mass/*SA:V* [mg cm]	
c_{DMC} [ppm]	$m_{V=24.5\,ml}$ [mg]	$m_{V=12.2\,ml}$ [mg]	$V_{total}= 24.5\,ml$	$V_{total}= 12.2\,ml$
100	2.04	1.02	1.02	0.43
200	4.09	2.04	(2.04)	0.85
300	6.13	3.06	(3.06)	1.28

Investigations of reaction temperature impact in DMC catalysis

In analogy to the above described investigations, temperature was examined as a reaction parameter. By variation of the polymerization temperature from 80 to 140 °C, the impact of the additional thermal energy concerning the initiation of polymerization, the resulting M_n and Đ as well as the unsaturation level was evaluated. Each polymerization was performed three times and the average from these values was calculated to minimize errors. The monitoring of pressure progression was evaluated in analogy to the concentration screening described in the previous paragraphs. Figure 4 shows the plot of t_{max} and p_{max} against T (Supporting Information: Single values in Table S 3, Pressure curves in Figure S 6).
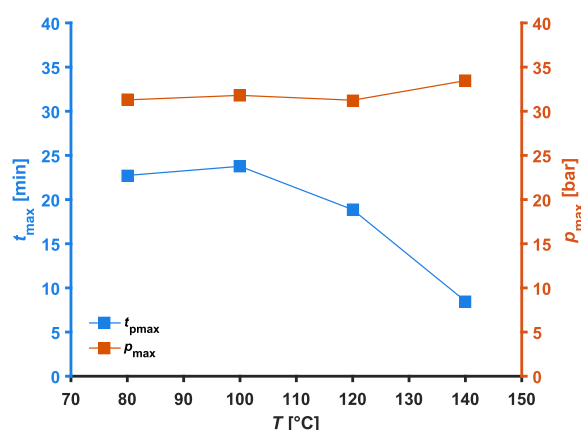
Figure 4. Diagram indicating the impact of reaction temperature on p_{max} and t_{max} in ring-opening polymerization of PO catalyzed by the DMC catalyst.

The values of pmax are slightly increased with higher reaction temperatures which can be accounted to the impact of T to the vapor pressure of PO. In contrast, t_{max} is significantly accelerated with increasing reaction temperatures from 22.7 (80 °C) to 8.5 min (140 °C). The

additional thermal energy and therefore increased pressure presumably lowers the energy needed for ring-opening of PO under the applied conditions. Nevertheless, it has to be mentioned that the exact regulation of heating rate and temperature of the heating plates in use is not feasible. Additional polymerizations performed with a thermostat can in future ensure precisely controllable temperatures and could therefore further certify these findings. The average values of Δt range from 27.6 to 28.9 min with no distinct trend (Table S3). Hence, no pronounced dependence of the time to reach full conversion of PO (t_{const}) to the reaction temperature applied in ROP catalyzed by DMC is indicated.

The synthesized polymers were analyzed by SEC to determine the molecular weights and corresponding distributions (Supporting Information: SEC in Figure S7, single values in Table S4). The plot of M_n^{SEC} and $Đ$ against T shows no explicit dependence of the molecular weight and the dispersity to the reaction temperature as no significant trend is apparent (Figure 5). Equally, determination of the high molecular weight tailing HMWT higher than 10k and 20k g mol^{-1} shows no significant impact of the reaction temperature to the molecular weight distribution.
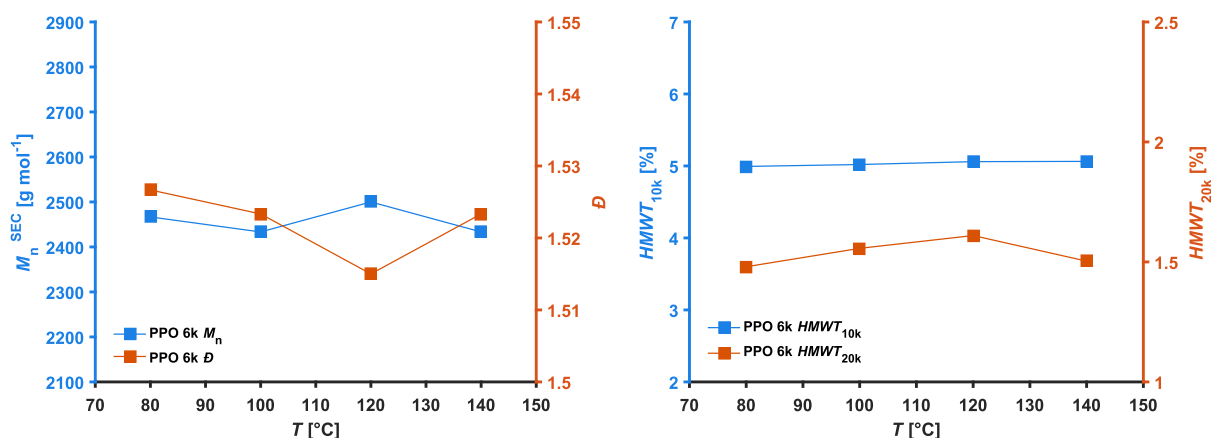
Figure 5. Analysis of the synthesized samples by SEC. Left: Impact of increasing reaction temperature on M_n^{SEC} and $Đ$. Right: Impact of increasing temperature on HMWT of 10k and 20k g mol^{-1}.

An exact evaluation of molecular weights via SEC was not applicable as a PPG calibration was not allocated. Thus, further polymer analysis was implemented by ^{1}H NMR spectroscopy to determine exact molecular weights and calculate the unsaturation level in regard to the benzylic methylene protons of the initiator 2-(benzyloxy)ethanol at 4.55 ppm (Supporting Information: Single spectra in Figure S8 to S11). The values of M_n^{NMR} significantly decreased from 5.9 to 5.4 kg mol^{-1} which corresponds to the unsaturation level increasing from 12.8 to 21.1 % with higher temperature (Figure 6). The generating of allylic species from PO as described in Scheme 2 leads to formation of additional alkoxides capable of initiation. Due to increased reaction temperatures, the activation energy of the proton abstraction is lowered and therefore the side reaction is enhanced. Accordingly, the molecular weights of the resulting polymer samples are decreased as the ratio of monomer to initiator is reduced.
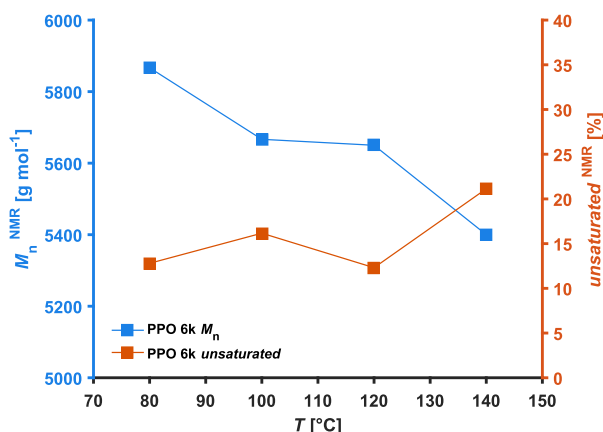
Figure 6. Analysis of the synthesized samples by ^{1}H NMR spectroscopy regarding M_n^{NMR} and the unsaturation level.

Summarizing, the herein performed investigations concerning the reaction temperature in DMC catalyzed ROP of PO reveal no explicit impact on the dispersity and the $HMWT_{>10k}$ and $HMWT_{>20k}$ of the synthesized polymers. The initiation time decreases expectedly with higher temperatures with the herein presented conditions. Additionally, p_{max} increased due to enhanced vapor pressure of PO. Nevertheless, with increasing reaction temperature the M_n evaluated by ^{1}H NMR spectroscopy is significantly decreased because of the enhanced unsaturation level.

Investigations of catalyst suspensions

The hitherto presented catalytic polymerizations of PO were performed using the pure and powdery catalyst. In industrial synthesis, the DMC catalyst is commonly utilized suspended in a suitable liquid media, hereafter denoted as suspension polyols. Suspension of the DMC catalyst in a liquid medium simplifies the utilization in industrial scales. Furthermore, the preference of the DMC catalyst to PO indicates a possible activating impact of PPO for ROP of PO by coordination. The possible coordination of PPO to the active Zn center of the catalyst must be denoted as speculative as to this date no theoretical considerations concerning this phenomenon have been published. Nevertheless, the following investigations aim to further examine this hypothesis.

To evaluate the impact of the polyol to the DMC catalyzed polymerization of PO, a variety of DMC suspensions were investigated. For this purpose, a bifunctional PPO macroinitiator with a M_n of 4.000 g mol^{-1} was utilized to initiate the polymerization of PO. The reaction scale, synthesis procedure and temperature as well as the $M_n^{th.}$ (4.000 g mol^{-1}) of the added PPO-block were kept constant for all polymerizations. The individual polymerizations using the different DMC suspensions were performed twice to minimize possible errors (Supporting Information: Single values in Table S5 and S6). Additional repetitions of experiments in the future could further minimize these possible errors and verify the herein presented results.

All suspensions consisted of PPO homopolymers with M_n^{SEC} of 1.000 g mol^{-1} with exception of **PPG** with 400 g mol^{-1}. The concentrations of catalyst c_{DMC} and c_{Zn} were approximately constant

for all suspensions, ranging from 5.10 to 5. % and 1.4 to 1.6 g, respectively. Each polyol can be classified into a linear or branched structure and its amount of hydroxy-functionalities ranging from 0 to 3. The polyols **L1100** and **PPG** represent linear, bifunctional PPO synthesized by DMC catalyzed autopolymerization of PO without an additional initiator. The polyol **mPPG** constitutes the dimethylated and therefore non-functional derivative of **L1100**. The linear **Tridecanol** was initiated by the monofunctional tridecan-1-ol and hence possess one hydroxy-functionality, the bifunctional, linear **DPG** on the other hand was initiated by dipropylene glycol (DPG) with its two terminal hydroxy groups. Utilization of the trifunctional initiators glycerin and 1,1,1-trimethylpppropane (TMP) resulted in star-shaped polyols hereafter revered to as **Glycerin** and **TMP**. The chemical structures of the individual suspension polyols are shown in Table 4. As the product of polymerization of PO, the amorphous and therefore liquid PPO represents the ideal solvent for these suspensions as the polarity of the polymer does not change the chemical environment of the reaction.

Table 4. Catalyst content of polyol suspensions and corresponding particle sizes. The polyol suspensions as well as the data of M_n, c_{DMC}, c_{Zn} and particle size were supplied by *BASF SE*.

polyol	chemical structure	properties	$M_n{}^{SEC}$ [kg mol^{-1}]	c_{DMC} [%]	c_{Zn} per 100 g [g]	particle size (D50) [nm]
L1100		linear, bifunctional	1.0	5.47	1.5	3009
PPG		linear, bifunctional	0.4	5.47	1.5	3840
DPG		linear, bifunctional	1.0	5.47	1.5	3050
Tridecanol		linear, monofunctional	1.0	5.47	1.5	3050
mPPG		linear, non-functional	1.0	5.83	1.6	-
Glycerin		branched, trifunctional	1.0	5.10	1.4	3008
TMP		branched, trifunctional	1.0	5.47	1.5	3580
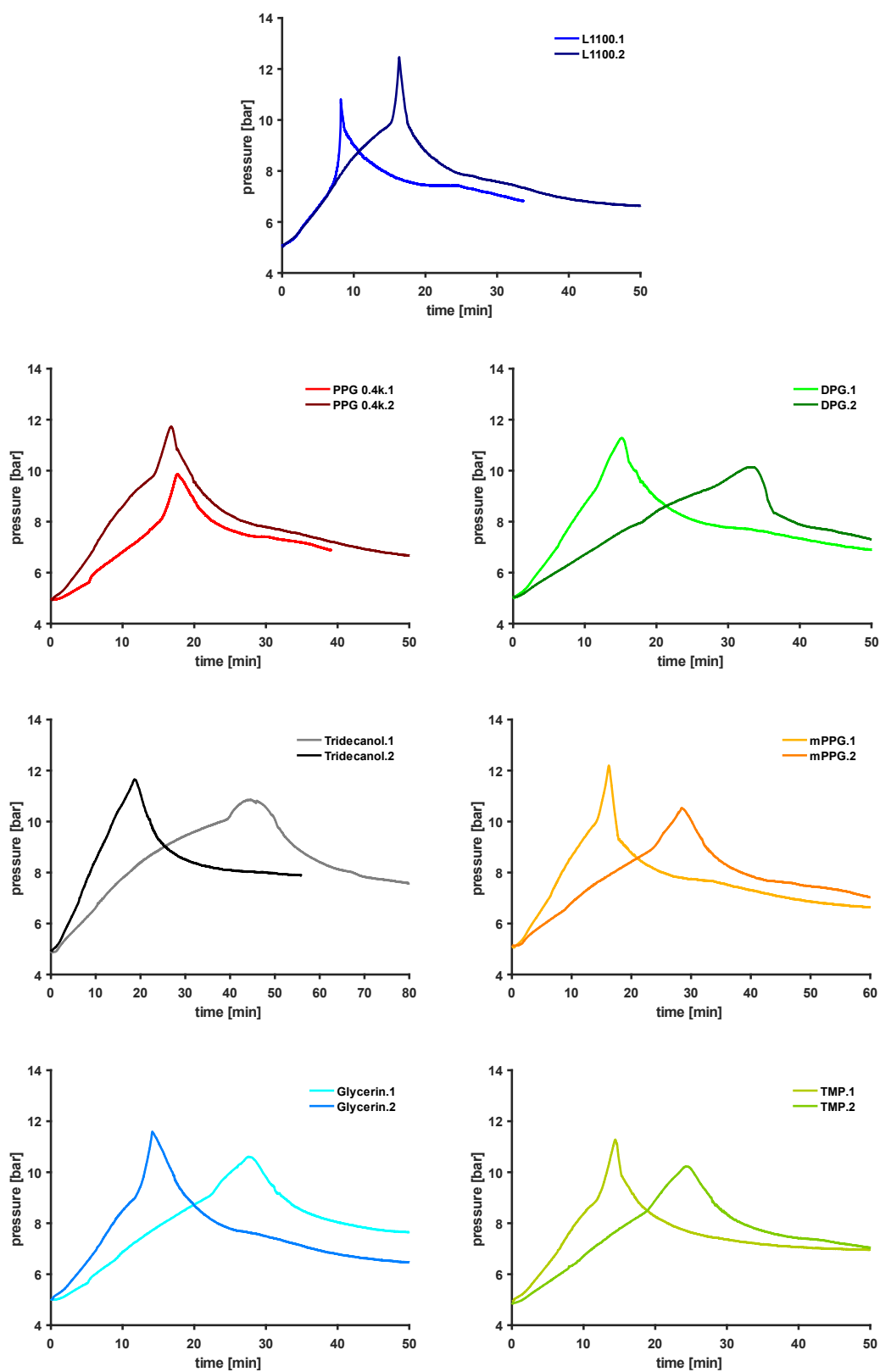
Figure 7. Pressure-time graph of the ring-opening polymerization of PO by utilization of varying suspensions of the DMC catalyst.

All polymerizations exhibit similar curve progressions typically obtained for DMC catalysis. After an induction time the pressure sharply increases within seconds and declines rapidly after reaching pmax. In contrast to the pressure progression observed investigating the c_{DMC} and reaction temperature (see Figure 1 and Support Information Figure S6), the curve reveals an irregular progression. Hence, due to the missing reproducibility, the evaluation of the period to reach a constant pressure value tconst for these polymerizations was foregone. The calculated medium slopes m roughly correlates with the observed maximum pressure but do not indicate a plausible trend (Table 5). Comparing the diagrams, the pressure progression of **PPG**, the polyol of the lowest M_n of the investigated suspension polyols, exclusively shows somewhat reproducible results with similar t_{max}. The exploration of c_{DMC} and temperature impact were performed using a powdery catalyst and a low molecular weight initiator 2-(benzyloxy)ethanol. In contrast, a polyol suspension of the catalyst and a macroinitiator of 4.000 g mol^{-1} were utilized for the presented polymerizations. Consequently, the 'bulky' curve progression suggests an impact of viscosity to the pressure development in DMC catalysis. The viscous reaction mixture seems to rather randomly be intercepting the pressure evolving from ring-opening of PO at the catalyst surface during polymerization. Thus, the polyol of the lowest M_n **PPG** shows a least incidental pressure progression.

Considering the speed of pressure decrease and accordingly a highly negative value of the medium slope m as an indicator for a full conversion of PO, a slower polymerization while using a more viscous reaction mixtures is verifiable. Theoretical considerations were performed to further evaluate the impact of viscosity of the reaction mixture to the polymerization kinetics in DMC catalysis. In regard to the M_n, the degree of branching and the number of hydroxy-functionalities, a ranking concerning the relative viscosity of the varying polyols is feasible. The viscosity is generally increased with increasing M_n, as well as with a higher number of terminal hydroxy-functionalities due to hydrogen bonding. Additionally, with a higher degree of branching, the hydrodynamic radius is reduced which results in lower viscosities.[18,19] Taking these aspects into account leads to the theoretical, chronological order $\eta_{th.}$ shown in Figure 8. Additional viscometric meausurements are necessary to verify these estimations by receiving definite viscosity-values and should therefore be considered.

PPG < TMP = Gylcerin < Tridecanol < DPG < mPPG < L1100

Increase of estimated viscosity $\eta_{\text{th.}}$

DPG < PPG = TMP < Glycerin < Tridecanol < mPPG < L1100

Increase of maximum pressure p_{max}

DPG < PPG < L1100 < mPPG < TMP < Glycerin < Tridecanol

Increase of high molecular weight tailing *HMWT*
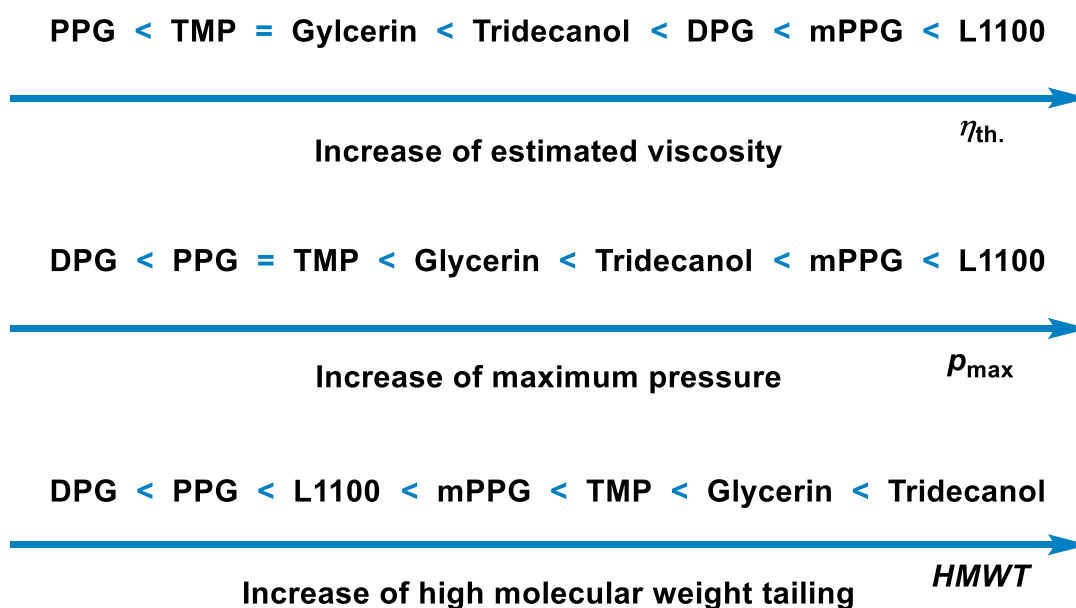
Figure 8. Comparison of the ordered estimated viscosities $\eta_{\text{th.}}$ of the utilized amorphous suspension polyols and obtained order by analysis of p_{max} and HMWT.

The obtained values of p_{max} of the investigated suspension polyols are shown in their ascending order from left to right in Figure 8. Comparing the order of $\eta_{\text{th.}}$ and p_{max} reveals a remarkable agreement between the classifications. With exception of **DPG**, which exhibited the lowest pmax, the obtained order of pmax correlates with $\eta_{\text{th.}}$. The observation indicates an inverse impact of the suspension polyols viscosity to the pressure increase during the initiation of the polymerization. A plausible explanation with an improved accessibility of the catalyst particle in a less viscos medium is contradicting with the observed findings. One would expect an increased maximum pressure less viscos reaction mixture as a result of the enhanced thermal energy development during the initiation process. A pronounced pressure development is desirable as it possibly indicates a faster and therefore uniform initiation of polymerization leading to low dispersities. The necessity of viscometric measurements is therefore underlined.

Table 5. Determined values of M_n PPO prepared by DMC catalyst suspended in varying polyols. Theoretical M_n for all samples was 8.0 kg mol⁻¹.

polyol	$M_n^{th.}$ [kg mol⁻¹]	M_n^1 [kg mol⁻¹]	$Đ^1$	HMWT$_{>10k}$ [%]	HMWT$_{>20k}$ [%]	t_{max} [min]	p_{max} [bar]	m [bar min⁻¹]
L1100	8.0	5.6	2.01	25.0	13.9	12.3	11.6	- 1.0
PPG	8.0	5.6	1.78	23.1	10.0	17.2	10.8	- 0.6
DPG	8.0	5.2	1.66	22.4	8.5	24.2	10.7	- 0.6
Tridecanol	8.0	5.5	2.30	31.4	18.1	31.7	11.3	- 0.3
mPPG	8.0	5.7	1.91	26.7	13.8	22.3	11.4	- 0.7
Glycerin	8.0	5.6	2.21	31.0	16.6	20.8	11.1	- 0.9
TMP	8.0	5.3	2.16	27.1	14.8	13.0	10.8	- 0.4

[1] Determined by SEC (DMF, Poly(ethylene glycol) calibration)

To further investigate this hypothesis, analysis by SEC of the resulting polymers regarding the molecular weights, dispersities and high molecular weight tailing was carried out (Table 5, Supplementary Information: SEC curves in Figure S12). Analysis of $Đ$ and HMWT greater than 10 and 20 kg mol⁻¹ revealed a pronounced tailing for all polymers. The lowest values were obtained for **DPG** and **PPG** although no explicit correlation of $Đ$/HMWT, p_{max} and $\eta_{th.}$ was obtained (Figure 8). For all polymerizations, the $M_n^{th.}$ was calculated by the ratio of macroinitiator to monomer feed. Despite the varying viscosities, the different suspension polyols in addition to the initiator can initiate the polymerization of PO due to their hydroxy-functionality. Accordingly, suspension polyols with a higher amount of hydroxy-functionalities should lead to a lower M_n as a higher number of initiating species is present. To illustrate the impact of the varying polyols and their hydroxy-functionalities, the M_n and $Đ$ versus the suspensions is shown in Figure 9.
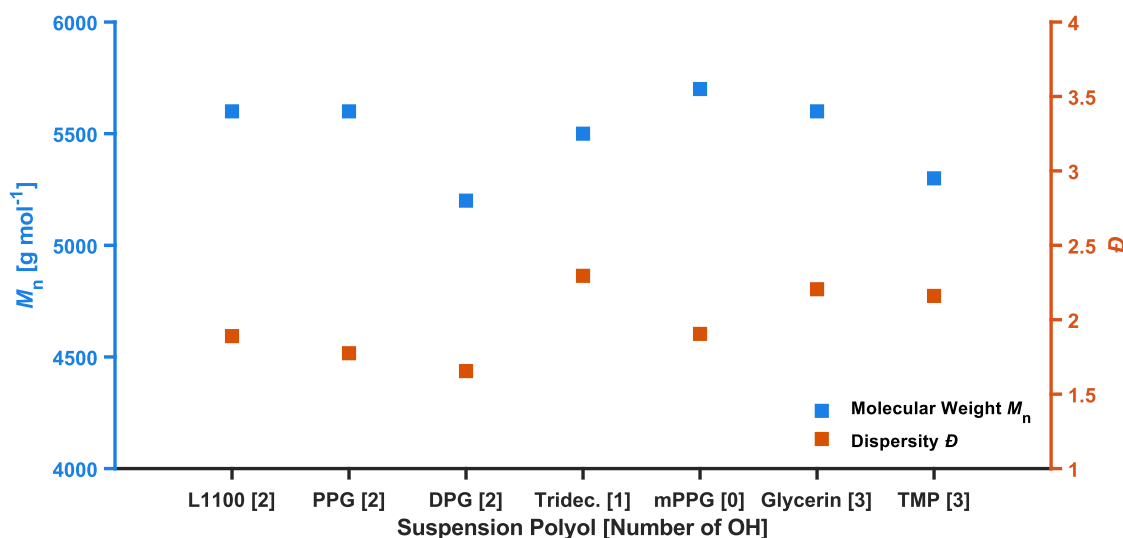
Figure 9. Comparison of M_n and $Đ$ of the polymer samples synthesized by varying DMC suspensions. The amount of hydroxy-functionalities is indicated by [X] for each polyol.

In accordance with the lowest number of initiating terminal groups (0), polymerizations using **mPPG** results in the highest M_n^{SEC} of 5.700 g mol^{-1} (Table 5). The M_n of the mono- and bifunctional polyols **L1100**, **PPG** and **Tridecanol** as well as the trifunctional **TMP** roughly correspond with the expected trend. In contrast, the polymers synthesized by **DPG** and **Glycerin** contradict the trend with relatively low (5.200 g mol^{-1}) and high molecular weights (5.600 g mol^{-1}), respectively. Additional evaluation of M_n^{NMR} and the unsaturation level, as demonstrated during the concentration and temperature investigations, is not feasible due to the absence of a definable initiator or end-group signal in ^{1}H NMR spectroscopy. By repeating the presented polymerization in future investigations, the obtained results can be confirmed and further specified.

In conclusion, the herein presented investigations could only identify the most promising suspension polyol for the DMC catalyzed polymerization of PO to some extent. Comparing the results of using catalyst suspensions with polymerizations utilizing the crude catalyst, could not confirm a positive impact of a possible PPO-coordination by the DMC catalyst. Investigations using the same macroinitiator with the powdery catalyst for polymerization of PO can verify these findings. However, the results indicate an enhanced control over M_n with lower dispersities for suspension polyols possessing less terminal hydroxy-functionalities. Considering our results, if aiming for the lowest amount of HMWT, the application of **DPG** and low molecular **PPG** (400 g mol^{-1}) is proposed. Further experiments are mandatory to gain a deeper understanding for utilization of the DMC catalysis in a polyol suspension.

Mechanistic perspective concerning HMWT

High molecular weight products remain to be a highly relevant side product in PPG polymerized by DMC catalysis. Although several justified ideas regarding the formation of HMWT have been

postulated in the past,[11,14] the mechanistic origin has not been discovered. In Scheme 3, we postulate a possible mechanism leading to high molecular weight polymers in DMC catalysis based on the findings presented throughout this article and the cationic-insertion mechanism described Scheme 1.
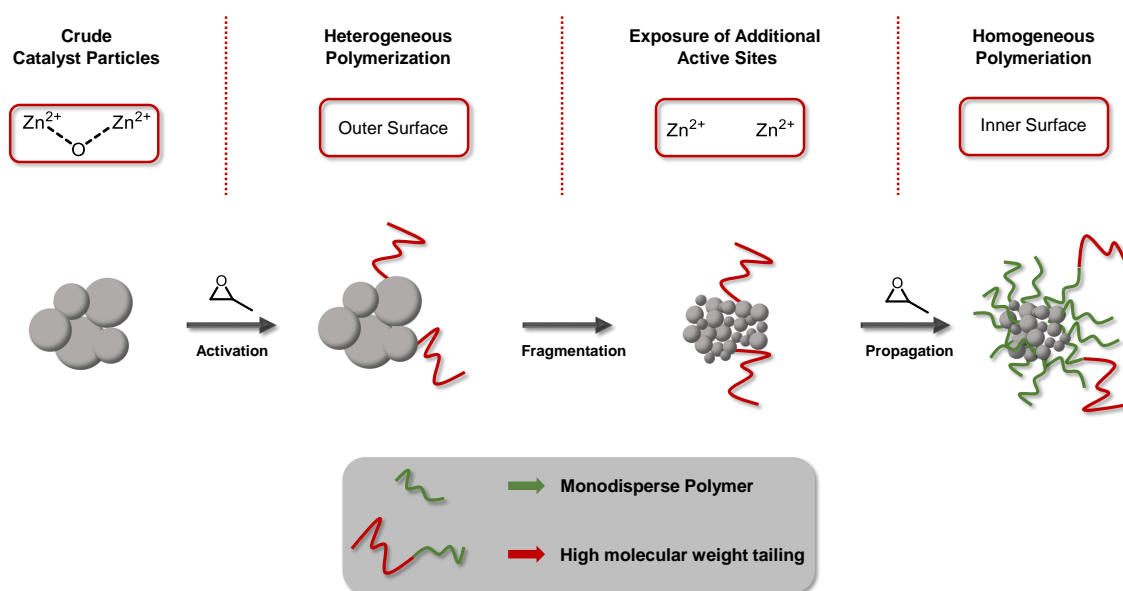
Scheme 3. Schematic illustration of the herein postulated mechanism regarding the formation of HMWT in ring-opening polymerization of PO by DMC catalysis.

Before the polymerization occurs, in each case two Zn^{2+} centers of the crude catalyst particles are linked to one oxygen atom. This oxygen atom is contributed by the utilized complexing agent which in this case is represented by *tert*-butanol. The crude catalyst is activated by addition of PO, followed by monomer conversion at Zn^{2+} centers located at the outer surface of the catalyst. A small number of chains are already formed during the activation step, indicated in red (Scheme 3). This first mechanistic step is herein considered to be heterogenous as the polymerization propagates at the catalyst surface and therefore uncontrolled in regard to the control of molecular weight. Following the activation step, fragmentation of the catalyst occurs leading to the exposure of additional active Zn^{2+} sites previously located at the inner particle surface. Simultaneously, the oxygen of the complexing agent is replaced by the epoxide which induces the breakage of the oxygen linkage between the Zn^{2+} atoms. Consequently, additional Zn^{2+} atoms are exposed providing new active centers for polymerization. The now highly active catalyst enhances the polymerization rate of PO resulting in the rapid consumption of the epoxide. After fragmentation, the small-sized catalyst particles are finely suspended in the growing polymer chains. The catalysis is considered to be homogeneous at this point, thus yielding a narrowly dispersed polyether. However, the polymer chains formed during the heterogeneous activation step equally grow after fragmentation. These "early" chains accordingly possess a higher and less defined molecular weight compared to the main polymer fraction and therefore represent the

HMWT of PPG synthesized by DMC catalysis. Collectively, to potentially suppress of the formation of HMWT pre-shredded catalyst particles could be utilized. Additionally, a pre-activation of the catalyst by exchange of the complexing agent possibly reduces the heterogeneous mechanistic pathway.

CONCLUSION

Herein, we examined several factors of the DMC catalyzed polymerization of the epoxide PO in a multiparameter analysis. Investigations concerning the catalyst concentration suggest a diminished performance with decreasing catalyst concentration. Furthermore, calculation of the surface-area-to-volume ratio (*SA:V*) of the used autoclave to the amount of catalyst indicated a minimum mass to *SA:V* ratio of 0.85 mg cm to obtain sufficient results. A confirmation of the performed calculations as well as its implementation to larger scales is feasible by applying the determined minimum of mass/*SA:V* to bigger reaction autoclaves. Additional reactions with a higher variety of catalyst concentrations can lead to specification of the obtained limits. Supplementary experiments concerning the reaction temperature exhibited no explicit impact concerning the dispersity and the high molecular weight tailing of the synthesized polymers. The unsaturation level was increased with higher temperatures resulting in significantly decreased molecular weights. The obtained results can be further verified by usage of heating devices enabling a precise control of temperature. Comparison of 7 different linear as well as branched DMC polyol suspensions displayed the accordance of the developed maximum pressure during initiation of DMC catalysis with the estimated viscosities of the suspensions. However, the most promising suspension among the varying polyols could not be explicitly identified. All parameters require further investigations to gain a full understanding of the DMC catalyzed polymerization of epoxides. Finally, the formation of HMWT in DMC catalysis is accounted to an initially heterogeneous and then homogeneous polymerization mechanism. Above all, a deeper understanding of the DMC catalysis mechanism is inevitable to further improve the efficiency of the DMC catalyst and the quality of the resulting polyethers.

EXPERIMENTAL SECTION

Reagents and Equipment

All chemicals and solvents were purchased from *Acros Organics*, *TCI*, *Sigma-Aldrich* and *Fluka*. Deuterated solvents were received from *Deutero GmbH*. The DMC catalyst and the DMC suspensions were provided by *BASF SE*. Propylene oxide (PO) was stirred over CaH_2 for 1 h and cryotransferred to a Schlenk flask. 2-(Benzyloxy)ethanol and the PPO macroinitiator (4 kg mol^{-1}) were dissolved in benzene and dried by azeotropic distillation. The crude DMC catalyst as well as the DMC suspensions were suspended in benzene and equally dried by azeotropic distillation. Polymerizations were performed in 100 ml high-pressure autoclaves purchased by *Carl Roth GmbH*. Pressure was monitored by wireless pressure transducer MEAS purchased from *TE connectivity*.

Polymerization Procedure for concentration screening

An exemplary synthesis protocol is described in the following. All polymerizations were performed accordingly three times each for the varying amounts of DMC catalyst. The prior dried monomer, initiator, the DMC catalyst and an autoclave were transferred to the glovebox to be handled under argon-atmosphere. 12 ml PO (171.5 mmol, 103 eq) 0,24 ml 2-(benzyloxy)ethanol (1.6 mmol, 1 eq) and the specific amount of DMC catalyst (100 – 300 ppm) were added to the autoclave. Then a pressure of 5 bar Ar was applied to the autoclave. The reactions mixture was stirred and heated to 120 °C overnight. After distillation of unreacted monomers, polymers were used without further purification.

^{1}H NMR (300 MHz, CDCl$_3$, δ): 7.35-7.27 (m, 5H, Ar H), 4.56 (s, 2H, Ph-CH$_2$), 3.79-3.09 (m, polyether backbone), 1.38-0.79 (m, propylene oxide -CH$_3$)

Polymerization Procedure for temperature screening

The polymerizations of the temperature screening were performed in analogy to the above described procedure. The amount of DMC catalyst was 300 ppm for all reactions and the temperature was varied between 80 and 120 °C.

^{1}H NMR (300 MHz, CDCl$_3$, δ): 7.35-7.27 (m, 5H, Ar H), 4.56 (s, 2H, Ph-CH$_2$), 3.79-3.09 (m, polyether backbone), 1.38-0.79 (m, propylene oxide -CH$_3$)

Polymerization Procedure for suspension screening

An exemplary synthesis protocol is described in the following. All polymerizations were performed accordingly two times each for the varying DMC catalyst suspensions. The prior dried monomer, macroinitiator, the DMC catalyst and an autoclave were transferred to the glovebox to be handled under argon-atmosphere. 5 ml PO (71.5 mmol, 69 eq) 4.15 g PPO (1.0 mmol, 1 eq) and the DMC suspension (75 ppm in regard to the catalyst concentration of each suspension) were added to the autoclave. Then a pressure of 5 bar Ar was applied to the autoclave. The reactions mixture

was stirred and heated to °C overnight. After distillation of unreacted monomers, polymers were used without further purification.

^{1}H NMR (300 MHz, CDCl$_3$, δ): 7.35-7.27 (m, 5H, Ar H), 4.56 (s, 2H, Ph-CH$_2$), 3.79-3.09 (m, polyether backbone), 1.38-0.79 (m, propylene oxide -CH$_3$)

Pressure Monitoring

Pressure Monitoring was performed by use of *MEAS M5600 Wireless Pressure Transducer* by *TE*. The Bluetooth sensor was attached to the autoclave under continuous argon flow outside the glovebox. Pressure values were measured every 100 ms. Size Exclusion Chromatography (SEC) measurements was performed in dimethylformamide (DMF) with 1 g L^{-1} lithium bromide as an eluent at °C. Agilent 1100 Series was used equipped with HEMA 300/100/40 column and calibration was carried out using polyethylene glycol standards, both provided by *Polymer Standard Service* (PSS), Mainz.

REFERENCES

(1) Jack Milgrom, *US Patent US3278457A*, **1963**. Method of Making a Polyether using a Double Metal Cyanide Complex Compound.

(2) Kim, I.; Ahn, J.-T.; Ha, C. S.; Yang, C. S.; Park, I. Polymerization of propylene oxide by using double metal cyanide catalysts and the application to polyurethane elastomer. *Polymer* **2003**, *44*, 3417–3428.

(3) Kim, I.; Byun, S. H.; Ha, C.-S. Ring-opening polymerizations of propylene oxide by double metal cyanide catalysts prepared with ZnX2 (X = F, Cl, Br, or I). *J. Polym. Sci. Part A: Polym. Chem.* **2005**, *43*, 4393–4404.

(4) Huang, Y.-J.; Qi, G.-R.; Wang, Y.-H. Controlled ring-opening polymerization of propylene oxide catalyzed by double metal-cyanide complex. *J. Polym. Sci. Part A: Polym. Chem.* **2002**, *40*, 1142–1150.

(5) Ionescu, M. Chemistry and technology of polyols for polyurethanes; Rapra Technology Ltd: *Shawbury*, U.K, **2005**.

(6) Chruściel, A.; Hreczuch, W.; Janik, J.; Czaja, K.; Dziubek, K.; Flisak, Z.; Swinarew, A. Characterization of a Double Metal Cyanide (DMC)-Type Catalyst in the Polyoxypropylation Process: Effects of Catalyst Concentration. *Ind. Eng. Chem. Res.* **2014**, *53*, 6636–6646.

(7) Blankenburg, J.; Kersten, E.; Maciol, K.; Wagner, M.; Zarbakhsh, S.; Frey, H. The poly(propylene oxide- co -ethylene oxide) gradient is controlled by the polymerization method: determination of reactivity ratios by direct comparison of different copolymerization models. *Polym. Chem.* **2019**, *116*, 2170.

(8) Zhang, X.-H.; Wei, R.-J.; Zhang, Y.; Du, B.-Y.; Fan, Z.-Q. Carbon Dioxide/Epoxide Copolymerization via a Nanosized Zinc–Cobalt(III) Double Metal Cyanide Complex: Substituent Effects of Epoxides on Polycarbonate Selectivity, Regioselectivity and Glass Transition Temperatures. *Macromolecules* **2015**, *48*, 536–544.

(9) Suh, H. S.; Ha, J. Y.; Yoon, J. H.; Ha, C.-S.; Suh, H.; Kim, I. Polyester polyol synthesis by alternating copolymerization of propylene oxide with cyclic acid anhydrides by using double metal cyanide catalyst. *Reactive and Functional Polymers* **2010**, *70*, 288–293.

(10) Sun, X.-K.; Zhang, X.-H.; Chen, S.; Du, B.-Y.; Wang, Q.; Fan, Z.-Q.; Qi, G.-R. One-pot terpolymerization of CO2, cyclohexene oxide and maleic anhydride using a highly active heterogeneous double metal cyanide complex catalyst. *Polymer* **2010**, *51*, 5719–5725.

(11) Tran, C. H.; Pham, L. T. T.; Lee, Y.; Jang, H. B.; Kim, S.; Kim, I. Mechanistic insights on Zn(II)−Co(III) double metal cyanide-catalyzed ring-opening polymerization of epoxides. *Journal of Catalysis* **2019**, *372,* 86–102.

(12) Zhang, X.-H.; Hua, Z.-J.; Chen, S.; Liu, F.; Sun, X.-K.; Qi, G.-R. Role of zinc chloride and complexing agents in highly active double metal cyanide catalysts for ring-opening polymerization of propylene oxide. *Applied Catalysis A: General* **2007**, *325*, 91–98.

(13) Pazos, J.; Browne, E. Catch-Up Kinetics: Selectivity based on equivalent weight in the polymerization of alkylene oxides by double metal cyanide catalysts. *Polymer Preprints,* **2008**, *434*.

(14) Almora-Barrios, N.; Pogodin, S.; Bellarosa, L.; García-Melchor, M.; Revilla-López, G.; García-Ratés, M.; Vázquez-García, A. B.; Hernández-Ariznavarreta, P.; López, N. Structure, Activity, and Deactivation Mechanisms in Double Metal Cyanide Catalysts for the Production of Polyols. *ChemCatChem* **2015**, *7*, 928–935.

(15) Bi Le-Khac, W. C.; Wei Wang, U. D.; Mahmoud K. Faraj, Newton Square, all of PA. US Patent. Acid-Treated Double Metal Cyanide Complex Catalysts.

(16) Jeffrey J. Lear, Oliver D. Sloan, Jose F. Pazos. US Patent. Method for decreasing the propensity for phase-out of the high molecular weight component of double metal cyanide-catalyzed high secondary hydroxyl polyoxypropylene polyols, **2000**.

(17) Wu, L.-C.; Yu, A.-F.; Zhang, M.; Liu, B.-H.; Chen, L.-B. DMC catalyzed epoxide polymerization: Induction period, kinetics, and mechanism. *J. Appl. Polym. Sci.* **2004**, *92*, 1302–1309.

(18) Kaiser, T.; Frey, H. Hyperbranched polymer architectures: From Flory's AB(f-1) polycondensates to controlled structures. *Polymer* **2020**, *211*, 123113.

(19) Schömer, M.; Schüll, C.; Frey, H. Hyperbranched aliphatic polyether polyols. *J. Polym. Sci. Part A: Polym. Chem.* **2013**, *51*, 995–1019.

(20) Wei, R.-J.; Zhang, Y.-Y.; Zhang, X.-H.; Du, B.-Y.; Fan, Z.-Q. Regio-selective synthesis of polyepichlorohydrin diol using Zn–Co(iii) double metal cyanide complex. *RSC Adv* **2014**, *4*, 21765–21771.

SUPPORTING INFORMATION
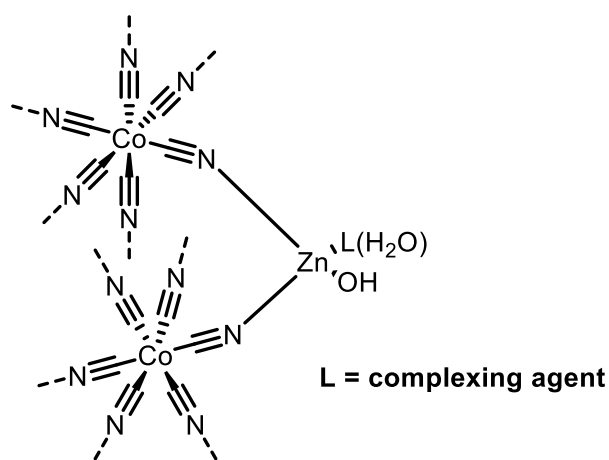
Figure S1. Proposed structure of the active site of Zn-Co(III) DMC catalyst.[20]
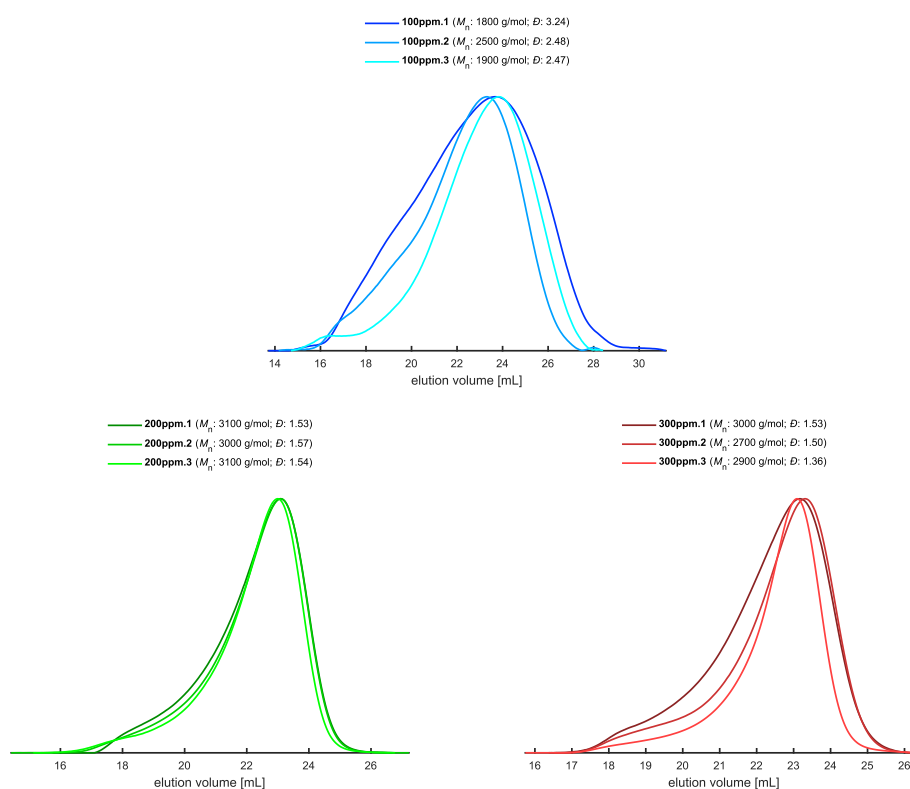
Figure S2. SEC traces of ring-opening polymerization of propylene oxide with varying amounts of DMC catalyst (DMF, PEG calibration).

Table S1. Single values of pressure monitoring of ring-opening polymerization of propylene oxide by varying amounts of DMC catalyst. The sample P1.2 differs from P1 by a doubled reaction scale by a constant catalyst concentration. Sample no. 1 of P3 was not considered for average evaluation retrospectively as technical issues in the glovebox potentially inhibited the crucial uniformity of the reaction procedure throughout the screening process.

sample	No.	c_{DMC} [ppm]	p_{max} [bar]	t_{max} [min]	t_{const} [min]	Δt [min]	m [bar min^{-1}]
P1	1	99	-	-	-	-	-
	2	101	-	-	-	-	-
ØP1		**100**	**-**	**-**	**-**	**-**	**-**
	1	103	43.0	33.9	63.3	29.4	- 9.4
P1.2	2	93	48.5	15.3	31.6	16.3	- 11.8
	3	98	49.7	12.0	22.8	10.8	- 12.4
ØP1.2		**98**	**47.1**	**20.4**	**39.2**	**18.8**	**- 11.2**
	1	206	30.2	12.0	28.9	17.0	- 6.6
P2	2	196	31.6	11.9	25.7	13.8	- 7.1
	3	196	30.6	11.3	24.8	13.6	- 7.0
ØP2		**199**	**30.8**	**11.7**	**26.5**	**14.8**	**- 6.9**
	1	313	30.9	21.2	57.8	36.6	- 6.7
P3	2	323	32.2	11.6	29.2	17.6	- 7.3
	3	304	32.4	10.9	28.3	17.4	- 7.7
ØP3		**313**	**31.8**	**11.3**	**28.8**	**17.5**	**- 7.2**

[1] $\Delta t = t_{const} - t_{max}$
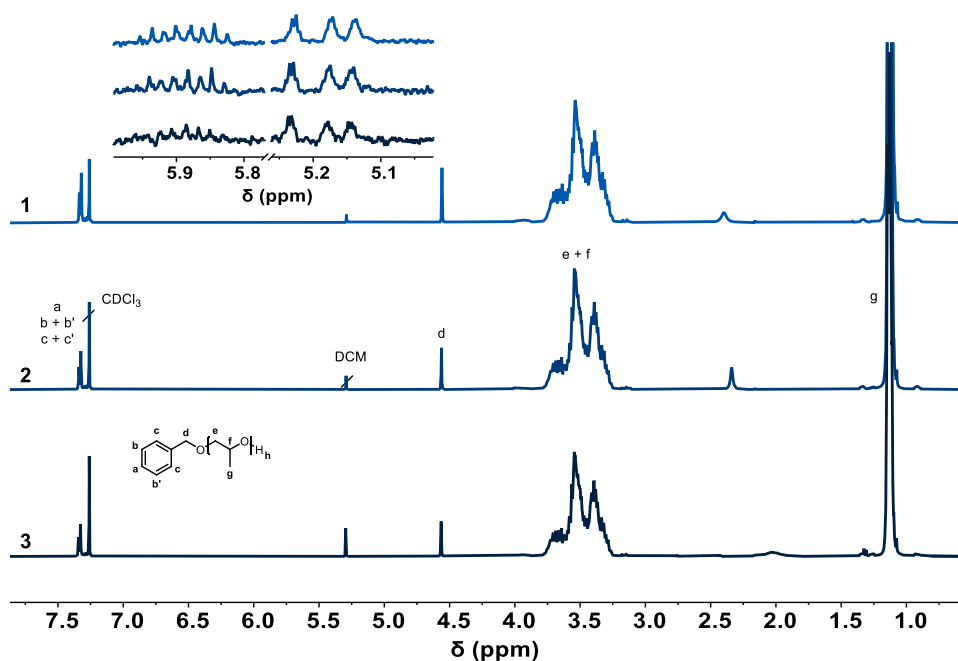
Figure S3. Stacked ¹H NMR spectra (300 MHz, CDCl$_3$) of the samples P1.2 1,2 und 3 of the ring-opening polymerization of propylene oxide with 100 ppm of DMC catalyst. The extracted region indicates the unsaturated species.
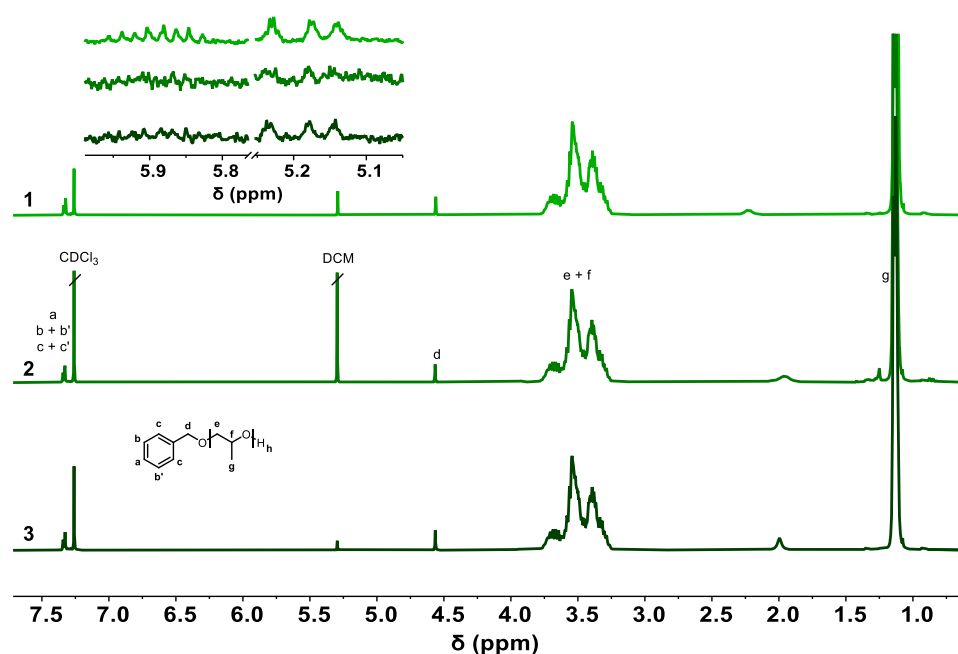
Figure S4. Stacked ¹H NMR spectra (300 MHz, CDCl$_3$) of the samples P2 1,2 und 3 of the ring-opening polymerization of propylene oxide with 200 ppm of DMC catalyst. The extracted region indicates the unsaturated species.

Figure S5. Stacked ^{1}H NMR spectra (300 MHz, CDCl$_3$) of the samples P3 1,2 und 3 of the ring-opening polymerization of propylene oxide with 300 ppm of DMC catalyst. The extracted region indicates the unsaturated species.

Table S2. Single values of molecular weight analysis of PPO prepared by varying amounts of DMC catalyst. The sample P1.2 differs from P1 by a doubled reaction scale by a constant catalyst concentration. Sample no. 1 of P3 was not considered for average evaluation retrospectively as technical issues in the glovebox potentially inhibited the crucial uniformity of the reaction procedure throughout the screening process.

sample	no.	c_{DMC} [ppm]	HMWT$_{>10k}$ [%]	HMWT$_{>20k}$ [%]	M_n[1] [kg mol⁻¹]	M_n[2] [kg mol⁻¹]	$Đ$[1]	unsat. [%]	yield [%]
P1	1	99	-	-	-	-	-	-	-
	2	101	-	-	-	-	-	-	-
ØP1		**100**	**-**	**-**	**-**	**-**	**-**	**-**	**-**
P1.2	1	103	15.02	5.35	1.8	2.6	3.24	8.0	42.2
	2	93	14.03	5.34	2.5	3.4	2.48	13.4	53.9
	3	96	7.60	3.09	1.9	3.3	2.47	10.4	42.3
ØP1.2		**98**	**12.22**	**4.59**	**2.1**	**3.1**	**2.73**	**10.6**	**46.1**
P2	1	206	9.48	2.09	3.1	5.2	1.53	3.5	82.2
	2	196	8.73	2.34	3.0	5.4	1.57	n.d.	89.2
	3	196	8.27	2.63	3.1	4.9	1.54	12.4	81.2
ØP2		**199**	**8.83**	**2.35**	**3.1**	**5.2**	**1.55**	**5.3**	**84.2**
P3	1	313	8.20	1.52	3.0	5.2	1.53	19.0	80.5
	2	323	6.89	1.38	2.7	5.0	1.50	23.8	78.8
	3	304	4.91	1.05	2.9	5.1	1.36	19.4	83.2
ØP3		**313**	**5.90**	**1.22**	**2.8**	**5.1**	**1.43**	**21.6**	**81.0**

[1] Determined by SEC (DMF, Poly(ethylene glycol) calibration)

[2] Determined by ^{1}H NMR spectroscopy (CDCl$_3$, 300 MHz)

[3] Unsaturation level calculated from the integral ratio (^{1}H NMR spectroscopy, CDCl$_3$, 300 MHz) between

the CH of the allyl end-groups (5.95 to 5.82 ppm) and the methyl group (4.56 ppm) of the propylene glycol units.
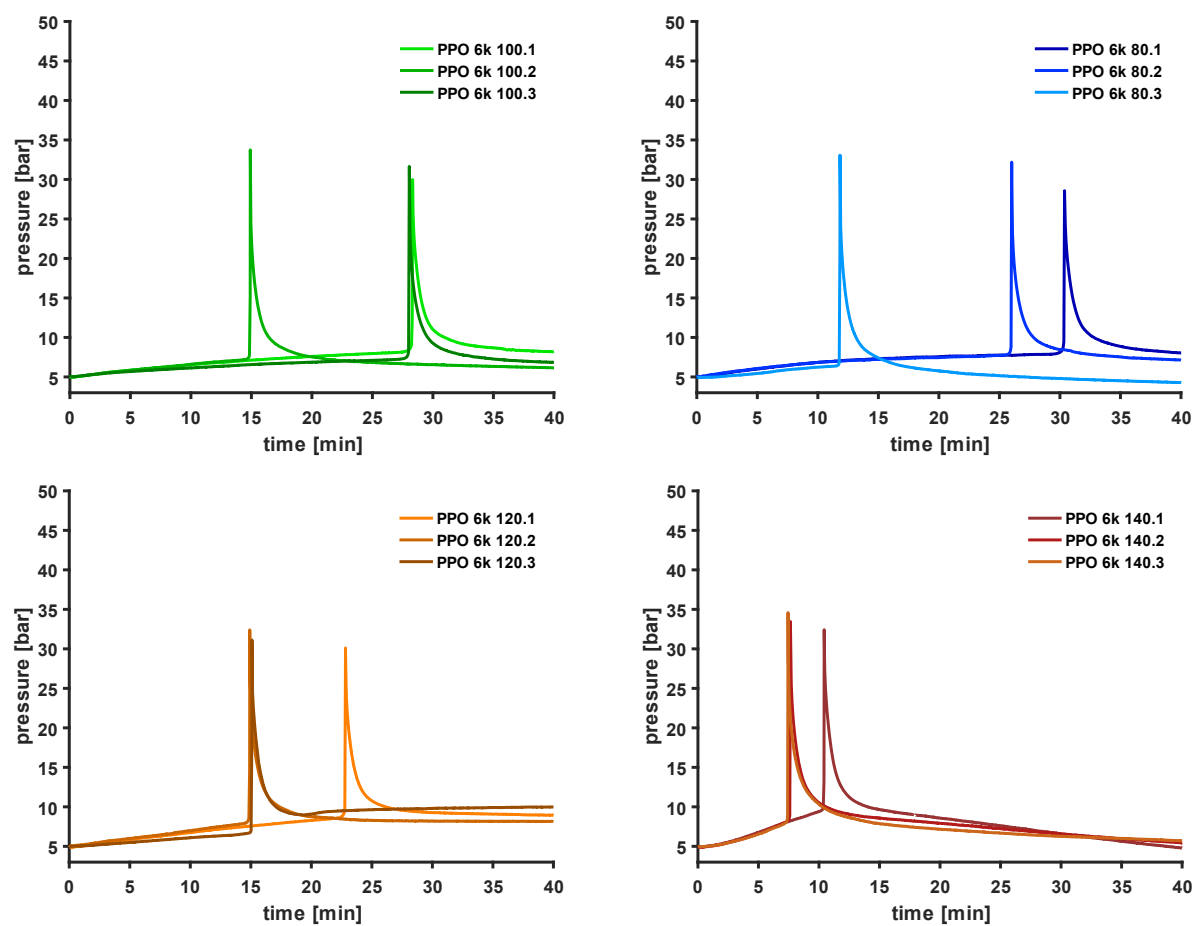
Figure S6. Separate plots of the pressure progression of the single reactions of ring-opening polymerization of propylene oxide with varying reaction temperatures.

Table S3. Single values of temperature screening of ring-opening polymerization of propylene oxide. Sample no. 3 of P120 was not considered for average evaluation retrospectively as technical issues in the glovebox potentially inhibited the crucial uniformity of the reaction procedure throughout the screening process.

sample	no.	T_{DMC} [ppm]	p_{max} [bar]	t_{max} [min]	t_{const} [min]	Δt^1 [min]	m [bar min^{-1}]
P80	1		28.6	30.4	58.2	27.8	- 6.3
	2	80	32.2	26.0	51.6	25.6	- 7.8
	3		33.1	11.8	41.1	29.3	- 8.5
ØP80			31.3	22.7	50.3	27.6	- 7.5
P100	1		30.0	28.3	59.5	31.2	- 6.7
	2	100	33.7	14.9	31.3	26.4	-8.4
	3		31.7	28.1	57.3	29.2	- 7.8
ØP100			31.8	23.8	52.7	28.9	- 7.6
P120	1		30.1	22.8	47.9	25.1	- 6.6
	2	120	32.4	14.9	45.3	30.4	-7.6
	3		31.1	15.1	50.0	34.9	- 7.3
ØP120			31.2	17.6	46.6	27.7	- 7.1
P140	1		32.4	10.4	42.1	31.7	- 7.4
	2	140	33.4	7.7	35.4	27.7	- 7.8
	3		34.6	7.4	32.7	25.3	- 8.3
ØP140			33.5	8.5	36.7	28.2	- 7.8

^{1} $\Delta t = t_{const} - t_{max}$
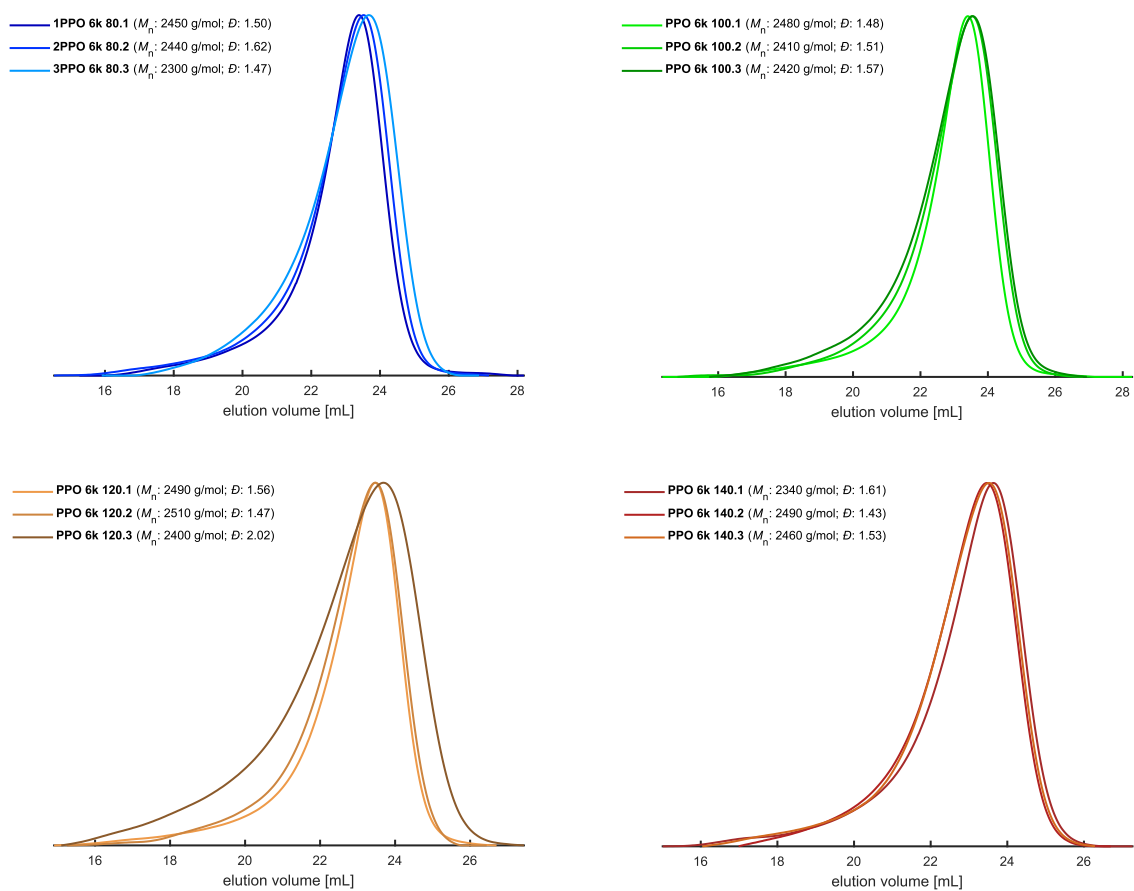
Figure S7. SEC traces of ring-opening polymerization of propylene oxide by DMC catalysis with varying reaction temperatures (DMF, PEG calibration).
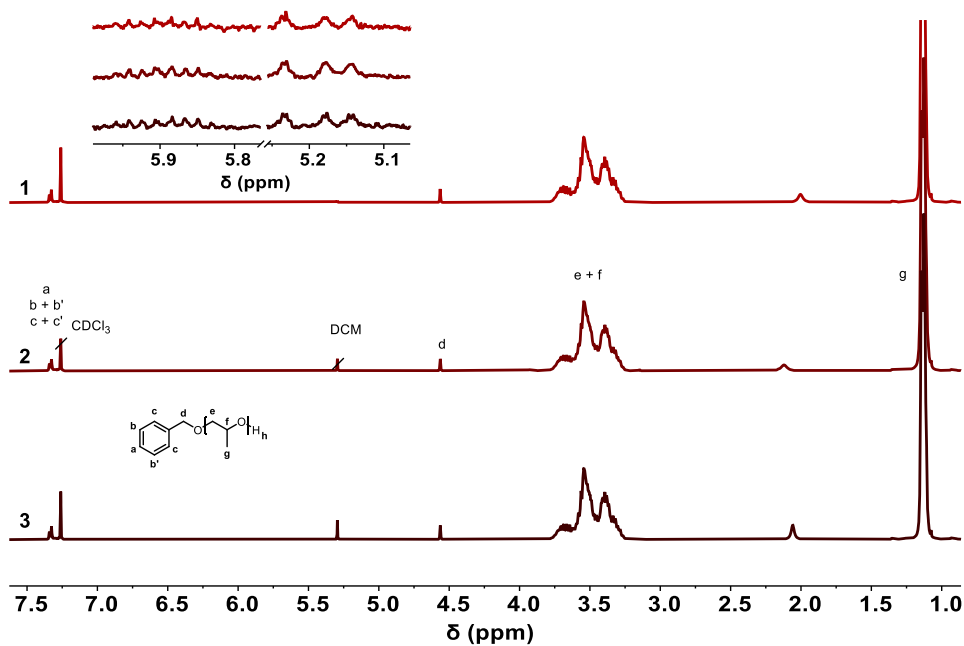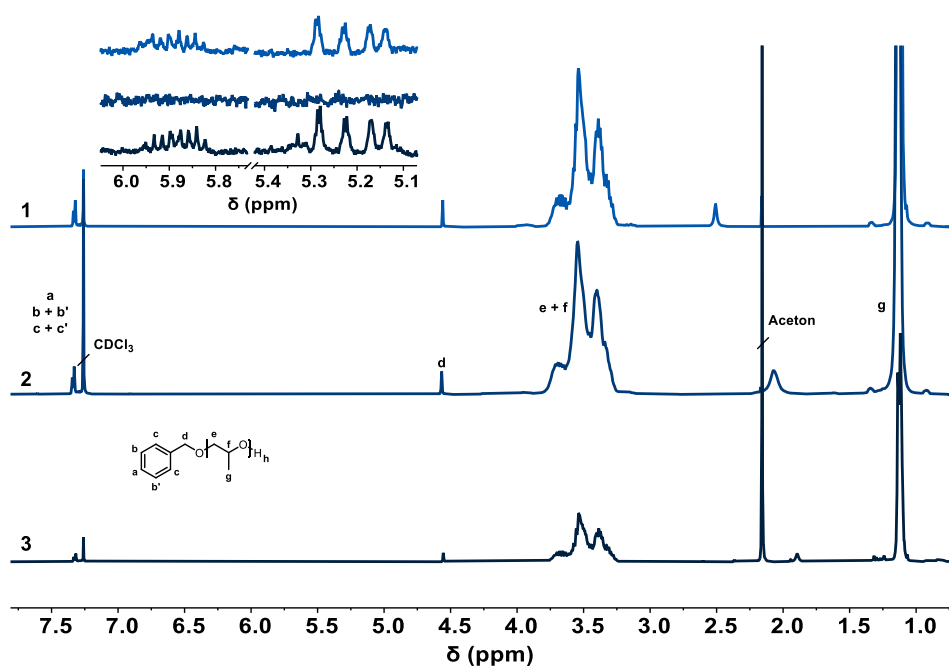
Figure S8. Stacked ¹H NMR spectra (300 MHz, CDCl₃) of the samples P80 1,2 und 3 of the ring-opening polymerization of propylene oxide catalyzed by the DMC catalyst at 80 °C. The extracted region indicates the unsaturated species.
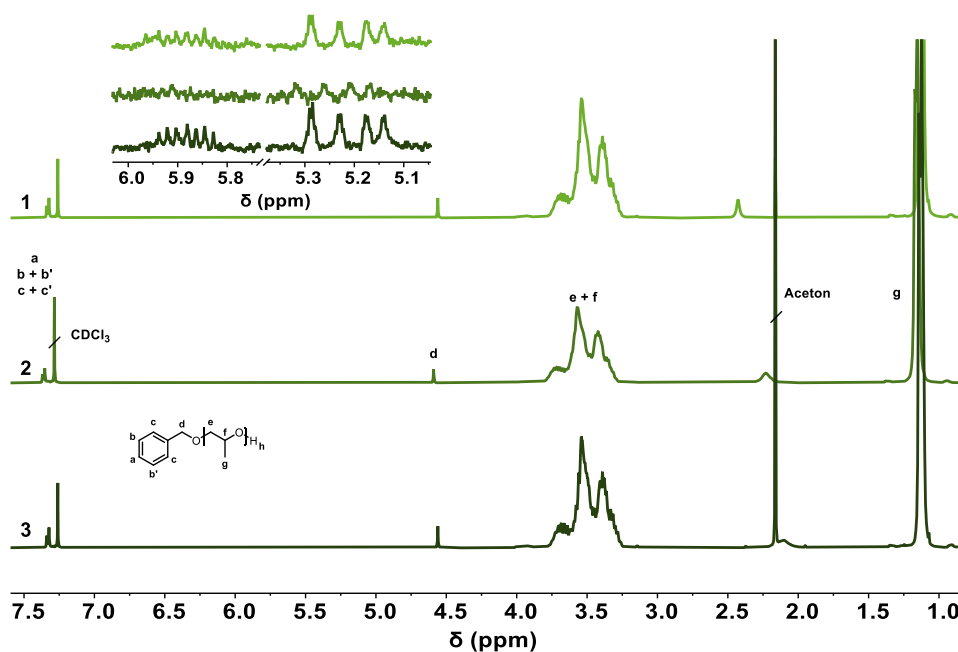
Figure S9. Stacked ¹H NMR spectra (300 MHz, CDCl₃) of the samples P100 1,2 und 3 of the ring-opening polymerization of propylene oxide catalyzed by the DMC catalyst at 100 °C. The extracted region indicates the unsaturated species.
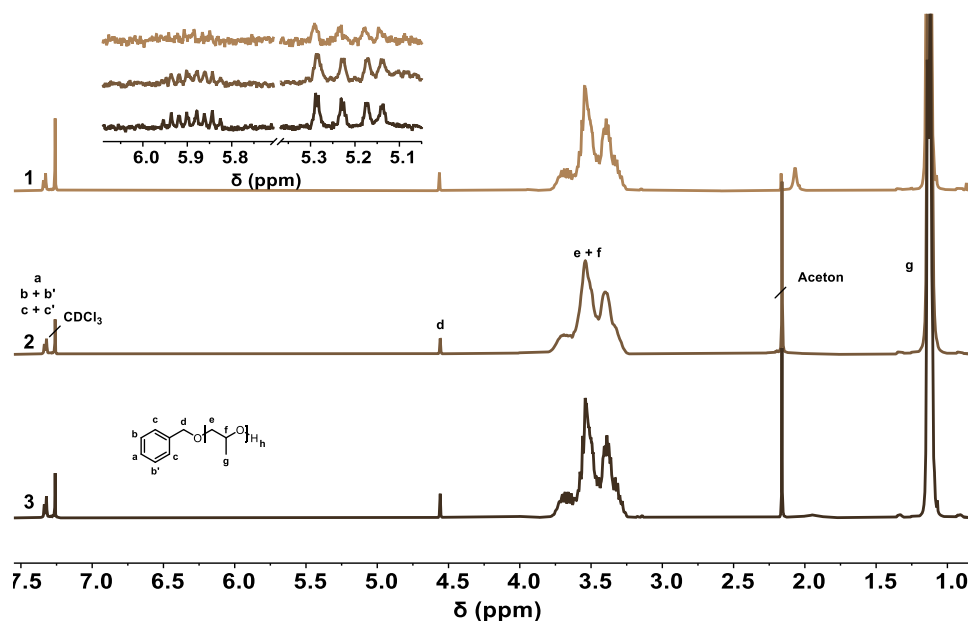
Figure S10. Stacked ^{1}H NMR spectra (300 MHz, CDCl$_3$) of the samples P120 1,2 und 3 of the ring-opening polymerization of propylene oxide catalyzed by the DMC catalyst at 120 °C. The extracted region indicates the unsaturated species.
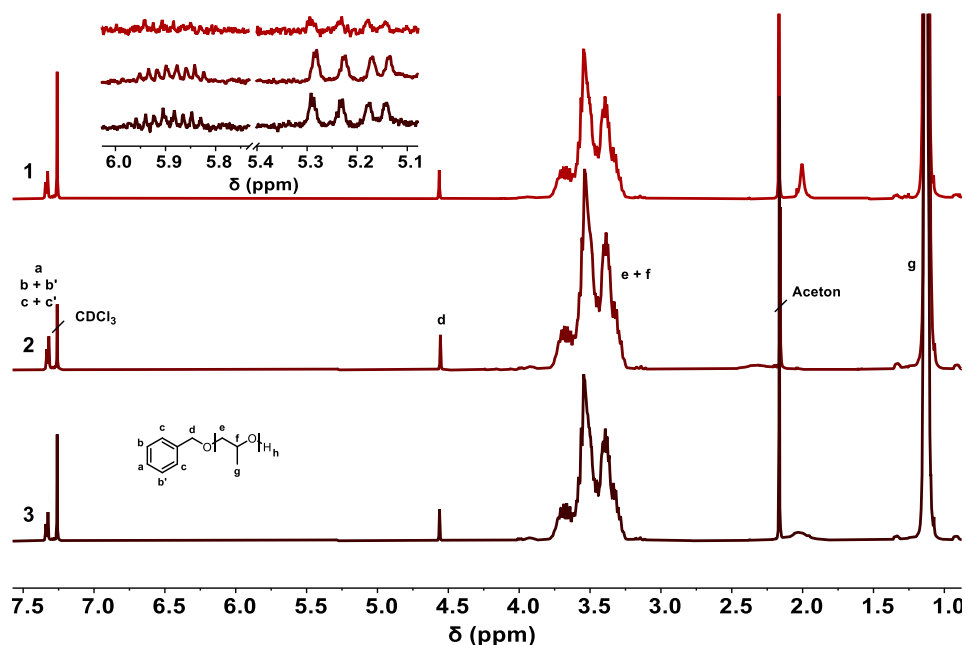
Figure S11. Stacked ^{1}H NMR spectra (300 MHz, CDCl$_3$) of the samples P140 1,2 und 3 of the ring-opening polymerization of propylene oxide catalyzed by the DMC catalyst at 140 °C. The extracted region indicates the unsaturated species.

Table S4. Single values of molecular weight analysis of PPO prepared by varying temperatures. Sample no. 3 of P120 was not considered for average evaluation retrospectively as technical issues in the glovebox potentially inhibited the crucial uniformity of the reaction procedure throughout the screening process.

| sample	no.	c_{DMC} [ppm]	HMWT$_{>10k}$ [%]	HMWT$_{>20k}$ [%]	M_n[1] [kg mol^{-1}]	M_n[2] [kg mol^{-1}]	$Đ$[1]	unsat.[3] [%]	yield [%]
P80	1		4.94	1.50	2.5	5.8	1.49	16.6	93
	2	80	5.68	2.14	2.5	6.0	1.62	n.d.	94
	3		4.36	0.80	2.4	5.8	1.47	21.8	96
ØP80			**4.99**	**1.48**	**2.4**	**5.9**	**1.53**	**12.8**	**94**
P100	1		4.96	1.74	2.5	5.9	1.49	22.1	96
	2	100	4.41	1.28	2.4	5.6	1.51	7.4	95
	3		5.69	1.65	2.4	5.5	1.57	19.0	97
ØP100			**5.02**	**1.56**	**2.5**	**5.7**	**1.52**	**16.2**	**96**
P120	1		5.31	2.01	2.5	5.8	1.56	7.8	90
	2	120	4.81	1.21	2.5	5.5	1.47	16.8	99
	3		10.82	4.71	2.4	5.0	2.02	13.2	84
ØP120			**5.06**	**1.61**	**2.5**	**5.7**	**1.52**	**12.3**	**94**
P140	1		5.40	1.91	2.3	5.2	1.61	8.1	87
	2	140	4.46	0.87	2.5	5.6	1.43	18.2	93
	3		5.33	1.73	2.5	5.4	1.53	37.1	96
ØP140			**5.06**	**1.50**	**2.4**	**5.4**	**1.52**	**21.2**	**92**

[1] Determined by SEC (DMF, Poly(ethylene glycol) calibration)

[2] Determined by ^{1}H NMR spectroscopy (CDCl$_3$, 300 MHz)

[3] Unsaturation level calculated from the integral ratio (^{1}H NMR spectroscopy, CDCl$_3$, 300 MHz) between

the CH of the allyl end-groups (5.95 to 5.82 ppm) and the methyl group (4.56 ppm) of the propylene glycol units.

Table S5. Single values of suspension screening of ring-opening polymerization of propylene oxide by DMC catalyst. Values for tconst. were not calculated as a definite tconst. could not be determined.

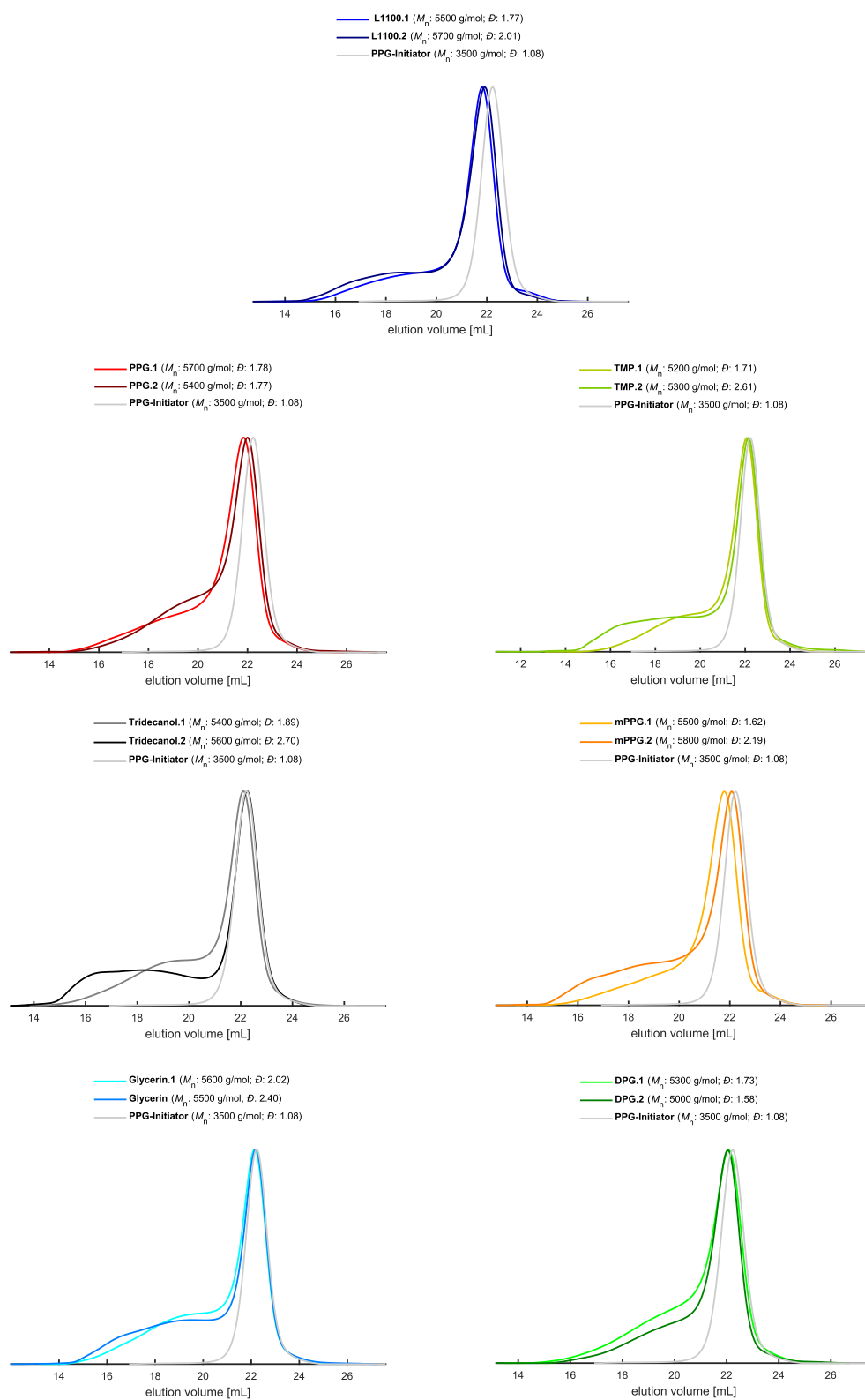| polyol	no.	p_{max} [bar]	t_{max} [min]	m [bar min^{-1}]
L1100	1	10.8	8.2	- 0.8
	2	12.5	16.3	- 1.2
ØL1100		**11.7**	**12.3**	**- 1.0**
PPG	1	9.9	17.6	- 0.4
	2	11.7	16.8	- 0.7
ØPPG		**10.8**	**17.2**	**- 0.6**
DPG	1	11.3	15.2	- 0.6
	2	10.1	33.3	- 0.6
ØDPG		**10.7**	**24.2**	**- 0.6**
Tridecanol	1	10.9	44.7	- 0.1
	2	11.7	18.6	- 0.5
ØTridecanol		**11.3**	**31.7**	**- 0.3**
mPPG	1	12.2	16.2	- 1.1
	2	10.5	28.4	- 0.4
ØmPPG		**11.4**	**22.3**	**- 0.7**
Glycerin	1	10.6	27.6	- 1.2
	2	11.6	14.1	- 0.6
ØGlycerin		**11.1**	**20.9**	**- 0.9**
TMP	1	11.3	14.4	- 0.8
	2	10.2	24.6	- 0.4
ØTMP		10.8	19.5	- 0.4

Figure S12. SEC traces of ring-opening polymerization of propylene oxide by varying DMC polyol suspensions and PPG Macroinitiator (DMF, PEG calibration).

Table S6. Single values of molecular weight analysis of PPO prepared by varying DMC polyol suspensions.

polyol	no.	HMWT$_{>10k}$ [%]	HMWT$_{>20k}$ [%]	M_n[1] [kg mol^{-1}]	$Đ$[1]
L1100	1	23.6	12.0	5.5	1.77
	2	26.5	15.7	5.7	2.01
ØL1100		**25.0**	**13.9**	**5.6**	**1.89**
PPG	1	20.5	9.9	5.7	1.78
	2	25.7	10.1	5.4	1.77
ØPPG		**23.1**	**10.0**	**5.6**	**1.78**
DPG	1	24.1	9.6	5.3	1.73
	2	20.6	7.5	5.0	1.58
ØDPG		**22.4**	**8.5**	**5.2**	**1.66**
Tridecanol	1	27.7	12.6	5.4	1.89
	2	35.1	23.6	5.6	2.70
ØTridecanol		**31.4**	**18.1**	**5.5**	**2.30**
mPPG	1	21.2	9.2	5.5	1.62
	2	32.2	18.3	5.8	2.19
ØmPPG		**26.7**	**13.8**	**5.7**	**1.91**
Glycerin	1	31.1	15.8	5.6	2.01
	2	31.0	17.3	5.5	2.40
ØGlycerin		**31.0**	**16.6**	**5.6**	**2.21**
TMP	1	22.9	9.9	5.2	1.71
	2	31.3	19.7	5.3	2.61
ØTMP		**27.1**	**14.8**	**5.3**	**2.16**

[1] Determined by SEC (DMF, Poly(ethylene glycol) calibration)

Chapter A2

Poly(ethylene glycol) having C1 to C3-alkyloxymethyl side chains, bioconjugates thereof, process for its preparation and its use

The author of this thesis contributed to this work by synthesis of the monomer, polymer analysis,^{1}H NMR kinetics, implementation of ELISA Assays and partially writing of the patent. The patent was submitted on 14.5.2021 and is currently reviewed by the european patent office (EPO).
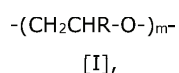
Title:

Poly(ethylene glycol) having C1 to C3-alkyloxymethyl side chains, bioconjugates thereof, process for its preparation and its use

Introduction

The present invention concerns polyether polymers represented by the following formula [I]:

$$-(CH_2CHR\text{-}O\text{-})_m-$$

[I],

wherein residues R are hydrogen or C1-C3 alkoxymethyl, 1 to 100 % are methoxymethyl and up to 50% of R may be C2-C3 alkoxymethyl with the proviso that at least one R is hydrogen, if at least one R is C2-C3 alkoxymethyl; and m is in the range of from 10 to 1000, wherein the dispersity is 1.15 or less. The invention further concerns a process for their preparation, conjugates thereof and the use thereof.

Background of the invention

The aliphatic polyether poly(ethylene glycol) (PEG) is the most widely employed polymer in pharmaceutics, medicine and drug delivery. PEGylation, i.e. the attachment of PEG to peptide drugs, was introduced in the 1970ies and has since then led to numerous highly efficient drugs. PEGylation is a form of conjugation, i.e. the attachment of a polymer to a molecule by a covalent bond. The main effect of the attachment of PEG chains is the so-called "stealth effect", which prevents close approach of and recognition by the immune system and subsequent binding and removal by the reticuloendothelial system (RES) in the liver. More simply, PEG attachment also prevents opsonization by proteins, when attached to the surfaces of nanocarriers for drug delivery. The inhibition of protein adsorption by PEG is further emphasized by fulfillment of the rules for protein-repellent surfaces derived by Whitesides (Yarovsky et al., "Quantitative design rules for protein-resistant surface coatings using machine learning", Scientific Rep. 2019, 9, 265). PEGylation is also used for "stealth liposomes" with long circulation times, low molecular weight drugs as well as for lipid nanoparticles. Such structures are employed for the transport and delivery of mRNA. Here the respective PEG-based lipids play a key role for the vaccination against the COVID-19 pandemic, enabling transport of mRNA to cells, avoiding undesired degradation

processes. The recently approved mRNA vaccines from Moderna and Pfizer-BioNTech require PEGylated lipids to ensure the stability of the mRNA in the lipid-based nanoparticle. PEGylation also prevents coalescence of liposomes and similar structures in aqueous systems. Commonly, molecular weights in the range of 2 to 40 kg/mol are preferred for the PEGylation of drugs or nanocarriers. To sum up, PEG has become a standard for water-soluble medical polymers for a vast variety of medical and pharmaceutical uses, particularly in the therapy of cancer, chronic diseases and recently also for RNA delivery vehicles. The success of PEG may have had several reasons. Among them are commercial availability in sufficient quality and in a wide range of molar masses from the anionic ring-opening polymerization of ethylene oxide as well as its extremely low toxicity and high biocompatibility. Further, PEG can be prepared in narrow molecular weight distributions.

However, an increasing number of studies summarize concerns related to the presence of so-called anti-PEG antibodies (APAs) that are present in a large and constantly growing part of the population. Such antibodies can lead to accelerated clearance of PEGylated drugs from the blood stream, i.e. loss of the stealth effect that is crucial for therapeutic success, allergic reactions and in extreme and rare cases even potentially fatal anaphylactic shock. This undesired effect is observed both for PEGylated peptide drugs, PEGylated liposomes and other PEGylated nanocarriers as well as PEGylated small molecule drugs. Anti-PEG antibodies are also problematic with respect to PEGylated lipids for RNA-transporting lipid nanoparticles, e.g. in the context of COVID-19 vaccines. PEG-antibodies are often mentioned in the context of potential PEG-alternatives as a motivation to look beyond PEG for alternatives. As an estimate, approximately 10% of the population experience allergic reactions when treated with PEGylated formulations. Only recently, the nature of the binding between PEG and anti-PEG antibodies has been studied by Lai et al (Lai et al, „Structure of an anti-PEG antibody reveals an open ring that captures highly flexible PEG polymers." *Commun Chem* 2020, *3, 124*). They concluded that binding of PEG is due to an open ring structure of PEG captured by the APAs. By counting the number of monomer repeats of the PEG polymer interacting with the interior and exterior paratope of the Fab, they found the size of the PEG antigen epitope to be ~700 g/mol, equivalent to 16 monomer subunits. Thus, at least 16 ethylene glycol units are required for binding by the APA. Other works suggest that also shorter regular chain segments of PEG as well as the methoxy end group of mPEG (α-methoxy poly(ethylene glycol)) structure play a key role for the recognition. US 8,129,330 B2 therefore discloses methods for the preparation of PEG conjugates that are based on end group modification of the PEG chains. Variation of the end group of PEG is disclosed, aiming at minimizing interaction of for example methoxy end groups with anti-PEG antibodies. The authors disclose conjugates, wherein a hydroxyl group is present on all of the distal polyalkylene glycol termini in said pure conjugate, and wherein

3

said conjugate exhibits reduced antigenicity compared to mPEG-protein conjugates. It has been reported that antibodies elicited by PEG-OH have similar affinity to both mPEG and PEG-OH, while antibodies induced by mPEG recognize mPEG more effectively than PEG-OH (Sherman et al, „Role of the methoxy group in immune responses to mPEG-protein conjugates." *Bioconjug Chem* 2012, 23(3), 485-499; Sherman et al, „Selectivity of binding of PEGs and PEG-like oligomers to anti-PEG antibodies induced by methoxyPEG-proteins." *Mol Immunol* 2014, 57(2), 236-246.). These results have been obtained by using competitive ELISA and imply that the anti-PEG antibodies elicited by PEG-OH-proteins are directed against the backbone of the PEG (backbone-specific), while antibodies induced by mPEG-protein conjugates are methoxy group specific. It can be concluded that regular segments of at least 4-5 to 16 regularly arranged ethylene glycol units are required to achieve recognition and immunogenic reaction by anti-PEG antibodies. Recent clinical works demonstrated that the presence of antibodies against PEG permits to predict Pegasparagase allergic reactions and failure of rechallenge, emphasizing the clinical importance of anti-PEG antibodies for the success of the treatment of leukemia in this case (Liu et al, "Antibodies Predict Pegasparagase Allergic Reactions and Failure of Rechallenge", *J. Clin. Oncol*. 2019, 37, 2051).

Three strategies for the modification of the PEG structure have been developed to counteract undesired APA interaction of PEGylated therapeutics. Replacing the methoxy end group of mPEG by a hydroxyl group led to a strong decrease in the affinity for anti-PEG antibodies, which was demonstrated by competitive ELISA tests. However, it is obvious that for large scale commercial applications the presence of a hydroxyl group at the terminus would require protected functional initiators, which complicates existing synthetic protocols. A second recent strategy is disclosed in US 2019/0015520 A1 and relies on PEG-bottlebrush structures, i.e. small PEG structures appended to a poly(hydroxyethyl methacrylate) backbone. The inventors state that this type of PEG-architecture minimizes anti-PEG antigenicity, while preserving the desired stealth properties for surface coating. However, the resulting PEG-grafted copolymers exhibit rather broad, multimodal molecular weight distributions, which represent a major obstacle for approval for medical application and PEGylation analogous bioconjugation with peptides or lipids. Narrow distributions (Mw/Mn < 1.15) were exclusively feasible by performing a cost- and time-consuming preparative size-exclusion chromatography (SEC).

Another strategy is to exchange PEG with the linear polyether polyglycerol to increase the blood circulation time of liposomes and to avoid accelerated blood clearance (see Abu Lila et al, "*Use of polyglycerol (PG), instead of polyethylene glycol (PEG), prevents induction of*

the accelerated blood clearance phenomenon against long-circulating liposomes upon repeated administration", International Journal of Pharmaceutics, 456 (2013) 235-242). However, the utilization of polyglycerol also results in the introduction of multiple hydroxyl functionalities to the liposome, which is in contrast to the aforementioned rules of Whitesides resulting in complex unspecific recognitions of peptides in the blood stream. Therefore, a targeted use of the conjugated drug or liposomes is not possible with polyglycerol.

Since PEGylated therapeutics are often used for chronic or in many cases otherwise fatal diseases, like in cancer therapy, in many cases repeated doses have to be administered over prolonged periods of time. PEG is a non-biodegradable polymer and has to be eliminated from the body through the kidneys. In studies on the renal filtration of PEGylated drugs, an undesirable accumulation of PEG in the kidneys and the associated pathological changes in the renal system could be demonstrated (see e.g. Bendele, A.; Seely, J.; Richey, C.; Sennello, G.; Shopp, G. Short Communication: Renal Tubular Vacuolation in Animals Treated with Polyethylene-Glycol-Conjugated Proteins. Toxicol.
Sei. 1998, 42, 152-157). The tendency of polyethylene to crystallize can therefore lead to deposits in the kidney. The elimination through the kidneys also limits the molecular weight of PEG for medical therapeutics to the renal cutoff size, which for globular proteins is approximately 50 to 60 kDa.

The present inventors have reported in 2014 on the copolymerization of ethylene oxide with glycidyl methyl ether (GME) by use of the monomer activation method and tetraoctylammonium bromide and tris-*iso*-butylaluminum as initiators (see Frey et al, A Challenging Comonomer Pair: *"Copolymerization of Ethylene Oxide and Glycidyl Methyl Ether to Thermoresponsive Polyethers"*, Macromolecules 2014, 47, 5492-5500). Rather broad molecular weight distributions were obtained (dispersity in the range of 1.21 to 1.5), which are clearly not suitable for medical applications. As discussed at the time, with the conventional anionic ring-opening method only molecular weights up to 3000 g/mol and high dispersities have been reported for the polymerization of GME. In previous studies regarding the homopolymerization of GME to poly(glycidyl methyl ether) (PGME) it was generally stated that polymerization causes difficulties, and no molecular weight control can be achieved by anionic ring-opening polymerization as employed for medical PEG (Frey et al., Biomacromolecules 2014, 15, 1935−1954). In all available reports regarding GME polymerization to date, either phosphazene bases were used as a catalyst or aluminum compounds had to be added in the way of a "monomer activated polymerization". None of these polymers or copolymers are suitable for medical applications for several reasons: (i) traces of phosphazene bases lead to toxicity and cannot be removed; (ii) dispersities exceed

1.1, which is prohibitive for most medical applications and (iii) end-group fidelity of the polymers derived from the methods is insufficient for attachment to peptides, drugs or lipids via bioconjugation. Therefore, neither PGME homopolymer nor copolymers of GME have been considered for PEGylation type applications to date.
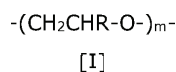
The retention of polymer end-groups (end-group fidelity) is a critical tool for chain extension and post polymerization reactions. End-group fidelity is also a decisive factor for the use of polymers in bioconjugates for pharmaceutical applications, in which the biomolecules are connected by means of the end-groups. Polymers with low end-group fidelity comprise a large amount of macromolecules that are not bound to the biomolecule and cannot be removed from the mixture without undue expenditure. The formed conjugates do not have the required purity. The loss of end-groups is therefore not desirable, but cannot be completely avoided. End-group fidelity varies greatly depending on the reaction conditions in the preparation of the polymers.

Purpose of the invention

It is the objective of the present invention to provide alternative polymers that are able to replace PEG in its applications and that can alleviate at least some of the aforementioned disadvantages of PEG. The alternative polymer should especially be suited to replace PEG in pharmaceutical applications. It is further an objective to provide polymers with low dispersity. A further objective is to provide polymers with high end-group fidelity. It is also desired to provide a process that allows preparation of such polymers in a simple and commercially feasible way. The alternative polymers should have a low affinity towards anti-PEG antibodies (APAs). A further goal is to provide polymers with a low immunogenicity.

Detailed description

The present invention concerns poly(ethylene glycol) having C1 to C3-alkyloxymethyl side chains. The present invention concerns polyether polymers represented by the following formula [I]:

$$-(CH_2CHR-O-)_m-$$
[I]

wherein residues R are independently from each other selected from the group consisting of hydrogen, methoxymethyl, ethoxymethyl, n-propoxymethyl and iso-propoxymethyl; 1

6

to 100% of the residues R are methoxymethyl; up to 50% of the residues R may be selected from the group consisting of ethoxymethyl, n-propoxymethyl and iso-propoxymethyl; with the proviso that at least one residue R is hydrogen, if at least one residue R is selected from the group consisting of ethoxymethyl, n-propoxymethyl and iso-propoxymethyl; and m is in the range of from 10 to 1000, characterized in that the dispersity is 1.15 or less. Herein the percentages of the residues R are based on the sum of all residues R, i.e. on m. These new polyether polymers are a new type of material, which behaves very different to PEG in regard to the affinity towards anti-PEG antibodies (APAs) and have a low immunogenicity. They also have a low crystallinity. But the polyether polymers of the present invention behave very similar to PEG with respect to various features that are important for pharmaceutical applications, including aqueous solubility, hydration, cell viability and biocompatibility.

Key to the reduced interaction with APAs is the use of substituents on the PEG backbone. The increased spatial requirements of the said PEG copolymers impede or disable interaction with anti-PEG antibodies according to the specific "lock and key principle". Besides the steric impact, the random distribution of the substituents over the polymer backbone and/or the random steric orientation of the substituents furthermore disable the development and formation of specific anti-polymer antibodies.

Key to the similarity of the features of PEG and the inventive polymers is the use of alkoxymethyl side chains. This maintains water solubility and other properties in view of PEG. A repeating group of the present polymer wherein R is a methoxymethyl group, i.e. (-CH$_2$-CH(-CH$_2$-OCH$_3$)-O)-, has the same molecular formula C$_4$H$_8$O$_2$ as two repeating units of PEG (-CH$_2$-CH$_2$-O)$_2$- and is therefore a constitutional isomer of two main chain repeating units of PEG. It comprises the same number of atoms and very similar functional groups. This leads to similar properties, especially to similar water solubility, which is important for applications in biological systems. The lack of reactive functional groups in the side chain like hydroxy, amino etc. reduces undesired interactions with biological systems.

Ethoxymethyl, n-propoxymethyl and iso-propoxymethyl may be used as residue R to adjust the properties of the polymers further, for example their solubility, interaction with lipids, properties in respect to the passage of biological membranes etc. However, these residues lead to a reduced solubility in water. The choice of such substituents also leads to a deviation from the behavior of PEG for other properties. For this reason, the amount of repeating units with the residues selected from the group consisting of ethoxymethyl, n-propoxymethyl and iso-propoxymethyl is limited to 50% of all residues R of the polymer of formula (I). Also in embodiments of the present invention in which at least one residue R

7

of the polymers is selected from the group consisting of ethoxymethyl, n-propoxymethyl and iso-propoxymethyl at least one residue R must be hydrogen, preferred at least 5 % are hydrogen in such embodiments, more preferred at least 10 % are hydrogen and most preferred at least 25 % are hydrogen. In a further preferred embodiment up to 20% of the residues R may be selected from the group consisting of ethoxymethyl, n-propoxymethyl and iso-propoxymethyl and even more preferred only up to 5% of the residues R may be selected from this group. These residues are not required for some of the uses of the polymers of the present invention in pharmaceutical applications. For this reason, polymers of the present invention are preferred where R is selected from the group consisting of hydrogen and methoxymethyl. Obviously, ethylene oxide repeating units in the inventive polymers also lead to similar properties with PEG. This selection therefore provides the polymers that are closest in behavior to PEG.

Higher homologues of methoxymethyl, i.e. where R is C4 alkoxymethyl and higher lead to increasingly low solubility in water and other detrimental properties and should therefore generally be avoided. They may however be used in small quantities when required, preferably in amounts of 10 % or less and more preferably in amounts of 3 % or less and most preferred 1 % or less, based on the sum of all residues R selected from the group consisting of hydrogen, methoxymethyl, ethoxymethyl, n-propoxymethyl and iso-propoxymethyl; i.e. on m. If the polyether of the present invention comprises higher homologues of methoxymethyl, where R is C4-alkoxymethyl or higher, the same proviso for the presence of hydrogen applies with the same preferred amounts. Various other co-monomers may be also used in small amounts, i.e. preferably less than 3 wt%, more preferably less than 1 wt% and most preferred in less than 0.1 wt% based on the weight average molecular weight of the polymer of formula [I], if necessary. They may for example be used to introduce functional groups or side chains into the polymer. Best suited for the use in pharmaceutical application are however usually polymers of the present invention that comprise only the repeating units of formula (I).

As mentioned before, ethylene oxide repeating units and glycidyl methyl ether repeating units, i.e. wherein R is methoxymethyl, provide polymers with very similar properties. Because of the very similar properties, the ethylene oxide repeating units in the backbone of PEG may be completely substituted by methoxymethyl substituted repeating units, i.e. 100% of the residues R may be selected from methoxymethyl groups, which constitutes the homopolymer of glycidyl methyl ether. This is however not preferred. The properties of the polymers of the present invention are still closer to the properties of PEG, when at least some of the residues R are selected to be hydrogen. Furthermore, immunogenicity of copolymers will be reduced as compared to the homopolymer of glycidyl methyl ether,

8

because they do not only differ in the orientation of side groups, but also side groups themselves. Preferred are therefore polymers for the present invention that are copolymers. The largest differences between the side groups and therefore the lowest immunogenicity is provided by polymers in which some of the repeating units have no side groups, i.e. where R is hydrogen. Most effective are therefore polymers of the present invention wherein 3 to 99% of the residues R are hydrogen and 1 to 97% of the residues R are independently from each other selected from the group consisting of methoxymethyl, ethoxymethyl, n-propoxymethyl and iso-propoxymethyl.

More preferred are 5 to 95% of the residues R hydrogen and 5 to 95% of the residues R are independently from each other selected from the group consisting of methoxymethyl, ethoxymethyl, n-propoxymethyl and iso-propoxymethyl. This will ensure a lower immunogenicity. More preferred 10 to 90% of the residues R are hydrogen and 10 to 90% of the residues R are independently from each other selected from the group consisting of methoxymethyl, ethoxymethyl, n-propoxymethyl and iso-propoxymethyl. Even more preferred are 20 to 80% of the residues R are hydrogen and 20 to 80% of the residues R are independently from each other selected from the group consisting of methoxymethyl, ethoxymethyl, n-propoxymethyl and iso-propoxymethyl. The lowest immunogenicity provide polymers of the present invention, where about 50 % of all ethylene oxide repeating units are substituted by alkyl glycidyl ethers. For this reason polymers are preferred where 30 to 70% of the residues R are hydrogen and 30 to 70% of the residues R are independently from each other selected from the group consisting of methoxymethyl, ethoxymethyl, n-propoxymethyl and iso-propoxymethyl and more preferred 40 to 60%. Especially useful in pharmaceutical applications is a polyether polymer of the present invention, wherein the polyether is a poly(glycidyl methyl ether-co-ethylene oxide) copolymer, i.e. wherein the residue R is selected from the group consisting of hydrogen and methoxymethyl. The same preferred ranges apply to embodiments where R is selected from the group consisting of hydrogen and methoxymethyl, i.e. wherein the polyether is a poly(glycidyl methyl ether-co-ethylene oxide) copolymer.

Especially preferred are polyether polymer of the present invention, wherein 30 to 70% of the residues R are hydrogen and the remaining residues R are methoxymethyl. These copolymers comprising repeating units where R is hydrogen combine most of the aforementioned advantageous properties. They have low immunogenicity, good water solubility, low crystallinity and are otherwise very similar to PEG.

m is preferably in the range of 20 to 900 and more preferably in the range of 30 to 800. Most preferably m is in the range of 30 to 700. These ranges correspond to the polymer
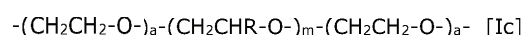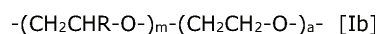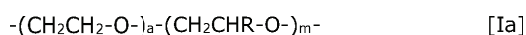
weights of PEG that are most suited for medical applications and that are used in existing medical application for PEG. Furthermore, the polymers of the present invention have preferably a molecular weight M_n as determined by MALDI-TOF in the range of 500 to 50.000 g/mol, more preferably in the range of 1.000 to 50.000 g/mol and most preferably in the range of 1.000 to 30.000 g/mol. These ranges apply to all embodiments of the present invention.

Copolymers of the present invention may be random copolymers. Such copolymers provide the lowest immunogenicity, as they do not provide a blueprint for the immune system for antibodies. They are intrinsically resistant to an immune response and are therefore preferred embodiments of the present invention. These polymers may be prepared by a process of the present invention as discussed below.

In one embodiment of the present invention the polymers of the present invention may be block copolymers or may have a block like structure or a tapered or gradient structure. The methods to prepare such polymers are known to the expert in the art. In such embodiments it is preferred that no more than 5% of the macromolecules of the polymers comprise blocks with more than 15 ethylene oxide repeating units, more preferably that no more than 5% of the macromolecules of the polymers comprise blocks with more than 8 ethylene oxide repeating units. This reduces immunogenicity.
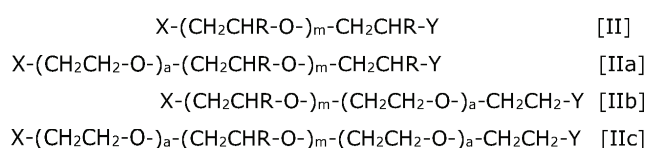
As described above, similarity to PEG is an important feature of the polymers of the present invention. This is especially true for the end groups of the polymer. Processing of PEG for the use in the pharmaceutical field, involves regularly the modification of the end groups. For this purpose, any end group known to be used for PEG can also be used for the present polymers. This includes not only the use of all known end groups for PEG, but also their modification including the kind of modification and the process of modification. If necessary, in order to allow the present polymers to function in this regard as similar or in fact identical to PEG, the present polymers may be provided with ethylene oxide repeating units on either end or both ends of the polymer, as depicted in Formula [Ia] to [Ic]. These are preferred embodiments of the present invention.

$$-(CH_2CH_2-O-)_a-(CH_2CHR-O-)_m- \qquad [Ia]$$
$$-(CH_2CHR-O-)_m-(CH_2CH_2-O-)_a- \quad [Ib]$$
$$-(CH_2CH_2-O-)_a-(CH_2CHR-O-)_m-(CH_2CH_2-O-)_a- \quad [Ic]$$

In these formulae the partial formulae $-(CH_2CHR-O-)_m-$ depicts a polymer of the present invention as described herein and a may be any number, but is preferable a number in the

range of 1 to 10 and more preferably in the range of 1 to 3. Polymers according to formulae [Ia] to [Ic] allow the modification of the termini of the present polymers exactly as PEG is modified in known processes and especially in present industrial processes. This allows for a smooth transition of established processes from PEG to the polymers of the present invention. Such can be prepared without much additional effort, as will be discussed below.

A further embodiment of the present invention, are polyether polymers represented by any of the following formula [II] and [IIa] to [IIc]:

$$X\text{-}(CH_2CHR\text{-}O\text{-})_m\text{-}CH_2CHR\text{-}Y \qquad\qquad \text{[II]}$$
$$X\text{-}(CH_2CH_2\text{-}O\text{-})_a\text{-}(CH_2CHR\text{-}O\text{-})_m\text{-}CH_2CHR\text{-}Y \qquad\qquad \text{[IIa]}$$
$$X\text{-}(CH_2CHR\text{-}O\text{-})_m\text{-}(CH_2CH_2\text{-}O\text{-})_a\text{-}CH_2CH_2\text{-}Y \quad \text{[IIb]}$$
$$X\text{-}(CH_2CH_2\text{-}O\text{-})_a\text{-}(CH_2CHR\text{-}O\text{-})_m\text{-}(CH_2CH_2\text{-}O\text{-})_a\text{-}CH_2CH_2\text{-}Y \quad \text{[IIc]}$$

wherein m is 19 to 999 and R is defined as in formula [I] and a is as defined in any of formulae [Ia] to [Ic]. X is the end group derived from the initiator of the reaction and the α-end group (alpha end group) and Y is the ω-end group (omega-end group).

X or Y or both may be chosen from any end group known for use in PEG. The same end groups may also be provided for the polymers of formulae [Ia] to [Ic].

X and Y may independently of each other or both comprise one or more functional group selected from the group consisting of acetal (dialkoxy), aldehyde (formyl), amide (carboxamido), azide, carbonate (alkoxycarbonyl)oxy), carboxyl (carboxy), carboxylic anhydride, ester (alkoxycarbonyl), ether, halo, haloformyl (carbonohaloridoyl), hemiacetal (alkoxyol), hemiketal (alkoxyol), hydroxy, imide (imido), imine (imino), ketal (dialkoxy), ketone (oyl), orthoester (trialkoxy), primary, secondary, tertiary amino group, primary, secondary and tertiary alkoxy group, sulfhydryl (sulfanyl, H-S-), thioether and combinations thereof. In a preferred embodiment X or Y may be selected from the group consisting of alkyl, hydrogen, hydroxy, alkoxy, sulfanyl, phthalimide, amide, amine and combinations thereof. X or Y or both may be a primary alkoxy group selected of the formulae $R\text{-}CH_n\text{-}O\text{-}$, wherein R is linear, branched or cyclic alkyl or phenyl and n equals 1 to 20. Preferred are X or Y or both selected from the group consisting of methoxy, ethoxy, propoxy, butoxy, pentoxy, hexoxy, heptoxy, octoxy, nonoxy, decanoxy, 3-ethyl-butoxy, 2,3-dialkoxypropoxy and a combination thereof. X or Y or both may also be the alkoxy residue of an alcohol of the following formula:
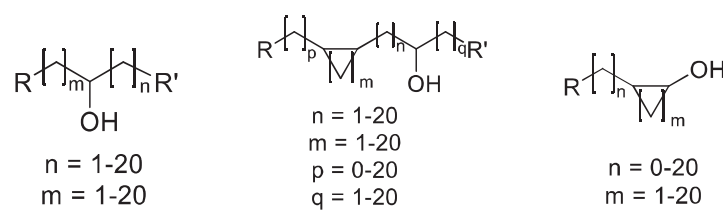
$$R \overbrace{}_{p} \bigtriangleup_{m} \overbrace{}_{n} OH$$
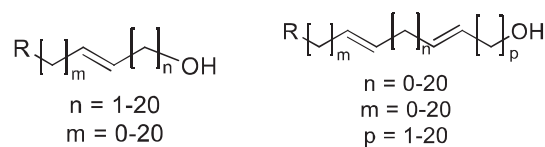
n = 1-20
m = 1-20
p = 0-20   ,
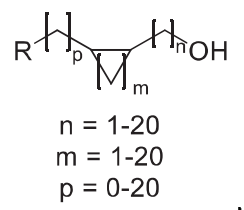
wherein R is hydrogen or linear, branched or cyclic alkyl or phenyl. X or Y or both may be the alkoxy residue of a secondary alcohol selected from any of the formulae

$$R \overbrace{}_{m} \underset{OH}{\overbrace{}}_{n} R'$$

n = 1-20
m = 1-20

$$R \overbrace{}_{p} \bigtriangleup_{m} \overbrace{}_{n} \underset{OH}{\overbrace{}}_{q} R'$$

n = 1-20
m = 1-20
p = 0-20
q = 1-20

$$R \overbrace{}_{n} \underset{\bigtriangleup_{m}}{\overbrace{}} OH$$
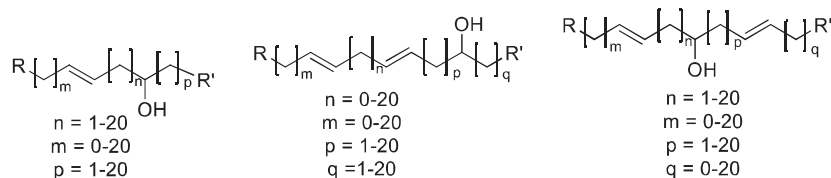
n = 0-20
m = 1-20   ,

wherein R and R' are independently from each other hydrogen or linear, branched or cyclic alkyl or phenyl. Among them a secondary alkoxy group is preferred that is selected from the group consisting of 2-propoxy, 2-butoxy, 2-pentoxy, 3-pentoxy, 2-hexoxy, 3-hexoxy, 2-heptoxy, 3-heptoxy, 4-heptoxy and cyclohexyloxy.

X or Y or both may also be selected from primary alkenyloxy groups, which may be linear, branched or cyclic. X or Y or both may also be the alkoxy residue of an alcohol of the following formula:

$$R \overbrace{}_{m} \overbrace{}_{n} OH$$

n = 1-20
m = 0-20

$$R \overbrace{}_{m} \overbrace{}_{n} \overbrace{}_{p} OH$$

n = 0-20
m = 0-20
p = 1-20   ,

wherein R is hydrogen or linear, branched or cyclic alkyl or phenyl. Among them a primary alkenyloxy group is preferred that is selected from the group consisting of 2-propenoxy (allyloxy), 3-butenoxy, 2-butenoxy, 3-methyl-2-butenoxy, 4-pentenoxy, 3-pentenoxy, 2-pentenoxy and 3,5-hexadienoxy.

X or Y or both may further be selected from secondary alkenyloxy groups, which may be branched or cyclic. X or Y or both may be the alkoxy residue of any of the following formulae:

n = 1-20
m = 0-20
p = 1-20

n = 0-20
m = 0-20
p = 1-20
q =1-20

n = 1-20
m = 0-20
p = 1-20
q = 0-20

,

wherein R and R' are independently from each other hydrogen or linear, branched or cyclic alkyl or phenyl. The secondary alkenyloxy group may be of any of the formulae 4-penten-2-oxy, 3-penten-2-oxy, 5-hexen-2-oxy, 4-hexen-2-oxy, 3-hexen-2-oxy, 4,6-heptadien-2-oxy, 1,4-pentadien-3-oxy.

X or Y or both may further be selected from aryloxy and heteroaryloxy groups. Benzyloxy groups are especially preferred. X or Y or both may be the aryloxy or benzyloxy residue of an alcohol of any of the following formulae:
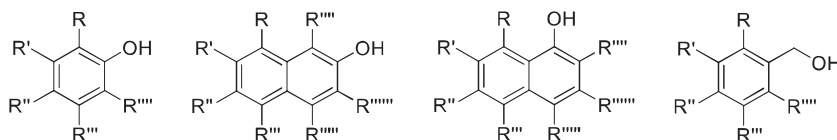
wherein R, R'', R''', R'''' R''''' and R'''''' are independently from each other hydrogen or linear, branched or cyclic alkyl or phenyl. X or Y or both are preferably selected from the group consisting of benzyloxy, phenyloxy and naphthyloxy.

X or Y or both may be multifunctional alkoxy groups, i.e. may have multiple ether bonds to the $\alpha-$ or ω-position of a plurality of macromolecules of the polymers of the present invention according to formulae [II] or [IIa] to [IIc]. Any suitable polyol may be selected therefore. X or Y or both may especially be selected from the group consisting of polyethers of carbohydrates, especially of Ribose, polyethers of 1,1,1-trimethylolpropane, polyethers of glycerol, polyethers of saccharides or hydrogenated saccharides.
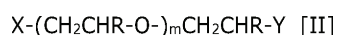
Further, Y may be selected from the group consisting of acrylamide, acrylates, aldehyde, alkyne, amine, aminooxy, azide, benzotriazole carbonate, carboxylic acid, chloroformate, cyanuric chloride, dithioester, epoxide, fluorescein, hydrazide, imidazoyl formate, iminoester, isocyanate, maleimide, mesylate, methacrylate, NHS ester, nitrobenzoate, nitrophenylcarbonate, succinimidyl active ester, succinimidyl carbonate, N-succinimidyl carbonate, succinimidyl succinate, thiocarbonate, thiol, thiol carboxylic acid, tosylate, triflate, vinyl sulfone and xanthate.

13

It is especially preferred that X is selected from the group consisting of hydrogen, alkyl, hydroxy, sulfanyl, C1-C10-alkoxy, C1-C10-thioalkoxy, amino, amino-C1-C10-alkoxy, dibenzylamino-C1-C10-alkoxy, amide, N-heterocyclic carbenes and N-heterocyclic olefins. It is also especially preferred that Y is selected from the group consisting of hydrogen, hydroxy, alkoxy, $-CH_2-C(=O)-R$ wherein R is as defined above, -CHO, alkylcarbonyloxy, alkyoxycarbonyloxy, amine, alkylamine, carboxamido, azide, halogen, sulfanyl, thioalkoxy and sulfonate. In addition, for any alkoxy rest defined herein for the residue X the corresponding thioalkoxy residue may be used, i.e. where a sulfur atom is present instead of the oxygen atom.

Most preferred are polymers of the present invention, where X and/or Y are selected from the group consisting of low molecular weight drugs, nanocarriers, liposomal structures, peptides, polypeptides, glycoproteins, polynucleotide, polysaccharides, lipid structures, liposomes, surfaces and interfaces, which are bonded directly by a covalent bond or by a spacer to the polymer. Nanocarriers usable in the present invention are for example selected from the group consisting of carbon nanotubes (CNT), dendrimers, gold nanorods, lipid nanoparticels, liposomes, micelles, nanocrystals, niosomes, polymeric nanoparticles (PNP), solid lipid nanoparticles (SLNs) and virus-based nanoparticles (VNP).

The polymers of the present invention have dispersities of 1.15 or less. They are suitable for applications where low dispersities are required, as for example in pharmaceutical, medical and biological applications. Dispersity of polymers in pharmaceutical, medical and biological applications is of great importance, as macromolecules of different molecular weight may behave differently in biological systems. They may for example differ in solubility in water, membrane permeability, crystallinity and renal clearance. Since a uniform behavior of all molecules is desired in medical applications, a low dispersity is often required. Most preferred are therefore polymers of the present invention that have a dispersity of 1.10 or less. This applies to all embodiments of the present invention. A dispersity of 1.10 or less is required for most medical and pharmaceutical applications. Most preferred are polymers of the present invention which have a dispersity that is lower than 1.08.

Preferred embodiments of the present invention are polyether polymers represented by the following formula [II]:

$$X-(CH_2CHR-O-)_mCH_2CHR-Y \quad [II]$$

wherein residues R are independently from each other selected from the group consisting of hydrogen, methoxymethyl, ethoxymethyl, n-propoxymethyl and iso-propoxymethyl; 1 to 100% of the residues R are methoxymethyl; up to 50% of the residues R may be selected from the group consisting of ethoxymethyl, n-propoxymethyl and iso-propoxymethyl; with the proviso that at least one residue R is hydrogen, if at least one residue R is selected from the group consisting of ethoxymethyl, n-propoxymethyl and iso-propoxymethyl; X is selected from the group consisting of hydrogen, alkyl, hydroxy, sulfanyl, C1-C10-alkoxy, C1-C10-thioalkoxy, amino, amino-C1-C10-alkoxy, dibenzylamino-C1-C10-alkoxy, amide, N-heterocyclic carbenes and N-heterocyclic olefins; Y is selected from the group consisting of hydrogen, hydroxy, alkoxy, $-CH_2-C(=O)-R$ wherein R is as defined above, -CHO, alkylcarbonyloxy, alkyoxycarbonyloxy, amine, alkylamine, carboxamido, azide, halogen, sulfanyl, thioalkoxy, N-succinimidyl carbonate and sulfonate; X and/or Y may also be selected from the group consisting of low molecular weight drugs, nanocarriers, liposomal structures, peptides, polypeptides, glycoproteins, polynucleotide, polysaccharides, lipid structures, liposomes, surfaces and interfaces, which are bonded directly by a covalent bond or by a spacer to the polymer, m is in the range of from 19 to 999, characterized in that the dispersity is 1.15 or less. Especially preferred is N-succinimidyl carbonate.

An especially preferred embodiment of the present invention is a polyether polymer of the present invention, wherein X is alkoxy and Y is hydroxy. Further preferably X is a C1-C10-alkoxy group and Y is hydroxy and even more preferably X is a C1-C3 linear alkoxy group and Y is hydroxy. These embodiments are analogous to commercially available PEG derivates. Most preferred X is methoxy and Y is OH, which is analogous to mPEG.

As discussed in regard to the dispersity, a unified behavior of all molecules in drugs and excipients used in pharmaceutical and medical applications is preferred. The end-group fidelity of the polymers of the present invention may be determined by MALDI TOF or by a combination of MALDI TOF with ^{1}H NMR by known methods. The polymers of the present invention have preferably an end-group fidelity of at least 95 % in regard to the group X and more preferably of at least 98 %. In a further embodiment the polymers of the present invention have preferably an end-group fidelity of at least 95 % in regard to the group Y and more preferably of at least 98 %. Even more preferred are polyether polymers of the present invention, wherein the end-group fidelity of the polymer in regard to group X and group Y is at least 95% and most preferably of at least 98 %. Especially preferred are polyether polymers of the present invention, wherein the end-group fidelity of the polymer in regard to group X and group Y is at least 95% and the dispersity is 1.10 or less and most preferred wherein the end-group fidelity of the polymer in regard to group X and group Y is at least 98% and the dispersity is 1.10 or less.

15

As aforementioned, the polymers of the present invention have similar properties as PEG, especially in biological systems. The present polymers may therefore substitute PEG in most of his applications. The polymers of the present invention are especially designed for use in the pharmaceutical and medical field. They may also be used with the same benefits in veterinary medicine and in other biological applications. In these fields the polymers of the present invention can fulfill the same functions as PEG, but have reduced immunogenicity and antigenicity. Because of their irregular structure, they do not elicit a strong immune response. The inventive polymers show especially a low response to anti-PEG antibodies, as evidenced by ELISA tests. Conjugates used for masking drugs and other pharmaceutically active compounds usually comprise PEG in addition to a physiologically active compound or an adjuvant. The polymers of the present invention may be used instead of PEG in any such application. At the same time the immune response elicited by the present polymers will be weak or non-existent thereby resolving one of the main problems in the use of PEG.

A further embodiment of the present invention is therefore a conjugate comprising a polyether polymer of any of the preceding claims and a substrate. The conjugates of the present invention may in the following also be named polyether-conjugated substrates or polymer-conjugated substrates. In the conjugates of the present invention a polymer of the present invention is bonded to a substrate directly or indirectly by a covalent bond. The polymer of the present invention may be bonded to the substrate by a spacer, which constitutes an indirect bond. The substrate may be selected from the group consisting of a pharmaceutically active compound, an adjuvant, a surface and interfaces. The pharmaceutically active compound is preferably selected from the group consisting of low molecular weight drugs, peptides, polypeptides, proteins, glycoproteins, polynucleotides and polysaccharides. The adjuvant is preferably a vesicle or carrier, which are preferably used to carry a pharmaceutically active compound. The adjuvant is preferably selected from the group consisting of nanocarriers, liposomal structures, lipid structures and liposomes. Nanocarriers usable in the present invention are for example selected from the group consisting of carbon nanotubes (CNT), dendrimers, gold nanorods, lipid nanoparticels, liposomes, micelles, nanocrystals, niosomes, polymeric nanoparticles (PNP), solid lipid nanoparticles (SLNs) and virus-based nanoparticles (VNP). In a further preferred embodiment the substrate is selected from the group consisting of low molecular weight drugs, nanocarriers, liposomal structures, peptides, polypeptides, proteins, glycoproteins, polynucleotides, polysaccharides, lipid structures, liposomes, surfaces and interfaces. Also in these embodiments the substrate may be bonded directly by a covalent bond or by a spacer to the polymer. Especially preferred are conjugates of the present invention with

2020-104 UMZ   2021-05-14

16

bovine serum albumin.

The polymer of the present invention may be bonded to the substrate directly by a covalent bond or by a spacer or any kind. Preferably a hydroxy-residue at the ω-terminal of the polymer of the present invention is used to bond a substrate or a spacer to the polymer. This is most economical, as the polymers of the present invention where X is an inert group and Y is OH can be most easily be prepared (see Examples). The conjugation of a substrate to the OH group at the ω-terminal end of PEG is well established. The same processes may be used for the polymers of the present invention. The substrate may however also be bonded to the α-terminal of the polymer. The polymers of the present invention can also be bonded to more than one substrate. This can be done by use of the α-terminal and the ω-terminal of the polymer and by using functional end groups of the polymer or spacer that can bond to a plurality of substrates. This may also be achieved by use of co-monomers with functional groups to which a substrate may be bonded. The bond between the polymers of the present invention and the substrate may be prepared by any means currently used for bonding PEG to substrates. It is also possible to bond a plurality of macromolecules of the polymers of the present invention to one substrate. This is especially useful for vesicle of all kinds including liposomes.

Typical examples for PEG conjugates are the lipid nanoparticles that are essential for vaccines against Covid-19 of the firms BioNTech SE and Pfizer Inc. and Moderna. It comprises a PEG conjugate of lipids, and the lipid nanoparticles (LNPs) are used to encapsulate and protect mRNA, which is the pharmaceutically active substance. The PEG in these conjugates may be substituted by the polymers of the present invention, thereby retaining the effects of the PEG polymer in the conjugate and at the same time reducing the immune response to the conjugate. A further vaccine of this kind is the Covid-19 vaccine of Curevac. Further drugs that comprise PEG conjugates wherein the PEG could be substituted by the present polymers are listed in the following.

Table 1

Trade names	Chemical Structure	Indication
Jivi®	60k-PEG recombinant Factor VII antihemophilic factor	Hemophilia A
Palynziq®	2K-PEG-rhu-Phenylalanine ammonia-lyase, Pegvaliase-pqpz	Phenyl-ketonuria
Adynovate®	20K-PEG-Factor VIII Antihemophilic Factor VIII	Hemophilia A
Revolixys® kit	40K-PEG-RNA aptamer + reverse agent, Factor-IXa blocker, Pegnivacogin /Anivamersen	Anti-coagulation

Onicyde®	2K-PEG-Liposomal irinotecan hydrochloride trihydrate	Metastatic pancreatic cancer
Plegridy®	20k PEG-Interferon β-1a	Relapsing from multiple sclerosis
Movantic®	<1k PEG-Naloxegol	Opioid-induced constipation
Omontys®	40K-PEG-Erythropoietin-mimetic peptide, Peginesatide	Anemia associated with chronic kidney disease
Sylatron®	12K-PEG-Interferon α-2b	Melanoma
Krystexxa®	10k-PEG-Uricase, Pegloticase	Gout
Cimzia®	40k-PEG-Certolizumab	Rheumatoid arthritis, Crohn's disease, Axial spondyloarthritis and psoriatic arthritis
Mircera®	30K-PEG- erythropoietin (epoetin) β	Anemia associated with chronic kidney disease
Macugen®	40K-PEG-anti-VEGF aptamer, Pegaptanib	Age-related macular degeneration
Somavert®	5K-PEG-rhuGH (human growth hormone), Pegvisomant	Acromegaly
Neulasta®	20K-PEG-Granulocyte colony stimulating factor, Pegfilgrastim	Neutropenia
Pegasys®	40K-PEG-interferon α-2	Hepatitis C und B
PegIntron®	12K-PEG-interferon α-2b	Hepatitis C und B
Doxil®/Caelyx®	2K-PEG-Liposomal doxorubicin HCl	Cancer
Oncaspar®	5K-PEGylated L-asparaginase, Pegaspargase	Acute lymphoblastic leukemia
Adagen®	5K-PEG-adenosine deaminase (bovine), Pegademase	Severe combined immunodeficiency disease (SCID)
Irinotecan®	PEGylated liposomal irinotecan hydrochloride trihydrate	Metastatic pancreatic cancer
Lonquez®	20k PEG-rhG-CSF	Neutropenia
Jintrolong®[1]	Branched 40k PEG hGH	hGH deficiency
Neulapeg®	20k-PEG rhG-CSF mutein	Neutropenia
Rebinyn®/ Refixia®	Branched 40k PEG Recombinant factor VIII	Hemophilia B
Asparlas®	5k-PEG L-Asparaginase	Acture lymphoblastic leukemia
Revcovi®	5k-PEG Recombinant B-domain truncated factor VIII	Hemophilia A
Besremi®[3]	Branched 40k PEG Proline-interferon α-2b	Polycythemia vera
PEGPH20®[3]	30k-PEG recombinant human hyaluronidase	Pancreatic cancer
Pegargiminase	20k PEG Arginine deiminase Interleukin-2	Hepatocellular carcinoma
NKTR-214	Branched PEG-20k Fmoc-succinimidyl carbonate	Melanoma, rencal cell carcinoma
PRX-201[3]	Bifunctional PEG2k α-Galactosidase A	Fabry disease
Peginterferon lambda-1a	20k PEG recombinant interferon lambda-1a	Hepatitis C and B[2], Hepatitis D[3]
Abicipar pegol	20k PEG anti-VEGF DARPin	Neovascular age related macular degeneration
TransCon GH®[3]	Four-arm-40PEG spacer hGH	Growth hormone deficiency
AM0010[2]	30k PEG-Interleukin-10	Metastatic pancreatic cancer

Rolontis®[3]	Bifunctional PEG rhG-CSF	Neutropenia
Efpeglenatide[3]	Bifunctional PEG Exendin-4 (glucagon-like peptide-1 receptor agonist)	Type-2 diabetes mellitus
Pegbelfermin[2]	30k PEG fibroblast growth factor-21 mutein	Fibrosis, liver disorders, nonalcoholic steatohepatitis, type 2 diabetes mellitus
Imrestor® (veterinary use)	20k PEG recombinant bovine G-CSF mutein	Reducing risk of clinical mastitis
Pegfilgrastim biosimilars: Fulphila (Mylan®) Lapelga/Pelgraz (Apobiologix®), Udenyca (Coherus Biosciences®), Pelmeg (Mundipharma®), Ziextenzo (Sandoz®)	20K-PEG-Granulocyte colony stimulating factor, Pegfilgrastim, rhG-CSF	Neutropenia
Esperoct®	Branched-PEG40k-SA-CMP, enzymatic glycopegylation at O-glycan on Ser-750	Hemophilia A

[1] only in China
[2] Phase II
[3] Phase III

Process for the preparation of a polyether polymer of the present invention, by anionic ring-opening copolymerization (AROP) comprising the steps of:

- Providing an anion An⁻,

- Adding at least one monomer of the formula ⟨triangle with O⟩-R, wherein R is as defined as described for any of formulae [I] or [II],

- Allowing the polymerization to proceed at a temperature in the range of -10 to 90 °C,

wherein the monomer comprises less than 1 wt% of epichlorohydrin.

In the process of the present invention the anion An⁻ must be an anion suitable for anionic ring-opening copolymerization (AROP). The expert in the art can easily choose among the known anions for this purpose. The An⁻ anion may be selected from the groups consisting of alkyl anion, hydride, OH⁻, alkoxy⁻, SH⁻, thioalkoxy⁻, amine anion, amide anion, imide anion and combinations thereof. Alkyl anions and hydride anions may be provided in the form of metal alkyl or metal hydride compounds. The alkoxy anion and the thioalkoxy anion may be the corresponding anion with the same structure as any of the alkoxy groups and aryloxy groups and aralkoxy groups defined herein for the residue X. Preferably however

the alkoxy anion and the thioalkoxy anion are not tertiary alkoxy anions. The imide anion is preferably a phthalimide anion. Polymers of the Formulae [Ia], [Ic], [IIa] and [IIc] may be prepared by first adding the corresponding amount of ethylene oxide to the anion An⁻ and allowing the polymerization to proceed at a temperature in the range of -10 to 90 °C until all of the ethylene oxide is consumed. Subsequently the steps of adding least one

monomer of the formula △-R, and allowing the polymerization to proceed at a temperature in the range of -10 to 90 °C are performed. In this manner the repeating units adjacent to the α-terminal of the polymers of the present invention are provided with exactly the same structure as PEG. Polymers of the Formulae [Ia], [Ic], [IIa] and [IIc] may also be prepared by use of anions of the formulae X-(CH$_2$CH$_2$-O-)$_a$⁻, wherein a is as defined for any of the Formulae [Ia], [Ic], [IIa] and [IIc] and X is any residue as defined herein for X. This is the preferred method. Especially preferred is the use of such anions of the formulae X-(CH$_2$CH$_2$-O-)$_a$⁻, in which X is alkyl, alkoxy, dialkylamin anion or (RCO)$_2$N⁻. Even more preferred is the use of anions selected from the group consisting of MeOCH$_2$CH$_2$O⁻, MeO(CH$_2$CH$_2$O)$_2$⁻, BenzylOCH$_2$CH$_2$O⁻, BzO(CH$_2$CH$_2$O)$_2$⁻, (Bz)$_2$N-CH$_2$CH$_2$O⁻, (Bz)$_2$N-(CH$_2$CH$_2$O)$_2$⁻, phthalimide-CH$_2$CH$_2$O⁻, phthalimide-(CH$_2$CH$_2$O)$_2$⁻, wherein Me is methyl and Bz is benzyl. Most preferred are MeO(CH$_2$CH$_2$O)$_2$⁻, BzOCH$_2$CH$_2$O⁻ and (Bz)$_2$N-CH$_2$CH$_2$O⁻.

Further, in a final step of the preparation, addition of a small amount of pure EO is possible to ensure primary hydroxyl end groups for the ω-terminal of the polymer that can undergo all established coupling strategies to therapeutic entities. This leads to polymers of the present invention with Formulae [Ib], [Ic], [IIb] and [IIc].

The counter ion to the An⁻ anion is preferably selected from the group consisting of Na⁺, K⁺ and Cs⁺. The anion An⁻ may be provided in an inert solvent. The solvent is preferably a non-protic solvent and most preferably dimethyl sulfoxide (DMSO). Also preferably the reaction is performed in the same solvent.

Anionic ring-opening polymerizations with alkyl glycidyl ethers are more prone to undergo chain transfer reactions as follows:
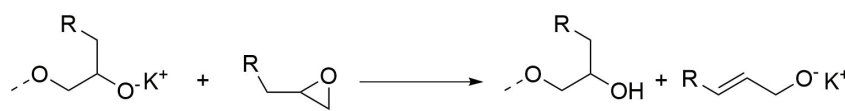
These side reactions increase with the temperature. Therefore, high molecular weight polymers can only be obtained, if the reaction temperature is not above 90°C. The chain transfer reaction results in a broad distribution of molecular weight and therefore in a high dispersity. Therefore, lower polymerization temperatures also provide polymers of the

present invention with lower dispersity. On the other hand, alkyl glycidyl ethers are as reactive in the anionic ring-opening polymerization as ethylene oxide. For this reason the polymerization may be performed at temperatures as low as -10°C. Preferably the polymerization is performed at a temperature in the range of 10 to 70°C and more preferred at a temperature in the range of 10 to 60°C.

A further problem in anionic ring-opening polymerizations is that commercially available alkyl glycidyl ethers are prepared from epichlorohydrin. Part of the epichlorohydrin remains in the alkyl glycidyl ether. Presence of alkyl glycidyl ethers leads to termination reactions as follows:

This in turn leads to low molecular weights and high dispersity of the product. The polymers of the present invention are therefore only accessible by reaction temperatures of -10 to 90°C or less and by the use of alkyl glycidyl ethers that comprise less than 1 wt% of epichlorohydrin. Preferably the alkyl glycidyl ethers comprise less than 0.5 wt% of epichlorohydrin and more preferably less than 0.1 wt%. Most preferably the alkyl glycidyl ether are free of epichlorohydrin. Removal of epichlorohydrin from the glycidyl methyl ether to the extent necessary is impossible, because the glycidyl methyl ether and epichlorohydrin have similar boiling points, e.g. epichlorohydrin 117.9°C, glycidyl methyl ether 110°C. Procedures for the preparation of epichlorohydrin free alkyl glycidyl ethers is provided in Example 1 of the present invention.

Furthermore, high temperatures also lead to side reactions of the starting anion An⁻ or the group X of the living polymer. Limitation of the temperature in the aforementioned range therefore also improves the end-group fidelity at the α-terminal of the polymers of the present invention and allows for end-group fidelities of 95% or more of the X residue. Other known methods for the polymerization of the alkyl glycidyl ethers do not provide the low dispersity required for the present polymers. They also do not allow for the same high end-group fidelity.

In order to provide random copolymers or the present invention, it is necessary to add at least two different kinds of monomers to the anion. The reactivity ratio for both alkyl glycidyl ether employed and ethylene oxide is in the range of 0.7 to 1.3. For glycidyl methyl ether and ethylene oxide the reactivity ratio is in the range of 0.98 to 1.02. This results in almost ideally random copolymers. Other forms of copolymers i.e. with a block structure, block like structure or a tapered or gradient structure can be prepared according to known

methods. Block copolymers can easily be prepared by subsequent additions of different monomers to the living polymer. Therefore, a process of the present invention is preferred, wherein the step of adding at least one monomer and the step of allowing the polymerization to proceed are repeated at least one time, whereby at least one different monomer is used than the first time.

A further embodiment of the present invention is the use of the polyether polymers of the present invention for the preparation of a conjugate of the polymers with a substrate. The substrate is as defined herein for the conjugates of the present invention. The substrate is preferably a bioactive compound. There is a well-developed chemistry for the preparation of conjugates of PEG, which is known to the expert in the art. The same chemistry may be used for the preparation of a conjugate of the present invention. Preferred is a use of the present invention, for the preparation of conjugated lipids for use in vaccines, in particular based on lipid nanoparticles. These nanoparticles are preferably nanoparticles, as used against COVID-19. Preferred are conjugates of polymers of the present invention with bovine serum albumin (BSA). Especially preferred are conjugates with polymers of the present invention where the y group of the polymer is a N-succinimidyl carbonate group. Even more preferred are conjugates of the present polymer where bovine serum albumin in conjugates by means of such a group Y to a polymer of the present invention. Conjugation of α-BzO-ω-N-succinimidyl carbonate-P(EG-co-GME) to bovine serum albumin if most preferred.

An additional embodiment for the present invention concerns the preparation of conjugates of the present invention. As discussed above, the conjugates may be prepared by any known process for the preparation of conjugates of PEG. The present invention provides additionally a process, where firstly the process for the preparation of the polymers of the present invention is performed and then a substrate is added to the living polymer, wherein the substrate has a functional group that reacts with the living polymer to form a conjugate.

Brief description of the figures:

Figure 1:   Figure 1 shows the results of ELISA test of three of the polymers of the present invention and mPEG.

Figures 2 to 8: These figures show the SEC traces of polymers of the present invention and Figure 8 shows in addition the SEC trace of commercially available mPEG.

Figure 9:   Figure 9 shows the ^{1}H NMR spectrum of α-BzO-P(EG0.51-co-GME0.49).

Figure 10: Figure 10 shows the MALDI-TOF spectrum of α-BzO-P(EG0.51-co-GME0.49).

Figure 11: Figure 11 shows cloud point of α-BzO-P(EG0.51-co-GME0.49).

Figure 12: Figure 12 shows the MALDI-TOF spectrum of α-DBzN-EtO-PGME, i.e. a homopolymer of the present invention.

Figure 13: Figure 13 shows the MALDI-TOF spectrum of α-MeO-P(PEG$_{0.88}$-b-PGME$_{0.22}$), i.e. a block copolymer of the present invention.

Figure 14: Figure 14 shows the MALDI-TOF spectrum of α-BzO-ω-Ts-P(EG$_{0.93}$-co-GME$_{0.07}$), i.e. a copolymer of the present invention that has been further functionalized at the ω-terminal ending.

Figure 15: Figure 15 shows the decreasing ^{1}H NMR signals of monomers during the preparation of a polymer of the present invention.

Figure 16: Figure 16 shows the result of a study of the relative reactivity of ethylene oxide and glycidyl methyl ether in the anionic ring opening polymerization.

Examples:

Reagents:

Chemicals were purchased from TCI, Acros Organics, Roth, Sigma Aldrich and Honeywell, unless otherwise noted. Ethylene oxide was obtained from Air Liquide. Deuterated solvents were purchased from Deutero GmbH. THF was flashed over basic aluminum oxide before usage. Glycidyl methyl ether was dried over CaH$_2$ and cryo-transferred before the polymerizations.

Measurements:

^{1}H and ^{13}C NMR spectra were recorded on a Bruker Avance III HD 300 spectrometer with 300 MHz and referenced internally to residual proton signals of the deuterated solvent.

Size-exclusion chromatography measurements were performed with dimethylformamide (DMF with 1 g/L LiBr) as the mobile phase (flow rate 1 mL/min) on 2-hydroxyethylmethacrylat (HEMA) 300/100/40 columns at 50 °C. Polymer concentrations were 1 mg/mL. Calibration was carried out using poly(ethylene glycol) standards (from Polymer Standard Service, Mainz, Germany).

Differential scanning calorimetry (DSC) measurements were carried out in the temperature range of -100 to 100 °C with a heating rate of 10 K/min at a PerkinElmer DSC 8500. The

thermal history of the samples was excluded via two cooling and two heating cycles. For each sample, the glass transition and the melting temperatures were obtained from the second heating curve.

MALDI-ToF MS measurements were carried out at a Bruker autoflex maX MALDI-TOF/TOF. The potassium salt of trifluoroacetic acid and trans-2-[3-(4-tert-Butylphenyl)-2-methyl-2-propenylidene]malononitrile (DCTB) were utilized as ionization salt and matrix, respectively.

Example 1: Synthesis of Glycidyl methyl ether (GME)
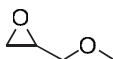
a)   Allyl methyl ether (10.0 g, 139 mmol) was dissolved in 274 mL dichloromethane (DCM) and m-chloroperoxybenzoic acid (m-CPBA, 70%, 37.6 g, 153 mmol (based on m-CPBA)) was added to the solution. After stirring overnight, the solution was filtrated and slowly concentrated under reduced pressure. Crude glycidyl methyl ether was separated from solid impurities via cryo-transfer. Slow evaporation of residual dichloromethane in vacuo gave pure glycidyl methyl ether as a colorless liquid; Yield 41%.

b)   1-Chloro-3-methoxy-propan-2-ol (3.00 g, 2.56 mL, 24.1 mmol) and anhydrous sodium sulfate (1.02 g, 7.23 mmol) were added to a flask equipped with a magnetic stirrer and cooled with a water bath. Finely grounded sodium hydroxide (1.25 g, 31.3 mmol) was added under stirring. After complete reaction (TLC control) the crude product was cryo-transferred in vacuo from the reaction flask and dried over CaH_2 under cooling. After an additional cryo-transfer, GME was obtained as a colorless liquid with a yield of 93 %.

Example 2:   General procedure for the preparation of random copolymers
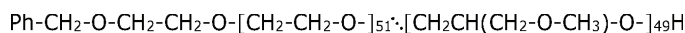   Synthesis of α-BzO-P(EG-co-GME)
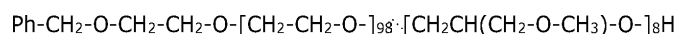
Ph-CH_2-O-CH_2-CH_2-O-[CH_2-CH_2-O-]$_{98}$·[$CH_2CH(CH_2$-O-CH_3)-O-]$_8$H

Potassium tert-butoxide (13.0 mg, 118 µmol) was dissolved in a tetrahydrofuran (THF) - water mixture and transferred into a reaction flask, equipped with a Teflon stopcock and a septum. 2-Benzyloxy-ethanol (20.0 mg, 18.7 µL, 131 µmol) was dissolved in benzene and added to the reaction flask. After slow evaporation of the solvent, the resulting solid was dried at 60 °C under high vacuum overnight. The residue was dissolved in dimethyl sulfoxide (DMSO, 5 mL) and the solution was cooled to -78 °C. Glycidyl methyl ether (119 mg, 122 µL, 1.35 mmol) was added via syringe and ethylene oxide (537 mg, 553 µL,

12.2 mmol) was cryo-transferred into the reaction flask. The solution was heated to 55 °C and stirred for 24 h under vacuum. Afterwards, the solution was poured into excess chloroform and the organic phase was extracted against water (3 times) and brine, dried over $MgSO_4$ and filtrated. After evaporation of the solvent α-BzO-P(EG0.92-co-GME0.08) was obtained as a colorless solid; yield quantitative.

The data of the polymer produced can be found in Tables 2 to 4 below (see entry b). Further examples have been prepared according to this procedure with varying amounts of the monomers (see Tables 2 to 3, entries a to d, f and g). Further, α-MeO-P(EG-co-GME) and α-DBzN-P(EG-co-GME) were prepared according to the same procedure with diethylene glycol monomethyl ether and N,N-dibenzyl-2-aminoethanol as initiators, respectively, instead of benzyloxy-ethanol (entries h and i of Tables 2 to 4).

Example 3:   Synthesis of

$$Ph\text{-}CH_2\text{-}O\text{-}CH_2\text{-}CH_2\text{-}O\text{-}[CH_2\text{-}CH_2\text{-}O\text{-}]_{51}\text{-}[CH_2CH(CH_2\text{-}O\text{-}CH_3)\text{-}O\text{-}]_{49}H$$

Cesium hydroxide monohydrate (28.0 mg, 118 μmol) was dissolved in a THF-water mixture and transferred into a reaction flask, equipped with a Teflon stopcock and a septum. 2-Benzyloxy-ethanol (20.0 mg, 18.7 μL, 131 μmol) was dissolved in benzene and added to the reaction flask. After slow evaporation of the solvent, the resulting solid was dried at 60 °C under high vacuum overnight. The residue was dissolved in DMSO (5 mL) and the solution was cooled to -78 °C. GME (367 mg, 374 μL, 4.16 mmol) was added via syringe and EO (183 mg, 189 μL, 4.16 mmol) was cryo-transferred from a graduated ampule into the reaction flask. The solution was stirred for 48 h at room temperature under vacuum. Afterwards, the solution was poured into excess chloroform and the organic phase was extracted against water (3 times) and brine, dried over $MgSO_4$ and filtrated. P(EG$_{0.51}$-co-GME$_{0.49}$) was obtained in quantitative yield as a viscous liquid after evaporation of the solvent and drying under high vacuo. The data of the product can be found in Tables 2 and 3, entry e.

Example 4: Synthesis of glycidyl methyl ether homopolymer

$$\alpha\text{-}Bz_2NCH_2CH_2O(CH_2CH(CH_2OCH_3)\text{-}O)_nH$$

Cesium hydroxide monohydrate (25.0 mg, 149 μmol) was dissolved in a THF-water mixture and transferred into a reaction flask, equipped with a Teflon stopcock and a septum. N,N-Dibenzyl-2-aminoethanol (40.0 mg, 166 μmol) was dissolved in benzene and added to the
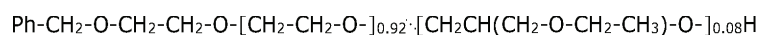
reaction flask. After slow evaporation of the solvent, the resulting solid was dried at 60 °C under high vacuum overnight. The residue was dissolved in DMSO (5 mL) and the solution was cooled to -78 °C. Glycidyl methyl ether (GME, 660 mg, 670 µL, 7.46 mmol) was added via syringe. The solution was stirred for 48 h at room temperature under vacuum. Afterwards, the solution was poured into excess chloroform and the organic phase was extracted against water (3 times) and brine, dried over $MgSO_4$ and filtrated. Poly(glycidyl methyl ether) (PGME) was obtained in quantitative yield as a viscous liquid after evaporation of the solvent and drying under high vacuo. The data of this polymer can be found in Table 2 and 3, entry j.

Example 5: Synthesis of α-BzO-P(EG-co-EGE)

$$Ph\text{-}CH_2\text{-}O\text{-}CH_2\text{-}CH_2\text{-}O\text{-}[CH_2\text{-}CH_2\text{-}O\text{-}]_{0.92}\text{-}[CH_2CH(CH_2\text{-}O\text{-}CH_2\text{-}CH_3)\text{-}O\text{-}]_{0.08}H$$

Potassium tert-butoxide (13.0 mg, 118 µmol) was dissolved in a THF-water mixture and transferred into a reaction flask, equipped with a Teflon stopcock and a septum. 2-Benzyloxy-ethanol (20.0 mg, 18.7 µL, 131 µmol) was dissolved in benzene and added to the reaction flask. After slow evaporation, the resulting solid was dried at 60 °C under high vacuum overnight. The residue was dissolved in DMSO (5 mL) and the solution was cooled to -78 °C. Ethyl glycidyl ether (EGE, 270 mg, 260 µL, 2.50 mmol) was added via syringe and ethylene oxide (440 mg, 450 µL, 9.99 mmol) was cryo-transferred from a graduated ampule into the reaction flask. The solution was heated to 55 °C and stirred for 24 h under vacuum. Afterwards, the solution was poured into excess chloroform, and the organic phase was extracted against water (3 times) and brine, dried over $MgSO_4$ and filtrated. P(EG0.92-co-EGE0.08) was obtained as a colorless solid after evaporation of the solvent and drying under high vacuo; yield > 96%. Table 2 and 3, entry k shows the data of this product.

Example 6: Synthesis of mPEG-b-PGME

$$Me\text{-}O\text{-}[CH_2\text{-}CH_2\text{-}O\text{-}]_{0.78}\text{-}[CH_2CH(CH_2\text{-}O\text{-}CH_3)\text{-}O\text{-}]_{0.22}H$$

Potassium tert-butoxide (13.0 mg, 118 µmol) was dissolved in a tetrahydrofuran (THF) - water mixture and transferred into a reaction flask, equipped with a Teflon stopcock and a septum. Methoxypoly(ethylene glycol) (mPEG, M_n 2 kg/mol; 250 mg, 125 µmol) was dissolved in benzene and added to the reaction flask. After slow evaporation, the residue was dried at 80 °C under high vacuum overnight. The residue was dissolved in dimethyl sulfoxide (DMSO, 5 mL) and the solution was cooled to -78 °C. Glycidyl methyl ether (253 mg, 258 µL, 2.88 mmol) was cryo-transferred into the reaction flask. The solution was

heated to 55 °C and stirred for 24 h under vacuum. Afterwards, the solution was poured into excess chloroform and the organic phase was extracted against water (3 times) and brine, dried over $MgSO_4$ and filtrated. mPEG-b-PGME 4k was obtained as a colorless solid after precipitation in ice-cold diethyl ether; yield quantitative. Table 2 and 3, entry j shows the data for this polymer.

Example 7: Synthesis of α-BzO-ω-Ts-P(EG-co-GME)

$$Ph-CH_2-O-CH_2-CH_2-O-[CH_2-CH_2-O-]_{98}-[CH_2CH(CH_2-O-CH_3)-O-]_8Ts$$
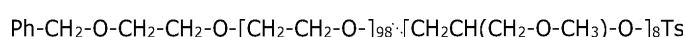
α-BzO-P(EG-co-GME) (50.0 mg, 4.6 µmol) from Example 2 was dissolved in dichloromethane (DCM) in a flask equipped with a reflux condenser and the solution was cooled to 0 °C. After addition of triethylamine (2.32 mg, 3.18 µL, 22.9 µmol), tosyl chloride (4.37 mg, 22.9 µmol) was added in portions to the solution. The ice-bath was removed and the solution was refluxed overnight. The reaction mixture was extracted with saturated $NaHCO_3$, water and brine, dried over $MgSO_4$ and filtrated. After precipitation in diethyl ether and drying in vacuo, α-BzO-ω-Ts-P(EG-co-GME) was obtained as a white solid; yield quantitative. Tables 2 and 3, entry m shows the data for this polymer.

Example 8: Synthesis of ɑ-BzO-ω-N-succinimidyl carbonate-P(EG-co-GME)
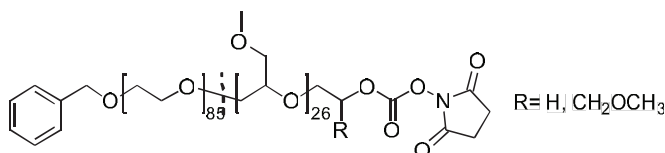
N,N'-disuccinimidyl carbonate (3.5 mg, 13.8 µmol) is added to a stirred solution of α-BzO-P(EG-co-GME) (50.0 mg, 4.6 µmol) from Example 2 in dry CH_3CN (1 ml) at room temperature for 18 h. The reaction mixture was dissolved in dichloromethane extracted with a saturated $NaHCO_3$, water and brine, dried over $MgSO_4$ and filtered. The solvent was removed under reduced pressure and the polymer dried under vacuum. The product was obtained as a white solid; yield quantitative.

Example 9: Conjugation of α-BzO-ω-N-succinimidyl carbonate-P(EG-co-GME) to bovine serum albumin (BSA).

2020-104 UMZ   2021-05-14

27
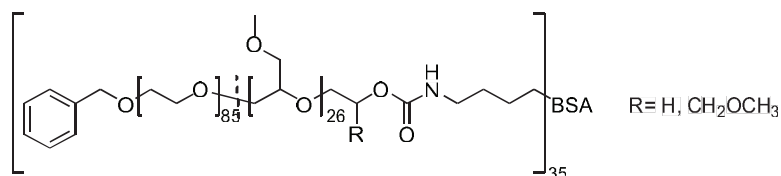
Bovine serum albumin (5 mg, 0.07 μmol) and α-BzO-ω-N-succinimidyl carbonate-P(EG-co-GME) (16.9 mg, 2.6 μmol) from Example 8 were stirred in phosphate-buffered saline (PBS buffer) for 1 h. The unreacted polymer was removed by dialysis in deionized water with a 25 kDa membrane filter. The conjugate was then dried by lyophilization and obtained in quantitative yield. In the preparation of this conjugate, the outer lysing group (30-35) are targeted for the conjugation.

Example 10: Competitive Enzyme-linked Immunosorbent Assay (ELISA)

The interaction of the copolymer samples entry c, d and e were evaluated by a competitive PEG ELISA kit using a murine monoclonal, horseradish peroxidase conjugated anti PEG antibody (HRP anti-PEG) (Life diagnostics, West Chester, PA, USA). Samples of concentrations ranging from 0 to 4600 μg ml-1 were prepared in dilution buffer. Additionally, mPEG with a molecular weight of 5000 g mol-1 was utilized as internal standard for comparison. 50 μl of each prepared sample was dispensed to a PEG pre-coated 96-well plate and 50 μl of HRP anti-PEG was added to each well. The solutions were incubated for 1h at 25 °C with a micro-plate shaker and then washed six times with 400 μl of wash buffer per each well. After removal of residual droplets, 100 μl of 3,3′,5,5′-Tetramethylbiphenyl-4,4'-diamine was added to each well and the solutions were mixed on a micro-plate shaker for 20 min. The reaction was stopped by addition of 100 μl of stop solution and the absorbance at 450 nm was read within 5 minutes.

Analysis of ELISA Data: The determined absorbance values were normalized to visualize the percent of maximal binding. The sample concentrations were transformed to a function of $\log_{10}$. The sigmoidal fits were calculated using the following equation with a representing the upper, b the lower limit, c the inflection point and d the hill slope.

$$y = a + (b\text{-}a) / 1 + 10^{(c\text{-}x)*d}$$

Example 11: Kinetic of the Synthesis of α-BzO-P(EG-co-GME)

The synthesis of α-BzO-P(EG-co-GME) was repeated in fully deuterated DMSO for an online

in situ ^{1}H NMR kinetic measurement. 95 mg glycidyl methyl ether (95 µl, 1.1 µmol) and 32 mg ethylene oxide (33 µl, 7.1 µmol), i.e. 60% glycidyl methyl ether and 40% ethylene oxide where solved in fully deuterated DMSO. The consumption of ethylene oxide and glycidyl methyl ether over time was measured by ^{1}H-NMR spectroscopy. As measure for the ethylene oxide concentration, the signal of the protons of ethylene oxide at about 2.6 ppm was used. For glycidyl methyl ether the signals of the protons at the oxirane ring with absorptions at about 2.75 and 3.1 ppm were used. Figure 15 shows the decrease of the selected ^{1}H NMR signals of the two monomers over time. Figure 16 shows plot of monomer consumption Mx,t/Mx,t=0 versus total conversion. As can be seen, ethylene oxide and glycidyl methyl ether are consumed at exactly the same rate. This data shows that the copolymers of the present invention are almost ideal random copolymers.

Discussion of the results

Tables 2, 3 and 4 and Figure 1 to 15 show the properties of the polymers prepared. They are discussed in the following.

Table 2: Composition of polymers prepared

Entry (Example)	*Sample*	DP_{EO} NMR	DP_{GE} NMR	*mol%$_{EO}$* NMR	*mol%$_{GME}$* NMR
a (2)	α-BzO-P(EG$_{0.96}$-*co*-GME$_{0.04}$)	108	4	96	4
b (2)	α-BzO P(EG$_{0.92}$-*co*-GME$_{0.08}$)	98	8	92	8
c (2)	α-BzO P(EG$_{0.84}$-*co*-GME$_{0.16}$)	112	21	84	16
d (2)	α-BzO P(EG$_{0.76}$-*co*-GME$_{0.24}$)	85	26	76	24
e (3)	α-BzO P(EG$_{0.51}$-*co*-GME$_{0.49}$)	35	33	51	49
f (2)	α-BzO P(EG$_{0.96}$-*co*-GME$_{0.04}$)	223	10	96	4
g (2)	α-BzO P(EG$_{0.93}$-*co*-GME$_{0.07}$)	175	13	93	7
h (2)	α-MeO-P(EG$_{0.97}$-*co*-GME$_{0.03}$)	147	5	97	3
i (2)	α-DBzN-P(EG$_{0.97}$-*co*-GME$_{0.03}$)	142	5	97	3
j (4)	α-DBzN-EtO-PGME	–	45	–	100
k (5)	α-BzO-P(EG$_{0.85}$-*co*-EGE$_{0.15}$)	106	18	85	15

| l (6) | α-MeO-PEG$_{0.88}$-b-PGME$_{0.22}$ | 50 | 14 | 88 | 22 |
| m (7) | α-BzO-ω-Ts-P(EG$_{0.93}$-co-GME$_{0.07}$) | 223 | 10 | 96 | 4 |

GE = Glycidyl ether; *DP* = degree of polymerization

Table 3: Characterization data of polymers prepared

Entry/ (Example)	Sample	$M_{n,NMR}$ [kg/mol]	$M_{n,MALDI}$ [kg/mol]	$M_{n,SEC}$ [kg/mol]	PDI_{SEC}	End-group fidelity MALDI
a (2)	α-BzO-P(EG$_{0.96}$-co-GME$_{0.04}$)	5.3	4.8	3.9	1.04	>99%
b (2)	α-BzO P(EG$_{0.92}$-co-GME$_{0.08}$)	5.2	5.3	4.5	1.05	>99%
c (2)	α-BzO P(EG$_{0.84}$-co-GME$_{0.16}$)	6.9	4.9	3.7	1.05	>99%
d (2)	α-BzO P(EG$_{0.76}$-co-GME$_{0.24}$)	6.0	5.2	3.8	1.06	>99%
e (3)	α-BzO P(EG$_{0.51}$-co-GME$_{0.49}$)	4.2	3.8	2.4	1.09	>99%
f (2)	α-BzO P(EG$_{0.96}$-co-GME$_{0.04}$)	10.9	8.5	7.5	1.08	>99%
g (2)	α-BzO P(EG$_{0.93}$-co-GME$_{0.07}$)	9.0	8.5	7.3	1.05	>99%
h (2)	α-MeO-P(EG$_{0.97}$-co-GME$_{0.03}$)	7.0	5.6	4.5	1.10	>99%
i (2)	α-DBzN-P(EG$_{0.97}$-co-GME$_{0.03}$)	6.9	5.1	4.0	1.08	>99%
j (4)	α-DBzN-EtO-PGME	4.2	4.0	2.7	1.05	>99%
k (5)	α-BzO-P(EG$_{0.85}$-co-EGE$_{0.15}$)	6.7	n.d.	4.2	1.09	n.d.
l (6)	α-MeO-PPEG$_{0.88}$-b-PGME$_{0.22}$	3.6	3.7	2.8	1.05	>99%
m (7)	α-BzO-ω-Ts-P(EG$_{0.93}$-co-GME$_{0.07}$)	11.1	8.8	n.d.	n.d.	>99%

M_n = molecular weight (number average molar mass), PDI = polydispersity.

Immunogenicity

As can be seen from Table 3, entries a to e show copolymers of the present invention which consisting of ethylene oxide repeating units and glycidyl methyl ether repeating units with about the same molecular weight, i.e. with an M_n of about 4 to 5 kg/mol. The amount of

GME$_{0.49}$), i.e. the polymer of Example 3 (entry e of Tables 2 and 3) with potassium and sodium cations. The only peaks visible here are the peaks of the product molecule. There are no peaks form macromolecules with a different end group. This shows that end-group fidelity of the polymers of the present invention is very high. In addition, the spectrum confirms the narrow molecular weight distribution.

Solubility

Figure 4 shows the cloud point measurement of α-BzO-P(EG0.51-co-GME0.49), i.e. the polymer of Example 3 (entry e of Tables 2 and 3). The cloud point determines the temperature at which immiscibility in water / in aqueous solution is observed upon heating. As an example, for the copolymer with 49% GME, the cloud point can be observed at 95 °C, showing excellent water solubility of the Poly(GME-co-EO) copolymers. The homopolymer PEG shows a cloud point of ca. 100°C. All other copolymers of the present invention with 26-49% GME are in between PEG and this copolymer, showing cloud points of 96-100°C. For copolymers of 25 mol% GME incorporation and lower no cloud point was detected in water at temperatures ranging from 0 to 99 °C. Thus, GME copolymerization hardly affects water solubility, which is a feature of the similar structure of polyethylene glycol and methyl ethyl ether. This is an important feature of the polymers of the present invention as it shows that they can substitute PEG in aqueous systems without causing problems with phase separation or even precipitation.

Homopolymers

Figure 12 shows the MALDI-TOF spectrum of the homopolymer of Example 4. The spectrum shows not only that the polymer has a low dispersity, but also that it is free from impurities deriving different end groups. The fact that besides the peaks of the product only white noise is visible shows that the end-group fidelity is about 100 %. Glycidyl methyl ether homopolymer has so far not been produced with these specifications.

Comparison of dispersity of end group fidelity of the polymers of the present invention with that of mPEG

Figure 13 shows an overlay of MALDI TOF spectra of commercially available mPEG and a block copolymer of the present invention (polymer of Example 6 (entry l of Tables 2 and 3). As can be seen, a clear shift between the macroinitiator mPEG and entry l is observed, indicating a successful block copolymer synthesis. Absence of macroinitiator in the MALDI-ToF MS of entry l further proves quantitative block copolymer formation. This is further proven by a distance of the signals of 44 g mol-1.

32

Modification of end groups

Figure 14 shows the MALDI TOF spectrum of α-BzO-ω-Ts-P(EG-co-GME), i.e. the polymer of Example 7 (see Tables 2 and 3, entry). In this polymer the ω-end group OH has been modified to a tosyl group. As can be seen from the spectrum, the modified polymer has the same narrow molecular weight distribution and the same high end-group fidelity. This shows that the polymers of the present invention can be modified as known for PEG.

Crystallinity

Table 4 shows thermal properties of some of the polymers of Tables 2 and 3:

Sample	T_g [°C]	T_m [°C]	ΔH_{PEG} [J/g]	$X_{c,PEG}$
a	-56	46	88.63	0.45
b	-56	45	76.79	0.39
c	-59	37	56.26	0.29
f	-59	35	58.22	0.30
g	-61	7	32.62	0.17
k	-56	46	88.63	0.45
l	-59	45	80.16	0.41

T_g = Glass transition temperature; T_m = Melting point; ΔH_{PEG} = Enthalpy of fusion; X_c = Crystallinity (all measurements by DSC)I

As can be seen, crystallinity of the inventive polymers is low. This prevents for example accumulation of the polymers in the kidney or in the liver.

Claims

1.   Polyether polymers represented by the following formula [I]:
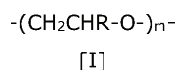
$$-(CH_2CHR-O-)_n-$$
$$[I]$$

wherein

-     residues R are independently from each other selected from the group consisting of hydrogen, methoxymethyl, ethoxymethyl, n-propoxymethyl and iso-propoxymethyl;

-     1 to 100% of the residues R are methoxymethyl;

-     up to 50% of the residues R may be selected from the group consisting of ethoxymethyl, n-propoxymethyl and iso-propoxymethyl;

-     with the proviso that at least one residue R is hydrogen, if at least one residue R is selected from the group consisting of ethoxymethyl, n-propoxymethyl and iso-propoxymethyl; and

-     m is in the range of from 10 to 1000,

characterized in that

the dispersity is 1.15 or less.

2.   Polyether polymer according to claim 1, wherein 5 to 95% of the residues R are hydrogen and 5 to 95% of the residues R are independently from each other selected from the group consisting of methoxymethyl, ethoxymethyl, n-propoxymethyl and iso-propoxymethyl.

3.   Polyether polymer according to any of the preceding claims, wherein the polyether is a poly(glycidyl methyl ether-co-ethylene oxide) copolymer.

4.   Polyether polymer according to any of the preceding claims, wherein 30 to 70% of the residues R are hydrogen and the remaining residues R are methoxymethyl.

5.   Polyether polymer according to any of the preceding claims, wherein the polymer is a random copolymer.

6.   Polyether polymers according to any of the preceding claims represented by the following formula [II]:

X-(CH$_2$CHR-O-)$_m$CH$_2$CHR-Y [II]
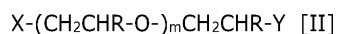
wherein X is selected from the group consisting of hydrogen, alkyl, hydroxy, sulfanyl, C1-C10-alkoxy, C1-C10-thioalkoxy, amino, amino-C1-C10-alkoxy, dibenzylamino-C1-C10-alkoxy, amide, N-heterocyclic carbenes and N-heterocyclic olefins;

Y is selected from the group consisting of hydrogen, hydroxy, alkoxy, -CH$_2$-C(=O)-R wherein R is as defined above, -CHO, alkylcarbonyloxy, alkyoxycarbonyloxy, amine, C1-C10-alkylamine, carboxamido, azide, halogen, sulfanyl, thioalkoxy, N-succinimidyl carbonate and sulfonate;

X and/or Y may also be selected from the group consisting of low molecular weight drugs, nanocarriers, liposomal structures, peptides, polypeptides, proteins, glycoproteins, polynucleotide, polysaccharides, lipid structures, liposomes, surfaces and interfaces, which are bonded directly by a covalent bond or by a spacer to the polymer,

m is in the range of from 9 to 999,

characterized in that

the dispersity is 1.15 or less.

7.   Polyether polymer according to claim 6, wherein X is alkoxy and Y is hydroxy.

8.   Polyether polymer according to any of claims 6 or 7, wherein end-group fidelity of the polymer in regard to group X and/or in regard to group Y is at least 95%.

9.   Conjugate, comprising a polyether polymer of any of the preceding claims and a substrate.

10.   Conjugate according to claim 9, wherein the substrate is selected from the groups consisting of low molecular weight drugs, nanocarriers, liposomal structures, peptides, polypeptides, proteins, glycoproteins, polynucleotides, polysaccharides, lipid structures, liposomes, surfaces and interfaces.

11.   Process for the preparation of a polyether polymer according to any of claims 1 to 8, by anionic ring-opening copolymerization comprising the steps of:

-       Providing an anion An$^-$,
-       Adding at least one monomer of the formula ◁-R, where in R is as defined in any

of claims 1 to 8,

-       Allowing the polymerization to proceed at a temperature in the range of -10 to 90 °C

wherein the monomer comprises less than 1 wt % of epichlorohydrin.

12.   Process according to claim 11, wherein the step of adding at least one monomer and the step of allowing the polymerization to proceed are repeated at least one time, whereby at least one different monomer is used than the first time.

13.   Process according to any of claims 11 or 12, wherein the counter ion to the An$^-$ anion is selected from the group consisting of Na$^+$, K$^+$ and Cs$^+$.

14.   Use of the polyether polymers according to any one of claims 1 to 8 for the preparation of a conjugate of the polymers with a bioactive compound.

15.   Use according to claim 14 for the preparation of conjugated lipids for use in vaccines, in particular based on lipid nanoparticles, wherein these nanoparticles are preferably nanoparticles, as used against COVID-19.

2020-104 UMZ   2021-05-14

36

Abstract

The present invention concerns polyether polymers represented by the following formula [I]:

$$-(CH_2CHR-O-)_m-$$

[I],

wherein residues R are hydrogen or C1-C3 alkoxymethyl, 1 to 100 % are methoxymethyl and up to 50% of R may be C2-C3 alkoxymethyl with the proviso that at least one R is hydrogen, if at least one R is C2-C3 alkoxymethyl; and m is in the range of from 10 to 1000, wherein the dispersity is 1.15 or less. The invention further concerns a process for their preparation, conjugates thereof and the use thereof.

2020-104 UMZ
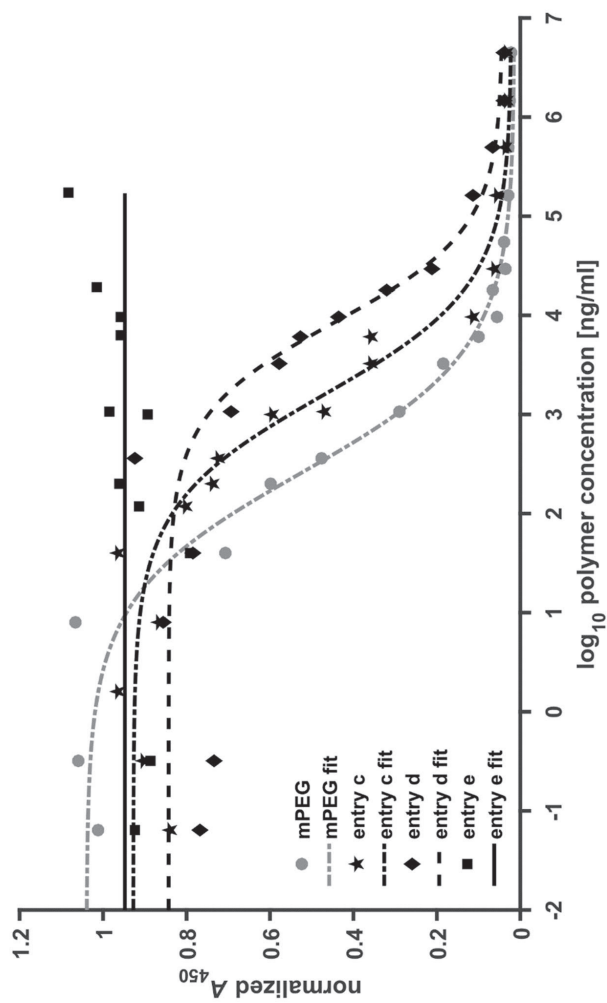
Figure 1
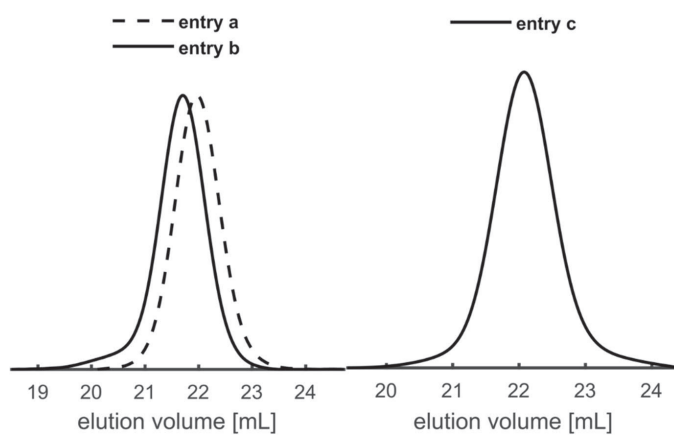
Figure 2

Figure 3

Figure 4

2
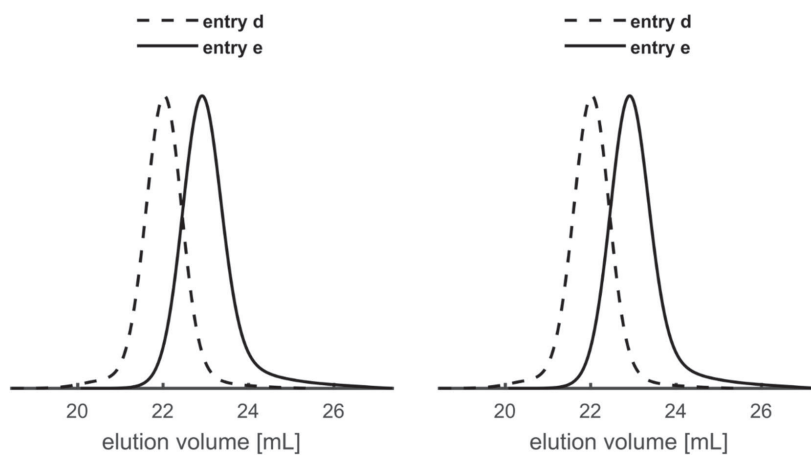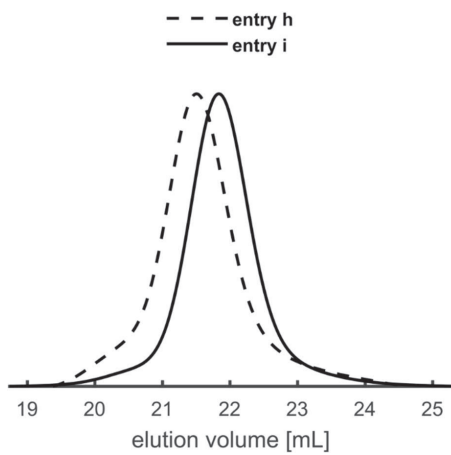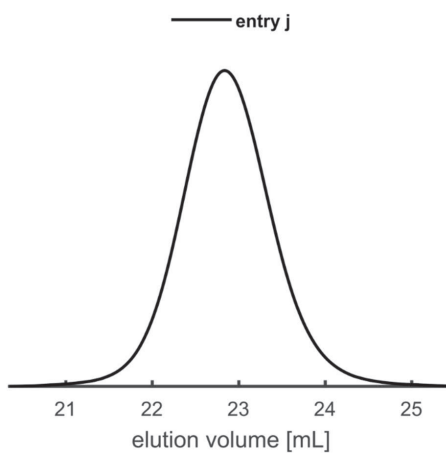
Figure 5

Figure 6

Figure 7
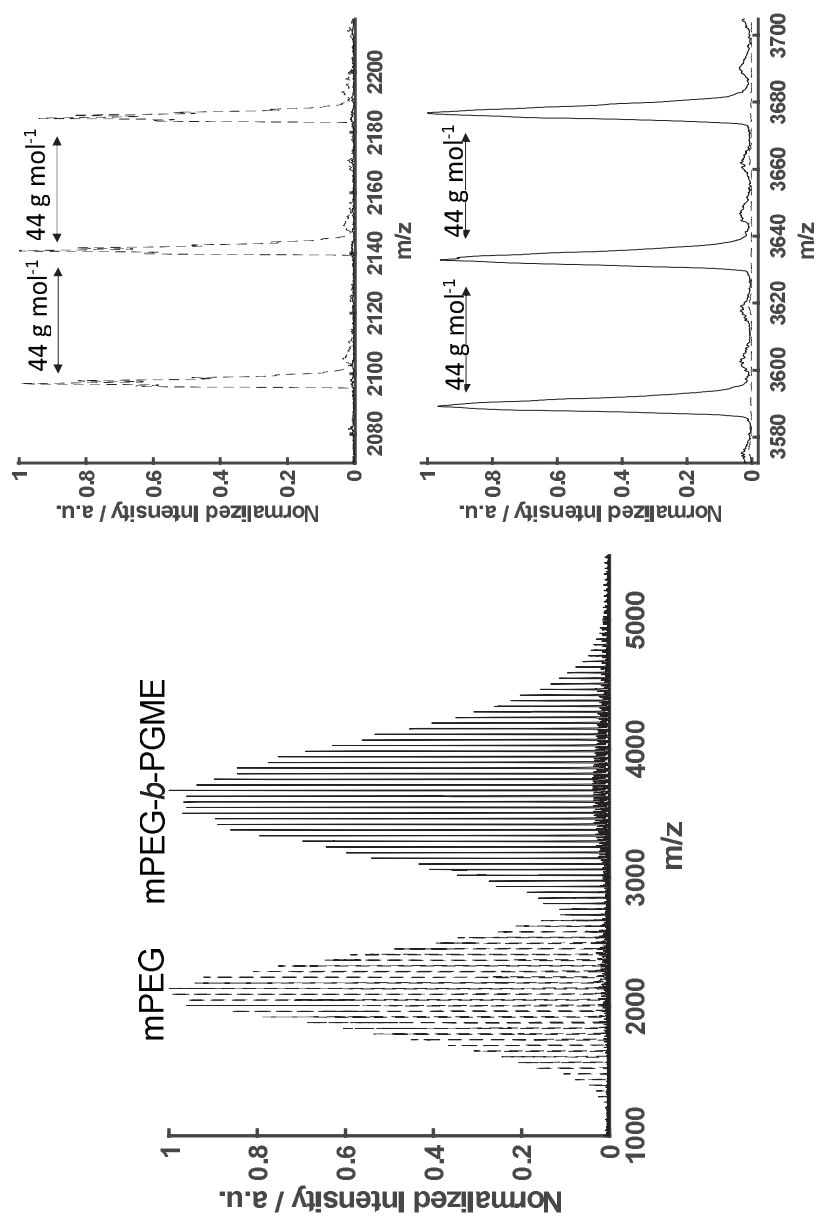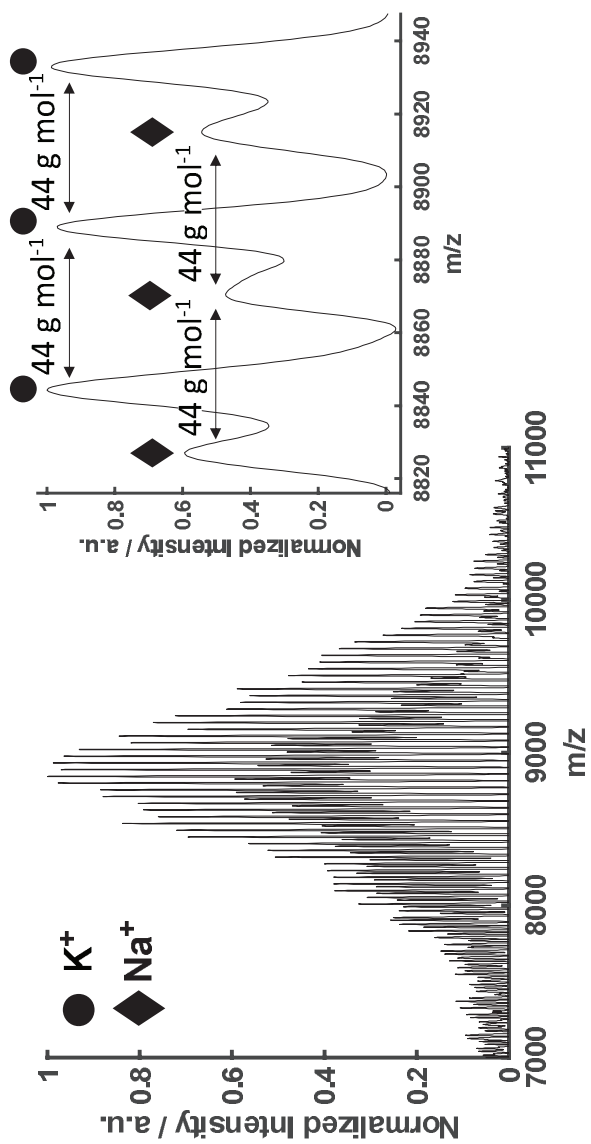

Figure 8

3

Figure 9

4
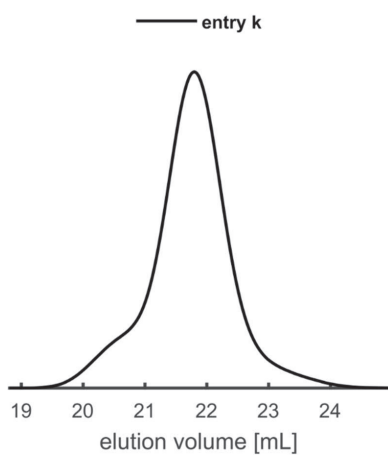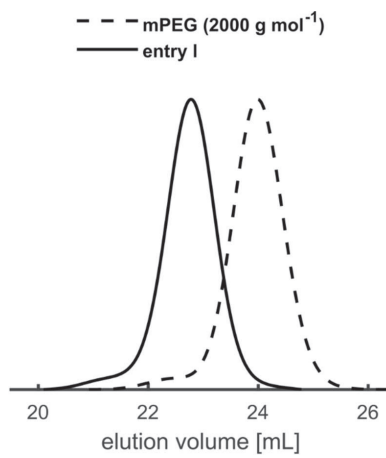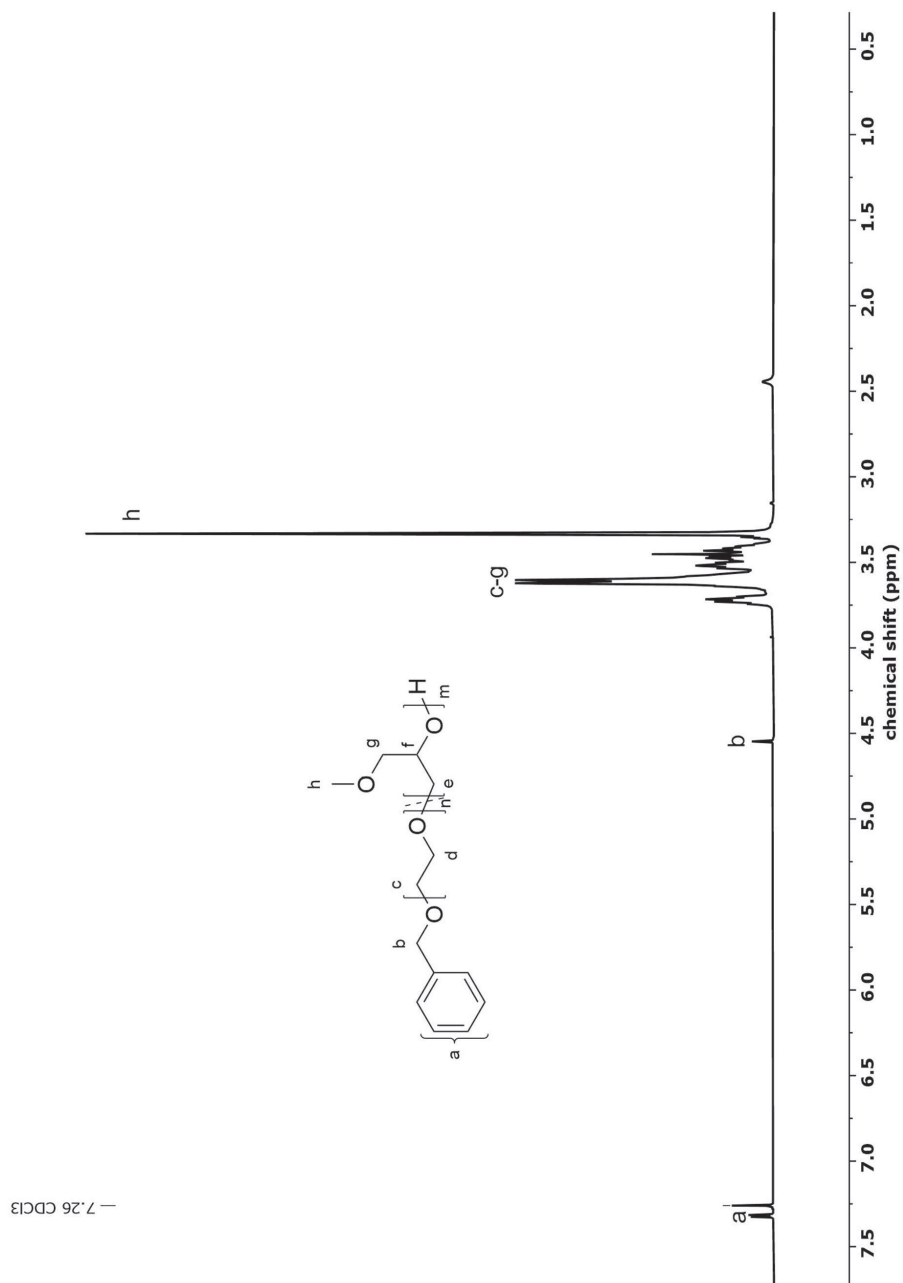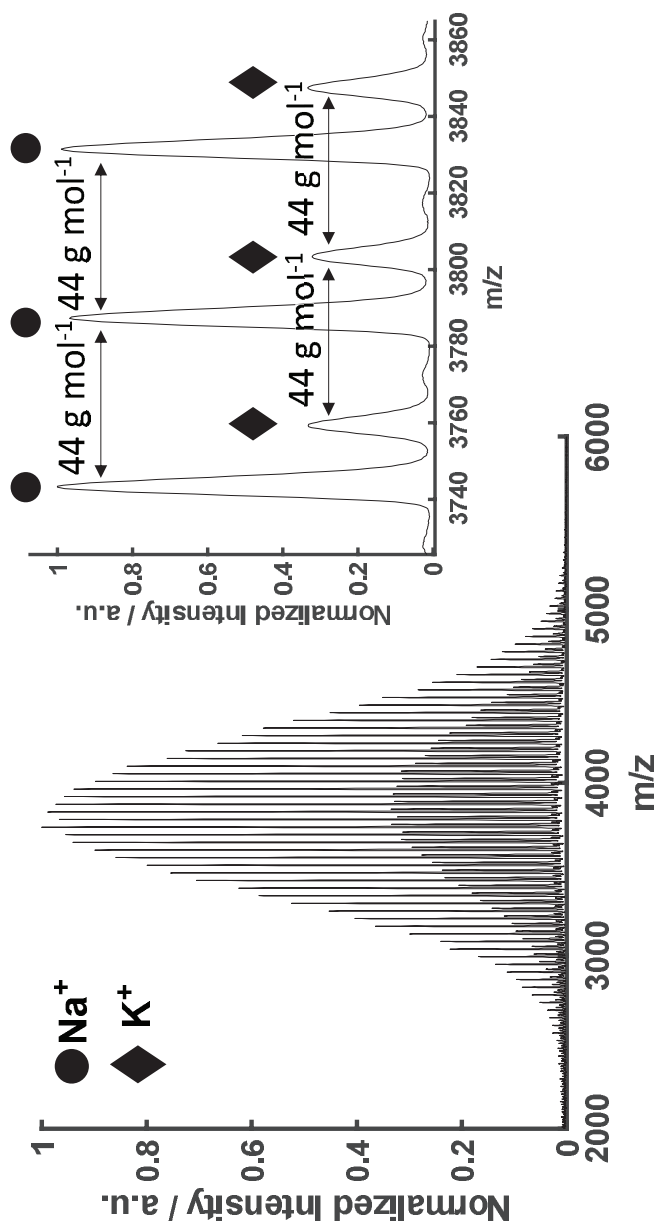
Figure 10

Figure 11

6
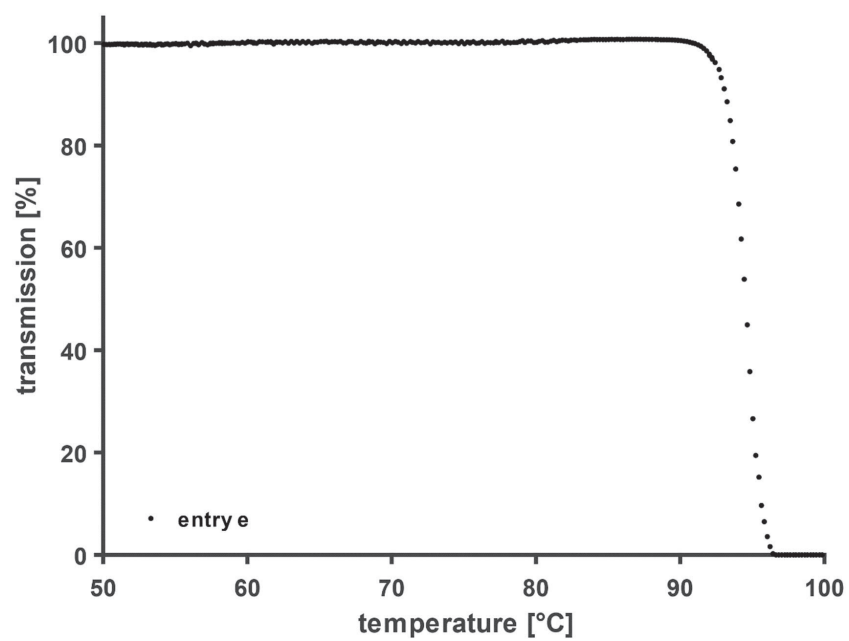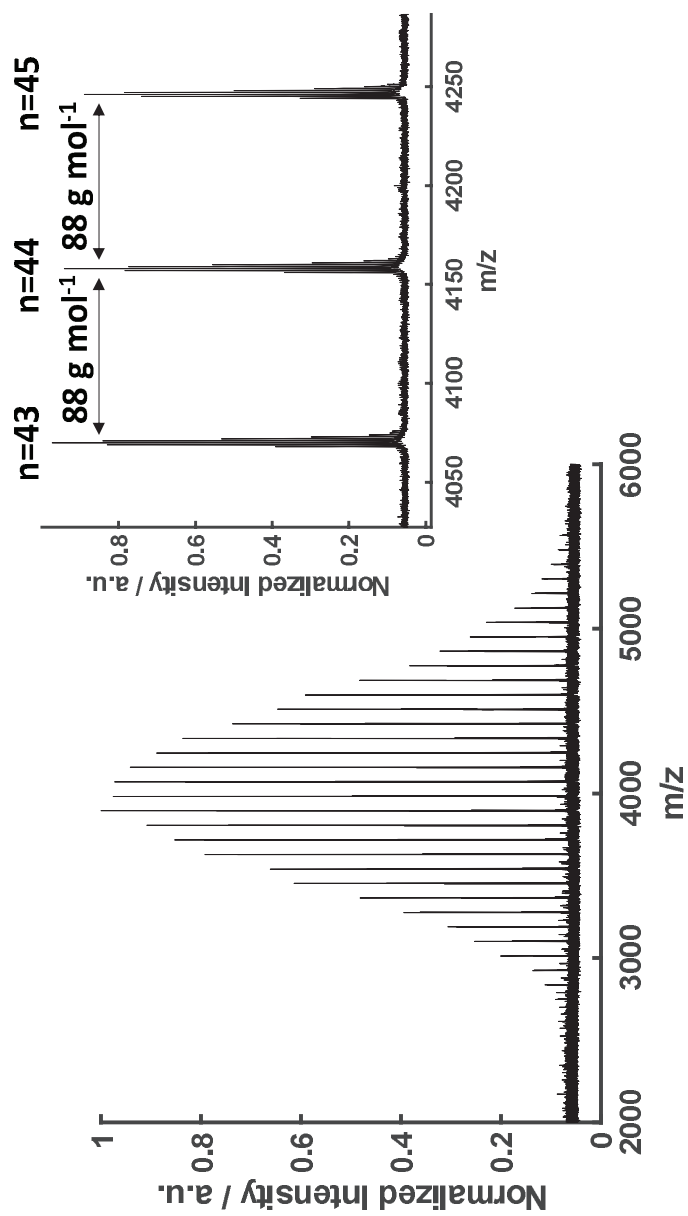
Figure 12

Figure 13

Figure 14

9

Figure 15

Figure 16

10